Natural Resources Canada | Ressources naturelles Canada

GEOLOGICAL SURVEY OF CANADA
OPEN FILE 8722

Targeted Geoscience Initiative 5: Advances in the understanding of Canadian Ni-Cu-PGE and Cr ore systems – Examples from the Midcontinent Rift, the Circum-Superior Belt, the Archean Superior Province, and Cordilleran Alaskan-type intrusions

Edited by
W. Bleeker and M.G. Houlé

2020

Canada

GEOLOGICAL SURVEY OF CANADA
OPEN FILE 8722

Targeted Geoscience Initiative 5: Advances in the understanding of Canadian Ni-Cu-PGE and Cr ore systems – Examples from the Midcontinent Rift, the Circum-Superior Belt, the Archean Superior Province, and Cordilleran Alaskan-type intrusions

Edited by
W. Bleeker and M.G. Houlé

Permanent link: https://doi.org/10.4095/326702

This publication is available for free download through GEOSCAN (https://geoscan.nrcan.gc.ca/)

Recommended citation

Bleeker, W. and Houlé, M.G. (ed.), 2020. Targeted Geoscience Initiative 5: Advances in the understanding of Canadian Ni-Cu-PGE and Cr ore systems – Examples from the Midcontinent Rift, the Circum-Superior Belt, the Archean Superior Province, and Cordilleran Alaskan-type intrusions; Geological Survey of Canada, Open File 8722, 225 p. https://doi.org/10.4095/326702

Publications in this series have not been edited; they are released as submitted by the author.

Contribution to the Geological Survey of Canada's Targeted Geoscience Initiative 5 (TGI-5) Program (2015-2020)

ACKNOWLEDGMENTS

Contributions to this TGI-5 synthesis volume on *Advances in the Understanding of Canadian Ni-Cu-PGE and Cr Ore Systems* are the culmination of five years of hard work by many individuals, including, of course, all individual authors, co-authors, and collaborators. The quality and clarity of each contribution were improved by critical reviewers and we would like to thank them for their efforts, specifically, Terry Boerboom of the Minnesota Geological Survey; Jim Miller, emeritus professor at the University of Minnesota, Duluth; James Moorhead, of the Ministère de l'Énergie et des Ressources naturelles du Québec (MERN); Thomas Clark, retired, formerly with the MERN; John Ayer, Laurentian University; Martin Tuchscherer, Tascan Geosciences Inc. and formerly with Freewest and Cliff Natural Resources; Charley Duran, with Independence Group; and Sarah Dare, Université du Québec à Chicoutimi. Furthermore, the editors of this volume provided additional critical reviews of each contribution, and a number of individuals critically read the manuscripts, among them Sarah Davey, GSC Ottawa; Tony LeCheminant, GSC Ottawa, retired; and Riku Metsaranta, Ontario Geological Survey. We sincerely thank them for taking the time to help improve the final products.

None of this research would have been possible without the active collaboration and assistance from countless individuals and organizations in industry. At Raglan, the geological staff of Glencore plc have been extremely helpful and accommodating over the years and we would like to mention in particular the following individuals: Benoit Soucy de Jocas, Adam White, Stéphanie Ouimet, Marilyn Rousseau, François Gagnon, François Baillargeon, and Mathieu Landry. The geological staff at Canadian Royalties are equally thanked for their assistance: Michael Li, Yueshi Lei, and Maxim Boisvert. For the research on the Midcontinent Rift around Lake Superior, we would like to sincerely thank the following individuals and industry partners for their keen interest, scientific input, and ongoing collaboration: Dean Rossel, Brian Goldner and Justin Laberge, at Rio Tinto; Steve Flank and Dave Peck, at North American Palladium; Grant Mourre and Scott McLean at Transition Metals; John McBride and Dave Good at Stillwater Canada; and numerous other individuals, including Bob Nowak and the geology staff at Eagle mine in Michigan. At the Ring of Fire, we would like to thank Ryan Weston, Geoff Heggie, Matt Deller, Matt Downey, and Alan Coutts, all at Noront; and Moe Lavigne, at KWG Resources. Other aspects of the research benefitted from the collaboration of Christine Vaillancourt and Ian Bliss at Northern Shield Resources; François Bissonnette and Jean-Marc Lulin at Azimut Exploration Inc.; Brigitte Dejou at Lasalle Exploration Corp.; Riku Metsaranta, at the Ontario Geological Survey; Christian Bohm, Chris Couëslan, and Marc Rinne, at the Manitoba Geological Survey; Patrice Roy, Andrea Amortegui, and Daniel Bandyayera, at the MERN, and Marc Choquette of Laval University. Many others we may have failed to mention here, but their time and efforts are much appreciated.

In putting the final volume together, two individuals deserve special praise, for countless hours of technical editing, lay-out production, and keeping track of hundreds of files and their various versions! Valérie Bécu, of the GSC Quebec, assisted with editing and oversaw the entire process, while Elizabeth Ambrose, of Ambrose & Associates, took care of overall editing and lay-out preparation, and correction of many small imperfections. Their professional efforts are reflected in the final volume.

Last but not least, we would like to thank our colleagues at the GSC and part of the TGI team, who assisted with a myriad of tasks to ensure the project remained on course: Kathleen Lauzière, for keeping track of the dollars, and Annick Morin, Gabriel Huot-Vézina, Étienne Girard, Pierre Brouillette, Marie-Pier Bédard, all of GSC Quebec, for GIS support and other technical assistance; and Rhian Evans and Christine Hutton, of GSC Ottawa, for much of the outreach and First Nations consultations. Thanks to all!

Wouter Bleeker and Michel Houlé
Ottawa, July 31, 2020

TABLE OF CONTENTS

Advances in the understanding of Canadian Ni-Cu-PGE and Cr ore systems – Examples from the Midcontinent Rift, the Circum-Superior Belt, the Archean Superior Province, and Cordilleran Alaskan-type intrusions

Preface

W. Bleeker

Geological Survey of Canada, 601 Booth Street, Ottawa, Ontario K1A 0E8
Author's e-mail: wouter.bleeker@canada.ca

INTRODUCTION

The present volume comprises a collection of nine papers summarizing research undertaken as part of the Geological Survey of Canada's Targeted Geoscience Initiative, Phase 5 (TGI-5). This 5-year thematic research program on Canadian ore systems ran from April 2015 to March 2020 with the broad aims of advancing the understanding of Canadian ore deposits and their broader ore system contexts, developing methods to help detect buried ore deposits, and providing public geoscience to increase the effectiveness of mineral exploration in both "brown fields" and "green fields" settings. The research program was designed around the concept of "ore systems" (e.g. Hronsky and Groves, 2008; Bleeker et al., 2014), i.e. the broader set of processes and their spatial-temporal context, and pre-history, that culminate in the formation and preservation of economic mineral deposits, often in clusters at the scale of a mining camp or at the larger scale of a mining district or geological province.

Implicit in this more holistic approach to ore deposit research, initially modelled on the system-scale approach typical of modern oil and gas exploration ("petroleum systems", see Wyborn et al., 1994), is the concept that individual constituents that make up an ore deposit are generally derived from dispersed sources, then transported by some medium, and finally precipitated and concentrated to ore levels at some depositional site, and under a highly specific set of circumstances (Fig. 1). The ore system approach thus involves the entire "process chain" from ultimate source reservoirs, such as the lower crust ("sources"), and transport pathways ("conduits"), to final depositional sites ("traps"). It also is cognizant of the post-depositional processes that play important roles in long-term preservation (e.g. sedimentary and/or tectonic burial), without which few ancient orebodies would be preserved.

For practical reasons, the thematic research of TGI-5 was organized into five major ore systems (orthomagmatic systems, gold systems, volcanic and sedimentary systems, porphyry-related systems, and uranium ore systems). This volume presents results from the orthomagmatic ore system that focused on Ni-Cu-PGE and Cr deposits. Some studies included here involved a detailed look at the Fe-Ti oxides associated with these deposits.

Of the nine individual contributions to this volume, eight were funded directly by the TGI-5 program and led by researchers from the Geological Survey of Canada (GSC). The final contribution to the present volume, on mineralized "Alaskan-type" intrusions (Irvine, 1974) in the Canadian Cordillera, was funded in part by the research grants component of the TGI-5 program—competitive grants that are awarded to selected researchers external to the GSC.

SYNOPSIS OF INDIVIDUAL CONTRIBUTIONS

The nine papers in this volume present research results on orthomagmatic ore systems across time and from across Canada, from Archean systems in the various subprovinces of the Superior craton, to komatiite-hosted magmatic sulphide deposits of the Paleoproterozoic "Circum-Superior Belt" on the margins of this craton, to the younger Proterozoic rift system of the ca. 1.1 Ga Midcontinent Rift, and finally the much younger Alaskan-type intrusions associated with Phanerozoic orogenic settings in the Canadian Cordillera (Fig. 2). For a complete list of peer-reviewed journal papers, government reports, and student theses stemming from the Orthomagmatic Ni-Cu-

Bleeker, W., 2020. Preface; *in* Targeted Geoscience Initiative 5: Advances in the understanding of Canadian Ni-Cu-PGE and Cr ore systems – Examples from the Midcontinent Rift, the Circum-Superior Belt, the Archean Superior Province, and Cordilleran Alaskan-type intrusions, (ed.) W. Bleeker and M.G Houlé; Geological Survey of Canada, Open File 8722, p. 1–6. https://doi.org/10.4095/326835

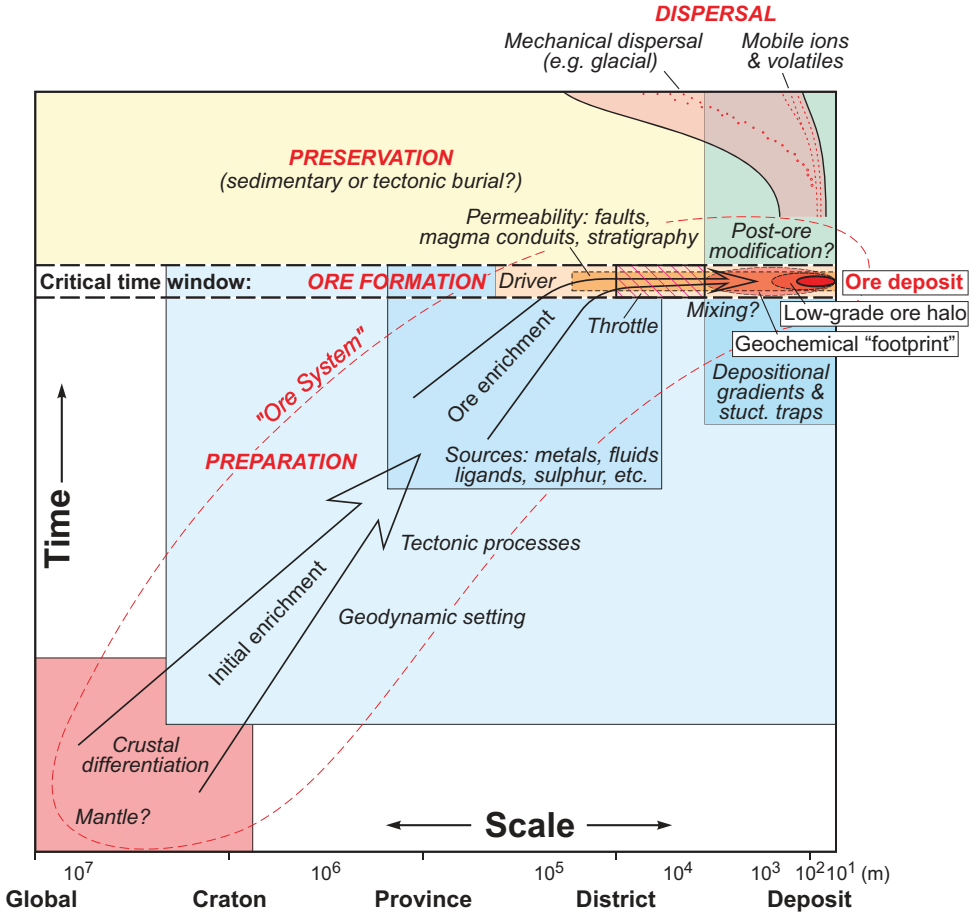

Figure 1. Diagram of geological time versus spatial scale illustrating the concept of complex mineral systems culminating in an economic ore deposit (small red ellipse along the right axis). The existence of an ore deposit accessible to mining typically involves initial preparatory processes (e.g. metal enrichment in the lower crust), a number of critically linked ore-formation processes (often with specific tectonic drivers, and typically operating in a narrow time-interval), and finally preservation (e.g. tectonic burial and/or sedimentary burial). These linked processes occur across a vast range of scales. Initially, large-scale geodynamic and tectonic processes concentrate elements of interest into a regional- to district-scale source region, from which they are stripped by hydrothermal fluids or magmas. Faults or other permeable zones (magmatic conduits, stratigraphy?) then focus metal-bearing fluids or magmas into depositional environments where chemical, physical, and/or thermal gradients lead to ore deposition. After passing through the depositional environment, spent fluids disperse into the environment. Many of these processes leave forensic evidence, such as hydrothermal alteration, that can be used to locate mineral deposits and their more extensive geochemical "footprints". Post-depositional dispersal of ore constituents or "pathfinder" elements, whether by chemical or mechanical means, may again enlarge the scale of the exploration target. (*from* Bleeker et al., 2014; *modified after* http://www.ga.gov.au/minerals/projects/current-projects/mineral-systems-of-australia.html#)[1].

PGE-Cr Ore Systems Project under TGI-5, the reader is referred to the Appendix at the end of this volume.

The ca. 1.1 Ga Midcontinent Rift System and its Mineralized Intrusions

(1) Starting with the Midcontinent Rift system, **Bleeker et al. (2020)** present an overview of this superbly preserved late Mesoproterozoic rift system thought to be associated with an upwelling mantle plume. A large and diverse set of intrusions is associated with this rift system, many of which are mineralized. Some of the key mineralized settings are described and new U-Pb ages are presented for several of the key intrusions, placing them in a more refined evolution of the rift system. Mineralized intrusions are not confined to a single magmatic pulse, but distributed through time and associated with each major magmatic pulse, from ca. 1117 to 1092 Ma. Many of the mineralized intrusions show

[1]This diagram is designed to illustrate, in particular, the process chain inherent to magmatic and hydrothermal ore systems. It is only partially applicable to some other ore systems, such as, for example, those forming on the seafloor due to selective scavenging of metals and adsorption onto highly condensed organic-rich black muds. The ore system of such deposits (HEBS: highly enriched black shales), involves a continental weathering cycle, delivery of metals to the global oceans, and finally highly specific adsorption processes. In that particular system there is again a lengthy preparatory stage, conduits in the sense or rivers, but no explicit "throttle".

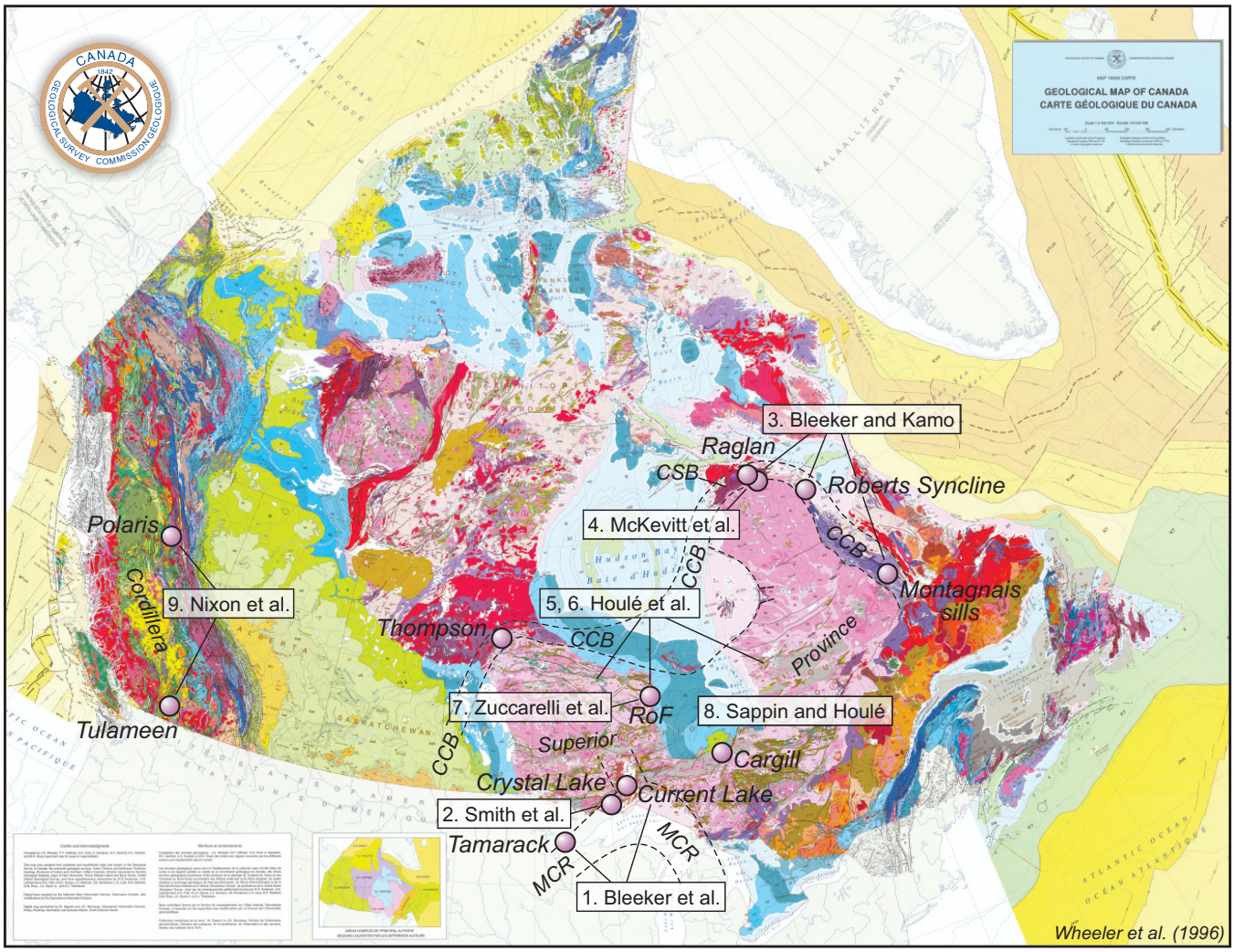

Figure 2. Geological map of Canada (*from* Wheeler et al., 1996) highlighting the project areas and deposit locations addressed by the present volume. The specific research areas for the nine papers in this volume are indicated. Abbreviations: CCB = the Paleoproterozoic Circum-Superior Belt (southern part of this belt not shown); CSB = Cape Smith Belt; MCR = the ca. 1.1 Ga Midcontinent Rift; RoF = the Ring of Fire area in northern Ontario. New high-precision ages for the Cargill carbonatite, internal to the Superior Province, and the Montagnais sills in the Labrador Trough are part of the Bleeker and Kamo study (2020).

evidence of a dynamic multi-phase intrusive history. This research involved numerous partners from industry, Canadian universities, the Ontario Geological Survey, and scientists from geological survey organizations south of the border.

(2) In a companion paper, **Smith et al. (2020)** focus in on one of the mineralized intrusions, the Crystal Lake intrusive complex ~40 km southwest of Thunder Bay. New high-precision geochronology on multiple phases of this interesting intrusive complex show this intrusion to be ca. 1093 Ma, and thus one of the youngest mineralized intrusions of the Midcontinent Rift. Sulphide mineralization is associated with varitextured "taxitic" gabbros and Smith et al. (2020) draw attention to peculiar spherical sulphide globules with silicate caps—thought to represent former vapour bubbles and attached sulphide globules—that have been described from other mineralized intrusions in recent years (Barnes et al., 2017). A detailed mineral deportment study of four samples is used to characterize the mineral assemblages and mineral characteristics of the platinum group element and precious metal phases. Modern laser ablation-inductively coupled plasma-mass spectrometry (LA-ICP-MS) mapping is used to further characterize compositional details of the various ore minerals and reveals a peculiar microfabric and metal redistribution in some of the sulphides. The authors conclude that sulphur assimilation from country rocks played a critical role in reaching S saturation but that this likely happened prior to final emplacement.

The Paleoproterozoic Circum-Superior Belt and its ca. 1882 Ma Magmatism

(3) Changing focus to the Paleoproterozoic Circum-Superior Belt (Baragar and Scoates, 1981), **Bleeker and Kamo (2020)** review and provide important new

details on the structural and stratigraphic setting of the Cape Smith Belt of northern Quebec. They show that the central part of the belt, hosting the mineralized "Raglan Horizon", is much less affected by thrust imbrication than previously thought and that the critical stratigraphy is relatively coherent, with the Raglan Horizon being a primary stratigraphic contact. New high-precision geochronology shows that the mineralized peridotite bodies, representing channelized komatiite lava flows, are ca. 1882 Ma, as are differentiated gabbro sills immediately below and above the ore-bearing horizon. This age is identical to that of mineralized komatiites in the Thompson Belt of northern Manitoba and mafic-ultramafic magmatic activity across the Superior craton and around its margins. The authors argue that the overall context appears to be one of mantle plume upwelling and continental breakup rather than one of arc and back-arc processes. The overall scale of this ca. 1882 Ma magmatic event was sufficient to perturb the global ocean-atmosphere system as it is shown that the onset of the major Sokoman iron formation of the Labrador Trough, and broadly correlative iron formations elsewhere along the Circum-Superior Belt, was exactly coeval with the climax of this magmatic event. At Raglan, the authors favour a model of several anastomosing komatiite lava channels that flowed to the north-northeast, rather than a single, giant, meandering lava channel. Finally, the authors show that the Cape Smith stratigraphy can be correlated with that of the northern Labrador Trough.

(4) **McKevitt et al. (2020)** present the initial results of a major compilation of geochemical data from a large number of sources (~18,800 unique whole-rock analyses, with metadata) on mafic-ultramafic volcanic and intrusive rocks of the Cape Smith Belt and neighbouring domains. These data are then used to expand on the geochemical differences and similarities among the major magmatic suites of the Cape Smith Belt, i.e. the Povungnituk Group and the Chukotat Group and their respective subvolcanic intrusive components. In particular, the geochemical data are used to explore the question whether the ultramafic dyke-like system in the southern part of the Cape Smith Belt, mineralized ultramafic occurrences that are known as the "Expo Trend", could have fed the on-average higher MgO komatiite lava channels of the "Raglan Trend" (i.e. the Raglan Horizon). Both important similarities and differences are identified, and highly incompatible trace element ratios show continuity in data points between the two trends, the main difference being that the mineralized komatiite lavas are more contaminated. Nevertheless, the authors favour an interpretation in which the Expo Trend dykes are not the exact feeders to the Raglan komatiite channels (cf. Bleeker and Kamo, 2020). This conclusion should be tempered, however, with the important realization that the large feeder dyke systems likely had an extended period of activity and that batches of magma that now fill the dyke system are not the same batches that erupted to the surface and fed the komatiite flows at the peak of the fissure eruptions. Furthermore, no other feeder dyke system has been identified.

The Archean Superior Province and its Mafic and Ultramafic Magmatism

(5) Moving to the Archean Superior Province, **Houlé et al. (2020a)** provide results to date of an on-going compilation of all Mesoarchean to Neoarchean mafic-ultramafic and ultramafic intrusives across this province, as well as all known komatiite occurrences. Regional groupings can be defined, some well known, others emerging or tentative. Using this compilation, the authors also summarize all known magmatic Ni-Cu-PGE, Cr-PGE, and Fe-Ti-V deposits and significant orthomagmatic mineral occurrences across the province. The age distribution of these deposits, to the extent it is known, is presented and discussed, as are the available resource estimates. Finally, the authors speculate on the tectonic and magmatic processes that may have shaped the overall distribution.

(6) In a second contribution, **Houlé et al. (2020b)** focus in on the so-called "Ring of Fire" area in northern Ontario, one of the most significant emerging mineral deposit regions in Canada, particularly for orthomagmatic chromite deposits, and also Ni-Cu-PGE sulphide deposits. The geology of the Ring of Fire area is briefly reviewed, before focusing in on the 2736–2732 Ma Esker intrusive complex of the arcuate McFaulds Lake greenstone belt (Metsaranta et al., 2015). This now-vertical, southeast-facing, intrusive complex, with a strike-length of ~15 to 20 km, consists of several composite ultramafic to mafic bodies (e.g. Black Thor and Double Eagle intrusions), now partly dismembered by faults, that host the very significant stratiform chromite deposits with chromitite layers up to 80 m thick. The authors argue for a model in which several large blade-shaped dykes intruded upwards and laterally across a footwall of older tonalites, then widened due to magma inflation, and finally coalesced into a differentiated layered complex, with the laterally extensive chromitite layers towards the upper parts of the composite intrusion. This model differs in detail from an earlier model of a single, large, dismembered layered intrusion (Mungall et al., 2010). Finally, the authors discuss their model in which the very significant chromitite layers of this intrusive complex are in part the result of assimilation and incorporation, and the reactive transformation into chromite, of magnetite xenocrysts derived from older iron formations in the footwall; a model that is not without its problems (Brenan et al., 2019, 2020). Pros and cons are discussed.

(7) **Zuccarelli et al. (2020)** present the results of a petrographic and sulphide textural study of Ni-Cu-PGE mineralized samples from the Eagle's Nest deposit, McFaulds Lake greenstone belt, in the Ring of Fire area of northern Ontario. The Eagle's Nest deposit is hosted by an ultramafic dyke-like body that is part of the ca. 2730 Ma Esker intrusive complex (Metsaranta et al., 2015). This study of 200 representative core samples helped to define the distribution of different ore types along the subvertical western margin of the conduit-like body. The relatively new technique of "high-resolution desktop microbeam scanning energy-dispersive X-ray fluorescence spectrometry" (μXRF), employing a ~40 μm X-ray beam, was then applied to a subset of polished core specimens to map the detailed compositional and textural features that are not easily visible by standard macroscopic and microscopic observation. The imaging technique also highlighted the presence of various inclusions (xenoliths) in some of the ore types, including chromitite, gabbro, and barren country rock clasts, supporting a dynamic evolution of the conduit-like body with multiple pulses of magma injection.

(8) **Sappin and Houlé (2020)** report on an investigation of minor and trace element compositions of Fe-Ti oxides from eleven Archean mafic to ultramafic intrusions from across parts of the Superior Province, specifically the Wawa-Abitibi subprovince and the Bird River-Uchi-Oxford-Stull-La Grande Rivière-Eastmain ("BUOGE") superdomain. Magnetite compositions depend on many factors, ranging from parental magma compositions and processes during crystal fractionation (e.g. what are the co-crystallizing phases) and the oxygen fugacity of the magma, to the history and degree of post-crystallization exsolution processes and redistribution of elements during metamorphism. Nevertheless, it may serve as a useful petrogenetic indicator and fractionation index. The authors collected both electron microprobe data and laser ablation data on their samples and compare the results of each approach. Finally, they evaluate their results in the context of previously established discrimination diagrams and discuss the implications of their work.

Mineralized Alaskan-type Intrusions in the Canadian Cordillera

(9) In the final contribution to this volume, **Nixon et al. (2020)** present new data and observations on a number of Mesozoic "Alaskan-type" ultramafic-mafic intrusions in the accreted arc terranes of the Canadian Cordillera, specifically the Tulameen and Polaris composite intrusions. New high-precision U-Pb age data of ca. 204–205 Ma are presented for two distinct phases of the Tulameen intrusion, ages that fall within a 6 Myr time interval during which the most important porphyry Cu-Au deposits in British Columbia were emplaced. The overall setting and internal structure of both intrusions are described in detail, as are details of sulphide mineralization. Traditionally these intrusions were better known for their chromitites and associated PGE mineralization and derived placer deposits (e.g. Cabri et al., 1973; Nixon et al., 1990). An interesting aspect of both intrusions is the complex relationships among ultramafic cumulate rocks and the associated chromitite occurrences, clearly indicating a dynamic environment where cumulate rocks and chromitites were disrupted and complexly intermingled. Chaotic blocks of chromitite and dunite of various sizes are mixed with clinopyroxenite cumulate rocks. Nixon et al. (2020) note that such relationships have been observed in many other Alaskan-type intrusions and attribute them to remobilization and magmatic avalanches during dynamic recharge of new magma pulses into the base of the intrusions.

ACKNOWLEDGMENTS

We would like to thank all the authors and their collaborators that contributed to the body of research contained in this volume, as well as the many reviewers that provided constructive criticism on initial manuscripts. Valérie Bécu assisted with the technical editing and Elizabeth Ambrose took care of final editing, correction of minor imperfections, and preparation for publication. Both are thanked for their skillful assistance. Last but not least, members of the TGI-5 team are thanked for taking care of a myriad of tasks from general project management to outreach and consultations, without which none of this research could have proceeded. Thanks to all!

REFERENCES

Baragar, W.R.A. and Scoates, R.F.J., 1981. The circum-Superior belt: A Proterozoic plate margin?; *in* Developments in Precambrian Geology, v. 4, (ed.) A. Kröner; Elsevier, Amsterdam, The Netherlands, p. 297–330.

Barnes, S.J., Mungall, J.E., Le Vaillant, M., Godel, B., Lesher, C.M., Holwell, D., Lightfoot, P.C., Krivolutskaya, N., and Wei, B., 2017. Sulfide-silicate textures in magmatic Ni-Cu-PGE sulfide ore deposits: Disseminated and net-textured ores; American Mineralogist, v. 102, p. 473–506.

Bleeker, W. and Kamo, S., 2020. Structural-stratigraphic setting and U-Pb geochronology of Ni-Cu-Co-PGE ore environments in the central Cape Smith Belt, Circum-Superior Belt; *in* Targeted Geoscience Initiative 5: Advances in the understanding of Canadian Ni-Cu-PGE and Cr ore systems – Examples from the Midcontinent Rift, the Circum-Superior Belt, the Archean Superior Province, and Cordilleran Alaskan-type intrusions, (ed.) W. Bleeker and M.G. Houlé; Geological Survey of Canada, Open File 8722, p. 65–98. https://doi.org/10.4095/326882

Bleeker, W., Mercier-Langevin, P., and Ames, D., 2014. Science Recommendations for Future Mineral Research Programs; Geological Survey of Canada, internal report, 33 p.

Bleeker, W., Smith, J., Hamilton, M., Kamo, S., Liikane, D., Hollings, P., Cundari, R., Easton, M., and Davis, D., 2020. The

Midcontinent Rift and its mineral systems: Overview and temporal constraints of Ni-Cu-PGE mineralized intrusions; *in* Targeted Geoscience Initiative 5: Advances in the understanding of Canadian Ni-Cu-PGE and Cr ore systems – Examples from the Midcontinent Rift, the Circum-Superior Belt, the Archean Superior Province, and Cordilleran Alaskan-type intrusions, (ed.) W. Bleeker and M.G. Houlé; Geological Survey of Canada, Open File 8722, p. 7–35.

Brenan, J.M., Woods, K., Mungall, J.E., and Weston, R., 2019. Origin of Chromitites in the Ring of Fire Part II: Trace element fingerprinting of contaminants; *in* Targeted Geoscience Initiative 5 Grant Program interim reports 2018–2019; Geological Survey of Canada, Open File 8620, p. 5–18.

Brenan, J.M., Woods, K., Mungall, J.E., and Weston, R., in press. Origin of chromitites in the Ring of Fire intrusive suite as revealed by chromite trace element chemistry and simple crystallization models; *in* Targeted Geoscience Initiative 5: Grant program final reports (2018–2020); Geological Survey of Canada, Open File 8734.

Cabri, L.J., Owens, D.R., and Laflamme, J.G., 1973. Tulameenite, a new platinum-iron-copper mineral from placers in the Tulameen River area, British Columbia; The Canadian Mineralogist, v. 12, p. 21–25.

Hronsky, J.M.A. and Groves, D.I., 2008. Science of targeting: definition, strategies, targeting and performance measurement; Australian Journal of Earth Sciences, v. 55, p. 3–12.

Houlé, M.G., Lesher, C.M., Sappin, A.-A., Bédard, M.-P., Goutier, J., and Yang, X.M., 2020a. Overview of Ni-Cu-(PGE), Cr-(PGE), and Fe-Ti-V magmatic mineralization in the Superior Province: Insights on metallotects and metal endowment; *in* Targeted Geoscience Initiative 5: Advances in the understanding of Canadian Ni-Cu-PGE and Cr ore systems – Examples from the Midcontinent Rift, the Circum-Superior Belt, the Archean Superior Province, and Cordilleran Alaskan-type intrusions, (ed.) W. Bleeker and M.G. Houlé; Geological Survey of Canada, Open File 8722, p. 117–139.

Houlé, M.G., Lesher, C.M., Metsaranta, R.T., Sappin, A.-A., Carson, H.J.E., Schetselaar, E.M., McNicoll, V., and Laudadio, A., 2020b. Magmatic architecture of the Esker intrusive complex in the Ring of Fire intrusive suite, McFaulds Lake greenstone belt, Superior Province, Ontario: Implications for the genesis of Cr and Ni-Cu-(PGE) mineralization in an inflationary dyke-chonolith-sill complex; *in* Targeted Geoscience Initiative 5: Advances in the understanding of Canadian Ni-Cu-PGE and Cr ore systems – Examples from the Midcontinent Rift, the Circum-Superior Belt, the Archean Superior Province, and Cordilleran Alaskan-type intrusions, (ed.) W. Bleeker and M.G. Houlé; Geological Survey of Canada, Open File 8722, p. 141–163.

Irvine, T.N., 1974. Petrology of the Duke Island ultramafic complex, southeastern Alaska; Geological Society of America, Memoir 138, 240 p.

McKevitt, D.J., Lesher, C.M., and Houlé, M.G., 2020. Regional lithogeochemical synthesis of mafic-ultramafic volcanic and intrusive rocks in the Cape Smith Belt, Nunavik, northern Quebec; *in* Targeted Geoscience Initiative 5: Advances in the understanding of Canadian Ni-Cu-PGE and Cr ore systems – Examples from the Midcontinent Rift, the Circum-Superior Belt, the Archean Superior Province, and Cordilleran Alaskan-type intrusions, (ed.) W. Bleeker and M.G. Houlé; Geological Survey of Canada, Open File 8722, p. 99–115.

Metsaranta, R.T., Houlé, M.G., McNicoll, V.J., and Kamo, S.L., 2015. Revised geological framework for the McFaulds Lake greenstone belt, Ontario; *in* Targeted Geoscience Initiative 4: Canadian Nickel-Copper-Platinum Group Elements-Chromium Ore Systems — Fertility, Pathfinders, New and Revised Models, (ed.) D.E. Ames and M.G. Houlé; Geological Survey of Canada, Open File 7856, p. 61–73.

Mungall, J.E., Harvey, J.D., Balch, S.J., Azar, B., Atkinson, J., and Hamilton, M.A., 2010. Eagle's Nest: A magmatic Ni-sulfide deposit in the James Bay Lowlands, Ontario, Canada; *in* The Challenge of Finding New Mineral Resources: Global Metallogeny, Innovative Exploration, and New Discoveries, Volume I: Gold, Silver, and Copper-Molybdenum, (ed.) R.J. Goldfarb, E.E. Marsh and T. Monecke; Society of Economic Geologists, Special Publication 15, p. 539–559.

Nixon, G.T., Cabri, L.J., and Laflamme, J.G., 1990. Platinum-group-element mineralization in lode and placer deposits associated with the Tulameen Alaskan-type complex, British Columbia; The Canadian Mineralogist, v. 28, p. 503–535.

Nixon, G.T., Scoates, J.S., Milidragovic, D., Nott, J., Moerhuis, N., Ver Hoeve, T.J., Manor, M.J., and Kjarsgaard, I.M., 2020. Convergent margin Ni-Cu-PGE-Cr ore systems: U-Pb petrochronology and environments of Cu-PGE versus Cr-PGE mineralization in Alaskan-type intrusions; *in* Targeted Geoscience Initiative 5: Advances in the understanding of Canadian Ni-Cu-PGE and Cr ore systems – Examples from the Midcontinent Rift, the Circum-Superior Belt, the Archean Superior Province, and Cordilleran Alaskan-type intrusions, (ed.) W. Bleeker and M.G. Houlé; Geological Survey of Canada, Open File 8722, p. 197–218.

Sappin, A.-A. and Houlé, M.G., 2020. The composition of magnetite in Archean mafic-ultramafic intrusions within the Superior Province; *in* Targeted Geoscience Initiative 5: Advances in the understanding of Canadian Ni-Cu-PGE and Cr ore systems – Examples from the Midcontinent Rift, the Circum-Superior Belt, the Archean Superior Province, and Cordilleran Alaskan-type intrusions, (ed.) W. Bleeker and M.G. Houlé; Geological Survey of Canada, Open File 8722, p. 181–196.

Smith, J.W., Bleeker, W., Hamilton, M., Petts, D., Kamo, S.L., and Rossell, D., 2020. Timing and controls on Ni-Cu-PGE mineralization within the Crystal Lake Intrusion, 1.1 Ga Midcontinent Rift; *in* Targeted Geoscience Initiative 5: Advances in the understanding of Canadian Ni-Cu-PGE and Cr ore systems – Examples from the Midcontinent Rift, the Circum-Superior Belt, the Archean Superior Province, and Cordilleran Alaskan-type intrusions, (ed.) W. Bleeker and M.G. Houlé; Geological Survey of Canada, Open File 8722, p. 37–63.

Wheeler, J.O., Hoffman, P.F., Card, K.D., Davidson, A., Sanford, B.V., Okulitch, A.V., and Roest, W.R., 1996. Geological map of Canada; Geological Survey of Canada, "A" Series Map 1860A, 3 sheets, 1 .zip file, scale 1:5 000 000.

Wyborn, L.A.I., Heinrich, C.A., and Jaques, A.L., 1994. Australian Proterozoic Mineral Systems: Essential Ingredients and Mappable Criteria; Geoscience Australia. Australian Institute of Mining and Metallurgy Annual Conference, Proceedings, p. 109–115.

Zuccarelli, N., Lesher, C.M., Houlé, M.G., and Barnes, S.J., 2020. Variations in the textural facies of sulphide minerals in the Eagle's Nest Ni-Cu-(PGE) deposit, McFaulds Lake greenstone belt, Superior Province, Ontario: Insights from microbeam scanning energy-dispersive X-ray fluorescence spectrometry; *in* Targeted Geoscience Initiative 5: Advances in the understanding of Canadian Ni-Cu-PGE and Cr ore systems – Examples from the Midcontinent Rift, the Circum-Superior Belt, the Archean Superior Province, and Cordilleran Alaskan-type intrusions, (ed.) W. Bleeker and M.G. Houlé; Geological Survey of Canada, Open File 8722, p. 165–179.

The Midcontinent Rift and its mineral systems: Overview and temporal constraints of Ni-Cu-PGE mineralized intrusions

Wouter Bleeker[1*], Jennifer Smith[1], Michael Hamilton[2], Sandra Kamo[2], Dustin Liikane[2,3], Pete Hollings[4], Robert Cundari[5], Michael Easton[6], and Don Davis[2]

[1]Geological Survey of Canada, 601 Booth Street, Ottawa, Ontario K1A 0E8
[2]Jack Satterly Geochronology Laboratory, University of Toronto, 22 Russell Street, Toronto, Ontario M5S 3B1
[3]Dynamic Earth, 122 Big Nickel Road, Sudbury, Ontario 53C 5T7
[4]Department of Geology, Lakehead University, 955 Oliver Road, Thunder Bay, Ontario P7B 5E1
[5]Ontario Geological Survey, 435 James Street South, Thunder Bay, Ontario P7E 6S7
[6]Ontario Geological Survey, 933 Ramsey Lake Road, Sudbury, Ontario P3E 6B5
*Corresponding author's e-mail: wouter.bleeker@canada.ca

ABSTRACT

In an effort to better understand the spatial and temporal distributions of mineralized intrusions of the Midcontinent Rift (MCR), and what controls their style of magmatic Ni-Cu-PGE sulphide mineralization, we have compiled an overview of all known intrusions and their ages. We provide new U-Pb ages for more than ten such intrusions and/or their associated dyke systems. A number of these investigations are still in progress, and all ages should be treated as preliminary. Nevertheless, we discuss new results on the mineralized Current Lake, Sunday Lake, Tamarack, and Crystal Lake intrusions, as well as the Bovine Igneous Complex on the southern flank of the MCR. These new results, as well as improved ages for a number of the associated major dyke swarms and sill complexes (e.g. the Logan Sills), favour a relatively sharp onset of high-volume mafic-ultramafic magmatism in the MCR at ca. 1110 to 1106 Ma, although a few of the older age "outliers" remain to be tested. Mineralized intrusions are not confined to any specific magmatic pulse but are distributed through time, correlating with the major magmatic pulses at 1110–1106 Ma (e.g. Current Lake), 1104 Ma (Tamarack), of course at 1099 Ma (Duluth Complex), to as young as 1093 Ma (Crystal Lake). All these intrusions are dynamic, multi-phase, feeder-type systems. A major "post-Duluth Complex" reorganization in the magmatic plumbing system is identified starting at ca. 1097–1096 Ma, with magmatism contracting into a linear feeding zone along the northwestern shore of Lake Superior—the "north shore magmatic feeder zone" or NSMFZ—cored by the major Pigeon River dyke swarm. This feeder zone, a major magmatic fissure system, likely fed the entire lava flow field of the Portage Lake Volcanic Group, which extends to both sides of Lake Superior.

INTRODUCTION

Straddling the Canada-USA border, North America's 1.1 Ga Midcontinent Rift (MCR; Fig. 1) is one of the best preserved and most accessible Proterozoic failed intra-cratonic rift systems in the world (Wold and Hinze, 1982; Green, 1983; Van Schmus and Hinze, 1985; Hutchinson et al., 1990; Cannon, 1992; Allen et al., 1997; Miller and Nicholson, 2013; Stein et al., 2018a,b). It thus represents a pre-eminent natural laboratory for understanding the evolution of complex rift systems in cratonic settings, what generates them, what makes them fail, and the myriad of processes associated with their magmatic, sedimentary, and structural evolution, including a wide variety of mineral systems (Nicholson et al., 1992).

The MCR, with its voluminous magmatic rocks (Fig. 1, Table 1), hosts one of the largest layered intrusions in the world, the Duluth Complex (e.g. Paces and Miller, 1993), with extensive low-grade Ni-Cu-Co-PGE resources, and possibly reef-type PGE mineralization (Hauck et al., 1997; Miller, 1998; Miller et al., 2002). Some of the deposits along the western basal contact of the Duluth Complex (*see* Fig. 1) are currently in an advanced exploration and permitting stage (e.g. PolyMet, 2019) and will likely be mined in the near future. Slightly younger discrete intrusions above that contact, so-called "OUIs" (oxide-rich ultramafic intrusion; Severson et al., 2002), are rich in Fe-Ti±V oxides and are being evaluated as a Ti±V resource.

Elsewhere, both in Canada and the USA, the rift system hosts a number of smaller, localized, conduit-type mafic-ultramafic intrusions ("chonoliths") that are mineralized with higher grade Ni-Cu sulphides (e.g. Tamarack; Goldner, 2011), one of which is currently

Bleeker, W., Smith, J., Hamilton, M., Kamo, S., Liikane, D., Hollings, P., Cundari, R., Easton, M., and Davis, D., 2020. The Midcontinent Rift and its mineral systems: Overview and temporal constraints of Ni-Cu-PGE mineralized intrusions; *in* Targeted Geoscience Initiative 5: Advances in the understanding of Canadian Ni-Cu-PGE and Cr ore systems – Examples from the Midcontinent Rift, the Circum-Superior Belt, the Archean Superior Province, and Cordilleran Alaskan-type intrusions, (ed.) W. Bleeker and M.G. Houlé; Geological Survey of Canada, Open File 8722, p. 7–35. https://doi.org/10.4095/326880

being mined (Eagle; *see* Ding et al., 2010, 2012; Ripley, 2014). These intrusions remain attractive but challenging targets for mineral exploration[1]. Consequently, there is significant on-going exploration, on both sides of the Canada-US border. The large, lopolith-like, multi-phase alkaline intrusion of the Coldwell Complex, on the northeast shore of Lake Superior, has long been a target for both disseminated Cu mineralization and, more recently, for platinum group elements (PGEs; Good and Crockett, 1994; Good et al., 2015, 2017; Ames et al., 2017).

The broader rift system and its cratonic hinterland also host a wide variety of other mafic-ultramafic, alkaline, and carbonatitic intrusions (e.g. Weiblen, 1982; Sage, 1991; Wu et al., 2017), many of which have been, or are being actively explored for a range of commodities, from rare metals (Nb, e.g. the Nemegosenda intrusion) to diamonds (Kyle Lake kimberlites). The overall age range of this compositionally diverse, intracratonic magmatic activity appears to span nearly 100 Myr, from ca. 1170 Ma to ca. 1070 Ma (Davis and Sutcliffe, 1985; Davis and Paces, 1990; Heaman and Machado, 1992; Paces and Miller, 1993; Davis and Green, 1997; Heaman et al., 2004, 2007; Fairchild et al., 2017; McCormick et al., 2017; Wu et al., 2017), with the early phases of magmatic activity generally seen as precursor events to the ca. 1115–1085 Ma main magmatic phases of the rift system (*see* Miller and Nicholson, 2013, for a discussion of the evolutionary phases of the MCR).

In the final stages of its evolution, during rift inversion as a consequence of moderate regional shortening, fluid systems transported base metals, particularly Cu, but also Ag, onto the thrust-imbricated flanks of the rift, forming a variety of Cu deposits (Bornhorst and Barron, 2011), particularly in Michigan on the Keweenaw Peninsula. Elsewhere, Ag-Co-bearing mineralization and a variety of other hydrothermal veins systems (e.g. Pb-Zn-Ba veins), are spatially associated with the MCR, its intrusions, and contemporaneous faults, including, of course, the well known amethyst deposits east of Thunder Bay (e.g. Smyk and Franklin, 2007).

Finally, the MCR and its mineral systems are superimposed on the complex older setting and substrate of the rifted Superior craton margin, which was intruded by several large igneous province-scale events (e.g. the ca. 2.1 Ga Marathon magmatic event) during the Paleoproterozoic, before being overlain by variably deformed sedimentary basins hosting classic "Superior-type" banded iron formations. All these exceptional characteristics enhance the value of the MCR as an outstanding natural laboratory.

RATIONALE FOR THE PRESENT STUDY

A critical data set fundamental to any deeper understanding of this well preserved but nevertheless complex rift system, including its mineral systems, consists of precise and accurate ages of all the components that make up this rift system. Already, there is a rich literature on dating (mostly U-Pb, some Ar-Ar) of the MCR (e.g. Heaman et al., 2007 and references therein; Bleeker et al., 2018, for a recent summary). Much recent progress has focused on improving the age resolution of volcanic rocks that fill the rift, in conjunction with detailed paleomagnetic investigations, to resolve the rapidly evolving apparent polar wander path and its implications (e.g. Swanson-Hysell et al., 2014, 2019; Fairchild et al., 2017). Nevertheless, many key components of the rift system, including a wide variety of intrusions that are part of the complex plumbing system of the MCR, remain undated or have ages that require refinement, and/or have dates that are clearly puzzling outliers in the temporal framework of U-Pb ages. Some of the published U-Pb ages (e.g. Heaman et al., 2007) were obtained on limited amounts of very small baddeleyite crystals and suffer from associated complications (Pb loss and variable discordance, elevated common Pb and associated corrections, ambiguity in choice of regression line and upper intercept, subtly different systematics between baddeleyite and zircon, etc.). In some cases, there exists doubt on the exact provenance or sample location of dated samples, or whether an intrusion of interest is part of the MCR at all or possibly much older (Bleeker et al., 2018).

[1] Many of the mineralized intrusions of the MCR have sulphides with favourable Cu/Ni ratio, additional Co, and appreciable precious metal contents (PGE+Au), which adds to the overall value of their potential sulphide ores.

Figure 1 opposite page. Summary map of the Midcontinent Rift, *modified after* Miller and Nicholson (2013) and previous authors (Miller and Chandler, 1997; Weiblen, 1982, and other contributors to the volume edited by Wold and Hinze, 1982), highlighting all the rift-related intrusions. Undated or poorly dated intrusions, and (or) ages that are otherwise problematic, are shown by stars with a yellowoutline. Only a selection of ages is specifically shown on this figure (space permitting), and the reader is referred to Table 1 for additional age data and references. High-precision U-Pb ages on volcanic rocks are shown for reference (Davis and Sutcliffe, 1985; Davis and Paces, 1990; Davis and Green, 1997; Zartman et al., 1997; Schoene et al., 2006; Swanson-Hysell et al., 2014, 2019; Fairchild et al., 2017). Dyke swarms are shown using red lines and font. Newly obtained U-Pb ages as part of the present study are shown in bold red font and are summarized in Table 2. The grey band along the northwestern shore of Lake Superior is the tentative "post-Duluth Complex" 1097–1092 Ma "north shore magmatic feeder zone" (NSMFZ) discussed in this paper. Abbreviations: BIF = banded iron formation, Cgl. = Conglomerate, Fm. = Formation, Gp = group, Is. = Island, Lk. = Lake, Mt = Mount, Qte = quartzite, Twp = Township.

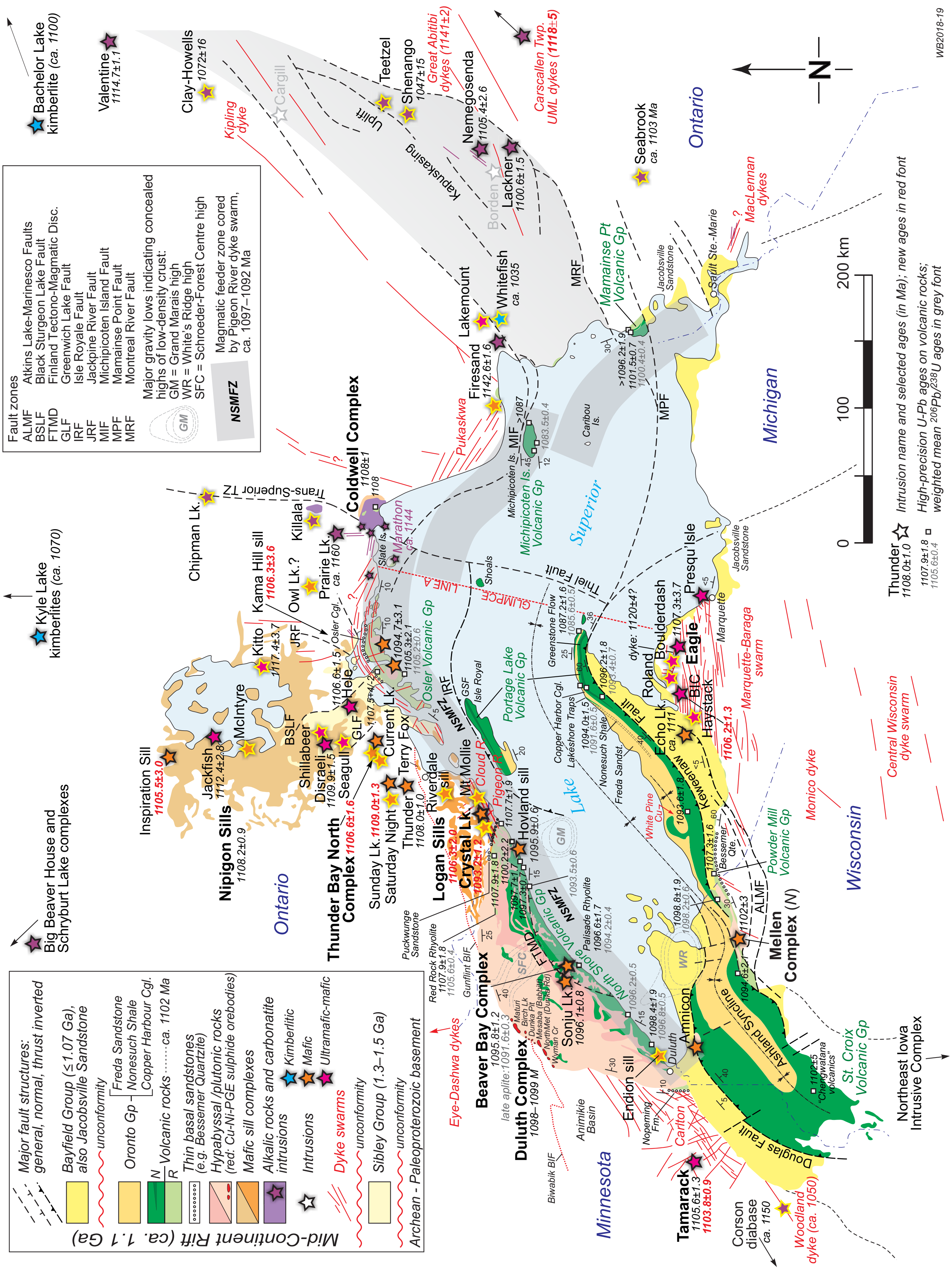
Mid-Continent Rift (ca. 1.1 Ga)
Major fault structures: general, normal, thrust inverted
Bayfield Group (≤1.07 Ga), also Jacobsville Sandstone
unconformity
Oronto Gp
Freda Sandstone
Nonesuch Shale
Copper Harbour Cgl.
N R Volcanic rocks ca. 1102 Ma
Thin basal sandstones (e.g. Bessemer Quartzite)
Hypabyssal /plutonic rocks (red: Cu-Ni-PGE sulphide orebodies)
Mafic sill complexes
Alkalic rocks and carbonatite intrusions
Intrusions Kimberlitic Mafic Ultramafic-mafic
Dyke swarms
unconformity
Sibley Group (1.3–1.5 Ga)
unconformity
Archean - Paleoproterozoic basement
Fault zones
ALMF Atkins Lake-Marinesco Faults
BSLF Black Sturgeon Lake Fault
FTMD Finland Tectono-Magmatic Disc.
GLF Greenwich Lake Fault
IRF Isle Royale Fault
JRF Jackpine River Fault
MIF Michipicoten Island Fault
MPF Mamainse Point Fault
MRF Montreal River Fault
Major gravity lows indicating concealed highs of low-density crust:
GM = Grand Marais high
WR = White's Ridge high
SFC = Schroeder-Forest Centre high
NSMFZ Magmatic feeder zone cored by Pigeon River dyke swarm, ca. 1097–1092 Ma
Thunder 1108.0±1.0 Intrusion name and selected ages (in Ma); new ages in red font
1107.9±1.8 1105.6±0.4 High-precision U-Pb ages on volcanic rocks; weighted mean $^{206}Pb/^{238}U$ ages in grey font
0 100 200 km
N
Lake Superior
Ontario
Michigan
Wisconsin
Minnesota
Coldwell Complex 1108±1
Duluth Complex 1098–1099 M
Beaver Bay Complex 1095.8±1.2
Thunder Bay North Complex 1106.6±1.6
Nipigon Sills 1108.2±0.9
Logan Sills 1106.3±2.0
Mellen Complex (N) 1102±3
Tamarack 1105.6±1.3 1103.8±0.9
Eagle
Crystal Lk. 1093.2±1.2
Inspiration Sill 1105.5±3.0
Kama Hill sill 1106.3±3.6
Marquette-Baraga swarm
Central Wisconsin dyke swarm
Eye-Dashwa dykes
Great Abitibi dykes (1141±2)
Carscallen Twp. UML dykes (1118±5)
Northeast Iowa Intrusive Complex
WB2018-19

Table 1. Listing of Midcontinent Rift-related intrusions, updated from Bleeker et al. (2018).

#	Intrusive Unit	Age (Ma)	Type of Age	Key References	Main Rock Types	Comments and Questions
MCR-related dyke swarms:						
1	Great Abitibi dykes	1141±2	U-Pb, bd, wm7/6 age	Krogh et al., 1987	Olivine diabase, gabbro, monzodiorite	Giant swarm, only one dyke dated
	Ultramfic lamprophyres:					
2	Ultramafic "Marathon dykes" (e.g., McKellar Harbour dyke)	ca. 1144 1145+15/-10	K-Ar U-Pb, prv	Platt and Mitchell., 1979, 1982; Platt et al., 1983; Queen et al., 1996	Ultramafic lamprophyre	Kimzeyite garnet in some dykes Age uncertainty allows link to Prairie Lake Complex
3	Lamprophyre dykes, Kapuskasing Uplift	ca. 1144	Ar-Ar	Queen et al., 1996	Ultramafic lamprophyre	Also age overlap with Abitibi dykes
4	Lamprophyre dykes, Carscallen Twp.	ca. 1118	Ar-Ar	This study	Ultramafic lamprophyre	Ultramafic lamprophyre intersected in core, west of Timmins
5	Woodland dyke, Minnesota (~060°)	ca. 1050	Ar-Ar	This study; T. Boerboom, pers. comm., 2016	Lamprophyre	Large, ~8 m wide lamprophyre dyke, reversely magnetized
	Various mafic dyke sets:					
6	ESE-trending diabase and lamprophyre dykes east of Sault Ste. Marie	undated		This study	Thin (ultramafic) lamprophyre dykes cut by slightly younger diabase dykes	Fresh lamprophyre and lamprophyre-diabase association is typical for MCR
7	ENE-trending dykes north of Wawa	undated		This study	Diabase	Trend ~070°, ~4–5 m wide, exposed along Hwy 17
8	NNE-trending dykes east of Coldwell	undated		OGS 1991a, Map 2543	Diabase	Distinct from Marathon dykes?
9	NNW-trending dykes west of Coldwell	undated		OGS 1991a, Map 2543; this study	Diabase	Observed in road outcrops; reversely magnetized
10	Pukaskwa dykes (~315°)	undated		OGS 1991a, Map 2543; Weiblen, 1982; Green et al., 1987	Diabase	Could be confused with parallel Matachewan dykes
11	NW- to N-trending dykes, Nipigon area	undated		OGS 1991b, Map 2542; Osmani, 1991; this study	Diabase	Some have been shown to be Marathon swarm dykes
12	E- to NE-trending diabase and lamprophyre east of Nipigon	undated		This study	Thin (ultramafic) lamprophyre dykes cut by slightly younger diabase dykes	Fresh lamprophyre and lamprophyre-diabase association is typical for MCR
13	E-trending diabase dykes cutting Osler Group flows	undated, 1096?		Giguerre, 1975; this study	Diabase dykes 3–30 m in width	Dykes cut and chilled against Osler Group basalt flows, and dip steeply north; tilted with flows; probably equivalents of Pigeon River dyke, and feeders to Portage Lake Group
14	Thin WNW-trending dykes north of Atikokan, cutting Eye-Dashwa pluton	1143±27	K-A	Osmani, 1991; Stone et al., 1992	Thin diabase dyke, trend ~290°	
	NW-trending dykes:					
15	Cloud River dykes (~330°), near Crooks	1109.2±4.2 1109.2±2.9	U-Pb, bd, wm6/8 age, n=2 U-Pb, bd, n=3	Hollings et al., 2010; Cundari, 2012 This study	Diabase Diabase, sparsely plagioclase megacrystic in centre	~80 m NW-trending (~318°) Cloud River dyke cut by ENE-trending Pigeon River dykes
16	NW-trending dyke at Mt. Josephine	1099.0±1.2	U-Pb, zr and bd, wm7/6 age, n=5	This study	Diabase	~100–150 m wide dyke, vertical, trend 330°
	Pigeon River swarm and parallel dykes:					
17	Pigeon River dyke (~070°), Crooks Twp. "Rita Bolduc dyke"	1141±20 1096.9±1.9	U-Pb, zr and bd, disc.	Heaman et al., 2007 This study	Diabase, gabbro	Higly discordant data, age interpretation likely too old
18	Arrow River dyke (~080°), Devon Twp.	1078±3 1096±12	U-Pb, bd, reverse disc., n=1	Heaman et al., 2007 This study	Diabase	Arrow River, Devon Township
19	Mount Mollie dyke (080-090°)	1109.3±6.3 1096.3±1.4	U-Pb, bd, wm7/6 age, n=2 U-Pb, zr and bd, u. intercept, n=6	Smyk and Hollings, 2009; Hollings et al., 2010 This study	Diabase, gabbro to leucogabbro, granophyre	Uncertainty on sample location; age in conflict with feeder to Crystal Lake Intrusion Mount Mollie dyke probably a member of the Pigeon River swarm
	Other dyke swarms:					
20	Carlton dykes (~030°, multiple trends)	undated		Weiblen, 1982; Green et al., 1987; Miller and Nicholson, 2013	Diabase	Multiple trends, i.e. likely more than one swarm
21	Marquette-Baraga dykes (080°)	ca. 1120±4	U-Pb bd, n=3, disc., u. intercept	Weiblen, 1982; Green et al., 1987; Miller and Nicholson, 2013; *see* Dunlop, 2013, for baddeleyite date	Diabase	Multiple trends, i.e. likely more than one swarm
22	NE-trending dykes south of MCR e.g., Monico dyke	undated		K. Schultz, pers. comm., 2019		Several NE-trending dyke below the ridge of the Bessemer Quartzite, also the Monico dyke farther south
23	Central Wisconsin dyke swarm	undated		Osmani, 1991		
24	NE-trending dykes, northeast Iowa	undated		Drenth et al., 2015		Associated with Northeast Iowa Intrusive Complex; some appear reversely magnetized
Various sills and sill complexes:						
	"Nipigon Sills", Nipigon area:					
25	Nipigon Sills	1109+4/-2 1108.2±0.9	U-Pb, zr (and bd), n=4 U-Pb, zr, u. intercept, recalculated	Davis and Sutcliffe, 1985; *see also* Krogh et al., 1987 *see* Davisand Green, 1997	Diabase, pegmatitic gabbro, granophyre	These were referred to as "Logan Sills" by Davis and Sutcliffe, 1985
26	Havoc Lake diabase (HAV02-02)	1110.1±2.5	U-Pb, bd, wm7/6, n=4	Heaman et al., 2007	Diabase	
27	Muskrat Lake diabase (ML01-01)	1112.7±2.4	U-Pb, bd, wm7/6, n=2	Heaman et al., 2007	Diabase	
28	Grand Bay diabase (GB01-01)	1114.4±8.3	U-Pb, bd, disc., scattered data	Heaman et al., 2007	Diabase	
29	North Bay diabase (LN08)	1110.1±2.1	U-Pb, bd, wm7/6, n=2	Heaman et al., 2007	Diabase	
30	Gull River troctolite (GR01-01)	1111±15	U-Pb, bd, wm7/6, n=2	Heaman et al., 2007	Troctolite	
31	South Bay diabase (LN139)	1106.8±1.9	U-Pb, zr, reversly disc., wm7/6, n=2	Heaman et al., 2007	Diabase	
32	Kama Hill, upper sill (KH10)	1008±29	U-Pb, zr, highly disc., n=2	Heaman et al., 2007	Diabase	Upper intercept through highly disc. zircon data
33	Inspiration (04RME-3210)	1159±33 1105.5±3.0	U-Pb, bd, disc., n=2, u. intercept U-Pb, bd, wm7/6, n=3	Heaman et al., 2007 This study	Diabase, gabbro	Upper intercept from 2 disc. baddeleyite fractions, likely too old Redated, see new age in line with other Logan and Nipigon sills
34	McIntyre	1100.8±4.4	U-Pb, bd, wm7/6 age, n=1	Heaman et al., 2007	Diabase	More likely to be ca. 1110 Ma based on wm6/8 age
	"Logan Sills", Thunder Bay area:					
35	Logan Sills	1114.7±1.1 1106.3±2.0	U-Pb, bd, 3.5-4.1% disc, wm7/6 U-Pb, zr and bd, u. intercept, n=5	Heaman et al., 2007 This study	Diabase	Clustered discordant data, age interpretation likely too old
36	Terry Fox sill	undated			Diabase, plagioclase phyric near roof contact	Interesting upper porphyry, with abundant xenoliths, melted roof rocks?
37	Riverdale	undated		Hollings et al., 2010; P. Hollings, pers. comm., 2017	Diabase, compositionally distinct	

Table 1 continued.

#	Intrusive Unit	Age (Ma)	Type of Age	Key References	Main Rock Types	Comments and Questions
	Intrusions in Minnesota, likely related to Logan Sills:					
38	Nathan's Layered Series	1106.9±0.6	U-Pb, zr, wm7/6, n=5	Weiblen et al., 1972; Paces and Miller, 1993	Olivine gabbro	Reversely magnetized, age suggest link with Logan Sills
39	Swamper Lake monzogabbro	1107.0±1.1	U-Pb, zr, wm7/6, n=3	Davis and Green, 1997	Monzogabbro	Reversely magnetized, age suggest link with Logan Sills
40	Cucumber Lake granophyre	1106.8±2.8	U-Pb, zr, u. intercept	Vervoort and Wirth, 2004; Vervoort et al., 2007	Granophyre	Reversely magnetized
41	Misquah Hills granophyre	1106.0±4.8	U-Pb, zr, u. intercept	Vervoort and Wirth, 2004; Vervoort et al., 2007	Granophyre	
42	Whitefish Lake granophyre	1109.4±5.1	U-Pb, zr, u. intercept	Vervoort and Wirth, 2004; Vervoort et al., 2007	Granophyre	
43	Mount Weber granophyre	1106.2±3.6	U-Pb, zr, u. intercept	Vervoort and Wirth, 2004; Vervoort et al., 2007	Granophyre	
44	Greenwood Lake granophyre	1106±3	U-Pb, zr, u. intercept	Vervoort and Wirth, 2004	Granophyre	
	Ultramafic intrusions:					
45	Kitto	1117.5±3.7	U-Pb, bd, wm7/6, n=2	Sutcliffe, 1986; Hart et al., 2002; Heaman et al., 2007; Larmaan, 2007	Peridotite, olivine websterite, and pyroxenite	Interstitial sulphides along basal contact and in websterite
46	Kitto diabase	1110.8±4.3	U-Pb, bd, disc., u. intercept	Heaman et al., 2007	Diabase thought to intrude Kitto ultramafic body	
47	Seagull	1112.8±1.4	U-Pb, bd, complex results	Heggie, 2005; Hart and Macdonald, 2007; Heaman et al., 2007	Dunite, peridotite to gabbro	Disseminated sulphides along basal contact, and reef-type PGE horizons
48	Jackfish	1112.4±2.8	U-Pb, bd, wm6/8 age, n=2	Heaman et al., 2007; Hollings et al., 2007	Melagabbro to peridotite core surrounded by olivine gabbro	
49	Disraeli	1109.9±1.4	U-Pb, bd, wm7/6, n=2	Hart and Magyarosi, 2004; Hart and Macdonald, 2007; Heaman et al., 2007	Peridotite to wehrlite core, with olivine gabbro marginal zone	Good baddeleyite age
50	Hele	1106.6±1.5	U-Pb, bd, wm7/6, n=2	Heaman et al., 2007; Hollings et al., 2007	Peridotite and wehrlite, interlayered with olivine gabbro	Minor sulphides in peridotite
51	Shillabeer	undated		Hollings et al., 2007	Ultramafic rocks	
	Thunder Bay North Complex:					
52	Current Lake	1120±23	U-Pb (unpubl.), no details	Smyk and Hollings, 2009; Chaffee, 2015	Feldspathic dunite to olivine melagabbro	Disseminated sulphides in peridotite, net-textured to massive sulphide in conduit
		1106.6±1.6	U-Pb, zr and bd, u. intercept, n=4	This study		
53	Steepledge Lake	undated		Thomas et al., 2011; D'Angelo, 2013	Peridotite to olivine gabbro	Basal peridotite hosts disseminated sulphides
54	Lone Island Lake	undated				
	Other intrusions:					
55	Thunder	1108.0±1.0	U-Pb, zr (bd), CA-ID-TIMS, conc.	Trevisan, 2014; Trevisan et al., 2015	Feldspathic peridotite, melagabbro, and upper massive gabbro	Disseminated sulphides in basal ultramafic rocks
56	Sunday Lake	1109.0±1.3		Flank, 2017; this study	Peridotite to monzogabbro (diorite)	Disseminated sulphides in basal ultramafic rocks
57	Tamarack Intrusive Complex	1105.6±1.3	U-Pb, bd, slightly disc.	Goldner, 2011; Taranovic et al., 2015, 2016	Peridotite to gabbro	Net-textured to massive sulphide; disseminated sulphides thoughout
		1103.8±0.9	U-Pb, zr, concordia age	This study, new age on pegmatitic gabbro of "southern bowl"		
58	Saturday Night	*in progress*		This study	Peridotite to monzogabbro (diorite)	Disseminated sulphides in basal ultramafic rocks
59	Crystal Lake Intrusion	1099.6±1.2	U-Pb, bd, wm7/6, n=2	Cogulu, 1993a,b; Heaman et al., 2007;	Vari-textured gabbro, troctolite, chromite layers	Some controversy on what part of the complex was dated
		1093.1±1.2	U-Pb, zr and bd, wm7/6, n=4	Smith et al., 2020; this study		
60	Blake Township Gabbro	1091.0±4.5	U-Pb, bd, wm6/8, 7/5 ages, n=2	Heaman et al., 2007	Gabbro	Blake Township
61	"Rainy River intrusion"	undated		W. Bleeker, unpublished observations on core	Peridotite-gabbro, metamorphosed, mineralized	Metamorphosed, cut by Fort Frances dyke, Archean; not MCR-related
	Younger gabbro intrusions in Osler Group:					
62	Moss Lake Gabbro	1094.7±3.1	U-Pb, bd, wm6/8, 7/5 ages, n=2	Heaman et al., 2007	Gabbro	Black Bay Peninsula, intrusive units emplaced in Osler Group
63	St. Ignace Island Complex Gabbro	1089.2±3.2	U-Pb, zr, unpubl.	Smyk et al., 2006	Gabbro	St. Ignace Island, intrusive units emplaced in Osler Group
	Duluth Complex and related intrusions, Minnesota:					
64	Duluth Complex	1099.0±0.6	U-Pb, zr, wm7/6, n=5	Paces and Miller, 1993; *see also* Hoaglund et al., 2010	Gabbroic anorthosite	
65	Duluth Complex	1099.1±0.5	U-Pb, zr, wm7/6, n=6	Paces and Miller, 1993	Gabbroic anorthosite	
66	Duluth Complex	1098.6±0.5	U-Pb, zr, wm7/6, n=8	Paces and Miller, 1993	Olivine gabbro	
67	Duluth Complex	1099.3±0.3	U-Pb, zr, wm7/6, n=6	Paces and Miller, 1993	Olivine ferrogabbro	
68	Kenwood Avenue granite	1098.2±1.4	U-Pb, zr, wm7/6, n=4	Davis and Green, 1997	Granite	One of the youngest phases clearly associated with the Duluth Complex
69	Pine Mountain granophyre	1095.3±3.8	U-Pb, zr, u. intercept	Vervoort and Wirth, 2004; Vervoort et al., 2007	Granophyre	
70	Eagle Mountain	1098.6±3.8	U-Pb, zr, u. intercept	Vervoort and Wirth, 2004; Vervoort et al., 2007	Granophyre	
71	Finland granophyre	1098.2±5.5	U-Pb, zr, u. intercept	Vervoort and Wirth, 2004; Vervoort et al., 2007	Granophyre	
72	Sonju Lake Intrusion (part of BBC)	1096.1±0.8	U-Pb, bd, wm7/6	Paces and Miller, 1993	Ferrodiorite	
73	Beaver Bay Complex (BBC), Silver Bay Intr.	1095.8±1.2	U-Pb, zr and bd, wm7/6, n=6	Paces and Miller, 1993	Granophyric ferrogabbro	
74	Intrusive aplites in Silver Bay Intr.	1091.6±0.3	U-Pb, zr, CA-TIMS, wm6/8 age	Fairchild et al., 2017	Aplite within granophyre	$^{206}Pb/^{238}U$ ages on multiple chemically abraded zircons
75	Wilson Lake ferrogabbro	1095.8±0.9	U-Pb, zr and bd, wm7/6, n=6	Hoaglund et al., 2010	Ferrogabbro	
76	Hovland Sill	1095.9±0.6	U-Pb, bd, wm7/6, n=6	Boerboom et al., 2014	Gabbro to granophyre	UTM: 722714E, 5301024N
77	Endion Sill	undated		Miller, 2016	Gabbro to granophyre	Exposed along the shore in Duluth
	Mafic-ultramafic intrusions south of Lake Superior:					
78	Amnicon gabbro intrusion	undated		Grout, 1918; J. Miller, pers. comm., 2019	Gabbro	
	Mellen Intrusive Complex:					
79	Mineral Lake Intrusion	1102.8±2.8	U-Pb, zr, wm7/6 age, n=2	Zartman et al., 1997	Olivine gabbro, ferrogabbro, granophyre, and late granite	Basal mineralization confined to Mineral Lake Intrusion

Table 1 continued.

#	Intrusive Unit	Age (Ma)	Type of Age	Key References	Main Rock Types	Comments and Questions
	Mellen Intrusive Complex continued:					
80	Mineral Lake Intrusion	1102.1±3.5	U-Pb, zr, u. intercept	Zartman et al., 1997	Granophyre	Wisconsin
81	Mellen Complex	1101.5±2.9	U-Pb, zr, u. intercept	Zartman et al., 1997	Granite	Wisconsin
82	Echo Lake	1110.8±1.5	U-Pb, unpubl.	Cannon and Nicholson, 2001; Koerber and Thakurta, 2017; S. Nicholson, pers. comm., 2018	Peridotite, troctolite, gabbro	Localized PGE horizons associated with disseminated sulphides
83	Bovine Igneous Complex (BIC)	1106.2±1.3	U-Pb, bd, u. intercept, n=3	Foley, 2011; Donoghue et al., 2014; this study	Feldspathic wehrlite overlain by melatroctolite and olivine gabbro	Basal, disseminated to locally massive sulphides, also reef-style PGE horizons
84	Roland Lake	undated		Dunlop, 2013	Feldspathic peridotite to pyroxenite	Minor sulphide mineralization, extent yet to be determined
85	Boulderdash	undated		Dunlop, 2013	Troctolite, melatroctolite	Minor sulphide mineralization, extent yet to be determined
86	Eagle	1107.3±3.7	U-Pb, bd, wm7/6 age	Ding et al., 2010, 2012; *see also* Ripley, 2014; Clow et al., 2017	Feldspathic peridotite sheet, underlain by melatroctolite and olivine gabbro	Relationship to Eagle East?
87	Eagle East	undated		As for Eagle, *see above*	Melatroctolite	High-grade massive to semi-massive sulphides concentrated above keel
	Coldwell Complex and nearby intrusions:					
88	Coldwell Complex	1108±1	U-Pb, zr, u. intercept	Mitchell et al., 1983, 1993; Heaman and Machado, 1992; Good et al., 2015, 2017	Gabbro, ferroaugite syenite, nepheline syenite, quartz syenite	Disseminated Cu and PGE mineralization in vari-textured Two Duck Lake gabbro; remnants of pre-intrusive basalts, preserved as hornfelsed roof pendants (xenoliths)
	Eastern marginal gabbro, Centre 1 (CL7)	1107+2/-1	U-Pb, bd and zr, u. intercept	Heaman and Machado, 1992	Gabbro	
	Two Duck Lake gabbro, Centre 1 (86CL1)	1108±1	U-Pb, bd and zr, u. intercept	Heaman and Machado, 1992	Coarse vari-textured gabbro	
	Syenite, Centre 1	ca. 1108	U-Pb, zr, some scatter	Heaman and Machado, 1992	Syenite	
	Nepheline syenite, Centre 2 (CL22)	1109+8/-4	U-Pb, zr and ti, disc.	Heaman and Machado, 1992	Nepheline syenite	
	Granite, Centre 3	≥1102	U-Pb, zr, disc.	Heaman and Machado, 1992	Granite	Centre 3 could be as young as 1102–1103 Ma
89	Prairie Lake	ca. 1163	U-Pb, bd and zr	Rukhlov and Bell, 2010; Wu et al., 2017	Pyroxenite, ijolite, carbonatite, syenite	Early precursor alkaline magmatism; plume incubation?
90	Killala	1050±35 1185	Rb-Sr K-Ar	Bell and Blenkinsop, 1980; Sage, 1988d Currie, 1976	Syenite, nepheline syenite, olivine gabbro, larvikite	Minor Nb and Ni-Cu sulphide mineralization
91	Owl Lake	undated				
92	Chipman Lake	1022±31	K-Ar	Sage, 1985	Carbonatite and lamprophyre dykes	Emplaced along the Trans-Superior Tectonic Zone
93	"Marathon dykes" (see under dykes)	ca. 1144				
	Ultramafic intrusions near Wawa:					
94	Firesand	1142.6±1.6 1019–1098	U-Pb, kmz K-Ar	Sage, 1988e, 1991; Rukhlov and Bell, 2010 Gittins et al., 1967	Carbonatite and related alkalic rocks	
95	Lakemount (a.k.a. Sunrise)	undated			Peridotite; basal Ni-Cu mineralization	Relation to MCR uncertain
	Alkaline and carbonatite intrusion east of Lake Superior:					
96	Seabrook Lake	1113±36	K-Ar	Gittins et al., 1967; Sage, 1988a	Carbonatite, mafic breccias, ijolite, syenite	Minor Nb mineralizaton
97	Lackner Lake	1100.6±1.5	U-Pb, bd, disc., n=3, intercept	Heaman et al., 2007	Carbonatite, ijolite and associated magnetite-apatite bodies, nepheline syenite	Minor Nb mineralizaton
98	Nemegosenda	1105.4±2.6	U-Pb, zr, u. intercept, n=3	Sage, 1987a; Heaman et al., 2007	Carbonatite, ijolite, nepheline syenite, syenite, gabbro	Nb mineralization
99	Shenango	1047±15	Rb-Sr	Bell and Blenkinsop, 1980; Sage, 1987b	Diorite, syenodiorite, monzonite and quartz monzonite	
100	Teetzel	1155±45	K-Ar	Currie, 1976; Weiblen, 1982		
101	Clay-Howells	1075±15	Rb-Sr	Bell et al., 1982; Sage, 1988b	Pyroxene syenite, intruded by magnetite-rich carbonatite dykes	REE, Nb and Fe (magnetite) mineralization
102	Valentine	1114.7±1.1	U-Pb, bd, u. intercept	Sage, 1988c; Rukhlov and Bell, 2010	Carbonatite	Widespread but sub-economic Nb and P mineralization
	Alkaline and carbonatite intrusion in NW Ontario:					
103	Big Beaver House	1093±2 1109±61	U-Pb, bd, disc., n=1 K-Ar, bi	Sage, 1991; Rukhlov and Bell, 2010 Sage, 1987c	Alkaline ultramafic rocks, carbonatite	Single 1.4% discordant bd fraction
104	Schryburt Lake	1084±3	U-Pb, bd, disc., n=2, intercept	Sage, 1988f, 1991; Rukhlov and Bell, 2010	Ultramafic lamprophyre, carbonatite	Weighted mean of the 2 bd analyses is 1083.0±1.2 Ma
	Kimberlites:					
105	Kyle Lake kimberlites	ca. 1070	U-Pb, prv, single analysis	Heaman et al., 2004	Kimberlite, diamondiferous	Northern Ontario, underneath Paleozoic cover
106	Whitefish Lake	1035±13 (1097±7)	Rb-Sr, phl	Kaminsky et al., 2000	Kimberlite, micaceous, diamondiferous	North east of Wawa, four kimberlite pipes
107	Bachelor Lake	1104±17	Rb-Sr, phl	Alibert and Albarede, 1988	Kimberlite	Western Quebec, underneath glacial till
	Distal events:					
108	Northeast Iowa Intrusive Complex	undated		Drenth et al., 2015	Various intrusion, both mafic and felsic	
109	Corson diabase	ca. 1150	U-Pb, bd	McCormick et al., 2017	Olivine diabase	Near border of South Dakota and Minnesota
110	Texaco-Poersch core, Kansas	1097.5±3.0	U-Pb, zr	Van Schmus, 1992	Gabbro	Kansas
111	Moore Lake gabbro	1109±2	U-Pb, bd and zr	French et al., 2002	Gabbro, diabase	Gabbro sills intruding the Athabasca Basin, Saskatchewan
112	Douglas River diabase dyke	1165±17	U-Pb, bd, in situ SIMS dating	Bleeker and Chamberlain, 2015	Diabase	Diabase dykes intruding the Athabasca Basin, Saskatchewan
113	SW USA Diabase Province	1115–1080	U-Pb, bd, various methods	Bright et al., 2014, and references therein	Diabase and gabbro sills, layered intrusion	Possibly a distal expression of the same MCR mantle upwelling?
114	Pahrump sills	1087±3	U-Pb, bd	Heaman and Grotzinger, 1992	Diabase, gabbro	Diabase sills in Parump Group, southern California
115	Salla dyke	1122±7	U-Pb, zr	Lauerma, 1995; Salminen et al., 2009	Medium- to coarse-grained diabase	A single large (distal), NE-trending diabase dyke, cutting across northern Karelia
116	Umkondo LIP, Kalahari craton	1112–1106	U-Pb, bd and zr	Hanson et al., 2004	Diabase, gabbro	Numerous diabase dykes and sills across Southern Africa

Notes: This is a compilation in progress; some unpublished information is currently included. In red, intrusions worked on during this study.
Abbreviations: bd = baddeleyite, bi = biotite, conc. = concordant, disc. = discodant, kmz = kimzeyite, n = number of analyses included, PGE = platinum group elements, phl = phlogopite, prv = perovskite, REE = rare earth elements, ti = titanite, u. intercept = upper intercept, wm6/8 = weighted mean $^{206}Pb/^{238}U$ date, wm7/6 = weighted mean $^{207}Pb/^{206}Pb$ date, zr = zircon.

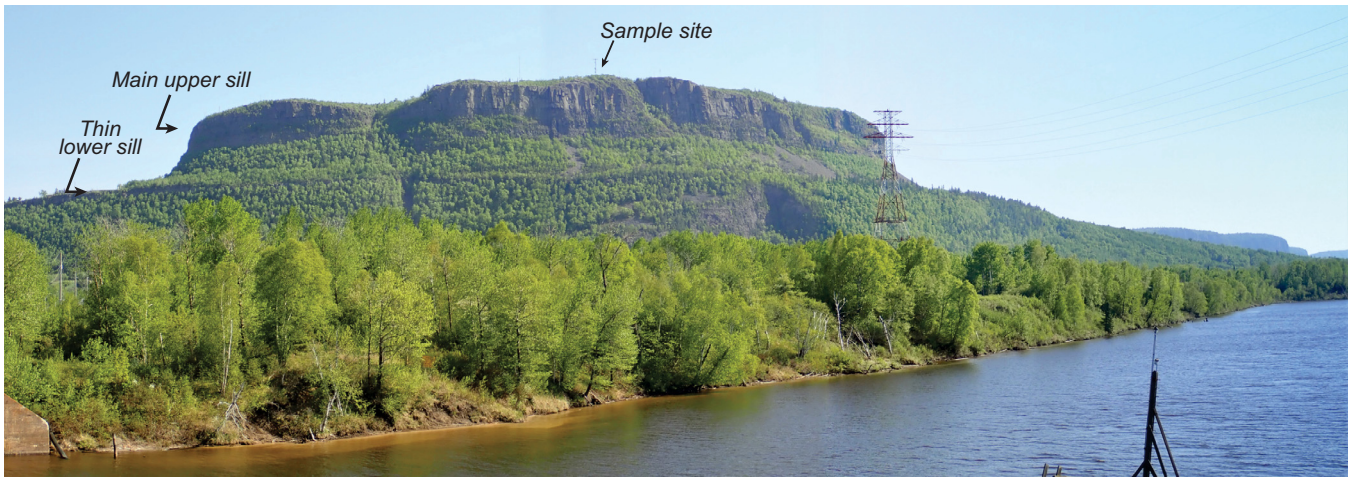

Figure 2. View of the iconic Logan Sills (s.s.) overlooking the Kaministiquia River and the city of Thunder Bay. Two sills are visible, having intruded mudstones and thinly bedded turbiditic wackes of the ca. 1.85 Ga Rove Formation, Animikie Basin: an upper main sill capping the mesas, and a thin lower sill forming a minor ledge in the trees. William Logan visited the area in 1846 during early geological reconnaissance work. Decades later, Lawson recognized that these were sills, rather than basaltic flows, and named them after Logan (Lawson, 1893).

The present research, therefore, aims to resolve some of the key questions on the timing of major magmatic pulses and, particularly, the ages of mineralized intrusions, thus allowing a more refined picture of the complex and evolving magmatic plumbing system of the rift. Resolving some of these key timing questions will set the stage for more detailed questions such as why some intrusions are mineralized whereas others are not, the spatial and temporal variation of their potential mantle sources and variable metal fertility, and what parts of the volcanic sequence the intrusions may have fed. We here present new U-Pb ages on ~10 key units and discuss their implications. In an accompanying contribution (Smith et al., 2020), we focus in more detail on one mineralized intrusion, the Crystal Lake Intrusion southwest of Thunder Bay.

SCOPE OF THE PROBLEM: KEY EXAMPLES

Here we introduce the scope of the problem by highlighting two key magmatic units on the northern flank of the MCR, the Logan Sills near Thunder Bay and the Inspiration sill of the northern Nipigon Embayment (Fig. 1, Table 1). The iconic "Logan Sills" (Fig. 2)—so named by Lawson (1893) after the founder and first director of the Geological Survey of Canada—represent extensive and voluminous sill complexes on the north shore of Lake Superior. Early U-Pb dating studies suggested an age of 1109 +4/-2 Ma[2]. (Davis and Sutcliffe, 1985), on samples from the Lake Nipigon area. Since then, subtle geochemical differences in incompatible element ratios have suggested that sills in the Nipigon area (now called "Nipigon Sills") and sills in the Thunder Bay area (now "Logan Sills", *sensu stricto*) may actually form two distinct sill complexes (Hollings et al., 2007, 2010). A tentative age of 1114.7 ± 1.1 Ma was determined from a Logan Sill on Mount McKay, using a limited selection of very small baddeleyite grains (Heaman et al., 2007). This and other older age "outliers", such as the suggested age for the Inspiration sill of 1159 ± 33 Ma (Heaman et al., 2007), raised the possibility of an older and drawn-out start of MCR mafic magmatism, a finding that is at odds with modern dating studies on many large igneous provinces. With better and more robust high-precision U-Pb data, these studies typically show a sharp onset of high-volume mafic magmatism, on a time scale of 1 to 2 Myr, sometimes followed by additional pulses of diminishing volume and/or more varied composition over a 5 to 25 Myr time scale.

To help settle this important question of "the age of onset of voluminous mafic magmatism", we resampled both the Mt. McKay sill overlooking Thunder Bay and the Inspiration sill in the Nipigon area. In the field, we spent time collecting the most optimum samples of late-stage, more fractionated, and Zr-enriched pegmatoidal gabbros towards the top of both sills. Both samples returned adequate baddeleyite and some magmatic zircons (Fig. 3). Although at this stage all our results should be treated as preliminary, our data indicate improved ages for these sills at 1106.3 ± 2.0 Ma for the main Logan Sill capping Mt. McKay, and 1105.5 ± 3.0 Ma for the Inspiration sill (Fig. 4), i.e. within uncertainty of each other and also the original Davis and Sutcliffe (1985) data, respectively; and, importantly, also within uncertainty of the oldest high-precision

[2] In a subsequent paper, the three collinear zircon fractions are regressed from the orign to an upper intercept age of 1108.2±0.9 Ma (*see* Davis and Green, 1997).

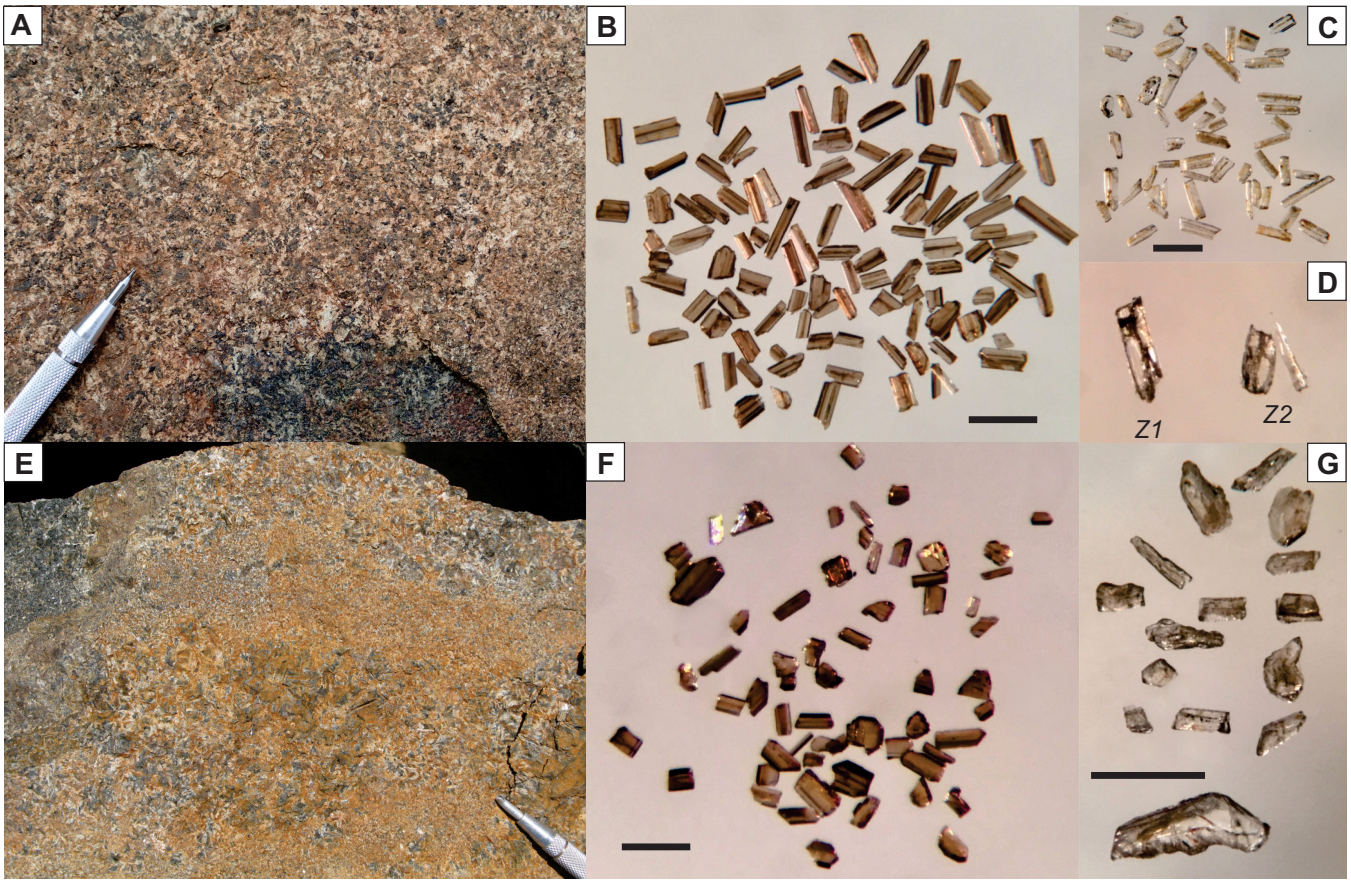

Figure 3. Typical baddeleyite and zircon recovery from pegmatitoidal gabbros near the top of Midcontinent Rift sills, the main Logan Sill at Mount McKay (a–d), and the Inspiration sill near Armstrong, Ontario (e-g). **a, e)** Photographs of sampled material, i.e. last-crystallizing differentiated pegmatoidal gabbro, which is typically underneath the chilled upper contact of the sills. **b, f)** Typical baddeleyite recovery. **c, d, g)** Blady late-stage magmatic zircons. All scale bars are 200 µm.

ages near the base of the volcanic successions around the rift at ca. 1107–1108 Ma (Davis and Sutcliffe, 1985; Davis and Green, 1997; Swanson-Hysell et al., 2019). These initial results confirm our intuition that the onset of the first high-volume mafic magmatism was indeed relatively sharply timed and occurred at ca. 1109–1107 Ma (*see also* Davis and Green, 1997), and that some of the more tentative results or interpretations on variably discordant small baddeleyite fractions from the Heaman et al. (2007) study were not quite accurate. Our results also demonstrate the remaining complexity, as few of the individual analyses are fully concordant. Although we recovered better baddeleyites than previous studies (Fig. 3), and also magmatic zircons in many cases, the blady magmatic zircon crystals in these types of samples do not withstand aggressive chemical abrasion and retain some discordance. If they are aggressively treated by chemical abrasion (Mattison, 2005), these crystals (Fig. 3c,d,g), with their cracks and accumulated damage, dissolve; with no or minimal chemical abrasion, they retain some discordance, requiring extrapolation to upper intercept ages. Nevertheless, these new improved ages represent a significant step forward.

In contrast to these improved, but nevertheless slightly discordant results on early high-volume diabase sill complexes, we here also discuss new zircon ages on well behaved gabbro samples from some of the mineralized intrusions, Tamarack in Minnesota and Crystal Lake in Ontario (Fig. 5). Both samples discussed here yielded abundant and relatively good quality zircons, which after chemical abrasion yielded fully concordant, overlapping data, and consequently highly precise and accurate ages on par with high-precision results on rhyolite samples in the volcanic successions. The sample from Tamarack, a differentiated pegmatoidal gabbro near the top of the "southern bowl" of this large composite intrusion, yielded a zircon concordia age (Ludwig, 1998, 2003) of 1103.8 ± 0.9 Ma based on three fully overlapping single zircon data (Fig. 5a). This age is clearly younger than the 1107–1109 Ma onset of high-volume mafic magmatism but could correlate with the nearby volcanic sequence of the "Chengwatana basalts" (Wirth and Gehrels, 1998) in the southwestern extension of the MCR (Fig. 1). A mineralized, pegmatoidal, vari-textured gabbro from the northern arm (or "limb") of the Crystal Lake Intrusion yields a fully concordant zircon and badde-

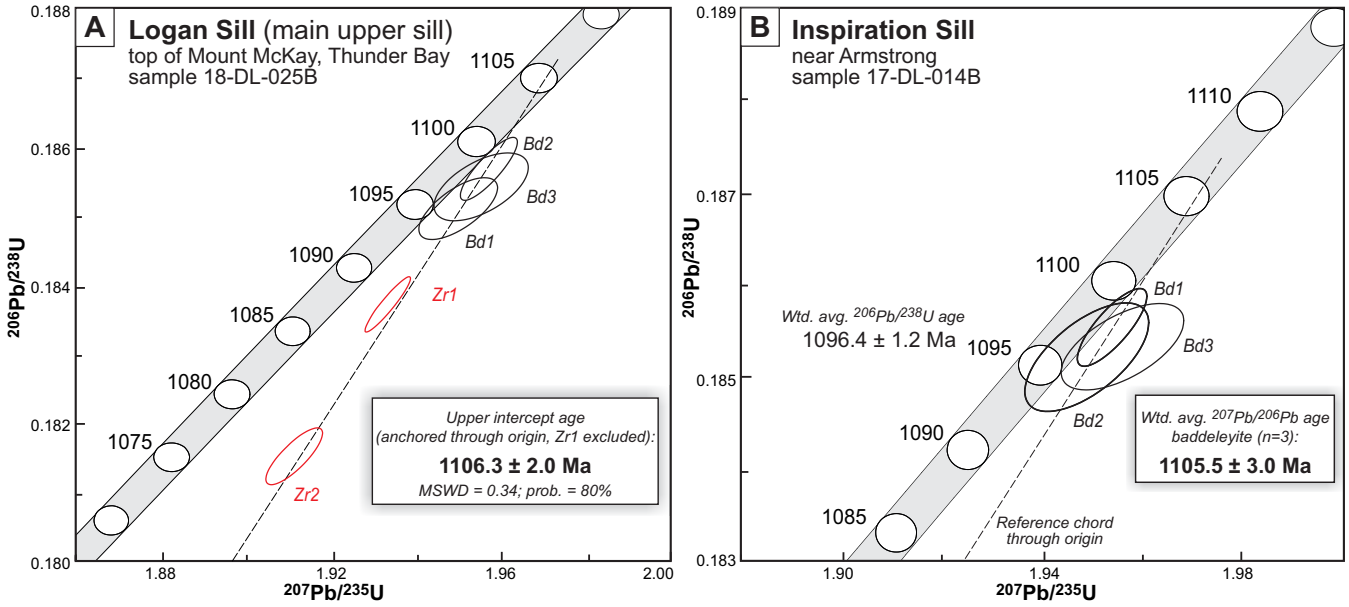

Figure 4. U-Pb concordia diagrams for **(a)** the Logan Sill at the top of Mt. McKay (sample 18-DL-025B) and **(b)** the Inspiration sill (sample 17-DL-014B) from the northern Nipigon Embayment. Zircon (Zr) data are shown as red ellipses and baddeleyite (Bd) as black ellipses. Preferred age picks are shown in bold font. All data-point error elipses are 2σ.

leyite age of 1093.2 ± 1.2 Ma (Fig. 5b), distinct and considerably younger than the 1099.6 ± 1.2 Ma date on discordant baddeleyite fractions reported by Heaman et al. (2007). This younger age suggests a correlation of the Crystal Lake Intrusion, not with the main Duluth Complex, but rather with the younger intrusions in the roof of that complex, such as the Beaver Bay Complex. Results on multiple samples from the Crystal Lake Intrusion and a more detailed interpretation is presented in Smith et al. (2020).

SAMPLING STRATEGY AND OVERVIEW OF RESULTS

Fieldwork over the last 2–3 years has allowed us to visit many of the key intrusive units, often with local experts. We have specifically targeted mineralized intrusions, and intrusions deemed of interest to exploration. We have also targeted representative units of some of the main magmatic pulses that were still lacking precise and accurate ages (e.g. Logan Sills), as well

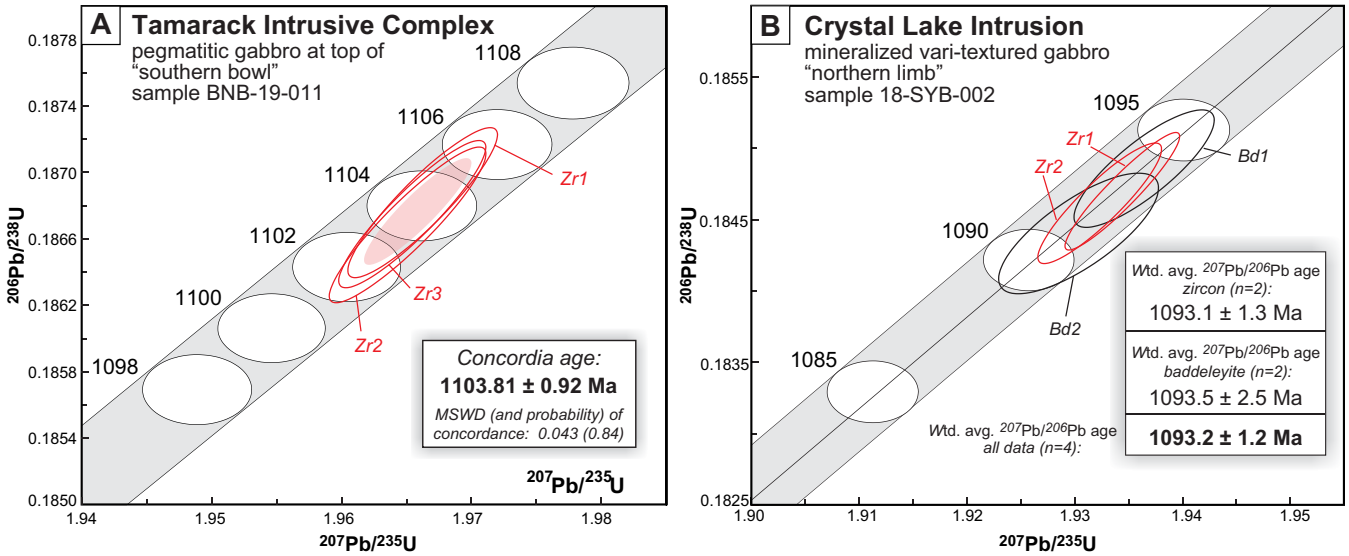

Figure 5. U-Pb concordia diagrams and preliminary ages for **(a)** the main "southern bowl" of the Tamarack Intrusion, Minnesota; and **(b)** the mineralized vari-textured gabbros from the northern limb of the Crystal Lake Intrusion. For the Tamarack sample, three fully concordant and overlapping zircon analyses define a concordia age (filled ellipse) of 1103.8 ± 0.9 Ma, distinctly younger than the earlier onset of high-volume basaltic magmatism in the Midcontinent Rift (at ca. 1106–1110 Ma). For Crystal Lake (b), we show one well behaved sample with concordant and overlapping zircon and baddeleyite results. Additional results are discussed in Smith et al. (2020). All data-point error elipses are 2σ.

as some of the problematic age "outliers" (e.g. Inspiration sill, and members of the Pigeon River dyke swarm). In all these cases, we spent time in the field to evaluate the overall complexity of the intrusions and their different phases, after which we sampled optimum material for U-Pb dating (~10 kg, sometimes multiple samples): typically coarser grained, slowly cooled, more fractionated units in which incompatible elements such as Zr (and U) show elevated abundances, thus increasing the likelihood that larger and more abundant baddeleyite and/or zircon crystals would have crystallized. In some of the composite or multi-phase intrusions, we sampled more than one phase, including both the presumed oldest and youngest phases—although the general expectation is that all of these will be within the resolution of the typical data, ideally ~1 Myr[3].

At the same time, we have compiled and evaluated all previous work (Table 1), feeding into our overall prioritization of samples. Needless to say, the requirement for accurate high-precision ages keeps increasing, as models are improving and associated questions are refined. Hence, this work is never finished and a number of samples are still in progress. Nevertheless, we can present here ~10 new ages for key units around the MCR, including some of the mineralized intrusions on the Canadian side of the border (Table 2). All results should be treated as preliminary, as additional fractions are still being analyzed. For analytical methods, the reader is referred to the accompanying paper by Smith et al. (2020, *see* their Appendix 1).

MINERALIZED INTRUSIVE COMPLEXES OF THE MIDCONTINENT RIFT: SOME KEY EXAMPLES

Sunday Lake Intrusion

The recently discovered Sunday Lake Intrusion, located in Jacques Township, ~25 km north of Thunder Bay, intrudes Archean metasedimentary rocks and granitoids of the Quetico Subprovince (Fig. 6). The intrusion, now dated at 1109.0 ± 1.3 Ma (this study; Table 2), is emplaced along the Crock Lake Fault, interpreted as a splay of the main Quetico Fault to the north (Flank, 2017), and is characterized by a distinct, elliptical, reversely magnetized anomaly. The morphology and true extent of the intrusion is yet to be fully determined; however, drilling indicates that the body is tabular in shape where emplaced into Quetico metasedimentary rocks, and more tube-like (cylindrical) to the northwest where it is hosted by Archean granitoids (Fig. 6). The differentiated intrusion is divided into an Ultramafic Series, a Lower Gabbro Series, and an Upper Gabbro Series (Flank, 2017) on the basis of petrographic and geochemical characteristics. The 10–120 m thick basal Ultramafic Series is composed of gabbroic breccia, melagabbro, olivine melagabbro, peridotite, and minor pyroxenite. The 250 m thick Lower Gabbro Series consists of gabbro, melagabbro, and peridotite. The evolved, coarse-grained Upper Gabbro Series is comprised of strongly hematized leucogabbro, oxide-rich gabbro, and evolved monzogabbro. The upper contact is commonly brecciated, containing subangular and partially resorbed quartz fragments and Quetico metasedimentary xenoliths within a chilled, hematized groundmass.

Sulphide mineralization within the Sunday Lake Intrusion is disseminated (2–10 vol.%) and mainly concentrated along the basal contact of the Ultramafic Series. The main mineralized body, which is enriched in Cu, Pt, Pd, and Au at typical levels of 3–10 g/t Pt+Pd+Au, contains disseminated, high PGE-tenor sulphides composed of chalcopyrite, pyrite, and pyrrhotite. Drilling has indicated that the main orebody can be traced over a 1500 x 900 m area, with a thickness of up to 43 m (Flank, 2017; S. Flank, pers. comm., 2019). Lower grade (<1 ppm Pt+Pd+Au), high-tenor sulphide mineralization (≥1200 ppm Pt+Pd+Au in 100% sulphide) has also been recognized within laterally continuous horizons at the upper and lower contacts of the Lower Gabbro Series (Flank, 2017). Footwall stringers, enriched in Cu and PGEs have also been noted.

Current Lake Intrusive Complex

The Thunder Bay North Igneous Complex, located ~50 km northeast of Thunder Bay, comprises a series of small, mineralized ultramafic-mafic intrusions that have been emplaced in proximity to the east-west-trending Quetico Fault, and are hosted within the Archean Quetico Subprovince (Fig. 7). Intrusions of the Thunder Bay North complex, which include the Current Lake, Steepledge, and Lone Island Lake intrusive complexes and possibly other bodies, are associated with the early stages of the MCR development and are prospective targets for Pt-Pd-Cu-Ni sulphide mineralization. The Current Lake Intrusive Complex, which we have dated at 1106.6 ± 1.6 Ma (this study; Table 2), is a tubular to tabular conduit-like deposit that is characterized by a "tadpole"-shaped aeromagnetic anomaly that extends for ~6 km in a northwest-southeast direction and widens to the southeast (Fig. 7a; Goodgame et al., 2010; Thomas et al., 2011). The Current Lake Complex, along with the adjacent paral-

[3] Most magmatic complexes are emplaced within the time span of a typical magmatic pulse of less than 1 Myr. Resolving complexity on shorter time scales, in Proterozoic rocks, remains very challenging. An interesting example is the study by Mungall et al. (2016) of the Bushveld Complex, although this study remains controversial.

Table 2. Summary of precise and robust U-Pb ages for key intrusions, including new results from the present study (results in bold font). The data are organized into two groups: intrusions on the northern flank of the Midcontinent Rift versus those on the southern flank. The age for the Kitto mafic-ultramafic intrusion is shown in red, as it remains one of the significant older age "outliers" for the onset of high-volume mafic magmatism still to be tested. Work on this sample is in progress. Intrusions known to have mineralization are preceded by an asterisk (*).

Rock Unit	New U-Pb Age (Ma)[1]	Method[2]	References	Sample ID	Easting (mE)	Northing (mN)	Zone	Description
Precisely dated intrusions on northern flank of MCR:								
* Kitto mafic-ultramafic intrusion	1117.4±3.7	Bd, wm7/6, n=2	Heaman et al., 2007					
* Seagull intrusion	1112.8±1.4	Bd, complex results	Heaman et al., 2007					
* Jackfish intrusion	1112.4±2.8	Bd, wm6/8, n=2	Heaman et al., 2007					
* Disraeli intrusion	1109.9±1.5	Bd, wm7/6, n=2	Heaman et al., 2007					
Cloud R. dyke	**1109.2±2.9**	**Bd, u. intercept, n=3**	**This study; *see also* Heaman et al., 2007**	**BNB-19-023**	**313140**	**5329177**	**16U**	**Main NNW-trending dykes, at Crooks; is cut by Pigeon River dykes**
***** Sunday Lk intrusion**	**1109.0±1.3**	**Bd, wm, n=5, slightly disc.**	**This study**	**BNB-17-050D**	**334842**	**5394958**	**16U**	**Sunday Lake Intrusion, coarser red monzogabbro; DDH SL-15-013, 481.0-485.4 m**
* Thunder Intrusion	1108.0±1.0	Zr, wm7/6, n=3, conc.	Trevisan et al., 2015					
* Coldwell Complex	1108.0±1.0	Zr, u. intercept	Heaman and Machado, 1992					
Nipigon Sills	1108.2±0.9	Zr, u. intercept, n=3	Davis and Sutcliffe, 1985; *see* Davis and Green, 1997					Diabase, pegmatitic gabbro, granophyre; these sills were referred to as "Logan Sills" by Davis and Sutcliffe, 1985; more precise upper intercept is quoted in Davis and Green, 1997.
Swamper Lk monzogabbro	1107.0±1.1	Zr, wm7/6, n=3	Davis and Green, 1997					Monzogabbro, reversely magnetized; age suggest link with Logan Sills
* Hele intrusion	1106.6±1.5	Bd, wm7/6, n=2	Heaman et al., 2007					
***** Current Lake Complex**	**1106.6±1.6**	**Zr and bd, u. intercept, n=4**	**This study**	**18-DL-035**			**16U**	**Coarser red monzogabbro near top of intrusion, Beaver Lake part of intrusive complex**
Logan Sills	**1106.3±2.0**	**Zr and bd, u. intercept, n=4**	**This study**	**18-DL-025B**	**330558**	**5357158**	**16U**	**Coarse-grained diabase, with incipient pegmatoidal segregations below uppper contact of upper sill**
Kama Hill sill	**1106.3±3.6**	**Zr, u. intercept, n=4**	**This study**	**BNB-19-024A**	**428116**	**5424370**	**16U**	**Coarse-grained to pegmatoidal diabase below upper contact of main sill**
Inspiration sill	**1105.5±3.0**	**Bd, wm7/6, n=3**	**This study**	**17-DL-014B**	**356197**	**5573323**	**16U**	**Pegmatoidal segregations in upper part of diabase sill**
* Nemegosenda	1105.4±2.6	Zr, u. intercept, n=3	Heaman et al., 2007					
* Tamarack Intr. Complex northern body "CGO"	1105.6±1.3	Bd, wm, n=3, slightly disc.	Goldner, 2011				15T	Feldspathic lherzolite from near margin of northern dyke-like body ("CGO")
***** Tamarack Intr. Complex northern body "CGO"**	**1105.9±0.9**	**Zr, u. intercept, n=4**	**This study**	**BNB-19-015**	**492042**	**5170155**	**15T**	**Pegmatoidal gabbro from upper part of northern dyke-like body ("CGO") DDH 15-TK-0221, 440.00–463.00 m: coarse-grained to pegmatoidal gabbro**
***** Tamarack Intr. Complex central body "FGO"**	**1103.7±0.8**	**Zr, conc. age, n=4**	**This study**	**BNB-19-013**	**492042**	**5170155**	**15T**	**Pegmatoidal gabbro from upper part of central dyke-like body ("FGO"), DDH 15-TK-0218, 503.46–510.30 m**
	1105.7±0.8	**Zr, wm7/6, n=4**		**BNB-19-014**				**Late crosscutting dyke of quartz dioritic pegmatoid, cutting FGO peridotite, DDH 15-TK-0218, 1059.55–1063.30 m**
***** Tamarack Intr. Complex southern bowl ("Bowl")**	**1103.8±0.9**	**Zr, conc. age, n=3**	**This study**	**BNB-19-011**	**496841**	**5163275**	**15T**	**Pegmatoidal gabbro from upper part of main southern part of intrusion ("the bowl") DDH 15-TK-0217, 193.60–199.80 m: coarse-grained to pegmatoidal gabbro**
* Duluth Complex	1099.0±1.0	Zr, wm7/6, several results	Paces and Miller, 1993					
Mt. Josephine dyke	**1099.0±1.2**	**Zr and bd, wm7/6, n=4**	**This study**	**18-DL-022**	**301962**	**5316973**	**16T**	**Coarse-grained, in part pegmatoidal, diabase from middle of ~100 m wide dyke**
Pigeon R. dykes	**1096.9±1.9**	**Zr, u. intercept, n=3**	**This study**	**17-DL-004B**	**310563**	**5324695**	**16U**	**Rita Bolduc dyke (~80–100 m), one of the main NNE-trending Pigeon River dykes**
Mount Mollie dyke	**1096.3±1.4**	**Zr and bd, u. intercept, n=6**	**Smith et al., 2020**					
* Sonju Lake Intrusion	1096.1±0.8	Bd, wm7/6, n=4	Paces and Miller, 1993					
* Beaver Bay Complex	1095.8±1.2	Zr and Bd, wm7/6, n=6	Paces and Miller, 1993					Beaver River Diabase complex
Hovland Sill	1095.9±0.6	Zr, wm6/8, concordant	Boerboom et al., 2014					
***** Crystal Lake Intrusion vari-text. gabbro, S limb**	**1094.1±1.4**	**Zr and bd, wm7/6, n=4**	**Smith et al., 2020**	**18-SYB-111**	**306239**	**5326523**		**Vari-textured gabbro, southern limb, minor sulphides and Cr-spinel; DDH CL0003, 556–562 m**
***** Crystal Lake Intrusion vari-text. gabbro, N limb**	**1093.1±1.2**	**Zr and bd, wm7/6, n=4**	**Smith et al., 2020; summarized in this paper**	**18-SYB-002**	**305453**	**5328330**		**Vari-textured gabbro, northern limb, minor sulphides and Cr-spinel; DDH CL0001, 412–417 m**
***** Crystal Lake Intrusion combined data**	**1092.3±0.7**	**Zr and bd, conc. age, n=6**	**Smith et al., 2020**	**18-SYB-001, 002, 111**				
***** Crystal Lake Intrusion Troctolite, unmineralized, N limb**	**1091.4±1.4**	**Zr, wm, n=2**	**Smith et al., 2020**	**18-SYB-001**	**305453**	**5328330**		**Homogeneous medium- to coarse-grained troctolite**
Moss Lake Gabbro	1094.7±3.1	Bd, wm6/8, n=2	Heaman et al., 2007					Intrusive complex emplaced within Osler Group, on Black Bay Peninsula
St. Ignace Isl. Complex	1089.2±3.2	Zr, no details available	Smyk et al., 2006					Intrusive complex emplaced within Osler Group
Precisely dated intrusions on southern flank of MCR:								
* Echo Lake Intrusion	1111.0±1.0	Zr, overlapping conc.	Canon and Nicholson, 2001; S. Nicholson, pers. comm., 2018					Large gabbroic layered intrusion with basal ultramafic units; buried
* Eagle - Eagle East complex	1107.3±3.7	Bd, wm7/6, n=4	Ding et al., 2010					Peridotite and gabbros, in feeder-like dykes
***** Bovine Igneous Complex**	**1106.2±1.3**	**Bd, wm, n=3, slighltly disc.**	**This study**	**18-DL-001**	**396985**	**5174336**	**16T**	**Coarse gabbro, from outcrop along southeastern rim of intrusion**
* Mellen Complex	1102.8±2.8	Zr, u. intercept.	Zartman et al., 1997					Layered intrusion with mafic lower part and granitic upper part

Notes and abbreviations: bd = baddeleyite, conc. = concordant, DDH = diamond drillhole, disc. = discordant, Gp = Group, Lk = Lake, Mt = Mount, n=x = number of analyses, R = River, u. intercept = upper intercept, wm = weighted mean, zr = zircon.

1: Ages in bold font are new ages obtained as part of the present study. The Kitto age of Heaman et al. (20017) is one of the remaining age "outliers" and shown in red font.

2: CA-ID-TIMS on single zircons or small fragments thereof, unless otherwise noted; baddeleyite untreated.

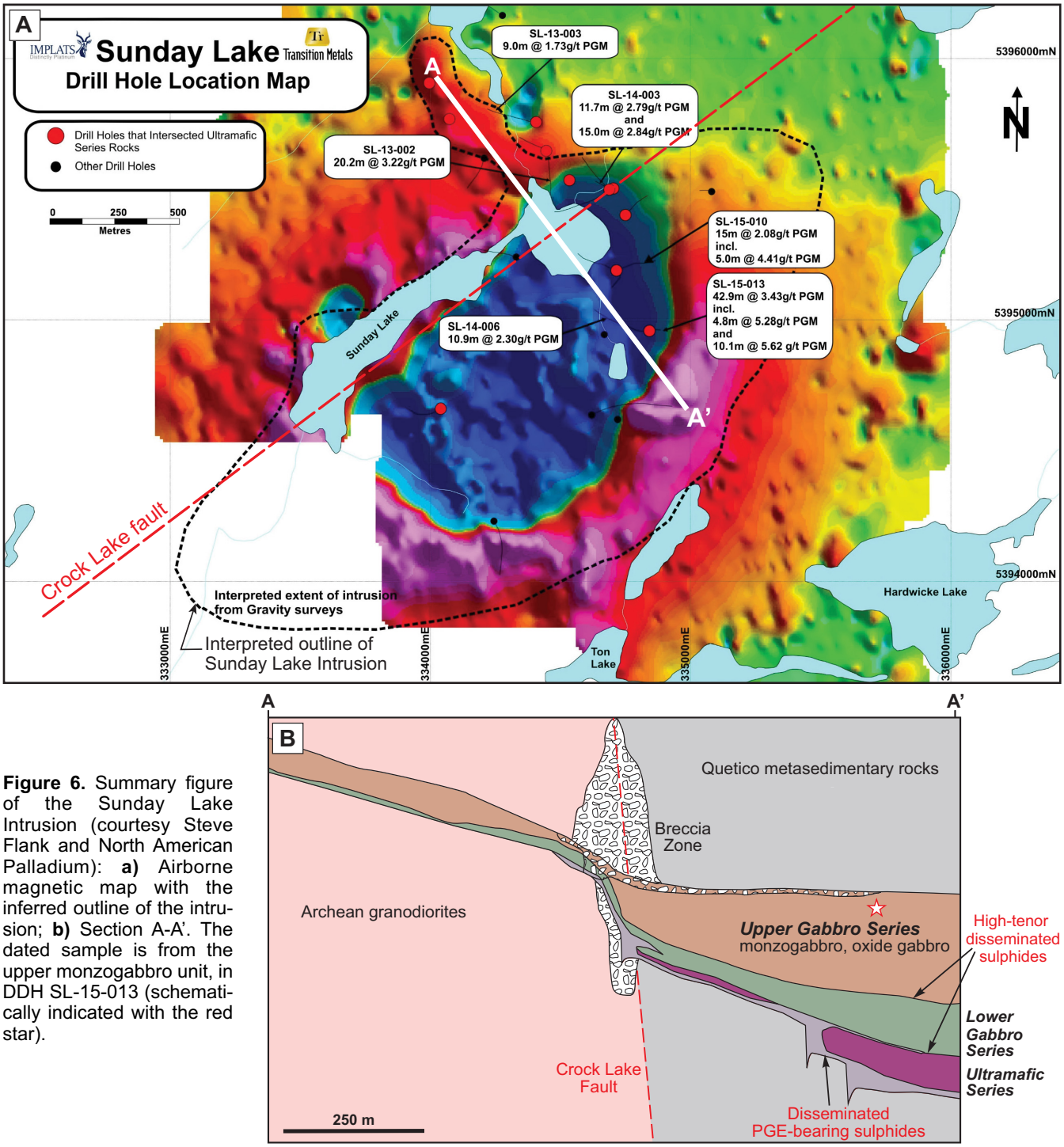

Figure 6. Summary figure of the Sunday Lake Intrusion (courtesy Steve Flank and North American Palladium): **a)** Airborne magnetic map with the inferred outline of the intrusion; **b)** Section A-A'. The dated sample is from the upper monzogabbro unit, in DDH SL-15-013 (schematically indicated with the red star).

lel Steepledge Complex, shows variation in shape, composition, orientation, and grade along its length. The change in morphology of the Current Lake Intrusive Complex from tubular to more tabular coincides with the contact between Archean granitoids in the north and Quetico metasedimentary rocks in the south. Pre-existing structures in the Quetico Subprovince are also thought to have strongly controlled the initial emplacement of the Thunder Bay North magmas.

Extensive drilling has delineated a 3.4 km long, continuously mineralized, disseminated sulphide body that is hosted within the ultramafic portion of the complex and is characterized by Pt/Pd ratios of >1 and Ni/Cu ratios of ~0.5 (Goodgame et al., 2010; Thomas et al., 2011). In the north, the Current Lake Intrusive Complex is a subhorizontal, sinuous, tubular body composed mainly of olivine melagabbro and lherzolite, ranging from ≥30 m in diameter, up to 50 m in width and 70 m in thickness (Goodgame et al., 2010;

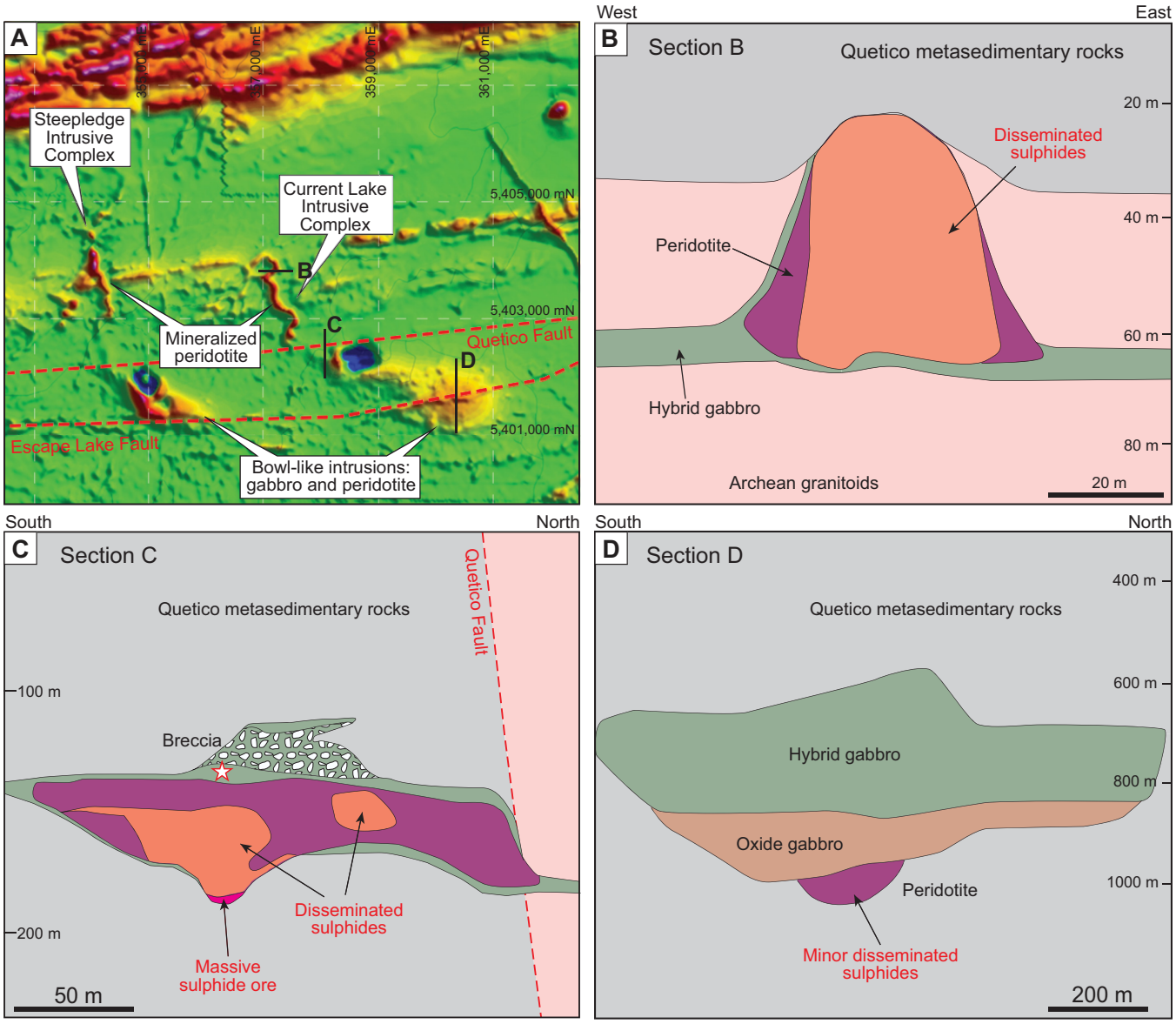

Figure 7. Summary figures of the Thunder Bay North Complex and its Current Lake Intrusive Complex. **a)** Summary magnetic map (total intensity) showing the various parts of the Current Lake complex (image courtesy of Allan MacTavish, Panoramic Resources, and pers. comm., 2018). The map highlights the NNW-SSE-trending "tadpole"-shape anomalies of the Current Lake and Steepledge Lake intrusive complexes. The locations of the cross-sections shown in figures (b) to (d) are also shown. **b)** Cross-section through the northern part of the Current Lake complex (looking north); in this section, the intrusion is tube-like in morphology with mineralization disseminated throughout the interior of the chonolith. **c)** Cross-section (looking east) through the Beaver Lake portion of the Current Lake Intrusive Complex. **d)** Cross-section (looking west) through the South-East anomaly. Cross-sections from Thomas et al. (2011) and A. MacTavish (Panoramic Resources, pers. comm., 2018). Approximate location of our dated sample shown by a red star.

Thomas et al., 2011). Here Pt-Pd-Cu-Ni sulphide mineralization is disseminated in nature and distributed throughout the entire tubular body (Fig. 7b). To the southeast, the peridotite intrusion progressively deepens and becomes a shallowly plunging tabular body in the Beaver Lake area, with dimensions up to 600 m wide and 200 m thick (Goodgame et al., 2010; Thomas et al., 2011). Sulphide mineralization is more localized in this area and is confined to the margins of the conduit. Semi-massive to massive sulphides have been locally intersected here, along the basal contact of the intrusion (Fig. 7c). Near the top of the intrusion, a different style of mineralization has been identified, characterized by finely disseminated, high-tenor Cu-bearing sulphides (Goodgame et al., 2010). The southeastern extent of the Current Lake Complex, defined by a circular magnetic anomaly, is represented by the differentiated, tabular, unmineralized "Southeast Anomaly", which is composed of a basal peridotite, overlain by an oxide gabbro, and a distinctive red, hybrid gabbro that is strongly hematized and contaminated.

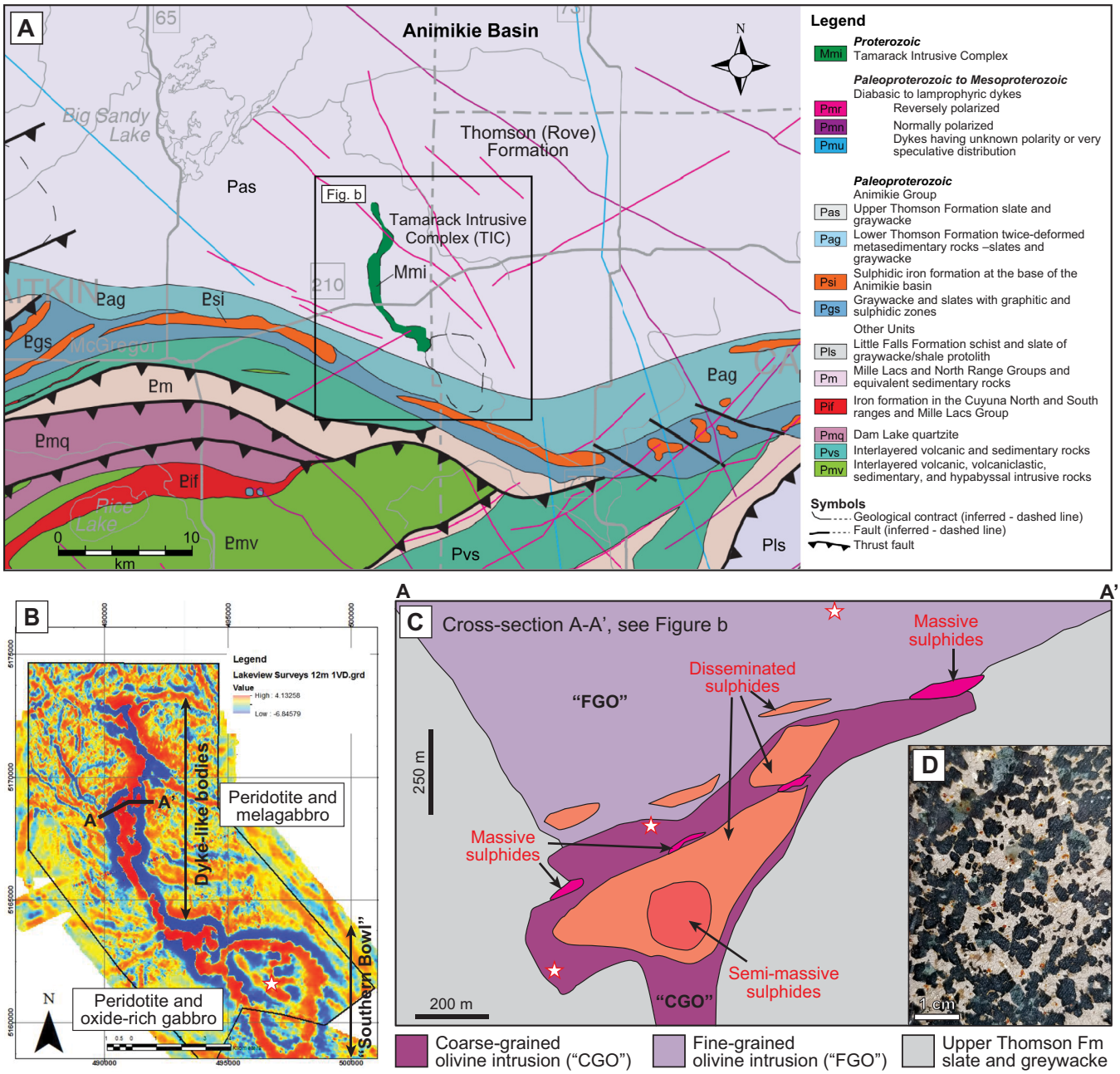

Figure 8. Summary figures of the Tamarack Intrusive Complex. **a)** Regional geological setting and location of the Tamarack complex, which intrudes slate and greywacke of the Rove Formation in the southern Animiki Basin (*from* the geological map of Minnesota; Jirsa et al., 2011). **b)** Airborne magnetic map image (1st vertical derivative) showing the overall shape of the Tamarack Intrusive Complex, with the northern dyke-like bodies and the "southern bowl". **c)** West-to-east cross-section A-A' (*see* Fig. (b) for location), showing the coarse-grained olivine ("CGO") and fine-grained olivine ("FGO") intrusions within the northern dyke-like part of the Tamarack Intrusive Complex (*after* Taranovic et al., 2015). **d)** Net-textured to semi-massive sulphide ore in drill core from the CGO intrusion.

Tamarack Intrusive Complex

The mafic-ultramafic Tamarack Intrusive Complex, located ~75 km to the southwest of the Duluth Complex, intrudes Paleoproterozoic slate and greywacke of the Upper Thomson Formation within the Paleoproterozoic Animikie Basin (Fig. 8). The complex is characterized by a tadpole-shaped aeromagnetic anomaly, which extends ~13 km in a northwest-southeast direction and varies from 1 to 4 km in width (Fig. 8; Goldner, 2011; Taranovic et al., 2015). The complex, interpreted as a dynamic open-system conduit that crystallized from a picritic parental magma (Taranovic et al., 2015), consists of three sub-intrusions: the "coarse-grained olivine" (CGO), the "fine-grained olivine" (FGO), and the southern "bowl" intrusions. The mineralized CGO and FGO intrusions are located in the north, where they form the dyke-like portion of the Tamarack Intrusive Complex, with an overall mor-

phology of an irregular funnel (Fig. 8c). The 1105 ± 1.2 Ma CGO intrusion (Goldner, 2011), which comprises the lower portion of the funnel-like dyke, is composed of coarse-grained peridotite, feldspathic peridotite, melatroctolite, and melagabbro (Taranovic et al., 2015). The overlying FGO intrusion is characterized by fine-grained peridotite, feldspathic peridotite, feldspathic pyroxenite, and melagabbro (Taranovic et al., 2015). The "bowl" intrusion, which appears barren of sulphide mineralization, is composed of peridotite and feldspathic peridotite overlain by a differentiated sequence of oxide-rich gabbronorites (Goldner, 2011). At present, uncertainty surrounds the relative timing of the three intrusions. Our new zircon concordia age of 1103.8 ± 0.9 Ma, based on three fully overlapping single zircon results (Fig. 5a), was obtained on pegmatoidal gabbro near the differentiated top of the southern bowl.

The Ni-Cu-PGE sulphide mineralization within the Tamarack Intrusive Complex (Fig. 8c) is hosted within the CGO and FGO intrusions and includes minor massive, disseminated, and net-textured sulphide ores characterized by Ni/Cu ratios of >1 (Taranovic et al., 2016). Current inferred resource estimates indicate 4.3 Mt at 1.58% Ni, 0.92% Cu, 0.29 g/t Pt, and 0.18 g/t Pd (Fletcher et al., 2018). The CGO intrusion hosts the majority of the mineralization as disseminated and semi-massive (net-textured) sulphides, which are typically localized within the core of the dyke. The FGO intrusion hosts disseminated and patchy net-textured sulphide mineralization that is confined to discrete layers near the base of the intrusion, above the FGO-CGO contact. Massive sulphide lenses are found at the contact between the FGO-CGO intrusions and in adjacent country rocks (Fig. 8c). The sulphide ores are characterized by variable proportions of the primary magmatic assemblage pyrrhotite, pentlandite, chalcopyrite, and magnetite, with accessory pyrite and cubanite (Taranovic et al., 2016). Platinum group element tenors are variable throughout the Tamarack Intrusive Complex ores (Taranovic et al., 2016), a feature attributed to variable R-factors. The highest PGE tenors, which are comparable to those of Noril'sk ores, are associated with disseminated ores of the CGO intrusion. It has been suggested that the high-tenor sulphides of the CGO intrusion formed as a result of upgrading of an earlier sulphide liquid, left in the conduit system by the inferred earlier FGO magma (Taranovic et al., 2016). Although crustal contamination is thought to have played a critical role in ore genesis and in attaining S saturation, this is not recognized within the preserved isotopic record. Sulphides within the Tamarack Intrusive Complex are characterized by mantle-like $\delta^{34}S$ values between -0.2 and 2.8‰ (Taranovic et al., 2018), which are in sharp contrast with those from the basal disseminated ores of the Duluth Complex ($\delta^{34}S$ 0–18‰; Ripley et al., 2007; Queffurus and Barnes, 2014). Furthermore, O and Re-Os isotope compositions indicate only low degrees of contamination (<3%). Taranovic et al. (2018) suggest that the isotopic characteristics of the Tamarack Intrusive Complex could be a function of either selective contamination of Paleoproterozoic sedimentary rocks or efficient isotopic exchange within the dynamic conduit system. If exchange reactions have operated to obliterate the initial isotopic signature, then such isotopes are no longer accurate proxies for estimating crustal contamination.

Eagle and Eagle East Intrusions

Prior to the discovery of extensive, high-grade, massive Ni-Cu sulphides at the Eagle intrusion in 2002, Ni-Cu-PGE mineralization in the MCR was thought to be hosted by larger, sheet-like mafic intrusions (e.g. Duluth Complex, Crystal Lake). The Eagle discovery changed this perspective, resulting in a wave of exploration for magmatic sulphide deposits focussed on smaller, early rift, conduit-type intrusions.

The small ultramafic Eagle intrusion and nearby Eagle East intrusion intrude Paleoproterozoic rocks of the Marquette Range Supergroup within the Baraga Basin, which is also host to the MCR east-west-trending Marquette-Baraga dyke swam (Fig. 9). The Eagle and Eagle East intrusions (formerly known as the Yellow Dog Peridotites; Morris, 1977), are characterized by prominent ellipse-shaped magnetic highs (long-axis parallel to the dyke swarm) and occur as separate subvertical, boat-shaped, dyke-like bodies (Fig. 9; Ding et al., 2010; Barnes et al., 2016). Barnes et al. (2016) suggest the morphology of these intrusions resulted from conduit widening of an initial blade-shaped dyke (cf. Savannah, Western Australia). The Eagle intrusion is 480 m long and 100–200 m wide, with a vertical extension of >300 m. The deeper Eagle East intrusion is ~600 m long, ~150 m wide, and >500 m thick (Ding et al., 2010). Both are emplaced above the unconformity with the Archean basement.

The Eagle and Eagle East intrusions contain significant Ni-Cu-PGE mineralization, with current estimates indicating a combined resource of 4.8 Mt at 2.8% Ni, 2.4% Cu, 0.7 g/t Pt, and 0.5 g/t Pd (Clow et al., 2017). The sulphide mineralization is characterized by disseminated, semi-massive and massive sulphide ores, which are composed of pyrrhotite, pentlandite, chalcopyrite, and cubanite (Ding et al., 2010, 2012). At Eagle, over 90% of the sulphide ore occurs in the irregular-shaped massive sulphide zone above the keel of the intrusion, with some ore also hosted within adjacent metasedimentary rocks (Fig. 9c,d). At Eagle East, high-grade semi-massive and massive sulphide ores are confined

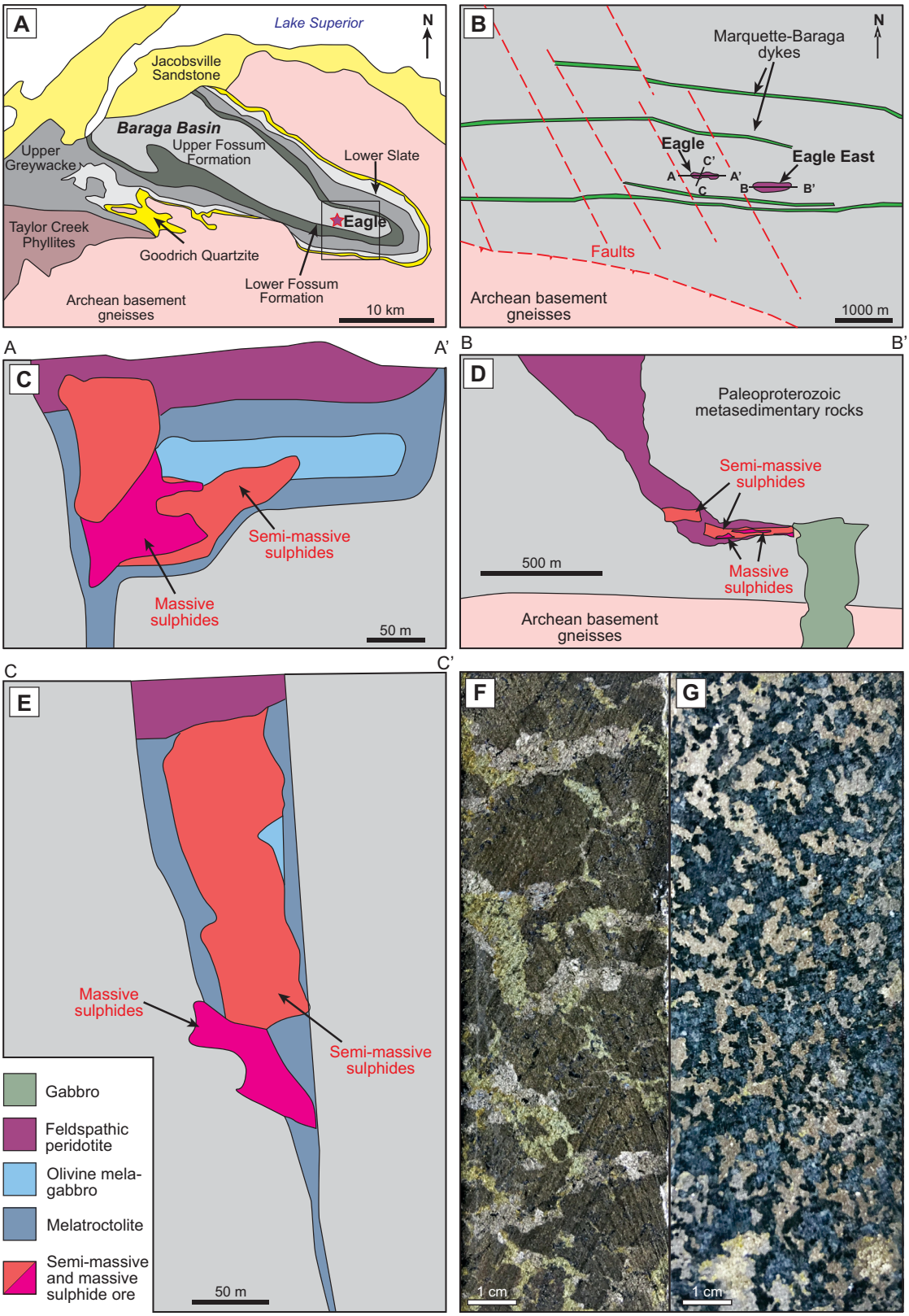

Figure 9. a) Geological setting of the Eagle deposit in the synclinorium of the Paleoproterozoic Baraga Basin (*after* Ding et al., 2010). **b)** Plan view of the Eagle and Eagle East intrusions in the eastern Baraga Basin. The intrusions are elongated in an east-west direction, parallel to the trend of nearby Marquette-Baraga dykes. **c, d, e)** Simplified cross-sections through the deposits showing the morphology of the Eagle and Eagle East intrusions and the distribution of mineralization. Locations of sections are shown on figure (b) (*after* Ding et al., 2010; Rose et al., 2018). **f, g)** Drill-core samples of typical Tamarack sulphide ore: (f) high-grade massive sulphides and (g) net-textured to semi-massive ore. In photograph (f) note the considerable pentlandite (brighter stringers) and chalcopyrite-cubanite (yellowish sulphides) content.

to the subhorizontal portion of the conduit, occurring close to the basal contact of the intrusion (Fig. 9e; Clow et al., 2017). The overlying funnel-shaped peridotite body contains negligible sulphide mineralization (Ding et al., 2010). The semi-massive to massive sulphide ores in both intrusions are characterized by elevated Ni/Cu ratios, relatively fractionated PGE patterns, and metal tenors comparable to those observed at Tamarack (Ding et al., 2012; Taranovic et al., 2016). Chalcopyrite-rich veins within the footwall show highly fractionated PGE patterns (Ding et al., 2012).

Within these conduit deposits, the addition of externally derived S is considered critical in producing the large sulphide accumulations characteristic of the Eagle deposits. Recent studies (e.g. Robertson et al., 2015) have shown that the addition of crustal S into these magmatic systems is controlled by the direct melting and assimilation of wall rock and xenoliths rather than through devolatilization reactions or dissolution of S in thermal aureoles. Thus, the Eagle and Eagle East ores are not considered to be contact-style deposits as external S is thought to have been derived distally from the present location of the ores. This notion is consistent with $\delta^{34}S$ and $\Delta^{33}S$ data of the sulphide ores, which indicate the addition of crustal-derived S, from both Paleoproterozoic and Archean sources distal to the deposits (Ding et al., 2012; Hink, 2016). The low $\delta^{34}S$ values ($\delta^{34}S$ 0–5 ‰) of the Eagle ores, which do not correspond to the high $\delta^{34}S$ values characteristic of the adjacent Michigamme Formation ($\delta^{34}S$ 4.6–29‰; Ding et al., 2012; Hink, 2016), could be attributed to selective assimilation of Michigamme Formation characterized by lower $\delta^{34}S$ values; isotopic exchange between the contaminated and pristine magma (Ripley and Li, 2003); or the extensive incorporation of Archean-derived S, as indicated by non-zero $\Delta^{33}S$ values (-0.86 to 0.86‰; Ding et al., 2012). Although isotopic data indicate <5% bulk contamination, possibly up to 20% locally, values are indicative of a contribution of S from country rocks of up to ~50% (Ding et al., 2012). Consequently, the sulphide liquid is viewed as being entrained and subsequently transported and deposited upwards through the magma conduit. Barnes et al. (2016) proposed, however, that the massive sulphide ores at Eagle accumulated as the result of the downward percolation of the sulphide liquid back into the former feeder dyke.

DISCUSSION

Onset of High-Volume Magmatism

As alluded to above, none of the new ages support an older and protracted onset of the main high-volume basaltic magmatism of the main MCR. All the ages of the Logan Sills (*sensu lato*) are compatible with a ca. 1106–1110 Ma onset, and the minor dispersion among the present ages (Table 2) may be in part analytical as uncertainties overlap. Only the reported date for olivine gabbro of the Kitto intrusion (*see* Fig. 1 for location), at 1117.5 ± 3.7 Ma (Heaman et al., 2007), remains as a suspected "outlier", and, hence, an important date we are still testing[4].

A sharp onset of the first high-volume basaltic magmatism sometime in the 1106 to 1110 Ma interval is also more in line with a similarly sharp onset of the main volcanic sequences at ca. 1107–1109 Ma[5], with the oldest recorded age being 1107.7 ± 1.9 Ma (Davis and Green, 1997) on a sample near the base of the volcanic sequence overlying the Puckwunge Sandstone along the Canada-USA border (Fig. 1), and a similar age of 1107.5 +4/-2 Ma for the base of the Osler Group (Davis and Sutcliffe, 1985).

This changed perspective on the older MCR units now draws renewed attention to the Echo Lake intrusion, a large layered gabbro complex with PGE mineralization buried below Jacobsville Sandstone on the southern flank of the MCR (Fig. 1). With a reported zircon age of 1110.8 ± 1.5 Ma on multiple near-concordant and concordant fractions (Cannon and Nicholson, 2001; S. Nicholson, pers. comm., 2018), this intrusion now stands as the oldest well dated intrusion in the MCR. As samples from this intrusion had robust zircons, new analysis of chemically abraded zircons may refine this age to better than 1 Myr precision.

Mineralized Mafic-Ultramafic Intrusion on the northern Flank of the Midcontinent Rift, Canada

On the northern flank of the MCR, north of Thunder Bay, there occur a number of localized mafic-ultramafic intrusions: the Thunder Bay North complex, including the chonolith-like Current Lake Intrusive Complex (with a narrow feeder and big bowl-shaped intrusion); the Sunday Lake intrusion; the Saturday Night intrusion; and the Thunder intrusion. All of these

[4] There are a few other older reported ages, either published or unpublished, but all are based on somewhat complicated and discordant baddeleyite data, such as the 1120 ± 4 Ma upper intercept age for a Baraga dyke near the Eagle deposit (Dunlop, 2013). Others are within error of a ca. 1109 Ma onset (e.g. Jackfish Island and other intrusions in Heaman et al., 2007).

[5] Note that in efforts to refine zircon ages on the volcanic sequences, using the latest innovations in high-precision U-Pb geochronology, there is a tendency towards reporting mean $^{206}Pb/^{238}U$ ages of multiple concordant zircon analyses, or concordia ages (e.g. Swanson-Hysell et al., 2019), which, in most cases, are just slightly younger than older $^{207}Pb/^{206}Pb$ ages on similar samples, thus shifting the age framework to slightly younger ages (by 1–2 Myr). This shift in absolute time is further magnified by using a modified U isotope ratio (Hiess et al., 2012).

intrude Archean basement of the Quetico Subprovince below the northern limb of the MCR, and all are variably mineralized. Some are being actively explored. They were discovered by probing distinct geophysical anomalies (reverse remanence magnetic anomalies), following the discovery in 2002 of high-grade Ni-Cu-PGE sulphide ore in another intrusion, the Eagle intrusion, on the south side of the MCR[6].

The larger bowl-shaped main parts of these various intrusive complexes typically show ultramafic cumulate rocks near the base, with or without basal sulphide mineralization, overlain by mafic cumulates that grade up into evolved monzogabbros underneath a chilled upper contact that shows extensive interaction with Archean roof rocks (e.g. Fig. 6b). The apparent negative magnetic anomalies associated with these intrusions, indicating a significant component of reverse paleomagnetic remanence, suggested that these intrusions were part of the early rift story. Few of them were dated, except for the Thunder intrusion (as part of a TGI-4 study; *see* Trevisan et al., 2015), which has a zircon age of 1108.0 ± 1.0 Ma. We therefore sampled the Current Lake intrusion of the Thunder Bay North Complex, the Sunday Lake intrusion, and the Saturday Night intrusion, two of which yielded good zircon and baddeleyite separates from evolved, coarsest grained samples of upper monzogabbros.

Baddeleyites (5 fractions) from the Sunday Lake intrusion yield a preliminary age of 1109.0 ± 1.3 Ma (weighted mean $^{207}Pb/^{206}Pb$ age); the Current Lake sample (from the Beaver Lake part of the intrusion), yields a 1106.6 ± 1.6 Ma age (upper intercept). It is too early to tell from these initial results (Table 2) whether the minor age dispersion is real or whether it reflects minor analytical differences (such as common Pb corrections on baddeleyites with lower radiogenic Pb content, or other complications). It is entirely possible that all these intrusions formed within a million years at ca. 1108 Ma. Given the shape of some of these intrusions, with tube-like conduits (i.e. "chonoliths"), it seems likely that they represent dynamic feeders to the major sill complexes on the northern flank of the MCR, and/or the lower parts of the basaltic volcanic sequences that may have extended well onto the northern flank of the MCR.

On the southern flank of the rift, the Eagle – Eagle East Complex and nearby intrusions also fall in this same older age group. We have newly dated one of these differentiated intrusions, the Bovine Igneous Complex), which yields a preliminary baddeleyite age of 1106.2 ± 1.3 Ma (Table 2). It seems likely that the linear array of intrusions, including Eagle and Bovine Igneous Complex, share a genetic relationship with major east-west-trending dykes of the Baraga-Marquette swarm, which still lack precise and concordant U-Pb ages in the published literature[7]. In detail, however, the Baraga-Marquette swarm shows at least two discrete trends (east-northeast, and east-southeast) and may represent more than one swarm and magmatic event.

Why the "Tadpole"-Shape? And Magma Flow/ Filling Direction?

A remarkable feature of the Current Lake and adjacent Steepledge Lake complexes is their composite shape with shallow dipping/plunging conduits in the north, widening into larger bowl-shaped intrusions to the southeast, over a distance of ~4 to 10 km. Even more remarkable is that the somewhat younger Tamarack Complex, hundreds of kilometres to the southwest in Minnesota, shows a similar morphology—a basic plan view that we refer to as a "tadpole". Also, Sunday Lake shows this basic plan view, although less pronounced, with a conduit-like appendage on its northwest side (Fig. 7). In addition to sharing this basic "tadpole" shape, the intrusions show a similar orientation and asymmetry, with the larger bowl-shaped bodies offset to the southeast (i.e. the tadpoles seem to be swimming in the same direction!).

Part of the explanation could be gentle southeast-directed tilting (e.g. ~5º into the rift), which could expose a somewhat deeper feeder dyke progressively to the north. Almost certainly this is part of the explanation and naturally leads to the question of flow or filling direction. Currently there are no hard data on the flow direction in these complexes, but an overall magma flow from northern conduit-like feeders into larger bowl-shaped intrusions in the south is our preferred[8]. This suggests that the larger bowl-shaped intrusions are the down-stream part of the complex that slowly filled and expanded by roof uplift and stoping, while undergoing internal crystal settling (cumulates at the base) and differentiation.

If our interpretation of flow direction is correct, it would suggest that sulphide ores are most likely to have accumulated in two places: 1) where narrow conduit-like feeders widened and fed into larger bodies to the southeast, due to decreasing magma flow rates and rapidly reduced transport capacity; and 2) localized

[6] At Current Lake, part of the Thunder Bay North Complex, the discovery of mineralized boulders on the lakeshore also contributed to the discovery of the Current Lake mineralized intrusion (A. MacTavish, pers. comm., 2018).

[7] Dunlop (2013) presented an upper intercept age of 1120 ± 4 Ma based on three discordant baddeleyite fractions.

[8] At the Current Lake Intrusive Complex, Panoramic Resources has generally been entertaining an opposite flow direction, i.e. from the southeastern bowl-shaped intrusion into the northern conduit (A. MacTavish, pers. comm., 2018).

sulphide accumulations along the bottom of the main bowls, due to local gravity settling of sulphide droplets and pooling in local footwall depressions. Neither of these targets is easy to find, particularly at depth. These predictions can be compared with the drill-defined sections shown in Figures 6 to 9.

Younger Mineralized Intrusions: Tamarack, Duluth Complex, Crystal Lake

Tamarack

We sampled several phases of the large Tamarack Intrusive Complex in Minnesota, parts of which hosts high-grade massive to semi-massive and disseminated Ni-Cu-PGE sulphides. An earlier date from the northern dyke-like feeder of the complex was determined at 1105.6 ± 1.3 Ma, using sparse baddeleyite from a feldspathic peridotite (Goldner, 2011). This date is based on three clustered, slightly discordant (1.1–1.5%) fractions. Some of our samples are still in progress, but zircons from the differentiated upper part of the large "southern bowl" of the complex yielded excellent concordant and overlapping results (Fig. 5a), resulting in a concordia age of 1103.8 ± 0.9 Ma. This precise and concordant result indicates that the Tamarack Complex is clearly younger than the ca. 1106–1109 Ma group of intrusions north of Thunder Bay. It is possible that it represents a feeder to the nearby "Chengwatana volcanics" that fill the southern part of the MCR (Fig. 1), for which Wirth and Gehrels (1998) reported a U-Pb zircon age of 1102 ± 5 Ma. The multi-lobed morphology of the Tamarack Intrusive Complex, suggesting three different phases and a dynamic, perhaps longer lived intrusive history, is compatible with a dynamic feeder-type system (Goldner, 2011; Taranovic et al., 2015).

Duluth Complex

The next younger intrusive complex is that of the very large Duluth Complex (Miller et al., 2001, 2002) dated by multiple samples at 1098–1099 Ma (Paces and Miller, 1993; Hoaglund, 2010). It has been described by numerous authors and will not be dealt with here in any detail, except for a few brief comments:

1. As recently reviewed by Cawthorn and Miller (2018), early work on the Duluth Complex by Grout (1918), then referred to as the "Duluth gabbro", recognized it as "a large, lenticular, centrally sunken, generally concordant, intrusive mass, with its thickness approximately one-tenth to one-twentieth of its width or diameter". Grout (1918) introduced the term "lopolith" (from the Greek word "lopos" meaning shell or dish) and interpreted the Mellen Complex across the lake (Fig. 1), now known to be slightly older, as the southern limb of his "lopolith". As explained by Cawthorn and Miller (2018), the modern view of the Duluth Complex has evolved significantly and the term "lopolith" is no longer appropriate, not here and possibly not elsewhere either (e.g. Bushveld).
2. In the modern literature, the Duluth Complex is commonly referred to as a "large layered intrusion", the second largest in the world after the Bushveld Complex. Therefore, it is often thought of as a laterally extensive layered complex (like the Bushveld), but a more detailed look at the Duluth Complex (Miller et al., 2001, 2002) reveals that it is indeed a "complex" in the very sense of the word—i.e., made up of several, if not many, more localized magmatic chambers or sub-intrusions, each with a slightly different magmatic history. This makes lateral correlation and a full understanding of the Duluth Complex inherently more difficult, in addition to the extensive glacial cover, and locally steep topography and thick tree cover.
3. Although there were no historic mines, the complex has been explored for many decades following the discovery of Cu-sulphide mineralization by F.W. Childers in 1948. Since then, exploration has involved numerous drilling campaigns and sinking of exploration shafts (Miller et al., 2002; Miller, 2011). Some projects along the basal contact of the complex (*see* Fig. 1), involving some massive but mainly large-tonnage disseminated Cu-Ni-PGE sulphide ores, are now in a final exploration and permitting stage. They are likely to go into modern production in the near future, as large bulk mining operations, in part using the existing infrastructure of adjacent iron mines (PolyMet, 2019).
4. These deposits along the base of the complex are among the largest undeveloped Cu-Ni-PGE sulphide resources in the world (e.g. Miller, 2011; Miller and Nicholson, 2013).

Given its dynamic evolution of multiple sub-intrusions or magma chambers, it seems likely that the Duluth Complex acted as staging chambers and feeders to parts of the volcanic sequence of the North Shore Volcanic Group, before magma supply contracted into a narrower feeding zone along the lakeshore (*see* Fig. 1 and below).

Crystal Lake Intrusion

The Crystal Lake Intrusion is a y-shaped, multi-phase, gabbroic intrusion ~40 km southwest of Thunder Bay and has been the target of past and on-going exploration programs. A detailed overview of the intrusion is given in another contribution to this volume by Smith et al. (2020). The absolute and relative age of this intrusion has been under debate, since the area also hosts a number of other gabbroic or diabase intrusions (Geul, 1970, 1973), in particular: the Logan Sills; the north-

northwest-trending Cloud River dykes; a dense development of major north-northeast-trending, rift-parallel Pigeon River dykes; and the locally internally differentiated, ~100–200 m wide Mount Mollie dyke (e.g. Cundari, 2012). In the field, we have established the following sequence of events in this area:

1. *North-northwest-trending Cloud River dykes:* 30–100 m wide diabase dykes. Our preliminary results for these dykes, based on baddeleyite data, suggest an age of 1109.2 ± 2.9 Ma, in general agreement with, but more precise than, the earlier result reported by Hollings et al. (2010).
2. *Logan Sills:* an extensive diabase (with local granophyre) sill complex now dated at 1106.3 ± 2.0 Ma. Only north-northeast-trending Pigeon River dykes demonstrably cut the Logan sills[9].
3. *Northwest-trending Mt. Josephine dyke:* a very large dyke (~100 m wide) just across the Canada–USA border, trending at right angles to the ridges defined by the Pigeon River dykes. We determined a combined zircon and baddeleyite upper intercept age for this dyke of 1099.0 ± 1.2 Ma (Table 2), which suggests a connection to Duluth Complex magmatism.
4. *Densely developed north-northeast-trending Pigeon River dykes and sheets:* major diabase to gabbroic dykes (and some dipping sheets), locally with internal differentiation (Geul, 1970, 1973). In the field, we established that Pigeon River dykes cut and are chilled against Cloud River dykes and thus younger (Bleeker et al., 2019; Smith et al., 2019). Our current results for Pigeon River dykes cluster at 1096 Ma, which suggest a broad connection with the younger intrusions in the roof of the Duluth Complex, i.e. Beaver Bay Complex and Sonju Lake Intrusion (Fig. 1, Tables 1, 2); and, in particular, the "Beaver River Diabase" (Miller and Chandler, 1997; Doyle, 2016), for which Paces and Miller (1993) established a crystallization age of 1095.8 ± 1.2 Ma. Large Pigeon River dykes form major topographic ridges in the area around Crystal Lake and our observations suggest that these ridges do not transect the Crystal Lake Intrusive Complex. We have searched the area of the Crystal Lake Intrusion for younger crosscutting diabase dykes, a search that came up negative. Hence, given that the dense Pigeon River swarm comprises numerous large, subparallel dykes, representing multiple intrusive pulses, and taking current dating uncertainties into consideration, the overall life span of this swarm is likely 1097–1094 Ma.
5. *Mount Mollie dyke:* a large, somewhat curved, east- to east-northeast-trending, internally differentiated dyke, locally with a core of fine- to coarse-grained granophyre. It has often been interpreted as a feeder dyke to the Crystal Lake Intrusion. Instead, we presently consider this dyke to be a member of the Pigeon River swarm and note that some other wide Pigeon River dykes in the area also show minor internal differentiation, with local granophyre (Geul, 1970, 1973). Our preliminary data on samples from the Mount Mollie dyke indicate an age of 1096.3 ± 1.4 (Smith et al., 2020), which is indistinguishable from our present Pigeon River dating results (Table 2). We have no explanation for the much older date reported by Hollings et al. (2010). We have searched for crosscutting relationships but, to date, have not identified conclusive field relationships, except for thin north-northeast-trending dykelets (with chilled margins) intruding into the Mount Mollie dyke, in agreement with multiple magma pulses within the overall Pigeon River swarm.
6. *Crystal Lake Intrusion:* and finally, the multiple gabbroic phases of the Crystal Lake Intrusion, a major keel-shaped to dyke-like, composite, intrusive body of both homogeneous gabbro/troctolite and mineralized vari-textured gabbros (Smith et al., 2020), not crosscut at surface by any of the dykes described earlier (but *see* cross-sections in Smith et al., 2020). Our most conclusive U-Pb results, on mineralized vari-textured gabbro from the northern limb of the intrusion indicates a crystallization age of 1093.2 ± 1.2 Ma (Fig. 5b).

Our preliminary results and observations thus suggest that the dense Pigeon River swarm and younger Crystal Lake Intrusion correlate in a broad sense with the Beaver Bay and Sonju Lake complexes in the roof of the Duluth Complex, and that the Mount Mollie dyke is not the direct feeder to the Crystal Lake Intrusion, but rather slightly older and part of the overall Pigeon River event. Specifically, the Pigeon River swarm appears to be the northeastern continuation of the Beaver River Diabase. The Crystal Lake Intrusion, at ca. 1093 Ma, represents a final intrusive pulse of this overall 1097–1092 Ma magmatic phase, which is also well represented in the volcanic sequences of the MCR.

[9] Our preliminary age for the main (upper) Logan Sill at Mount MacKay is within error of other nearby results. One that is robust and precise is the zircon age for the "Swamper Lake monzogabbro" at 1107.0 ± 1.1 Ma (Davis and Green, 1997), just across the Canada–USA border. These same authors also recalculated the original "Logan Sill" age (obtained at Lake Nipigon) to 1108.2 ± 0.9 Ma and considered this the age of onset of voluminous mafic magmatism. All these key ages are within uncertainty.

A few other gabbroic intrusions with this relatively young age are the Blake Township gabbro (Heaman et al., 2007) and the gabbroic complexes intruding the Osler Group volcanic rocks, i.e. the Moss Lake Gabbro and St. Ignace Island Complex (Table 2, and references therein). The older Cloud River dykes, with their distinct north-northwest-trend, at high angles to the Pigeon River swarm, represent a different magmatic phase related to the onset of high-volume magmatism. These various ages and trends of associated dykes (i.e. principal stress directions) indicate a significant reorganization of the system occurred at ca. 1096 Ma.

Post-Duluth Complex Contraction of Magma Supply into the Central Rift

It is interesting to note that the rift-parallel Pigeon River dykes (1097–1094 Ma) and the various younger "post-Duluth Complex" gabbroic intrusions discussed above all occur closer to the northwestern shore of Lake Superior (Fig. 1), i.e. closer to the rift axis, than many of the older intrusions (e.g. Thunder Bay North Complex, Tamarack, etc.), suggesting that the focus of magmatism contracted into the central rift as the lithosphere thinned and rifted apart. The Pigeon River dyke swarm, and the Beaver River Diabase to the south (Miller and Chandler, 1997), likely are the surface expression of this more focussed, rift-parallel, translithospheric feeder zone, which we here refer to as the "North Shore Magmatic Feeder Zone" (NSMFZ, identified in Figure 1 by the grey zones along the northern shore of Lake Superior)[10]. It seems likely that the major Pigeon River dykes and the NSMFZ may have fed thick lava flows as far away as the Keweenaw Peninsula. There, the thick Greenstone Flow (Portage Lake Group) has a U-Pb age of 1094.0 ± 1.5 Ma (Davis and Paces, 1990), an age that is, within uncertainty, coeval with the Pigeon River dykes and the more localized gabbroic intrusions that occur along its trend (e.g. Crystal Lake, Moss Lake). Doyle (2016) arrived at a similar conclusion but focussed on the Beaver River Diabase of the Beaver Bay Complex. Our conclusion would extend this feeder zone into a more extensive linear zone (NSMFZ). Doyle (2016) draws attention to the presence of very calcic plagioclase megacrysts in both the Beaver River Diabase, where they can be tied to large, lower crustal anorthosite xenoliths, and in the basalts of the Greenstone Flow. Large plagioclase megacrysts have also been noted in some Pigeon River dykes but require further study to determine their anorthite content and whether they are xenocrysts from a similar source.

Implications for Midcontinent Rift "Magmatic Stages"

Miller and Nicholson (2013) and other authors have divided the magmatic evolution of the MCR into various phases or stages. A full review of this important topic is beyond the scope of this report and should await the completion of all our dating results. Nevertheless, a few comments are in order. Their "Initiation Stage" (1115–1110 Ma) remains somewhat nebulous as some of the older ages have been revised, and others remain under discussion and to be tested. Beyond the problematic ca. 1110–1120 Ma baddeleyite ages, there are, however, various "precursor events", often alkaline, throughout the wider region (Fig. 1, Table 1), which need to be included in the overall consideration.

Also, as more precise ages emerge, some of their later stages, and particularly their age boundaries, will require some revision. The "Early Stage" of Miller and Nicholson (2013: 1110–1106 Ma) encompasses the onset of high-volume mafic magmatism, which is supported by our study, but the new Tamarack ages challenge the boundary of the following "Hiatus Stage (1106–1101 Ma). Perhaps more importantly, the new insights into the major Pigeon River swarm and younger gabbroic intrusions, and the reorganization into a linear magmatic feeder zone (NSMFZ), argue for a distinct 1097–1092 Ma stage, correlating with the eruption of the entire Portage Lake lava sequence. An unconformity may mark the beginning of this sequence (*see also* Swanson-Hysell, 2019).

Tholeiitic Versus Alkaline Intrusion and Mantle Sources

With more complete and accurate age control, and the spatial distribution of intrusions, as shown in Figure 1, an interesting aspect of the overall MCR evolution is the predominance of alkaline intrusions in the eastern part of the rift. The well dated Coldwell Complex (Heaman and Machado, 1992; G. Dunning and D. Good, pers. comm., 2017), and also the reasonably well dated Nemegosenda alkaline complex farther east (Heaman et al., 2007), overlap in age with the 1106–1110 Ma onset of high-volume basaltic magmatism but are compositionally distinct from the mafic-ultramafic intrusions in the western MCR. Many of the low-volume, alkaline precursor events (e.g. Great Abitibi swarm, and various lamprophyric to kimberlitic intrusions) are also concentrated in the eastern part (Fig. 1). This spatial dichotomy may speak to the nature of the underlying mantle lithosphere as well as issues discussed below.

[10] The presence of this zone is probably also the reason why the northwest shore of Lake Superior is overall more linear as compared to, for instance, the southern shore of Lake Superior.

Mantle Plume Centre and Potential Plume Track?

With the overall diversity of intrusions, and the various dyke swarms of different trends but in many cases still with poorly defined ages, we caution against drawing any simple radiating patterns that might indicate a hypothetical centre of mantle plume impact. The Great Abitibi dyke swarm (1141 Ma: Krogh et al, 1987) has featured prominently in such conjecture (Ernst and Buchan, 1997) but is much older than many dyke swarms proximal to the MCR, such as the rift-parallel Pigeon River swarm (1096 Ma: this study), and predates high-volume mafic magmatism by >30 Myr. Also, the evidence for lateral emplacement of the main Great Abitibi dyke, from a magmatic source south of the MCR (Ernst, 1990), should be treated as speculative at this stage. The Kipling dyke, which perhaps may define a fanning pattern and plays an important role in this debate, has no U-Pb age. Furthermore, in this general area east and northeast of the MCR, both ca. 2110 Ma Marathon dykes and ca. 2170 Ma Biscotasing dykes have similar northeast-trends and complicate the tracing of MCR-related dykes, and associated paleopoles are not fully distinct (e.g. Great Abitibi poles and Biscotasing poles overlap). Clearly, more complete and precise ages, as well as compositional data, on many of the dyke swarms of the MCR are needed to better infer overall emplacement patterns and define the entire tectonomagmatic system and its evolution.

To determine a possible centre of plume impact, and a potential plume track, it is also important to zoom out to the full scale of the North American continent (and beyond, Rodinia) and to consider all the mafic magmatism on a >1000 km scale that could be related (Table 1). To highlight the potential scale of MCR-related magmatism, some of the key pulses of magmatic activity, at ca. 1160 Ma and 1108 Ma, are echoed as far away as northern Saskatchewan in the form of diabase intrusions in the Athabasca sandstone basin (French et al., 2002; Bleeker and Chamberlain, 2015). Are these separate events or are they distant manifestations of the same overall tectonomagmatic system? Similarly, the southwestern arm of the MCR, extending far into the mid-continent, may be connected with the essentially contemporaneous southwest USA diabase province (Hammond, 1990; Bright et al., 2014). It is interesting to note that this latter magmatic province may extend to somewhat younger ages than the MCR (e.g. Heaman and Grotzinger, 1992), perhaps providing a hint of a plume track. Any such speculation would also need to be reconciled against the paleomagnetic data and apparent polar wander path derived from the MCR (Swanson-Hysell et al., 2019). Finally, in this overall context, it is worth drawing attention to the study of Edwards and Blackburn (2018), who recorded a distinct 1.1 Ga heating pulse at the base of the lithosphere (from xenoliths in the Victor kimberlite) far to the northeast of Lake Superior (~600 km) in the James Bay Lowlands.

CONCLUSIONS

Our ongoing research has added critical details, field observations, and U-Pb data to the magmatic evolution of the MCR, with new high-precision U-Pb ages for ~10 of the mineralized intrusions and associated feeder dyke swarms, while a number of samples is still in progress. Our results favour a relatively sharp onset of high-volume basaltic magmatism at ca. 1106–1110 Ma in the main part of the rift, with coeval more alkaline magmatism in the eastern MCR. Only the older date on the Kitto intrusion (ca. 1117 Ma: Heaman et al., 2007) in the Lake Nipigon area remains as an older age "outlier", one that we are still testing.

The mineralized Sunday Lake Intrusion, north of Thunder Bay, dated at 1109.0 ± 1.3 Ma, is one of the oldest differentiated intrusions on the northern flank of the MCR. On the southern flank, the large Echo Lake layered intrusion has the oldest robust zircon age of 1110.8 ± 1.5 Ma (Cannon and Nicholson, 2001), and for this reason alone should be a target for age refinement using modern chemical abrasion-isotope dilution-thermal ionization mass spectrometry (CA-ID-TIMS) methods, especially as it is known to contain relatively good zircons.

Mineralized intrusions of the MCR do not all fall in this early age group, but show a temporal distribution that correlates with all the main volcanic phases of the rift. Through time, they can be grouped as follows:

1. Early MCR intrusions, ca. 1110–1106 Ma: Sunday Lake, Thunder, Thunder Bay North (Current Lake), and many of the intrusion on the southern flank, such as Eagle, Bovine Igneous Complex, and Echo Lake; also the large Coldwell Complex.
2. The Tamarack Intrusive Complex at ca. 1105–1103 Ma.
3. The Mellen Complex at ca. 1102 Ma[11].
4. The main part of the Duluth Complex at 1099 Ma.
5. Younger intrusions along the northwestern shore of Lake Superior at ca. 1097–1094 Ma: Beaver Bay and Sonju Lake intrusions and the main Pigeon River dykes, including Mount Mollie at 1096 Ma.
6. Crystal Lake Intrusion at ca. 1094–1092 Ma.

[11] This large complex on the southern flank of the MCR has not been a focus of our study, but clearly could benefit from age refinement. Could it be coeval with the Duluth Complex, as Grout (1918) initially inferred, both emplaced near the base of the overlying volcanic sequences?

All of the mineralized intrusions that so far have received detailed studies appear more complex than single-phase intrusions and all are part of dynamic feeder systems that likely fed coeval parts of the volcanic stratigraphy of the rift. Hence, there is scope for detailed geochemical and isotopic studies (e.g. *see* Doyle, 2016) to reveal some of these connections in more detail and to better understand the overall dynamics.

As the age database improves, it is clear that the focus of magmatic activity, including emplacement of mineralized intrusions, contracted into the developing rift after the emplacement of the Duluth Complex. The major rift-parallel ca. 1096 Ma Pigeon River swarm, in particular, marks this contraction into a major feeder zone along the northwest shore of Lake Superior (our NSMFZ), perhaps stretching from the Duluth Complex in the southwest all the way to St. Ignace Island in the northeast. The southwest-trending Carlton dykes (Fig. 1) may extend this zone farther to the southwest. This zone and its major dykes likely were the major fissure system that fed the entire 1097–1092 Ma Portage Lake lava pile, including the thick Greenstone Flow. Following multiple pulses of dyke emplacement into the NSMFZ, this feeder zone was then intruded by several more localized gabbroic complexes, such as Crystal Lake.

Finally, at the higher precision that is likely to advance understanding of rift processes (~1 Myr or better), a number of challenging geochronology-related problems remain, first among which are the remaining discordance in some of the data (Fig. 4) and the sometimes minor offset of slightly discordant baddeleyite data to marginally older $^{207}Pb/^{206}Pb$ ages as compared to zircon data (Fig. 10). This offset was first noted decades ago in Nipigon sills (Davis and Sutcliffe, 1985); it also revealed itself in the data for the Thunder intrusion (Trevisan et al., 2015), and it is also present in some of our data. We are still working on this problem, but it is one reason to keep searching for well behaved zircons that respond well to chemical abrasion. Another approach would be to identify samples with relatively robust baddeleyite populations that could withstand air abrasion. This could test whether this issue with baddeleyite is related to the surface of the crystals or to other factors.

In comparison, a minor problem is the tendency in modern high-precision U-Pb dating to concentrate on potentially more precise $^{206}Pb/^{238}U$ data from multiple overlapping concordant zircon analyses (e.g. Swanson-Hysell et al., 2019), which typically are slightly younger than $^{207}Pb/^{206}Pb$ upper intercept ages on similar samples, creating an offset among data sets. Similarly, switching to a more refined U isotopic ratio amplifies this offset (Hiess et al., 2012). This may be useful in terms of the best possible absolute age control on key units of the MCR, but it complicates correlation between data sets and published ages at a ~1–2 Myr time scale for an area such as the MCR.

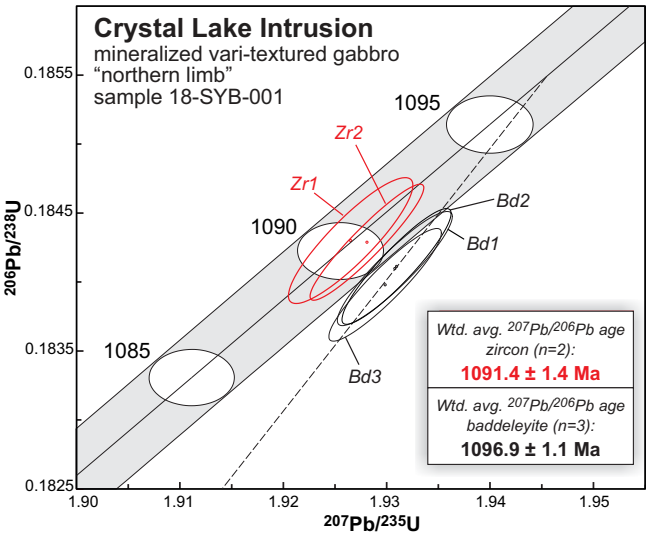

Figure 10. Standard U-Pb concordia diagram showing an example of the relative offset of baddeleyite data (n = 3, black ellipses) with respect to zircon (n = 2, red ellipses). The apparent offset to the right results in older $^{207}Pb/^{206}Pb$ ages for the baddeleyite, well beyond the uncertainties of the individual analyses. Several factors could contribute to this offset, some of which are presently not fully understood in each case study. It remains as a significant hindrance to obtaining accurate and highly precise ages on zircon-poor rock units (e.g. many diabase dykes). The example shown is from the unmineralized troctolite of the northern limb of the Crystal Lake Intrusion, but this issue is known to occur in many Midcontinent Rift data sets, including high-resolution data on zircon and baddeleyite standards from the Duluth Complex (K. Chamberlain, pers. comm., 2019). All data-point error elipses are 2σ.

ACKNOWLEDGMENTS

This report is a contribution to NRCan's Targeted Geoscience Initiative Program (TGI). Support for this study was provided through the Orthomagmatic Ni-Cu-PGE-Cr Ore Systems Project's 'Activity NC-1.3: Controls on the localization and timing of mineralized intrusions in intra-continental rift systems, with a specific focus on the ca. 1.1 Ga Mid-continent Rift system'. The authors thank our partners at Rio Tinto (Dean Rossell, Brian Goldner, Justin Laberge), North American Palladium (Steve Flank, Dave Peck), Transition Metals (Grant Mourre, Scott McLean), Panoramic (Al McTavish), and Stillwater Canada (Dave Good, John McBride) for their help, access to drill core, and constructive discussions. Terry Boerboom from the Minnesota Geological Survey is thanked for his detailed knowledge of and input on Minnesota geology, in the field and otherwise, and Jim Miller for various discussions on MCR geology.

Colleagues from the USGS (Klaus Schultz, Suzanne Nicholson) provided key information on units in Michigan and Wisconsin, and shared the unpublished data on the Echo Lake intrusion. Reviews by Terry Boerboom and Tony LeCheminant improved the manuscript. Valérie Bécu assisted with the technical editing and Elizabeth Ambrose took care of final editing and correction of minor imperfections. Both are thanked for their skillful assistance. Last but not least, members of the TGI-5 team are thanked for taking care of a thousand little tasks from general project management to outreach and consultations, without which none of this research could have proceeded. Thank you all.

REFERENCES

Alibert, C. and Albarede, F., 1988. Relationships between mineralogical, chemical and isotopic properties of some North American kimberlites; Journal of Geophysical Research, v. 93, p. 7643–7671.

Allen, D.J., Hinze, W.J., Dickas, A.B., and Mudrey, M.G., Jr., 1997. Integrated geophysical modeling of the North American Midcontinent Rift System: New interpretations for western Lake Superior, northwestern Wisconsin, and eastern Minnesota; *in* Middle Proterozoic to Cambrian Rifting, Central North America, (ed.) R.J. Ojakangas, A.B. Dickas, and J.C. Green; Geological Society of America, Special Paper 312, p. 47–72.

Ames, D.E., Kjarsgaard, I.M., McDonald, A.M., and Good, D.J., 2017. Insights into the extreme PGE enrichment of the W Horizon, Marathon Cu-Pd deposit, Coldwell Alkaline Complex, Canada: Platinum-group mineralogy, compositions and genetic implications; Ore Geology Reviews, v. 90, p. 723–747.

Barnes, S.J., Cruden, A.R., Arndt, N., and Saumur, B.M., 2016. The mineral system approach applied to magmatic Ni–Cu–PGE sulphide deposits; Ore geology reviews, v. 76, p. 296–316.

Bell, K. and Blenkinsop, J., 1980. Ages and initial 87Sr/86Sr ratios from alkali complexes of Ontario; *in* Geoscience Research Grant Program, Summary of Research 1979–1980, (ed.) E.G. Pye; Ontario Geological Survey, Miscellaneous Paper 93, p. 16–23.

Bleeker, W. and Chamberlain, K., 2015. Robust U-Pb age for the Douglas River dyke, Athabasca Basin – Further indications of a significant magmatic event in western Laurentia at 1165 Ma; *in* Reconstruction of supercontinents back to 2.7 Ga using the Large Igneous Province (LIP) Record: With implications for mineral deposit targeting, hydrocarbon exploration, and Earth system evolution – Year 5 Confidential Summary for Project Sponsors, (ed.) R.E. Ernst and W. Bleeker; Report A203, 9 p.

Bleeker, W., Liikane, D.A., Smith, J., Hamilton, M., Kamo, S.L., Cundari, R., Easton, M., and Hollings, P., 2018. Activity NC-1.3: Controls on the localisation and timing of mineralized intrusions in intra-continental rift systems, with a specific focus on the ca. 1.1 Ga Mid-continent Rift (MCR) system; *in* Targeted Geoscience Initiative: 2017 Report of Activities, Volume 2, (ed.) N. Rogers; Geological Survey of Canada, Open File 8373, p. 15–27.

Bleeker, W., Hamilton, M., Kamo, S., Liikane, D., Smith, J., Hollings, P., Cundari, R., Easton, M., and Davis, D., 2019. High-resolution dating of the magmatic plumbing system of the Midcontinent Rift System—Insights into rift evolution and mineralization processes; Institute on Lake Superior Geology Proceedings, 51st Annual Meeting, Abstracts and Proceedings, v. 65, p. 10–11.

Boerboom, T.J., Wirth, K.R., and Evers, J.F., 2014. Five newly acquired high-precision U-Pb age dates in Minnesota, and their geologic implications; *in* Institute on Lake Superior Geology Proceedings, 60th Annual Meeting, Abstracts and Proceedings, v. 60, pt. 1, p. 13–14.

Bornhorst, T.J. and Barron, R.J., 2011. Copper deposits of the western Upper Peninsula of Michigan; *in* Archean to Anthropocene: Field Guides to the Geology of the Mid-Continent of North America, (ed.) J.D. Miller, G.J. Hudak, C. Wittkop, and P.I. McLaughlin; Geological Society of America, Field Guide 24, p. 83–99. https://doi.org/10.1130/2011.0024(05)

Bright, R.M., Amato, J.M., Denyszyn, S.W., and Ernst, R.E., 2014. U-Pb geochronology of 1.1 Ga diabase in the southwestern United States: Testing models for the origin of a post-Grenville large igneous province; Lithosphere, v. 6, p. 135–156.

Cannon, W.F., 1992. The Midcontinent rift in the Lake Superior region with emphasis on its geodynamic evolution; Tectonophysics, v. 213, p. 41–48.

Cannon, W.F. and Nicholson, S.W., 2001. Geology map of the Keweenaw Peninsula and adjacent area; U.S. Geological Survey, Geological Investigations Series, Map I-2696, scale 1:100 000.

Chaffee, M.R., 2015. Petrographic and geochemical study of the hybrid rock unit associated with the Current Lake Intrusive Complex; M.Sc. thesis, University of Minnesota, Minneapolis, Minnesota, 139 p.

Clow, G.G., Normand L.L., Rennie, D.W., and Scholey, B.J.Y., 2017. Technical Report on the Eagle Mine, Michigan, U.S.A, NI 43-101 Report; Roscoe Postle Associates Inc. for Lundin Mining Corporation. <www.lundinmining.com/site/assets/files/2640/2017-04-26-eagle-ni-43-101.pdf[accessed December 1, 2019]

Cogulu, E.H., 1993a. Factors controlling postcumulus compositional changes of chrome-spinels in the Crystal Lake Intrusion, Thunder Bay, Ontario; Geological Survey of Canada, Open File 2748, 77 p.

Cogulu, E.H., 1993b. Mineralogy and chemical variations of sulphides from the Crystal Lake Intrusion, Thunder Bay; Ontario. Geological Survey of Canada, Open File 2749, 52 p.

Cawthorn, R.G. and Miller, J., 2018. Lopolith–A 100 year-old term. Is it still definitive?; South African Journal of Geology, v. 121, p. 253–260.

Cundari, R., 2012. Geology and geochemistry of Midcontinent Rift-related igneous rocks; M.Sc. thesis, Lakehead University, Thunder Bay, Ontario, 142 p.

Currie, K.L., 1976. The alkaline rocks of Canada; Geological Survey of Canada, Bulletin 239, 228 p., incl. Map 1369A, scale 1:5 000 000.

D'Angelo, M., 2013. Mineralogy, petrology and geochemistry of the Steepledge Intrusion; B.Sc. thesis, Lakehead University, Thunder Bay, Ontario, 83 p.

Davis, D.W. and Green, J.C., 1997. Geochronology of the North American Midcontinent rift in western Lake Superior and implications for its geodynamic evolution; Canadian Journal of Earth Sciences, v. 34, p. 476–488.

Davis, D.W. and Paces, J.B., 1990. Time resolution of geologic events on the Keweenaw Peninsula and implications for development of the Midcontinent Rift system; Earth and Planetary Science Letters, v. 97, p. 54–64.

Davis, D.W. and Sutcliffe, R.H., 1985. U-Pb ages from the Nipigon plate and northern Lake Superior; Geological Society of America Bulletin, v. 96, p. 1572–1579.

Ding, X., Li, C., Ripley, E.M., Rossell, D., and Kamo, S., 2010. The Eagle and East Eagle sulfide ore-bearing mafic-ultramafic intrusions in the Midcontinent Rift System, Upper Michigan: Geochronology and petrologic evolution; Geochemistry, Geophysics, Geosystems, v. 11, 22 p.

Ding, X., Ripley, E.M., and Li, C., 2012. PGE geochemistry of the Eagle Ni–Cu–(PGE) deposit, Upper Michigan: Constraints on ore genesis in a dynamic magma conduit; Mineralium Deposita, v. 47, p. 89–104.

Donoghue, K.A., Ripley, E.M., and Li, C., 2014. Sulfur isotope and mineralogical studies of Ni-Cu sulfide mineralization in the Bovine Igneous Complex intrusion, Baraga Basin, Northern Michigan; Economic Geology, v. 109, p. 325–341.

Doyle, M.S., 2016. Geologic and geochemical attributes of the Beaver River Diabase and Greenstone Flow: Testing a possible intrusive-volcanic correlation in the 1.1 Ga Midcontinent Rift; M.Sc. thesis, University of Minnesota, Duluth, Minnesota, 176 p.

Drenth, B.J., Anderson, R.R., Schulz, K.J., Feinberg, J.M., Chandler, V.W., and Cannon, W.F., 2015. What lies beneath: geophysical mapping of a concealed Precambrian intrusive complex along the Iowa–Minnesota border; Canadian Journal of Earth Sciences, v. 52, p. 279–293.

Dunlop, M., 2013. The Eagle Ni-Cu-PGE magmatic sulfide deposit and surrounding mafic dikes and intrusions in the Baraga Basin, Upper Michigan: Relationships, petrogenesis and implications for magmatic sulfide exploration; M.Sc. thesis, Indiana University, Bloomington, Indiana, 93 p.

Edwards, G.H. and Blackburn, T., 2018. Detecting the extent of ca. 1.1 Ga Midcontinent Rift plume heating using U-Pb thermochronology of the lower crust; Geology, v. 46, p. 911–914.

Emst, R.E., 1990. Magma flow directions in two mafic Proterozoic dyke swarms of the Canadian Shield: As estimated using anisotropy of magnetic susceptibility data; *in* Mafic dykes and Emplacement Mechanisms, (ed.) A.J. Parker, P.C. Rickwood, and D.H. Tucker; Balkema, Rotterdam, p. 231–235.

Ernst, R.E. and Buchan, K.L., 1997. Giant radiating dyke swarms: their use in identifying pre-Mesozoic large igneous provinces and mantle plumes; American Geophysical Union, Geophysical Monograph 100, p. 297–334.

Fairchild, L.M., Swanson-Hysell, N.L., Ramezani, J., Sprain, C.J., and Bowring, S.A., 2017. The end of Midcontinent Rift magmatism and the paleogeography of Laurentia; Lithosphere, v. 9, p. 117–133.

Flank, S., 2017. The petrography, geochemistry and stratigraphy of the Sunday Lake Intrusion, Jacques Township, Ontario; M.Sc. thesis, Laurentian University, Sudbury, Ontario, 71 p.

Fletcher, T., Peters, O., and Thomas B., 2018. Second Independent Technical Report on the Tamarack North Project – Tamarack, Minnesota, NI 43-101 Technical Report; DRA Americas Inc. for Talon Metals Corp., 213 p. <https://talonmetals.com/wp-content/uploads/2018/10/20180326_Talon_Tamarack_NI_43-101.pdf> [accessed December 1, 2019]

Foley, D.J., 2011. Petrology and Cu-Ni-PGE mineralization of the Bovine Igneous Complex, Baraga County, Northern Michigan; M.Sc. thesis, University of Minnesota, Minneapolis, Minnesota, 109 p.

French, J.E., Heaman, L.M., and Chacko, T., 2002. Feasibility of chemical U–Th–total Pb baddeleyite dating by electron microprobe; Chemical Geology, v. 188, p. 85–104.

Geul, J.J.C., 1970. Geology of Devon and Pardee Townships and the Stuart Location, District of Thunder Bay; Ontario Department of Mines, Geological Report 87, 58 p.

Geul, J.J.C., 1973. Geology of Crooks Township, Jarvis and Prince Locations, and Offshore Islands, District of Thunder Bay; Ontario Department of Mines, Geological Report 102, 46 p.

Giguerre, J.F., 1975 Geology of St. Ignace Island and Adjacent Islands, District of Thunder Bay; Ontario Division of Mines, Geological Report 118, 35 p. Accompanied by Map 2285, scale 1:63 360 or l inch to l mile.

Gittins, J., Macintyre, R.M., and York, D., 1967. The ages of carbonatite complexes in eastern Canada; Canadian Journal of Earth Sciences, v. 4, p. 651–655.

Goldner, B.D., 2011. Igneous petrology of the Ni-Cu-PGE mineralized Tamarack intrusion, Aitkin and Carlton Counties, Minnesota; M.Sc. thesis, University of Minnesota, Minneapolis, Minnesota, 156 p.

Good, D.J. and Crocket, J.H., 1994. Genesis of the Marathon Cu-platinum-group element deposit, Port Coldwell alkalic complex, Ontario; a Midcontinent rift-related magmatic sulfide deposit; Economic Geology, v. 89, p. 131–149.

Good, D.J., Epstein, R., McLean, K., Linnen, R.L., and Samson, I.M., 2015. Evolution of the Main Zone at the Marathon Cu-PGE sulfide deposit, Midcontinent Rift, Canada: Spatial relationships in a magma conduit setting; Economic Geology, v. 110, p. 983–1008.

Good, D.J., Cabri, L.J., and Ames, D.E., 2017. PGM facies variations for Cu-PGE deposits in the Coldwell Alkaline Complex, Ontario, Canada; Ore Geology Reviews, v. 90, p. 748–771.

Goodgame, V.R., Johnson, J.R., MacTavish, A.D., Stone, W.E., Watkins, K.P., and Wilson, G.C., 2010. The Thunder Bay North Deposit: Chonolith-hosted Pt-Pd-Cu-Ni mineralization related to the Midcontinent Rift; *in* Abstracts; 11th International Platinum Symposium, Extended Abstracts, p. 21–24.

Green, J.C., 1983. Geologic and geochemical evidence for the nature and development of the Middle Proterozoic (Keweenawan) Midcontinent Rift of North America; Tectonophysics, v. 94, p. 413–437.

Green, J.C., Bornhorst, T.J., Chandler, V.W., Mudrey, M.G., Jr., Myers, P.R., Pesonen, L.V., and Wilband, J.T., 1987. Keweenawan dykes of the Lake Superior region: Evidence for the evolution of the Middle Proterozoic Midcontinent Rift of North America; *in* Mafic Dyke Swarms, (ed.) H.C. Hall and W.F. Fahrig; Geological Association of Canada, Special Paper 34, p. 289–302.

Grout, F.F., 1918. The lopolith; an igneous form exemplified by the Duluth gabbro; American Journal of Science, v. 46, p. 516–22.

Hammond, J.G., 1990. Middle Proterozoic diabase intrusions in the southwestern U.S.A. as indicators of limited extensional tectonism; *in* Mid-Proterozoic Laurentia-Baltica, (ed.) C.F. Gower, T. Rivers, and B. Ryan; Geological Association of Canada, Special Paper 38, p. 517–531.

Hanson, R.E., Crowley, J.L., Bowring, S.A., Ramezani, J., Gose, W.A., Dalziel, I.W., Pancake, J.A., Seidel, E.K., Blenkinsop, T.G., and Mukwakwami, J., 2004. Coeval large-scale magmatism in the Kalahari and Laurentian cratons during Rodinia assembly; Science, v. 304, p. 1126–1129.

Hart, T.R. and MacDonald, C.A., 2007. Geology and structure of the western margin of the Nipigon Embayment; Canadian Journal of Earth Sciences, v. 44, p. 1021–1040.

Hart, T.R. and Magyarosi, Z., 2004. Precambrian geology of the northern Black Sturgeon River and Disraeli Lake area, Nipigon Embayment, northwestern Ontario; Ontario Geological Survey, Open File 6138, 56 p.

Hart, T.R., terMeer, M., and Jolette, C., 2002. Precambrian geology of Kitto, Eva, Summers, Dorothea and Sandra townships, northwestern Ontario–Phoenix Bedrock Mapping Project; Ontario Geological Survey, Open File 6095, 206 p.

Hauck, S.A., Severson, M.J., Zanko, L., Barnes, S.J., Morton, P., Alminas, H., Foord, E.E., and Dahlberg, E.H., 1997. An overview of the geology and oxide, sulfide, and platinum-group element mineralization along the western and northern contacts

of the Duluth Complex; *in* Middle Proterozoic to Cambrian Rifting, Central North America, (ed.) R.W. Ojakangas, A.B. Dickas, and J.C. Green; Geological Society of America, Special Paper 312, p. 137–185.

Heaman, L.M. and Grotzinger, J.P., 1992. 1.08 Ga diabase sills in the Pahrump Group, California: Implications for development of the Cordilleran miogeocline; Geology, v. 20, p. 637–640.

Heaman, L.M. and Machado, N., 1992. Timing and origin of mid-continent rift alkaline magmatism, North America: evidence from the Coldwell Complex; Contributions to Mineralogy and Petrology, v. 110, p. 289–303.

Heaman, L.M., Kjarsgaard, B.A., and Creaser, R.A., 2004. The temporal evolution of North American kimberlites; Lithos, v. 76, p. 377–397.

Heaman, L.M., Easton, R.M., Hart, T.R., Hollings, P., MacDonald, C.A., and Smyk, M., 2007. Further refinement to the timing of Mesoproterozoic magmatism, Lake Nipigon region, Ontario; Canadian Journal of Earth Sciences, v. 44, p. 1055–1086.

Heggie, G.J., 2005. Whole rock geochemistry, mineral chemistry, petrology and Pt, Pd mineralization of the Seagull intrusion, Northwestern Ontario; M.Sc. thesis, Lakehead University, Thunder Bay, Ontario, 156 p.

Hiess, J., Condon, D.J., McLean, N., and Noble, S.R., 2012. $^{238}U/^{235}U$ systematics in terrestrial uranium-bearing minerals; Science, v. 335, p. 1610–1614.

Hink, B.D., 2016. Geochemical and Petrological Studies on the Origin of Nickel-Copper Sulphide Mineralization at the Eagle Intrusion in the Marquette County, Michigan; M.Sc. thesis, Western Michigan University, Kalamazoo, Michigan, 129 p.

Hoaglund, S., Miller, J.D., Crowley, J.L., and Schmitz, M.D., 2010. U-Pb zircon geochronology of the Duluth Complex and related hypabyssal intrusions: Investigating the emplacement history of a large multiphase intrusive complex related to the 1.1 Ga Midcontinent Rift; Institute on Lake Superior Geology Proceedings, 56th Annual Meeting, Abstracts and Proceedings, v. 56, pt. 1, p. 25–26.

Hollings, P., Hart, T., Richardson, A., and MacDonald, C.A., 2007. Geochemistry of the Mesoproterozoic intrusive rocks of the Nipigon Embayment, northwestern Ontario: evaluating the earliest phases of rift development; Canadian Journal of Earth Sciences, v. 44, p. 1087–1110.

Hollings, P., Smyk, M., Heaman, L.M., and Halls, H., 2010. The geochemistry, geochronology, and paleomagnetism of dikes and sills associated with the Mesoproterozoic Midcontinent Rift near Thunder Bay, Ontario, Canada; Precambrian Research, v. 183, p. 553–571.

Hutchinson, D., White, R., Cannon, W., and Schulz, K., 1990. Keweenaw hot spot: Geophysical evidence for a 1.1 Ga mantle plume beneath the Midcontinent Rift system; Journal of Geophysical Research, v. 95, p. 10 869–10 884.

Jirsa, M.A., Boerboom, T.J., Chandler, V.W., Mossler, J.H., Runkel, A.C., and Setterholm, D.R., 2011. S-21 Geologic map of Minnesota – bedrock geology; Minnesota Geological Survey, University of Minnesota Digital Conservancy <https://conservancy.umn.edu/handle/11299/101466> [accessed December 1, 2019].

Kaminsky, F.V., Sablukov, S.M., Sablukova, L.I., and Shchukin, V.S., 2000. Petrology of kimberlites from the newly discovered Whitefish Lakefield in Ontario; GeoCanada 2000: the Millennium Geoscience Summit Conference CD, Abstract no. 1203.

Kent, R.W., Storey, M., and Saunders, A.D., 1992. Large igneous provinces: Sites of plume impact or plume incubation?; Geology, v. 20, p. 891–894.

Koerber, A. and Thakurta, J., 2017. Geochemical and petrological investigation of the prospective Ni-Cu-PGE mineralization at the Echo Lake intrusion in the upper peninsula of Michigan, USA; Geological Society of America Annual Meeting, Abstracts with Programs, v. 49. https://doi.org/10.1130/abs/2017AM-304314

Krogh, T.E., Corfu, F., Davis, D.W., Dunning, G.R., Heaman, L.M., Kamo, S.L., Machado, N., Greenough, J.D., and Nakamura, E., 1987. Precise U-Pb isotopic ages of diabase dykes and mafic to ultramafic rocks using trace amounts of baddeleyite and zircon; *in* Mafic Dyke Swarms, (ed.) H.C. Halls and W.F. Fahrig; Geological Association of Canada, Special Paper 34, p. 147–152.

Laarman, J.E., 2007. Geochemistry and PGE mineralization of the Kitto intrusion: A product of Mesoproterozoic plume magmatism through fault bounded Archean crust, east Nipigon Embayment, northern Ontario; M.Sc. thesis, Lakehead University, Thunder Bay, Ontario, 276 p.

Lauerma, R., 1995. Kursun ja Sallan kartta-alueiden kallioperä. Summary: Pre-Quaternary rocks of the Kursu and Salla map-sheet areas; Geological map of Finland, scale 1:100 000, Explanation to the map of Pre-Quaternary Rocks, Sheets 3643, 4621, 4623.

Lawson, A.C., 1893. The laccolith sill of the north-west coast of Lake Superior; Geological and Natural History Survey of Minnesota, Bulletin No. 8, Section II, p. 24–48.

Ludwig, K.R., 1998. On the treatment of concordant uranium-lead ages; Geochimica et Cosmochimica Acta, v. 62, p. 665–676.

Ludwig, K.R., 2003. User's manual for Isoplot 3.00: A geochronological toolkit for Microsoft Excel; Berkeley Geochronology Center, Special Publication No. 4, 71 p.

Mattinson, J.M., 2005. Zircon U/Pb chemical abrasion (CA-TIMS) method: Combined annealing and multi-step partial dissolution analysis for improved precision and accuracy of zircon ages; Chemical Geology, v. 220, p. 47–66.

McCormick, K.A., Chamberlain, K.R., and Paterson, C.J., 2017. U-Pb baddeleyite crystallization age for a Corson diabase intrusion: possible Midcontinent Rift magmatism in eastern South Dakota; Canadian Journal of Earth Sciences, v. 55, p. 111–117.

Miller, J.D., 1998. Potential for reef-type PGE mineralization in the Duluth Complex: Evidence from the Layered Series at Duluth; The Minnesota Prospector, Special Issue, p. 8–12.

Miller, J.D., 2011. Geology and mineral deposits of the Duluth Complex, Minnesota; United States Geological Survey. <https://mn.water.usgs.gov/projects/tesnar/2011/Presentations/MillerDC%20Min_USGS%20workshop.pdf> [accessed December 1, 2019]

Miller, J.D., 2016. Geology of the Endion Sill, Duluth; Institute on Lake Superior Geology, Proceedings - Field Trips, v. 62, pt. 2, p. 80–101.

Miller, J.D. and Chandler, V.W., 1997. Geology, petrology, and tectonic significance of the Beaver Bay Complex, northeastern Minnesota; *in* Middle Proterozoic to Cambrian Rifting, Central North America, (ed.) R.W. Ojakangas, A.B. Dickas, and J.C. Green; Geological Society of America, Special Paper 312, p. 73–96.

Miller, J.D. and Nicholson, S.W., 2013. Geology and mineral deposits of the 1.1 Ga Midcontinent Rift in the Lake Superior region – An overview; *in* Field Guide to the Cu-Ni-PGE Deposits of the Lake Superior Region, (ed.) J.D. Miller; Precambrian Research Center Guidebook 13-1, p. 1–50.

Miller, J.D., Jr., Green, J.C., Severson, M.J., Chandler, V.W., and Peterson, D.M., 2001. Geologic map of the Duluth Complex and related rocks, northeastern Minnesota; Minnesota Geological Survey, Miscellaneous Map M-119, scale 1:200 000.

Miller, J.D., Jr., Green, J.C., Severson, M.J., Chandler, V.W., Hauck, S.A., Peterson, D.M., and Wahl, T.E., 2002. Geology and mineral potential of the Duluth Complex and related rocks

of northeastern Minnesota; Minnesota Geological Survey, Report of Investigations 58, 207 p.

Mitchell, R.H., Platt, R.G., and Cheadle, S.P., 1983. A gravity study of the Coldwell Complex, northwestern Ontario and its petrological significance; Canadian Journal of Earth Sciences, v. 20, p. 1631–1638.

Mitchell, R.H., Platt, R.G., Lukosius-Sanders, J., Artist-Downey, M., and Moogk-Pickard, S., 1993. Petrology of syenites from center III of the Coldwell alkaline complex, northwestern Ontario, Canada; Canadian Journal of Earth Sciences, v. 30, p. 145–158.

Morris, W.J., 1977. Geochemistry and origin of the Yellow Dog Plains peridotite, Marquette Country, Northern Michigan; M.S. thesis. Michigan State University, East Lansing, Michigan.

Mungall, J.E., Kamo, S.L. and McQuade, S., 2016. U-Pb geochronology documents out-of-sequence emplacement of ultramafic layers in the Bushveld Igneous Complex of South Africa; Nature Communications, v. 7, 13 p. https://doi.org/10.1038/ncomms13385

Nicholson, S.W., Cannon, W.F., and Schulz, K.J., 1992. Metallogeny of the Midcontinent rift system of North America; Precambrian Research, v. 58, p. 355–386.

Ojakangas, R.W. and Morey, G.B., 1982. 7A: Keweenawan prevolcanic quartz sandstones and related rocks of the Lake Superior region; *in* Geology and Tectonics of the Lake Superior Basin, (ed.) R.J. Wold and W.J. Hinze; Geological Society of America, Boulder, Colorado, Memoir 156, p. 85–96.

Ontario Geological Survey, 1991a. Bedrock map of Ontario, east-central sheet; Ontario Geological Survey, Map 2543, scale 1: 1 000 000.

Ontario Geological Survey, 1991b. Bedrock map of Ontario, west-central sheet; Ontario Geological Survey, Map 2542, scale 1: 1 000 000.

Osamani, L.A., 1991. Proterozoic mafic dike swarms in the Superior Province; *in* Geology of Ontario, (ed.) P.C. Thurston, H.R. Williams, R.H. Sutcliffe, and G.M. Stott; Ontario Geological Survey, Special Volume 4, Part 1, p. 661–681.

Paces, J.B. and Miller, J.D., 1993. Precise U-Pb ages of Duluth complex and related mafic intrusions, northeastern Minnesota: Geochronological insights to physical, petrogenetic, paleomagnetic, and tectonomagmatic processes associated with the 1.1 Ga midcontinent rift system; Journal of Geophysical Research: Solid Earth, v. 98, p. 13 997–14 013.

Platt, R.G. and Mitchell, R.H., 1979. The Marathon Dikes. I: Zirconium-rich titanian garnets and manganoan magnesian ulvoespinel-magnetite spinels; American Mineralogist, v. 64, p. 546–550.

Platt, R.G. and Mitchell, R.H., 1982. The Marathon Dikes: ultrabasic lamprophyres from the vicinity of McKellar Harbour, NW Ontario; American Mineralogist, v. 67, p. 907–916.

Platt, R.G., Mitchell, R.H., and Holm, P.M., 1983. Marathon dikes: Rb–Sr and K–Ar geochronology of ultrabasic lamprophyres from the vicinity of McKellar Harbour, northwestern Ontario, Canada; Canadian Journal of Earth Sciences, v. 20, p. 961–967.

PolyMet, 2019. The NorthMet Project Overview. <https://polymetmining.com/operations/northmet-snapshot/> [accessed December 1, 2019]

Queen, M., Hanes, J.A., Archibald, D.A., Farrar, E., and Heaman, L.M., 1996. 40Ar/39Ar phlogopite and U–Pb perovskite dating of lamprophyre dykes from the eastern Lake Superior region: evidence for a 1.14 Ga magmatic precursor to Midcontinent Rift volcanism; Canadian Journal of Earth Sciences, v. 33, p. 958–965.

Queffurus, M. and Barnes, S.J., 2014. Selenium and sulfur concentrations in country rocks from the Duluth Complex, Minnesota, USA: Implications for formation of the Cu-Ni-PGE sulphides; Economic Geology, v. 109, p. 785–794.

Ripley, E.M., 2014. Ni-Cu-PGE mineralization in the Partridge River, South Kawishiwi, and Eagle intrusions: A review of contrasting styles of sulfide-rich occurrences in the Midcontinent rift system; Economic Geology, v. 109, p. 309–324.

Ripley, E.M. and Li, C., 2003. Sulfur isotope exchange and metal enrichment in the formation of magmatic Cu-Ni-(PGE) deposits; Economic Geology, v.98, p. 635–641.

Ripley, E.M., Taib, N.I., Li, C., and Moore, C.H., 2007. Chemical and mineralogical heterogeneity in the basal zone of the Partridge River Intrusion: implications for the origin of Cu–Ni sulphide mineralization in the Duluth Complex, midcontinent rift system; Contributions to Mineralogy and Petrology, v. 154, p. 35–54.

Robertson, J., Ripley, E.M., Barnes, S.J., and Li, C., 2015. Sulfur liberation from country rocks and incorporation in mafic magmas; Economic Geology, v. 110 p. 1111–1123.

Rose, K., Essig, W., and Thakurta, J., 2018. Variation trends in sulphide isotope ratios at the Eagle and East Eagle intrusions and the surrounding country and basement rocks of the Baraga Basin, Upper Peninsula, Michigan; Institute of Lake Superior Geology, 64th Annual Meeting, Abstracts, p. 87.

Rukhlov, A.S. and Bell, K., 2010. Geochronology of carbonatites from the Canadian and Baltic Shields, and the Canadian Cordillera: Clues to mantle evolution; Mineralogy and Petrology, v. 98, p. 11–54.

Sage, R.P., 1985. Geology of carbonatite-alkalic rock complexes of Ontario: Chipman Lake Area. Districts of Thunder Bay and Cochrane; Ontario Ministry of Northern Affairs and Mines, Ontario Geological Survey, Study 44, 44 p.

Sage, R.P., 1987a. Geology of carbonatite-alkalic rock complexes in Ontario: Nemegosenda Lake Alkalic Rock Complex. District of Sudbury; Ontario Ministry of Northern Development and Mines, Ontario Geological Survey, Study 34, 132 p.

Sage, R.P., 1987b. Geology of carbonatite-alkalic rock complexes in Ontario: Shenango Township Alkalic Rock Complex. District of Sudbury and Algoma; Ontario, Ministry of Northern Development and Mines, Ontario Geological Survey, Study 35, 119 p.

Sage, R.P., 1987c. Geology of carbonatite-alkalic rock complexes in Ontario: Big Beaver House Carbonatite Complex. District of Kenora; Ontario Ministry of Northern Development and Mines, Ontario Geological Survey, Study 51, 71 p.

Sage, R.P., 1988a. Geology of carbonatite-alkalic rock complexes in Ontario: Seabrook Lake Carbonatite Complex. District of Algoma; Ontario Ministry of Northern Development and Mines, Ontario Geological Survey, Study 31, 45 p.

Sage, R.P., 1988b. Geology of carbonatite-alkalic rock complexes in Ontario: Clay-Howells Alkalic Rock Complex. District of Sudbury and Algoma; Ontario Ministry of Northern Development and Mines, Ontario Geological Survey, Study 37, 104 p.

Sage, R.P., 1988c. Geology of carbonatite-alkalic rock complexes in Ontario: Valentine Township Carbonatite Complex. District of Cochrane; Ontario Ministry of Northern Development and Mines, Ontario Geological Survey, Study 39, 37 p.

Sage, R.P., 1988d. Geology of carbonatite-alkalic rock complexes of Ontario: Killala Lake Alkalic Rock Complex. District of Thunder Bay; Ministry of Northern Development and Mines, Ontario Geological Survey, Study 45, 120 p.

Sage, R.P., 1988e. Geology of carbonatite-alkalic rock complexes in Ontario: Firesand River Carbonatite Complex. District of Algoma; Ontario Ministry of Northern Development and Mines, Ontario Geological Survey, Study 47, 82 p.

Sage, R.P., 1988f. Geology of carbonatite-alkalic rock complexes in Ontario: Schryburt Lake Carbonatite Complex. District of Kenora; Ontario Ministry of Northern Development and Mines, Ontario Geological Survey, Study 50, 43 p.

Sage, R.P., 1991. Alkaline rocks, carbonatite and kimberlite complexes of Ontario, Superior Province; *in* Geology of Ontario, Ontario Geological Survey, Special Volume 4, p. 683–709.

Salminen, J., Pesonen, L.J., Mertanen, S., Vuollo, J., and Airo, M.L., 2009. Palaeomagnetism of the Salla diabase dyke, northeastern Finland, and its implication for the Baltica-Laurentia entity during the Mesoproterozoic; Geological Society, London, Special Publications, v. 323, p. 199–217.

Schoene, B., Crowley, J.L., Condon, D.J., Schmitz, M.D., and Bowring, S.A., 2006. Reassessing the uranium decay constants for geochronology using ID-TIMS U-Pb data; Geochimica et Cosmochimica Acta, v. 70, p. 426–445.

Severson, M.J., Miller, J.D., Peterson, D.M., Green, J.C., Hauck, S.A., Chandler, V.W., and Wahl, T.E., 2002. Mineral potential of the Duluth Complex and related intrusions. Geology and Mineral Potential of the Duluth Complex and Related Rocks of Northeastern Minnesota; Minnesota Geological Survey, Report of Investigations 58, p. 164–200.

Shirey, S.B., 1997. Re-Os isotopic compositions of Midcontinent rift system picrites: implications for plume–lithosphere interaction and enriched mantle sources; Canadian Journal of Earth Sciences, v. 34, p. 489–503.

Smith, J., Bleeker, W., Liikane, D.A., Hamilton, M., Cundari, R., and Hollings, P., 2019. Characteristics of Ni-Cu-PGE sulphide mineralization within the 1.1 Ga Midcontinent Rift; *in* Targeted Geoscience Initiative: 2018 report of activities, (ed.) N. Rogers; Geological Survey of Canada, Open File 8549, p. 421–432.

Smith, J.W., Bleeker, W., Hamilton, M., Petts, D., Kamo, S.L., and Rossell, D., 2020. Timing and controls on Ni-Cu-PGE mineralization within the Crystal Lake Intrusion, 1.1 Ga Midcontinent Rift; *in* Targeted Geoscience Initiative 5: Advances in the understanding of Canadian Ni-Cu-PGE and Cr ore systems – Examples from the Midcontinent Rift, the Circum-Superior Belt, the Archean Superior Province, and Cordilleran Alaskan-type intrusions, (ed.) W. Bleeker and M.G. Houlé; Geological Survey of Canada, Open File 8722, p. 37–63.

Smyk, M.C. and Franklin, J.M., 2007. A synopsis of mineral deposits in the Archean and Proterozoic rocks of the Lake Nipigon Region, Thunder Bay District, Ontario; Canadian Journal of Earth Sciences, v. 44, p. 1041–1053.

Smyk, M.C., Hollings, P., and Heaman, L.M., 2006. Preliminary investigations of the petrology, geochemistry and geochronology of the St. Ignace Island Complex, Midcontinent Rift, northern Lake Superior, Ontario; Institute of Lake Superior Geology, 52nd Annual Meeting, Proceedings and Abstracts, v. 52, p. 61–62.

Smyk, M.C. and Hollings, P., 2009. Mesoproterozoic Midcontinent Rift-related mafic intrusions near Thunder Bay: Update; *in* Summary of Field Work and Other Activities 2009, Ontario Geological Survey, Open File Report 6240, p. 11–15.

Stein, C.A., Stein, S., Elling, R., Keller, G.R., and Kley, J., 2018a. Is the "Grenville Front" in the central United States really the Midcontinent Rift?; GSA Today, v. 28, p. 4–10.

Stein, S., Stein, C.A., Elling, R., Kley, J., Keller, G.R., Wysession, M., Rooney, T., Frederiksen, A., and Moucha, R., 2018b. Insights from North America's failed Midcontinent Rift into the evolution of continental rifts and passive continental margins; Tectonophysics, v. 74, p. 403–421.

Stone, D., Kamineni, D.C., and Jackson, M.C., 1992. Precambrian geology of the Atikokan area, northwestern Ontario; Geological Survey of Canada, Bulletin 405, 115 p., 1 sheet. https://doi.org/10.4095/134053 (this publication contains Stone, D, and Kamineni, D.C., 1989. Geology, Atikokan area, Ontario; Geological Survey of Canada, Map 1666A, scale 1:50 000).

Sutcliffe, R.H., 1986. The petrology, mineral chemistry and tectonics of Proterozoic rift-related igneous rocks at Lake Nipigon, Ontario; Ph.D. thesis, University of Western Ontario, London, Ontario, 326 p.

Swanson-Hysell, N.L., Burgess, S.D., Maloof, A.C., and Bowring, S.A., 2014. Magmatic activity and plate motion during the latent stage of Midcontinent Rift development; Geology, v. 42, p. 475–478.

Swanson-Hysell, N.L., Ramezani, J., Fairchild, L.M., and Rose, I.R., 2019. Failed rifting and fast drifting: Midcontinent Rift development, Laurentia's rapid motion and the driver of Grenvillian orogenesis; Geological Society of America Bulletin, v. 131, p. 913–940. https://doi.org/10.1130/B31944.1

Taranovic, V., Ripley, E.M., Li, C., and Rossell, D., 2015. Petrogenesis of the Ni–Cu–PGE sulfide-bearing Tamarack Intrusive Complex, Midcontinent Rift System, Minnesota; Lithos, v. 212, p. 16–31.

Taranovic, V., Ripley, E.M., Li, C., and Rossell, D., 2016. Chalcophile element (Ni, Cu, PGE, and Au) variations in the Tamarack magmatic sulfide deposit in the Midcontinent Rift System: implications for dynamic ore-forming processes; Mineralium Deposita, v. 51, p. 937–951.

Taranovic, V., Ripley, E.M., Li, C., and Shirey, S.B., 2018. S, O, and Re-Os isotope studies of the Tamarack Igneous Complex: melt-rock interaction during the early stage of Midcontinent Rift development; Economic Geology, v. 113, p. 1161–1179.

Thomas, D.G., Melnyk, J., Gormely, L., Searston, S., and Kulla, G., 2011. Magma Metals Limited, Thunder Bay North polymetallic project, Ontario, Canada, NI 43-101 Technical Report on Preliminary Assessment; AMEC Americas Ltd for Magma Metals Ltd, p. 10-14 – 10-18. <https://www.miningdataonline.com/reports/Thunder_Bay_North_2011_PEA.pdf> [accessed December 1, 2019]

Trevisan, B.E., 2014. The petrology, mineralization and regional context of the Thunder mafic to ultramafic intrusion, Midcontinent Rift, Thunder Bay, Ontario; M.Sc. thesis, Lakehead University, Thunder Bay, Ontario, 285 p.

Trevisan, B.E., Hollings, P., Ames, D.E., and Rayner, N.M., 2015. The petrology, mineralization, and regional context of the Thunder mafic to ultramafic intrusion, Midcontinent Rift, Thunder Bay, Ontario; *in* Targeted Geoscience Initiative 4: Canadian nickel-copper-platinum group elements-chromium ore systems – fertility, pathfinders, new and revised models, (ed.) D.E. Ames and M.G. Houlé: Geological Survey of Canada, Open File 7856, p. 139–149.

Van Schmus, W.R., 1992. Tectonic setting of the Midcontinent Rift System; Tectonophysics, v. 213, p. 1-15.

Van Schmus, W.R. and Hinze, W.J., 1985. The midcontinent rift system; Annual Review of Earth and Planetary Sciences, v. 13, p. 345–383.

Vervoort, J.D. and Wirth, K.R., 2004. Origin of the rhyolites and granophyres of the Midcontinent Rift, northeast Minnesota. Institute on Lake Superior Geology Proceedings, 50th Annual Meeting, 52nd Annual Meeting, Proceedings and Abstracts, v. 52, p. 160–161.

Vervoort, J., Wirth, K., Kennedy, B., Sandland, T., and Harpp, K., 2007. The magmatic evolution of the Midcontinent Rift: New geochronologic and geochemical evidence from felsic magmatism; Precambrian Research, v. 157, p. 235–268.

Weiblen, P.W., 1982. 6: Keweenawan intrusive igneous rocks; *in* Geology and Tectonics of the Lake Superior Basin, (ed.) R.J. Wold and W.J. Hinze; Geological Society of America, Boulder, Colorado, Memoir 156, p. 57–82.

Weiblen, P.W., Mathez, E.A., and Morey, G.B., 1972. Logan intrusions; *in* Geology of Minnesota: A Centennial Volume, (ed.) P.K. Sims and G.B. Morey; Minnesota Geological Survey, St. Paul, Minnesota, p. 394–410.

Wirth, K.R. and Gehrels, G.E., 1998. Precise U–Pb zircon ages of Midcontinent rift rhyolite (Chengwatana Volcanics), Clam Falls, WI; Institute on Lake Superior Geology, Proceedings, v. 44, pt. 1, p. 124-125.

Wold, R.J. and Hinze, W.J., 1982. Geology and Tectonics of the Lake Superior Basin; Geological Society of America, Boulder, Colorado, Memoir 156, 280 p.

Wu, F.Y., Mitchell, R.H., Li, Q.L., Zhang, C., and Yang, Y.H., 2017. Emplacement age and isotopic composition of the Prairie Lake carbonatite complex, Northwestern Ontario, Canada; Geological Magazine, v. 154, p. 217–236.

Zartman, R.E., Nicholson, S.W., Cannon, W.F., and Morey, G., 1997. U-Th-Pb zircon ages of some Keweenawan Supergroup rocks from the south shore of Lake Superior; Canadian Journal of Earth Science, v. 34, p. 549–561.

Timing and controls on Ni-Cu-PGE mineralization within the Crystal Lake Intrusion, 1.1 Ga Midcontinent Rift

J.W. Smith[1]*, W. Bleeker[1], M. Hamilton[2], D. Petts[1], S.L. Kamo[2], and D. Rossell[3]

[1]Geological Survey of Canada, 601 Booth Street, Ottawa, Ontario K1A 0E8
[2]Jack Satterly Geochronology Laboratory, University of Toronto, 22 Russell Street, Toronto, Ontario M5S 3B1
[3]Rio Tinto Exploration Canada Inc., 1300 Walsh Street, Thunder Bay, Ontario P7E 4X4
*Corresponding author's e-mail: jennifer.smith6@canada.ca

ABSTRACT

North America's 1.1 Ga Midcontinent Rift (MCR) hosts a diverse range of ultramafic and mafic intrusions, many of which contain Ni-Cu-PGE mineralization. The gabbroic, sulphide-bearing Crystal Lake Intrusion was emplaced between 1095–1091 Ma during the 'main-stage' of rift evolution. The Ni-Cu-PGE mineralization shows a close spatial association with contaminated, Cr-spinel-bearing, vari-textured gabbros. Despite the MCR having a rich legacy of research, the temporal and spatial controls on ore formation, in addition to the processes critical for ore genesis, remain poorly constrained. Here we present new field, petrographic, and mineralogical observations, with preliminary U-Pb zircon and baddeleyite isotope dilution-thermal ionization mass spectrometry (ID-TIMS) results for various phases of the Crystal Lake Intrusion to resolve questions regarding the timing of emplacement and its relationship to other MCR magmatic events, such as the Mount Mollie dyke, the Pigeon River dykes, and the Cu-Ni-bearing Duluth Complex.

Results suggest that the sulphide ores at Crystal Lake were formed under low confining pressures from a magma saturated in volatiles through contamination. The addition of crustal S prior to emplacement, by assimilation and melting of wall rocks and xenoliths entrained in the magma, is considered critical for the genesis of the ores. The local addition of S in situ, as indicated by S/Se ratios, likely contributed only minor S into the system and is not considered essential for S saturation. Reworking of the magmatic system is indicated within the taxitic units by local brecciation, 'ripped' sulphide clasts and large (>1 cm) globular sulphides, which may indicate minimal transportation of the ores and the potential of a deeper sulphide pool/source. The pronounced magnetic anomaly of the southern limb may suggest the presence of a feeder dyke in the south.

Palladium (91–99%) and Pt (>99%) reside primarily as platinum group minerals (PGMs) in association with sulphides. The PGM assemblage, which is largely controlled by the availability of semi-metals through contamination, is dominated by Pt arsenides, Pd-Bi-Sb±Te phases, Pd-Sn±Sb phases, Pd bismuthides, and Pd antimonides. The similarity of the PGM assemblage throughout the Crystal Lake Intrusion indicates crystallization from compositionally similar magmas. The distribution of elements is consistent with the fractionation of a sulphide liquid, with later low-temperature alteration locally remobilizing elements at the micro-scale. The preferential partitioning of Mo, As, Bi, Re, and Pd into discrete parallel linear features and the development of a micro-fabric within unaltered sulphide globules suggests localized remobilization of select elements post-sulphide fractionation.

INTRODUCTION

North America's Midcontinent Rift (MCR) represents one of the best preserved intra-continental rift systems of the late Mesoproterozoic (Wold and Hinze, 1982; Green, 1983; Van Schmus and Hinze, 1985; Hutchinson et al., 1990; Miller and Nicholson, 2013). The ca. 1.1 Ga 'failed rift' system hosts a range of mafic-ultramafic, carbonatitic and alkaline intrusions (*see* compilation in Bleeker et al., 2020), many of which are actively being explored for a range of commodities (e.g. Ni, Cu, PGE, Co, Cr, V, Ti, Fe, Nb). The magmatic Ni-Cu-PGE sulphide deposits occur in association with a variety of mafic and mafic-ultramafic intrusions. Like many other world-class Ni-Cu deposits (e.g. Norilsk, Voisey's Bay, Raglan), this mineralization shows a close spatial and temporal relationship with large volumes of magma erupted at or near the margins of Archean cratons and/or in association with trans-lithospheric faults (e.g. Naldrett, 1997; Begg et al., 2010; Lightfoot and Evans-Lamswood, 2015, and references therein).

The MCR mafic and mafic-ultramafic intrusions that host Ni-Cu-PGE mineralization not only show considerable variability in their size, shape, and internal igneous stratigraphy but also in their style of mineralization (*see* Bleeker et al., 2020 and references

Smith, J.W., Bleeker, W., Hamilton, M., Petts, D., Kamo, S.L., and Rossell, D., 2020. Timing and controls in Ni-Cu-PGE mineralization within the Crystal Lake Intrusion, 1.1 Ga Midcontinent Rift; *in* Targeted Geoscience Initiative 5: Advances in the understanding of Canadian Ni-Cu-PGE and Cr ore systems – Examples from the Midcontinent Rift, the Circum-Superior Belt, the Archean Superior Province, and Cordilleran Alaskan-type intrusions, (ed.) W. Bleeker and M.G. Houlé; Geological Survey of Canada, Open File 8722, p. 37–63. https://doi.org/10.4095/326881

therein). The Ni-Cu-PGE sulphide mineralization within the MCR can be broadly classified into four types: 1) disseminated sulphide mineralization associated with gabbroic to troctolitic intrusions (e.g. Duluth Complex, Crystal Lake Intrusion); 2) high-tenor, disseminated to massive sulphide occurrences hosted by small 'early-rift' ultramafic intrusions (e.g. Eagle and Eagle East, Tamarack); 3) low-sulphide, PGE-enriched reef-style mineralization within well differentiated layered intrusions (e.g. Sonju Lake, Echo Lake); and 4) disseminated, sulphide-poor, PGE-Cu-enriched mineralization associated with 'early-rift' conduit-type ultramafic and mafic intrusions (e.g. Marathon Deposit, Current Lake, Sunday Lake). The reader is referred to Bleeker et al. (2020) and references therein for more detailed summaries of the key features of the various styles of Ni-Cu-PGE mineralization developed within the MCR.

In addition to refining the geochronological framework of the MCR magmatism and thus providing insights into the spatial and temporal controls on the various styles of ore formation, this TGI activity also characterizes the nature and timing of Ni-Cu-PGE mineralization within the Crystal Lake Intrusion to gain further insight into key ore-forming processes. The Crystal Lake Intrusion is an interesting case study as, unlike many other MCR Ni-Cu-PGE deposits, the mineralization shows a close spatial association with contaminated 'taxitic' rocks, a feature common in many other Ni-Cu deposits around the world, including the ores of Norilsk and Voisey's Bay[1]. This study combines field, petrographic, and mineralogical observations of the Crystal Lake ores, with high-precision U-Pb geochronology on various phases of the intrusion to examine/review (1) the role of contamination in ore formation; (2) the source and timing of S saturation; (3) the controls on the distribution of metals; and (4) the timing of ore formation relative to other MCR intrusions. This paper presents new field observations, mineralogical/laser ablation-inductively coupled plasma-mass spectrometry (LA-ICP-MS) results, and preliminary zircon and baddeleyite U-Pb ID-TIMS results for the Crystal Lake Intrusion and Mount Mollie dyke. The new ages begin to answer some unresolved questions regarding the timing of emplacement of the Crystal Lake Intrusion and its relationship to other MCR magmatic events, such as the Mount Mollie dyke, the north-northeast-trending Pigeon River dykes, and the Cu-Ni-bearing Duluth Complex. With a growing database of ages of MCR intrusions and continued efforts being made to refine the overall temporal framework of the MCR, we can start to delineate how ore formation relates in time and space to the overall evolution of the rift system and whether particular styles of mineralization are restricted to discrete magmatic episodes.

To gain insights into the behaviour and mobility of chalcophile elements during syn- and post-magmatic processes, we detail the mineral and trace element characteristics of precious metal-bearing minerals (PMM) and base metal sulphides within the Crystal Lake Intrusion. This has been achieved through combining a mineralogical deportment study with LA-ICP-MS analysis and element mapping. Although in the past metal deportment studies were largely utilized for optimizing metallurgical processing, they have also shown potential for applications to mineral exploration (e.g. Marathon deposit: Good et al., 2017). In addition, deportments also provide insights into the geological processes responsible for the concentration of metals, and thus ore formation (e.g. Holwell et al., 2006; Yudovskaya et al., 2011; Smith et al., 2014; Ames et al., 2017; Good et al., 2017) and are particularly insightful when combined with novel techniques such as quantitative LA-ICP-MS element mapping, which provides unparalleled spatial information at the microscopic scale.

GEOLOGICAL SETTING

The MCR represents a >2500 km arcuate tract of largely buried igneous and sedimentary rocks that extend from the Lake Superior region, where rift rocks are exposed, to the southwest and southeast (Van Schmus and Hinze, 1985; Stein et al., 2018). Geophysical anomalies, previously inferred as the Grenville Front, are now considered to represent the southward continuation of the MCR's eastern arm (Stein et al., 2018). Current U-Pb dates suggest that the extensive, plume-related, largely tholeiitic volcanism (~1.5 million km^3: Cannon, 1992) within the MCR was initiated at ca. 1109 Ma and continued intermittently to ca. 1083 Ma (Swanson-Hysell et al., 2019 and references therein). Geochronology of some of the intrusions (Heaman et al., 2007) may extend the onset of the main rift magmatism to ca. 1117 Ma (*see* Bleeker et al., 2018, 2020 for a detailed discussion). On the basis of existing geochronology and geochemical data, the MCR is conventionally divided into five stages: an initiation stage (ca. 1115–1109 Ma), an early stage (ca. 1109–1104), a latent stage (ca. 1104–1098 Ma), a main stage (ca. 1098–1090 Ma), and a late stage (ca. 1090–1083 Ma; Miller and Nicholson, 2013; Swanson-Hysell et al., 2019). The ca. 1144 Ma lamprophyre dykes and 1141 Ma Abitibi dyke swarm located to the northeast of Lake Superior are considered precursors to the main rifting event at ca. 1115 Ma (Krogh et al., 1987; Queen et al., 1996; Piispa et al., 2018). Although

[1] The close spatial association with taxitic-textured, hydrothermal mineral-rich marginal gabbro is also observed in basal mineralization of the Duluth Complex intrusions (J. Miller, pers. comm., 2019).

a number of dating studies have been undertaken on the MCR, there are continued efforts to improve and refine the temporal framework of the MCR magmatism. Recent studies include those by Bleeker et al. (2020), Swanson-Hysell et al. (2014, 2019), and Fairchild et al. (2017), which provide new high-precision chemical abrasion-ID-TIMS (CA-ID-TIMS) ages for both the MCR volcanic and intrusive rocks. The ongoing research by Bleeker et al. (2018, 2020) is continuing to refine the overall age distribution of the MCR magmatism, and as a result, previously anomalous ages (e.g. Inspiration sill, Pigeon River dykes, Current Lake Intrusion; Heaman et al., 2007; Smyk and Hollings, 2009) have now been constrained to within the ca. 1115–1084 Ma main rifting event. Furthermore, the new and refined ages of mineralized intrusions suggest that ore formation within the rift system was constrained to multiple episodes.

THE CRYSTAL LAKE INTRUSION

Geological Setting and Timing of Emplacement

The Crystal Lake Intrusion, located 47 km southwest of Thunder Bay, outcrops as a prominent Y-shaped body (Fig. 1) within the Animikie basin, intruding sulphur-bearing greywacke and mudstone of the Paleoproterozoic Rove Formation (Geul, 1970, 1973). Cross-sections, provided in Figure 2, illustrate the interpreted morphology of the intrusion, which is generally eastward plunging and thought to be lopolithic to dyke-like in shape. Whereas the northern limb has no strong magnetic expression, the southern limb is characterized by a magnetic anomaly. This could indicate that the intrusion extends deeper, potentially into a feeder dyke in the south (Fig. 2). Representative sections of the igneous stratigraphy of the northern and southern limbs are provided in Figure 3. Although the composition of the upper portion of the 'limbs' differs, both limbs are broadly comparable, characterized by a basal, sulphide-bearing vari-textured gabbro unit, overlain by a thick succession of homogeneous, unmineralized troctolite or magnetite-bearing olivine gabbro in the northern and southern limbs, respectively. With no chilled margin recognized at the upper contact of the mineralized vari-textured gabbros with the overlying barren troctolite/gabbro, which is represented by a distinct geochemical break, it is difficult to resolve the relative timing of these units. Fine-grained porphyritic diabase to coarse-grained, plagioclase-rich megacrystic sheet-like bodies, (Fig. 2, 3) intersect the Crystal Lake stratigraphy at depth. With a potential chilled margin recognized at the basal contact of the megacrystic sill (borehole CL003; Fig. 2, 3), these are thought to postdate emplacement of the main phases of the Crystal Lake Intrusion (however, see the comment in the caption to Fig. 2). For detailed petrographic descriptions of the Crystal Lake Intrusion, the reader is referred to Geul (1970), Mainwaring and Watkinson (1981), Smith and Sutcliffe (1987), Cogulu (1993a,b), Thomas (2015), and O'Brien (2018). Note that the geology of the Crystal Lake Intrusion is no longer subdivided into a basal, lower, middle/layered, and upper zones as defined in the earlier literature (Smith and Sutcliffe, 1987).

Geochemically, the Crystal Lake Intrusion can be distinguished from the more primitive conduit-type bodies of the MCR (e.g. Tamarack, Eagle), by olivine composition (Fo_{51-79}; Thomas, 2015; O'Brien, 2018), lower Ni/Cu and Pt/Pd ratios (<1), higher rare earth element (REE) abundances, light REE enrichment, and minimal fractionation of heavy REEs (Gd/Yb <2). In contrast to the high-grade, massive sulphide ores of Eagle and Tamarack, the mineralization at Crystal Lake is more comparable to the low-grade but extensive, disseminated ores of the Duluth Complex (Ripley 2014, and references therein).

At present, the timing of emplacement of the Crystal Lake Intrusion, which was previously dated at 1099.1 ± 1.2 Ma (Heaman et al., 2007), and its relationship with the MCRs north-northeast-trending Pigeon River dykes, the northwest-trending Cloud River dykes, the east- to northeast-trending Mount Mollie dyke, as well as the Duluth Complex, is poorly constrained (Fig. 1). This is largely resultant from poor exposure, lack of observed crosscutting relationships, and imprecise U-Pb ages. Based on Geul's (1970) interpretation, the Crystal Lake Intrusion crosscuts the Pigeon River dykes, which have been re-dated at ca. 1096.6 ± 2.2 Ma (Bleeker et al., 2020). With this notion supported by our own field observations and the apparent abrupt termination of Pigeon River dykes at the edge of the Crystal Lake Intrusion, the Heaman et al. (2007) age of 1099.1 ± 1.2 Ma may not reflect the true crystallization age of the Crystal Lake Intrusion. Newly recognized crosscutting relationships (Fig. 1), in addition to new U-Pb ages, indicate that the ca. 1097 Ma Pigeon River dykes post-date emplacement of the northwest-trending Cloud River dykes (Smith et al., 2019; Bleeker et al., 2020), which at ca. 1109 Ma may be related to the emplacement of the Logan sill complex. The Mount Mollie dyke, which comprises olivine gabbro, pegmatitic gabbro, and a granophyre core, is located immediately to the east of the Crystal Lake Intrusion. The relationship between these two intrusions has long been debated and, due to unreliable age constraints, remains unresolved. Although they have been suggested to be coeval (Smith and Sutcliffe, 1987; O'Brien, 2018), with Mount Mollie potentially representing a feeder dyke, this is not consistent with Hollings et al.'s (2010) reported baddeleyite age of 1109.3 ± 6.3 Ma. However, this older age is in dis-

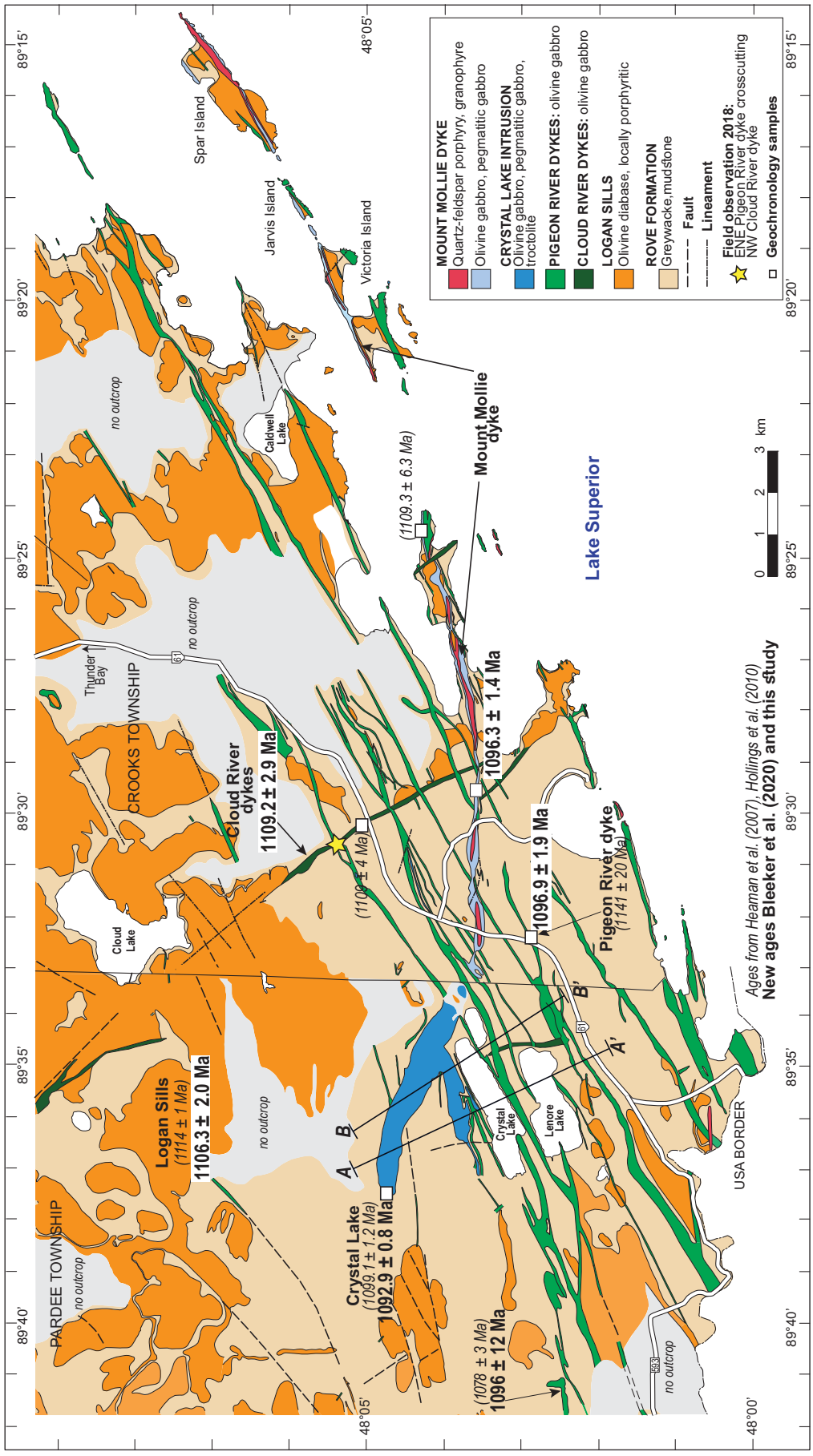

Figure 1. Geological map of Pardee and Crook townships showing the location and relationship of the Crystal Lake Intrusion with other Midcontinent rift intrusions. New U-Pb ages for the north-northeast-trending Pigeon River dykes, northwest-trending Cloud River dykes, and Logan sills (Bleeker et al., 2020) are shown, with previously determined ages by Heaman et al. (2007) and Hollings et al. (2010) in brackets. Map is *modified from* Geul (1970, 1973) on the basis of new field observations and age constraints.

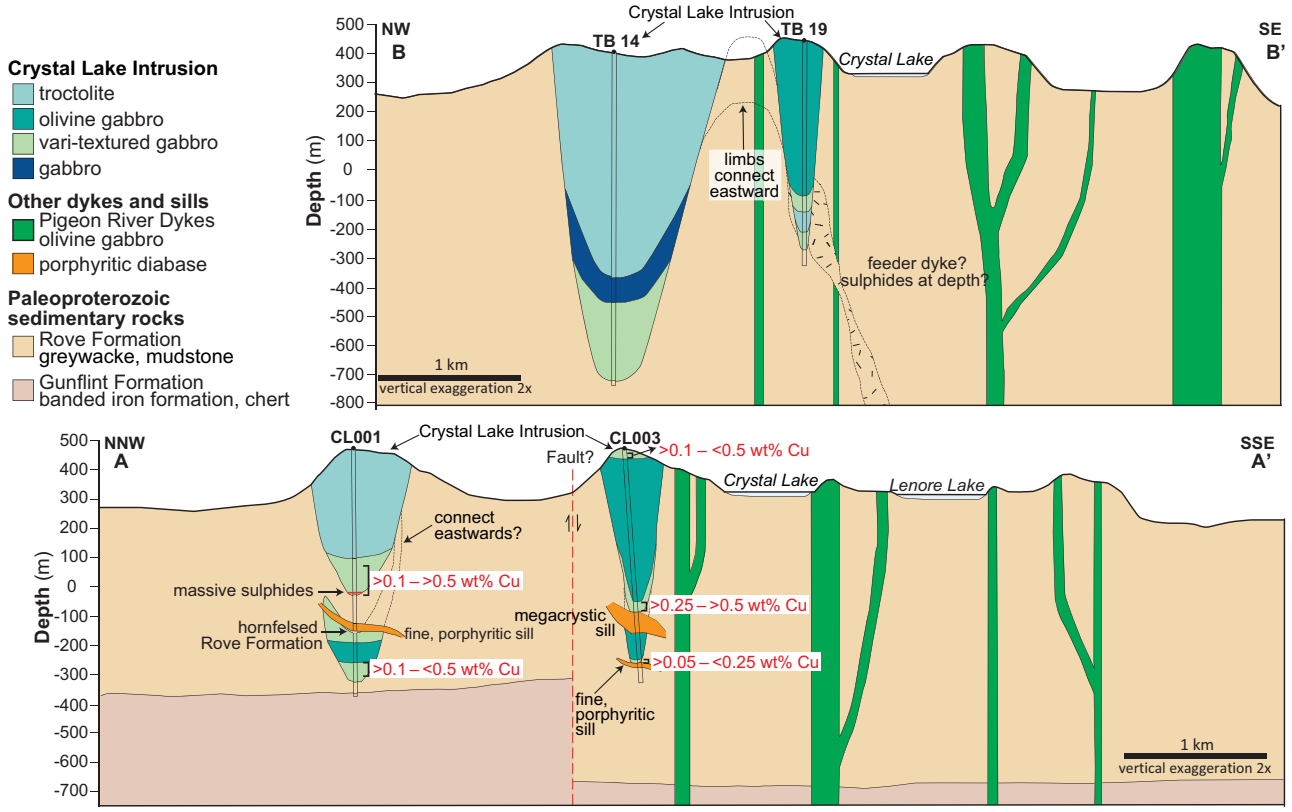

Figure 2. Cross-sections showing the interpreted morphology of the Crystal Lake Intrusion. Location of the sections are shown on Figure 1. Note that the "porphyritic diabase" units intersected at depth in section A-A' may be older Logan sills that predate the Crystal Lake Intrusion, rather than post-date the intrusion (J. Miller, pers. comm., 2019). No diabase sills in the area are known to be younger than the Crystal Lake Intrusion, whereas Logan Sills are abundant in the area.

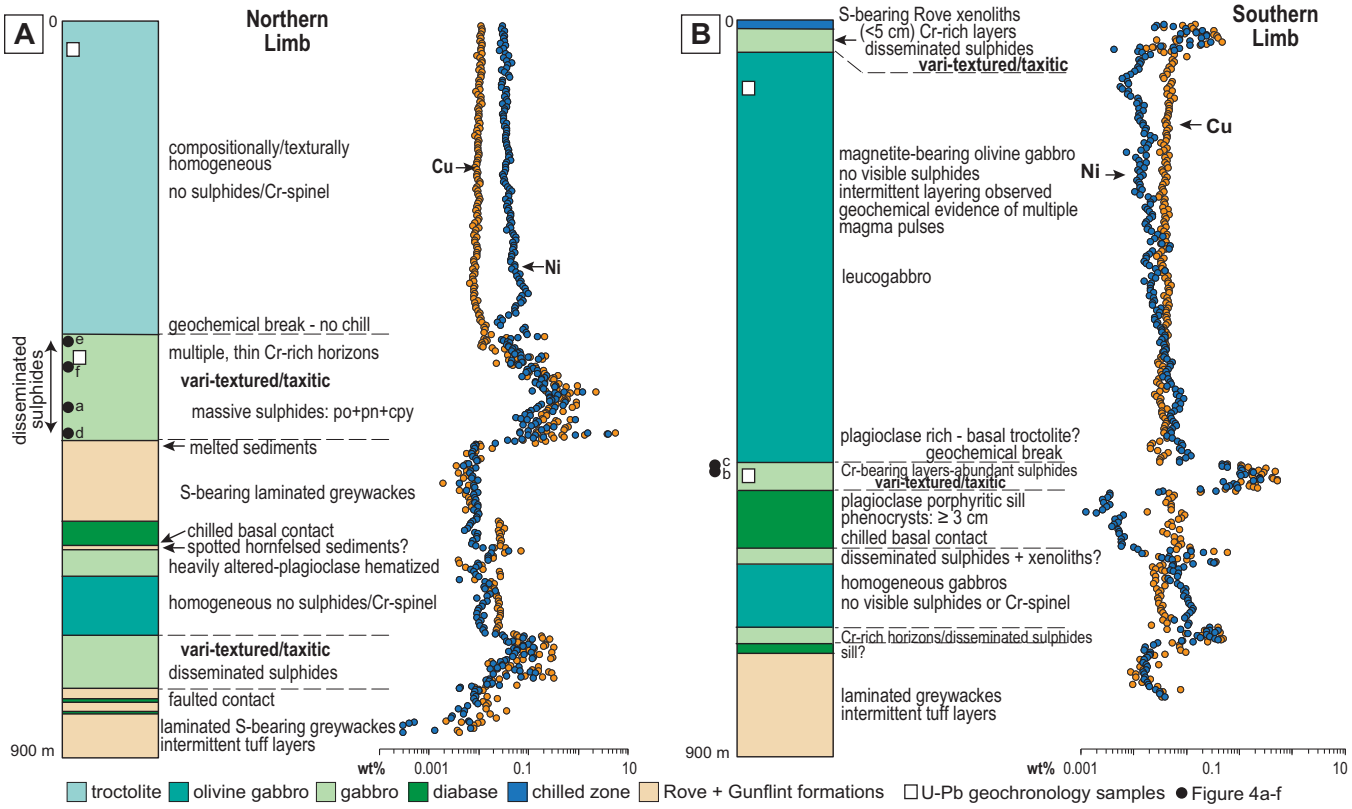

Figure 3. Representative stratigraphic columns of the **(a)** northern and **(b)** southern limbs of the Crystal Lake Intrusion. Metal concentrations from Goldner (2015, 2016). Location of geochronology samples and photographs provided in Figure 4 are also shown.

agreement with the normal polarity of the Mount Mollie dyke, a feature characteristic of younger rift rocks (<1100 Ma).

Vari-textured Gabbros: Textural Features

Vari-textured gabbros of the Crystal Lake Intrusion, referred to as 'taxites' in Norilsk literature (e.g. Lightfoot, 2007), are heterogeneous in nature, characterized by irregular variations in texture (fine-grained to pegmatitic) and composition, in addition to the presence of sulphides, Cr-spinel, and sedimentary/gabbroic xenoliths (Fig. 4). In the northern limb, discrete and sulphide-free troctolite layers are recognized near the upper contact of the vari-textured gabbro unit (Fig. 4f). These layers, which are comparable to the overlying troctolite unit, are in sharp (but not chilled) contact with the pegmatitic/vari-textured gabbros. The vari-textured gabbros also contain rare, spherical segregation vesicles (Fig. 5d). These vesicles are infilled with prehnite, biotite, amphiboles, and rare calcite, and are typically <1.5 cm in diameter. Although many of the segregation vesicles occur in association with sulphide droplets (*see* Discussion *below*), some occur without any sulphide attachment (Fig. 5d). Many deposits exhibit an association of sulphides with taxitic rocks, with the latter often interpreted to have crystallized from a volatile-rich, highly contaminated magma indicating significant wall-rock interaction (e.g. Norilsk, Voisey's Bay, Merensky Reef; Barnes and Campbell, 1988; Lightfoot, 2007; Cawthorn, 2010; Barnes et al., 2016).

Within the Crystal Lake Intrusion, Cr-spinel is found in association with the vari-textured gabbros, occurring as discrete, massive layers and stringers (<1 to ~100 cm thick) with sharp and diffuse contacts, and as irregular patches and xenoliths with both sharp and angular contacts (Fig. 4c, 5b,c,g). Cr-spinel also occurs as fine disseminations within the gabbroic rocks. The Cr-spinel layers are often brecciated and heterogeneous in appearance (Fig. 4c), containing sulphide-bearing and sulphide-free gabbro xenoliths and lenses (often elongated) of anorthositic material. Disseminated interstitial, blebby and globular sulphides are identified within the Cr-rich rocks. From the boreholes studied, it appears that the distribution of Cr-spinel differs between the two limbs of the intrusion. Within the northern limb, Cr-spinel primarily occurs as fine disseminations and as thin (<10 cm thick), undisturbed layers/stringers that do not contain significant sulphide mineralization and are associated with the upper portion of the vari-textured gabbro unit. In contrast, the southern limb vari-textured gabbros are characterized by thicker (<1 m), denser, Cr-spinel layers that are massive in nature, brecciated, and contain abundant sulphides (e.g. Fig. 4c). Towards the upper contact of the taxitic gabbros in the southern limb, the Cr-spinel horizons decrease in thickness and irregular Cr-rich patches/xenoliths are recognized (Fig. 5b).

Sedimentary xenoliths, some of which contain disseminated sulphides, are common near the margins of the intrusion (Fig. 5a; Geul, 1970, Mainwaring and Watkinson, 1981). They are irregular in shape with rounded contacts and are often characterized by an altered and sulphide-bearing rim. Interaction of the Crystal Lake magma(s) with the Rove Formation is also indicated by the high $\delta^{34}S$ signature of the Crystal Lake sulphides ($\delta^{34}S$ +1.4 to +21‰; Thomas, 2015; O'Brien, 2018) and the higher than mantle S/Se ratios (2850–4350; Eckstrand and Hulbert, 1987), which suggests a significant crustal S component throughout the ores. Mafic fragments, which are rounded to angular, are commonly identified within the vari-textured gabbros and Cr-spinel bearing horizons (Fig. 4a,b, 5e–g). Within the northern limb, these fragments are sulphide-free; however, in the southern limb sulphide-bearing and sulphide-free fragments are observed.

Ni-Cu-PGE Mineralization: New Petrographic Observations

Within the Crystal Lake Intrusion, sulphide mineralization is largely disseminated, with massive sulphide intervals (<50 cm thick) intersected locally within the northern limb (Fig. 4b–d). The disseminated ores, which are hosted by the vari-textured gabbros and Cr-bearing horizons, are variable in texture (Fig. 4a–c) with globular (silicate capped and uncapped), blebby, and interstitial sulphides identified. Globular sulphides (represented by sulphide aggregates that are convex and subspherical; Barnes et al., 2017, 2019) are irregularly distributed throughout the mineralized horizons.

The sulphide ores are dominated by the magmatic assemblage pyrrhotite, chalcopyrite, pentlandite ±cubanite with minor primary magnetite (Fig. 6a,b) and accessory nickel arsenides (Fig. 6f). Within the disseminated ores, sulphide grains are composed primarily of pyrrhotite and/or chalcopyrite. Pentlandite occurs as granular grains within pyrrhotite, around the margins of the composite grains, or along the contact between pyrrhotite and chalcopyrite (Fig. 6a–d). Exsolution flames/fans of pentlandite within pyrrhotite are also observed and are preferentially concentrated along fractures (Fig. 6e,j). Within the blebby/globular ores, curved lamellar exsolutions of an iron sulphide phase are occasionally observed within pyrrhotite (e.g. Fig. 6d,j). In areas where chalcopyrite and cubanite occur adjacent to or around the margins of pyrrhotite, rounded relics of pyrrhotite are observed within the Cu-rich phases (Fig. 6c). Within pyrrhotite-dominated blebs, chalcopyrite is restricted to the margins of the grains. Chalcopyrite (with minor pyrrhotite) is also

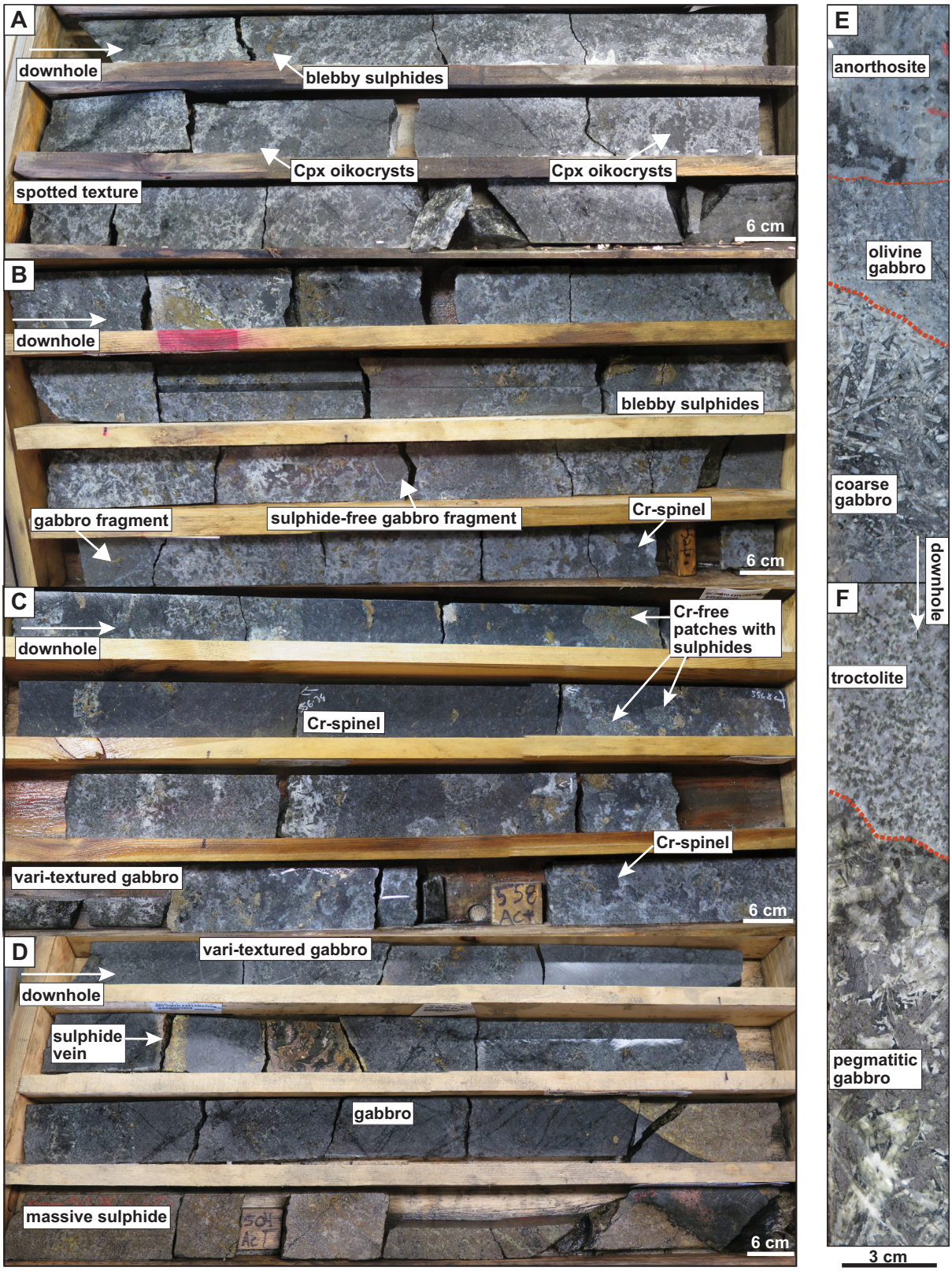

Figure 4. Representative photographs of Ni-Cu-PGE mineralization within the Crystal Lake Intrusion. **a, b)** Vari-textured gabbros from the northern limb, showing textural variations and associated interstitial/blebby sulphide mineralization. **c)** Chrome-spinel-rich horizon from the southern limb. Sulphide mineralization is disseminated and blebby in nature and is associated with the Cr-rich and Cr-free gabbro pockets. **d)** Massive sulphides developed within the northern limb. Note the sharp upper contact with gabbro and the presence of sulphide veins. **e)** Sharp layering observed near the upper contact of the vari-textured gabbro unit in the northern limb. **f)** Sharp contact observed between pegmatitic gabbro and troctolite near the upper contact of the vari-textured gabbro. Abbreviation: Cpx = clinopyroxene.

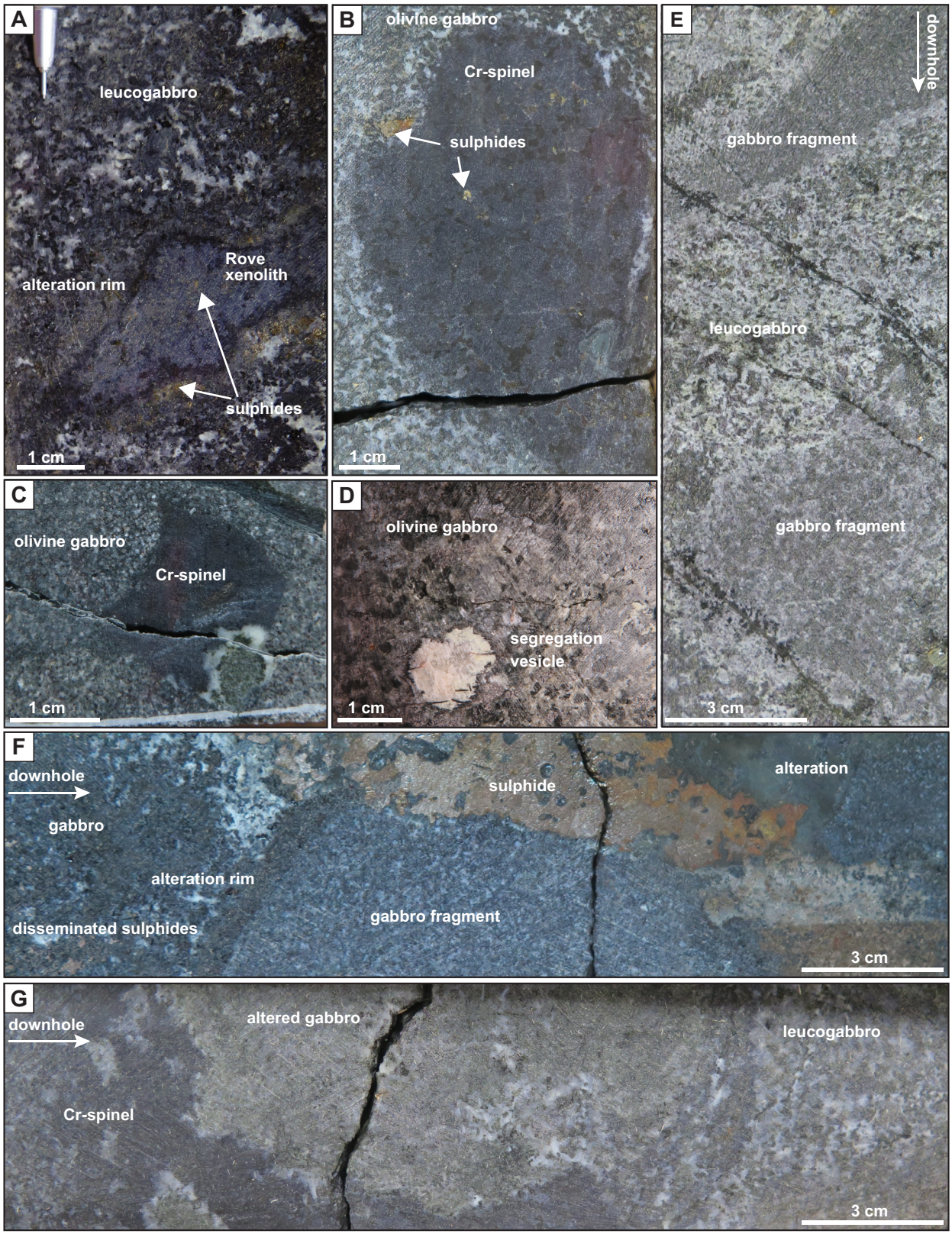

Figure 5. A representative selection of xenoliths/fragments observed within the Crystal Lake Intrusion. **a)** Irregular sedimentary xenolith within the Crystal Lake Intrusion; sulphides are abundant around the margin of the xenolith. **b)** Rounded chrome-spinel-rich xenolith with disseminated sulphides, within an olivine gabbro. **c)** Angular chrome-spinel clast within fine gabbro containing minor disseminated sulphides. **d)** Segregation vesicle composed of prehnite within an olivine gabbro from within the vari-textured gabbro unit. **e)** Textural variations commonly observation within the vari-textured gabbro units. **f)** A rounded gabbro fragment with massive sulphides and alteration around its margin. **g)** A rounded altered gabbro fragment, partially rimmed by chrome-spinel and hosted by leucogabbro.

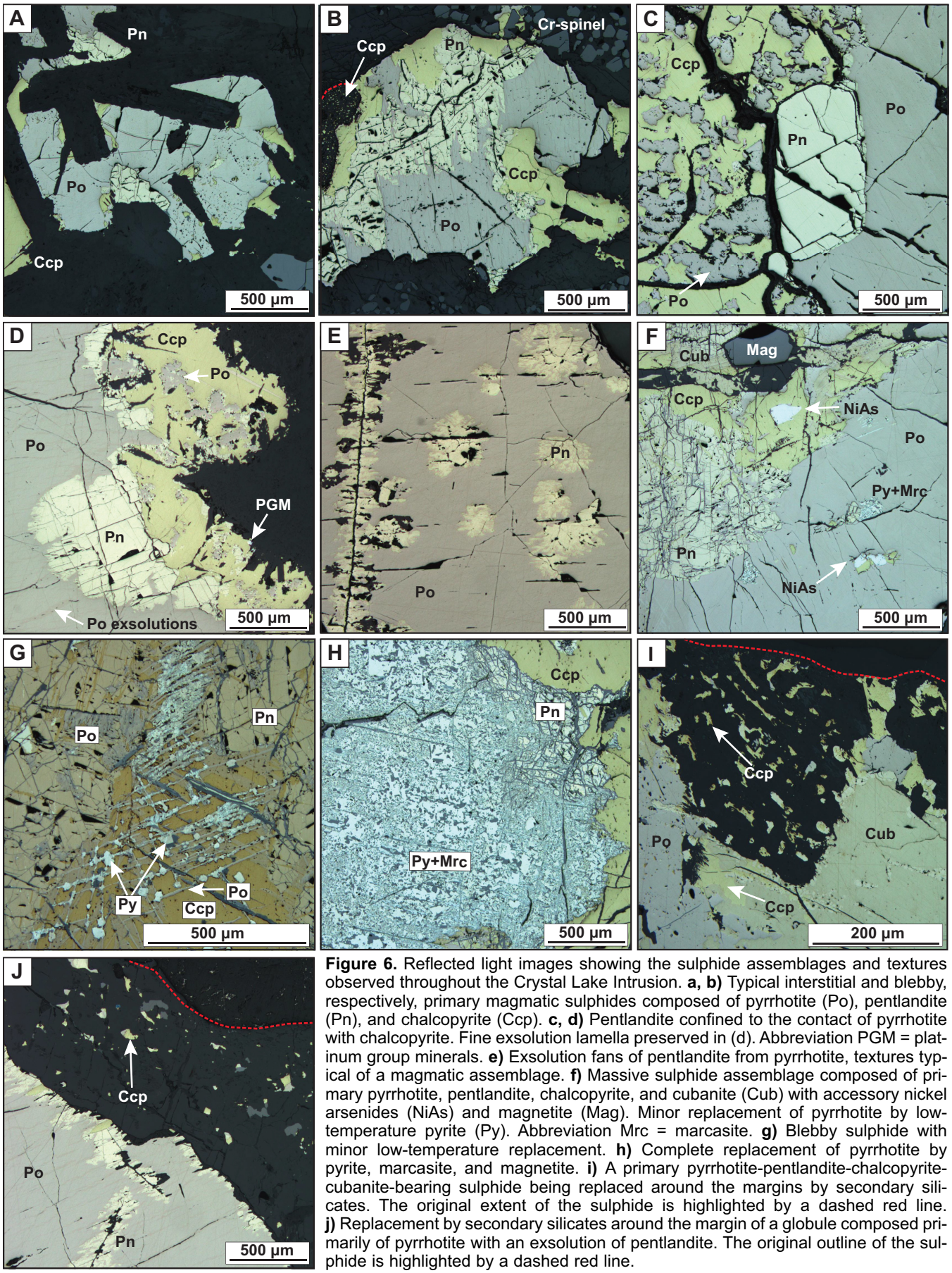

Figure 6. Reflected light images showing the sulphide assemblages and textures observed throughout the Crystal Lake Intrusion. **a, b)** Typical interstitial and blebby, respectively, primary magmatic sulphides composed of pyrrhotite (Po), pentlandite (Pn), and chalcopyrite (Ccp). **c, d)** Pentlandite confined to the contact of pyrrhotite with chalcopyrite. Fine exsolution lamella preserved in (d). Abbreviation PGM = platinum group minerals. **e)** Exsolution fans of pentlandite from pyrrhotite, textures typical of a magmatic assemblage. **f)** Massive sulphide assemblage composed of primary pyrrhotite, pentlandite, chalcopyrite, and cubanite (Cub) with accessory nickel arsenides (NiAs) and magnetite (Mag). Minor replacement of pyrrhotite by low-temperature pyrite (Py). Abbreviation Mrc = marcasite. **g)** Blebby sulphide with minor low-temperature replacement. **h)** Complete replacement of pyrrhotite by pyrite, marcasite, and magnetite. **i)** A primary pyrrhotite-pentlandite-chalcopyrite-cubanite-bearing sulphide being replaced around the margins by secondary silicates. The original extent of the sulphide is highlighted by a dashed red line. **j)** Replacement by secondary silicates around the margin of a globule composed primarily of pyrrhotite with an exsolution of pentlandite. The original outline of the sulphide is highlighted by a dashed red line.

present within thin veinlets, which are most commonly observed within the disseminated blebby/globular ores.

A low-temperature, alteration assemblage, characterized by pyrite, marcasite, chalcopyrite, and magnetite, is recognized in both the disseminated and massive sulphide ores. The degree of replacement of the primary assemblage is variable (e.g. Fig. 6f–h) with alteration more pervasive in the disseminated ores of the northern limb with increasing proximity to the basal footwall contact. The altered assemblages are texturally more complex and characterized by the partial to complete replacement of pyrrhotite and pentlandite by subhedral to euhedral pyrite, marcasite, and magnetite (Fig. 6f–h). In places, chalcopyrite contains crosscutting lamellae of pyrrhotite with which subhedral pyrite grains are associated with (Fig. 6g).

Alteration of sulphides by secondary silicates is largely confined to the margins of the grains and is a feature observed in both the primary and altered sulphide assemblages. The silicate alteration rim is variable in thickness and contains relics of pyrrhotite, pentlandite, chalcopyrite and magnetite (Fig. 6i,j). Platinum-group minerals also reside within these alteration halos.

Globular sulphides have been recognized in numerous intrusions, komatiites, and flood basalts including Sudbury, Norilsk, Black Swan, the Insizwa Complex, and dykes from East Greenland and Uruguay (Lightfoot et al., 1984; Dowling et al., 2004; Prichard et al., 2004; Holwell et al., 2012; Barnes et al., 2017, 2019; Le Vaillant et al., 2017). Within the Crystal Lake Intrusion, disseminated globular sulphides form only a minor component (Fig. 7). The lower contact of the globules is generally rounded with no evidence of the sulphide liquid infiltrating/penetrating downwards into the intercumulus framework. The globules are generally >1 cm in diameter and are composed of pyrrhotite and chalcopyrite with minor pentlandite. None of the globules investigated as part of the present study have experienced any low-temperature replacement by pyrite/marcasite. Internal differentiation of sulphide globules into a Cu-rich upper zone and Cu-poor, Ni-rich lower zone is commonly observed (e.g. Fig. 7a,d). Pentlandite is predominantly confined to the contact between chalcopyrite and pyrrhotite or the margins of the sulphide grains.

Silicate-capped globules have been documented in various intrusions and komatiitic bodies (e.g. Norilsk, Black Swan, macrodykes in East Greenland; Barnes et al., 2017 and references therein), and have been interpreted as remnants of a former magmatic vapour phase (Barnes et al., 2017). Silicate caps are also recognized in association with globular sulphides in the Crystal Lake Intrusion (Fig. 7c–f). The polymineralic caps are

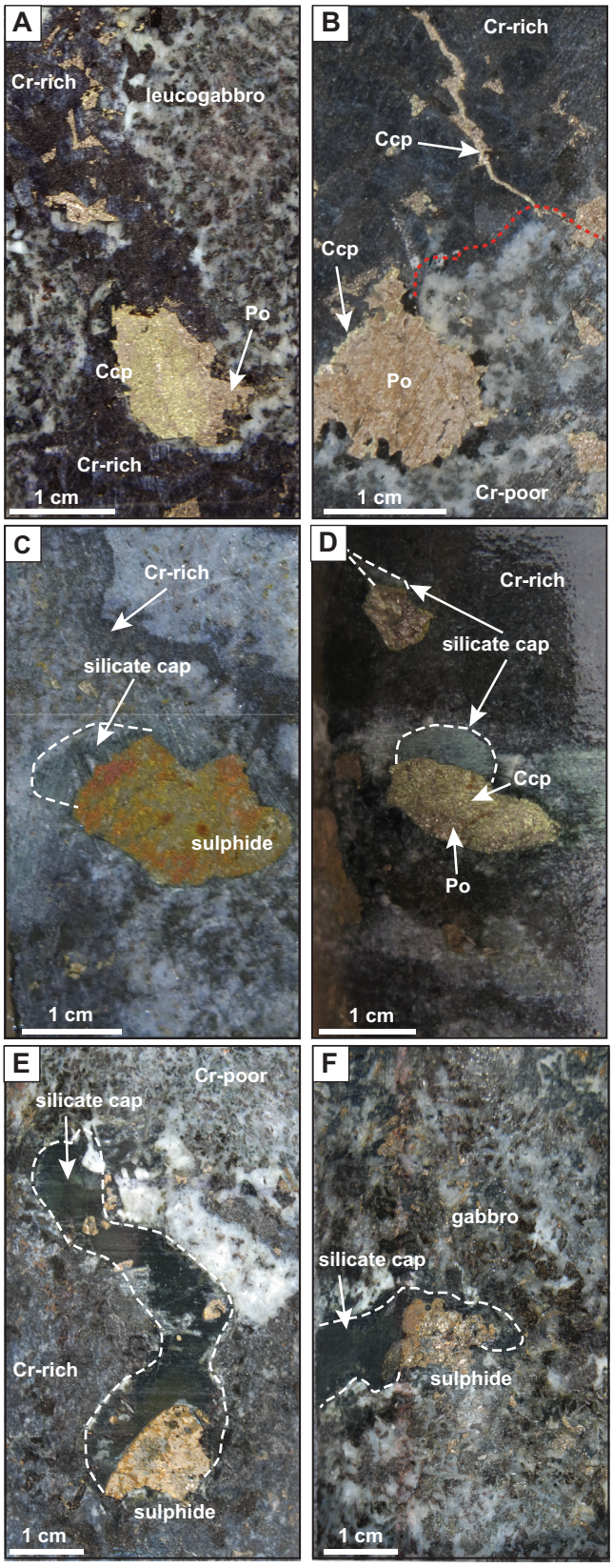

Figure 7. Examples of globular sulphides observed within the Crystal Lake Intrusion. **a, b)** Uncapped, sulphide globules within chrome-spinel-bearing horizons. **c, d)** Capped globules with regular silicate attachments. **e, f)** Capped sulphide globules with irregular-shaped attachments. Abbreviations: Ccp = chalcopyrite, Po = pyrrhotite.

Table 1. Preliminary U-Pb results for the Crystal Lake Intrusion and Mount Mollie dyke.

#	Description	Sample Number	Sample type/ Borehole/ Depth	Easting	Northing	Details	Age (Ma)
1	Northern limb Homogeneous, medium troctolite, unmineralized	18-SYB-001	drillcore CL0001 21–35 m	305453.19	5328330.35	Ab z, n=2, wm 7/6	1091.4 ± 1.4
2	Northern limb Vari-textured gabbro, minor sulphides, and Cr-spinel	18-SYB-002	drillcore CL0001 412–417 m	305453.19	5328330.35	Ab z, n=2, b, n=2, wm 7/6	1093.2 ± 1.2
3	Southern limb Coarse, vari-textured gabbro, minor sulphides, and Cr-spinel	18-SYB-111	drillcore CL0003 556–562 m	306239.91	5326523.72	Ab z, n=2, wm 7/6	1094.1 ± 1.4
4	Coarse, pink granophyre from centre of dyke	18-SYB-149	outcrop	313981.00	5325871.74	Ab z, n=2, bd=5, upper intercept	1096.3 ± 1.4

Abbreviations: Ab z = abraded zircon, bd = baddeleyite, n = number of fractions, wm 7/6 = weighted mean $^{207}Pb/^{206}Pb$ age.

completely filled with secondary amphibole, prehnite, and biotite, with accessory calcite and apatite. In comparison to the segregation vesicles described in the Norilsk ores, no primary magmatic phases have been recognized within the caps (Barnes et al., 2019). The silicate caps are typically attached to the upper margin of the sulphide bleb (Fig. 7c–e), although some droplets appear to be fully surrounded/encased by a secondary silicate halo. The morphology of the vapour phase is variable. Spherical, convex-up silicate caps, identical to those modelled by Mungall et al. (2015), are present (Fig. 7c,d) along with very irregular silicate attachments (Fig. 7e,f).

PRELIMINARY U-Pb RESULTS

New U-Pb results for the Crystal Lake Intrusion and Mount Mollie dyke are presented below. Note that many of these ages are preliminary, with additional analyses still in progress. The results of the four samples are summarized in Table 1. The reader is referred to Appendix 1 for details on U-Pb methods, and to Appendix 2 for a table of complete analytical data. Three samples from the Crystal Lake Intrusion were dated to determine (1) whether any age difference exists among the different phases and limbs; and (2) the relationship of the intrusion with the Pigeon River dykes and Mount Mollie dyke.

Crystal Lake Intrusion

The three samples from the Crystal Lake Intrusion yielded abundant, high-quality, fresh baddeleyite and magmatic zircon. For each sample, a population of the best quality, clear, and generally anhedral to subhedral zircon grains were selected for chemical abrasion pretreatment. Two single zircon grains of roughly prismatic form were analyzed for each sample and produced overlapping, concordant results, with good agreement among all three samples (Table 1, Fig. 8a–c). The mineralized vari-textured gabbro from the northern limb (sample 18-SYB-002; Fig. 8b) also includes the analyses of two multigrain baddeleyite fractions. Here, the baddeleyite data are concordant and show a high degree of overlap with the zircon data, producing a combined weighted average $^{207}Pb/^{206}Pb$ age of 1093.2 ± 1.2 Ma (Fig. 8b). Concordant zircons from the mineralized horizon of the southern limb yield a comparable weighted average $^{207}Pb/^{206}Pb$ age of 1094.1 ± 1.4 Ma (mean square weighted deviation (MSWD) = 2.6; Fig. 8c). The zircon data from the upper, unmineralized, homogenous troctolite unit is also concordant, producing a weighted average $^{207}Pb/^{206}Pb$ age of 1091.4 ± 1.4 Ma (MSWD = 1.3; Fig. 8a).

Combined U-Pb results for the best, concordant zircon and baddeleyite data from the three samples (including the following six fractions: 18-SYB-001 Z2; 18-SYB-002 Z1, Z2, B1, B2; and 18-SYB-111 Z2; Appendix 2) are presented in Figure 8d. They yield a weighted average $^{207}Pb/^{206}Pb$ age of crystallization of 1092.9 ± 0.8 Ma (MSWD = 0.55), and a concordia age (Ludwig, 2003) of 1092.3 ± 0.7 Ma. These new, preliminary ages are notably younger than the 1099.6 ± 1.2 Ma age reported by Heaman et al. (2007), which represents the weighted average $^{207}Pb/^{206}Pb$ age of the two more precise baddeleyite data points. Although less precise, Heaman's et al. (2007) upper intercept age of 1095.2 ± 3.7 Ma, overlaps within uncertainty with the new ages presented here.

Mount Mollie Dyke

A modest amount of zircon and baddeleyite crystals were recovered from sample 18-SYB-149, a coarse granophyre sampled from the centre of the Mount Mollie dyke on the mainland. Both the zircon and baddeleyite populations include altered grains of varying quality, with some of the zircon containing elevated

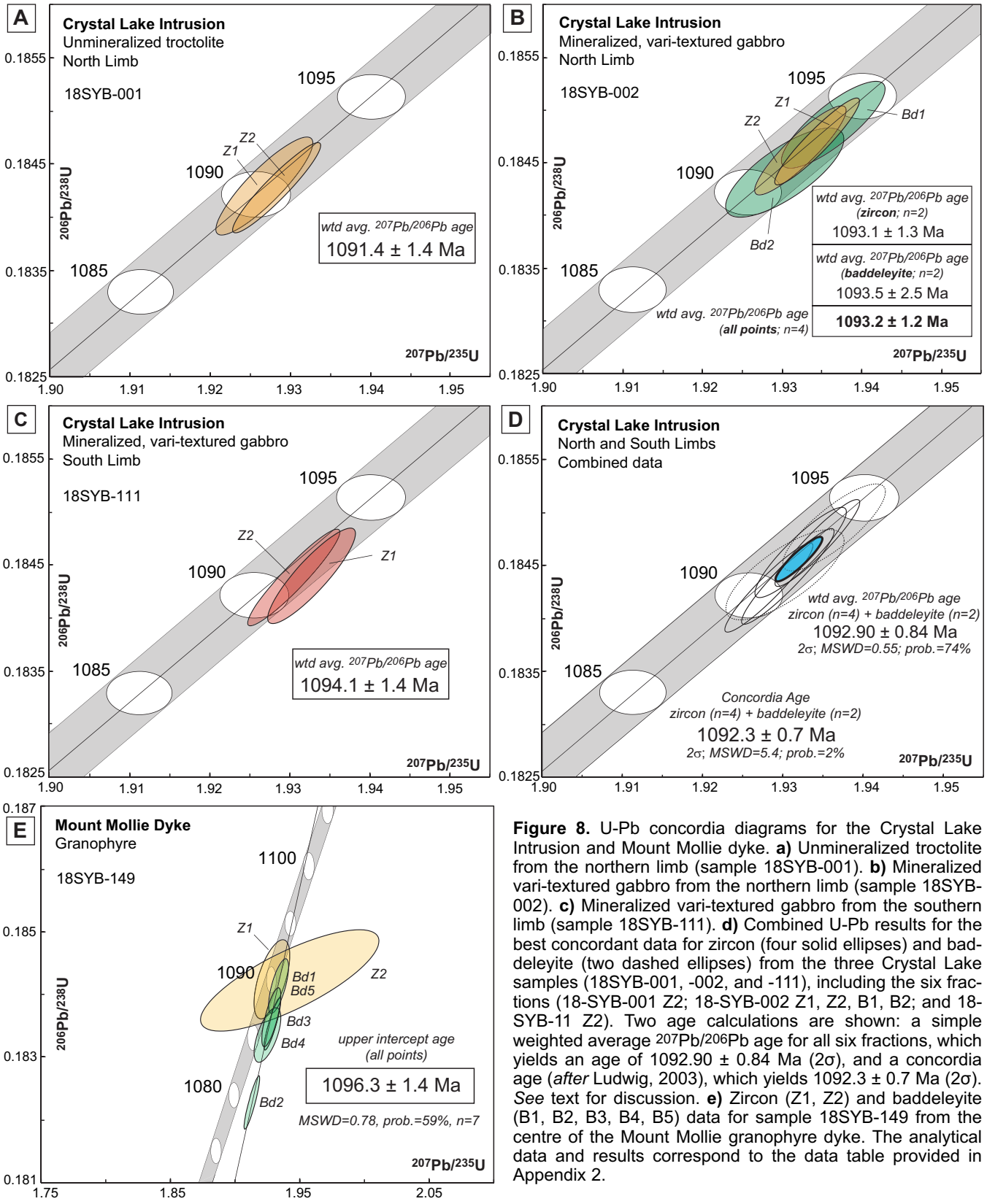

Figure 8. U-Pb concordia diagrams for the Crystal Lake Intrusion and Mount Mollie dyke. **a)** Unmineralized troctolite from the northern limb (sample 18SYB-001). **b)** Mineralized vari-textured gabbro from the northern limb (sample 18SYB-002). **c)** Mineralized vari-textured gabbro from the southern limb (sample 18SYB-111). **d)** Combined U-Pb results for the best concordant data for zircon (four solid ellipses) and baddeleyite (two dashed ellipses) from the three Crystal Lake samples (18SYB-001, -002, and -111), including the six fractions (18-SYB-001 Z2; 18-SYB-002 Z1, Z2, B1, B2; and 18-SYB-11 Z2). Two age calculations are shown: a simple weighted average $^{207}Pb/^{206}Pb$ age for all six fractions, which yields an age of 1092.90 ± 0.84 Ma (2σ), and a concordia age (*after* Ludwig, 2003), which yields 1092.3 ± 0.7 Ma (2σ). *See* text for discussion. **e)** Zircon (Z1, Z2) and baddeleyite (B1, B2, B3, B4, B5) data for sample 18SYB-149 from the centre of the Mount Mollie granophyre dyke. The analytical data and results correspond to the data table provided in Appendix 2.

common Pb. The two single zircon grains overlap in concordia space and straddle the concordia band (Fig. 8e). Fraction Z1 of sample 18SYB-149 is perfectly concordant with a $^{207}Pb/^{206}Pb$ age of 1089.6 Ma, whereas fraction Z2 is 1.5% discordant and yields a $^{207}Pb/^{206}Pb$ age of 1104.8 Ma, with the larger error associated with elevated common Pb. The five multi-grain, good quality, baddeleyite fractions are collinear

and, in this case, more precise than the zircon data. These fractions overlap concordia and yield an upper intercept age, anchored at 0 Ma, of 1096.4 ± 1.4 Ma (Fig. 8e). Together, the seven zircon and baddeleyite fractions (Z1, Z2, B1, B2, B3, B4, B5) have an upper intercept age of 1096.3 ± 1.4 Ma (MSWD = 0.78; Fig. 8e). This age is considerably younger than the previously reported age of 1109.3 ± 6.3 Ma (Hollings et al., 2010), which was a weighted average $^{207}Pb/^{206}Pb$ age from two less precise baddeleyite fractions.

PLATINUM GROUP MINERALOGY OF THE CRYSTAL LAKE INTRUSION

Over 8000 platinum group minerals (PGMs) and PMMs (total area of 1,625,255 μm^2) have been characterized. Results indicate that 91 to 99% of Pd is hosted by PMMs, with the rest residing in solid solution within sulphides. Platinum occurs almost exclusively (>99%) as discrete mineral phases. Precious metal-bearing minerals were successfully liberated when milled to P80 of 75 μm (80% material passing 75 μm), with the majority of grains occurring either completely free or attached to sulphides/silicates. Platinum-group minerals completely enclosed in sulphide or silicate phases were rare, although submicron PGM inclusions (too small to measure on the SEM) were commonly identified in nickel arsenide minerals.

The PMM assemblage of the Crystal Lake Intrusion is dominated by Pt-As (22%) and Pd-Pd±Sb±Te (41%)-bearing minerals. Of all PMMs classified, Pt- and Pd-bearing phases constitute 23% and 69% (by area), respectively. The PGMs and PMMs were grouped into seven types (in order of abundance by area): 1) Pd bismuthides (±Sb, ±Te); 2) Pt arsenides; 3) Pd/Pt-Sn±Sb minerals; 4) Pd antimonides; 5) composite grains; 6) Au-Ag minerals; and 7) Pd-nickel arsenides. Other minor mineral types identified (each constituting <1% of the assemblage) include Pd tellurides, Pd-Pt alloys (including rare Pt-Fe alloys), Pd bismuth-selenides, Pd/Pt bismuth-tellurides, and Rh/Ru sulphur-arsenides (Table 2). As recognized within many other Ni-Cu-PGE sulphide deposits, the PMMs reside in close proximity to sulphides (Fig. 9a–d). The PGMs typically occur (1) fully enclosed in sulphides, near the margins of the sulphide; (2) attached to sulphides; and (3) as satellite grains within secondary silicates surrounding sulphides (Fig. 9a–d).

The PMM assemblage of the Crystal Lake Intrusion is summarized in Table 2. By area, the most significant Pd-bearing minerals are unconstrained Pd-Bi-Sb±Te phases, froodite ($PdBi_2$), unconstrained Pd-Sn-Sb phases, stibiopalladinite (Pd_5+xSb_{2-x}), paolovite (Pd_2Sn), sobelevskite (PdBi), and electrum, all of which form >4% of the total PMM assemblage. Grains characterized by the exsolution of multiple minerals (Fig. 9e–h) were classified as composites and represent 5% (by area) of the total mineral assemblage. Composite grains, although variable in their mineralogy, are overwhelmingly dominated by the exsolution of froodite with unconstrained Pd-Bi±Sb±Te phases and Pd-Sb-Sn phases exsolved with electrum (Fig. 9f,h). Sperrylite ($PtAs_2$) represents the most important Pt-bearing phase. Platinum has also been identified as rare Pt-Fe alloys, rustenburgite ($(Pd,Pd)_3Sn$), and nigglite (PtSn).

The presence of abundant Cr-spinel does not appear to have any significant control over the mineralogy of PGMs, with the Cr-rich and Cr-poor samples characterized by near comparable PMM assemblages (Table 2, Fig. 10). A noticeable difference among the four samples studied is the greater abundance of PMMs identified in the Cr-bearing rocks of the northern limb, which have a total area of 659,555 μm^2, in comparison to <390,000 μm^2 in the other three samples. Furthermore this sample is also characterized by the abundance of Pd/Pt-Sn±Sb±As phases, which form 36% of the PMM assemblage. Elsewhere Sn-bearing phases represent only 0.6–3.2% of the overall mineral assemblage. Although the assemblages of the northern and southern limbs are broadly comparable, some subtle differences are recognized (Table 2, Fig. 10). Occurrences of Pd arsenides (e.g. palladoarsenide (Pd_2As) and unconstrained Pd-As phases), Pd tellurides, Pt-Pd alloys, and Pd bismuth-selenides (padmaite PdBiSe) are restricted to the northern limb assemblages (Table 2). The southern limb assemblages are characterized by Pd/Pt bismuth-tellurides (e.g. michenerite PdBiTe, maslovite PtBiTe), and Pd bismuth-arsenides and greater abundances of Pd-Ni arsenides (menshikovite $Pd_3Ni_2As_3$, majakite PdNiAs).

DISTRIBUTION OF ELEMENTS WITHIN SULPHIDES: LA-ICP-MS RESULTS

The precious metal and chalcophile element contents of sulphides from the Crystal Lake Intrusion, determined by LA-ICP-MS analyses, are summarized in Figure 11. The preliminary data show that the concentration of metals and trace elements is variable, not only between the primary sulphide phases but also among the different ore textures (i.e. contact, granular, and fan-textured pentlandite). Primary sulphide phases typically contain low concentrations of PGEs, with Os, Ir, and Pt, in addition to Au, measuring close to or below the limit of detection. Concentrations of Ru, Rh, and Pd are also low in pyrrhotite and chalcopyrite, but are elevated in pentlandite (>1–150 ppm Pd). The data suggests Mo, As, and Bi are preferentially concentrated in pyrrhotite and pentlandite (Fig. 11). Other elements, including Se, appear more comparable throughout the various sulphide phases.

Table 2. Summary of the platinum group minerals (PGMs) and precious metal-bearing mineral (PMM) assemblages (by area μm2) of the composite samples studied from the Crystal Lake Intrusion.

		Southern Limb		Northern Limb		Total Area
PMMs	Formula	Cr-rich	Cr-poor	Cr-rich	Cr-poor	
Pd bismuthides		***35,779***	***32,380***	***191,262***	***98,537***	**357,957**
Froodite	$PdBi_2$	35,087	28,384	128,545	96,771	
Sobelevskite	PdBi	692	3995	62,717	1765	
Pd-Bi-Sb±Te	unconstrained	***44,799***	***157,768***	***77,040***	***46,178***	***325,785***
Pt arsenide		***85,330***	***86,262***	***59,622***	***137,031***	***368,245***
Sperrlyite	$PtAs_2$	85,330	86,262	59,622	137,031	
Pd/Pt-Sn±Sb±As		***3320***	**2180**	***240,557***	***11,142***	***257,200***
Atokite	$(Pd,Pt)_3Sn$	25	765	474	158	
Palarstanide	$Pd5(Sn,As)_2$	1827	1324			
Paolovite	Pd_2Sn	516		102,629	1619	
Rustenburgite	$(Pt,Pd)_3Sn$		91			
Niggliite	PtSn				20	
Unconstrained	Pd-Sn-Sb	843		137,454	9345	
Unconstrained	Pd-Sn-As	109				
Pd antimonides±As		***37,295***	***76,049***	***26,026***	***4123***	**143,493**
Stibiopalladanite	$Pd_{5+x}Sb_{2-x}$	36,328	62,250	26,026	4123	
Sudburyite	$Pd_{0.75}Ni_{0.25}Sb$		13,528			
Isomertieite	$Pd_{11}Sb_2As_2$	232				
Mertieite	$Pd_{11}(Sb,As)_4$	225				
Unconstrained	Pd-Sb-As	510	271			
Composite		***10,740***	***2853***	***31,924***	***31,384***	**76,902**
Au-Ag minerals	Au(Ag)	***8507***	***15,453***	***28,563***	***15,527***	**68,050**
Pd nickel arsenides		***3581***	***6348***	***348***	***118***	**10,395**
Menshikovite	$Pd_3Ni_2As_3$	2433	2512	348		
Majakite	PdNiAs	1149	3836		118	
Pd bismuth-tellurides		***853***	***8234***			**9087**
Unconstrained	Pd-Bi-Te	507	617			
Michenerite	PdBiTe	346	7617			
Pd-Pt alloys				***3079***		**3079**
Zvyagintsevite	Pd_3Pb			2152		
Pt-Fe				928		
Pd-Bi-Se					***1641***	**1641**
Padmaite	PdBiSe				1641	
Rh/Ru sulphur-arsenides		***872***	***119***	***185***	***38***	**1214**
Hollingworthite	RhAsS	813	71	185	38	
Ruarsite	RuAsS	59	47			
Pd arsenides		***85***		***438***	***567***	**1090**
Stillwaterite	Pd_8As_3	85		119		
Palladoarsenide	Pd_2As			99	47	
Unconstrained Pd-As	Pd-As			220	520	
Sn oxide (Cassiterite)	SnO_2			***393***		**393**
Pt bismuth-telluride (Maslovite)	PtBiTe		***376***			**376**
Pd bismuth-arsenide	Pd-Bi-As	***39***	***114***			**153**
Unconstrained Pd-Bi-As						
Pd telluride (Keithconnite)	$Pd_{3-x}Te$ (x=0.14 to 0.43)			***118***		**118**
Bismuthide (Bismuthinite)	Bi_2S_3				***79***	**79**

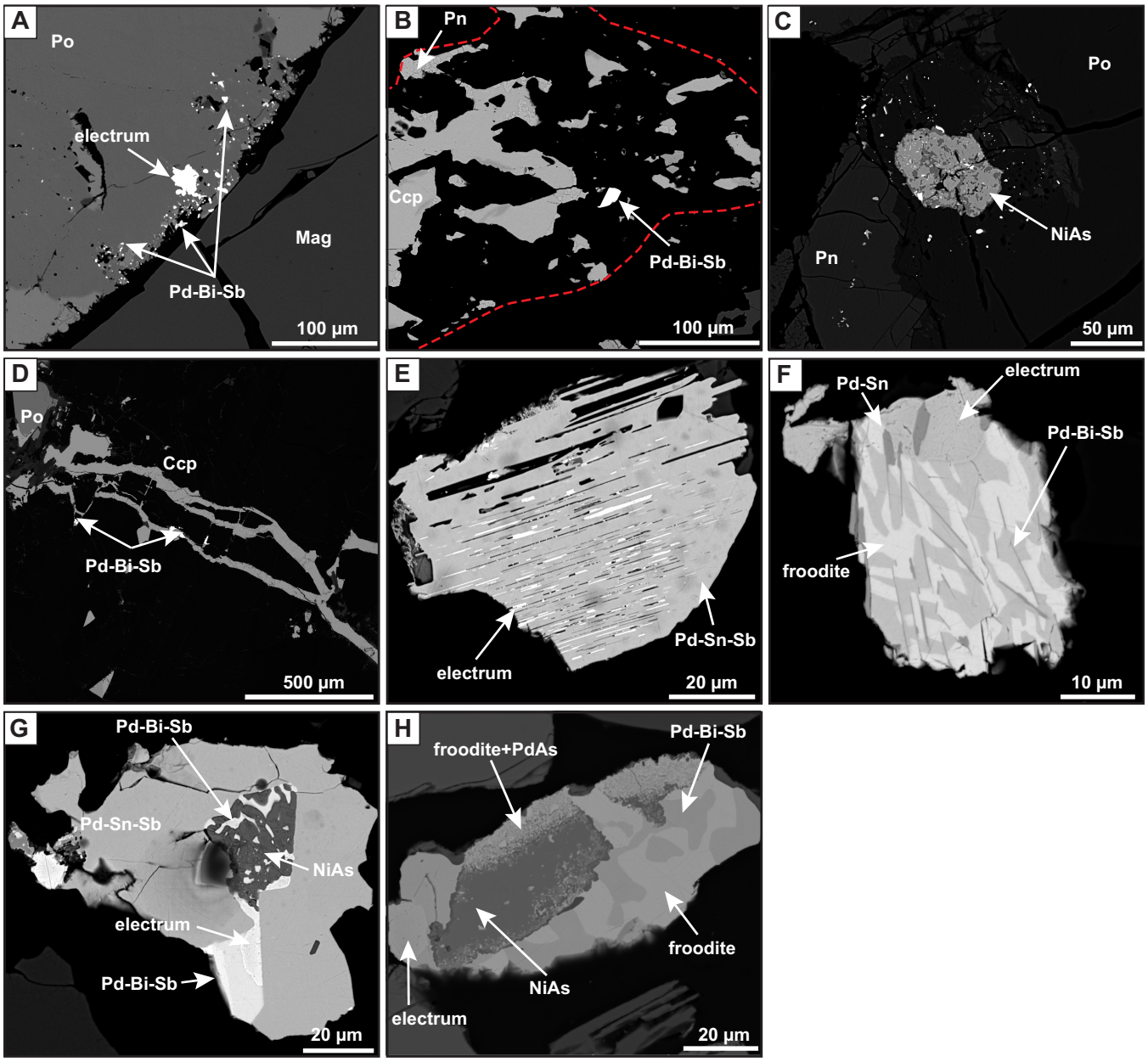

Figure 9. a–d) Back-scattered electron images showing the associations of precious metal-bearing minerals observed within the Crystal Lake Intrusion. **a)** A cluster of platinum group minerals (PGMs) and electrum enclosed within pyrrhotite, near the margin of a sulphide bleb. **b)** A PGM located within secondary silicates, in close proximity to a sulphide bleb. **c)** A cluster of PGMs occurring in close association with a nickel arsenide within the massive sulphide horizon. PGMs are also enclosed within pyrrhotite and pentlandite. **d)** PGMs associated with chalcopyrite veinlets. e–h) Back-scattered electron images of composite PGMs. **e)** Exsolution of electrum within a Pd-Sn-Sb-bearing mineral. **f)** Composite grain containing electrum (Au-Ag), froodite (PdBi2), Pd-Bi-Sb, and Pd-Sn phases. **g)** Pd-Sn-Sb-bearing mineral with electrum, Pd-Bi-Sb, and nickel arsenide. Note the inclusions of PGMs within nickel arsenide. **h)** A composite PGM grain associated with nickel arsenide. Note the fine-grained nature of the froodite and Pd-As-bearing phase occurring in association with the nickel arsenide. Abbreviations: Ccp = chalcopyrite, Mag = magnetite, Pn = pentlandite, Po = pyrrhotite,

Within the Crystal Lake Intrusion, pentlandite represents the main carrier of Pd in solid solution (>1–150 ppm) and accounts for 1–9% of the total Pd contents, with the rest residing in discrete PGMs. The Pd and trace element contents of pentlandite are variable among the massive, globular, and blebby sulphide ores (Fig. 11). The globular ores, which contain the lowest Co concentrations, are characterized by significantly elevated Pd concentrations (up to 150 ppm, mean 79 ppm). The blebby and massive ores, which contain comparable Co concentrations, contain <38 ppm and <3 ppm Pd, respectively. Though the globular and blebby ores appear to have similar As, Te, Bi, and Se contents, the massive ores are characterized by elevated Bi and As contents. The Pd content of the three distinct pentlandite textures (contact, granular, and fan;

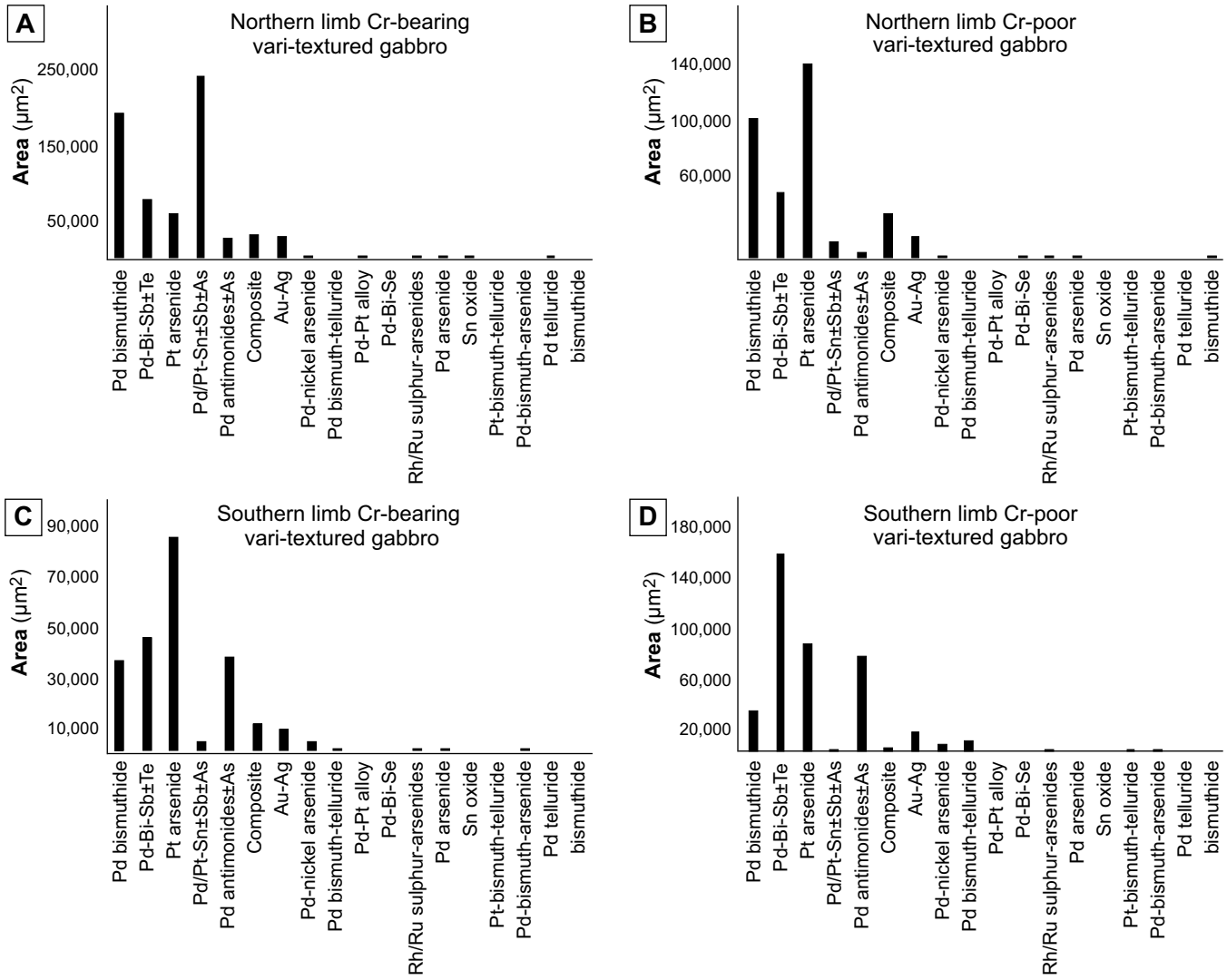

Figure 10. Histograms showing the platinum group mineral assemblage (by area): **a)** Cr-spinel-bearing rocks of the northern limb; **b)** vari-textured gabbros of the northern limb with no visible Cr-spinel; **c)** Cr-spinel bearing rocks of the southern limb; and **d)** vari-textured gabbros of the southern limb with no visible Cr-spinel.

Fig. 11) is variable. Palladium concentrations are noticeably elevated in the contact and granular pentlandite. Within a single sulphide droplet/bleb, the Pd contents of contact pentlandite are often elevated relative to granular or fan pentlandite.

Laser ablation ICP-MS imaging (Fig. 12) of the different sulphide ore textures, provides further insights into the spatial distribution of PGE and trace-elements at the microscopic scale. Within the unaltered primary magmatic assemblage, Pd is uniformly distributed within pentlandite regardless of its concentration (Fig. 12a,c,d). Pentlandite within the secondary sulphide assemblages is characterized by more heterogeneous element distributions (e.g. Pd, As, Bi; Fig. 12b) with evidence of remobilization of Pd and As, which appear to be broadly related. Complex zoning of several elements (e.g. As, Mo, Rh, Ru, Ir, and Re) is most commonly observed in pentlandite that is developed at the contact between pyrrhotite and chalcopyrite (Fig. 12a, c–d). These elements are depleted in pentlandite adjacent to the contact with chalcopyrite and enriched towards the pyrrhotite. Within some samples, the zonation is marked by a very distinctive, sharp boundary that clearly crosscuts the pentlandite grain (Mo in Fig. 12c). Although some zonation of Mo and Te are observed in chalcopyrite, elements are uniformly distributed throughout pyrrhotite, except where elements are preferentially concentrated into a microfabric.

A strong microfabric (Fig. 12d), which runs parallel to small micro-fractures, has been observed within some of the primary magmatic globular sulphides. The fabric is defined by several elements, including As, Mo, Pd, Re, Pb, Bi, V, and Cr, which appear to be preferentially concentrated along thin, parallel, linear features that are best developed within pyrrhotite and pentlandite (contact, granular, and fan), and occasionally extend into adjacent chalcopyrite. This fabric is not confined to a particular sulphide phase, with As, Mo,

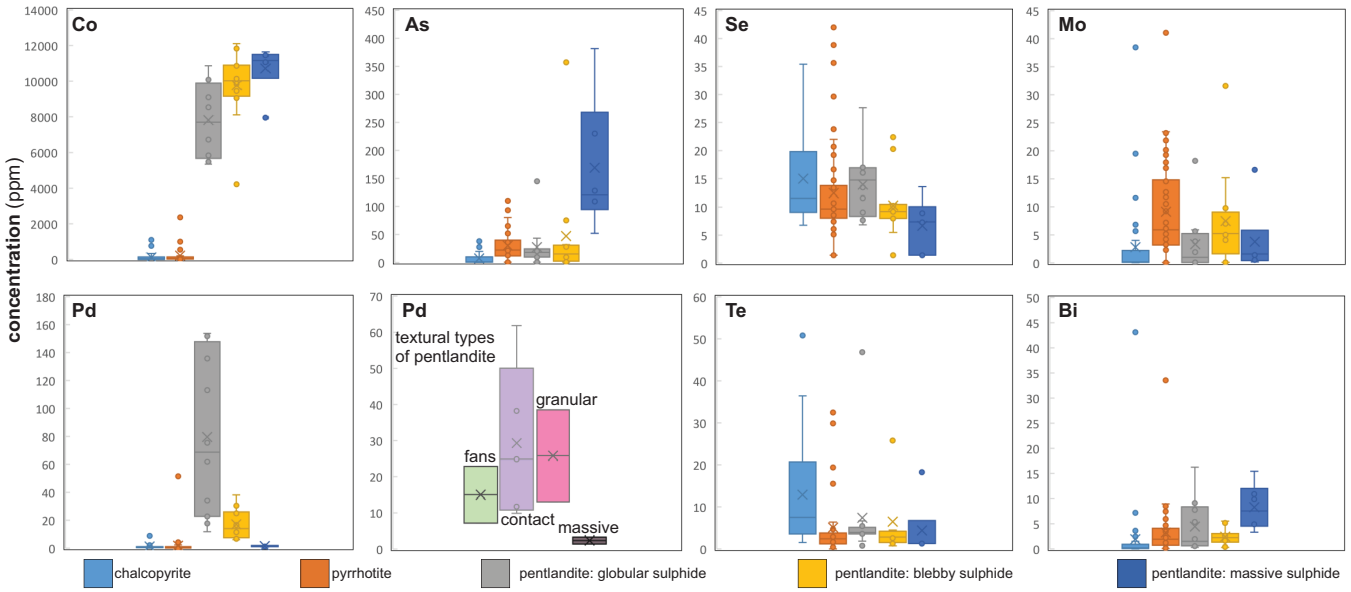

Figure 11. LA-ICP-MS results showing the compositional differences between the different sulphide phases. Palladium concentration for the various textures of pentlandite are also shown. The mean of the data set is represented by X.

and Re clearly crosscutting the primary sulphide contacts (Fig. 12d). This suggests preferential remobilization of these elements subsequent to fractionation of monosulphide solid solution (mss) and intermediate solid solution (iss). Late silicate-infilled fractures clearly cut the fabric as shown in the As map (Fig. 12d).

DISCUSSION

Emplacement of the Crystal Lake Intrusion and Mount Mollie Dyke

New ages for the Crystal Lake Intrusion and Mount Mollie dyke are not in agreement with those previously reported, therefore our data provide new temporal constraints for magmatism and ore formation within the MCR. The newly refined 1092.9 ± 0.8 Ma age for the Crystal Lake Intrusion is significantly younger than the previously reported age of 1099.6 ± 1.2 Ma (Heaman et al., 2007), and places it towards the end of the 'mainstage' of the rift's development. The Crystal Lake Intrusion thus appears to be the final intrusive pulse of a ca. 1097–1092 Ma magmatic episode that is represented by the dense Pigeon River swarm, the Mount Mollie dyke (*see below*), and the Beaver Bay Complex (*see* Bleeker et al., 2020). This magmatic episode is also well represented within the volcanic sequences of the North Shore and Portage Lake volcanic groups. The new ages confirm that the Crystal Lake Intrusion is not related to the ca. 1099 Ma Duluth Complex and northwest-trending Cloud River dykes (Bleeker et al., 2020). Furthermore, the age reported here is in better agreement with field observations, suggesting emplacement post-dates the ca. 1096 Ma north-northeast-trending Pigeon River dykes (Bleeker et al., 2020).

Our data also indicates that the Mount Mollie dyke is considerably younger than previously estimated (1109.3 ± 6.3 Ma; Hollings et al., 2010). Our new preliminary age of 1096.3 ± 1.4 Ma is now consistent with its normal polarity and suggests that it is coeval with the Pigeon River dyke swarm (Bleeker et al., 2020). Although the southern limb of the Crystal Lake Intrusion (sample 18-SYB-111) is just within error of the preliminary Mount Mollie age, our overall data suggests that these two intrusions are not directly related. Thus from the data currently available, Mount Mollie is thought to not be a feeder dyke to the Crystal Lake Intrusion. With additional zircon and baddeleyite analyses still in progress for both the Crystal Lake Intrusion and the Mount Mollie dyke, we hope to better resolve this relationship and provide a more refined (i.e. concordant) age for the latter.

From the newly refined ages presented here and in Bleeker et al. (2020), it is becoming increasingly apparent that the Ni-Cu-PGE mineralization is associated with multiple magmatic episodes throughout the evolution of the rift. Furthermore, ore formation appears to show a close temporal relationship with the various volcanic packages. From the current data, we are unable to conclude whether there is any evident age difference between the northern and southern limbs, or the unmineralized and mineralized phases of the Crystal Lake Intrusion, although there is a hint in the data that the unmineralized troctolite of the northern limb may be the youngest phase (compare Fig. 8a,b). Only additional high-precision analyses of well behaved zircons can settle this issue by reducing the errors on the weighted means to well below 1 Myr.

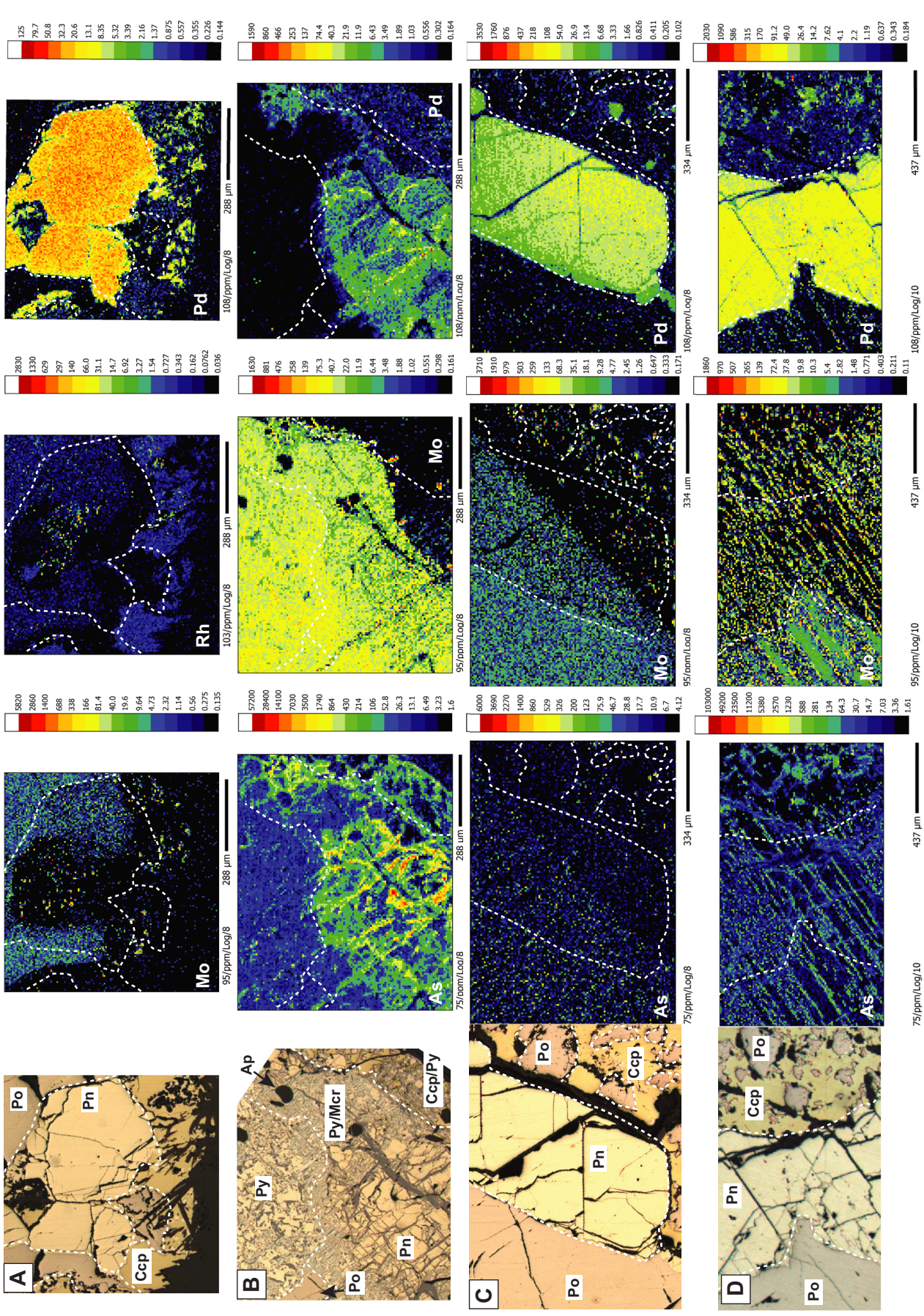

Figure 12. LA-ICP-MS element maps of primary magmatic **(a–c)** and **(d)** secondary sulphide assemblages. Abbreviations: Ap = apatite, Ccp = chalcopyrite, Mcr = marcacite, Pn = pentlandite, Po = pyrrhotite, Py = pyrite.

Conditions During Ore Formation: Sulphur Saturation, Contamination, and Volatiles

Within magmatic Ni-Cu-PGE sulphide systems, the addition of crustal S is considered critical for ore genesis. Although limited, S isotope data for the Crystal Lake Intrusion is consistent with the incorporation of significant sedimentary-derived S, with $\delta^{34}S$ values ranging from +1.4 to +21‰ (Thomas, 2015; O'Brien, 2018). The addition of crustal S has in the past been attributed to two key processes: 1) devolatilization and release of S from a thermal aureole; and 2) by direct melting and assimilation of wall rocks and sulphide-bearing xenoliths. After consideration of mass balance constraints and the time-scale of these processes, Robertson et al. (2015) concluded that S liberated from thermal aureoles is negligible in terms of ore formation, with dynamic wall-rock and xenolith melting being the most efficient and dominant mechanism for S transfer into the magma. With partially digested S-bearing xenoliths associated with the S-bearing taxitic rocks of the Crystal Lake Intrusion, in addition to a lack of any footwall control on the S isotopic data, we propose that crustal S was largely incorporated into the Crystal Lake magma through the melting of S-bearing xenoliths and wall rock, likely occurring both within the feeder dyke and during emplacement. Although S is available in the immediate footwall rocks, the heterogeneous nature of the S isotopic data set is more consistent with crustal S being derived distally relative to the final magma emplacement site. Therefore, like the Duluth Complex, the Crystal Lake Intrusion is interpreted to have been emplaced in S-saturated host rocks. Consequently, we therefore interpret the observed increase in S/Se ratios (Eckstrand and Cogulu, 1986) with proximity to the basal footwall contact as evidence of localized, in situ S contamination. This contamination event likely only contributed minor amounts of S into the system and is not considered critical for ore formation.

Within the Crystal Lake Intrusion, the contact of the mineralized taxitic rocks with the overlying unmineralized troctolite and olivine gabbro is marked by a distinct shift in the Cu/Pd ratio, from mantle-like signatures to greater than mantle or 'depleted' values (>10^4), respectively. The elevated Cu/Pd values within the upper, unmineralized units of both the northern and southern limbs, are consistent with PGE depletion of the magma through removal/segregation of sulphides. These ratios could indicate the early segregation of sulphides at depth, prior to final emplacement, as is also indicated by the preservation of large (>1 cm) globular sulphides (discussed below) and identification of 'ripped' sulphide clasts. Alternatively, the elevated Cu/Pd ratios could be indicative of in situ depletion of Pd through genesis of the underlying mineralization. This interpretation is only supported by several boreholes where a decrease in the Cu/Pd ratio towards the contact with the sulphide-bearing taxitic rocks is observed.

Constraining the initial source(s) of crustal S is extremely difficult within Ni-Cu-PGE systems as the transport and settling of xenoliths and the release of S is controlled by many factors (e.g. flow rate, temperature, density, size of xenoliths). Barnes and Robertson (2019), however, have recently shown that dissolution and melting rates of sulphide droplets and xenoliths, respectively, are slow relative to magma flow rates. The implications of this are that xenoliths, in addition to sulphide droplets, can be transported significant distances within a mafic system and that S can be released from the xenoliths both during transport and post-deposition. Considering the Crystal Lake Intrusion, it is feasible that the S-bearing sedimentary xenoliths (which were likely more buoyant than the carrier magma) were assimilated some distance (up to kilometres) from the final site of deposition. The observed association of mineralization, both with xenoliths and taxitic rocks, could suggest deposition of sulphide liquid together with the partially dissolved xenoliths, which continued to melt and release S (and volatiles) after deposition. As indicated by Barnes and Robertson (2019), this may provide some explanation for the close association of the ores, such as those at Crystal Lake, with contaminated/taxitic rocks.

Magmatic Ni-Cu-PGE sulphide deposits form in highly dynamic systems where there is prolonged magma flow (e.g. Lesher 1989; Bleeker, 1990a,b; Naldrett, 2004; Barnes et al., 2016). Continued recycling of the sulphide and thus multiple cycles of deposition, migration, re-entrainment, and re-deposition, are also thought to be critical in generating the high tenors of many deposits (e.g. Norilsk, Voisey's Bay). This notion is supported by computational fluid dynamic modelling, which shows that a segregated sulphide pool can be easily entrained back into the magma (Barnes and Robertson, 2019). At Crystal Lake, a degree of reworking is indicated by the presence of brecciated ores and fragments of Cr-spinel and gabbro within the taxitic units. Direct evidence of reworking of a deeper sulphide pool is potentially provided by the preservation of large sulphide droplets (>1 cm in size), which have been shown to be indicative of limited transport distance and thus proximity to a sulphide source or a reworked sulphide pool (Robertson et al., 2016). The internal differentiation (Cu-rich and Cu-poor) observed in many of these larger sulphide droplets (e.g. Fig. 7d) suggests that they were emplaced while molten, rather than being derived from a previously solidified sulphide liquid.

One of the more unique features of the ore-bearing taxites of the Crystal Lake Intrusion, is the presence of

segregation vesicles. Although vapour saturation and degassing are not common features of mafic Ni-Cu-PGE systems, segregation vesicles similar to those described here, have also been identified within the Norilsk ores, where they are interpreted to indicate shallow emplacement under low confining pressures (Barnes et al., 2019). The segregation vesicles within the Crystal Lake Intrusion could be interpreted to have formed under similar conditions. However, the lack of flattened bubble-droplet geometries, which Barnes et al. (2019) use as evidence for first boiling, in addition to the presence of irregular gas bubble attachments, and the identification of vesicles in the absence of sulphide could indicate that volatile saturation resulted from second boiling. Regardless of the timing of vapour saturation, it appears that within both the Norilsk and Crystal Lake Intrusions evidence of degassing is limited to the taxitic rocks, suggesting vapour saturation is favoured by the assimilation of volatile-rich sediments within these systems.

The role of volatiles within the Crystal Lake Intrusion and many other magmatic systems is indicated by the presence of distinctive pegmatitic-bearing units. Whereas the pegmatites of the Merensky Reef and other intrusions are interpreted to result from the crystallization of late-stage, ultra-fractionated volatile-rich material derived from trapped liquid in the cumulus pile (Barnes and Campbell, 1988), the marginal pegmatoidal units in the Norilsk intrusions, are thought to result from the local assimilation of volatiles during prolonged magma flow (Barnes et al., 2016). In the Crystal Lake Intrusion, taxitic rocks are widespread, occurring primarily at the margins of the intrusion and are thus also interpreted to be derived by local assimilation of volatile-rich sediments. Thermal modelling demonstrates that preheating of the basement facilitates partial melting and incorporation of volatiles into the magma (Karykowski et al., 2018), thus multiple magma influxes or prolonged flow are required to generate the significant volumes of pegmatitic material. The Crystal Lake Intrusion was therefore likely emplaced as a series of magmatic pulses, as suggested by Mainwaring and Watkinson (1981), Thomas (2015), and O'Brien (2018). Although the relationship of the taxitic rocks with the overlying unmineralized troctolites and olivine gabbros is not well constrained, preheating of the basement may have resulted from the earlier emplacement of these upper unmineralized units.

Controls on Metal and Trace Element Distributions

The distribution of PGEs within the Crystal Lake Intrusion, as revealed by detailed characterization of the PGM assemblages and LA-ICP-MS analyses, is consistent with the fractionation and crystallization of a magmatic sulphide liquid (Cabri and Laflamme, 1976; Fleet et al., 1993; Li et al., 1996; Ballhaus et al., 2001; Mungall et al., 2005; Holwell and McDonald, 2010). The abundance of Pd- and Pt-bearing PGMs, which account for >91% of these elements, in addition to the close association of PGMs with base metal sulphides, reflects the preferential partitioning of these elements from a fractionating sulphide liquid into a late-stage semi-metal-rich melt (Fleet et al., 1993; Helmy et al., 2007, 2010; Tomkins, 2010). The availability of Te, As, Bi, Sb, and Sn (referred to as TABS) within the magma and therefore the ability for a semi-metal-rich melt to fractionate from the sulphide liquid is thought to be primarily controlled by the assimilation of country rocks (Samalens et al., 2017). Although not significant to the overall metal budget at Crystal Lake, appreciable concentrations of Pd (<150 ppm) in pentlandite suggests that Pd was also concentrated within the fractionating sulphide liquid, which, upon cooling, was preferentially partitioned into exsolved pentlandite. For ore processing and extraction, the distribution of Pd and Pt primarily as PGMs in base metal sulphides is favourable for effective recovery as by-products of the Ni-Cu ores. Platinum group minerals hosted in sulphides rather than silicates are more easily liberated and are thus amenable for recovery by gravity concentration and flotation methods. For the Crystal Lake ores, we show that the majority of PGMs are liberated from their host when milled to P80 of 75 μm.

The PGM assemblage of the Crystal Lake Intrusion is dominated by varying proportions of Pd bismuthides, Pd-Bi-Sb-Te phases, Pt arsenides, and Pd antimonides (Table 2, Fig. 10). The observed similarity of the PGM assemblages of the northern and southern limbs suggests that the magma from which these ores crystallized was not distinct in its composition, and that the distribution and mineralogy of PGMs was controlled by the same processes throughout the intrusion. Furthermore, it is evident that the precipitation of Cr-spinel, which in some PGE-rich deposits (e.g. Merensky Reef) is known to effectively concentrate PGEs (Kinloch, 1982; von Gruenewaldt et al., 1989: Kinloch and Peyerl, 1990; Barnes and Maier, 2002; Godel et al., 2007), has no effect on the PGM assemblage in the Crystal Lake Intrusion. Whereas some variation in the proportion of the main PGM types is noted among the four samples studied: the Cr-rich ores of the northern limb are notably more abundant in Pd/Pd-Sn±Sb±As-bearing phases. This could potentially reflect a local footwall control. To understand whether the local footwall plays an important role in controlling the final PGM assemblage, a detailed comparison of MCR deposits hosted both within Paleoproterozoic sediments and Archean basement would be required.

The presence of significant concentrations of Pd in solid solution within pentlandite is a well documented feature of many Ni-Cu-PGE deposits (Norilsk, Voisey's Bay) and is considered a function of texture and therefore the temperature at which pentlandite exsolved (Piña et al., 2012; Mansur et al., 2019). Until recently, pentlandite was commonly interpreted to exsolve directly from mss, however, this model can not account for the preferential partitioning of Pd into pentlandite due to its incompatibility with mss (Liu and Brenan, 2015). Thus, a model that invokes some interaction/diffusion with the fractionating sulphide liquid is required (e.g. Piña et al., 2012; Mansur et al., 2019). Experimental studies have shown that a high-temperature Ni-rich phase can form via a peritectic reaction of mss with the fractionating sulphide liquid between 800 and 870°C (Waldner and Pelton, 2004; Kosyakov and Sinyakova, 2012; Kitakaze et al., 2016). This phase, which had previously not been documented in nature, is recognized in the Norilsk and Merensky ores by contact-style pentlandite that is characterized by zonation of Mo, Rh, Ru, Re, Os, and Ir along the pentlandite-chalcopyrite contact (Mansur et al., 2019). In the Crystal Lake Intrusion, three distinct textures of Pn are documented and referred to as contact, granular, and flame/fan. The homogeneous distributions of elements in granular and fan pentlandite, which contain comparable concentrations of Pd in a single sample, are interpreted to have exsolved from mss at <650°C and 200°C, respectively (Kelly and Vaughan, 1983). The depletion of Mo, Rh, Ru, and Re in the contact-style pentlandite along the contact with chalcopyrite (Fig. 12a,c,d) is consistent with Mansur's et al. (2019) observations and could be indicative of formation at ~870°C through peritectic reaction. Within a sulphide droplet, the elevated Pd concentrations in contact pentlandite relative to the lower temperature granular and fan textures support this interpretation and indicate partitioning of Pd, which is concentrated in the fractionated liquid into pentlandite during the peritectic reaction with mss.

The preferential concentration of various elements, including As, Mo, Pd, Re, and Bi into discrete linear features (Fig. 12d), is a rather interesting and unique feature of the Crystal Lake sulphide ores and is thought to be related to either sulphide fractionation, low-temperature alteration or deformation. Several observations indicate that the preferential remobilization of elements at the micro-scale occurred at low temperatures, post-sulphide fractionation: 1) the fabric is not confined to a single phase and crosscuts sulphide boundaries; 2) the fabric is preserved in high- and low-temperature pentlandite (contact, granular, and fans); 3) exsolutions within pyrrhotite do not correspond with the fabric; and 4) the linear features coincide with submicroscopic fractures. At this point, it is difficult to reconcile the exact process controlling the observed element distribution patterns. However, with the microfabric being restricted to globular droplets, and thus not being observed throughout the primary magmatic sulphide assemblage, this may indicate that it is a localized feature and not representative of a deposit-scale deformation event.

Like many other Ni-Cu-PGE deposits, the Crystal Lake ores have experienced some degree of low-temperature alteration, as indicated by the replacement of primary sulphides by low-temperature phases. The more heterogeneous distributions of Pd and As in the altered secondary sulphide assemblages (Fig. 12b) suggests these elements were locally remobilized during low-temperature alteration. The close association of PGMs with sulphides in addition to PGMs residing within silicate alteration halos around sulphides suggests remobilization was localized. This is further supported by whole-rock data, which shows strong positive correlations between Pd, Ni, Cu, and S (R = >0.7).

SUMMARY

The initial U-Pb results of this study indicate that the Crystal Lake Intrusion should now be considered as the youngest known mineralized intrusion within the MCR, representing the last intrusive phase of a major magmatic episode at ca. 1097 to 1092 Ma. This younger age suggests a correlation of the Crystal Lake Intrusion, not with the Duluth Complex, but rather with the younger intrusive phases of the Beaver Bay Complex.

The new field, petrographic, and mineralogical observations show that the Ni-Cu-PGE mineralization of the Crystal Lake Intrusion is broadly comparable to the ores of Norilsk, and are associated with reworked, volatile-rich, contaminated taxitic rocks that crystallized under low confining pressures. The similarity of the platinum group mineral assemblage, which is largely controlled by the availability of semi-metals through contamination, indicates crystallization from compositionally similar magmas. With evidence of reworking of the mineralized horizons and of a potentially deeper sulphide source/pool in the southern limb, the Crystal Lake ores appear to have formed in a more dynamic setting than previously thought and could possibly represent a conduit-type setting rather than a more stable intrusive environment. The addition of crustal S, through assimilation and melting of wall rocks and xenoliths prior to final emplacement, is considered critical for ore genesis. The local addition of S during emplacement is not considered critical for inducing S saturation. To gain a more comprehensive understanding of the timing of S saturation relative to emplacement, a more detailed S isotopic study of the intrusion is required.

With our new U-Pb results indicating that the Mount Mollie dyke is not a specific feeder to the Crystal Lake intrusion, we suggest that at least part of the feeder system may extend beneath the southern limb of the intrusion, which is characterized by a distinct magnetic anomaly.

ACKNOWLEDGMENTS

This report is a contribution to NRCan's Targeted Geoscience Initiative Program (TGI-5). Support for this study was provided through the Orthomagmatic Ni-Cu-PGE-Cr Ore Systems Project's 'Activity NC-1.3: Controls on the localization and timing of mineralized intrusions in intra-continental rift systems, with a specific focus on the ca. 1.1 Ga Midcontinent Rift system'.

The authors thank our partners at Rio Tinto (Dean Rossell, Brian Goldner) for providing access to drill core and constructive discussions. The Ontario Geological Survey, particularly Robert Cundari, Mike Easton, Mark Puumala, Mark Smyk, and Greg Paju, are also thanked for their logistical support throughout the 2018 and 2019 field seasons and for sharing their knowledge of the geology of the Thunder Bay area. We also thank Sarah Davey and Dustin Liikane for their assistance during fieldwork. Numerous discussions with Jim Miller, on the geology of the MCR, are acknowledged and have been beneficial. Similarly, his review of a draft of this report helped sharpen some points. Valérie Becu assisted with the technical editing and Elizabeth Ambrose took care of final editing and correction of minor imperfections. Both are thanked for their skillful assistance.

REFERENCES

Ames, D.E., Kjarsgaard, I.M., McDonald, A.M., and Good, D.J., 2017. Insights into the extreme PGE enrichment of the W Horizon, Marathon Cu-Pd deposit, Coldwell Alkaline Complex, Canada: platinum-group mineralogy, compositions and genetic implications; Ore Geology Reviews, v. 90, p. 723–747.

Ballhaus, C., Tredoux, M., and Spath, A., 2001. Phase relations in the Fe-Ni-Cu-PGE-S system at magmatic temperature and application to massive sulphide ores of the Sudbury Igneous Complex; Journal of Petrology, v. 42, p. 1911–1926.

Barnes, S.J. and Campbell, I.H., 1988. Role of late magmatic fluids in Merensky-type platinum deposits: A discussion; Geology, v. 6, p. 488–491.

Barnes, S.J. and Robertson, J.C., 2019. Time scales and length scales in magma flow pathways and the origin of magmatic Ni–Cu–PGE ore deposits; Geoscience Frontiers, v. 10, p. 77–87.

Barnes, S.J., Cruden, A.R., Arndt, N., and Saumur, B.M., 2016. The mineral system approach applied to magmatic Ni–Cu–PGE sulphide deposits; Ore Geology Reviews, v.76, p. 296–316.

Barnes, S.J., Mungall, J.E., Le Vaillant, M., Godel, B., Lesher, C.M., Holwell, D., Lightfoot, P.C., Krivolutskaya, N., and Wei, B., 2017. Sulfide-silicate textures in magmatic Ni-Cu-PGE sulfide ore deposits: Disseminated and net-textured ores; American Mineralogist, v. 102, p.473–506.

Barnes, S.J., Le Vaillant, M., Godel, B., and Lesher, C.M., 2019. Droplets and Bubbles: Solidification of Sulphide-rich Vapour-saturated Orthocumulates in the Norilsk-Talnakh Ni–Cu–PGE Ore-bearing Intrusions; Journal of Petrology, v. 60, p. 269–300.

Barnes, S.-J. and Maier. W.D., 2002. Platinum-group element distributions in the Rustenburg Layered Suite of the Bushveld Complex, South Africa; Canadian Institute of Mineralogy, Metallurgy and Petrology, v. 54, p. 553–580.

Begg, G.C., Hronsky, J.A., Arndt, N.T., Griffin, W.L., O'Reilly, S.Y., and Hayward, N., 2010. Lithospheric, cratonic, and geodynamic setting of Ni-Cu-PGE sulphide deposits; Economic Geology, v. 105, p. 1057–1070.

Bleeker, W., 1990a. Evolution of the Thompson Nickel Belt and its nickel deposits, Manitoba, Canada; Ph.D. thesis, University of New Brunswick, Fredericton, New Brunswick, 400 p.

Bleeker, W., 1990b. Thompson Area—General geology and ore deposits; *in* Geology and Mineral Deposits of the Flin Flon and Thompson Belts, Manitoba; *in* Field Trip no. 10 Guidebook, 8th IAGOD Symposium, p. 93–125.

Bleeker, W., Liikane, D.A., Smith, J., Hamilton, M., Kamo, S.L., Cundari, R., Easton, M., and Hollings, P., 2018. Activity NC-1.3: Controls on the localisation and timing of mineralized intrusions in intra-continental rift systems, with a specific focus on the ca. 1.1 Ga Mid-continent Rift (MCR) system; *in* Targeted Geoscience Initiative: 2017 Report of Activities, Volume 2, (ed.) N. Rogers; Geological Survey of Canada, Open File 8373, p. 15–27.

Bleeker, W., Smith, J., Hamilton, M., Kamo, S., Liikane, D., Hollings, P., Cundari, R., Easton, M., and Davis, D., 2020. The Midcontinent Rift and its mineral systems: Overview and temporal constraints of Ni-Cu-PGE mineralized intrusions; *in* Targeted Geoscience Initiative 5: Advances in the understanding of Canadian Ni-Cu-PGE and Cr ore systems – Examples from the Midcontinent Rift, the Circum-Superior Belt, the Archean Superior Province, and Cordilleran Alaskan-type intrusions, (ed.) W. Bleeker and M.G. Houlé; Geological Survey of Canada, Open File 8722, p. 7–35.

Cabri, L.J. and Laflamme, J.H.G., 1976. The mineralogy of the platinum-group elements from some copper–nickel deposits of the Sudbury area, Ontario; Economic Geology, v. 71, p. 1159–1195.

Cannon, W.F., 1992. The Midcontinent rift in the Lake Superior region with emphasis on its geodynamic evolution; Tectonophysics, v. 213, p. 41–48.

Cawthorn, R.G., 2010. The platinum group element deposits of the Bushveld Complex in South Africa; Platinum Metals Review, v. 54, p. 205–215.

Cogulu, E., 1993a. Factors controlling postcumulus compositional changes of chrome-spinels in the Crystal Lake intrusion, Thunder Bay, Ontario; Geological Survey of Canada, Open File 2748, 28 p.

Cogulu, E., 1993b. Mineralogy and chemical variations of sulphides from the Crystal Lake intrusion, Thunder Bay, Ontario; Geological Survey of Canada, Open File 2749, 21 p.

Dowling, S.E., Barnes, S.J., Hill, R.E.T., and Hicks, J., 2004. Komatiites and nickel sulfide ores of the Black Swan area, Yilgarn Craton, Western Australia. 2. Geology and Genesis of the Orebodies; Mineralium Deposita, v. 39, p. 707–728.

Eckstrand, O.R. and Cogolu, E., 1986. Se/S evidence relating to genesis of sulphides in the Crystal Lake gabbro, Thunder Bay, Ontario; Geological Association of Canada-Mineralogical Association of Canada, Abstracts, v. 11, p. 66.

Eckstrand, O.R. and Hulbert, L.J., 1987. Selenium and the source of sulfur in magmatic nickel and platinum deposits; Geological Association of Canada-Mineralogical Association of Canada, Abstracts,. v. 12, p. 40.

Fairchild, L.M., Swanson-Hysell, N.L., Ramezani, J., Sprain, C.J., and Bowring, S.A., 2017. The end of Midcontinent Rift magmatism and the paleogeography of Laurentia; Lithosphere, v. 9, p. 117–133.

Fleet, M.E., Chryssoulis, S.L., Stone, W.E., and Weisener, C.G., 1993. Partitioning of platinum-group elements and Au in the Fe–Ni–Cu–S system: experiments on the fractional crystallization of sulfide melt; Contributions to Mineralogy and Petrology, v. 115, p. 36–44.

Geul, J.J.C., 1970. Geology of Devon and Pardee Townships and the Stuart Location, District of Thunder Bay; Ontario Department of Mines, Geological Report 87, 58 p.

Geul, J.J.C., 1973. Geology of Crooks Township, Jarvis and Prince Locations, and Offshore Islands, District of Thunder Bay; Ontario Department of Mines, Geological Report 102, 46 p.

Godel. B., Barnes, S.-J., and Maier, W.M., 2007. Platinum-group elements in sulfide minerals, platinum-group minerals, and whole-rocks of the Merensky Reef (Bushveld Complex, South Africa) Implications for the formation of the reef; Journal of Petrology, v. 48, p, 1569–1604.

Goldner, B., 2015. Rio Tinto Exploration Canada Inc. Assessment Report on the Cu-Ni-PGE Crystal Lake Project. Pardee, Devon and Crooks Township, NTS 52A/04; Thunder Bay Mining Division, Ontario, 825 p.

Goldner, B., 2016. Rio Tinto Exploration Canada Inc. Assessment Report on the Cu-Ni-PGE Crystal Lake Project. Pardee, Devon and Crooks Township, NTS 52A/04; Thunder Bay Mining Division, Ontario, 219 p.

Good, D.J., Epstein, R., McLean, K., Linnen, R.L., and Samson, I.M., 2015. Evolution of the Main Zone at the Marathon Cu-PGE sulphide deposit, Midcontinent Rift, Canada: spatial relationships in a magma conduit setting; Economic Geology, v. 110, p. 983–1008.

Good, D.J., Cabri, L.J., and Ames, D.E., 2017. PGM facies variations for Cu-PGE deposits in the Coldwell Alkaline Complex, Ontario, Canada; Ore Geology Reviews, v. 90, p. 748–771.

Green, J.C., 1983. Geologic and geochemical evidence for the nature and development of the Middle Proterozoic (Keweenawan) Midcontinent Rift of North America; Tectonophysics, v. 94, p. 413–437.

Heaman, L.M., Easton, R.M., Hart, T.R., Hollings, P., MacDonald, C.A., and Smyk, M., 2007. Further refinement to the timing of Mesoproterozoic magmatism, Lake Nipigon region, Ontario; Canadian Journal of Earth Sciences, v. 44, p. 1055–1086

Helmy, H.M., Ballhaus, C., Berndt, J., Bockrath, C., and Wohlgemuth-Ueberwasser, C., 2007. Formation of Pt, Pd and Ni tellurides; experiments in sulfide-telluride systems; Contributions to Mineralogy and Petrology, v. 153, p. 577–591.

Helmy, H.M., Ballhaus, C., Wohlgemuth-Ueberwasser, C., Fonseca, R.O.C., and Laurenz, V., 2010. Partitioning of Se, As, Sb, Te and Bi between monosulfide solid solution and sulfide melt—application to magmatic sulfide deposits; Geochimica et Cosmochimica Acta v. 74, p. 6174–6179.

Hollings, P., Smyk, M., Heaman, L.M., and Halls, H., 2010. The geochemistry, geochronology, and paleomagnetism of dikes and sills associated with the Mesoproterozoic Mid-continent Rift near Thunder Bay, Ontario, Canada; Precambrian Research, v. 183, p. 553–571.

Holwell, D.A. and McDonald, I., 2010. A review of the behaviours of platinum group elements within natural magmatic sulfide ore systems; Platinum Metal Reviews, v. 54, p. 26–36.

Holwell, D.A., McDonald, I., and Armitage, P.E.B., 2006. Platinum-group mineral assemblages in the Platreef at the South Central pit, Sandsloot mine, northern Bushveld Complex, South Africa; Mineralogical Magazine, v. 70, p. 83–101.

Holwell, D.A., Abraham-James, T., Keays, R.R., and Boyce, A.J., 2012. The nature and genesis of marginal Cu-PGE-Au sulphide mineralization in Paleogene Macrodikes of the Kangerlussuaq region, East Greenland; Mineralium Deposita, v. 47, p. 3–21.

Hutchinson, D., White, R., Cannon, W., and Schulz, K., 1990. Keweenawan hot spot: Geophysical evidence for a 1.1 Ga mantle plume beneath the Midcontinent Rift system; Journal of Geophysical Research, v. 95, p. 10 869–10884.

Karykowski, B.T., Maier, W.D., Groshev, N.Y., Barnes, S.J., Pripachkin, P.V., McDonald, I., and Savard, D., 2018. Critical controls on the formation of contact-style PGE-Ni-Cu mineralization: Evidence from the Paleoproterozoic Monchegorsk Complex, Kola Region, Russia; Economic Geology, v. 113, p. 911–935.

Kelly, D.P. and Vaughan, D.J., 1983. Pyrrhotine-pentlandite ore textures: A mechanistic approach; Mineralogical Magazine, v. 47, p. 453–463.

Kinloch, E.D., 1982. Regional trends in the platinum-group mineralogy of the critical zone of the Bushveld Complex, South Africa; Economic Geology, v. 77, p. 1328–1347.

Kinloch, E.D. and Peyerl, W., 1990. Platinum-group minerals in various rock types of the Merensky Reef: genetic implications; Economic Geology, v. 85, p. 537–555.

Kitakaze, A., Machida, T., and Komatsu, R., 2016. Phase relations in the Fe-Ni-S system from 875 to 650°C; The Canadian Mineralogist, v. 54, p. 175–1186.

Kosyakov, V.I. and Sinyakova, E.F., 2012. Physicochemical prerequisites for the formation of primary orebody zoning at copper-nickel sulfide deposits (by the example of the systems Fe-Ni-S and Cu-Fe-S); Russian Geology and Geophysics, v. 53, p. 861–882.

Krogh, T.E., 1973. A low contamination method for hydrothermal decomposition of zircon and extraction of U and Pb for isotopic age determinations; Geochimica et Cosmochimica Acta, v. 37, p. 485–494.

Krogh, T.E., Corfu, F., Davis, D.W., Dunning, G.R., Heaman, L.M., Kamo, S.L., Machado, N., Greenough, J.D., and Nakamura, E., 1987. Precise U-Pb isotopic ages of diabase dykes and mafic to ultramafic rocks using trace amounts of baddeleyite and zircon; *in* Mafic Dyke Swarms, (ed.) H.C. Halls and W.F. Fahrig; Geological Association of Canada, Special Paper 34, p. 147–152.

Le Vaillant, M., Barnes, S.J., Mungall, J.E. and Mungall, E., 2017. Role of de-gassing of the Noril'sk nickel deposits in the Permo-Triassic mass extinction event; Proceedings of the National Academy of Sciences, v. 114, p. 2485–2490.

Lesher, C.M., 1989. Komatiite-associated nickel sulfide deposits; Reviews in Economic Geology, v. 4, p. 45–101.

Li, C., Barnes, S.-J., Makovicky, E., Rose-Hansen, J., and Makovicky, M., 1996. Partitioning of nickel, copper, iridium, rhenium, platinum, and palladium between monosulfide solid solution and sulfide liquid: effects of composition and temperature; Geochimica et Cosmochimica Acta, v. 60, p. 1231–1996.

Lightfoot, P.C., 2007. Advances in Ni-Cu-PGE sulphide deposit models and implications for exploration technologies; *in* Proceedings of Exploration 07, (ed.) B. Milkereit; Fifth Decennial International Conference on Mineral Exploration, 2007, p. 629–646.

Lightfoot, P.C. and Evans-Lamswood, D.M., 2015. Structural controls on the primary distribution of mafic–ultramafic intrusions containing Ni–Cu–Co–(PGE) sulfide mineralization in the roots of large igneous provinces; Ore Geology Reviews, v. 64, p. 354–386.

Lightfoot, P.C., Naldrett, A.J., and Hawkesworth, C.J. 1984. The geology and geochemistry of the Waterfall Gorge section of the Insizwa Complex with particular reference to the origin of the

nickel sulphide deposits; Economic Geology, v. 79, p. 1857–1879.

Liu, Y. and Brenan, J., 2015. Partitioning of platinum-group elements (PGE) and chalcogens (Se, Te, As, Sb, Bi) between monosulfide-solid solution (MSS), intermediate solid solution (ISS) and sulfide liquid at controlled fO_2-fS_2 conditions; Geochimica et Cosmochimica Acta, v. 159, p. 139–161.

Ludwig, K.R., 2003. User's manual for Isoplot 3.00: A geochronological toolkit for Microsoft Excel; Berkeley Geochronology Center, Special Publication No. 4, 71 p.

Mainwaring, P.R. and Watkinson, D.H., 1981. Origin of chromian spinel in the Crystal Lake Intrusion, Pardee Twp., Ontario; *in* Geoscience Research Grant Program, Summary of Research, (ed,) E.G. Pye; Ontario Geological Survey, Miscellaneous Paper 98, p. 180–186.

Mansur, E.T., Barnes, S.J., and Duran, C.J., 2019. Textural and compositional evidence for the formation of pentlandite via peritectic reaction: Implications for the distribution of highly siderophile elements; Geology, v. 47, p. 351–354.

Miller, J.D. and Nicholson, S.W., 2013. Geology and mineral deposits of the 1.1 Ga Midcontinent Rift in the Lake Superior region – An overview; *in* Field Guide to the Cu-Ni-PGE Deposits of the Lake Superior Region, (ed.) J.D. Miller; Precambrian Research Center Guidebook 13-1, p. 1–50.

Mungall, J.E., Andrews, D.R.A., Cabri, L.J., Sylvester, P.J., and Tubrett, M., 2005. Partitioning of Cu, Ni, Au, and platinum-group elements between monosulfide solid solution and sulfide melt under oxygen and sulfur fugacities; Geochimica et Cosmochimica Acta, v. 69, p. 4349–4360.

Mungall, J.E., Brenan, J.M., Godel, B., Barnes, S.J., and Gailard, F., 2015. Transport of S, Cu and Au in magmas by flotation of sulphide melt on vapour bubbles; Nature Geoscience, v. 8, p. 216–219.

Naldrett, A.J., 1997. Key factors in the genesis of Noril'sk, Sudbury, Jinchuan, Voisey's Bay and other world-class Ni–Cu–PGE deposits: Implications for exploration; Australian Journal of Earth Science, v. 44, p. 283–315.

Naldrett, A.J., 2004. Magmatic Sulfide Deposits: Geology, geochemistry and exploration; Springer Verlag, Heidelberg, Germany, 728 p. doi:10.1007/978-3-662-08444-1

O'Brien, S., 2018. Geology of the Crystal Lake Gabbro and the Mount Mollie Dyke, Midcontinent Rift, Northwest Ontario; M.Sc. thesis, Lakehead University, Thunder Bay, Ontario, 350 p.

Piispa, E.J., Smirnov, A.V., Pesonen, L.J., and Mitchell, R.H., 2018. Paleomagnetism and geochemistry of ~1144 Ma lamprophyre dikes, Northwestern Ontario; Implications for the North American polar wander and plate velocities; Journal of Geophysical Research, Solid Earth, v. 123, p. 6195–6214.

Piña, R., Gervilla, F., Barnes, S.-J., Ortega, L., and Lunar, R., 2012. Distribution of platinum-group and chalcophile elements in the Aguablanca Ni-Cu sulfide deposit (SW Spain): Evidence from a LA-ICP-MS study; Chemical Geology, v. 302, p. 61–75.

Prichard, H.M., Hutchinson, D., and Fisher, P.C., 2004. Petrology and crystallization history of multiphase sulfide droplets in a Mafic Dike from Uruguay: Implications for the origin of Cu-Ni-PGE sulfide deposits; Economic Geology and the Bulletin of the Society of Economic Geologists, v. 99, p. 365–376.

Queen, M., Hanes, J.A., Archibald, D.A., Farrar, E., and Heaman, L.M., 1996. $^{40}Ar/^{39}Ar$ phlogopite and U-Pb perovskite dating of lamprophyre dykes from the eastern Lake Superior region; Evidence for a 1.14 Ga magmatic precursor to Midcontinent Rift volcanism; Canadian Journal of Earth Sciences, v. 33, p. 958–965.

Ripley, E.M., 2014. Ni-Cu-PGE mineralization in the Partridge River, South Kawishiwi, and Eagle intrusions: A review of contrasting styles of sulfide-rich occurrences in the Midcontinent rift system; Economic Geology, v. 109, p. 309–324.

Robertson, J., Ripley, E.M., Barnes, S.J., and Li, C., 2015. Sulfur liberation from country rocks and incorporation in mafic magmas; Economic Geology, v. 110, p. 1111–1123.

Robertson, J.C., Barnes, S.J., and Le Vaillant, M., 2016. Dynamics of magmatic sulphide droplets during transport in silicate melts and implications for magmatic sulphide ore formation; Journal of Petrology, v. 56, p. 2445–2472.

Samalens, N., Barnes, S.J., and Sawyer, E.W., 2017. A laser ablation inductively coupled plasma mass spectrometry study of the distribution of chalcophile elements among sulfide phases in sedimentary and magmatic rocks of the Duluth Complex, Minnesota, USA; Ore Geology Reviews, v. 90, p. 352–370.

Smith, A.R. and Sutcliffe, R.H., 1987. Keweenawan intrusive rocks of the Thunder Bay area; Ontario Geological Survey, Miscellaneous Paper 137, p. 248–255.

Smith, J.W., Holwell, D.A., and McDonald, I., 2014. Precious and base metal geochemistry and mineralogy of the Grasvally Norite–Pyroxenite–Anorthosite (GNPA) member, northern Bushveld Complex, South Africa: implications for a multistage emplacement; Mineralium Deposita, v. 49, p. 667–692.

Smith, J., Bleeker, W., Liikane, D.A., Hamilton, M., Cundari, R., and Hollings, P., 2019. Characteristics of Ni-Cu-PGE sulphide mineralization within the 1.1 Ga Midcontinent Rift; *in* Targeted Geoscience Initiative: 2018 report of activities, (ed.) N. Rogers; Geological Survey of Canada, Open File 8549, p. 421–432.

Smyk, M.C. and Hollings, P., 2009. Mesoproterozoic Midcontinent Rift-related mafic intrusions near Thunder Bay: Update; *in* Summary of Field Work and Other Activities 2009, Ontario Geological Survey, Open File Report 6240, p. 11–15.

Stein, C.A., Stein, S., Elling, R., Keller, G.R., and Kley, J., 2018. Is the "Grenville Front" in the central United States really the Midcontinent Rift?; GSA Today, v. 28, p. 4–10.

Swanson-Hysell, N.L., Burgess, S.D., Maloof, A.C., and Bowring, S.A., 2014. Magmatic activity and plate motion during the latent stage of Midcontinent Rift development; Geology, v. 42, p. 475–478.

Swanson-Hysell, N.L., Ramezani, J., Fairchild, L.M., and Rose, I.R., 2019. Failed rifting and fast drifting: Midcontinent rift development, Laurentia's rapid motion and the driver of Grenvillian orogenesis; Geological Society of America Bulletin, v. 131, p. 913–940.

Thomas, B., 2015. Geochemistry, sulfur isotopes and petrography of the Cu-Ni-PGE mineralized Crystal Lake intrusion, Thunder Bay, Ontario; M.Sc. thesis, Indiana University, Indiana, 94 p.

Tomkins, A.G., 2010. Wetting facilitates late-stage segregation of precious metal-enriched sulfosalt melt in magmatic sulfide systems; Geology, v. 38, p. 951–954.

Van Schmus, W.R. and Hinze, W.J., 1985. The midcontinent rift system; Annual Review of Earth and Planetary Sciences, v. 13, p. 345–383.

von Gruenewaldt, G., Hulbert, L.J., and Naldrett, A.J., 1989. Contrasting platinum group element concentration patterns in cumulates of the Bushveld Complex; Mineralium Deposita, v. 24, p. 219–229.

Waldner, P. and Pelton, A.D., 2004. Critical thermodynamic assessment and modeling of the Fe-Ni-S system; Metallurgical and Materials Transactions B: Process Metallurgy and Materials Processing Science, v. 35, p. 897–907.

Wold, R.J. and Hinze, W.J., 1982. Geology and Tectonics of the Lake Superior Basin; Geological Society of America, Boulder, Colorado, Memoir 156, 280 p.

Yudovskaya, M., Kinnaird, J., Naldrett, A.J., Mokhov, A.V., McDonald, I., and Reinke, C., 2011. Facies variation in PGE

mineralization in the central Platreef of the Bushveld Complex, South Africa; The Canadian Mineralogist, v. 49, p. 1349–1384.

ADDITIONAL REFERENCES

Gerstenberger, H. and Haase, G., 1997. A highly effective emitter substance for mass spectrometric Pb isotope ratio determinations; Chemical Geology v. 136, p. 309–312.

Guillong, M., Hametner, K., Reusser, E., Wilson, S.A., and Günther, D., 2005. Preliminary characterisation of new glass reference materials (GSA-1G, GSC-1G, GSD-1G and GSE-1G) by laser ablation-inductively coupled plasma-mass spectrometry using 193 nm, 213 nm and 266 nm wavelengths; Geostandards and Geoanalytical Research, v. 29, p. 315–331.

Jackson, S.E., 2008. Calibration strategies for elemental analysis by LA-ICP-MS; *in* Short Course Series; Mineralogical Association of Canada, v. 40, p. 169–188.

Jaffey, A.H., Flynn, K.F., Glendenin, L.E., Bentley, W.C., and Essling, A.M., 1971. Precision measurement of half-lives and specific activities of ^{235}U and ^{238}U; Physical Review, v. 4, p. 1889–1906.

Jochum, K.P., Nohl, U., Herwig, K., Lammel, E., Stoll, B., and Hofmann, A.W., 2005. GeoReM; A new geochemical database for reference materials and isotopic standards; Geostandards Geoanalytical Research, v. 29, p. 333–338.

Lawley, C.J.M., Petts, D.C., Jackson, S.E., Zagorevski, A., Pearson, D.G., Kjarsgaard, B.A., Savard, D., and Tschihart, V., 2019. Precious metal mobility during serpentinization and breakdown of base metal sulphide; Lithos.

Lawley, C., Creaser, R., Jackson, S. E., Yang, Z., Davis, B., Perhsson, S., Dubé, B., Mercier-Langevin, P., and Vaillancourt, D., 2015. Unraveling the Western Churchill Province Paleoproterozoic gold metallotect: Constraints from Re-Os arsenopyrite and U-Pb xenotime geochronology and LA-ICP-MS arsenopyrite trace element chemistry at the BIF-hosted Meliadine Gold District, Nunavut, Canada; Economic Geology, v. 110, p. 1425–1454.

Ludwig, K.R., 2003. User's manual for Isoplot 3.00: A geochronological toolkit for Microsoft Excel; Berkeley Geochronology Center, Special Publication No. 4, 71 p.

Mattinson, J.M., 2005. Zircon U-Pb chemical abrasion ("CA-TIMS") method: combined annealing and multi-step partial dissolution analysis for improved precision and accuracy of zircon ages; Chemical Geology, v. 220, p. 47–66.

Söderlund, U. and Johansson, L., 2002. A simple way to extract baddeleyite (ZrO_2); Geochemistry, Geophysics, Geosystems, v. 3, 7 p. doi:10.1029/2001GC000212

Sylvester, P.J., Cabri, L.J., Tubrett, M.N., Peregoedova, A., McMahon, G., and Laflamme, J.H.G., 2005. Synthesis and evaluation of a fused pyrrhotite standard reference material for

APPENDIX 1

METHODS

U-Pb Geochronology

Three samples from the Crystal Lake Intrusion and one from the Mount Mollie dyke, weighing ~8–12 kg each, were prepared and analyzed at the Jack Satterly Geochronology Laboratory at the University of Toronto. The coarse pegmatoidal gabbro, troctolite, and granophyre samples were crushed and milled using standard methods (jaw crusher and Bico disk mill, respectively). A concentrate of heavy minerals was produced by re-processing the heavy mineral splits on a Wilfley table until a significantly reduced sample size of ~5–10 g was achieved. This was followed by standard mineral separation procedures using magnetic separation and methyn iodide methods. Baddeleyite and zircon crystals were recovered using a Wilfley table following the method of Söderlund and Johanssen (2002). U-Pb analysis was carried out using isotope dilution thermal ionization mass spectrometry methods (ID-TIMS). Prior to analysis, zircon crystals were thermally annealed and chemically etched (Mattinson 2005). The pre-treatment involved placing zircon grains in a muffle furnace at 900–1000°C for ~24–60 hours to repair radiation damage and anneal the crystal lattice, followed by a modified single-step partial dissolution procedure in ~0.10 ml of ~50% HF and 0.020 ml 7N HNO_3 in Teflon dissolution vessels at 200°C for between 2 and 12 hours.

Zircon and baddeleyite grains were rinsed with 8N HNO_3 at room temperature prior to dissolution. A ^{205}Pb-^{235}U spike solution was added to the Teflon dissolution capsules during sample loading. Minerals were dissolved using ~0.10 ml of concentrated HF acid and ~0.02 ml of 7N HNO_3 at 195°C for 3 to 5 days, then dried to a precipitate and re-dissolved in ~0.15 ml of 3N HCl overnight (Krogh, 1973). Uranium and Pb were isolated from zircon and baddeleyite in 50 µl anion exchange columns using HCl, deposited onto outgassed rhenium filaments with silica gel (Gerstenberger and Haase, 1997), and analyzed with a VG354 mass spectrometer using a Daly detector in pulse counting mode. Corrections to the ^{206}Pb-^{238}U ages for initial ^{230}Th disequilibrium in the zircon have been made assuming a Th/U ratio in the magma of 4.2. All common Pb was assigned to procedural Pb blank for zircon and baddeleyite. Dead time of the measuring system for Pb and U was 16 and 14 ns, respectively. The mass discrimination correction for the Daly detector was constant at 0.05% per atomic mass unit. Amplifier gains and Daly characteristics were monitored using the SRM 982 Pb standard. Thermal mass discrimination corrections are 0.10% per atomic mass unit. Decay constants are those of Jaffey et al. (1971). All age errors are given at the 95% confidence interval. Plotting and age calculations were achieved using Isoplot 3.00 (Ludwig, 2003).

Platinum Group Element Deportment

To fully characterize the precious metal-bearing mineral (PMM) assemblage within the Crystal Lake Intrusion, four mineralized composite samples from

drill core were selected from high-grade intervals (∑PGE+Au 1.3–3.3 ppm) for mineral separation and upgrading. Representative samples were collected from selected intervals from the vari-textured gabbros (<200 ppm Cr) and chrome-spinel-bearing units (>3000 ppm Cr) developed within the northern and southern limbs of the intrusion. Composite samples were crushed and milled to P80 of 75 µm (80% of material passing 75 µm) with 500 g splits of each sample wet sieved into +75 µm, 40–75 µm, 20–40 µm, 10–20 µm, and -10 µm size fractions. Heavy mineral concentrates were prepared at Advanced Mineral Technology Laboratory (AMTEL) through heavy liquid separation, magnetic separation, and panning of the non-magnetic concentrates. The pan tip of each size fraction was mounted in epoxy on a 1 inch monolayer polished block.

Polished mounts were analyzed at the Geological Survey of Canada using a Tescan Mira-3 field emission-scanning electron microscope (FE-SEM). Sections were scanned using the *Feature* function in Oxford Instruments Aztec software package. Automated scans were set at various magnifications (dependant on the size fraction) to identify high-density minerals, including precious-bearing minerals. An automated SEM-EDS analysis (0.5 s/element, normalized to 100 wt%) was performed on each identified feature. The data generated from each scan was subsequently reviewed and verified, with semi-quantitative analyses of representative grains obtained by SEM-EDS. Composite grains were reclassified and analyzed. The apparent area of each PMM was calculated from the measured two dimension equivalent-circle diameter. All data on PMM assemblages are presented in percentage of total area, which reflects more accurately the relative proportions of each PMM type. To obtain textural information about mineral associations and to characterize the PMMs in situ, a selection of polished thin sections representative of each composite sample were also studied using automated SEM-EDS analysis.

LA-ICP-MS Methodology

Quantitative elemental mapping of sulphides was carried out on selected areas of thick sections by laser ablation - inductively coupled plasma - mass spectrometry (LA-ICP-MS), at the Geological Survey of Canada. Analyses were conducted using a Photon Machines Analyte G2 excimer laser ablation system (λ = 193 nm), with a Helex II ablation cell, and an Agilent 7700x quadrupole ICP-MS.

The mapping procedure closely follows the method of Lawley et al. (2015, 2019). Elemental maps were constructed by rastering a focused laser beam across the sample surface to form a series of line scans. Laser conditions during the analytical sessions include a fluence of 4.25 J/cm^2, a repetition rate of 30 Hz, a spot size of 6–10 µm, and a scan speed of 6–10 µm/s. The spot size and scan speed were synchronized for each map such that the laser beam would advance one equivalent spot diameter in 1.0 second (i.e. 8 µm @ 8 µm/s). Prior to each ablation pass, the sample surface was cleaned by rastering the laser across the sample at a rate of 2–3 pulses every equivalent spot diameter. The cleaning step was followed by 50 s of washout, and then each analysis began with 20 s of background measurement (gas blank). The ablation aerosol was transported out of the Helex II cell using 1 L/min of helium gas, and was transported to the ICP-MS using ~ 1 m of Teflon tubing (2 mm I.D.), with no SQUID device attached. The carrier gas (He + ablation aerosol) was subsequently mixed with ~ 1 L/min of argon gas before entering the ICP-MS. To reduce the interference of the metal-argide species on the light PGEs (e.g. $^{65}Cu^{40}Ar$ on ^{105}Pd), a collision cell was used in the ICP-MS with a He flowrate of 4.0 ml/min. The instrumentation was tuned on NIST-612 to achieve >7000 cps/ppm on ^{175}Lu (in collision cell mode; 50 µm spot, ~7 J/cm^2 at 10 Hz), while minimizing the production of oxides (<0.2% for ThO/Th) and maintaining a U/Th ratio of ~1.0. Dwell times were optimized to 1–4 ms for major and minor elements and 3–8 ms for trace elements. The total duty cycle time to measure all masses on the ICP-MS (in time-resolved analysis mode) was 250 ms. Utilizing these settings, every 1.0 second of data collection, or the equivalent of one full spot diameter, included four isotopic measurements. These four isotopic measurements were then subsequently averaged to form one pixel/data point on the map.

The calibration procedures described by Jackson (2008) were followed during the mapping sessions to produce quantitative elemental maps. Standardization was achieved by calibrating the signals of unknowns (i.e. treating each pixel as a separate analysis) against analyses of GSE-1G (Guillong et al., 2005; for most major and trace elements) and synthetic pyrrhotite standard Po726 (Sylvester et al., 2005; for the calibration of sulphur and PGEs), and normalizing the total element, or element oxide, concentrations to 100%. Reference materials were analyzed every 20 unknowns to account for instrumental drift during the mapping session. A secondary standard, NIST-610, was analyzed every 20 unknowns and routinely yielded calculated concentrations within 15% of the accepted values for most elements. In addition, the major element compositions of all sulphide phases were routinely within 10 and 15% of the stoichiometric values (based on end-member sulphide phases). Reference values for standards GSE-1G and NIST-610 are taken from the online geological and environmental reference materials database (GeoReM; Jochum et al., 2005).

All data processing was performed using the in-house software *LAMTrace* and *PixeLAte*, and maps were constructed using an in-house *Python* script that converted concentration profiles into 2-D images. The elemental concentration maps are displayed using logarithmic and percentile colour scaling, with red colours representing the highest concentrations.

APPENDIX 2

Table A2.1. Summary of U-Pb CA-ID-TIMS isotopic data for zircon and baddeleyite from the Crystal Lake Intrusion and Mount Mollie dyke.

Sample/ Number	Fraction	U (ppm)	Th/U	Pbtot (pg)	Pbc (pg)	$^{206}Pb/^{204}Pb$	$^{207}Pb/^{235}U$	2σ	$^{206}Pb/^{238}U$	2σ	Error Corr.	$^{207}Pb/^{206}Pb$	2σ	Age (Ma) $^{206}Pb/^{238}U$	2σ	Age (Ma) $^{207}Pb/^{235}U$	2σ	Age (Ma) $^{207}Pb/^{206}Pb$	2σ	% Disc
18-SYB-001 - Unmineralized, homogeneous troctolite, northern limb; 305453.19 E, 5328330.35 N (Zone 16), 21–35 m																				
MH19055	Z1	253	1.478	61.02	0.32	9371	1.92656	0.00493	0.184297	0.000374	0.8782	0.075816	0.000094	1090.4	2.0	1090.3	1.7	1090.2	2.5	0.0
MH19056	Z2	484	1.533	118.23	0.26	21670	1.92812	0.00448	0.184288	0.000344	0.9366	0.075881	0.000066	1090.4	1.9	1090.9	1.6	1091.9	1.7	0.2
18-SYB-002 - Mineralized, vari-textured gabbro, northern limb; 305453.19 E, 5328330.35 N (Zone 16), 412–417 m																				
MH19057	Z1	615	1.315	144.02	0.18	39903	1.93414	0.00435	0.184712	0.000337	0.9324	0.075944	0.000065	1092.7	1.8	1093.0	1.5	1093.6	1.7	0.1
MH19058	Z2	329	1.315	76.90	0.35	11084	1.93207	0.00467	0.184627	0.000349	0.8977	0.075897	0.000084	1092.2	1.9	1092.3	1.6	1092.4	2.2	0.0
MH19113	Bd1	900	0.060	78.21	0.97	5510	1.93618	0.00528	0.184864	0.000336	0.8230	0.075961	0.000122	1093.5	1.8	1093.7	1.8	1094.1	3.2	0.1
MH19114	Bd2	949	0.056	128.59	2.24	3936	1.93009	0.00604	0.184414	0.000346	0.7524	0.075907	0.000161	1091.0	1.9	1091.6	2.1	1092.6	4.2	0.2
18-SYB-111 - Mineralized, vari-textured gabbro, southern limb; 306239.91 E, 5326523.72 N (Zone 16), 556–562 m																				
MH19059	Z1	567	0.792	118.32	0.21	32323	1.93275	0.00446	0.184406	0.000368	0.8851	0.076015	0.000082	1091.0	2.0	1092.5	1.5	1095.5	2.2	0.4
MH19060	Z2	414	1.243	95.22	0.20	24648	1.93047	0.00468	0.184396	0.000371	0.9404	0.075929	0.000066	1090.9	2.0	1091.7	1.6	1093.2	1.7	0.2
18-SYB-149 - Coarse granophyre, Mount Mollie dyke; 313981.01 E, 5325871.74 N (Zone 16)																				
MH19064a	Z1	185	0.218	10.06	0.42	1595	1.92532	0.01173	0.184233	0.000525	0.6097	0.075794	0.000372	1090.1	2.9	1089.9	4.1	1089.6	9.8	0.0
MH19065a	Z2	241	0.217	13.10	3.07	297	1.93971	0.05663	0.184207	0.000666	0.7775	0.076371	0.002025	1089.9	3.6	1094.9	19.7	1104.8	53.4	1.5
MH19066a	Bd1	1006	0.019	463.44	9.59	3352	1.93041	0.00654	0.184122	0.000356	0.7029	0.076040	0.000186	1089.5	1.9	1091.7	2.3	1096.1	4.9	0.7
MH19109	Bd2	1092	0.034	603.24	3.68	11264	1.91003	0.00468	0.182245	0.000351	0.8995	0.076012	0.000084	1079.2	1.9	1084.6	1.6	1095.4	2.2	1.6
MH19110	Bd3	632	0.016	358.96	3.10	8000	1.92584	0.00491	0.183508	0.000349	0.8805	0.076114	0.000096	1086.1	1.9	1090.1	1.7	1098.1	2.5	1.2
MH19111	Bd4	806	0.026	151.12	4.80	2184	1.92239	0.00861	0.183335	0.000361	0.6339	0.076049	0.000272	1085.2	2.0	1088.9	3.0	1096.4	7.2	1.1
MH19112	Bd5	883	0.014	229.51	3.75	4245	1.92467	0.00600	0.183615	0.000387	0.7467	0.076023	0.000159	1086.7	2.1	1089.7	2.1	1095.7	4.2	0.9

Notes:
All zircon grains have been thermally annealed and etched in HF (Mattinson, 2005).
Z = zircon; Bd = baddeleyite.
Th/U calculated from radiogenic $^{208}Pb/^{206}Pb$ ratio and $^{207}Pb/^{206}Pb$ age, assuming concordance.
Pbc is total common Pb, assuming the isotopic composition of laboratory blank ($^{206}Pb/^{204}Pb$=18.49±0.4%; $^{207}Pb/^{204}Pb$=15.59±0.4%; $^{208}Pb/^{204}Pb$=39.36±0.4%).
$^{206}Pb/^{204}Pb$ corrected for fractionation and common Pb in the spike.
Pb/U ratios corrected for fractionation, common Pb in the spike, and blank.
Correction for ^{230}Th disequilibrium in $^{206}Pb/^{238}U$ and $^{207}Pb/^{206}Pb$ assuming a Th/U of 4.2 in the magma.
% Disc. is percent discordance for the given $^{207}Pb/^{206}Pb$ age.
Error Corr. is the correlation coefficient for X-Y errors in the concordia plot.
Decay constants are those of Jaffey et al. (1971): ^{238}U = 1.55125 x 10^{-10}/yr, ^{235}U = 9.8485 x 10^{-10}/yr.

Structural-stratigraphic setting and U-Pb geochronology of Ni-Cu-Co-PGE ore environments in the central Cape Smith Belt, Circum-Superior Belt

Wouter Bleeker[1]* and Sandra Kamo[2]

[1]Geological Survey of Canada, 601 Booth Street, Ottawa, Ontario K1A 0E8
[2]Jack Satterly Geochronology Laboratory, University of Toronto, 22 Russell Street, Toronto, Ontario M5S 3B1
*Corresponding author's e-mail: wouter.bleeker@canada.ca

ABSTRACT

The economically important Cape Smith Belt of northern Quebec represents a key segment of the "Circum-Superior Belt", preserving a ~12–15 km thick record of Paleoproterozoic stratigraphy in a south-vergent, mostly north-dipping fold-thrust belt. The central part of this belt is only moderately deformed and experienced merely sub-biotite grade metamorphism. It hosts world-class Ni-Cu-Co-PGE mineralization in both extrusive and intrusive settings that, at present, form the basis for two integrated mining operations. Collectively, these attributes make this belt unique in Canada and the world.

A detailed, holistic understanding of this belt has been hampered, however, by conflicting interpretations on the degree of thrust stacking, and a lack of accurate and precise ages for critical elements of the stratigraphy. Here we report on new fieldwork and drill core observations—collected over several summers—that resolve many of the outstanding questions and provide a more detailed stratigraphic framework for the mineralization and the belt as a whole. We integrate these data and observations with new high-precision U-Pb ages for ~10 critical rock units, from the Cape Smith Belt and other parts of Circum-Superior Belt, as well as relevant parts of the overall craton-scale ore system.

We briefly describe the different ore settings of the Cape Smith Belt and place these in the structural-stratigraphic framework. We show that the central part of the Cape Smith Belt is more coherent and less imbricated by thrusts than previously interpreted. The important Nuvilik Formation of thinly bedded distal turbidites and sulphidic mudstones forms a stratigraphic unit at the top of the Povungnituk Group, reflecting a phase of basin formation and deepening following volcanism of the ca. 1959 Ma Cécilia Formation. Neither the lower contact nor the upper contact of the Nuvilik Formation is a regional thrust. At 1883–1882 Ma, the Nuvilik sulphidic mudstones formed the ambient seafloor across which high-volume, hot, Mg-rich lavas of the Chukotat Group were emplaced, which included high-flow rate, turbulent, channelized komatiite flows, thus bringing into direct contact the most dynamic magma system of the belt with a ubiquitous, prolific sulphur source. Although Chukotat magmas may have been at sulphur saturation on final ascent, thermo-mechanical erosion of the lava channels into underlying Nuvilik mudstones, and mixing and melting of sulphidic sediments into the channels, led to massive sulphur oversaturation and accumulation of net-textured and massive sulphides. Our ages show that all of this happened during the onset and climax phase of the Chukotat magmatic event, which lasted ~2 Myr and occurred at the same time as similar events more than 1500 km away, in Thompson, Manitoba. At Raglan, we describe one well preserved lava and ore channel where, in present coordinates, flow was demonstrably down-dip and to the north-northeast. This is the first observation of flow polarity. We prefer an overall model of several anastomosing, subparallel lava channels presently plunging down to the north-northeast, not a single, giant, meandering lava channel subparallel to the trace of the basal Chukotat lavas on the present erosion surface. The observed flow direction makes it feasible, if not likely, that the channelized komatiite flows were fed from an eruptive fissure system ~25 km to the south, which would suggest a "processing length" of ~25 km to achieve optimal mixing, sulphide saturation, and segregation at high R-factors.

At the craton scale, the overall model that best explains the rich spectrum of phenomena is that of a hot mantle upwelling ascending from a deep thermal boundary layer to impinge on the base of the lithosphere of the Superior craton, or rather its ancestral supercraton Superia, prior to final breakup. Rapid lateral flow of hot buoyant mantle to lithospheric "thin spots", such as active or pre-existing rifts or delamination scars, caused nearly synchronous, high-volume, ultramafic-mafic magmatism around what ultimately became the margins of a fully separated Superior craton. Although the overall magmatic event has a younger tail, to as young as 1878 Ma, and also a distinct younger pulse at ca. 1870 Ma, the early onset and climax phase of high-volume ultramafic-mafic magmatism is most prospective for economic Ni-Cu-Co-PGE mineralization.

Bleeker, W. and Kamo, S., 2020. Structural-stratigraphic setting and U-Pb geochronology of Ni-Cu-Co-PGE ore environments in the central Cape Smith Belt, Circum-Superior Belt; *in* Targeted Geoscience Initiative 5: Advances in the understanding of Canadian Ni-Cu-PGE and Cr ore systems – Examples from the Midcontinent Rift, the Circum-Superior Belt, the Archean Superior Province, and Cordilleran Alaskan-type intrusions, (ed.) W. Bleeker and M.G. Houlé; Geological Survey of Canada, Open File 8722, p. 65–98. https://doi.org/10.4095/326882

INTRODUCTION

The Paleoproterozoic Circum-Superior Belt (Baragar and Scoates, 1981), encircling the Archean Superior craton, represents one of Canada's principal mineral belts, particularly in terms of orthomagmatic Ni-Cu-Co-PGE sulphide ores and resources. It hosts both the ~100 Mtonne Thompson district in northern Manitoba and the ~30 Mtonne Raglan camp in the Cape Smith Belt of northernmost Quebec, as well as a number of significant prospects elsewhere, particularly in Manitoba and in the Labrador Trough. Less obvious is the connection of the Circum-Superior Belt with other mineral systems such as rare metal and industrial mineral (apatite) deposits in alkaline intrusions interior to the Superior craton, and the globally significant peak in Superior-type banded iron formations, all essentially of the same age at ca. 1880 Ma. The iron formations support the long active iron mining districts in Labrador, Minnesota, and Michigan, and their scale indicates that the ca. 1880 Ma Circum-Superior Belt magmatism affected the ocean-atmosphere system at the global scale.

Despite significant progress in the general understanding of this global mineral system, numerous key questions remained unresolved. Foremost among these were questions of detailed timing and regional- to deposit-scale stratigraphy in key belts, such as Raglan. Detailed timing of ore-forming processes, at the ~1 Myr scale, is essential for linking the various processes involved in the right time sequence: a cause must precede the effect. A correct interpretation of stratigraphy is equally essential for singling out key ore-forming processes, understanding the relationships among different rock units, subtracting out the interfering effects of later deformation, and correctly identifying ore horizons and where they may occur next. Many of these aspects were controversial at Raglan, particularly the question of detailed timing and the degree to which the ore-hosting stratigraphy is imbricated by thrust faulting, and thus which contacts are primary and which are structural (Bleeker, 2013; Bleeker and Ames, 2017; Bleeker and Kamo, 2018).

In this report, we present significant progress in resolving these questions, particularly for the Raglan camp of the central Cape Smith Belt in northern Quebec (Fig. 1). We show that the key magmatic pulse of komatiitic magmatism was short-lived at ca. 1882 Ma, with new U-Pb ages on ore-hosting units and on gabbro sills that immediately pre- and post-date the formation of major lenses of massive sulphide ore. We integrate these new data with structural and stratigraphic observations to arrive at a more refined understanding of the deposit- to regional-scale stratigraphy and the setting of the various ore-hosting environments. The stratigraphy at Raglan is more coherent than previously interpreted, and the ore-bearing "Raglan Horizon" resulted from the direct superposition, in space and time, of the most dynamic, high-volume part of the Chukotat magmatic system (large channelized komatiite flows; *see also* Lesher, 2007 and references therein) with the most prolific sulphur source in the belt, the sulphidic mudstones of the uppermost Nuvilik Formation. From Raglan and the Cape Smith Belt, we zoom out to the scale of the craton and the larger magmatic system of a hot mantle upwelling that ascended underneath the Archean lithosphere of the Superior craton, prior to final breakup of the ancestral craton. A number of predictions follow from this model. In an appendix, we explore interesting questions of correlation with the stratigraphy in the ~900 km long Labrador Trough of Quebec and Labrador.

STRATIGRAPHY OF THE CENTRAL CAPE SMITH BELT, RAGLAN

General Structural Considerations

The central Cape Smith Belt of northernmost Quebec (Low, 1902; Gunning, 1934; Bergeron, 1957, 1959; Stam, 1961; Taylor, 1982) preserves ~12 to 15 km of Paleoproterozoic lithostratigraphy across a number of structural panels in the core of an approximately east–west-trending synclinorium (Fig. 1, 2; Bergeron, 1957, 1959; Dimroth et al., 1970; Hynes and Francis, 1982). The belt forms an integral part of the Circum-Superior Belt (Baragar and Scoates, 1981), which extends all around the Ungava promontory of the northern Superior craton, and indeed around much of the craton. The southern part of the Cape Smith Belt, dominated by two major mafic volcanic sequences that have long been referred to as the mostly Fe-tholeiitic Povungnituk Group and the more Mg-rich Chukotat Group (Bergeron, 1959), respectively, is largely homoclinal and dipping moderately to the north. Some structural-stratigraphic repetition (e.g. Stam, 1961; Hynes and Francis, 1982) and a major north-dipping shear zone along the basal contact with the underlying granitoid gneisses of the Superior craton (Stam, 1961; St-Onge et al., 1992) indicate significant thrusting onto the craton in a generally south-vergent fold-thrust belt. Only a few small, fully autochthonous outliers of basal sedimentary rocks, lying unconformably on Archean crystalline basement, occur along the southern and eastern margin of the thrust belt (e.g. Taylor et al., 1982).

The first-order synclinorium that preserves the fold-thrust belt is ~50 km wide, being flanked by gently north-dipping basement to the south, and a major basement-cored antiformal ridge to the north, the Kovik Antifom (Fig. 1, 2). Archean granitoid gneisses of the Kovik Antiform are deformed into planar tectonites for ~1 km adjacent to the contact with the Paleoprotero-

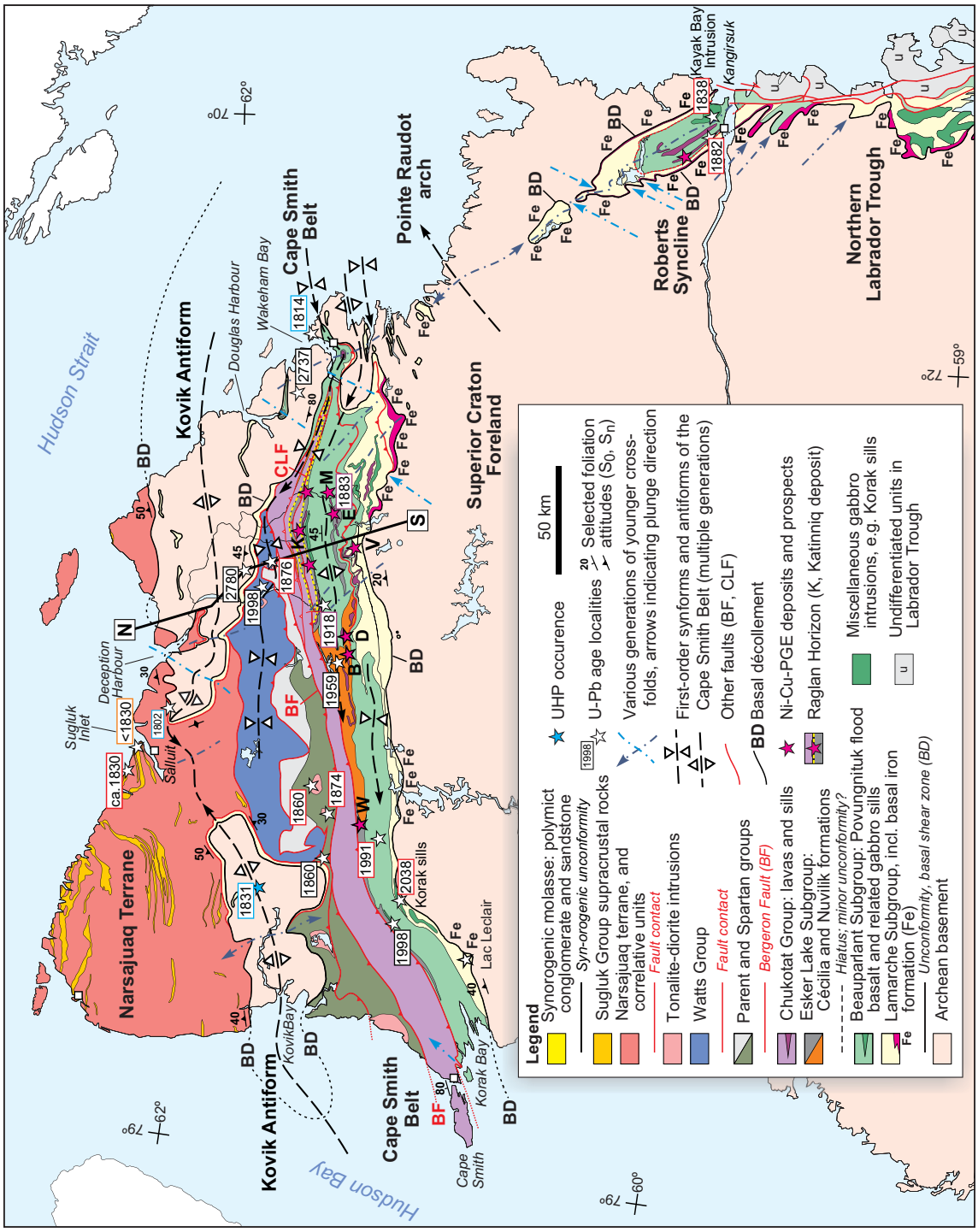

Figure 1. Generalized map of the Ungava promontory, northern Quebec, showing the Cape Smith Belt, Roberts Syncline area, and the northern Labrador Trough (*modified and simplified from* MRN (2002), St-Onge et al. (2006), and Lamothe (2007), with data from the present study). Only major faults are shown and most are thrusts, including early movement on the basal décollement (BD); however, faults that define the flanks of the major Kovik Antiform were reactivated as major extensional faults. The Cross Lake Fault (CLF) and Bergeron Fault (BF) are in red, with thrust teeth on their north side. Line S–N is the cross-section line discussed in the text (e.g. Fig. 2). Basal iron formations in the various belts are highlighted with "Fe". Stars indicate localities mentioned in the text, as well as previous U-Pb geochronology sites: Lac Leclair and Korak sills (white stars); UHP locality of Weller and St-Onge (2017) in Kovik Antiform (blue); main areas of mineralization (magenta): K = Katinniq deposit on the main Raglan Horizon; also shown along the main Raglan Horizon are the Kikialik deposit in the west, and Donaldson deposit in the east. Abbreviations: B = Bravo sill, D = Delta sill, E= Expo-Ungava, M = Mesamax, V = Lac Vaillant sill, W = West Raglan. U-Pb ages (in Ma) are colour-coded: black outline = plutonic and volcanic ages, red = intrusive and thus minimum ages for host rocks, purple = Chukotat ultramafic sills and dykes, orange = maximum depositional age from detrital zircon grains, blue = metamorphic ages. *See* the text for references.

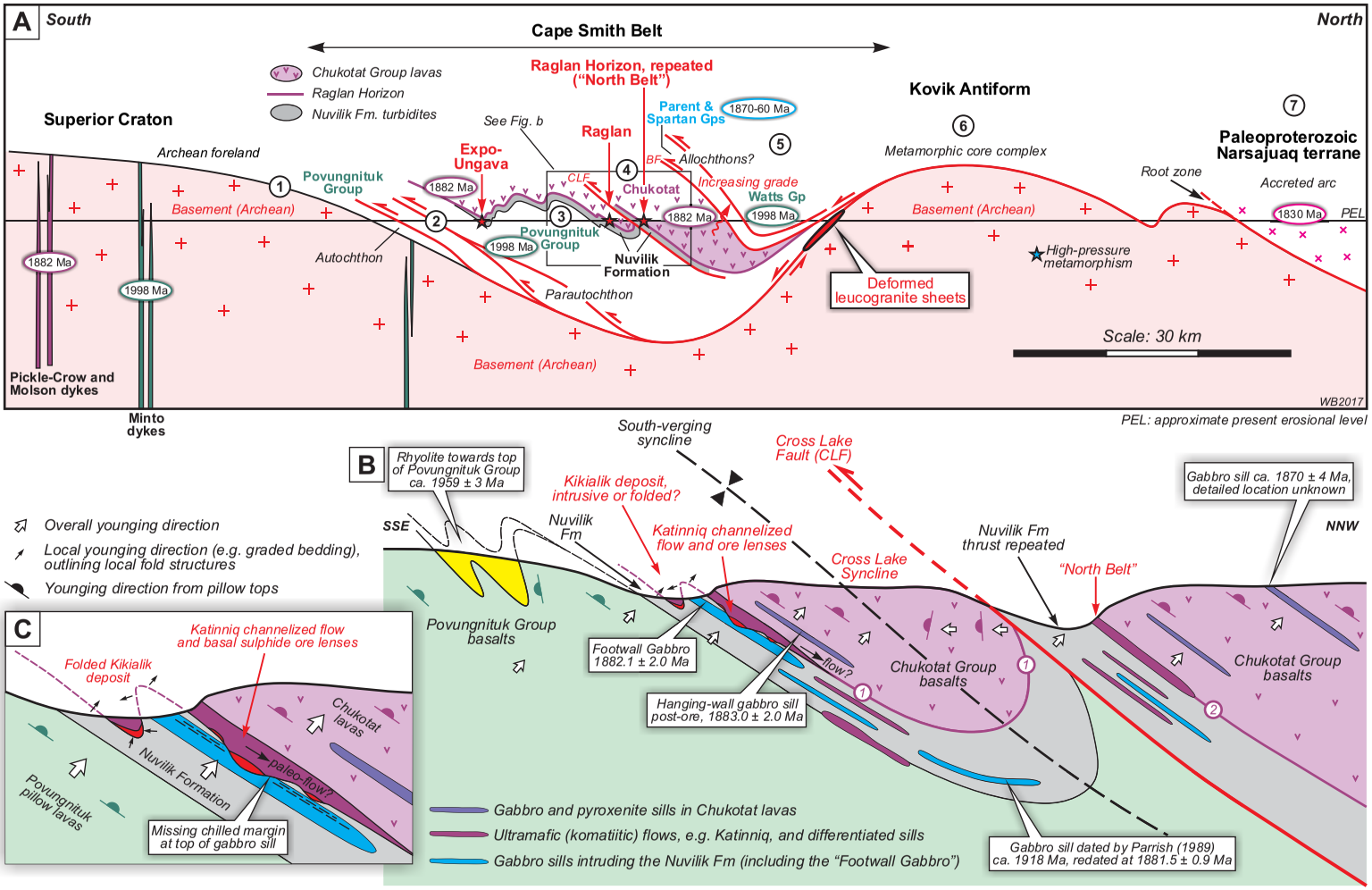

Figure 2. a) Generalized south-to-north regional-scale cross-section through the central Cape Smith Belt, northern Quebec. Circled numbers (1 to 7) refer to tectonostratigraphic domains: 1) the Archean foreland of the Superior craton; 2) parautochthonous thrust sheets of ca. 1998 Ma Povungnituk Group and its >2038 Ma basal units; 3) top of the Povungnituk Group and the overlying sedimentary rocks of the Nuvilik Formation (the latter in grey); 4) Chukotat lava flows exposed in a faulted syncline-anticline pair; 5) structurally higher thrust sheets in the core of the synform on the south side of the major Kovik Antiform; 6) the basement-cored Kovik Antiform; and 7) the younger Narsajuaq terrane. The mineralized "Raglan Horizon", in the well preserved north-dipping central part of the belt, is shown as a solid purple line, on the stratigraphic contact between turbiditic Nuvilik Formation mudstones and siltstones (in grey) and the overlying Chukotat Group lava flows. Ni-Cu-Co-PGE sulphide deposits and prospects are identified by red stars. **b)** Zoomed-in view of the central part of the Raglan belt, with the Katinniq orebodies at the base of channelized basal komatiite flows. The Kikialik deposit, situated in a tight fold structure, is also shown but off-section to the west. Some of the available high-precision ages are shown for reference. Note that the overall structure is that of a faulted syncline-anticline pair, the overturned limb of which has evolved into the Cross Lake Fault (CLF, in red), a fault of moderate displacement (reverse, north over south). The footwall syncline, a well defined structure in the belt, is known as the Cross Lake Syncline. The overall structure leads to repetition of the Raglan Horizon (1) across the Cross Lake Fault into the "North Belt" (2). **c)** Inset that zooms in further to highlight the stratigraphic and structural relationships of the Raglan Horizon at the Katinniq and Kikialik deposits. Note the localization of some of the larger sulphide lenses (red) at Katinniq in channels that have eroded down into the "Footwall Gabbro Sill" (gabbro sill in blue). A primary contact that formed by thermal erosion is indicated by a missing chilled margin at the top of the gabbro sill (*see* Bleeker and Ames, 2017).

zoic supracrustal rocks to the south, but become less tectonized in the core of the antiform. These gneisses host remarkably few major mafic dykes, which is one of several lines of evidence arguing against early views that the Cape Smith Belt developed in situ in a largely ensialic setting (cf. Dimroth et al., 1970; Hynes and Francis, 1982); rather, the entire fold-thrust belt of the Cape Smith Belt must have been transported over a basal décollement to the south into its current position (Hoffman, 1985), with a net displacement of >100 km, from a root zone well to the north. The complete set of arguments that favour significant structural transport of the thrust belt onto the craton, from a more northerly position towards to south, can be summarized as follows:

- A lack of "syn-rift" or synvolcanic basement-derived conglomerate-sandstone wedges in the Povungnituk and Chukotat lavas, which could indicate proximity to major rift fault scarps[1].
- No major, dense, mafic-ultramafic dyke systems in the nearby basement that could represent proximal feeder zones to the very thick lava sequences of the Povungnituk and Chukotat groups of the thrust belt. All such proximal feeder systems are contained within the thrust belt and thus transported with it.
- In most localities along the basal contact of the supracrustal thrust belt, there is a major shear zone hundreds of metres wide (e.g. Stam, 1961), involving complete transposition, i.e. a classic basal décollement, indicating very significant displacement (St-Onge et al., 1992).
- Crystalline basement of the Superior craton, and the décollement, can be mapped all around the eastern closure of the Cape Smith fold-thrust belt (Taylor, 1982), in what defines the broad hinge zone of a westerly plunging synclinorium (Lucas and St-Onge, 1992).
- Kinematic indicators and a general fold and thrust vergence that indicate structural transport towards the south.

This overall context for the supracrustal rocks of the central Cape Smith Belt is now generally agreed upon. What is more controversial, and worthy of debate, are the following aspects:

1. What is the nature of the uppermost thrust sheets (Fig. 2a), involving basaltic rocks, gabbros, and ultramafic cumulate rocks of the ca. 1998 Ma Watts Group? Do these rocks represent a fully allochthonous ophiolite assemblage as proposed by Scott et al. (1989, 1991, 1992)? The age of this assemblage remains problematic and, remarkably, it is identical to that of the Povungnituk Group basaltic rocks.
2. What is the nature of the ca. 1870–1860 Ma Parent Group volcanic rocks and the associated Spartan Group greywackes and intercalated volcanic rocks? Do they represent an accreted arc assemblage as per the various arc accretion models (Picard et al., 1989, 1990; St-Onge et al., 1992). If so, why then the apparently smooth age transition from the ca. 1883–1870 Ma Chukotat Group rocks into the 1870–1860 Ma Parent Group?
3. Where is the sediment prism representing the time between hypothesized basin opening (end Chukotat Group) and arc accretion? There is none and only the Parent and Spartan groups satisfy the constraints.
4. Which contact represents a suture, if any? Is it the basal contact of the Parent Group volcanic rocks, i.e. the Bergeron Fault (BF in Fig. 2)?
5. What is the nature of the major Kovik Antiform? Is it simply a basement-cored antiformal fold that formed as part of the early, progressive, deformation and shortening history ("D3" of Lucas and St. Onge, 1992; Hoffman, 1985), or do the significant scale and amplitude of this antiform indicate a different origin, i.e. as a late-stage core complex as proposed by Bleeker and Kamo (2018)? This important question is relevant to the major shear zone on its southern flank, which shows late-stage south-side-down kinematics and in which the entire thrust belt is reduced to narrow widths, including the complete pinching out of the Chukotat Group (Fig. 2).
6. And finally, what is the degree of internal thrust stacking (i.e. relative to normal stratigraphic superposition and some fold duplication) in the southern part of the fold-thrust belt?

Some of these questions will be touched upon later in this report. The last question, however, is immediately relevant to the stratigraphic understanding of the central Cape Smith Belt, and has important implications for understanding the Ni-Cu-Co-PGE ore system associated with its voluminous ultramafic rocks. As in any deformed belt with less than complete exposure and less than perfect age control, some degree of interpretation is involved in compiling the complete stratigraphic framework. In particular, the question of thrust

[1] Immature conglomerate units do occur in the Cape Smith Belt, but none are "syn-rift" in age and coeval with the thick lava sequences. They occur (1) at the very base of the stratigraphic sequence and thus are among the oldest of the preserved supracrustals; and (2) as thin panels of syn-orogenic conglomerates and sandstones within the Chukotat lavas, which are among the youngest rocks in the belt. *See* later in this report.

stacking pertains to which, and how many, of the sedimentary packages in the belt are unique, and part of regular depositional stratigraphic development, versus thrust repeats of the basal sedimentary section. It also pertains to what is the true thickness and geochemical evolution of the lava sequences of the Povungnituk and Chukotat groups.

Lithostratigraphy and Summary of U-Pb Ages

A synopsis of the lithostratigraphy of the southern homoclinal part of the Cape Smith Belt is shown in Figure 3. This figure contrasts previous understanding of the (tectono-) stratigraphy, based on the work of St-Onge et al. (1992, 2006) and St-Onge and Lucas (1993) (Fig. 3a), with our current understanding (Fig. 3b). The fundamental difference, other than significantly improved U-Pb age control, is that essentially all sedimentary packages in the north-dipping homoclinal belt were interpreted as thrust repeats of sedimentary units representative of the lower Povungnituk Group (i.e. Lamarche Subgroup, in the stratigraphic nomenclature of Picard et al., 1995). It is for this reason that all the various sedimentary intercalations in both the Povungnituk and also the Chukotat groups are "riding on top" of a thrust (Fig. 3a) in both the tectonostratigraphic interpretation and the mapping of St-Onge et al. (1992, 2006). This extreme interpretation also makes the important Nuvilik Formation, at the top of the Povungnituk Group, a thrust slice and its upper contact with the ore-bearing komatiites of the Chukotat Group a first-order, large-displacement thrust (Fig. 3a). Perhaps part of the motivation for this model was the early idea that there was a long-lived continuum in magmatic activity from the Povingnituk Group into the more magnesian lava flows of the Chukotat Group (e.g. Taylor, 1982[2]; Hynes and Francis, 1982), with the latter representing a more advanced stage of rifting and basin opening, and having been transported from a more northerly, outboard position. However, even as this end-member thrust model was being formulated, most other researchers considered the Nuvilik Formation greywackes and mudstones as the final stage of the Povungnituk Group (e.g. Coats, 1982; Moorhead, 1989) and essentially in place (relative to underlying and overlying lavas).

In the evolving understanding of the stratigraphy, a particularly problematic (apparent) age has been the baddeleyite upper intercept date for large mafic-ultramafic differentiated sills in the Nuvilik Formation, dated at ca. 1918 Ma (Parrish, 1989). We have previously reinterpreted those same data to reflect an age of ca. 1884 Ma (Bleeker, 2014), and, since then, reanalyzed zircon grains from this same sill[3]. The new data conclusively show this sill to be 1881.5 ± 0.9 Ma based on multiple concordant zircon analyses (Bleeker and Kamo, 2018). All currently available age data (Fig. 3b) thus show that flood basalts of the Povungnituk Group, representing a ~3–5 km thick lava sequence, are ca. 2000 to 1990 Ma, whereas Chukotat Group magmatism was initiated more than a 100 Myr later at 1883 to1882 Ma (Bleeker and Kamo, 2018). These two major magmatic events and lava sequences do not, therefore, represent a continuum but rather independent melting events below the northern Superior craton, and their lava sequences are stratigraphically stacked.

The sedimentary base of the Povungnituk Group stratigraphy, including platformal-type sedimentary rocks, overlain by finer grained sandy to silty semipelites, is locally intruded by gabbro sills that have a robust zircon age of ca. 2038 Ma (Korak sills, *see* Fig. 3b; Machado et al., 1993), thus indicating that basin formation on this part of the Superior craton (or rather its precursor, supercraton Superia; Bleeker, 2003, 2004; Bleeker and Kamo, 2018) had started well before this date of 2038 Ma and at least 40 Myr prior to eruption of the Povungnituk flood basalt sequence. Two other important deductions follow: 1) iron formation near the base of Povungnituk Group, which thickens eastward (Fig. 1), is older than 2038 Ma and likely correlates with the basal iron formation in the northernmost Labrador Trough, the Roberts Syncline area (Hardy, 1976; Madore and Larbi, 2001). It is therefore much older than the main ca. 1880 Ma Sokoman iron formation of the southern Labrador Trough; and 2) the basal part of the Povungnituk Group likely correlates in some ways with the older stratigraphy ("Cycle 1") of the Labrador Trough. These important issues are explored further in the Appendix.

Significantly post-dating the Povungnituk basaltic event, there was a flare-up of more localized alkalic volcanism, involving basanites, nephelinites, phonolites (Gaonac'h et al., 1989, 1992), and some rhyolites which have been dated at 1953 ± 3 Ma (Parrish, 1989). This is the Cécilia Formation, which is now complexly infolded into the rest of the Povungnituk Group (Fig. 1, 2), and, given its interesting makeup and importance stratigraphically, remains insufficiently documented. Besides volcanic and volcaniclastic rocks, the Cécilia Formation also involves minor carbonates and other shallow-water deposits. Early reports by Beall (1959) and Bergeron (1959) also mention conglomerates and

[2] In his more regional synthesis, Taylor (1982) saw little evidence for a break between the lower (Povungnituk) and upper (Chukotat) volcanic rocks and argued for discontinuing these two group names altogether. All of this work was undertaken prior to the first U-Pb ages in the belt.

[3] The thick lowermost differentiated sill in the Cross Lake area, also known as the "Romeo I" sill.

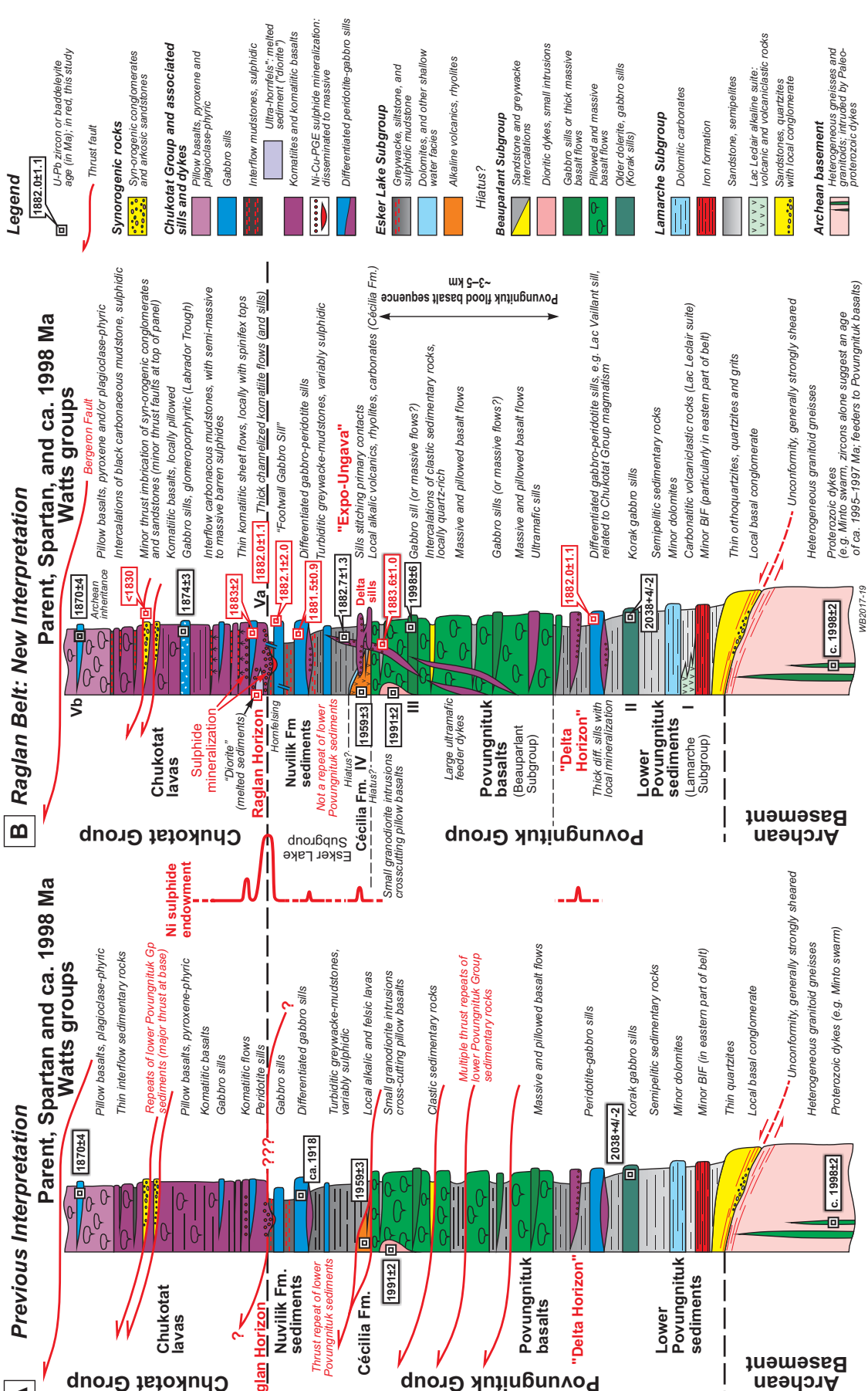

Figure 3. Lithostratigraphy of the Raglan belt. **a)** Previous interpretation, compiled from St-Onge et al. (1992) and St-Onge and Lucas (1993), with thrusts at the base of each sedimentary unit (based on a model of thrust imbrication and the repeated reappearance of lower Povungnituk sedimentary units). **b)** New interpretation based on this study, with far fewer thrust contacts. Most of the sedimentary members in the stratigraphy represent unique stratigraphic units rather than thrust repeats, in particular the important Nuvilik Formation. Conglomerate panels in the Chukotat Group are imbricated synorogenic clastic rocks. All available U-Pb ages (in Ma), as well as other details, are highlighted. Ages shown in red are from this study. See the text for references. Abreviations: BIF = banded iron formation, diff. = differentiated, Fm. = Formation, Gp = Group.

possibly some angular discordance with underlying Povungnituk basalts.

The important Nuvilik Formation is mostly younger than the Cécilia Formation and represents renewed basin formation and general basin deepening. Its lower part may interfinger with Cécilia Formation volcanic rocks, and locally includes tuffs (J. Moorhead, pers. comm., 2020). To some extent the two formations may be lateral facies equivalents. The Nuvilik Formation is overall upward fining and its upper part is characterized by thinly bedded distal turbidites and black, carbonaceous, sulphidic mudstones that formed in a below-storm wave-base setting. We have grouped the Cécilia and Nuvilik formations in an upper "Esker Lake Subgroup" to set them apart from the two lower, previously defined subgroups of the Povungnituk Group (Fig. 3b). The Esker Lake Subgroup spans a minimum of 75 Myr, from the single Cécilia Formation rhyolite age to the onset of the Chukotat event, and there could well be an important time hiatus in this part of the stratigraphy, perhaps at the base of the Cécilia Formation and (or) near its top (Fig. 3b).

All current data indicate a rapid and sudden onset of Chukotat high-volume ultramafic-mafic magmatism at ca. 1883–1882 Ma, and much of the ~3–4 km Chukotat lava pile could have developed within 1–2 Myr, as essentially all the high-precision ages overlap within uncertainty.

In summary then, no continuum exists between the magmatic evolution of the Povungnituk Group and that of the Chukotat Group. These major lava sequences are separated in time by more than 100 Myr. Just the Cape Smith Belt section of the Circum-Superior Belt experienced at least five discrete magmatic events (*see* Roman numerals I to V in Fig. 3b): early alkaline magmatism of the Lac Leclair suite (Baragar et al., 2001); Korak sill mafic magmatism at 2038 Ma (Machado et al., 1993); 2000–1990 Ma Povungnituk flood basalt eruption (Machado et al., 1993; Kastek et al., 2018) and intrusion of Minto dykes in the distal foreland (Buchan et al., 1998); ca. 1959 Ma Cécilia Formation alkaline and bimodal volcanism (Gaonac'h et al., 1989; Parrish, 1989); and the ca. 1883–1882 Ma onset of the Chukotat magmatic event (Bleeker and Kamo, 2018; this study). All of these events and the resulting stratigraphy (Fig. 3b) can be tied to Superior craton basement and/or its margin.

Returning to the issue of thrust repetition of basal Povungnituk sedimentary rocks, in the field the evidence for discrete thrust faults at the base of sedimentary panels is absent or at least ambiguous. We have walked through a number of these interpreted thrust panels and found no obvious thrust fault at their base. Many of the key contacts are stitched by synvolcanic intrusions and are thus primary. Some thrust repeats likely exist in the southernmost part of the belt (St-Onge et al., 1992, 2006), but much of the central part of the belt lacks major thrusts. Instead, many of the sedimentary intercalations of siliciclastic rocks, and the Nuvilik Formation in particular, represent regular stratigraphy. Both the lower and the upper contact of the Nuvilik Formation are stitched by mafic-ultramafic sills and dykes (Fig. 3b). A typical traverse across the transition from the Povungnituk Group to the Chukotat Group shows intense hornfelsing of uppermost Nuvilik Formation silt- and mudstones by hot, thick, basal ultramafic flows and sills of the Chukotat Group, without significant shearing, thus tying both groups together (*see also* Coats, 1982; Lesher, 1999, 2007 and references therein). This contact between the Nuvilik sulphidic silt- and mudstones and the overlying Chukotat komatiites, which defines the main ore-bearing "Raglan Horizon", is therefore a primary stratigraphic contact (Bleeker and Ames, 2017; Bleeker and Kamo, 2018). It is locally defined by thermo-mechanical erosion channels (Lesher, 1999, 2007) where hot komatiite lava flows eroded down into the Nuvilik Formation substrate and into marginally older footwall gabbro sills (Fig. 2c, 3b). Many of these channels host Ni-Cu-Co-PGE sulphides near the base of the komatiite flows, and some of the largest ore lenses occur within the deepest lava channels, on a footwall of gabbro sills that lack their upper chilled margin (e.g. Bleeker and Ames, 2017).

Higher in the stratigraphic section, several coarse clastic panels are observed within the Chukotat lavas. The fact that they consist solely of polymict conglomerate and arkosic sandstone, without also bringing Povungnituk basalts back into the section, rules out the possibility that they represent thrust repeats ramped up from the base of the Povungnituk Group. They are significantly deformed, however, and we therefore proposed that they represent synorogenic clastic wedges that were shed from a northerly source across the developing fold-thrust belt, and then captured by later, minor thrust faults, along the top of the panels (north side). These minor thrusts imbricated them within the Chukotat section (Bleeker and Kamo, 2018)[4]. We have tested this by dating detrital zircon grains, which indeed indicate that these conglomerates are younger than ca. 1830 Ma (*see* geochronology section *below*).

[4] The same explanation may equally apply to other reported occurrences of conglomerate in the belt, but we have not had an opportunity to test this for such occurrences other than the ones discussed here. The young polymict conglomerates discussed here were interpreted in some early reports (e.g. Bergeron, 1959; Beall, 1977) to indicate a significant unconformity at the base of the Chukotat Group.

U-Pb GEOCHRONOLOGY

In this section we briefly review and discuss existing geochronological data, in addition to introducing half a dozen new ages for units associated with the onset of the Chukotat magmatic event. We also present detrital zircon data for young synorogenic conglomerate panels interleaved within the Chukotat Group lavas. Ages will be discussed from oldest to youngest and going up stratigraphy, with reference to Figure 3b. A selection of the new age data are shown by means of concordia diagrams in Figures 4 and 5.

Lac Leclair Suite (Magmatic Event I)

Baragar et al. (2001) described the interesting occurrence of the alkaline (carbonatitic) volcaniclastic rocks of the Lac Leclair suite, in the same general area as the Korak sills, western Cape Smith Belt (Fig. 1). No age is available for this early magmatic suite, but it must be considerably older than 2038 Ma. Considering other magmatic events in the northern Superior craton (e.g. Ernst and Bleeker, 2010), it could be as old as ca. 2170 Ma or 2216 Ma and could perhaps assist in clarifying correlations with Cycle 1 stratigraphy of the Labrador Trough.

Korak Gabbro Sills (Magmatic Event II)

Machado et al. (1993) determined a crystallization age of 2038 +4/-2 Ma for the Korak gabbro sills, from near the base of the western Cape Smith Belt (Fig. 1). This sill was intruded towards the top of the Lamarche Subgroup. The age is based on three concordant to slightly discordant air-abraded zircon analyses and is robust within the quoted uncertainty. It demonstrates that much of the Lamarche Subgroup sedimentary units are older than 2038 Ma.

Povungnituk Flood Basalt Sequence and Minto Dyke Swarm (Magmatic Event III)

An upper intercept age of 1991 ± 2 Ma was determined for a small granodiorite intrusion or dyke cutting across pillow basalts of the Povungnituk flood basalt sequence, again by Machado et al. (1993). This age is based on three slightly discordant but collinear fractions of air-abraded zircon grains, with a near zero-age lower intercept, and is therefore robust. It probably indicates the end stage of Povungnituk basaltic volcanism. Recently, this age was confirmed by a baddeleyite upper intercept age of 1998 ± 6 Ma for a massive doleritic unit within the uppermost Povungnituk basalt sequence (Kastek et al., 2018). Well to the south, intruding Archean basement of the Superior craton, large northwest-trending mafic dykes, referred to as the Minto swarm (Buchan et al., 1998), have yielded a similar upper intercept age of ca. 1998 Ma. These dykes likely represent a major dyke swarm associated with the Povungnituk basaltic magmatism and may point to a magmatic centre in the Hudson Bay area (Ernst and Bleeker, 2010). This age was partly defined by a cluster of slightly discordant zircon fractions and we are currently refining the age of these zircons using chemical abrasion techniques. Preliminary results indicate an age that may be marginally younger but within error of the result of Buchan et al. (1998). Thus, all these Povungnituk ages cluster between 2000 and 1990 Ma and there is currently no evidence for Povungnituk basaltic volcanism to have continued to much younger ages. As dating methods have improved, protracted basaltic flood volcanism spanning tens of millions of years is rare, if not absent, in the modern record. We thus view the alkaline volcanism of the Cécilia Formation as a discrete younger magmatic pulse after a ~30 Myr hiatus.

We note that ages for the Watts Group basalts and ultramafic cumulate rocks, along the northern margin of the fold-thrust belt, also fall within the same 1990 to 2000 Ma interval as that of the Povungituk basaltic volcanism. It seems likely that this age equivalence points to a connection that yet remains to be fully understood. Could the Watts Group represent a northern rifted margin of essentially Povungnituk basaltic units, including layered ultramafic rocks?

Cécilia Formation Volcanism (Magmatic Event IV)

The interesting Cécilia Formation (Gaonac'h et al., 1989, 1992; Picard et al., 1990) remains insufficiently documented. It occurs in the central part of the Cape Smith Belt, overlying and infolded with the Povungnituk Group. It is described as alkaline and comprising mostly volcaniclastic rocks. A rhyolite associated with this volcanic package has been dated at 1959 ± 3 Ma (Parrish, 1989), but data remain unpublished.

Onset of the Chukotat Event, Lac Vaillant Sill and Expo-Ungava Dyke (Magmatic Event Va)

Differentiated gabbro-peridotite sills with thick lower sections of ultramafic rocks occur at various levels within the stratigraphy (Fig. 3b). These have long been correlated with the Mg-rich Chukotat lava sequence based on geochemical similarity (e.g. Hynes and Francis, 1982). We have dated gabbros from near the top of the ~400–500 m thick "Lac Vaillant sill"[5], exposed immediately east of Lac Vaillant in the southern part of the belt, at 1882.0 ± 1.1 Ma (Fig. 4a). This age is based on several chemically abraded single zir-

[5] This large sill east of Lac Vaillant also goes by the name "Gulf Sill" (M. Houlé, pers. comm., 2020).

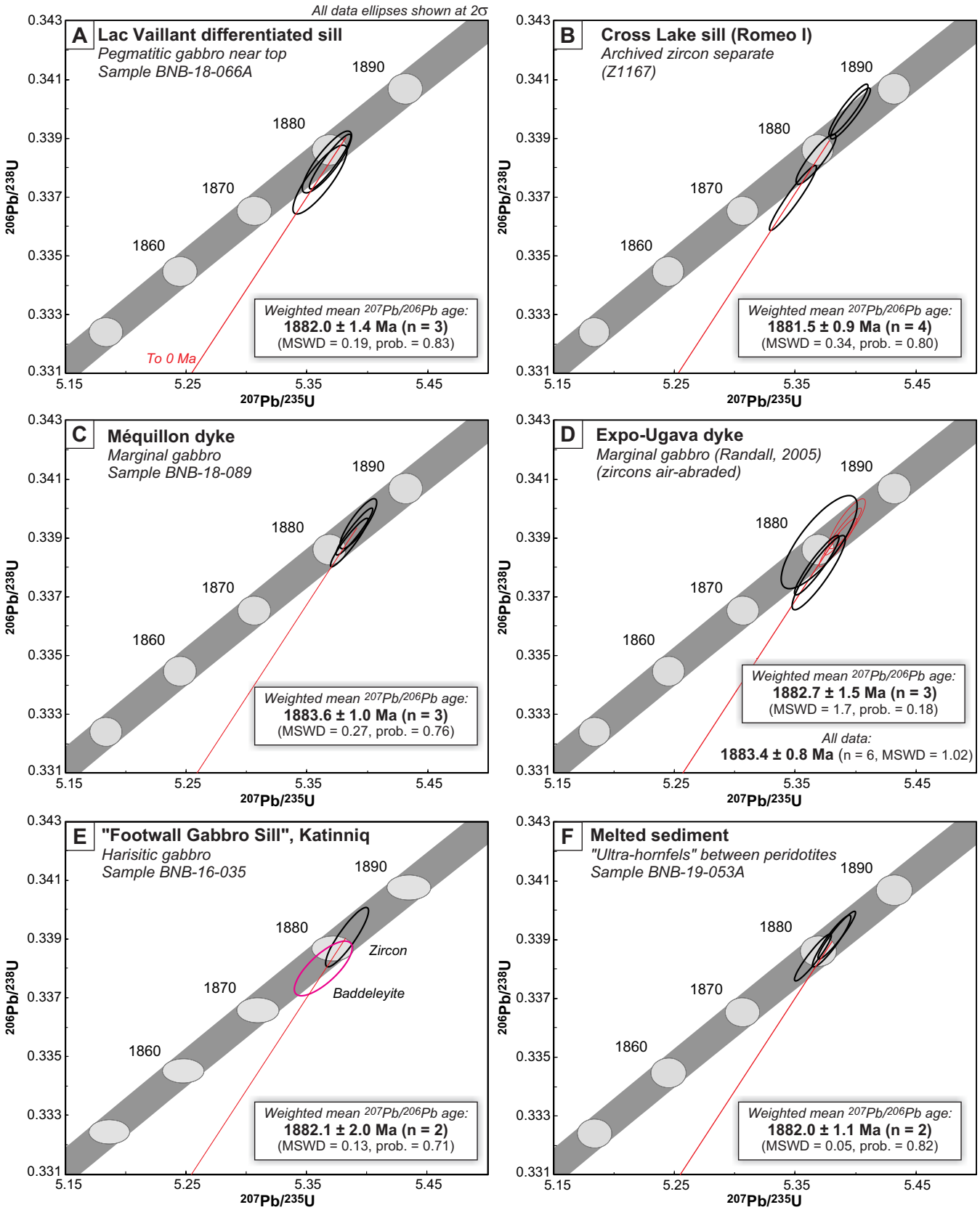

Figure 4. U-Pb concordia diagrams for selected results from this study. All data are from chemically abraded zircons and mostly single crystals, unless otherwise indicated. Abbreviations: MSWD = mean square weighted deviation, prob. = probability.

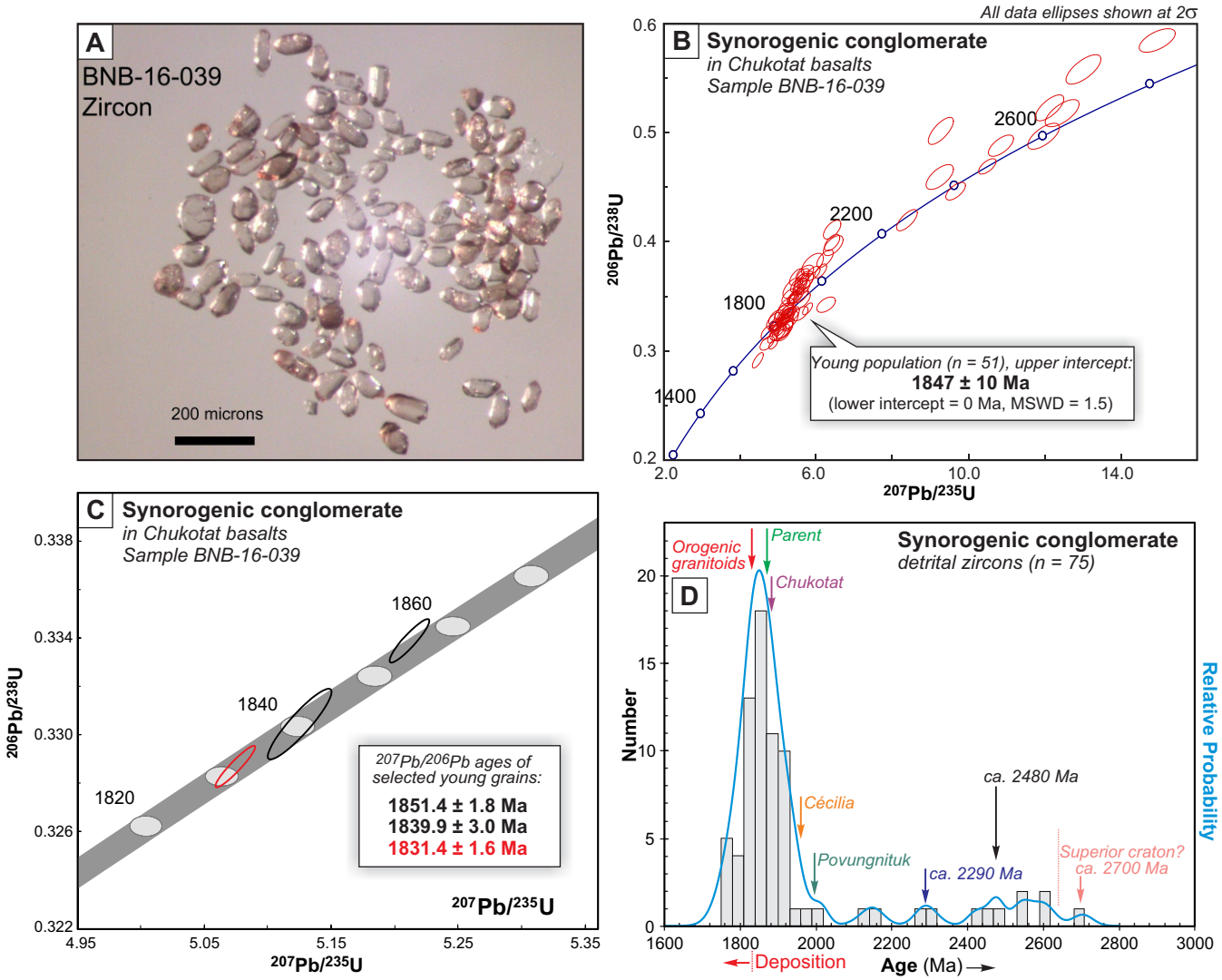

Figure 5. U-Pb results for ~80 detrital zircons from the synorogenic clastic rocks imbricated with the Chukotat lavas. **a)** Image of zircon grains selected for laser ablation analysis. The selection was more or less random but favoured clearer grains to optimize chances for good results. **b)** Summary of the laser ablation data presented on a standard Wetherill U-Pb concordia plot; note the dominant young population and the relative absence of grains >2650 Ma that would indicate a Superior basement source. **c)** CA-ID-TIMS results for three selected grains from the young population, with the youngest concordant zircon analysis indicating a maximum depositional age of 1831 Ma. **d)** Relative probability plot of all the laser ablation data showing the dominant young "orogenic" population and relative absence of Superior basement-derived grains. Abbreviation: MSWD = mean square weighted deviation.

con grains, all of which are concordant. This high-precision age confirms the connection with the Chukotat event.

Higher in the stratigraphy, linear outcrops of ultramafic rocks, with an overall west-southwest trend, define a large, steeply dipping, dyke-like body that can be followed for several tens of kilometres (e.g. Mungall, 2007; *see* Fig. 1). It is the host of disseminated Ni-Cu-PGE sulphide mineralization, including the Expo and Ungava orebodies which have been mined by open pit, as well as several other prospects. Randall (2005) presented an age of 1882.7 ± 1.5 Ma[6] for this dyke based on air-abraded zircon analyses on a sample of marginal gabbro from the Expo area (Fig. 4d). We have dated a second sample from the western continuation of this locally >300 m wide dyke in the Méquillion area[7]. This sample also contained zircon. Using modern chemical abrasion (CA) ID-TIMS methods[8], these zircon grains yield a crystallization age of 1883.6 ± 1.0 Ma (Fig. 4c), within error of the previous result presented by Randall

[6] Mineral separation and U-Pb analyses done at the Jack Satterly Lab, University of Toronto, by S. Kamo.

[7] A sample of coarse-grained gabbro was collected from the northern margin of the dyke at the Méquillon showing by M. Houlé.

[8] Chemical abrasion-isotope dilution-thermal mass spectrometry (CA-ID-TIMS).

(2005). Combining six data points from these two data sets of the same overall body, and all done at the same laboratory, these data defines a weighted mean $^{207}Pb/^{206}Pb$ age of 1883.4 ± 0.8 Ma (Fig. 4d).

Given the size and steep attitude of this very large differentiated dyke (~30 km long, steep, and at high angles to stratigraphy), and that it intrudes across the Povungnituk Group and into the base of the Nuvilik Formation, it is very likely to have reached the surface at the time of intrusion. Thus, it likely acted as a major fissure-like feeder to the lowermost Chukotat komatiite lava flows.

Although at the limit of what we can currently resolve, there is a hint in the overall U-Pb data set that this well dated dyke, at least its margin, with a crystallization age of 1883.4 ± 0.8 Ma, is among the oldest Chukotat-related units and that it is marginally older than the precisely dated Cross Lake sill with an age of 1881.5 ± 0.9 Ma (Fig. 4b; *see below*). It is possible therefore that many of the ultramafic sills are marginally younger, and that the Chukotat event was initiated by dyke intrusion and eruption of high-volume komatiite flows. As the lava pile thickened, silling may have become more important.

Footwall Gabbro Sills (Magmatic Event Va, continued)

The Nuvilik Formation is intruded by numerous gabbro and differentiated gabbro-peridotite sills. One of these large differentiated sills, at Cross Lake, near the western end of the Raglan belt proper, produced the earlier 1918 +9/-7 Ma upper intercept age interpretation of Parrish (1989). Using modern CA-ID-TIMS methods, we have redated the remaining zircon grains from this same sample, showing it to be 1881.5 ± 0.9 Ma (Bleeker and Kamo, 2018; Fig. 4b). We have also dated several other gabbro sills, including the main "Footwall Gabbro Sill" below the main komatiitic lava channel at Katinniq, which forms the immediate footwall to some of the larger ore lenses (e.g. Barnes et al., 1982; Lesher, 2007). The sample from this sill returned an age of 1882.1 ± 2.0 Ma (Fig. 4e). All of these sills are metamorphosed and the zircons recovered from these samples vary in quality, abundance, and how they respond to the chemical abrasion pre-treatment, a procedure that is critical to achieving concordance by removing open system domains (Mattinson, 2005). Some of the minor dispersion among the various dating results is therefore, in all likelihood, largely a function of this variability in zircon quality. All the ages overlap within uncertainty. In some samples we also recovered baddeleyite, but in most cases they display minor secondary zircon overgrowths and generally returned more complex data than those zircon grains that could be successfully treated with chemical abrasion.

Melted Sediments Interleaved with Main Komatiite Flows and Sills

From the many hundreds of exploration drillholes that intersect the lowermost Chukotat Group, in search of and to delineate the lenses of basal sulphide mineralization, some holes intersect anomalous rocks of igneous aspect but of more intermediate composition than the komatiites. Some of these intersections have been logged as "diorite" or "leucogabbro" (Raglan exploration staff, pers. comm., 2019), and in some cases can be shown to be grading into high-temperature hornfelsed sedimentary rocks of the Nuvilik Formation between thick peridotite bodies. Their mineralogy is dominated by randomly orientated, zoned, plagioclase crystals, granophyre with K-feldspar but little quartz, dark mica (both biotite and stilpnomelane), and accessory minerals such as titanite, zircon, and disseminated sulphides (Fig. 6). They clearly represent in situ melting and subsequent crystallization of siltstone and mudstone between thick (~100 m), hot, peridotite bodies—most likely a thick komatiite lava channel above and a sill-like invasive flow below. Heat input from both sides led to wholesale melting of the silt- and mudstones; we like to refer to this distinctive rock type as "ultra-hornfels". One of the intersections of such ultra-hornfels studied in detail contained newly crystallized zircon crystals of sufficient size to be separated, thus allowing dating of the actual mineralized komatiite lava channels. Zircon cystals from this sample yield an age of 1882.0 ± 1.1 Ma (Fig. 4f).

Hanging-wall Gabbro Sills (Magmatic Event Va, continued)

Gabbro sills also intrude the komatiite flows above the basal contact of the Chukotat Group, and above some of the lowermost sulphide lenses. One such gabbro sill showed chilled margins against both underlying and overlying komatiite flows, and must have intruded some time after the effusion of the lowermost komatiite lava flows and, therefore, after the formation of the basal ore lenses. Pegmatitic gabbro from near the top of this sill returned a zircon age of 1883.0 ± 2.0 Ma, somewhat less precise but within uncertainty of all the other dated gabbro-peridotite sills (and dykes).

Gabbro Sills at Higher Stratigraphic Levels (Magmatic Event Vb)

At yet higher stratigraphic levels, one gabbro sill has returned a reported age of 1870 ± 4 Ma based on preliminary zircon analyses (R. Parrish, unpubl. data; mentioned in Lucas and St-Onge, 1992; *see* Fig. 3b). Interestingly, this sample was reported to also contain inherited Archean zircon crystals. We have not yet independently confirmed this younger age. We do note, however, that at the larger scale of the Circum-Superior

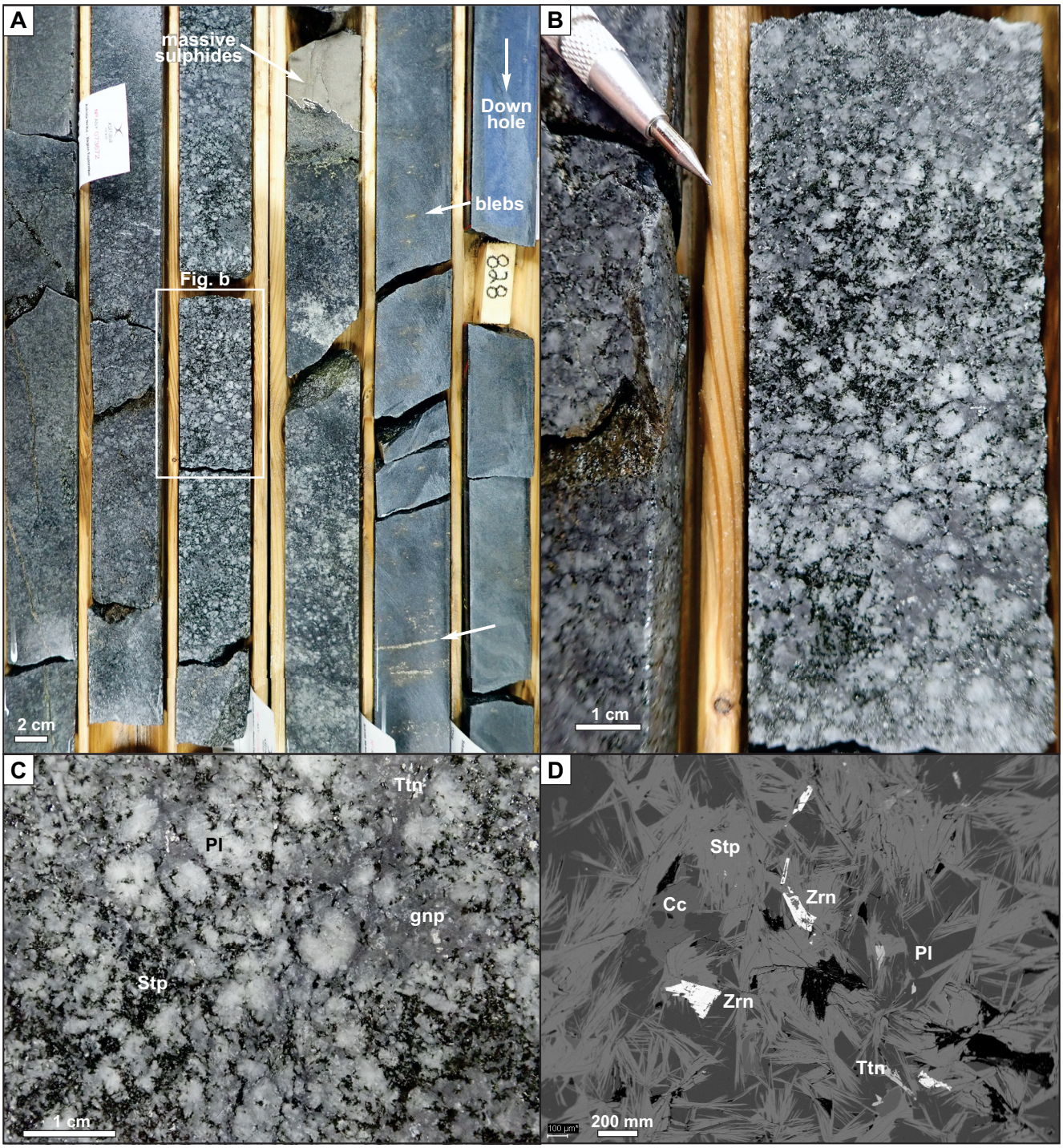

Figure 6. Images of the melted sedimentary units between large peridotite channels or sills. **a)** Overview of drill core through the base of a komatiite channel with basal sulphide blebs (~829.5 m) in contact with the melted sedimentary unit at ~831.0 m. The contact is characterized by ~5 cm of massive sulphide on the underlying unit, with the sulphides having infiltrated down to some extent. Note the pseudo-porphyritic texture in the melted sedimentary unit, in the middle of the image, which is shown in detail in (b). **b)** Close-up of the melted sedimentary "ultra-hornfels", which is dominated by feldspar (white to grey) and stilpnomelane (black) in a randomly orientated texture. **c)** Further close-up with minerals identified. **d)** Backscattered-electron image showing the skeletal morphology of zircon crystals that were used for dating. Also note the fan-like sheaves of stilpnomelane. Abbreviations: Cc = calcite; gnp = granophyric intergrowth of plagioclase and K-feldspar; Pl = plagioclase; Stp = stilpnomelane; Ttn = titanite; Zrn = zircon.

Belt, there occur a number of well dated dykes and sills in this same time interval of 1874 to 1870 Ma (Fig. 7). Hence there was a discrete younger magmatic pulse at the tail end of the Chukotat event. One such younger gabbro sill is the Haig Sill on the Belcher Islands (Hamilton et al., 2009). Another example occurs in the

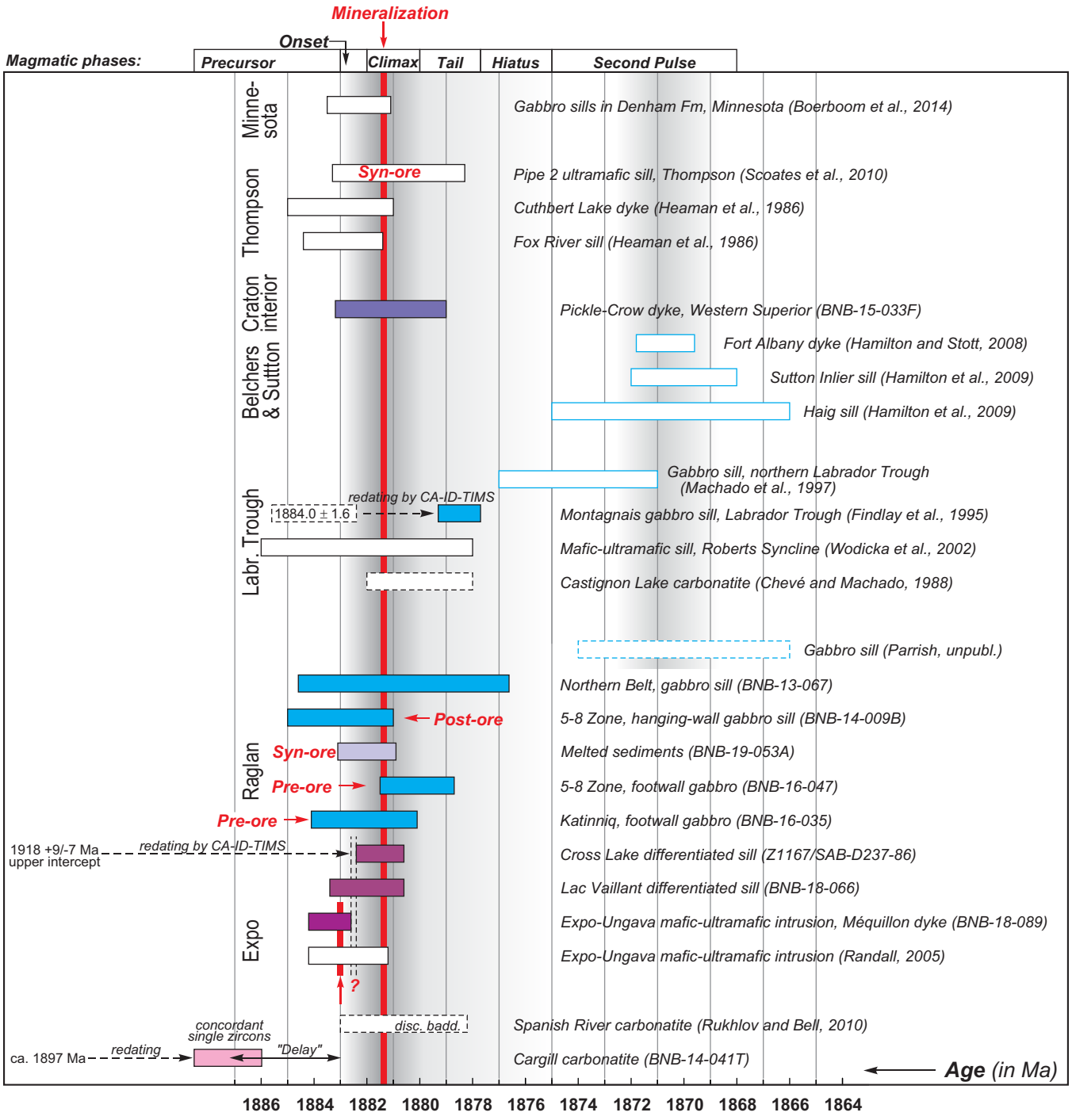

Figure 7. Summary of selected U-Pb zircon ages for Raglan and other segments of the Circum-Superior Belt. New data that were obtained as part of the present study are represented by the coloured (filled) age bars; others are referenced to the original publication as indicated. Units specifically redated for this study are identified and discussed in the text. Dates that explicitly bracket ore formation are highlighted (pre-, syn- and post-ore). The large igneous province-scale event started at 1883 Ma or shortly thereafter, and, at Raglan, peak komatiite effusion and ore formation (mineralization) occurred at 1882 ±1 Ma. The "Chukotat magmatic event" can be divided into several magmatic phases as shown at the top of the diagram. Data for a number of units across the Superior craton also indicate a distinct younger pulse at ca. 1870 Ma. Abbreviations: CA-ID-TIMS = chemical abrasion-isotope dilution-thermal ionization mass spectrometry; disc. badd. = age based on discordant baddeleyite; Fm = Formation; Labr. = Labrador.

northern Labrador Trough, where Machado et al. (1997) dated one of the glomeroporphyritic gabbro sills intruding the Hellancourt Formation, which can likely be correlated with the Chukotat Group. This sill returned a zircon age of 1874 ± 3 Ma (Fig. 3b). Further south in the Labrador Trough, we have refined the age of one of the type samples of these glomeroporphyritic "Montagnais" gabbro sills to 1878.6 ± 0.8 Ma (Bleeker

and Kamo, 2018; *see* Findlay et al., 1995, for original date of 1884 Ma). These plagioclase porphyritic gabbro sills are therefore clearly younger and more evolved than the earlier komatiitic magmas at the onset of the Chukotat event (*see* Appendix for regional correlations with the Labrador Trough).

Synorogenic Conglomerates and Sandstones Structurally Interleaved within the Chukotat Group

Several panels of polymict conglomerate and pink arkosic sandstone occur within the Chukotat Group (St-Onge et al., 2006). These panels are deformed with a composite cleavage fabric compatible with north-over-south deformation. As essentially all other sedimentary intercalations in the Chukotat Group lavas consist of either sulphidic mudstone or komatiitic-basaltic volcaniclastic material (the latter interpreted as proximal debris flows of reworked lava flows), these polymict conglomerates and sandstones appear distinctly out of place. As these panels do not bring back other Povungnituk Group rocks, we can rule out that they are brought up by thrusts from the very base of the sequence (cf. St-Onge et al., 1992). An alternative possibility is that these panels are lenses of synorogenic clastic rocks that were shed across the fold-thrust belt in alluvial fans and subsequently imbricated within it by later thrust movement. We have tested this prediction by investigating the detrital zircons from one of these panels. A selection of ~80 whole zircon grains was mounted on tape and analyzed by laser ablation to determine approximate ages, without destroying most of the grains[9]. We then analyzed a selection of the youngest grains by CA-ID-TIMS, with the youngest grains being ca. 1831 Ma (Fig. 5). These grains must indeed have been derived from orogenic granitoid rocks towards the north, with the compositionally immature conglomerate representing an apron of molasse being shed to the south across the Cape Smith fold-thrust belt. That the conglomerate now occurs imbricated within the Chukotat lavas indicates that there was a renewed, late, thrusting event, younger than 1830 Ma, most likely associated with the uplift of the Kovik Antiform core complex (Bleeker and Kamo, 2018).

INTEGRATING STRATIGRAPHY AND STRUCTURAL DEVELOPMENT

Here we elaborate on the structural development of the Cape Smith fold-thrust belt, and in particular the setting of the Raglan Horizon in the central part to the thrust belt. A generalized cross-section was already introduced in Figure 2.

All observations support the interpretation that the Cape Smith Belt represents a fold-thrust belt that was transported to the south onto the craton, and preserved by down-folding into a broad synclinorium on the south side of the Kovik Antiform. In Figure 8, we explain in more detail some of the key features of the structural development, again using a cross-sectional perspective.

Figure 8a shows a south-to-north model cross-section of the Cape Smith Belt, with ~7 main thrust sheets, stacked in a moderately north-dipping homoclinal thrust stack. Key features are the flexed-down basement of the northern Superior craton in the south, the main shear zone (basal décollement), across which progressively more transported thrust slices were emplaced onto the craton, the progressive thickening of the thrust stack towards the north, and the potentially allochthonous thrust sheets at the highest structural level (structural panels 6 and 7). The inset shows the general stratigraphic template of the imbricated cover succession, which was implicit to earlier interpretations, with a single sediment package at the base of the stratigraphic sequence. Importantly, each major thrust sheet is marked by the reappearance of basal Povungnituk sedimentary rocks in the section.

Figure 8b shows a more detailed version of this same cross-section, which is essentially the end-member interpretation proposed by St-Onge et al. (1992) and St-Onge and Lucas (1993). In this section, going from south to north, each sedimentary panel is interpreted as riding on a thrust that ramped up basal Povungnituk sedimentary rocks. No less than 13 major thrust sheets are required by this interpretation. The sedimentary unit between the Povungnituk and Chukotat volcanic sequence is incorporated in this section, and St-Onge et al. interpreted yet another major thrust fault at the base of this unit (thrust fault #5 in Fig. 8b). As the Chukotat sequence was seen as a more outboard (distal) volcanic package, perhaps in part oceanic (following Hynes and Francis, 1982), and emplaced on these sediments, a major thrust was also introduced at the top of this sediment package (fault #6), going against such field observations as sills stitching contacts and hornfelsing that clearly tie these units together stratigraphically.

At Raglan (*see* arrow indicating the position of the Katinniq orebody), it is easy to demonstrate, based on numerous pillow top directions, that the Chukotat lavas sit in a south-vergent synclinal fold that is truncated on its north side by a fault (fault #7, the Cross Lake Fault) and thrust over by north-facing siltstones and mudstones (e.g. Coats, 1982), followed again by north-dip-

[9] Laser spot size of ~25 μm, and pits of ~15 μm deep; we estimate that, on average, only ~20 vol.% of the analyzed zircon grain is consumed during this process, and therefore much of the grain remains available for follow-up CA-ID-TIMS analysis.

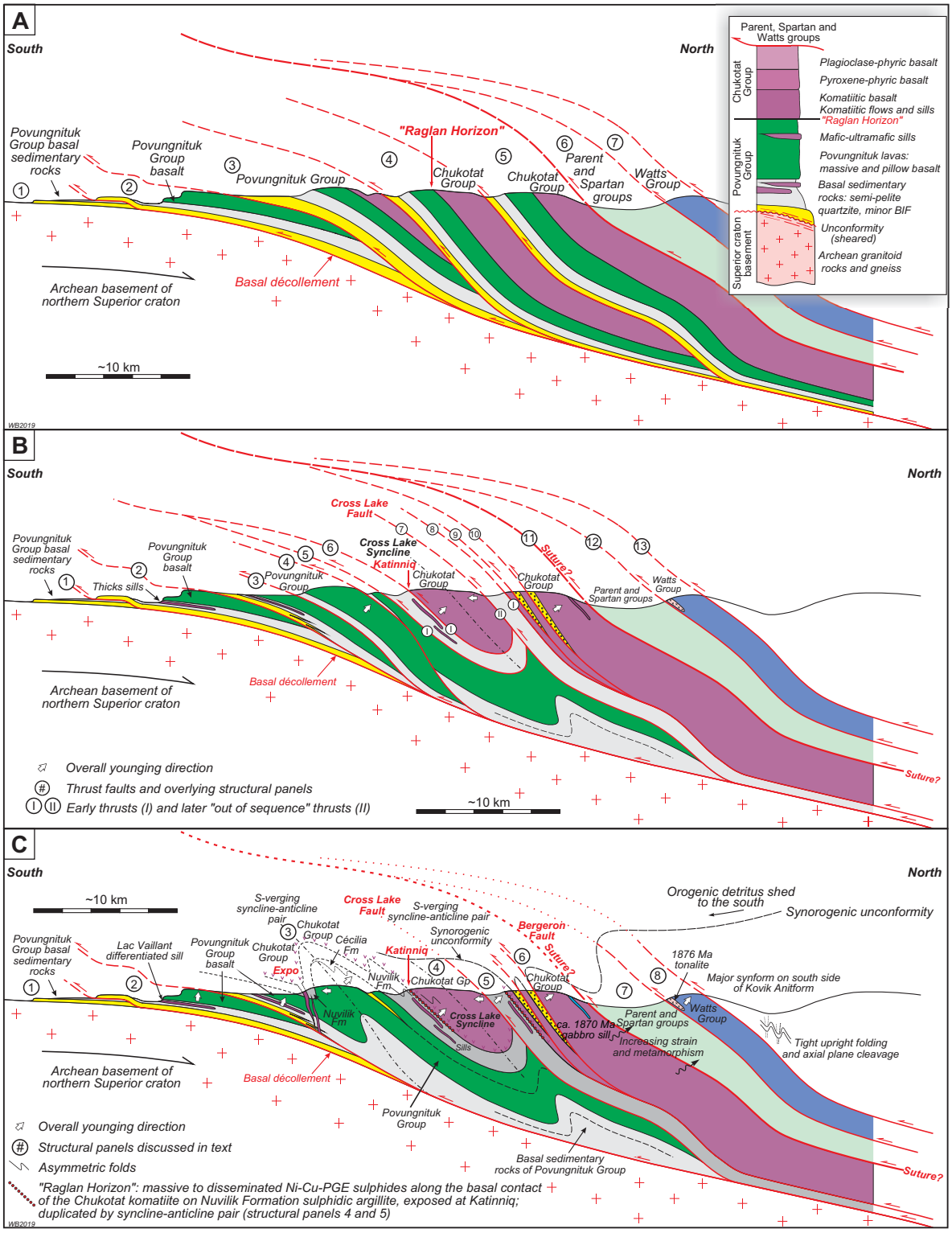

Figure 8. Model section (a) and more detailed cross-sections (b, c), all south to north, across the central Cape Smith Belt; compare with Figure 2. Many of the details are not to scale. **a)** Model section of the north-dipping homoclinal part of the Central Cape Smith Belt, using the interpretation that is implicit in the model of St-Onge et al. (1992), in which each panel of sedimentary rocks was identified as representing units ramped up from the base of the sequence (Lamarche Subgroup), following the stratigraphic template as shown in the inset. **b)** Section similar to (a) but incorporating the sedimentary unit between the Povungnituk and Chukotat lavas (i.e. the Nuvilik Formation), also bounded by thrusts. *See* the text for discussion. **c)** Reinterpretation of the same section (b) based on the present study. In this section the important Nuvilik Formation is a stratigraphic unit that marks the transition from the Povungnituk Group to the Chukotat Group, with primary depositional contacts. The upper contact with the Chukotat komatiites defines the “Raglan Horizon”. The central part of the section has far fewer thrusts and is more coherent. Two major syncline-anticline pairs define key parts of the section.

ping and north-younging Chukotat lava flows. Hence, as the Cross Lake Fault clearly cuts the Nuvilik Formation upper and lower contacts, two ages of thrust faults (I and II, *see* Fig. 8b) were hypothesized to maintain this overall model (Lucas and St-Onge, 1992; St-Onge et al., 1992).

Abundant evidence, summarized in earlier sections, argues against many of these thrust faults, and specifically against the thrust faults at the base and top of this sedimentary package, i.e. the Nuvilik Formation that separates the Povungnituk and Chukotat lava sequences. Hence, Figure 8c shows a more accurate cross-section that honours the field observations obtained as part of the current study. Other than significantly less thrust duplication, another key feature is that the mostly north-dipping fold-thrust belt incorporates two significant syncline-anticline pairs that repeat and thicken both the Povungnituk and Chukotat lava sequences. The first of these exposes the main Povungnituk basalt belt in an asymmetric anticlinal core, and brings back the Nuvilik Formation in the Expo-Ungava area to the south (*see also* Mungall, 2007). The second syncline-anticline pair involves the Cross Lake Syncline and duplicates the Raglan Horizon from Katinniq into what is known as the "North Belt" (*see also* Fig. 2). Given the stratigraphic linkages and the nature of this overall syncline-anticline pair, with the Cross Lake Syncline representing a "footwall syncline" and the Cross Lake Fault representing merely a faulted overturned limb, the net displacement on the Cross Lake Fault is probably on the order of one to a few kilometres, rather than many tens or a hundred kilometres as in the model proposed by St-Onge et al. (1992). Figure 8c also shows, in context, the position of the dated Lac Vaillant gabbro-peridotite sill in the south; the major ultramafic dykes that host the Expo and Ungava orebodies, also dated; orebody-scale asymmetric folds at Raglan (Katinniq) that repeat the Raglan Horizon on a mine scale and, off-section to the west, host the Kikialik deposit (Bleeker, 2013; *see* Fig. 2b,c); the synorogenic conglomerate panels in the Chukotat Group, in the hanging wall of the Cross Lake Fault (*see* panel #6); the required synorogenic unconformity across which molasse-type deposits were shed to the south; and the possible suture at the base of panel #7, the Bergeron Fault[10], which brings in the Parent Group volcanic rocks and associated Spartan Group greywackes.

In Figure 9, the cross-section is completed by adding the Kovik Antiform to the north and drawing attention to the major shear zone on its southern flank that eliminates much of the thrust belt. Shear fabrics along the basement-cover contact on this southern flank indicate late-stage, south-side down kinematics (Fig. 9d) and we interpret this overall structure as being due to uplift of a metamorphic core complex (the broad domal Kovik Antiform), and extensional thinning of the thrust belt on its uplifted southern flank. Extension and core complex uplift may also be related to the exhumation of high-pressure rocks in the core of the antiform further west (Weller and St-Onge, 2017; *see* Fig. 1 for location). Thin orthoquartzite units on the contact of the Kovik Antiform must be all that is left of the basal part of the Povungnituk Group, whereas prominent kilometre-scale peridotite knobs just above this contact are likely the highly extended leftovers of Lac Vaillant-equivalent sills.

At the highest structural level, peridotitic, dunitic, and pyroxenitic layered cumulates of the Lac Watts Group overlie basaltic units and may well be facing down (Fig. 9a, structural panel #9). The exact age equivalence of the Watts Group with the Povungnituk flood basalt sequence argues for these units being related, perhaps in the sense of the Watts Group being derived from a northernmost rift-type basin, and perhaps of transitional oceanic character. A key question is whether the peridotites of the Watts Group represent true mantle rocks, versus perhaps the lower cumulate parts of a layered intrusion associated with a northern extent of the Povungnituk Group. If indeed the latter, it would require significant revision of the various arc collision models (Picard et al., 1989; St-Onge et al., 1992).

Figure 9 also draws attention to some other intriguing aspects that are relevant to any accurate interpretation of these uppermost thrust sheets and what they mean in terms of a tectonic model. Near the top of the Chukotat Group (panel #6), a gabbro sill has been dated at 1870 ± 4 Ma (R. Parrish, unpubl. data) and is reported to contain inherited Archean zircon grains, suggesting a link to Archean basement even at this stratigraphic level and relative (original) position on the Superior margin. As final Chukotat magmatism, at ca. 1870 Ma, must still represent an overall extensional setting, and basin opening rather than closing, thrusting must have started well after 1870 Ma.

At approximately the same time, small tonalitic intrusions were intruded into the Watts Group (Fig. 9, panel #8). Parrish (1989) reports ages for several of these, which overlap with the tail end of Chukotat magmatism. One specifically has been dated at ca. 1876.1 ± 1.5 Ma. It seems fortuitous to link this to random events in an offshore arc, particularly as the mafic host rocks of the Watts Group already have an exact age

[10] Named after R. Bergeron, whose early mapping in the 1950s identified this major fault structure (Bergeron, 1957a,b, 1958, 1959).

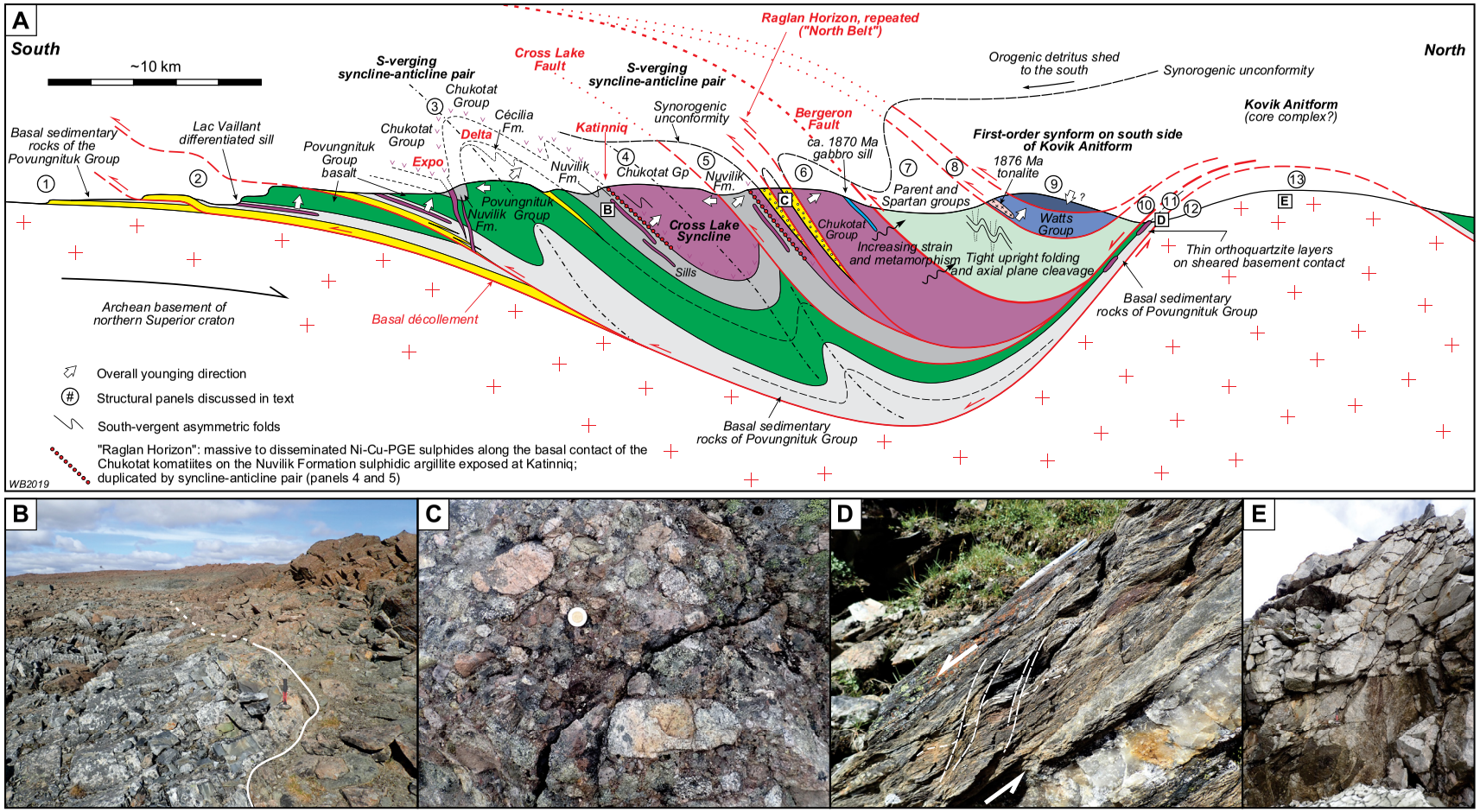

Figure 9. a) Final cross-section, incorporating the first-order basement-cored Kovik Antiform that flanks the north side of the Cape Smith Belt. Structural panels in the section are (1) Autochthonous foreland with local outliers of lowermost sedimentary rocks overlying Archean basement. 2) Parautochthonous belt of lower Povungnituk Group rocks, with some thrust repeats. 3) The central part of the belt is dominated by the Povungnituk flood basalt sequence, outlining a major south-verging syncline-anticline pair. 4) Cross Lake Syncline hosting Chukotat flows and sills that stratigraphically overlie the Nuvilik Formation. 5) Thrust repeat of Nuvilik Formation and overlying Chukotat lavas. Panels 4, 5, and 6 define a south-verging, faulted syncline-anticline pair. 6) Uppermost Chukotat panel with imbricated synorogenic clastic rocks (*see* Fig. c). Note also the gabbro sill dated at 1870 ± 4 Ma near the top. 7) Upper thrust sheet of possible arc rocks, the Parent and Spartan groups. The major fault at the base of this panel is the Bergeron Fault. 8) Watts Group basalts, gabbros and dykes, with ca. 1876 Ma tonalite intrusions. 9) Upper panel of the Watts Group comprising ultramafic rocks, perhaps facing down? 10) More strongly deformed and metamorphosed Spartan and Parent group rocks on the flank of the Kovik Antiform. 11) Highly deformed amphibolites and schists, including quartzites, overlying tectonized Archean basement; likely thinned and highly deformed equivalents of Povungnituk Group rocks. Kilometre-scale peridotite boudins occur in this belt, which are remnants of some of the large sills. 12) Tectonized Archean basement gneisses. 13) The less tectonized core of the Kovik Antiform. Note the remarkable thinning of the fold-thrust belt on the flank of the Kovik Antiform. We interpret the Kovik Antiform as a metamorphic core complex that was uplifted and exhumed at a late orogenic stage, perhaps at ca. 1820–1790 Ma. **b)** Basal contact of the Romeo I sill, cutting across but subparallel to hornfelsed thinly bedded wackes of the Nuvilik Formation, indicating a primary contact; view to the west. Hammer for scale. **c)** Polymict synorogenic conglomerate panels imbricated in Chukotat lavas. Diameter of the coin for scale is 28 mm. d) Late, south-side-down, extensional shear zone on the south flank of the Kovik Antiform; view to the west. Pencil for scale is 15 cm. **e)** Heterogeneous Archean gneisses and granitoid rocks in the core of the Kovik Antiform. Hammer for scale.

match to the Povungnituk basalts. More likely perhaps, Chukotat magmatism led to melting of Povungnituk/Watts group units, locally producing tonalitic magmas. More detailed work on the zircon populations in these various units may help solve these questions.

In summary, in the stratigraphic framework as currently understood (Fig. 3b), the entire Chukotat Group appears tied to the Povungnituk Group and, in turn, to Archean basement. This basement was likely thinned by synmagmatic extension, providing the lithospheric thin spot that allowed large-scale decompression melting. Even the MORB-like upper Chukotat lava flows cannot be fully oceanic, as hypothesized by earlier authors (Hynes and Francis, 1982; St-Onge et al., 1992). This link to basement is supported by inherited Archean zircon grains in the youngest gabbro sills with ages of 1870 ± 4 Ma. As Chukotat magmatism was still active at 1870 Ma, thrusting (and subduction?) must have started much later, not prior to 1870 Ma (cf. Lucas and St-Onge, 1992). Late re-imbrication occurred after 1830 Ma.

The presence of an accreted arc and a true suture, indeed most likely at the base of the Parent Group (the fault at the base of panel #7, the Bergeron Fault), depends entirely on an accurate interpretation of the Parent and Spartan groups. In the model of St-Onge et al. (1992), these units represent the leading edge of the Narsajuak Arc, and the boundary between panels #6 and #7 would be the remnants of a north-dipping subduction interface.

As is clear from this brief review, a number of observations remain to be explained and significantly complicate the details of published arc collision models. Resolution of some of these issues could greatly benefit from a more detailed follow-up, using SHRIMP, on the various archived zircon populations of such samples as the late gabbro sills and the tonalite/diorite intrusions, as well as various Watts and Parent group units. A full review of these issues is beyond the scope of this report and best deferred to a later date when such data are available.

THE SETTING OF MINERALIZATION

Ni-Cu-Co-PGE Ore Systems

With a more refined stratigraphic and structural framework, we can now return to the detailed setting of Ni-Cu-Co-PGE mineralization. In previous publications, the mineralization has often been discussed as occurring along two different belts or trends: 1) a main northern belt at Raglan, i.e. the "Raglan Horizon" (e.g. the Katinniq orebody shown in Fig. 8, 9; *see also* Fig. 1, 3b), and 2) a southern belt associated with various ultramafic sills, particularly the Delta sill and thus generally referred to as the "Delta Horizon" (e.g. Giovenazzo et al., 1989; St-Onge and Lucas, 1994). It is evident from the stratigraphic and structural sections shown here that this view needs some modification.

The "Raglan Horizon" is clearly structurally duplicated by the faulted syncline-anticline pair involving the Cross Lake footwall syncline and Cross Lake Fault, with the northern structural repeat of the Raglan Horizon referred to as the "North Belt" by exploration staff at Raglan Mine. The southern "Delta Horizon" is a collection of different ultramafic sills, not all at the same stratigraphic level. The Delta sill *sensu stricto*, intruding the Cécilia Formation, is just one of these sills, but other sills such as the large Lac Vaillant sill occur lower in the lithostratigraphy (Fig. 1, 3b). None of these have been mined to date. The Delta sill, specifically, has received attention for PGE mineralization (Picard et al., 1995).

Finally, the Expo, Ungava, and Cominga orebodies, and other showings such as Kehoe and Méquillon (*see* Mungall, 2007; McKevitt et al., 2020) are associated with the major ultramafic feeder dyke system in the south, with variable amounts of disseminated sulphides occurring in parts of this ~30 km long dyke. Examples of this mineralization are shown in Figure 10. This dyke cuts at high angles through Povungnituk Group units, reaching up into the southern synclinal outlier of the Nuvilik Formation (Fig. 2, 3b, 8c, 9). Therefore, it is very likely to have acted as one of the feeders to the Chukotat lava flows. No other potential feeder dyke system is known in the belt.

From all these different settings, the main Raglan Horizon, along which major, very hot, high-volume and high flow-rate channelized komatiite lavas flowed out across a substrate of sulphidic sediments of the Nuvilik Formation, is by far the most dynamic setting and, consequently, hosts the largest amount of high-grade sulphide ore (Fig. 11, 12). It is this stratigraphic ore horizon that elevates the Cape Smith Belt to a world-class Ni-Cu-Co-PGE district with several operating mines (~30 Mtonnes of ore). Large komatiite lava flows will inevitably channelize (gravity!), and thus thermo-mechanically erode into their footwall or substrate due to very high temperatures and turbulent flow (Huppert et al., 1984; Lesher et al., 1984; Huppert and Sparks, 1985; Williams et al., 1998), and thus necessarily interact with proximal sulphide sources (i.e. the Nuvilik deep-water mudstones). Such interaction is much less predictable in sill or dyke settings, if any occurs at all. Many of the sills are devoid of sulphide mineralization and appear to represent less dynamic magma inflation events, perhaps just a single pulse, followed by in situ differentiation and crystallization (*see also* Lesher, 2007).

Sulphide-bearing mudstone of the uppermost Nuvilik Formation, the stratigraphic substrate (ambient seafloor) across which the Chukotat komatiite flows

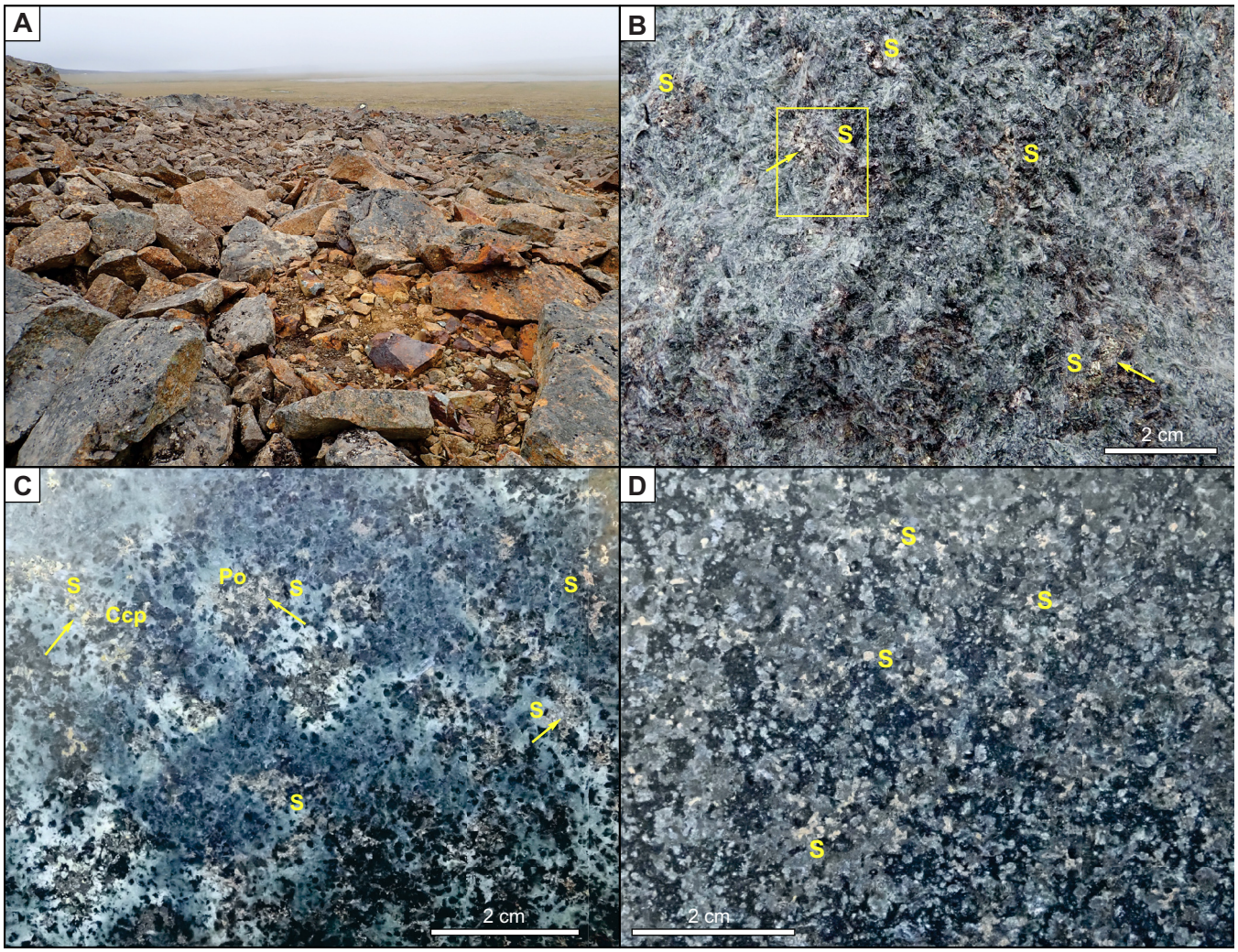

Figure 10. The ore environment of the Expo-Ungava ultramafic dyke system. **a)** Field photograph along the northern margin of the large ultramafic-mafic dyke intrusion, Kehoe showing; view towards the west. Note the gossanous blocks among the frost-heaved material. **b)** Fresh surface of one of the gossanous blocks showing ~5–10% sulphides in amphibole-altered pyroxenitic host rock. Sulphide aggregates (S) are highlighted. **c)** Polished slab from the same locality. Sulphide aggregates (S) show both chalcopyrite (Ccp) and Fe-Ni sulphides (Po), with an overall grade of ~2 wt% combined Ni and Cu. **d)** More olivine-rich rock, further into the dyke, with ~3–5 wt% disseminated sulphides.

were emplaced, acted as a proximal sulphide source for the Raglan Ni-Cu-Co-PGE sulphide orebodies, as has long been surmised empirically (Barnes et al., 1982; Coats, 1982;). This is supported by S isotopic data (Lesher, 2007). The numerous mafic-ultramafic differentiated sills, now all dated to the same short-lived event and spatially correlated with the komatiite flows on a regional scale, must be part of a complex and extensive feeder system that tapped into a deeper translithospheric plumbing system (e.g. Fig. 13b) somewhere in the northern root zone of the thrust belt. Dynamic parts of this feeder system could host economic mineralization, such as in the Expo-Ungava dyke setting, but the base of the komatiite lava pile, in direct contact with Nuvilik Formation sulphidic mudstones, is more prospective and predictable.

Raglan is perhaps unique, certainly in Canada, in terms of the scale and preservation of the komatiite lava channels (e.g. Lesher, 1999, 2007). It bears many similarities to the Thompson camp (~100 Mtonnes), northern Manitoba, generated by komatiitic magmatism of identical age (see Fig. 7) and resulting from the same overall large-scale magmatic event, but where many of the primary relationships have been destroyed by intense polyphase deformation and high-grade metamorphism (Bleeker, 1990a,b,c). Lessons from Raglan may change some of the interpretations of the Thompson geology, and perhaps the role of large, deeply eroding komatiitic lava channels has been under-estimated at Thompson. Worldwide, some of the best developed komatiitic lava channels and associated Ni-Cu-PGE mineralization occur, of course, in the late Archean greenstone belts of the Yilgarn craton, particularly at Kambalda and Perseverence, where the critical concept of lava channels and dynamic interaction with sulphidic footwall rocks was first recognized and

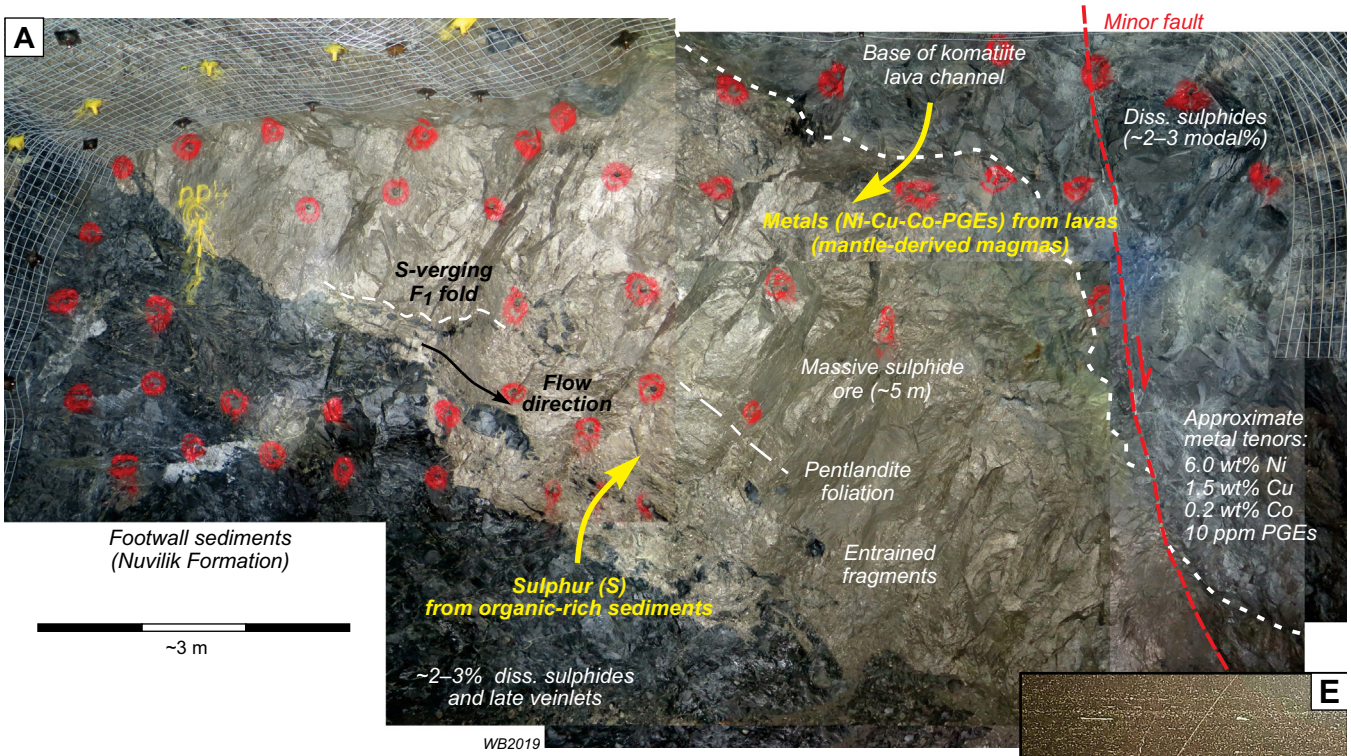

Raglan lava channel: cross-section through base of 7C Lens
(*face of Access Drift 7D-1130, view towards 230°*)

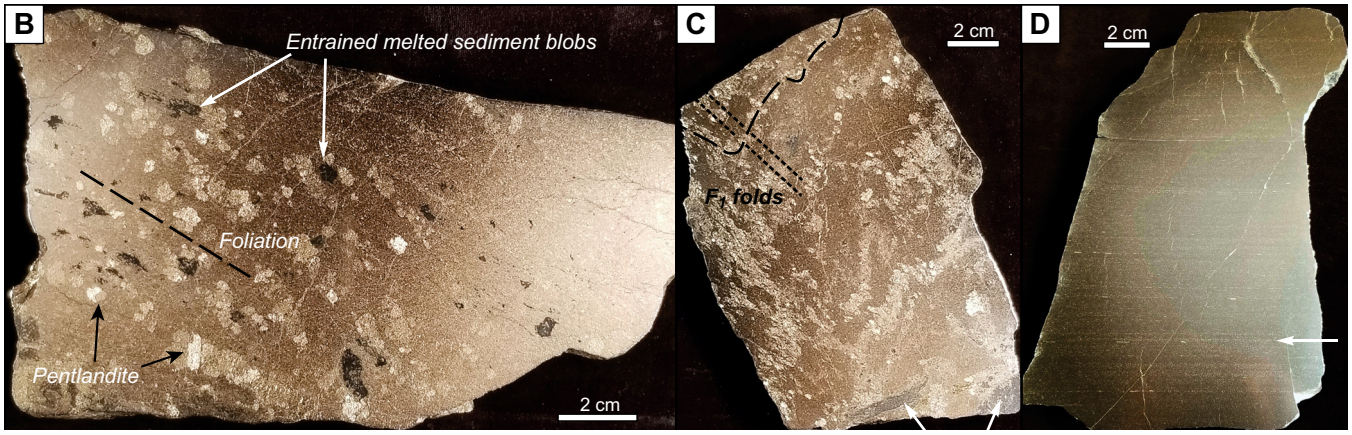

Figure 11. Cross-sectional view of one of the main komatiite lava channels with thick basal sulphide accumulation at Raglan, at the base of the 7C Lens, Qakimajurq deposit (5-8 Zone). **a)** A nearly 5 m thick massive sulphide zone occurs at the base of a thick komatiite lava channel, overlying and interacting with sulphidic, graphitic, footwall sedimentary rocks (black) of the uppermost Nuvilik Formation. Note entrainment of fragments of the footwall sedimentary rocks into the sulphide ore, indicating an original flow direction in the channel to the north (to the right in photo). The ore lens shows minor south-vergent folding (F_1), and is offset by a minor fault on the right side. **b)** Massive sulphide ore from this ore lens, showing entrained blobs of sedimentary rocks in the process of melting into the ore. Bright blotches are pentlandite ($(Fe,Ni)_9S_8$) crystals. The ore contains considerable graphite, which tracks the high degree of footwall assimilation. **c)** Massive ore with the pentlandite foliation being folded by minor south-verging folds, with development of a new foliation. **d)** A polished slab of Nuvilik Formation sulphidic mudstone, highlighting the considerable sulphide content of finely disseminated barren sulphides (pyrrhotite) along the primary bedding and lamination. **e)** Zoomed-in view of the sulphide lamination of the mudstone, showing 2–3 modal% barren sulphides along the lamination. Some remobilization of sulphides can be seen along late fractures, some of which may be originating from the overlying ore lens.

described (Gresham and Loftus-Hills, 1981; Marston et al., 1981; Lesher et al., 1984; Barnes et al., 1988; Gole et al., 1989; Lesher, 1989; *see also* Naldrett, 2005).

Interestingly, as at Raglan, the recognition of eroding lava channels at Kambalda, and thus of a somewhat more distal volcanic setting, came in several steps. At

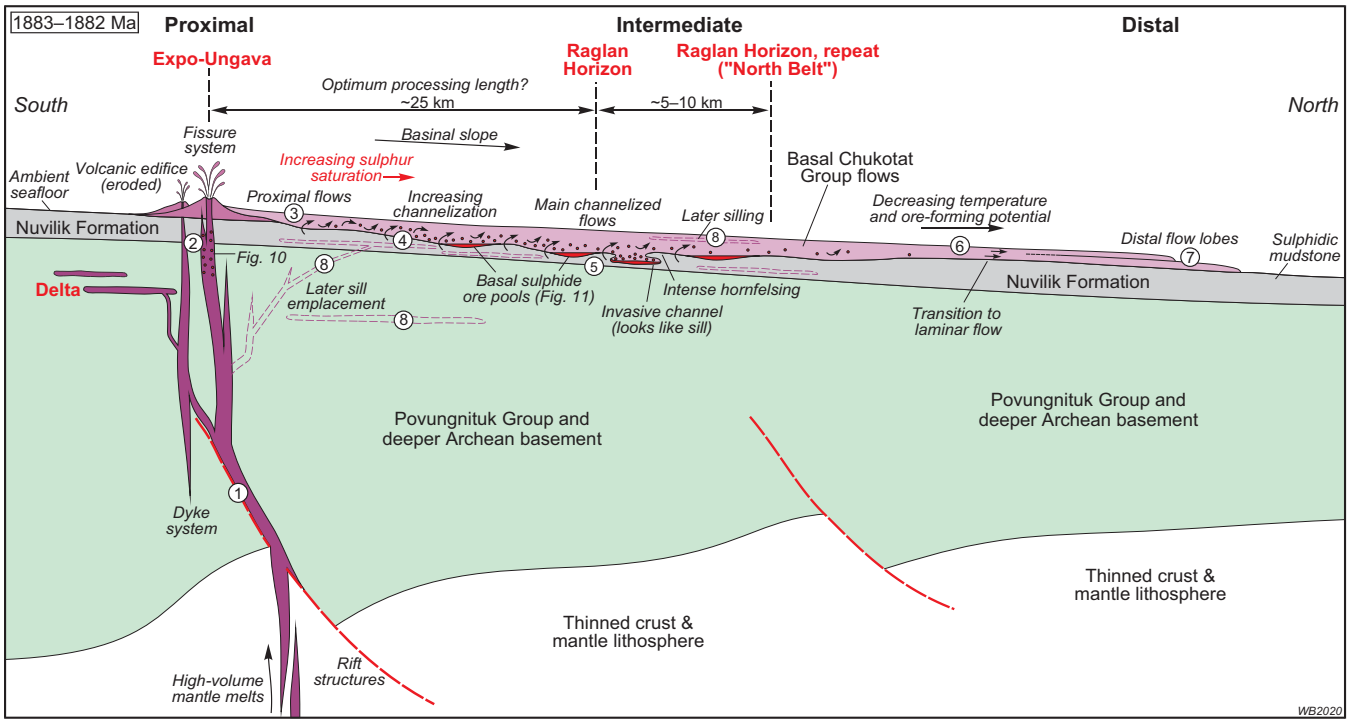

Figure 12. Key elements of the Chukotat magmatic system that generated the Raglan Horizon, in south-to-north cross-sectional view; details are not to scale. A major ultramafic feeder dyke system intruded in the south, guided by rift faults (1), resulting in a fissure system from which komatiite flows were erupted (2). These high-volume lavas flowed down a weak basinal slope in a northerly direction (3), and progressively channelized (4), while thermo-mechanically eroding into the underlying substrate of Nuvilik Formation mudstone. Channelization, erosion, and efficient mixing led to massive oversaturation of sulphides, with sulphide ore pooling out in embayments along the channel floor (5). The current position of the Raglan Horizon is indicated at a horizontal distance of ~25 km north-northeast of the fissure system. Downstream from Raglan, at an unconstrained distance, the lava flow field became less channelized (6) and terminated in lower temperature distal flow lobes of komatiitic basalt (7), devoid of mineralization. As the lava pile thickened, after multiple eruptive pulses, the emplacement mechanism transitioned to a mode where dense ultramafic magmas were emplaced as sills (8). The approximate position of the Delta sills is also shown, as are the locations of Figures 10 and 11.

first, the mineralized peridotite bodies were universally interpreted as sills and the ore environment was seen as proximal and intrusive. As spinifex textures and flow-top breccia units were recognized, the realization grew that the mineralized bodies were likely komatiite lava flows rather than sills (e.g. Barnes and Barnes, 1990 in the case of Raglan). Yet, the footwall troughs were still seen as primary topographic features filled in by the komatiite flows (Gresham and Loftus-Hills, 1981; Lesher et al., 1984; Barnes and Barnes, 1990), and a link to proximal feeding sills was maintained. A growing understanding of hot komatiite lavas, and the modelling of their turbulent flow (Huppert et al., 1984; Huppert and Sparks, 1985), and modern volcanological studies of lava channels in places such as Hawaii, finally led to the critical insight that the basal trough shapes and the elimination of flanking stratigraphy (thin sulphide-rich shale and iron formation at Kambalda; sulphidic Nuvilik mudstone at Raglan) were entirely a product of thermo-mechanical erosion. This important realization thus allows the ore-forming environment to occur in an entirely distal volcanic environment of hot channelized lava flows, decoupled from proximal feeder sills (e.g. Lesher, 2007).

This critical change in perspective naturally leads to several important next-level questions: how big can these channels be; how deep can they erode; what is their cross-sectional shape; and how far can they flow and remain prospective for sulphide mineralization? The Raglan camp may provide partial answers to these questions. If indeed the Expo-Ungava dyke and fissure system acted as the feeder system to the channels at Raglan, the basal komatiite flows occur ~25 km downstream (corrected for fold structures) from their feeder system, allowing direct interaction with sulphidic Nuvilik mudstone for part of that "processing length" (Fig. 12). Cross-sectional shapes of the channels may be complex (Huppert et al., 1984; Huppert and Sparks, 1985), perhaps locally leading to "invasive flows" that eroded laterally into the footwall strata for a limited distance. In typical drill core intersections, or in terrain of incomplete exposure, these invasive flows would be easily misinterpreted as shallow sills.

Other Ore Systems

A number of other ore systems may be represented in the Cape Smith Belt, among them various types of base

metal mineralization, as well as orogenic gold mineralization (e.g. Orford Mining's Qiqavik project, *see* https://orfordmining.com/projects/qiqavik/). The refined cross-section of Figure 9 certainly draws attention to the association of a potentially deep-reaching fault zone or suture (Bergeron Fault), multiply deformed and metamorphosed volcano-sedimentary rocks (Parent-Spartan assemblages), synorogenic magmatism, and a synorogenic unconformity and associated clastic rocks that are imbricated in the thrust belt. This overall setting bears strong similarities to Archean settings of major lode gold systems (e.g. Bleeker, 2015).

SOME REGIONAL CORRELATIONS

The stratigraphy of the Cape Smith Belt, and specifically the Raglan belt in terms of mafic-ultramafic sills with an age of 1882 Ma, can be followed further east into the northern Labrador Trough, specifically the Roberts Syncline around the northern hamlet of Kangirsuk (Hardy, 1976; Madore and Larbi, 2001; *see* Fig. 1). There, Wodicka et al. (2002) dated a differentiated mafic-ultramafic sill at 1882 ± 4 Ma (Fig. 7). This same sill, somewhat further north along the syncline, was drilled for low-grade Ni-Cu sulphide mineralization. The entire Roberts Syncline with its basal sedimentary units, including iron formation, and a thick upper sequence of massive and pillowed flows, equivalent to the Povungnituk basalts and intruded by Chukotat age sills, represents a straightforward continuation of the Cape Smith stratigraphy (*see also* Taylor, 1982), less so of the typical cyclic Labrador Trough stratigraphy described much further south (e.g. Dimroth et al., 1970; Rohon et al., 1993; Findlay et al., 1995; Clark and Wares, 2006). Where and how the transition to more typical Labrador Trough stratigraphy occurs, somewhere well south of Kangirsuk, remains to be resolved in detail (*see* Appendix).

ZOOMING OUT TO THE SCALE OF THE CRATON

Most of the U-Pb data for units associated with the Raglan Horizon, from the northern Labrador Trough to the western Cape Smith Belt, suggest a short-lived, large igneous province-scale magmatic event that initiated at 1883–1882 Ma (*see also* Ernst and Bleeker, 2010). As far as can currently be resolved (~1–2 Myr), this age is identical to that of komatiitic magmatism along the western margin of the Superior craton (Thompson, Manitoba: Bleeker, 1990 a,b,c; Scoates et al., 2017), and to the age of large intra-cratonic dykes that intruded the craton (Molson swarm: Heaman et al., 1986, 2009; Pickle-Crow dyke: Bleeker and Kamo, this study). Recently, 1882 Ma gabbro sills have also been documented from the southern margin of the Superior Craton, in Minnesota (Boerboom et al., 2014). Many of the key ages have been summarized in Figure 7.

The overall scale and volume of this magmatic event, its short-lived nature of ~1–2 Myr, its synchroneity at the craton scale, and the involvement of initial high-temperature magmas compares well to modern large igneous provinces. Consequently, we interpret the overall geodynamic setting in terms of a hot mantle upwelling, possibly a deep-seated mantle plume, that impinged on the base of the Superior craton's subcontinental lithosphere (Fig. 13). The initial ascent of this mantle upwelling may have been somewhat slower (tens of millions of years; *see* Davies, 1999; Fig. 13a), but accelerated in the uppermost mantle with overall lower viscosities. A buoyant plume head, first flattening and then rapidly spreading (~1–2 Myr) underneath thick cratonic lithosphere (Fig. 13b), flowed to "thin spots" in the lithosphere where high-volume decompression melting led to the large-scale emplacement of mafic and ultramafic magmas, and ultimately ore formation. This overall model (*see* Sleep (1997) and Griffin et al. (2013) for more background) most easily explains the rich spectrum of phenomena at the scale of the Superior craton, in particular the nearly contemporaneous emplacement of mafic-ultramafic magmatic rocks along the entire length of the Circum-Superior Belt (Baragar and Scoates, 1981).

The model also makes many predictions, a few of which are highlighted below:

- Alkaline complexes, possibly including early kimberlite clusters, were likely one of the first manifestations of the impingement of a hot mantle upwelling underneath ancient Superior craton subcontinental lithosphere (Fig. 13a; *see also* Fig. 7). Indeed, kimberlitic rocks of this age are known in the Castignon area (Chevé and Machado, 1988).
- Precise ages of such alkaline complexes (e.g. David et al., 2006; Rukhlov and Bell, 2010; this study), at the scale of the craton, may provide information on the earliest interaction and potentially outline a plume track across the Superior craton as the Superior plate (i.e. supercraton Superia: *see* Bleeker, 2003, 2004) migrated over the mantle upwelling. This could be a rich avenue of further investigation and, at a global scale, will help to identify which cratonic blocks represent the conjugate margins to specific segments of the Circum-Superior Belt (Bleeker and Ernst, 2006).
- The markedly linear trend of large, ca. 1880–1890 Ma, alkaline and carbonatite complexes across the centre of the Superior craton from James Bay to Lake Superior, and following the Kapuskasing Structural Zone (Sage, 1991), must be related to this overall event and our model (Fig. 13b) provides a context for it. This trend must have initiated as a rift zone in cratonic lithosphere just prior to 1883 Ma. We have obtained a new, concordant,

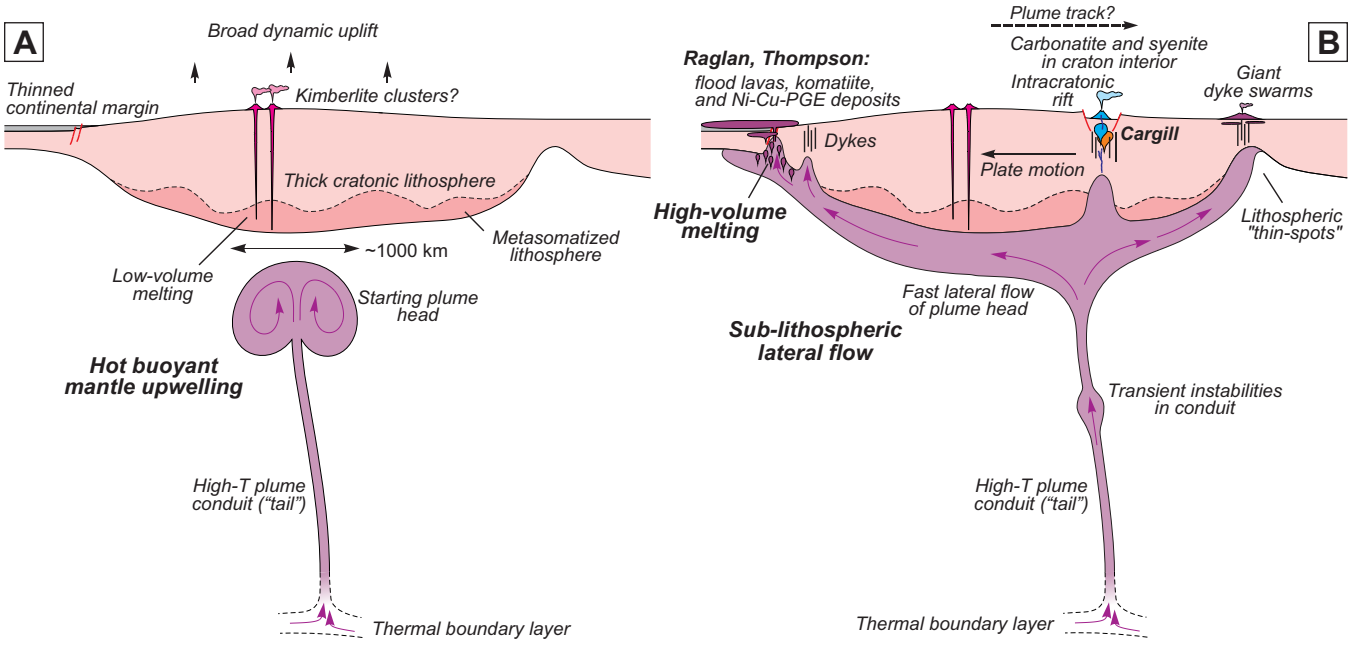

Figure 13. Interpreted geodynamic setting of the Chukotat magmatic event, at Raglan, and the broader Circum-Superior Belt magmatism. **a)** Initial slow rise of a hot mantle upwelling, possibly a mantle plume from a deep thermal boundary layer, below ancient continental lithosphere of the Superior craton. The latter was likely still part of a larger Superia plate at the time. The initial manifestations of the arrival of the hot upwelling or plume were broad uplift, possibly localized rifting, and low-volume melting of metasomatized lithosphere. **b)** Flattening and rapid spreading of the hot, buoyant, plume head below the subcontinental lithosphere and lateral flow to "thin spots", where large-volume decompression melting led to LIP-scale volumes of ultramafic and mafic magmatic rocks. Elsewhere, carbonatite complexes intruded into local rift structures in the craton interior, and giant dyke swarms intruded into fracture patterns in the crust. Events can be essentially contemporaneous on the craton scale, over a ~1 to 2 Myr interval. Transient instabilities in the plume conduit may have led to new arrivals of hot ultramafic magmas in younger pulses (e.g. Waterton et al., 2017). Overall, the spectrum of phenomena is suggestive of a continental breakup setting rather than a back-arc tectonic environment.

high-precision age of 1887 Ma for the large Cargill Complex along this zone (Fig. 7), suggesting intracratonic rifting and carbonatite magmatism preceded high-volume mafic magmatism by ~4–5 Myr, a similar delay as is seen between the Phaloborwa (2060 Ma) and Bushveld (2056 Ma) complexes in South Africa (Heaman, 2009; Mungall et al., 2016). This rifting provided the preparation and weakening for the later intra-cratonic thrusting documented along the Kapuskasing Zone (e.g. Percival and West, 1994), which was probably driven by collisions along the margin of the craton at ca. 1830–1800 Ma. This modified rift was later reactivated, again with intrusion of alkaline complexes, during ca. 1.1 Ga Midcontinent rifting (e.g. Bleeker et al., 2020).

- The overall geodynamic setting as portrayed in Figure 13 is more suggestive of a continental breakup setting than one of subduction-driven back-arc magmatism and associated upper mantle flow. Attempts to explain the ca. 1883–1882 Ma Circum-Superior Belt events in the latter context (i.e. back-arcs) may be misguided (cf. Corrigan et al., 2007, 2009). Not only are there no arcs built on the Circum-Superior margins, but arcs in general cannot explain the remarkable synchroneity of mafic-ultramafic magmatism around the Superior craton. We thus suggest that along some segments of the Circum-Superior Belt final breakup of supercraton Superia was delayed until about 1880–1878 Ma, after which the Superior craton fragment was finally isolated as an independently drifting plate.

CONCLUSIONS

We have resolved some of the persistent problems and contradictions in the stratigraphic and structural interpretation, and geochronology, of the central Cape Smith Belt, thus providing a more accurate context for the setting of world-class Ni-Cu-Co-PGE mineralization along the Raglan Horizon on the contact between the sulphidic Nuvilik Formation and the overlying Chukotat Group lavas. Neither the lower contact nor the upper contact of the important Nuvilik Formation is a thrust. Instead this formation of distal, thinly bedded turbidites and sulphidic mudstone defines the transition from the Povungnituk Group to the komatiitic Chukotat Group and represents the substrate and ambient seafloor across which the basal Chukotat komatiite flows were erupted and channelized. The Nuvilik sulphidic mudstones provided a proximal sulphur source

for the komatiitic lava channels, invasive flows, and sills.

We have dated differentiated gabbro sills, both below and above the critical contact at ca. 1883–1882 Ma, showing that the onset of the high-volume and high-temperature Chukotat magmatic event occurred at that age. To this we have now added precise zircon ages from melted sedimentary rocks ("ultra-hornfels") sandwiched between thick komatiite channels and their invasive flows, thus dating the channels and mineralization themselves. This age is 1882.0 ± 1.1 Ma based on two overlapping, concordant single zircon analyses. Our observations on one of the lava channels with thick basal sulphide ore (7C lens, Fig. 11) also provide the first robust indication of flow direction (polarity) in the channel: down-dip to the north-northeast. This important observation, together with the new ages, allows for the following scenario (*see* Fig. 12): (1) A major ultramafic feeder dyke system, perhaps guided by deep-reaching rift faults, intruded well to the south of Raglan; (2) these dykes, with a precise age at 1883.4 ± 0.8 Ma, formed an eruptive fissure system that fed the hot basal komatiite flows. From there, the high-volume komatiite lavas flowed down a gentle basinal slope in a northerly direction (3), and progressively channelized (4), while thermo-mechanically eroding into the underlying substrate of Nuvilik Formation mudstone. Channelization, erosion, and efficient mixing led to massive oversaturation of sulphides, with sulphide ore pooling out in embayments along the channel floor (5). A horizontal flow distance of ~20 to 25 km to Raglan, downstream to the northeast, may have provided an ideal "processing length" to achieve large degrees of assimilation, sulphur saturation, turbulent mixing, and final sulphide segregation and pooling, at high R-factors[11], to form the main high-grade ore lenses of the Raglan Horizon. Downstream from Raglan, at an unconstrained distance, the lava flow field became less channelized (6), and terminated in lower temperature distal flow lobes of komatiitic basalt (7), devoid of mineralization. As the lava pile thickened, after multiple eruptive pulses, the emplacement mechanism transitioned to a mode where dense ultramafic magma was emplaced mainly as sills (8), with the most precisely dated sill being emplaced at 1881.5 ± 0.9 Ma. The Raglan Horizon likely represents several subparallel lava channels, each with a cross-sectional width of ~1 km. Typical channel depths are ~100 to 150 m, and lateral erosion of the channels into the Nuvilik Formation may have taken place locally on a similar scale. In typical drill sections, such lateral expansions of the channels ("invasive flows") are likely to be misinterpreted as shallow sills.

The lithostratigraphy of the central Cape Smith Belt is more coherent and less disrupted by numerous thrusts than previously interpreted, simplifying the overall structural-stratigraphic interpretation. Clearly there are some thrusts in the belt, however, and one of these, the Cross Lake Fault just north of Raglan, duplicates the Raglan Horizon into the "North Belt". This thrust is a relatively minor reverse fault that evolved from the overturned limb of what was originally a south-vergent syncline-anticline pair. Thrust displacement on this fault is probably on the order of one to a few kilometres, rather than many tens or hundreds of kilometres. Another south-vergent syncline-anticline pair duplicates and thickens the stratigraphy further south, particularly the main belt of Povungnituk basalts and the infolded Cécilia Formation and Delta sills.

It appears the entire stratigraphy of Povungnituk and Chukotat groups, as shown in Figure 3b, is coherent and tied to the basement of the Superior craton or its margin, perhaps with some lateral offset in the sense of the youngest, uppermost lavas of the Chukotat Group being concentrated along a more extended northern margin. Whether a short-lived basin opened towards the end of the Chukotat Group deposition, at ca. 1875–1870 Ma, and to what extent the Parent-Spartan and Watts groups are allochthonous remain problematic issues. The ca. 1870–1860 Ma Parent Group and the associated sedimentary rocks of the Spartan Group represent the fill of this basin, which may simply reflect a volcano-sedimentary rift basin on thinned Superior craton crust. Ages of the Watts Group are remarkably similar to those of the Povungnituk flood basalts and may suggest a link to the Superior craton, rather than indicating some exotic, outboard, oceanic crust.

The Kovik Antiform likely reflects late uplift of low-density sialic basement from below the thickened thrust belt, as a metamorphic core complex, resulting in the formation of a major extensional shear zone on its flank and necking of nearly the entire fold-thrust belt. This uplift also drove significant re-imbrication of the thrust belt, with slices of synorogenic molasse deposits, with detrital zircon grains as young as 1831 Ma, being captured in the thrust belt. The age of this re-imbrication could be as young as ca. 1820 to 1790 Ma.

At the scale of the craton, the concept of a Circum-Superior Belt, envisioned by Baragar and Scoates (1981) almost four decades ago, is coming into focus. The new high-precision ages demonstrate essentially synchronous magmatic activity across the craton and

[11] The R-factor is defined as the mass ratio of silicate magma to sulphide magma (Campbell and Barnes, 1984). Intimate interaction and mixing of segregated sulphides with a large volume (mass) of host silicate magma (i.e. high R-factors) leads to higher grade (tenor) ores, particularly of the more chalcophile elements.

around its (present) margins at ca. 1883–1882 Ma. This magmatism is best explained by a model of a mantle plume impinging on the base of the lithosphere of supercraton Superia, prior to final breakup, with initial alkaline magmatism as early as 1887 Ma (e.g. Cargill carbonatite), followed by lateral flow of hot mantle to lithospheric thin spots, and the essentially synchronous onset of high-volume mafic-ultramafic magmatism at 1883–1882 Ma. The overall context is one of final continental break-up, with possible arc accretion and foredeep deposition occurring much later, after ca. 1850 Ma.

A wide variety of mineral deposits can be linked to this likely globally significant event, from rare metal and apatite deposits associated with early alkaline intrusions, to the Ni-Cu-Co-PGE magmatic ore systems at 1882 Ma, and the return of major Superior-type iron formation deposition at ca. 1880 Ma, all around the Superior craton (*see* Appendix). If indeed these processes are linked, it indicates that the ca. 1882 Ma Circum-Superior magmatism was of a scale sufficient to affect the global ocean-atmosphere system. At Raglan and Thompson, high-volume ultramafic magmatism caused the direct juxtaposition of dynamic hot magma systems with a prolific, crustal, and proximal sulphur source in the form of carbonaceous sulphide-rich mudstone, resulting in some of the largest Ni-sulphide deposits in Canada and the world.

FUTURE RESEARCH

An important remaining question relevant to the Raglan Horizon is the overall shape and flow direction of the komatiite lava channels (or channel?). Did the various deposits form in a single, giant, meandering lava channel, subparallel to the present surface trend of the horizon (Fig. 14b), as has been suggested by some authors (Green and Dupras, 1999; Osmond and Watts, 1999)? Or were there several subparallel anastomosing channels, now plunging, in present day coordinates, in a north- to northeasterly direction (Fig. 14c). The magnetic image that suggests that the various deposit areas are connected in a single giant west-to-east meandering channel (Fig. 14a,b), although spectacular, very likely is an artefact of more magnetic komatiite channels dipping to the north underneath a thickening hanging wall of less magnetic flows, with the magnetic anomalies merging to depth and then fading out. Our preferred interpretation is of multiple, subparallel, anastomosing lava channels flowing in an overall northeasterly direction (i.e. Fig. 14c).

Equally important, what was the flow direction in the main lava channels? In other words, what was (and is) downstream and upstream in these channels, and in terms of magmatic assimilation processes and evolving compositions? Currently, few data on flow direction are available from any of the channels or ore lenses; merely long axes of main ore lenses, which generally plunge to the northeast to north. Our observation of flow direction in the channel of Figure 11, down-dip to the north, is the first hard observation of this kind, but similar observations are needed for other key channels. These questions are relevant to how the structurally repeated North Belt relates to the main Raglan trend, and thus to its prospectivity. If the paleo-flow direction in the channels was to the north or northeast, as we indeed observed in the 7C ore lens, the North Belt would be ~5–10 km downstream from the main deposits such as Katinniq and Qakimajurq (5-8 Zone), and the major ultramafic dyke system in the southern part of the belt (Expo-Ungava) could be the principal fissure system from which the komatiite lavas were erupted. This is currently our preferred interpretation. If correct, it would indicate, after unfolding, that the main ore-forming channels such as at Katinniq were ~20–25 km downstream from their feeding fissure system, thus providing ~20–25 km of "processing length" for the intimate interaction and assimilation of the carbonaceous, sulphidic mudstone of the sedimentary substrate by the hot, eroding komatiitic lavas (Fig. 12). In addition to a local sulphide source (Nuvilik mudstone), this processing length may be critical to generating world-class orebodies.

Regionally, the interesting geology of the Cécilia Formation, and the relationships of the Parent, Spartan, and Watts groups remain insufficiently understood. Additional high-precision geochronology using more refined modern methods (e.g. chemical abrasion on single zircon grains), and detailed investigations of zircon populations (e.g. inheritance patterns, core and overgrowth relationships; detrital populations and provenance) on new and existing samples, together with detailed field studies, may help solve these problems. Some of this work is in progress, i.e. detrital zircon studies of units up through the stratigraphic column, and revisiting archived zircon populations. At the same time, the Quebec geological survey (MERN, Ministère de l'Énergie et des Ressources naturelles du Québec) is engaged in a remapping program, with geochronology support, of the Watts, Parent and Spartan groups to the north.

Farther afield, the stratigraphic and structural transitions into the Labrador Trough in the southeast (*see* Appendix), and into Hudson Bay and its various island groups to the southwest, remain to be resolved in detail. Our end goal is a full, modern integration and synthesis of all the Circum-Superior stratigraphy.

ACKNOWLEDGMENTS

This report is a contribution to NRCan's Targeted Geoscience Initiative Program (TGI). Support for this

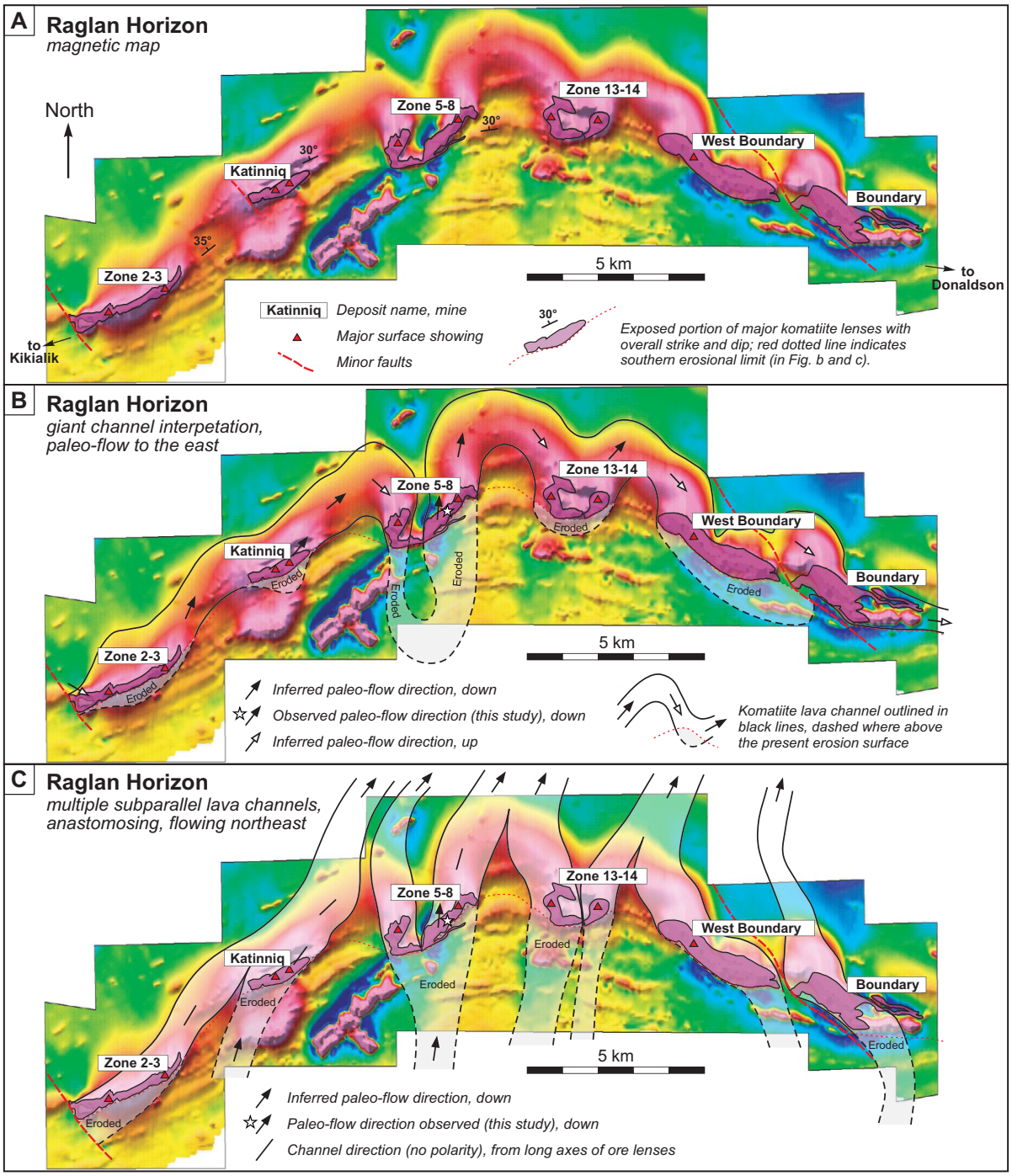

Figure 14. Magnetic map (total intensity) of the central Raglan belt highlighting the alternative komatiite lava channel interpretations; channels outlined by black lines, with dashed lines where eroded (map image *after* Osmond and Watts, 1999; and *modified after* Fig. 28 in Lesher, 2007). Hot colours (red to purple) are magnetic highs. **a)** Magnetic map image showing the exposed portions of the main peridotitic komatiite bodies. Stratigraphy generally dips ~30° in a northerly direction. **b)** The giant, single, channel interpretation of Green and Dupras (1999), locally up to 2 km wide, with tight meanders. Inferred paleo-flow directions as indicated, based on general elongation of ore lenses (but without flow polarity). Our observation of flow direction (at star), including polarity (to the north, Zone 7; *see* Fig. 11) is also shown. The overall curvature of the surface trace of the Raglan Horizon is due to late cross-folding of the belt. Therefore, the Green and Dupras (1999) interpretation is that of a giant channel flowing from west to east, parallel to the surface trace of the horizon. **c)** Our alternative interpretation of multiple, subparallel, anastomosing channels flowing down a weak basinal slope to the north-northeast. This preferred interpretation is equally in agreement with flow indicators, allows linking to the ultramafic fissure system in the south, fits an inferred basinal slope, and is less fortuitous in the sense of a single channel being exactly parallel to the present erosion surface. Broadening and merging of the magnetic highs is simply an artefact of the peridotite channels dipping and plunging to depth, below a less magnetic hanging wall of basalts. If correct, it would mean that the "North Belt" ultramafic bodies, in the structurally repeated panel north of the Cross Lake Fault, is more likely to include, at least in part, the downstream continuation of some of the main Raglan channels.

study was provided through the Orthomagmatic Ni-Cu-PGE-Cr Ore Systems Project's 'Activity NC-1.1: Extent, origin, and deposit-scale controls of the 1883 Ma Circum-Superior large igneous province, northern Manitoba, Ontario, Québec, Nunavut, and Labrador'.

The authors thank Glencore plc for their on-going logistical support for this project, without which this study would have been impossible. Many individual staff members at Raglan are sincerely thanked for their input, help with drill core sampling, and numerous discussions. Chelsea Sutcliffe of the Jack Satterly Geochronology Laboratory, University of Toronto, did the laser ablation analyses of the detrital zircon grains extracted from the synorogenic conglomerate. Sarah Davey provided skilled and efficient GIS assistance in preparing the summary map of Figure 1. Natasha Wodicka and Julie Peressini, both at GSC Ottawa, are thanked for their help and discussions on previously dated samples. Michel Houlé, GSC Quebec, provided the marginal gabbro sample from the Méquillon dyke locality, and both Michel and Mike Lesher, Laurentian University, are thanked for some of the shared fieldwork and helicopter logistics, and for discussions on Raglan geology and the history of past research. Jim Mungall provided permission to discuss the unpublished data on the Expo-Ungava dyke, as well as detailed coordinates for that sample, which were part of the unpublished thesis by Randall (2005).

This report benefited from the thoughtful review by James Moorhead, of the Ministère de l'Énergie et des Ressources naturelles du Québec (MERN). Sarah Davey and Michel Houlé critically read the manuscript. Valérie Bécu assisted with the technical editing and Elizabeth Ambrose took care of the final editing and correction of minor imperfections. Both are thanked for their skillful assistance. Last but not least, members of the TGI-5 team are thanked for taking care of a thousand little tasks from general project management to outreach and consultations, without which none of this research could have proceeded. Thank you all.

REFERENCES

Baragar, W.R.A., 1967. Wakuach Lake map-area, Quebec – Labrador; Geological Survey of Canada, Memoir 344, 174 p.

Baragar, W.R.A. and Scoates, R.F.J., 1981. The circum-Superior belt: A Proterozoic plate margin?; *in* Developments in Precambrian Geology, volume 4, (ed.) A. Kröner; Elsevier, Amsterdam, The Netherlands, p. 297–330.

Baragar, W.R., Mader, U., and LeCheminant, G.M., 2001. Paleoproterozoic carbonatitic ultrabasic volcanic rocks (meimechites?) of Cape Smith Belt, Quebec; Canadian Journal of Earth Sciences, v. 38, p. 1313–1334.

Barnes, S.J. and Barnes, S.-J., 1990. A new interpretation of the Katiniq nickel deposit, Ungava, northern Quebec; Economic Geology, v. 85, p. 1269–1272.

Barnes, S.J., Coats, C.J.A., and Naldrett, A.J., 1982. Petrogenesis of a Proterozoic nickel sulfide-komatiite association: the Katiniq sill, Ungava, Quebec; Economic Geology, v. 77, p. 413–429.

Barnes, S.J., Gole, M.J., and Hill, R.E., 1988. The Agnew nickel deposit, Western Australia; Part I, Structure and stratigraphy; Economic Geology, v. 83, p. 524–536.

Beall, G.H., 1959a. Preliminary report on Cross Lake area, New Quebec; Quebec Department of Mines, Preliminary Report 396, 9 p., Preliminary Map 1267.

Beall, G.H., 1959b. Final report on Cross Lake and Laflamme Lake areas; Ministère de l'Énergie et des Ressources naturelles du Québec, DP 460, 79 p., 2 plans.

Bergeron, R., 1957a. Preliminary report on Cape Smith - Wakeham Bay Belt, New Quebec; Quebec Department of Mines, Preliminary Report 355, 8 p., Preliminary Maps 1090 and 1196.

Bergeron, R., 1957b. Proterozoic rocks of the northern part of the Labrador Geosyncline, the Cape Smith Belt and the Richmond Gulf area; *in* The Proterozoic in Canada, (ed) J.E. Gill; Royal Society of Canada, Special Publication 2, p. 101–111.

Bergeron, R., 1958. The Cape Smith – Wakeham Bay Belt; Canadian Mining Journal, v. 79, p. 115–117.

Bergeron, R., 1959. Preliminary report on Povungnituk range area, New Quebec; Quebec Department of Mines, Preliminary Report 392, 9 p., Preliminary Map 1279.

Bleeker, W., 1990a. Evolution of the Thompson Nickel Belt and its nickel deposits, Manitoba, Canada; Ph.D. thesis, University of New Brunswick, Fredericton, New Brunswick, 400 p.

Bleeker, W., 1990b. New structural-metamorphic constraints on Early Proterozoic oblique collision along the Thompson Nickel Belt, Manitoba, Canada; *in* The Early Proterozoic Trans-Hudson Orogen of North America, (ed.) J.F. Lewry and M.R. Stauffer; Geological Association of Canada, Special Paper 37, p. 57–73.

Bleeker, W., 1990c. Thompson Area — General geology and ore deposits; Geology and Mineral Deposits of the Flin Flon and Thompson Belts, Manitoba (Field Trip 10), Field Trip Guidebook 8th IAGOD Symposium, p. 93–125.

Bleeker, W., 2003. The late Archean record: A puzzle in ca. 35 pieces; Lithos, v. 71, p. 99–134.

Bleeker, W., 2004. Taking the pulse of planet Earth: A proposal for a new multi-disciplinary flagship project in Canadian solid earth sciences; Geoscience Canada, v. 31, p. 179–190.

Bleeker, W., 2013. Report on Visit to Raglan Mine, Cape Smith Belt, Northern Quebec; Unpublished report for Glencore Xstrata Plc, Raglan Mine geology and exploration team, 9 p. Available on request from the author.

Bleeker, W., 2014. The quest for better precision and more accuracy: Revisiting upper intercept ages; Geological Association of Canada. Abstract Volume 37, p. 31–32.

Bleeker, W., 2015. Synorogenic gold mineralization in granite-greenstone terranes: the deep connection between extension, major faults, synorogenic clastic basins, magmatism, thrust inversion, and long-term preservation; *in* Targeted Geoscience Initiative 4: Contributions to the Understanding of Precambrian Lode Gold Deposits and Implications for Exploration, (ed.) B. Dubé and P. Mercier-Langevin; Geological Survey of Canada, Open File 7852, p. 25–47.

Bleeker, W. and Ames, D.E., 2017. System-scale and deposit-scale controls on Ni-Cu-PGE mineralisation in cratonic areas and their margins; *in* Targeted Geoscience Initiative, 2017: report of activities, (ed.) N. Rogers; Geological Survey of Canada, Open File 8199, p. 47–53.

Bleeker, W. and Ernst, R.E., 2006. Short-lived mantle generated magmatic events and their dyke swarms: The key unlocking Earth's palaeogeographic record back to 2.6 Ga; *in* Dyke Swarms—Time Markers of Crustal Evolution: Selected Papers

of the Fifth International Dyke Conference in Finland, Rovaniemi, Finland, 31 July -– 3 Aug 2005 & Fourth International Dyke Conference, Kwazulu-Natal, South Africa 26–29 June 2001, (ed.) E. Hanski, S. Mertanen, T. Rämö, and J. Vuollo; A.A. Balkema, Rotterdam, p. 3–26.

Bleeker, W. and Kamo, S.L., 2018. Extent, origin, and deposit-scale controls of the 1883 Ma Circum-Superior large igneous province, northern Manitoba, Ontario, Quebec, Nunavut and Labrador; *in* Targeted Geoscience Initiative, 2017: report of activities, volume 2, (ed.) N. Rogers; Geological Survey of Canada, Open File 8373, p. 5–14.

Bleeker, W., Smith, J., Hamilton, M., Kamo, S., Liikane, D., Hollings, P., Cundari, R., Easton, M., and Davis, D., 2020. The Midcontinent Rift and its mineral systems: Overview and temporal constraints of Ni-Cu-PGE mineralized intrusions; *in* Targeted Geoscience Initiative 5: Advances in the understanding of Canadian Ni-Cu-PGE and Cr ore systems – Examples from the Midcontinent Rift, the Circum-Superior Belt, the Archean Superior Province, and Cordilleran Alaskan-type intrusions, (ed.) W. Bleeker and M.G. Houlé; Geological Survey of Canada, Open File 8722, p. 7–35.

Boerboom, T.J., Wirth, K.R., and Evers, J.F., 2014. Five newly acquired high-precision U-Pb age dates in Minnesota, and their geologic implications; *in* Institute on Lake Superior Geology Proceedings, 60th Annual Meeting, May 14–17, 2014, Hibbing, Minnesota, v. 60, part 1, p. 13–14.

Buchan, K.L., Mortensen, J.K., Card, K.D., and Percival, J.A., 1998. Paleomagnetism and U-Pb geochronology of diabase dyke swarms of Minto block, Superior Province, Quebec, Canada; Canadian Journal of Earth Sciences, v. 35, p. 1054–1069.

Campbell, I.H. and Barnes, S.J., 1984. A model for the geochemistry of the platinum-group elements in magmatic sulfide deposits; The Canadian Mineralogist, v. 22, p. 151–160.

Chevé, S.R. and Machado, N., 1988. Reinvestigation of the Castignon Lake carbonatite complex, Labrador Trough, New Quebec; Geological Association of Canada - Mineralogical Association of Canada, Annual Meeting, Program with Abstracts, v. 13, p. 20.

Clark, T. and Wares, R., 2006. Lithotectonic and metallogenic synthesis of the New Québec Orogen (Labrador Trough); Ministère de l'Énergie et des Ressources naturelles du Québec, MM 2005-01, 180 p.

Coats, C.J.A., 1982. Geology and nickel sulphide deposits of the Raglan area, Ungava, Quebec; Ministère de l'Énergie et des Ressources naturelles du Québec, GM 40480, 130 p., 26 plans.

Corrigan, D., Galley, A.G., and Pehrsson, S., 2007. Tectonic evolution and metallogeny of the southwestern Trans-Hudson Orogen; *in* Mineral Deposits of Canada: A Synthesis of Major Deposit-Types, District Metallogeny, the Evolution of Geological Provinces, and Exploration Methods, (ed.) W.D. Goodfellow; Geological Association of Canada, Mineral Deposits Division, Special Publication No. 5, p. 881–902.

Corrigan, D., Pehrsson, S., Wodicka, N., and de Kemp, E., 2009. The Palaeoproterozoic Trans-Hudson Orogen: A prototype of modern accretionary processes; *in* Ancient Orogens and Modern Analogues, (ed.) J.B. Murphy, J.D. Keppie, and A.J. Hynes; Geological Society, London, Special Publications, v. 327, p. 457–479.

David, J., Dion, C., Goutier, J., Roy, P., Bandyayera, D., Legault, M., and Rhéaume, P., 2006. Datations U-Pb effectuées dans la Sous-province de l'Abitibi à la suite des travaux de 2004-2005; Ministère de l'Énergie et des Ressources naturelles du Québec, RP 2006-04, 22 p.

Davies, G.F., 1999. Dynamic Earth: Plates, Plumes and Mantle Convection; Cambridge University Press, Cambridge, United Kingdom, 458 p.

Dimroth, E., Baragar, W.R.A., Bergeron, R., and Jackson, G.D., 1970. The filling of the Circum-Ungava Geosyncline; *in* Basins and Geosynclines of the Canadian Shield, (ed.) A.J. Baer; Geological Survey of Canada, Paper 70-40, p. 45–143.

Ernst, R. and Bleeker, W., 2010. Large igneous provinces (LIPs), giant dyke swarms, and mantle plumes: Significance for breakup events within Canada and adjacent regions from 2.5 Ga to the Present; Canadian Journal of Earth Sciences, v. 47, p. 695–739.

Findlay, J.M., Parrish, R.R., Birkett, T.C., and Watanabe, D.H., 1995. U-Pb ages from the Nimish Formation and Montagnais glomeroporphyritic gabbro of the central New Québec Orogen, Canada; Canadian Journal of Earth Sciences, v. 32, p. 1208–1220.

Gaonac'h, H., Picard, C., Ludden, J.N., and Francis, D.M., 1989. Alkaline rocks from a Proterozoic volcanic island in the Cape Smith Thrust Belt, New Quebec; Geoscience Canada, v. 16, p. 137–139.

Gaonac'h, H., Ludden, J.N., Picard, C., and Francis, D., 1992. Highly alkaline lavas in a Proterozoic rift zone: Implications for Precambrian mantle metasomatic processes; Geology, v. 20, p. 247–250.

Giovenazzo, D., Picard, C., and Guha, J., 1989. Tectonic setting of Ni-Cu-PGE deposits in the central part of the Cape Smith Belt; Geoscience Canada, v. 16, p. 134–136.

Gole, M.J., Barnes, S.J., and Hill, R.E.T., 1989. The geology of the Agnew nickel deposit, Western Australia; Canadian Institute of Mining and Metallurgy Bulletin, v. 82, p. 46–56.

Green, A.H. and Dupras, N., 1999. Exploration model for komatiitic peridotite-hosted Ni-Cu-(PGE) mineralization in the Raglan Belt; *in* Komatiitic Peridotite-Hosted Fe-Ni-Cu-(PGE) Sulphide Deposits in the Raglan Area, Cape Smith Belt, New Québec, (ed.) C.M. Lesher; Laurentian University, Mineral Exploration Research Centre, Guidebook Series, v. 2, p. 191–199.

Gresham, J.J. and Loftus-Hills, G.D., 1981. The geology of the Kambalda nickel field, Western Australia; Economic Geology, v. 76, p. 1373–1416.

Griffin, W.L., Begg, G.C., and O'Reilly, S.Y., 2013. Continental-root control on the genesis of magmatic ore deposits; Nature Geoscience, v. 6, p. 905–910.

Gunning, H.C., 1933. Sulphide deposits at Cape Smith, east coast of Hudson Bay; Geological Survey of Canada, Summary Report 1939, Part D, p. 139–154.

Hamilton, M.A. and Stott, G.M., 2008. Project Unit 04-018. The significance of new U/Pb baddeleyite ages from two Paleoproterozoic diabase dikes in northern Ontario; *in* Summary of Fieldwork and Other Activities 2008,; Ontario Geological Survey, Open File Report 6226, p. 17-1–17-7.

Hamilton, M.A., Buchan, K.L., Ernst. R.E., and Stott, G.M., 2009. Widespread and short-lived 1870 Ma mafic magmatism along the northern Superior craton margin; Geological Association of Canada, 2009 Joint Assembly, 24–27 May 2009, Toronto, Ontario, Canada.

Hardy, R., 1976. Région des lacs Roberts, des Chefs (Roberts, des Chefs Lakes area); Ministère de l'Énergie et des Ressources naturelles du Québec, RG 171, 99 p., 2 plans.

Heaman, L.M., 2009. The application of U–Pb geochronology to mafic, ultramafic and alkaline rocks: An evaluation of three mineral standards; Chemical Geology, v. 261, p. 43–52.

Heaman, L.M., Machado, N., Krogh, T.E., and Weber, W., 1986. Precise U-Pb zircon ages for the Molson dyke swarm and the Fox River sill: Constraints for Early Proterozoic crustal evolu-

tion in northeastern Manitoba, Canada; Contributions to Mineralogy and Petrology, v. 94, p. 82–89.

Heaman, L.M., Peck D., and Toope, K., 2009. Timing and geochemistry of 1.88 Ga Molson Igneous Events, Manitoba: Insights into the formation of a craton-scale magmatic and metallogenic province; Precambrian Research, v. 172, p. 143–162.

Henrique-Pinto, R., Guilmette, C., Bilodeau, C., and McNicoll, V., 2017. Evidence for transition from a continental forearc to a collisional pro-foreland basin in the eastern Trans-Hudson Orogen: Detrital zircon provenance analysis in the Labrador Trough, Canada; Precambrian Research, v. 296, p. 181–194.

Hoffman, P.F., 1985. Is the Cape Smith belt (northern Quebec) a klippe?; Canadian Journal of Earth Sciences, v. 22, p. 1361–1369.

Huppert, H.E. and Sparks, R.S.J., 1985. Komatiites I: Eruption and flow; Journal of Petrology, v. 26, p. 694–725.

Huppert, H.E., Sparks, R.S.J., Turner, J.S., and Arndt, N.T., 1984. Emplacement and cooling of komatiite lavas; Nature, v. 309, p. 19–22.

Hynes, A. and Francis, D.M., 1982. A transect of the early Proterozoic Cape Smith foldbelt, New Quebec; Tectonophysics, v. 88, p. 23–59.

Kastek, N., Ernst, R.E., Cousens, B.L., Kamo, S.L., Bleeker, W., Söderlund, U., Baragar, W.R.A., and Sylvester, P., 2018. U-Pb geochronology and geochemistry of the Povungnituk Group of the Cape Smith Belt: Part of a craton-scale circa 2.0 Ga Minto-Povungnituk large igneous province, northern Superior craton; Lithos, v. 320, p. 315–331.

Lamothe, D., 2007. Lexique stratigraphique de l'Orogène de l'Ungava; Ministère de l'Énergie et des Ressources naturelles du Québec, DV 2007-03, 61 p., 1 plan.

Le Gallais, C.J. and Lavoie, S., 1982. Basin evolution of the lower Proterozoic Kaniapiskau Supergroup, Central Labrador Miogeocline (trough), Quebec; Bulletin of Canadian Petroleum Geology, v. 30, p. 150–166.

Lesher, C.M., 1989. Komatiite-associated nickel sulphide deposits; *in* Ore Deposition Associated with Magmas, (ed.) J.A. Whitney and A.J. Naldrett; Society of Economic Geologists, Reviews in Economic Geology, v. 4, p. 45–101.

Lesher, C.M. (ed.), 1999. Komatiitic Peridotite-Hosted Fe-Ni-Cu-(PGE) Sulphide Deposits in the Raglan Area, Cape Smith Belt, New Québec; Laurentian University, Mineral Exploration Research Centre, Guidebook Series, v. 2, 212 p.

Lesher, C.M., 2007. Ni-Cu-(PGE) deposits in the Raglan area, Cape Smith Belt, New Québec; *in* Mineral Deposits of Canada: A Synthesis of Major Deposit-Types, District Metallogeny, the Evolution of Geological Provinces, and Exploration Methods, (ed.) W.D. Goodfellow; Geological Association of Canada, Mineral Deposits Division, Special Publication No. 5, p. 351–386.

Lesher, C.M., Arndt, N.T., and Groves, D.I., 1984. Genesis of komatiite-associated nickel sulphide deposits at Kambalda, Western Australia: A distal volcanic model; *in* Sulphide Deposits in Mafic and Ultramafic Rocks, (ed.) D.L. Buchanan and M.J. Jones; Institute of Mining and Metallurgy, London, p. 70–80.

Low, A.P., 1902. Report on an exploration of the east coast of Hudson Bay from Cape Wolstenholme to the south end of James Bay; Geological Survey of Canada, Annual Report, v. 13, Part D, 84 p. and 4 map sheets.

Lucas, S.B. and St-Onge, M.R., 1992. Terrane accretion in the internal zone of the Ungava orogen, northern Quebec. Part 2: Structural and metamorphic history; Canadian Journal of Earth Sciences, v. 29 p. 765–782.

Machado, N., Goulet, N., and Gariépy, C., 1989. U–Pb geochronology of reactivated Archean basement and of Hudsonian metamorphism in the northern Labrador Trough; Canadian Journal of Earth Sciences, v. 26, p. 1–15.

Machado, N., David, J., Scott, D.J., Lamothe, D., Philippe, S., and Gariepy, C., 1993. U-Pb geochronology of the western Cape Smith Belt, Canada: New insights into the age of initial rifting and arc magmatism; Precambrian Research, v. 63, p. 211–223.

Machado, N., Clark, T., David, J., and Goulet, N., 1997. U–Pb ages for magmatism and deformation in the New Quebec Orogen; Canadian Journal of Earth Sciences, v. 34, p. 716–723.

Madore, L. and Larbi, Y., 2001. Geology of the Riviere Arnaud area (25D) and adjacent coastal areas (25C, 25E and 25F); Ministère de l'Énergie et des Ressources naturelles du Québec, RG 2001-06, 33 p.

Marston, R.J., Groves, D.I., Hudson, D.R., and Ross, J.R., 1981. Nickel sulfide deposits in Western Australia; a review; Economic Geology, v. 76, p. 1330–1363.

Mattinson, J.M., 2005. Zircon U/Pb chemical abrasion (CA-TIMS) method: Combined annealing and multi-step partial dissolution analysis for improved precision and accuracy of zircon ages; Chemical Geology, v. 220, p. 47–66.

McKevitt, D.J., Lesher, C.M., and Houlé, M.G., 2020. Regional lithogeochemical synthesis of mafic-ultramafic volcanic and intrusive rocks in the Cape Smith Belt, Nunavik, northern Quebec; *in* Targeted Geoscience Initiative 5: Advances in the understanding of Canadian Ni-Cu-PGE and Cr ore systems – Examples from the Midcontinent Rift, the Circum-Superior Belt, the Archean Superior Province, and Cordilleran Alaskan-type intrusions, (ed.) W. Bleeker and M.G. Houlé; Geological Survey of Canada, Open File 8722, p. 99–115.

Melezhik, V., Fallick, A., and Clark, T., 1997. Two billion year old isotopically heavy carbon: evidence from the Labrador Trough, Canada; Canadian Journal of Earth Sciences, v. 34, p. 271–285.

MRN, 2002. Carte géologique du Québec, Édition 2002; Ministère de l'Énergie et des Ressources naturelles du Québec; DV 2002-06, 1 map, scale 1:2 000 000.

Moorhead, J., 1989. Géologie de la région du lac Chukotat (Fosse de l'Ungava); Ministère de l'Énergie et des Ressources naturelles du Québec, ET 87-10, 64 p., 2 plans.

Mungall, J.E., 2007. Crustal contamination of picritic magmas during transport through dikes: the expo intrusive suite, Cape Smith Fold Belt, New Quebec; Journal of Petrology, v. 48, p. 1021–1039.

Mungall, J.E., Kamo, S.L., and McQuade, S., 2016. U-Pb geochronology documents out-of-sequence emplacement of ultramafic layers in the Bushveld Igneous Complex of South Africa; Nature Communications, v. 7, 13385, 13 p.

Naldrett, A.J., 2005. A history of our understanding of magmatic Ni–Cu sulfide deposits; The Canadian Mineralogist, v. 43, p. 2069–2098.

Osmond, R. and Watts, A., 1999. 3D geophysical model of the Raglan Belt; *in* Komatiitic Peridotite-Hosted Fe-Ni-Cu-(PGE) Sulphide Deposits in the Raglan Area, Cape Smith Belt, New Québec, (ed.) C.M. Lesher; Laurentian University, Mineral Exploration Research Centre, Guidebook Series, v. 2, p. 185–190.

Parrish, R.R., 1989. U-Pb geochronology of the Cape Smith Belt and Sugluk block, northern Quebec; Geoscience Canada, v. 16, p. 126–130.

Percival, J.A. and West, G.F., 1994. The Kapuskasing uplift: a geological and geophysical synthesis; Canadian Journal of Earth Sciences, v. 31, p. 1256–1286.

Picard, C., Giovenazzo, D., and Lamothe, D., 1989. Geotectonic evolution by asymmetric rifting of the Proterozoic Cape Smith Belt, New Quebec; Geoscience Canada, v. 16, p. 130–134.

Picard, C., Lamothe, D., Piboule, M., and Oliver, R., 1990. Magmatic and geotectonic evolution of a Proterozoic oceanic basin system: The Cape Smith thrust-fold belt (New-Quebec); Precambrian Research, v. 47, p. 223–249.

Picard, C., Amossé, J., Piboule, M., and Giovenazzo, D., 1995. Physical and chemical constraints on platinum-group element behavior during crystallization of a basaltic komatiite liquid; example of the Proterozoic Delta Sill, New Quebec, Canada; Economic Geology, v. 90, p. 2287–2302.

Randall, W., 2005. U-Pb geochronology of the Expo Intrusive Suite, Cape Smith Belt, and the Kyak Bay intrusion, New Quebec Orogen: Implications for the tectonic evolution of the northeastern Trans-Hudson Orogen; M.Sc. thesis, University of Toronto, Toronto, Ontario, 51 p.

Rohon, M.L., Vialette, Y., Clark, T., Roger, G., Ohnenstetter, D., and Vidal, P., 1993. Aphebian mafic–ultramafic magmatism in the Labrador Trough (New Quebec): Its age and the nature of its mantle source; Canadian Journal of Earth Sciences, v. 30, p. 1582–1593.

Rukhlov, A.S. and Bell, K., 2010. Geochronology of carbonatites from the Canadian and Baltic Shields, and the Canadian Cordillera: Clues to mantle evolution; Mineralogy and Petrology, v. 98, p. 11–54.

Sage, R.P., 1991. Alkalic rock, carbonatite and kimberlite complexes of Ontario, Superior Province; *in* Geology of Ontario, (ed.) P.C. Thurston, H.R. Williams, R.H. Sutcliffe, and G.M. Stott; Ontario Geological Survey, Special Volume 4, Part 1, p. 683–709.

Scoates, J.S., Wall, C.J., Friedman, R.M., Booth, K., Scoates, R.F.J., Couëslan, C., and Macek, J., 2010. Recent progress in determining the precise age of ultramafic sills and mafic dikes associated with mineralization in the Thompson nickel belt, Manitoba, Canada; 11th International Platinum Symposium, Sudbury, Ontario, Canada, June 21–24, 2010, Ontario Geological Survey, Miscellaneous Release– Data 269, 4 p.

Scoates, J.S., Scoates, R.J., Wall, C.J., Friedman, R.M., and Couëslan, C.G., 2017. Direct dating of ultramafic sills and mafic intrusions associated with Ni-sulphide mineralization in the Thompson Nickel Belt, Manitoba, Canada; Economic Geology, v. 112, p. 675–692.

Scott, D.J., St-Onge, M.R., Lucas, S.B., and Helmstaedt, H., 1989. The 1998 Ma Purtuniq ophiolite: imbricated and metamorphosed oceanic crust in the Cape Smith Thrust Belt, northern Quebec; Geoscience Canada, v. 16, p. 144–147.

Scott, D.J., St-Onge, M.R., Lucas, S.B. and Helmstaedt, H., 1991. Geology and chemistry of the early Proterozoic Purtuniq ophiolite, Cape Smith belt, northern Quebec, Canada; *in* Ophiolite Genesis and Evolution of the Oceanic Lithosphere, (ed.) T. Peters, A. Nicolas, and R.G. Coleman; Springer, Petrology and Structural Geology Series, v. 5, p. 817–849.

Scott, D.J., Helmstaedt, H., and Bickle, M.J., 1992. Purtuniq ophiolite, Cape Smith belt, northern Quebec, Canada: A reconstructed section of Early Proterozoic oceanic crust; Geology, v. 20, p. 173–176.

Skulski, T., Wares, R.P., and Smith, A.D., 1993. Early Proterozoic (1.88–1.87 Ga) tholeiitic magmatism in the New Quebec orogeny; Canadian Journal of Earth Sciences, v. 30, p. 1505–1520.

Sleep, N.H., 1997. Lateral flow and ponding of starting plume material; Journal of Geophysical Research, Solid Earth, v. 102, p. 10 001–10 012.

Stam, J.C., 1961. On the geology and petrology of the Cape Smith-Wakeham Bay belt, Ungava, Quebec; Geologie en Mijnbouw, v. 40, p. 412–421.

St-Onge, M.R. and Lucas, S.B., 1993. Geology of the Eastern Cape Smith Belt: Parts of the Kangiqsujuaq, Cratere du nouveau-Quebec, and Lacs Nuvilik map areas, Quebec; Geological Survey of Canada, Memoir 438, 110 p.

St-Onge, M.R. and Lucas, S.B., 1994. Controls on the regional distribution of iron–nickel–copper–platinum-group element sulfide mineralization in the eastern Cape Smith Belt, Quebec; Canadian Journal of Earth Sciences, v. 31, p. 206–218.

St-Onge, M.R., Lucas, S.B., and Parrish, R.R., 1992. Terrane accretion in the internal zone of the Ungava orogen, northern Quebec. Part 1: Tectonostratigraphic assemblages and their tectonic implications; Canadian Journal of Earth Sciences, v. 29, p. 746–764.

St-Onge, M.R., Henderson, I., and Baragar, W.R.A., 2006. Geology, Cape Smith Belt and adjacent domains, Ungava Peninsula, Quebec-Nunavut; Geological Survey of Canada, Open File 4930, 2 sheets.

Taylor, F.C., 1982. Reconnaissance geology of a part of the Canadian Shield, northern Quebec and Northwest Territorie; Geological Survey of Canada, Memoir 399, 32 p. and 7 maps, 1:250 000.

Wares, R.P. and Goutier, J., 1990. Deformational style in the foreland of the northern New Quebec Orogen; Geoscience Canada, v. 17, p. 244–249.

Waterton, P., Pearson, D.G., Kjarsgaard, B., Hulbert, L., Locock, A., Parman, S., and Davis, B., 2017. Age, origin, and thermal evolution of the ultra-fresh ~1.9 Ga Winnipegosis Komatiites, Manitoba, Canada; Lithos, v. 268, p. 114–130.

Weller, O.M. and St-Onge, M.R., 2017. Record of modern-style plate tectonics in the Palaeoproterozoic Trans-Hudson orogen; Nature Geoscience, v. 10, p. 305–311.

Williams, D.A., Kerr, R.C., and Lesher, C.M., 1998. Emplacement and erosion by Archean komatiite lava flows: Revisited; Journal of Geophysical Research, v. 103, p. 27,533–27,549.

Wodicka, N., Madore, L., Larbi, Y., and Vicker, P., 2002. Geochronologie U-Pb de filons-couches mafiques de la Ceinture de Cape Smith et de la Fosse du Labrador; Ministère de l'Énergie et des Ressources naturelles du Québec, Résumés des Conférences et des Photoprésentations, DV 2002-10, p. 48.

APPENDIX

Here we explore important questions of regional correlation of the Cape Smith Belt stratigraphy with that of the Labrador Trough to the southeast (*see* Fig. 1 for a regional map). The Labrador Trough is a ~900 km long belt along the eastern margin of the Superior craton with perhaps the best preserved and most extensive record of Paleoproterozoic craton-margin stratigraphy of the entire Circum-Superior Belt. The preserved stratigraphy thickens towards the east and is asymmetric. It has been divided into several lithotectonic zones, with generally more allochthonous units towards the east. Given its considerable length, the different lithotectonic zones, and the fact that it spans two jurisdictions (the provinces of Quebec and Labrador), the literature on the Labrador Trough is extensive (e.g. Baragar, 1967; Dimroth et al., 1970; Le Gallais and Lavoie, 1982; Wares and Goutier, 1990; Clark and Wares, 2006) and involves a bewildering variety of formation names, some of which are essentially duplicates from one mapping area to another, whereas others involve important questions of correlation from north to south or across lithotectonic zones. All of this we attempt to summarize in one lithostratigraphic column, a column that is necessarily imperfect but aims to highlight the essential elements (Fig. 15c). Quoted U-Pb zircon ages are from Chevé and Machado et al. (1988), Krogh (1988, unpub. data, mentioned in Machado et al., 1989), Parrish (1989), Rohon et al. (1993), Findlay et al., (1995), Machado et al. (1997), Buchan et al. (1998), Henrique-Pinto et al. (2017), and Bleeker and Kamo (2018).

In Figure 15a, we show the lithostratigraphic synthesis of the Cape Smith Belt, as presented earlier (Fig. 3b of this report). Again, key ages are shown, and those outlined in red are from the present study. As described earlier in this report, key features of the Cape Smith stratigraphy are the two major mafic volcanic sequences of the ca. 1998 Ma Povungnituk basalts and the much younger 1883–1870 Ma Chukotat komatiites and basalts, as well at the basal sedimentary Lamarche Subgroup. Unless there are undocumented structural-stratigraphic complexities, these basal sedimentary rocks must be older than 2038 Ma, the age of the intrusive Korak gabbro sills. This >2038 Ma age must also apply to the iron formations near the base of the sequence, which generally become more prominent in the eastern part of the Cape Smith Belt (St-Onge and Lucas, 1993; M. St-Onge, pers. comm., 2020).

Figure 15b shows the lithostratigraphy of the Roberts Syncline area, based on a traverse across the entire syncline in 2013 and the mapping of Hardy (1976). Although the entire section is moderately to strongly deformed and overlies a basal décollement, as in the Cape Smith Belt, it probably reflects, to a first degree, a primary stratigraphic succession. Top indicators from graded beds, pillows, and differentiated sills are all into the core of the syncline. The area generally has been considered as the northernmost parts of the Labrador Trough, but is only a mere 125 km to the southeast of the easternmost Cape Smith Belt where similar units are exposed. In the main part of the Roberts Syncline, the basal section is essentially similar to that of the Lamarche Subgroup of the Cape Smith Belt and, coming from Cape Smith (Fig. 15a,b), there is no compelling reason to not correlate the various units (*see also* Taylor, 1982). The iron formation near the base is thicker than in the Cape Smith Belt but this agrees with the general trend observed farther north, where the iron formation becomes thicker towards the east. The erosional remnant in the core of the Roberts Syncline, which is obviously truncated at its top, is occupied by a ~3–5 km thick sequence of massive and pillowed basalt flows that are intruded by mafic and ultramafic sills. Gabbro at the top of one of these sills has been dated at 1882 ± 4 Ma (Wodicka et al., 2002), as shown in Figure 15b. Importantly, several distinct quartzitic intercalations occur in this basaltic sequence and help to correlate it with the Povungnituk basalts. Detrital zircon grains from these quartzites are all derived from Archean basement (D. Davis, pers. comm., 2016: preliminary laser ablation data from samples collected in 2013). No such intercalations of sialic basement-derived, mature quartzite are known from the Chukotat sequence.

Figure 15c attempts to summarize the extensive and rather complex lithostratigraphy of the Labrador Trough proper, which can be divided into several major depositional cycles and subcycles (Dimroth et al., 1970; Le Gallais and Lavoie, 1982; Clark and Wares, 2006) that progress from shelf-like facies, including stromatolitic carbonates, to basinal facies dominated by greywackes and shale, with associated mafic volcanic rocks. Two major cycles are recognized, separated, at least locally, by a low-angle unconformity. A third cycle of synorogenic siliciclastic rocks occurs at the top. In large parts of the trough, the units of "Cycle 2" overstep units of "Cycle 1" to the west and onlap onto basement of the Superior craton, as schematically shown in Figure 15c.

With the three lithostratigraphic columns side by side, the first-order problem of correlation is immediately clear: the major Sokoman iron formation of the central and southern Labrador Trough, the age of which is reasonably well constrained to ca. 1880 Ma (Chevé and Machado, 1988; Findlay et al., 1995) and thus coeval with the climax of Chukotat magmatism, cannot be the same iron formation unit as near the base of the Roberts Syncline, even though essentially all previous authors have made this correlation. One solution would

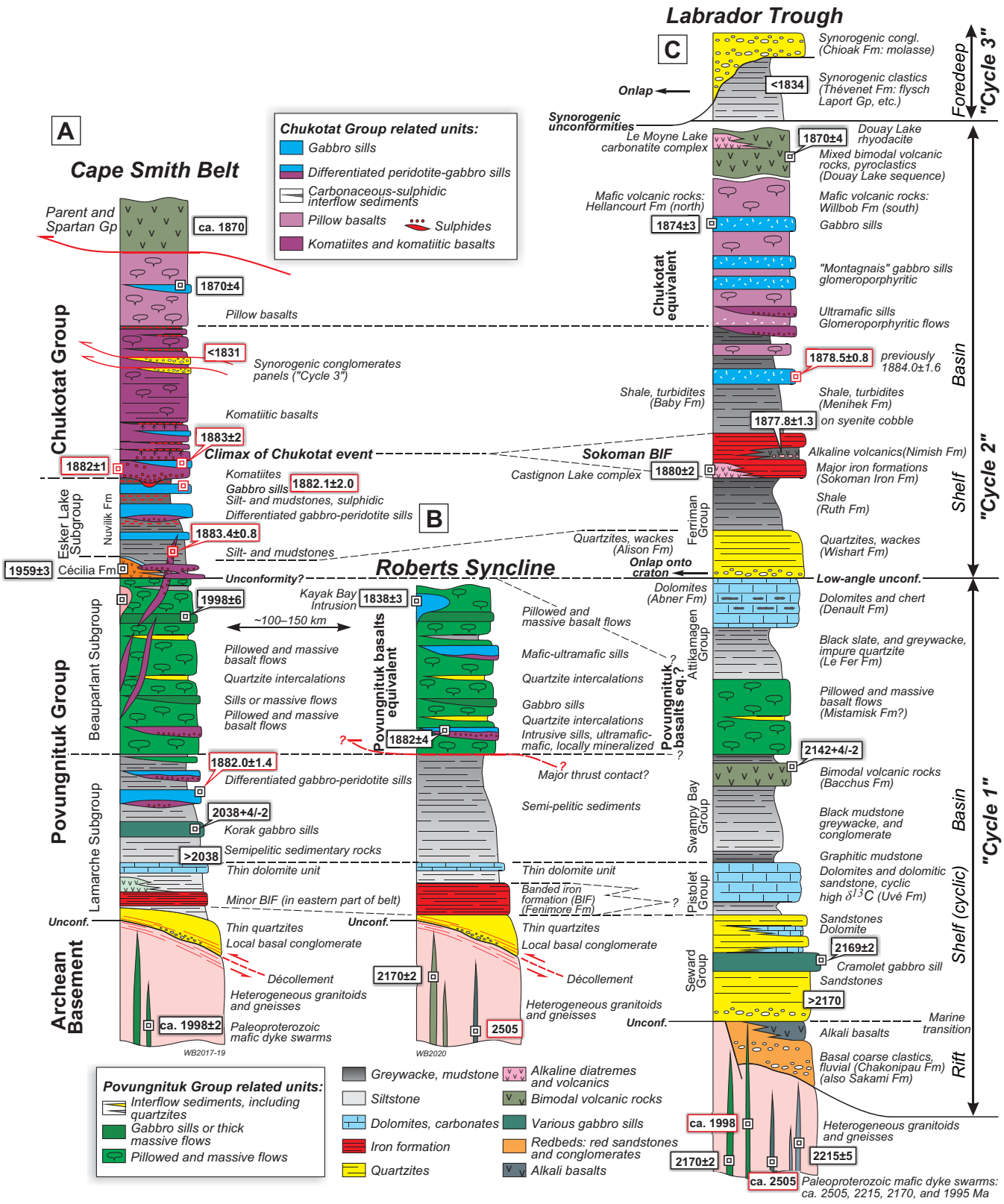

Figure 15. Composite lithostratigraphic columns for **(a)** the Cape Smith Belt; **(b)** the Roberts Syncline area ~100–150 km to the southeast; and **(c)** the Labrador Trough. Dashed lines indicate tentative correlations. The age of the major iron formation of the Labrador Trough, the Sokoman Iron Formation, in "Cycle 2" is constrained to ca. 1882–1877 Ma and overlaps in age with the climax of the Chukotat magmatic event. Iron formations near the base of the Cape Smith stratigraphy represent an older cycle of chemical sedimentation.

be to make the entire Roberts Syncline stratigraphy part of Cycle 2, with the basalt sequence in the core of the syncline being equivalent to the Chukotat and Hellancourt sequences, but we do not favour this view. It ignores the important observation of mature quartzite intercalations in the Roberts Syncline volcanic sequence and forces the question of why the major, ~3–5 km- thick Povungnituk basalt sequence is suddenly missing over a lateral distance of just over 100 km from the Cape Smith Belt. Furthermore, the basal sedimentary section of the Roberts Syncline is not a perfect match to the Menihek shales and turbidites that overlie the Sokoman Formation further south. A thin dolomitic carbonate unit near the base of the Roberts Syncline is identical to a thin carbonate unit in the lower Povungnituk Group. We thus favour the correlations as shown in Figure 15, acknowledging that a there are a number of questions that remain to be resolved:

1. Is there a Povungnituk basalt equivalent in the northern and central Labrador Trough, as part of Cycle 1? Only one widely quoted U-Pb zircon age (unpub.; T. Krogh, pers. comm., mentioned in Machado et al., 1989), on a rhyolite, occurs in the relevant part of the Labrador Trough column and the associated volcanic rocks appear to be older, i.e. 2142 Ma, and too old to be part of the Povungnituk sequence. Many volcanic packages remain undated, however, and the different lithotectonic zones complicate overall correlations.
2. Could the major sequence boundary between Cycle 1 and Cycle 2 stratigraphy perhaps be ca. 1960 Ma and correlate with the hiatus at either the base or the top of the Cécilia Formation in the Cape Smith Belt?

In the Labrador Trough, we have redated, using CA-ID-TIMS on single zircon grains, the glomeroporphyritic "Montagnais" gabbro sill that intruded the Menihek Formation greywackes. The previously reported age for this sill, based on discordant but collinear zircon fractions, was 1884.0 ± 1.6 Ma (Findlay et al., 1995). Even though the quoted upper intercept age was relatively precise, from the nature of these data we predicted that it was an over-estimate and too old. Our new, refined and concordant zircon age of 1878.5 ± 0.8 Ma erases the apparent age reversal in the previous data—an 1884 Ma intrusive sill above ca. 1880–1878 Ma iron formation and volcanic rocks. No part of the Sokoman iron formation is therefore older than 1884 Ma.

Towards the top of Cycle 2, the primitive Hellancourt basalts, generally correlated with the Willbob Formation further south, are a relatively straightforward continuation of the upper Chukotat sequence (e.g. Skulski et al., 1993).

The major Sokoman iron formation, and broadly correlative Superior-type iron formations elsewhere along the Circum-Superior Belt (e.g. Gunflint and Biwabik formations in Ontario and Minnesota), are coeval with the climax of the 1883–1880 Ma Chukotat event, indicating the likely global scale of perturbations in the ocean-atmosphere system. Iron formations near the base of the Cape Smith Belt, and the Roberts Syncline, and into the northern Labrador Trough (Fenimore Formation), must represent an older cycle of chemical sedimentation and possibly overlap in time with major perturbations such as the Lomagundi event. Melezhik et al. (1997) demonstrated that carbonates in the middle of Cycle 1 (Pistolet Group; subgroup in previous publications) are characterized by heavy $\delta^{13}C$ signatures above 10‰.

As is evident from this preliminary correlation exercise, numerous questions remain and the scope for exciting new work is enormous. High-precision zircon dating of key stratigraphic units, intrusive sills, and carefully selected detrital zircon samples is probably the most efficient way forward to test many of the questions and predictions raised here.

Regional lithogeochemical synthesis of mafic-ultramafic volcanic and intrusive rocks in the Cape Smith Belt, Nunavik, northern Quebec

D.J. McKevitt[1]*, C.M. Lesher[1], and M.G. Houlé[2]

[1]Mineral Exploration Research Centre, Harquail School of Earth Sciences, Goodman School of Mines, Laurentian University, 935 Ramsey Lake Road, Sudbury, Ontario P3E 2C6
[2]Geological Survey of Canada, 490 rue de la Couronne, Québec, Quebec G1K 9A9
*Corresponding author's e-mail: dmckevitt@laurentian.ca

ABSTRACT

More than a century of geological reconnaissance, mapping, and mineral exploration across the Cape Smith Belt has yielded a wealth of geochemical data. However, as is the case with much "big data" that span many years, sources, methodologies, and file types, the data have not been compiled in their entirety in a common format. This research component of the TGI-5 Ni-Cu-PGE-Cr Project was to compile, harmonize, and interpret publicly available lithogeochemical data for volcanic and associated intrusive rocks in the Cape Smith Belt. The current data set includes ~18,800 unique whole-rock analyses from the Cape Smith Belt (87%) and surrounding domains in Nunavik (13%) with major ± trace elements and accompanying metadata (drillhole collars and depths, sample locations, rock descriptions, and references) from 130 sources. Duplications of records from different sources allowed cross-validation and identification of transcription errors, and preliminary QA-QC of data generated for the same rock units using multiple methods revealed differences in sample preparation and analytical methods employed at various laboratories.

Analysis of the collated data reveals significant differences in lithogeochemistry, and therefore petrogenesis, of several lithostratigraphic units. In the Southern Domain of the Cape Smith Belt, major and trace element contents can be used to readily distinguish between the major volcanic events; for example, the Povungnituk Group volcanic rocks have higher incompatible (e.g. Th, Nb, LREE, Zr, Ti) and lower compatible (e.g. Mg, Cr, Ni) element contents than those of the Chukotat Group, which have generally lower incompatible and higher compatible element contents. Fractionations in Th/Nb/Yb suggest that the Povungnituk Group formed from magmas derived by low-moderate degree partial melting of a depleted mantle source, whereas the Chukotat Group formed from magmas derived by higher degrees of partial melting of a depleted mantle source with variable degrees of contamination by crustally-derived sediments. Within the Povungnituk Group, coarser grained mafic (gabbroic) rocks of the Lac Bélanger Suite are geochemically indistinguishable from the surrounding finer grained mafic (basaltic) rocks of the Beauparlant Formation, consistent with the coarser grained Lac Bélanger units being thick flows or high-level synvolcanic sills that are geochemically related to but cooled more slowly than the finer grained Beauparlant volcanic rocks.

Similarly, thicker and coarser grained olivine orthocumulate-mesocumulate units of the Lac Esker Suite are geochemically related to thinner olivine- and pyroxene-phyric mafic (komatiitic basaltic) volcanic rocks of the Chukotat Group. The units of the Lac Esker Suite can be subdivided into an upper Raglan Trend, comprising poorly differentiated lava channels/invasive channels (Ni-Cu-PGE mineralized) and well differentiated sheet flows/sills (unmineralized), and a lower Expo Trend that includes poorly differentiated blade-shaped dykes (Cu-Ni-PGE mineralized) and well to poorly differentiated sills (unmineralized). Raglan units are characterized by higher Mg, Cr, and Th contents, higher La/Sm ratios, and generally higher Ni/Cu ratios than Expo units. Contrary to some previous interpretations, these geochemical differences suggest that the pyroxene peridotite/melagabbro blade-shaped dykes in the Expo Trend did not feed the peridotite/pyroxenite lava channels in the Raglan Trend. These lithogeochemical characteristics of the stratigraphic units provide important constraints on petrogenetic and metallogenic relationships and therefore the nature of the volcanic-subvolcanic-intrusive plumbing system, and should aid in categorizing potentially prospective units in areas along strike from known sulphide deposits.

INTRODUCTION

More than a century of activity by government, industry, and academia has generated a wealth of data through whole-rock and ore geochemical analyses, geophysical surveys, diamond drilling, and geological mapping. A major goal of this component of the

McKevitt, D.J., Lesher, C.M., and Houlé, M.G., 2020. Regional lithogeochemical synthesis of mafic-ultramafic volcanic and intrusive rocks in the Cape Smith Belt, Nunavik, northern Quebec; *in* Targeted Geoscience Initiative 5: Advances in the understanding of Canadian Ni-Cu-PGE and Cr ore systems – Examples from the Midcontinent Rift, the Circum-Superior Belt, the Archean Superior Province, and Cordilleran Alaskan-type intrusions, (ed.) W. Bleeker and M.G. Houlé; Geological Survey of Canada, Open File 8722, p. 99–115. https://doi.org/10.4095/326883

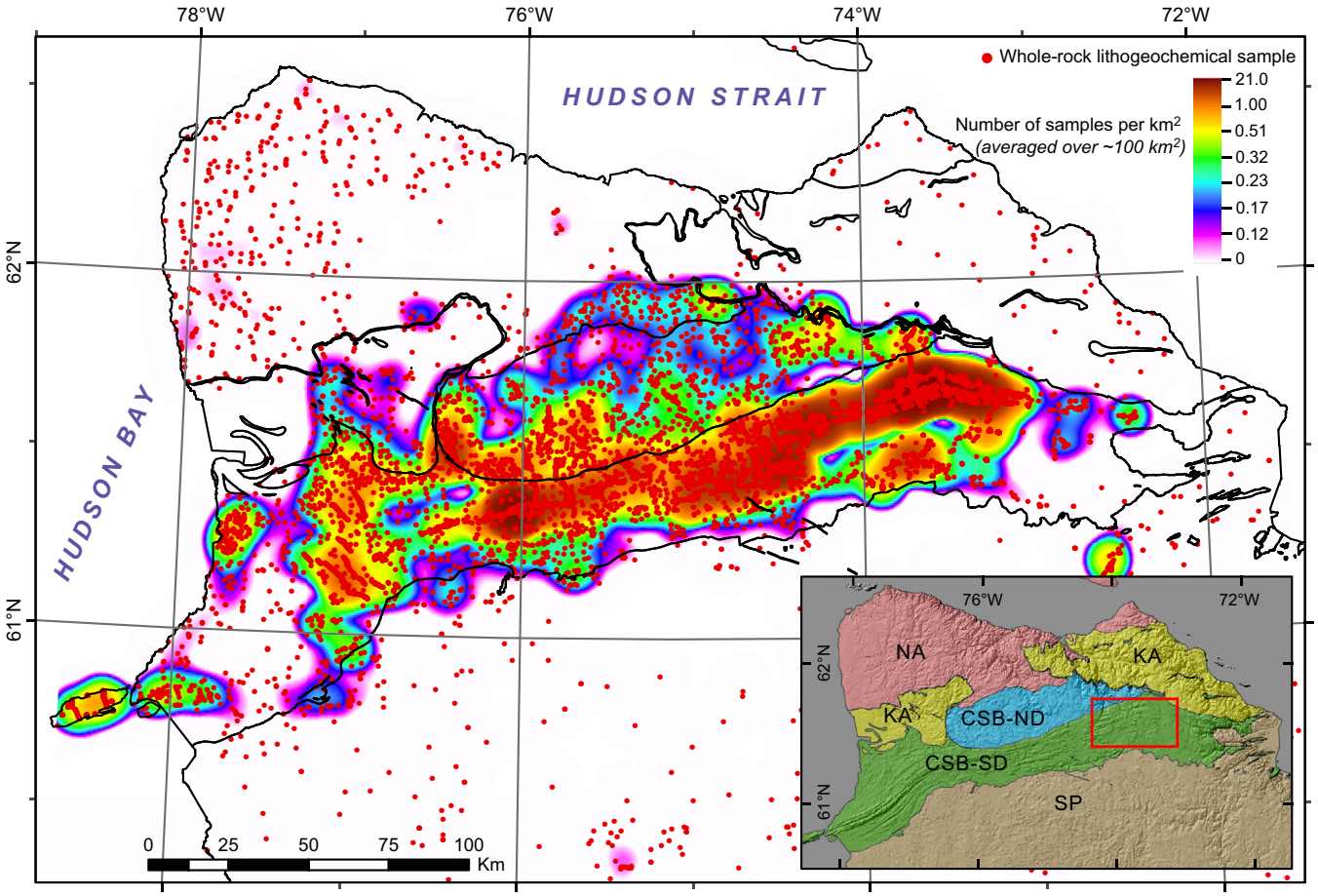

Figure 1. Locations of whole-rock samples in Nunavik, northern Quebec, for which lithogeochemical data are included in the present compilation. The colour scale shows sample density (samples per km², averaged over ~100 km²; at a larger map scale, the largest number of samples per km² is ~160 and includes drill core and surface samples). Most samples come from the Cape Smith Belt. The red rectangle in the inset map outlines the map area shown in Figure 2. Abbreviations on inset map: CSB-ND = Cape Smith Belt, Northern Domain; CSB-SD = Cape Smith Belt, Southern Domain; KA = Kovik Antiform; NA = Narsajuaq Arc; SP = Superior Province.

research activity studying mafic and ultramafic magmatic architecture under the Ni-Cu-PGE-Cr Project of the Targeted Geoscience Initiative-Phase V (TGI-5) of the Geological Survey of Canada was to compile, harmonize, and interpret publicly available lithogeochemical data for rocks in the Cape Smith Belt.

Since the early geological reconnaissance, mapping, and exploration activity of A.P. Low by the Geological Survey of Canada (1898–1899) and the Cyril Knight Prospecting Company Ltd. (1931–1933) in the western end of the Cape Smith Belt, this Paleoproterozoic volcano-sedimentary succession has become well known for its Ni-Cu-PGE magmatic sulphide deposits (Dupras and Green, 1999). Currently, there are mining activities in the Southern Domain (Fig. 1, inset) of the eastern Cape Smith Belt by Glencore Canada Corp. in the Raglan area and by Canadian Royalties Inc. in the Expo area. Exploration for magmatic sulphide mineralization is ongoing throughout the region and along strike to the east and west (e.g. Orford Mining's West Raglan project), while exploration for shear-zone-hosted Au mineralization is progressing in the Cape Smith Belt's Northern Domain (e.g. Orford Mining's Qiqavik project).

This synthesis report presents preliminary results of the belt-scale compilation for mafic-ultramafic volcanic-subvolcanic-intrusive rocks in the eastern part of the Southern Domain of the Cape Smith Belt and is a part of a Ph.D. study at Laurentian University in Sudbury (Canada). For a description of the specific goals and fieldwork that was completed in the course of this study, the reader is referred to McKevitt et al. (2018, 2019).

RESULTS

Data Compilation Methodology

Types and sources

Compilation of whole-rock lithogeochemical data (excluding solely assay data) from both public and private sources began in September 2016. Previous compilations by government, academia, and industry (*see*

St-Onge et al., 2007 and SIGÉOM records; Ministère de l'Énergie et des Ressources naturelles du Québec, 2019) did not include some of the geochemical data from published and unpublished theses, scientific articles, and company reports. Additionally, these previous compilations often lacked metadata, including location and drilling information, analytical details, rock types/descriptions, and sources. Therefore, to obtain a more comprehensive, useful, and harmonized data set, original materials were obtained (including unpublished theses, digital reports, and scientific articles), and much of the data was extracted manually before comparison and integration with previous compilations. Table 1 lists the 130 sources that were used and the geological regions covered by this study.

Validation

A drawback of including so many sources was that many sample records were duplicated, however, this did facilitate the cross-validation and identification of multiple analytical methods and laboratories that had been used to analyze the same samples/rock units and individual elements; it also permitted the discovery of numerous transcription errors and some print/publication errors. Data quality assurance-quality control (QA-QC) was performed manually and with Excel, ArcGIS, and ioGAS software. Much older location data were reported in North American Datum 27 (NAD27); these coordinates were converted to NAD83 using the NRCan NTv2 National Transformation tool (https://www.nrcan.gc.ca/maps-tools-publications/tools/geodetic-reference-systems-tools/tools-applications/10925#ntv2). Duplicate sample records were identified both by element values and location coordinates. After the removal of duplicate sample records, the resulting data set comprises 17,000 public (or unpublished but public-pending) records, spanning all major geological domains in Nunavik, Quebec, north of latitude 60ºN (*see* Fig. 1 and Table 2).

Data Analysis

Classification

Samples were classified using a combination of original rock descriptions and locations (e.g. from drillhole logs) and geochemistry. They were categorized by geological domains, groups, and formations after the terminology of St-Onge et al. (2007) and Lamothe (2007). Mafic-ultramafic samples from units of exploration interest were classified using those same resources, detailed geological mapping that was undertaken as part of this current Ph.D. research (over the summers of 2017, 2018, and 2019), and publicly available mining exploration/assessment (GM) reports filed with the Ministère de l'Énergie et des Ressources naturelles du Québec, as well as validated with the aid of private Glencore Canada Corp. and Canadian Royalties Inc. geological maps. Samples from mineralized mafic-ultramafic lithologies of the Lac Esker Suite were subdivided into the "Raglan Trend" (after the informally defined Raglan formation of Lesher, 1999, 2007) and the "Expo Trend" (after the informally defined Expo intrusive suite of Mungall, 2007) based on the stratigraphic position, geometry of the units, and types of sulphide mineralization (Fig. 2). The geochemical data plotted in this article represent samples collected from the eastern Southern Domain of the Cape Smith Belt, east of longitude 75ºW, because this region is the main focus of the current research activity and contains the greatest concentration of lithogeochemical data (Fig. 1).

Geochemistry

Rocks in the Cape Smith Belt are generally metamorphosed from the lower greenschist facies to the lower amphibolite facies, but metamorphism is restricted to the greenschist facies in the eastern portion of the Southern Domain where this study is focused. Geochemical plots revealed that some elements are mobile during alteration (e.g. Cs, Rb, K, Na, Ba, Sr, Ca, Si, U) and show variable amounts of spread unrelated to magmatic processes; these elements are ignored here. Bivariate plots with MgO display geochemical variations in mafic-ultramafic rocks useful for the interpretation of petrogenetic processes.

Some of the geochemical variations observed in samples from the same rock unit result from differences in sample preparation (e.g. non-digestion versus 4-acid digestion versus alkali fusion) and variations in the lower limits of detection for individual elements by different analytical methods[1] (e.g. pressed-pellet XRF versus INAA versus ICP-AES versus ICP-MS) employed at various laboratories. Less reliable data, especially older analyses (e.g. from the 1980s) and cumulate rocks with abundances near lower limits of detection, have been flagged and filtered from the geochemical plots. In some cases, samples have been reanalyzed in recent years by alternate methods and/or improved techniques (e.g. samples collected from the western Cape Smith Belt by P.-D. Barrette and analyzed for trace elements by ICP-AES or XRF in 1987 were reanalyzed by ICP-MS and INAA in 2018). In such instances, the most recent, reliable, and complete data are utilized in plotting.

After considering and allowing for such analytical variations, the data revealed significant differences in the lithogeochemistry and therefore petrogenesis of some lithostratigraphic units and domains. In the east-

[1] XRF = X-ray fluorescence, INAA = instrumental neutron activation analysis, ICP-AES = inductively coupled plasma-atomic emission spectroscopy, ICP-MS = inductively coupled plasma-mass spectrometry.

Table 1. Sources of whole-rock lithogeochemical data compiled for the region located north of latitude 60°N in Nunavik, Quebec.

Reference	Data Privacy	Number of Samples	CSB Southern Domain	*Raglan Trend*	*Delta Trend*	*Expo Trend*	CSB Northern Domain	Narsajuaq Arc	Kovik Antiform	Superior Province
Albino (1984) - Colorado State U.; M.Sc. thesis	public (unpub.)	69	X	X						
***Arndt et al. (1987)** - Geol. Society of London Spec. Pub. 33	public	1	X							
Barnes et al. (1982) - Economic Geology	public	25	X	X						
Barnes and Giovenazzo (1990) - The Canadian Mineralogist	public	17	X		X					
***Barnes (1979)** - U. of Toronto; M.Sc. thesis	public (unpub.)	53	X	X						
Bédard (1981) - McGill U.; M.Sc. thesis	public	116	X							
Burnham et al. (1998) - Camiro final report	public (unpub.-pending)	340	X	X		X				
***Ciborowski et al. (2017)** - Precambrian Research	public	25	X							
Clark (2008) - McGill U.; M.Sc. thesis	public	58	X	X						
Dionne-Foster (2007) - U. du Québec à Chicoutimi; M.Sc. thesis	public	71	X	X						
Dunphy and Ludden (1998) - Precambrian Research	public	76					X	X		
Dunphy (1995) - U. de Montréal; Ph.D. thesis	public	76					X	X		
Francis et al. (1981) - Contributions to Mineralogy and Petrology	public	19	X							
Francis et al. (1983) - Journal of Petrology	public	17	X							
Gillies (1993) - U. of Alabama; M.Sc. thesis	public (unpub.)	206	X	X						
Giovenazzo (1991) - U. du Québec à Chicoutimi; Ph.D. thesis	public	65	X		X					
Harvey (1995) - U. de Montréal; M.Sc. thesis	public (unpub.)	55							X	X
***Kastek et al. (2018)** - Lithos	public	86	X							
Lévesque (2000–2003) - Laurentian U.; unfinished M.Sc. thesis	public (unpub.-pending)	192	X	X						
McKevitt (2017-present) - Laurentian U.; pending Ph.D. thesis	public (unpub.-pending)	345	X	X	X	X				
Miller (1977) - U. of Western Ontario; Ph.D. thesis	public	72	X	X						
Modeland et al. (2003) - Lithos	public	156	X							
***Mungall (2007)** - Journal of Petrology	public	118	X			X				
Nadeau (1984) - U. de Montréal; M.Sc. thesis	public (unpub.)	78	X							
Picard (1989) - MERNQ publication ET 87-07	public	216	X							
Picard (1989) - MERNQ publication ET 87-14	public	163	X							
***Picard (1995)** - MERNQ publication MB 95-01	public	457	X		X					
Picard et al. (1994) - MERNQ publication MB 94-30	public	653	X	X	X	X				
Picard et al. (1990) - Precambrian Research	public	522	X				X			
Scott (1990) - Queen's U.; Ph.D. thesis	public (unpub.)	87					X			
Shepherd (1960) - U. of Toronto; Ph.D. thesis	public (unpub.)	5	X	X						
Stewart (2002) - McGill U.; M.Sc. thesis	public	118	X	X						
Stilson (2000) - U. of Alabama; M.Sc. thesis	public (unpub.)	197	X	X						
St-Onge et al. (2007) - GSC Open File 5117	public	2728	X	X	X	X	X	X	X	X
Thacker (1995) - U. of Alabama; M.Sc. thesis	public (unpub.)	68	X	X						
Thibert (1993) - U. de Montréal; M.Sc. thesis	public (unpub.)	73	X	X	X					
Tremblay (1990) - U. du Québec à Chicoutimi; M.Sc. thesis	public	27	X		X					
Van Hoof (2000) - U. of Ottawa; H.B.Sc. thesis	public	25	X	X						
Wilson et al. (1969) - Society of Economic Geologists, Monograph 4	public	59	X	X						
Glencore Canada Corp. Raglan Mine files (1981–2007), *including* Xstrata, Falconbridge, New Québec Raglan Mines records Talkington (1988) Falconbridge Ltd. Report Tremblay (1990) Falconbridge Ltd. Report	private	~1900	X	X	X	X	X			

Table 1 continued.

Reference	Data Privacy	Number of Samples	CSB Southern Domain	*Raglan Trend*	*Delta Trend*	*Expo Trend*	CSB Northern Domain	Narsajuaq Arc	Kovik Antiform	Superior Province
SIGÉOM, *including*	public	13,695	X	X	X	X	X	X	X	X
Barrette, P.-D. (1987)	public	384	X						X	
Budkewitsch, P. (1987)	public	36	X							
Carrier, J.A. (1988–1989)	public	87					X	X		
Giovenazzo, D. (1984–1985–1987)	public	543	X	X	X	X	X			X
Hervet, M. (1984)	public	293					X	X	X	
Lamothe, D. (1983–1984–1988–1989–1990)	public	1142	X				X	X	X	X
Lefebvre, C. (1986)	public	218	X				X	X		
Moorhead, J. (1986–1987)	public	460	X				X	X	X	X
Picard, C. (1984–1985–1987–1988)	public	805	X				X			
Roy, C. (1984)	public	165	X				X			
Tremblay, C. (1987)	public	115	X				X	X		
Tremblay, G. (1985–1986)	public	400	X				X	X	X	
Mining exploration/assessment reports filed with the Ministère de l'Énergie et des Ressources naturelles du Québec (*# samples in parentheses*):	public	7462	X	X	X	X	X	X	X	X
GM53072 (36); GM53312 (50); GM53313 (33); GM53314 (41); GM53966 (49); GM53968 (10); GM54025 (82); GM54774 (37); GM54904 (27); GM54911 (106); GM55418 (3); GM55652 (102); GM55666 (16); GM55667 (33); GM55835 (328); GM56016 (100); GM56017 (42); GM56057 (3); GM56113 (66); GM56137 (86); GM56228 (24); GM56643 (17); GM57830 (163); GM57914 (16); GM58002 (45); GM58098 (14); GM58155 (15); GM58329 (6); GM58535 (3); GM58538 (5); GM58539 (63); GM58541 (36); GM58542 (38); GM58543 (7); GM58544 (84); GM58561 (70); GM58565 (51); GM58566 (285); GM59703 (26); GM59704 (21); GM59705 (3); GM59708 (108); GM59709 (23); GM60528 (138); GM60665 (205); GM60677 (46); GM60678 (19); GM60679 (89); GM60680 (50); GM60977 (216); GM61450 (49); GM61451 (6); GM61458 (15); GM61459 (9); GM61624 (3); GM61628 (137); GM61828 (10); GM61982 (63); GM61990 (11); GM62276 (1); GM62288 (766); GM62602 (52); GM62619 (74); ***GM62809** (529); GM62855 (194); GM62857 (23); GM63002 (49); GM63073 (102); GM63115 (156); ***GM64449** (1118); ***GM64611** (136); GM64736 (10); GM64843 (118); GM64953 (389); GM65441 (306).										

NB: Many samples were found in numerous sources; after eliminating duplicates, the total number of samples is fewer than what is listed here (*see* Table 2).
***Reference:** Source of high-quality major, minor, and trace element data plotted in Figures 3 to 5 and discussed in the text.
Abbreviations: CSB = Cape Smith Belt, MERNQ = Ministère de l'Énergie et des Ressources naturelles du Québec, U. = University or Université.

Table 2. Summary of whole-rock lithogeochemical data compiled for the region located north of latitude 60°N in Nunavik, Quebec.

Geological Domain	Number of sample records		Number of public sample records with particular group of elements analyzed			
	All (private + public)	Public	majors ± traces	traces (no majors)	REEs	PGEs
Narsajuaq Arc	572 (3.1%)	572 (3.4%)	543 (3.7%)	29 (1.3%)	546 (5.2%)	8 (0.1%)
Kovik Antiform	271 (1.4%)	271 (1.6%)	180 (1.2%)	91 (4.0%)	234 (2.2%)	112 (1.5%)
CSB Northern Domain	1877 (10.0%)	1809 (10.6%)	1737 (11.8%)	72 (3.1%)	1429 (13.7%)	498 (6.8%)
CSB Southern Domain	14,453 (76.8%)	12,710 (74.8%)	11,134 (75.8%)	1553 (67.7%)	7432 (71.1%)	6283 (85.8%)
New Québec Orogen, Core Zone	25 (0.1%)	25 (0.1%)	16 (0.1%)	9 (0.4%)	17 (0.2%)	3 (0.04%)
New Québec Orogen, Labrador Trough	669 (3.6%)	669 (3.9%)	536 (3.7%)	133 (5.8%)	215 (2.1%)	214 (2.9%)
Superior Province	902 (4.8%)	902 (5.3%)	500 (3.4%)	402 (17.5%)	547 (5.2%)	176 (2.4%)
references + Franklin dyke swarm	44 (0.2%)	40 (0.2%)	37 (0.3%)	5 (0.2%)	28 (0.3%)	26 (0.4%)
Totals	18,813 (100.0%)	17,000 (100.0%)	14,683 (100.0%)	2294 (100.0%)	10,448 (100.0%)	7320 (100.0%)

NB: "Public" includes some records that are currently unpublished but are planned for release (*see* Table 1). "Majors" includes major + minor element oxides.
Abbreviations: PGEs = platinum group elements, REEs = rare earth elements.

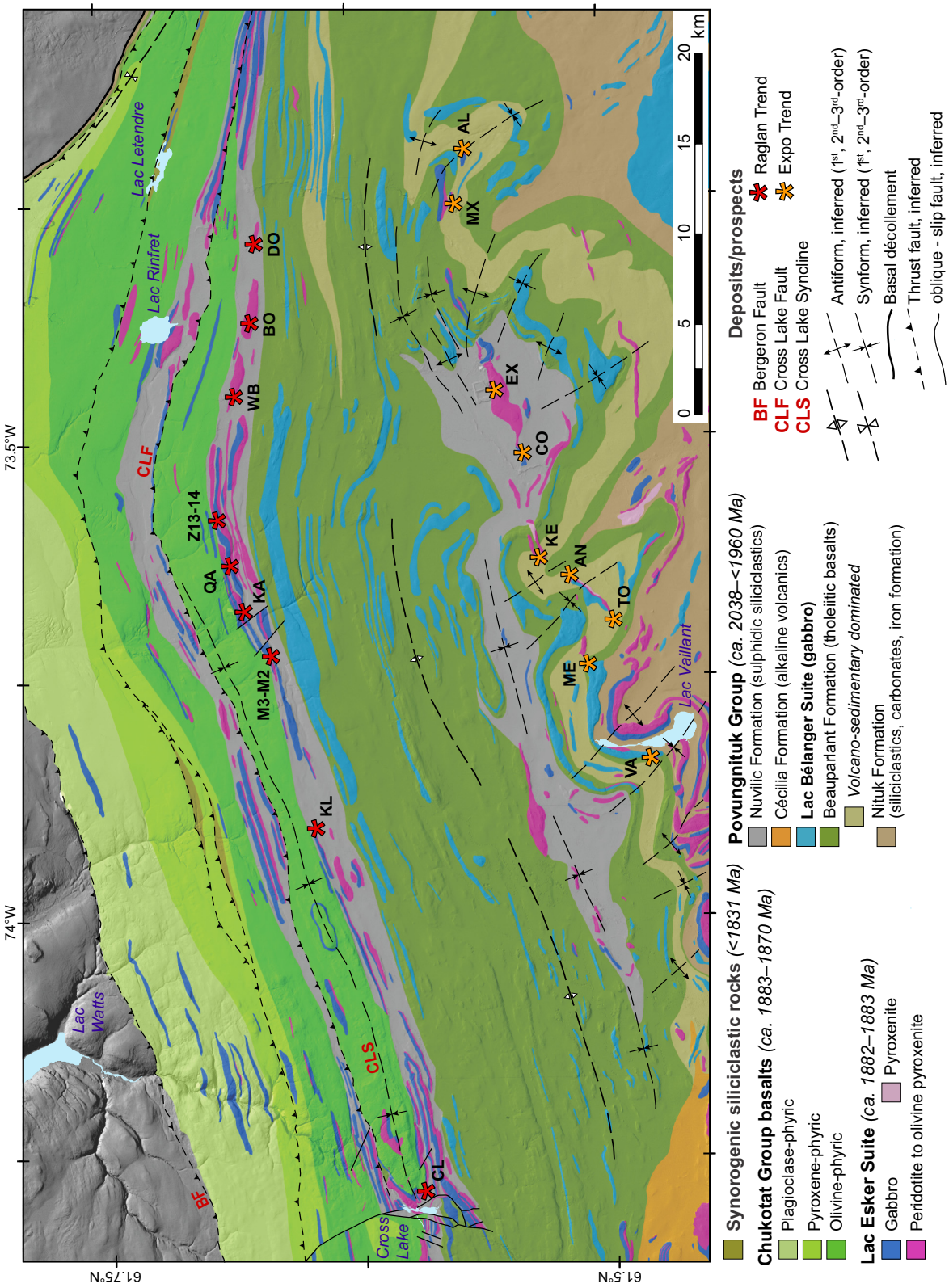

Figure 2. Regional geological map of the eastern part of the Southern Domain within the Paleoproterozoic Cape Smith Belt. The geology is *modified from* St-Onge et al. (2007) and Mungall (2007), and follows the structural interpretation of Bleeker and Kamo (2020). The underlying digital elevation model is from Porter et al. (2018). Deposits and prospects along the Raglan Trend, from west to east: CL = Cross Lake, KL = Kikialik, M3-M2 = Mine 3 and Mine 2, KA = Katinniq, QA = Qakimajurq, Z13-14 = Zone 13-14, WB = West Boundary, BO = Boundary, DO = Donaldson. Deposits and prospects along the Expo Trend, from west to east: VA = Vaillant, ME = Méquillon, TO = Tootoo, AN = Annie, KE = Kehoe, CO = Cominga, EX = Expo, MX = Mesamax, AL = Allammaq. Note: many lower order (2nd–3rd order), younger generation faults and folds are omitted for clarity.

ern portion of the Cape Smith Belt's Southern Domain, significant differences in major and trace element concentrations distinguish the various mafic-ultramafic volcanic and intrusive units. The following observations and discussion utilize a representative subset of 1,368 samples with high-quality major and trace element geochemical data from 9 sources (*see* Table 1).

Figure 3 shows major and trace element concentrations for volcanic and high-level intrusive rocks of the Povungnituk Group. The stratigraphically lowest and oldest volcanic rocks comprise the 1998–1991 Ma Beauparlant Formation tholeiitic basalt with continental flood basalt affinity and the associated microgabbro ("diabase") rocks (e.g. Picard et al., 1990, 1994; Modeland et al., 2003; Kastek et al., 2018), referred to as the Lac Bélanger Suite by Lamothe (2007). These samples contain 5–10 wt% MgO, 1–4 wt% TiO_2, and 20–300 ppm Cr. Primitive mantle-normalized rare earth element (REE) values of Beauparlant Formation and Lac Bélanger Suite samples average 10–30 for the light REEs (LREEs) and 5–7 for the heavy REEs (HREEs). The conformably overlying and slightly younger alkaline volcanic rocks of the Cécilia Formation (ca. 1959 Ma: Parrish, 1989; Gaonac'h et al., 1992), in comparison to Beauparlant Formation and Lac Bélanger Suite rocks, generally display similar concentrations of MgO and Cr, greater than 3 wt% TiO_2, similar or higher concentrations of high-field-strength elements (HFSEs) (e.g. >400 ppm Zr, >70 ppm Nb), and significantly higher concentrations of REEs (particularly greater La/Sm ratios). Phonolite samples from the Cécilia Formation contain ~2 wt% MgO, <20 ppm Cr, <1 wt% TiO_2, >500 ppm Zr, and Nb and REE concentrations similar to those of the other alkaline volcanic rocks.

The stratigraphically higher ca. 1883–1870 Ma Chukotat Group basalt transitions upward (in general) from olivine-phyric komatiitic basalt through pyroxene-phyric to plagioclase-phyric tholeiitic basalt, although different series are interlayered throughout the stratigraphy (Francis and Hynes, 1982; Hynes and Francis, 1982; St-Onge et al., 1992; St-Onge and Lucas, 1993; Bleeker and Kamo, 2018). Figure 3 displays the continuous geochemical variation of major and trace elements among these series in terms of MgO (~5–18 wt%; samples with >18 wt% represent channelized komatiitic basalt lava flows with cumulus olivine), TiO_2 (0.5–1 wt%), Cr (50–2000 ppm), Zr (30–90 ppm), and Nb (<10 ppm). Primitive mantle-normalized REE values average 4–5 for the LREEs and 3–4 for the HREEs.

Mafic to ultramafic dykes and sills[2], referred to as the Lac Esker Suite by Lamothe (2007), occur throughout the stratigraphy from the lower Povungnituk Group to the base of the Chukotat Group. Generally, non-mineralized samples from units hosting deposits/prospects/showings fall along similar trends on MgO bivariate plots, implying similar parental magma(s) and petrogenetic/magmatic processes for the Raglan Trend and Expo Trend units. However, Figure 4 shows some clear differences: 1) the most magnesian Raglan cumulate rocks range up to 44 wt% MgO, whereas the most magnesian Expo cumulate rocks only range up to 35 wt% MgO; 2) many Expo samples have lower TiO_2 and Cr concentrations than Raglan samples at >15 wt% MgO; 3) mineralized Raglan samples have higher Ni/Cu ratios than Expo samples; 4) Raglan samples have significantly higher La/Sm ratios and more positive primitive mantle-normalized Th and Zr-Hf anomalies than Expo samples.

Figure 5 utilizes Nb/Yb versus Th/Yb bivariate plots, which are ideal for identifying crustal input (i.e. direct crustal contamination or subduction-related crustal recycling in the magma source region) because Th and Nb behave similarly during most petrogenetic processes and are both immobile during lower amphibolite-facies metamorphism (Pearce, 2008). Sedimentary rock samples and Cécilia Formation alkaline volcanic/phonolite rocks plot at high values of Nb/Yb and Th/Yb, values typical of continental upper crust and ocean island basalt (OIB), respectively. Chukotat Group and Beauparlant Formation basaltic rocks plot in two distinct regions. The Chukotat field extends from low values of Th/Yb and Nb/Yb, located halfway between normal mid-ocean ridge basalts (N-MORB) and enriched mid-ocean ridge basalts (E-MORB), to higher Th/Yb and Nb/Yb values, outside of the oceanic basalt array. The Beauparlant samples plot in two fields located almost entirely within the oceanic basalt array: a "less-enriched" field between N-MORB and E-MORB comprising samples from the lower Beauparlant Formation and a "more-enriched" field between E-MORB and OIB comprising samples mostly from the middle-upper Beauparlant Formation. Ultramafic–gabbroic–basaltic samples from Raglan Trend and Expo Trend units together form an array that overlaps Chukotat samples and extends to high values of Th/Yb and Nb/Yb, similar to values for upper crustal rocks and sedimentary rocks derived from the upper continental crust. Raglan samples, classified as sedimentary "xenomelts" (Stilson, 2000) or "ultrahornfels" (*see* Fig. 6 in Bleeker and Kamo, 2020), plot within or close to the field of metasedimentary samples. We pre-

[2] Units that belongs to the Lac Esker Suite have been classified as intrusive by Lamothe (2007), however, many of these, especially units at the interface between the Povungnituk and the Chukotat groups, are lava flows as suggested by the presence of polyhedral jointing and flow top breccias (*see* Lesher, 1999, 2007; Lesher and Houlé, 2017).

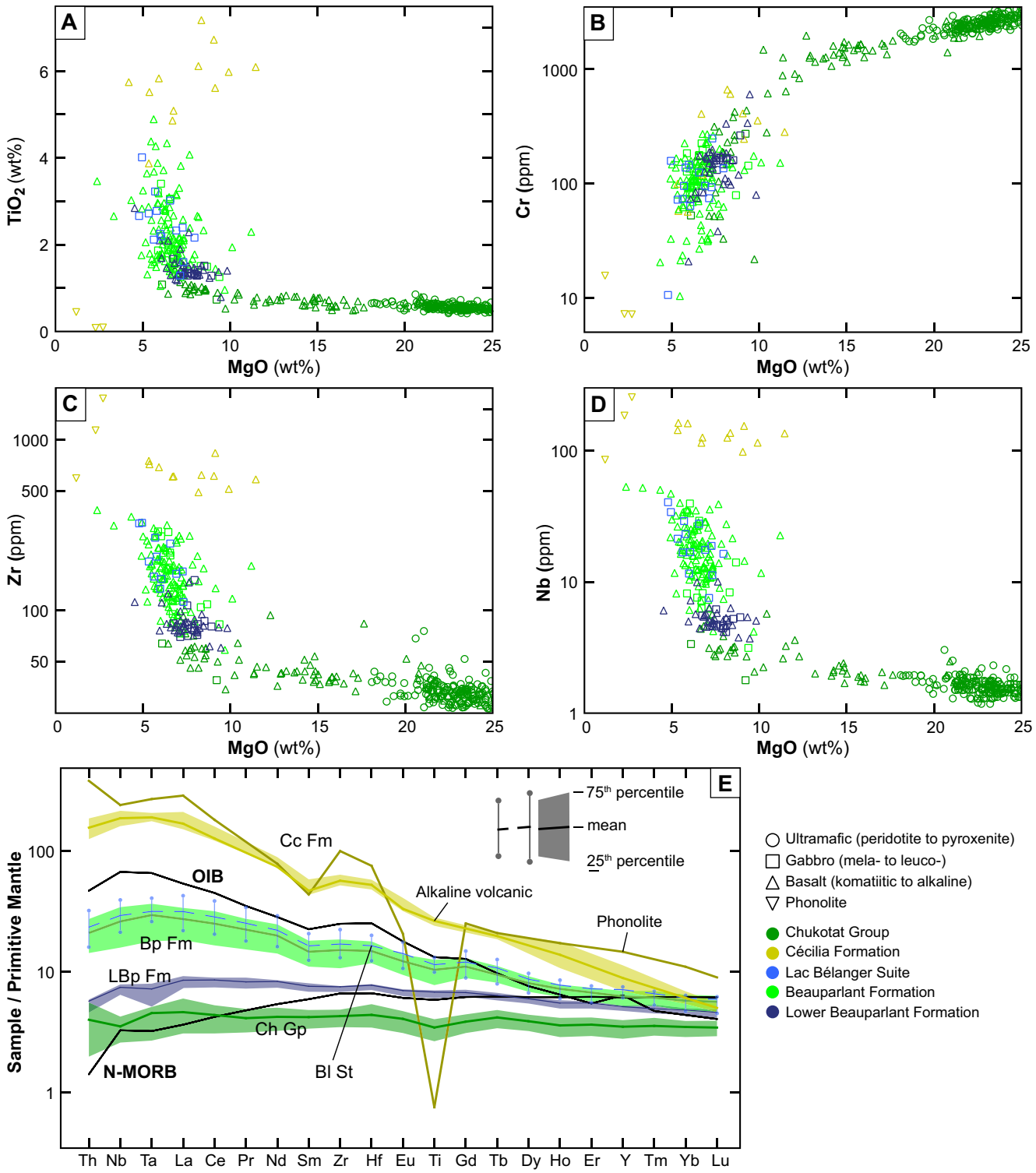

Figure 3. Geochemical plots for distinguishing volcanic-subvolcanic rocks of the Povungnituk and Chukotat groups in the Southern Domain of the eastern Cape Smith Belt (east of longitude 75ºW). bivariate plots of **(a)** MgO (wt%) versus TiO_2 (wt%); **(b)** MgO (wt%) versus Cr (ppm); **(c)** MgO (wt%) versus Zr (ppm); and **(d)** MgO (wt%) versus Nb (ppm) bivariate plot. **e)** High field strength elements (HFSE) and rare earth element (REE) primitive mantle-normalized diagram showing Povungnituk Group lower and middle to upper Beauparlant Formation basalt (LBp Fm and Bp Fm, n = 44 and 129, respectively), Cécilia Formation alkaline basalt (Cc Fm, n = 12) and phonolite (n = 7), Lac Bélanger Suite "gabbro" (Bl St, n = 14), and Chukotat Group basalt (Ch. Gp, n = 85). The thick, dark lines indicate the average values within the lighter coloured fields, which represent the 25th to 75th percentiles. All plotted data are publicly available (*see* text and Table 1). Chukotat Group basalts with >18 wt% MgO contain cumulus olivine in channelized lava flows or feeders; the samples averaged in (e) contain <18 wt% MgO. Abbreviations: N-MORB = normal mid-ocean ridge basalt, OIB = oceanic island basalt. Primitive mantle normalization and reference values are from Sun and McDonough (1989).

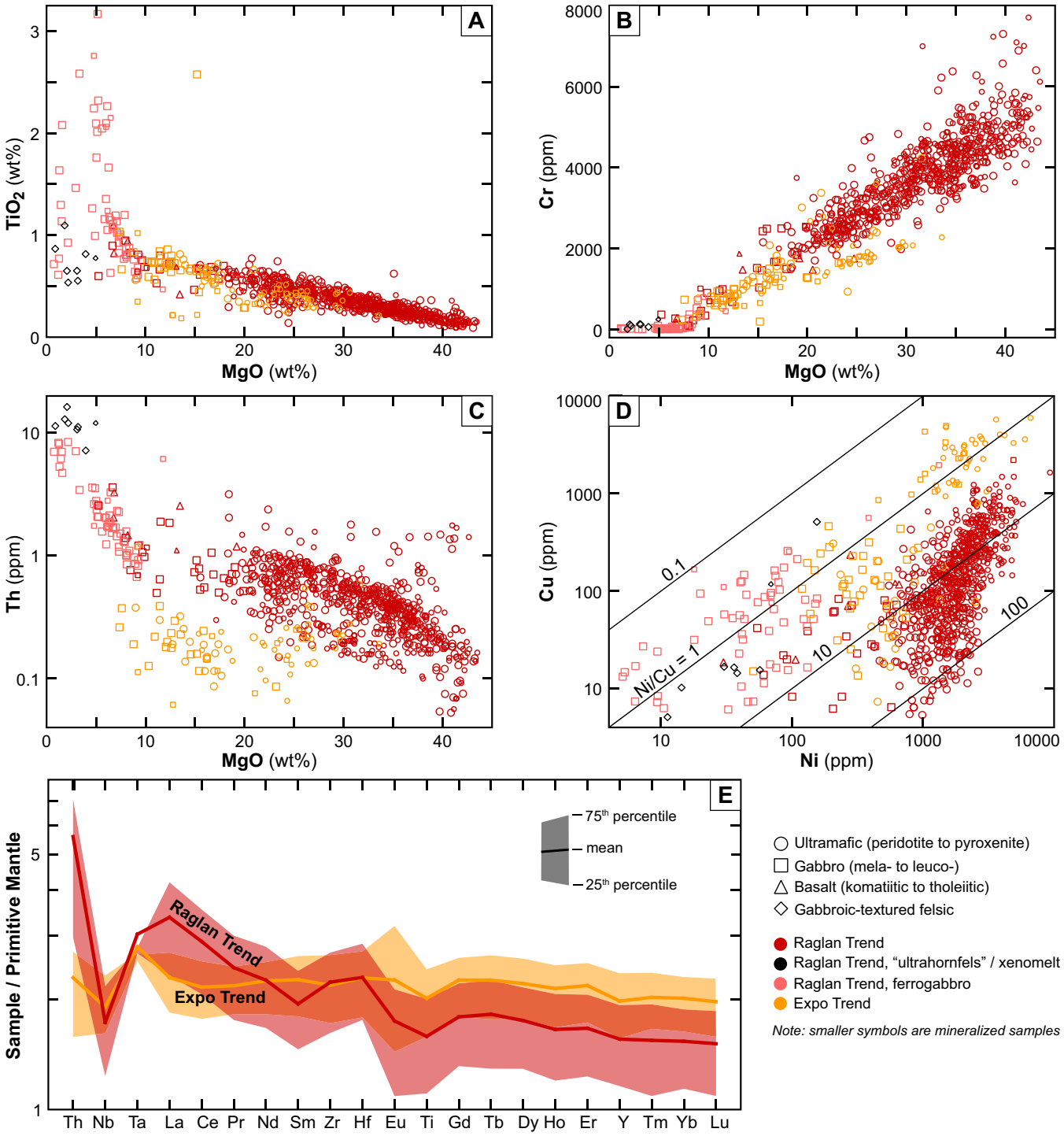

Figure 4. Geochemical plots for distinguishing volcanic-subvolcanic-intrusive units along the Raglan and Expo trends of the mafic-ultramafic Lac Esker Suite in the Southern Domain of the eastern Cape Smith Belt (east of longitude 75°W). Bivariate plots of **(a)** MgO (wt%) versus TiO_2 (wt%); **(b)** MgO (wt%) versus Cr (ppm); **(c)** MgO (wt%) versus Th (ppm); and **(d)** Ni (ppm) versus Cu (ppm) bivariate plot. **e)** High field strength elements (HFSE) and rare earth element (REE) primitive mantle-normalized diagram showing compositions of the Expo Trend (n = 70) and Raglan Trend (n = 665) for samples with >15 wt% MgO. The thick, dark lines indicate average values within the lighter coloured fields, which represent the 25th to 75th percentiles. All plotted data are publicly available (*see* text and Table 1). In plots (a) to (d), the smaller symbols represent mineralized samples with at least one value greater than 5000 ppm S, 2500 ppm Ni, 500 ppm Cu, and 250 ppb Pt+Pd. Primitive mantle normalization values are from Sun and McDonough (1989).

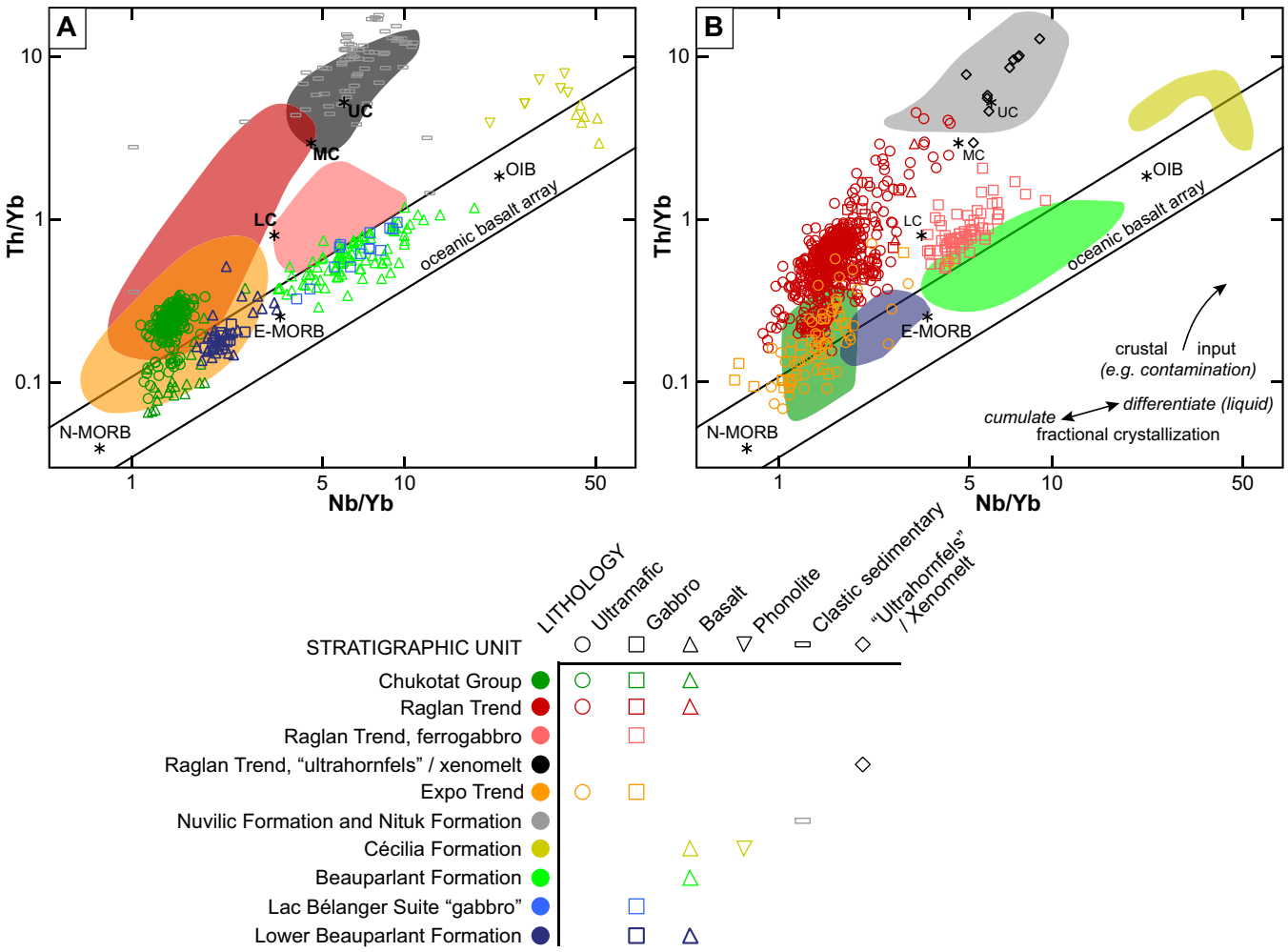

Figure 5. Geochemical plots of Nb/Yb versus Th/Yb (*after* Pearce, 2008) for characterizing magma source regions and crustal input. The legend applies to plots (a) and (b). **a)** Sedimentary and volcanic/high-level synvolcanic intrusive rock samples from the Povungnituk and Chukotat groups. Shaded fields correspond to samples plotted in (b). **b)** Volcanic/intrusive ultramafic-mafic rock samples from the Raglan Trend and Expo Trend units. Inset arrows indicate possible (but not exclusive) processes that may control trends. Shaded fields correspond to samples plotted in (a). All plotted data are publicly available (*see* text and Table 1). Abbreviations: E-MORB = enriched mid-ocean ridge basalt, N-MORB = normal mid-ocean ridge basalt, OIB = oceanic island basalt, LC = lower crust, MC = middle crust, UC = upper crust. Reference values are from Sun and McDonough (1989) and Rudnick and Gao (2003).

fer the former interpretation, as the most strongly hornfelsed rocks at Raglan are bleached, recrystallized, or spotted (*see* Fig. 4D in Lesher, 2007; Fig. 3E–H in Lesher, 2017), whereas these rocks have gabbroic igneous textures.

DISCUSSION

Volcanism in the eastern Cape Smith Belt

Povungnituk Group

Volcanic rocks in the Povungnituk Group have traditionally been separated into the Beauparlant Formation, with dominantly tholeiitic pillowed and massive basalt flows of continental-flood basalt geochemical affinity (Hynes and Francis, 1982; Modeland et al., 2003), and the concordantly overlying (in the central Cape Smith Belt area) Cécilia Formation alkaline basalt and lesser intermediate-felsic volcaniclastic rocks, characterized by high concentrations of LREEs and HFSEs such as Zr and Nb (Gaonac'h et al., 1992). These geochemical distinctions are evident in major and trace elements in the current geochemical compilation (Fig. 3). Modeland et al. (2003) and Kastek et al. (2018) note two end-member varieties within the Beauparlant basalts: enriched (highly incompatible lithophile elements: HILE, e.g. Th, LREE) and unenriched or depleted (lower HILE) basalt. Figure 3a–d shows relatively constant MgO concentrations (6–8 wt%) and a continuous variation between "enriched" and "unenriched" samples. Notably, some Beauparlant samples range up to ~10 wt% MgO (possibly a pyroxenephyric population), but they are readily distinguished from Chukotat Group basalt by higher TiO_2 (>1 wt%) and lower Cr (<200 ppm) contents at a given MgO concentration. The samples plotted in Figure 5a

suggest two geochemically distinct magma source regions (unenriched or depleted and enriched); however, this is likely an artifact of sampling. Other data sets (e.g. Modeland et al., 2003), although less precise (not plotted), suggest that a continuum exists between these fields, possibly representing variable degrees of partial melting (more in less enriched samples, less in more enriched samples).

Numerous coarser grained units that often exhibit columnar jointing and stand in stark topographic relief relative to surrounding interflow sedimentary rocks and pillowed basalt within the Beauparlant Formation have been interpreted as subvolcanic microgabbro ("dolerite") sills of the Lac Bélanger Suite (St-Onge and Lucas, 1993; Picard et al., 1994). Recent field observations (Mungall, 2007; McKevitt et al., 2019) have confirmed that these units are conformable with underlying and overlying massive and/or pillowed basalt flows. Additionally, what are often mapped at regional-scale (Fig. 2) as extensive, thick, entirely "gabbroic" units are, in fact, at outcrop scale units with rapid transitions in grain size with coarse-grained "gabbroic" columnar-jointed sections grading upwards into fine-grained, massive and/or pillowed basalt. Considering that the major and trace element concentrations of these gabbro units are indistinguishable from the surrounding basalt (Fig. 3, 5), this raises the possibility that at least some of the Lac Bélanger Suite intrusions are thick, coarse-grained texturally/compositionally differentiated basaltic flows.

Chukotat Group

The majority of the lower and middle Chukotat Group volcanic rocks (e.g. olivine-phyric and pyroxene-phyric basalts with >8 wt% MgO) are easily distinguished from Povungnituk Group volcanic rocks by higher MgO concentrations and a trend in Nb/Yb versus Th/Yb space that is oblique to the mantle array (and to the trend of Povungnituk basalt) but project to a point on the mantle array between N-MORB and E-MORB (Fig. 3, 5; Francis et al., 1983; Modeland et al., 2003). Although some Chukotat basalt samples have similar MgO contents to those of Beauparlant Formation basalt, they are distinguished by having lower TiO_2 and higher Cr concentrations (Fig. 3a,b) at equivalent MgO contents. Additionally, the averages of primitive mantle-normalized REE abundances of all Povungnituk Group volcanic and subvolcanic units are significantly higher than those of Chukotat Group basalt (Fig. 3e). Most of the more primitive Chukotat basalt and ultramafic cumulate rocks (from the lowermost series) plot outside of the MORB-OIB oceanic basalt array in Figure 5a, suggesting some degree of crustal input in the magma source region (less likely) and/or crustal contamination during flow through/over continental crust or sediments derived from continental crust (more likely) (Lesher et al., 2001; Lesher, 2007; *see* discussion by Pearce, 2008). The Chukotat basalt samples that plot within the oceanic basalt array between N-MORB and E-MORB are likely most representative of the primary magma source region (*see also* Lesher et al., 2001).

Mineralized Lac Esker Suite Units in the eastern Cape Smith Belt

The geometry of the host units and location and style of sulphide mineralization differ between the Expo and Raglan trends of the Lac Esker Suite: net-textured to disseminated Cu-Ni-PGE sulphide mineralization occurs along the lower margins and keels of blade-shaped dykes within the Expo Trend (Mungall, 2007), whereas massive to net-textured Ni-Cu-PGE sulphide mineralization occurs within embayments at the bases of channelized lava flows within the Raglan Trend (Lesher, 2007). As shown here, a combination of major and trace element geochemistry of mineralized or barren host rocks is useful in distinguishing between units of these two trends. They are also readily distinguished by the Ni and Cu concentrations of mineralized samples.

The geochemical differences in major and trace elements among samples from units throughout the Expo-Raglan transcrustal magmatic plumbing system(s) may result from a combination of factors: 1) differential evolution of magma(s) within different parts of the plumbing system(s) driven by variable pressure, temperature, flow dynamics, magma flux, assimilation of country rock, fO_2, and fS_2 (e.g. Lesher et al., 2001; Lesher, 2007, 2019); and 2) magma evolution within a rising mantle plume (Ciborowski et al., 2017; Bleeker and Kamo, 2018). Any explanation for the varying metal concentrations between ores of the Expo and Raglan trends should also consider the effective magma:olivine:sulphide ratios (R' factors: *as modified by* Lesher and Burnham, 2001 *from* Campbell and Naldrett, 1979) and possible assimilation and subsequent upgrading of pre-existing sulphides from an upstream part of the system (*see* Barnes and Giovenazzo, 1990).

The similar HFSE-REE primitive mantle-normalized patterns in Figure 4e and the overlap of Expo and Raglan fields in Figure 5b suggest that the parental magmas of these two trends may have come from the same primary mantle source but with varying degrees of crustal contamination: the Raglan Trend samples ranging to more contaminated compositions. There is evidence of some crustal contamination in the Chukotat Group (Fig 5; *see also* Lesher et al., 2001; Lesher, 2007; Ciborowski et al., 2017), but it is minor compared to that in the Raglan and Expo units. The restriction of significant contamination to Raglan and

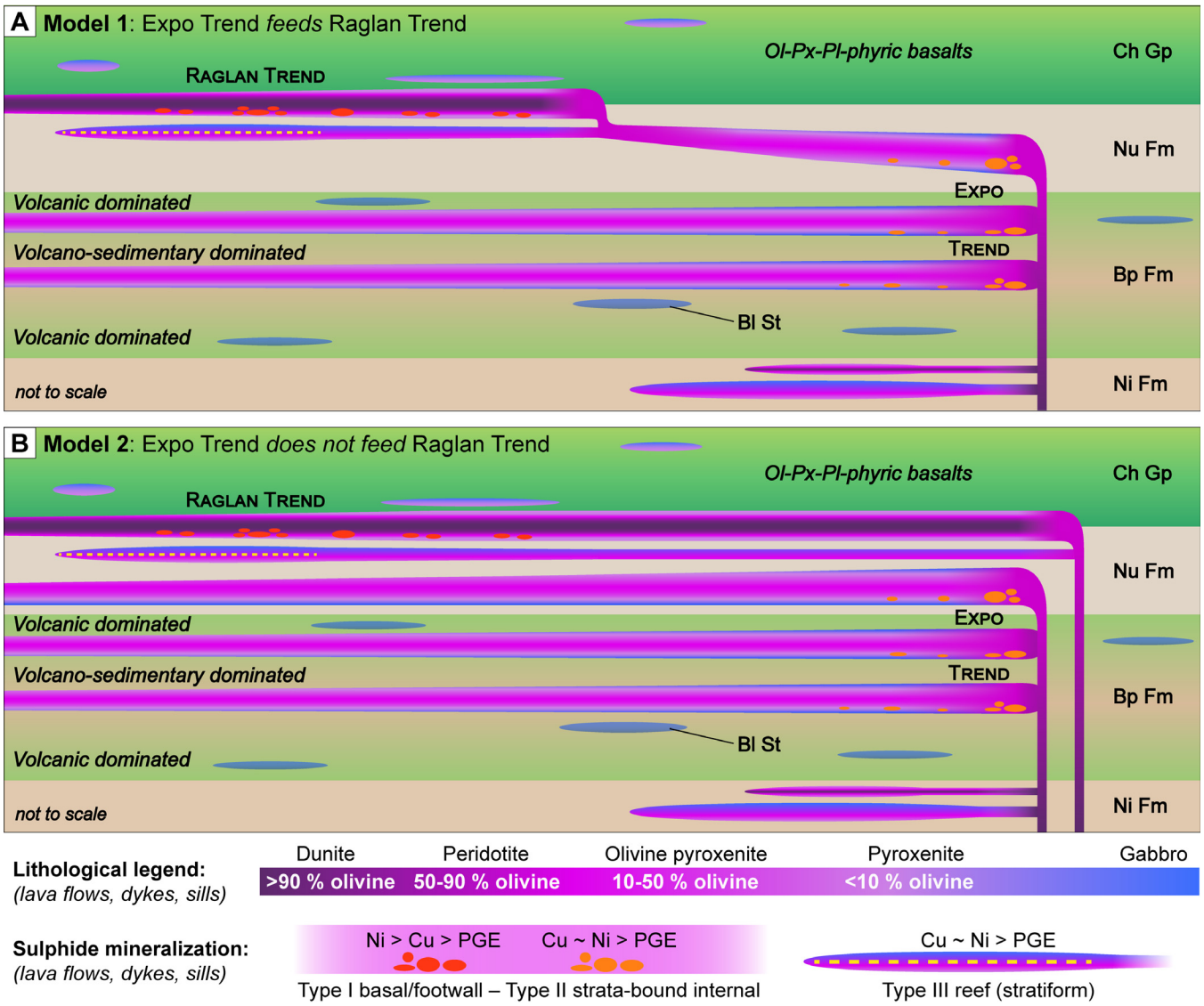

Figure 6. Schematic models of the magmatic plumbing systems (before deformation and erosion) for the Lac Esker Suite intrusive/extrusive mafic-ultramafic units of the eastern part of the Southern Domain of the Cape Smith Belt. **a)** Model 1 illustrates Expo Trend magmatism directly feeding the Raglan Trend units; **b)** model 2 illustrates Expo Trend magmatism *not* directly feeding Raglan Trend units. Specific deposits/prospects are not shown, but in the Expo Trend, those hosted by the lower to middle Beauparlant Formation include Vaillant, Méquillon, Tootoo, and Annie; those in the middle to upper Beauparlant Formation include Kehoe, Mesamax, and Allammaq; those in the Nuvilic Formation include Cominga and Expo. Deposits and prospects along the Raglan Trend include Cross Lake, Kikialik, Mine 3 and Mine 2, Katinniq, Qakimajurq, Zone 13-14, West Boundary, Boundary, and Donaldson. Abbreviations: Ch Gp = Chukotat Group, Bl St = Lac Bélanger Suite, Bp Fm = Beauparlant Formation, Ni Fm = Nituk Formation, Nu Fm = Nuvilic Formation.

Expo units, rather than the Chukotat Group as a whole, indicates that most of the contamination in those units was from Nuvilic sediments (which were derived by erosion of upper continental crust) and did not result from passage through upper continental crust (*see* discussion by Lesher and Arndt, 1995). After allowance for crustal contamination, there are no systematic variations in Th/Yb and Nb/Yb values in Raglan or Expo units—of the type observed in the Beauparlant Formation in Figure 5—that could be attributed to differences in the composition of the mantle source and/or degree of partial melting.

Figure 6 shows two possible models for the relationship between the magmatism of the Expo and Raglan trends, and Table 3 summarizes the criteria and actual observations by which the relative merits of these models can be tested. Model 1 (Fig. 6a), favoured by Francis et al. (1983), Bédard et al. (1984), Giovenazzo et al. (1989), Mungall (2007), and most recently by Bleeker and Kamo (2020), suggests that the subvolcanic parts (i.e. Expo) of the magmatic plumbing system fed the volcanic-dominated parts (i.e. Raglan). The models of Mungall (2007) and Bleeker and Kamo (2020), in particular, suggest that Expo represents a

Table 3. Summary of the key criteria expected and observed in each magmatic plumbing system model used to evaluate the relative merits of each model (*see* Fig. 6).

Criteria	Expected Observations/Characteristics (actual in **bold**)		Actual Observations/Characteristics	
	MODEL 1	**MODEL 2**	**RAGLAN**	**EXPO**
	Expo feeds Raglan	Expo DOES NOT feed Raglan		
Age	must be the **same**	may be the **same** or different	1882–1883 Ma[1,2]	1882–1883 Ma[1,3]
Maximum MgO margins	Raglan ≤ Expo	**Raglan > Expo**, but may be different	18–20 wt%[4,5,7–8] pyroxenite	15-17 wt%[6,8–9] gabbro
Maximum MgO cumulates	Raglan ≤ Expo	**Raglan > Expo**, but may be different	44 wt%[4,5,7–9]	34 wt%[6–9]
$[La/Sm]_{MN}$ (proxy for crustal contamination)	Raglan ≤ Expo, but depends on flow rate *see* [7]	**Raglan > Expo**, but depends on flow rate *see* [7]	average ~1.8[4–9]	average ~1.0[6–9]
Primary magma source	must be the **same**	may be the **same** or different	between N-MORB and E-MORB[4–9]	between N-MORB and E-MORB[4–9]
Ni/Cu ratios of ores	Raglan ≤ Expo	**Raglan > Expo**, but may be different	average ~10[4–7,9]	average ~1[4–7,9]

References: [1]Bleeker and Kamo (2020), [2]Wodicka et al. (2002), [3]Randall (2005), [4]Lesher (1999), [5]Lesher (2007), [6]Mungall (2007), [7]Lesher et al. (2001), [8]McKevitt et al. (2019), [9]McKevitt et al. (this study).
Abbreviations: E-MORB = enriched mid-ocean ridge basalt, N-MORB = normal mid-ocean ridge basalt.

volcanic/intrusive centre that sits within the same sedimentary formation that underlies/hosts Raglan Trend units (i.e. that it is a southern synclinal outlier of the Nuvilic Formation sediments underlying Raglan units: *see* Fig. 2), and that Raglan units are "downflow" equivalents of Expo magmas. Model 2 (Fig. 6b), which has been favoured by Lesher (1999, 2007) and Lesher and Houlé (2017), suggests that the subvolcanic (i.e. Expo) and volcanic (i.e. Raglan) parts were fed separately. Although the criteria and observations, thus far, are insufficient to unequivocally prove or disprove either model, the current weight of evidence greatly favours Model 2 (Table 3). The less magnesian "chilled" margins and olivine cumulates of the host units combined with the lower Ni/Cu ratios of the ores at Expo indicate that the host units crystallized from and the ores equilibrated with cooler, less magnesian, and more evolved magmas, and could not have supplied the hotter, more magnesian, and more primitive magmas required to produce the more magnesian "chilled" margins and olivine cumulates of the host units and the higher Ni/Cu ratios of the ores at Raglan. Although the degree of crustal contamination increases then decreases with increasing magma/lava flux (*see* discussion by Lesher et al., 2001), the higher degree of contamination of Raglan host units—despite their higher magnesium contents—and the greater ore tonnages at Raglan are also consistent with higher temperatures, higher magma fluxes, and greater degrees of thermomechanical erosion.

Ongoing evaluation of these observations, models, and possible factors noted above will continue to yield insights into the source and evolution of this well exposed, well endowed Paleoproterozoic volcanic-subvolcanic-intrusive magmatic plumbing system. The findings may apply to Archean greenstone belts within the Superior Province, Circum-Superior Paleoproterozoic volcanic belts, and other Paleoproterozoic volcanic belts worldwide.

Geodynamic Setting

The geodynamic setting of the mafic-ultramafic magmatism in the Cape Smith Belt is not yet clear. Several authors have suggested that Chukotat magmas were generated in a mantle plume (e.g. Ciborowski et al., 2017; Kastek et al., 2018) that was "steered" toward the Superior Craton margin (Begg et al., 2010; *see also* Bleeker and Kamo, 2020), but Chukotat lavas have non-unique PRIMELT3-calculated compositions with 18–19% MgO that could also be generated by decompression melting of mantle peridotite in a hot rift (*see* Herzberg, 2004). It is not yet clear which model is more consistent with the presence of mafic-ultramafic magmas that extend more than 3500 km along the Circum-Superior Belt (Baragar and Scoates, 1981, 1987).

IMPLICATIONS FOR EXPLORATION

Important considerations during exploration for magmatic Ni-Cu-PGE sulphide mineralization include proximity to sulphur-rich horizons of country rock and magma flux in different parts of the magmatic plumbing system (Lesher, 2019; Fig. 6). These considerations especially apply in the eastern Cape Smith Belt, where

[3] PRIMELT software, designed by Herzberg and O'Hara (2002) and Herzberg and Asimow (2008, 2015), can be used to determine the primary magma composition and mantle potential temperature from an observed lava composition.

deposits along the Expo and Raglan trends show stratigraphic control. The clear geochemical distinctions (in both major and trace elements) between the Povungnituk Group and Chukotat Group volcanic rocks thus may aid a surface or underground exploration program in establishing the relative stratigraphic position. Additionally, especially in examining drill core, some non-prospective gabbroic-textured units in the Povungnituk Group (i.e. Lac Bélanger Suite) may be mistaken for gabbro of prospective Lac Esker Suite units; however, the geochemical distinction between these two types of gabbro is possible by considering major elements (e.g. TiO_2) or trace element contents.

The major and trace element geochemistry of mineralized or barren samples from the Lac Esker Suite can be used to discriminate between units of the Expo or Raglan trends. Such data can aid in categorizing potentially prospective units as volcanic or intrusive (i.e. channelized flows or dykes/sills) and thereby improve targeting for sulphide mineralization within units.

The geochemical data shown here come from samples collected in the eastern Southern Domain of the Cape Smith Belt (east of longitude 75°W). However, the resulting distinctions may apply to similar lithologies located along strike to the west and east (e.g. West Raglan). Furthermore, as the rocks considered here are part of the Circum-Superior Large Igneous Province (e.g. Baragar and Scoates, 1987; Ciborowski et al., 2017), similar geochemical distinctions between prospective and less prospective units may be true in other parts of the Circum-Superior Large Igneous Province (e.g. western Cape Smith Belt and Labrador Trough).

ONGOING WORK

This research is part of a Ph.D. project, planned for completion in 2021. The project seeks to understand the temporal, geochemical, and architectural evolution of the transcrustal Expo-Raglan mineralized magmatic plumbing system. Additional geochemical data collection, QA-QC, classification, and interpretation will continue. Petrographic analyses, whole-rock and mineral geochemical analyses, and modelling are ongoing to evaluate the many possible factors and models that may explain the observed differences between the Expo Trend and Raglan Trend units. Compilation of regional mineral chemical data is also ongoing; hundreds of records have already been compiled from the same references sourced for the whole-rock lithogeochemical data presented here. Most of the whole-rock lithogeochemical data compilation referenced in this report, the largest and most comprehensive for this region, will be released as a GSC Open File.

ACKNOWLEDGMENTS

This report is a contribution to NRCan's Targeted Geoscience Initiative Program (TGI). Support for this study was provided through the Orthomagmatic Ni-Cu-PGE-Cr Ore Systems Project's 'Activity NC-1.1: Extent, origin, and deposit-scale controls of the 1883 Ma Circum-Superior large igneous province, northern Manitoba, Ontario, Québec, Nunavut, and Labrador'.

The authors greatly appreciate logistical support—including room and board, and truck and helicopter transportation—from Glencore's Raglan Mine (especially from Mathieu Landry, Véronique Gauthier, and the exploration team) and Canadian Royalties' Nunavik Nickel Project (particularly from Yueshi Lei, Maxim Boisvert, and the exploration team). This support has been critical for fieldwork and essential for the collection of new data. Additionally, access to some of Glencore's and CRI's private data compilations has been useful for validating publicly available data. Additional logistical and field support (including field assistants) has been provided by the GSC and the Metal Earth research initiative at the Harquail School of Earth Sciences, Laurentian University (ME-HES). The Natural Resources of Canada Research Affiliate Program (NRCan RAP), the GSC, and ME-HES have provided financial support (including analytical costs) for this project. CML thanks Claude Herzberg for stimulating discussions. CML and MGH thank Jim Mungall and Danielle Giovenazzo for many helpful discussions. The authors appreciate constructive scientific review and comments from Thomas Clark and Wouter Bleeker but also technical and editorial review by Elizabeth Ambrose and Valérie Bécu. This is Harquail School of Earth Sciences, Mineral Exploration Research Centre contribution MERC-ME-2019-227.

REFERENCES

Albino, G.V., 1984. Petrology, geochemistry and mineralization of the Boundary ultramafic complex, Quebec, Canada; M.Sc. thesis, Colorado State University, Fort Collins, Colorado, 220 p.

Arndt, N.T., Brügmann, G.E., Lehnert, K., Chauvel, C., and Chappell, B.W., 1987. Geochemistry, petrogenesis and tectonic environment of Circum-Superior Belt basalts, Canada; *in* Geochemistry and Mineralization of Proterozoic Volcanic Suites, (ed.) T.C. Pharaoh, R.D. Beckinsale, and D. Rickard; Geological Society of London, Special Publication 33, p. 133–145.

Baragar, W.R.A. and Scoates, R.F.J., 1981. The Circum-Superior Belt: A Proterozoic Plate Margin?; Chapter 12 *in* Precambrian Plate Tectonics, (ed.), A. Kroner; Elsevier, Netherlands, Developments in Precambrian Geology no. 4, p. 297–330.

Baragar, W.R.A. and Scoates, R.F.J., 1987. Volcanic geochemistry of the northern segments of the Circum-Superior Belt of the Canadian Shield; *in* Geochemistry and Mineralization of Proterozoic Volcanic Suites, (ed.) T.C. Pharaoh, R.D. Beckinsale, and D. Rickard; Geological Society of London, Special Publication no. 33, p. 113–131.

Barnes, S.J., 1979. Petrology and geochemistry of the Katiniq nickel deposit and related rocks, Ungava, Northern Quebec; M.Sc. thesis, University of Toronto, Toronto, Ontario, 220 p.

Barnes, S.J., Coats, C.J.A., and Naldrett, A.J., 1982. Petrogenesis of a Proterozoic nickel sulfide-komatiite association; the Katiniq Sill, Ungava, Quebec; Economic Geology, v. 77, p. 413–429.

Barnes, S.-J. and Giovenazzo, D., 1990. Platinum-group elements in the Bravo Intrusion, Cape Smith Belt, northern Quebec; The Canadian Mineralogist, v. 28, p. 431–449.

Bédard, J.H., 1981. Fractional crystallization and intrusion mechanisms, Spur Slice (Block 4), Cape Smith, New Quebec; M.Sc. thesis, McGill University, Montreal, Quebec, 260 p.

Bédard, J.H., Francis, D.M., Hynes, A.J., and Nadeau, S., 1984. Fractionation in the feeder system at a Proterozoic rifted margin; Canadian Journal of Earth Sciences, v. 21, p. 489–499.

Begg, G.C., Hronsky, J.A.M., Arndt, N.T., Griffin, W.L., O'Reilly, S.Y., and Hayward, N., 2010. Lithospheric, cratonic and geodynamic setting of Ni-Cu-PGE sulfide deposits; Economic Geology, v. 105, p. 1057–1070.

Bleeker, W. and Kamo, S.L., 2018. Extent, origin, and deposit-scale controls of the 1883 Ma Circum-Superior large igneous province, northern Manitoba, Ontario, Quebec, Nunavut and Labrador; *in* Targeted Geoscience Initiative 5: 2017 report of activities, volume 2, (ed.) N. Rogers; Geological Survey of Canada, Open File 8373, p. 5–14.

Bleeker, W. and Kamo, S., 2020. Structural-stratigraphic setting and U-Pb geochronology of Ni-Cu-Co-PGE ore environments in the central Cape Smith Belt, Circum-Superior Belt; *in* Targeted Geoscience Initiative 5: dvances in the understanding of Canadian Ni-Cu-PGE and Cr ore systems – Examples from the Midcontinent Rift, the Circum-Superior Belt, the Archean Superior Province, and Cordilleran Alaskan-type intrusions, (ed.) W. Bleeker and M.G. Houlé; Geological Survey of Canada, Open File 8722, p. 65–98.

Burnham, O.M., Keays, R.R., Lesher, C.M., and Hulbert, L., 1998. Application of PGE geochemistry to exploration for komatiite-hosted Ni sulphide deposits in Canada; CAMIRO project 94E04 final report, Laurentian University, Sudbury, Ontario, 310 p.

Campbell, I.H. and Naldrett, A.J., 1979. The influence of silicate:sulfide ratios on the influence of magmatic sulfides; Economic Geology, v. 74, p. 1503–1506.

Ciborowski, T.J.R., Minifie, M.J., Kerr, A.C., Ernst, R.E., Baragar, B., and Millar, I.L., 2017. A mantle plume origin for the Palaeoproterozoic Circum-Superior Large Igneous Province; Precambrian Research, v. 294, p. 189–213.

Clark, D., 2008. Petrogenetic and economic significance of the whole-rock chemistry of ultramafic cumulates in the Cape Smith foldbelt, northern Quebec; M.Sc. thesis, McGill University, Montreal, Quebec, 67 p.

Dionne-Foster, C., 2007. Géologie et indices de Ni-Cu-ÉGP de la Zone Frontier dans la Ceinture de Cape Smith, Nouveau Québec; M.Sc. thesis, Université du Québec à Chicoutimi, Chicoutimi, Quebec, 320 p.

Dunphy, J.M., 1995. Magmatic evolution and crustal accretion in the Early Proterozoic: The geology and geochemistry of the Narsajuaq terrane, Ungava Orogen, northern Quebec; Ph.D. thesis, Université de Montréal, Montreal, Quebec, 402 p.

Dunphy, J.M. and Ludden, J.N., 1998. Petrological and geochemical characteristics of a Paleoproterozoic magmatic arc (Narsajuaq terrane, Ungava Orogen, Canada) and comparisons to Superior Province granitoids; Precambrian Research, v. 91, p. 109–142.

Dupras, N. and Green, A.H., 1999. Exploration and development history of the Raglan Ni-Cu-(PGE) deposits, Cape Smith Belt, New Quebec; *in* Komatiitic Peridotite-Hosted Ni-Cu-(PGE) Deposits of the Raglan Area, Cape Smith Belt, New Quebec, (ed.) C.M. Lesher; Mineral Exploration Research Centre, Laurentian University, Guidebook Series, v. 2, p. 1–21.

Francis, D. and Hynes, A., 1982. Komatiitic basalts of the Cape Smith foldbelt, New Quebec, Canada; *in* Komatiites, (ed.) N.T. Arndt and E.G. Nisbet; George Allen & Unwin, United Kingdom, p. 159–170.

Francis, D.M., Hynes, A.J., Ludden, J.N., and Bédard, J., 1981. Crystal fractionation and partial melting in the petrogenesis of a Proterozoic high-MgO volcanic suite, Ungava, Québec; Contributions to Mineralogy and Petrology, v. 78, p. 27–36.

Francis, D., Ludden, J., and Hynes, A., 1983. Magma evolution in a Proterozoic rifting environment; Journal of Petrology, v. 24, p. 556–582.

Gaonac'h, H., Ludden, J.N., Picard, C., and Francis, D., 1992. Highly alkaline lavas in a Proterozoic rift zone: implications for Precambrian mantle metasomatic processes; Geology, v. 20, p. 247–250.

Gillies, S.L., 1993. Physical volcanology of the Katinniq Peridotite Complex and associated Fe-Ni-Cu-(PGE) mineralization, Cape Smith Belt, northern Québec; M.Sc. thesis, University of Alabama, Tuscaloosa, Alabama, 146 p.

Giovenazzo, D., 1991. Géologie et caractéristiques géochimiques des minéralisations Ni-Cu-EGP de la région de Delta, Ceinture de Cape-Smith, Nouveau-Québec; Ph.D. thesis, Université du Québec à Chicoutimi, Chicoutimi, Quebec, 238 p.

Giovenazzo, D., Picard, C., and Guha, J., 1989. Tectonic setting of Ni-Cu-PGE deposits in the central part of the Cape Smith Belt; Geoscience Canada, v. 16, p. 134–136.

Harvey, D., 1995. Géochimie et traceur isotopique du néodyme dans les intrusifs Archéens de la partie nord-est de la péninsule d'Ungava; M.Sc. thesis, Université de Montréal, Montreal, Quebec.

Herzberg C., 2004. Geodynamic information in peridotite petrology; Journal of Petrology, v. 45, p. 2507–2503.

Herzberg, C. and O'Hara, M.J., 2002. Plume-associated ultramafic magmas of Phanerozoic age; Journal of Petrology, v. 43, p. 1857–1883.

Herzberg, C. and Asimow, P.D., 2008. Petrology of some oceanic island basalts: PRIMELT2.XLS software for primary magma calculation; Geochemistry Geophysics Geosystems, v. 9, Q09001. https://doi:10.1029/2008GC002057

Herzberg, C. and Asimow, P.D., 2015. PRIMELT3 MEGA.XLSM software for primary magma calculation: Peridotite primary magma MgO contents from the liquidus to the solidus; Geochemistry Geophysics Geosystems, v. 16, p. 563–578. https://doi.org/10.1002/2014GC005631

Hynes, A. and Francis, D., 1982. A transect of the early Proterozoic Cape Smith foldbelt, New Quebec; Tectonophysics, v. 88, p. 23–59.

Kastek, N., Ernst, R.E., Cousens, B.L., Kamo, S.L., Bleeker, W., Söderlund, U., Baragar, W.R.A., and Sylvester, P., 2018. U-Pb geochronology and geochemistry of the Povungnituk Group of the Cape Smith Belt: Part of a craton-scale circa 2.0 Ga Minto-Povungnituk Large Igneous Province, Northern Superior Craton; Lithos, v. 320–321, p. 315–331.

Lamothe, D., 2007. Lexicon stratigraphique de l'Orogène de l'Ungava; Ministère des Ressources naturelles et de la Faune du Québec, DV 2007-03, 63 p.

Lesher, C.M. (ed.), 1999. Komatiitic peridotite-hosted Ni-Cu-(PGE) deposits of the Raglan area, Cape Smith Belt, New Québec; Mineral Exploration Research Centre, Laurentian University, Guidebook Series, v. 2, 205 p.

Lesher, C.M., 2007. Ni-Cu-(PGE) deposits in the Raglan area, Cape Smith Belt, New Québec; *in* Mineral Deposits of Canada: A

Synthesis of Major Deposit-Types, District Metallogeny, the Evolution of Geological Provinces, and Exploration Methods, (ed.) W.D. Goodfellow; Geological Association of Canada, Mineral Deposits Division, Special Publication no. 5, p. 351–386.

Lesher, C.M., 2017. Roles of residues/skarns, xenoliths, xenocrysts, xenomelts, and xenovolatiles in the genesis, transport, and localization of magmatic Fe-Ni-Cu-PGE sulfides and chromite; Ore Geology Reviews, v. 90, p. 465–484 (and erratum, 2020. Ore Geology Reviews, v. 119, 103374). https://doi.org/10.1016/j.oregeorev.2017.08.008

Lesher, C.M., 2019. Up, down, or sideways: emplacement of magmatic Fe–Ni–Cu–PGE sulfide melts in large igneous provinces; Canadian Journal of Earth Sciences, v. 56, p. 756–773.

Lesher, C.M. and Arndt, N.J., 1995. REE and Nd isotope geochemistry, petrogenesis and volcanic evolution of contaminated komatiites at Kambalda, Western Australia; Lithos, v. 34, p. 127–157.

Lesher, C.M. and Burnham, O.M., 2001. Multicomponent elemental and isotopic mixing in Ni-Cu-(PGE) ores at Kambalda, Western Australia; The Canadian Mineralogist, v. 39, p. 421–446.

Lesher, C.M. and Houlé, M.G., 2017. Geology, physical volcanology, and Ni-Cu-(PGE) deposits of the Raglan area, Cape Smith Belt, Nunavik, Québec, Canada: A Field Trip to the 14th Biennial Society for Geology Applied to Mineral Deposits meeting; Geological Survey of Canada, Open File 8350, 110 p.

Lesher, C.M., Burnham, O.M., Keays, R.R., Barnes, S.J., and Hulbert, L., 2001. Trace element geochemistry and petrogenesis of barren and ore-associated komatiites; The Canadian Mineralogist, v. 39, p. 673–696.

McKevitt, D.J., in prep. Localization of Ni-Cu-(PGE) mineralization in an early Proterozoic trans-crustal dike-sill-lava channel system, Cape Smith Belt, Nunavik; Ph.D. thesis, Laurentian University, Sudbury, Ontario.

McKevitt, D.J., Houlé, M.G., and Lesher, C.M., 2018. Investigation of ultramafic to mafic komatiitic units within the Raglan Block within the Cape Smith Belt, Nunavik, northern Quebec; *in* Targeted Geoscience Initiative 5: 2017 report of activities, volume 1, (ed.) N. Rogers; Geological Survey of Canada, Open File 8358, p. 169–172.

McKevitt, D.J., Lesher, C.M., and Houlé, M.G., 2019. Volcanology, geochemistry and petrogenesis of the Expo - Raglan magmatic system in the eastern Cape Smith Belt, Nunavik, northern Quebec; *in* Targeted Geoscience Initiative 5: 2018 report of activities, (ed.) N. Rogers; Geological Survey of Canada, Open File 8549, p. 393–401.

Miller, A.R., 1977. Petrology and geochemistry of the 2-3 ultramafic sill and related rocks, Cape Smith-Wakeham Bay fold belt, Quebec; Ph.D. thesis, University of Western Ontario, London, Ontario, 219 p.

Modeland, S., Francis, D., and Hynes, A., 2003. Enriched mantle components in Proterozoic continental-flood basalts of the Cape Smith foldbelt, northern Québec; Lithos, v. 71, p. 1–17.

Mungall, J.E., 2007. Crustal contamination of picritic magmas during transport through dikes: The expo intrusive suite, Cape Smith Fold Belt, New Quebec; Journal of Petrology, v. 48, p. 1021–1039.

Nadeau, S., 1984. La pétrologie, la géochimie et le rôle de la contamination dans l'évolution magmatique du Sill No-Name, Cape-Smith Baie de Wakeham, Nouveau Québec; M.Sc. thesis, Université de Montréal, Montreal, Quebec, 115 p.

Parrish, R.R., 1989. U-Pb geochronology of the Cape Smith Belt and Sugluk block, northern Quebec; Geoscience Canada, v. 16, p. 126–130.

Pearce, J.A., 2008. Geochemical fingerprinting of oceanic basalts with applications to ophiolite classification and the search for Archean oceanic crust; Lithos, v. 100, p. 14–48.

Picard, C., 1989. Pétrologie et volcanologie des roches volcaniques protérozoïques de la partie centrale de la Fosse de l'Ungava; Ministère des Ressources naturelles du Québec, ET 87-07, 98 p.

Picard, C., 1989. Lithochimie des roches volcaniques protérozoïques de la partie occidentale de la Fosse de l'Ungava (région au sud du lac Lanyan); Ministère des Ressources naturelles du Québec, ET 87-14, 81 p.

Picard, C., Lamothe, D., Piboule, M., and Oliver, R., 1990. Magmatic and geotectonic evolution of a Proterozoic oceanic basin system: the Cape Smith Thrust-Fold Belt (New-Quebec); Precambrian Research, v. 47, p. 223–249.

Picard, C., Giovenazzo, D., Tremblay, C., and Thibert, F., 1994. Pétrographie, géochimie et gîtologie des roches plutoniques ultramafiques et mafiques protérozoïques de la partie centrale de la Fosse de l'Ungava : implications sur la distribution des éléments du groupe des platinoïdes; Ministère des Ressources naturelles du Québec, MB 94-30, 402 p.

Picard, C., 1995. Synthèse pétrogéochimique des roches volcanique protérozoïques de la ceinture orogénique de l'Ungava: évolution géologique des groupes de Povungnituk, de Chukotat et de Parent; Ministère des Ressources naturelles du Québec, MB 95-01, 257 p.

Porter, C., Morin, P., Howat, I., Noh, M.-J., Bates, B., Peterman, K., Keesey, S., Schlenk, M., Gardiner, J., Tomko, K., Willis, M., Kelleher, C., Cloutier, M., Husby, E., Foga, S., Nakamura, H., Platson, M., Wethington, M., Jr., Williamson, C., Bauer, G., Enos, J., Arnold, G., Kramer, W., Becker, P., Doshi, A., D'Souza, C., Cummens, P., Laurier, F., and Bojesen, M., 2018. ArcticDEM, Harvard Dataverse, V1; Polar Geospatial Center, University of Minnesota. <https://www.pgc.umn.edu/data/arcticdem/> [accessed January, 2018]

Randall, W., 2005. U-Pb geochronology of the Expo Igneous Suite, Cape Smith Belt, and the Kyak Bay intrusion, New Quebec Orogen: implications for the tectonic evolution of the northeastern Trans-Hudson Orogen; M.Sc. thesis, University of Toronto, Toronto, Ontario, 52 p.

Rudnick, R.L. and Gao, S., 2003. Composition of the continental crust; Treatise On Geochemistry, v. 3, p. 1–64.

Scott, D.J., 1990. Geology and geochemistry of the Early Proterozoic Purtuniq ophiolite, Cape Smith Belt, northern Quebec, Canada; Ph.D. thesis, Queen's University, Kingston, Ontario, 289 p.

SIGÉOM, 2019. Système d'information géominière du Québec; Ministère de l'Énergie et des Ressources naturelles du Québec. <http://sigeom.mines.gouv.qc.ca> [accessed November 15, 2019]

Shepherd, N., 1960. The petrography and mineralogy of the Cross Lake area, Ungava, New Quebec; Ph.D. thesis, University of Toronto, Toronto, Ontario.

Stewart, A.J., 2002. The geochemistry and physical volcanology of the East Lake Ultramafic Zone, Cape Smith Belt, northern Quebec; M.Sc. thesis, McGill University, Montreal, Quebec, 116 p.

Stilson, C.M., 2000. Geology of the Boundary Ultramafic Complex and genesis of associated Fe-Ni-Cu-(PGE) sulfide mineralization, Cape Smith Belt, New Québec; M.Sc. thesis, University of Alabama, Tuscaloosa, Alabama, 267 p.

St-Onge, M.R. and Lucas, S.B., 1993. Geology of the eastern Cape Smith Belt: Parts of the Kangiqsujuaq, Cratère du Nouveau-Quebec, and Lacs Nuvilik Map Areas, Quebec; Geological Survey of Canada, Memoir 438, 110 p.

St-Onge, M.R., Lucas, S.B., and Parrish, R.R., 1992. Terrane accretion in the internal zone of the Ungava orogen, northern Quebec. Part 1: Tectonostratigraphic assemblages and their tec-

tonic implications; Canadian Journal of Earth Sciences, v. 29, p. 746–764.

St-Onge, M.R., Lamothe, D., Henderson, I., and Ford, A., 2007. Digital geoscience atlas of the Cape Smith Belt and adjacent domains, Ungava Peninsula, Quebec–Nunavut / Atlas géoscientifique numérique, ceinture de Cape Smith et environs, péninsule d'Ungava, Québec–Nunavut; Geological Survey of Canada, Open File 5117.

Sun, S.-s. and McDonough, W.F., 1989. Chemical and isotopic systematics of oceanic basalts: implications for mantle compositions and processes; *in* Magmatism in the Oceanic Basins, (ed.) A.D. Saunders and M.J. Norry; Geological Society of London, Special Publication 42, p. 313–345.

Thacker, J.L., 1995. Geology of the 5-8 peridotite complex, Cape Smith Belt, New Quebec; M.Sc. thesis, University of Alabama, Tuscaloosa, Alabama, 173 p.

Thibert, F., 1993. Pétrogénese du filon-couche différencié Roméo 1 situé dans la Ceinture Plissée-faillée du Cap Smith, Nouveau-Quebec; M.Sc. thesis, Université de Montréal, Montreal, Quebec, 145 p.

Tremblay, C., 1990. Les éléments du groupe du Platine dans le dyke de Méquillon Ceinture de Cape Smith, Nouveau-Québec; M.Sc. thesis, Université du Québec à Chicoutimi, Chicoutimi, Quebec, 76 p.

Van Hoof, C., 2000. Petrology of Zone 3, of the Raglan Horizon, Cape Smith Belt, Ungava (Québec); H.B.Sc. thesis, University of Ottawa, Ottawa, Ontario, 39 p.

Wilson, H.D.B., Kilburn, L.C., Graham, A.R., and Ramlal, K., 1969. Geochemistry of some Canadian nickeliferous ultrabasic intrusions; *in* Magmatic Ore Deposits – A Symposium, (ed.) H.D.B. Wilson; Society of Economic Geologists, Monograph 4, p. 294–309.

Wodicka, N., Madore, L., Larbi, Y., and Vicker, P., 2002. Geochronologie U-Pb de filons-couches mafiques de la Ceinture de Cape Smith et de la Fosse du Labrador; Ministère de l'Énergie et des Ressources naturelles du Québec, Programme et Résumés 2002, DV 2002-10, p. 48.

Overview of Ni-Cu-(PGE), Cr-(PGE), and Fe-Ti-V magmatic mineralization in the Superior Province: Insights on metallotects and metal endowment

Michel G. Houlé[1]*, C. Michael Lesher[2], Anne-Aurélie Sappin[1], Marie-Pier Bédard[1], Jean Goutier[3], and Eric (Xue-Ming) Yang[4]

[1]Geological Survey of Canada, 490 rue de la Couronne, Québec, Quebec G1K 9A9
[2]Mineral Exploration Research Centre, Harquail School of Earth Sciences, Goodman School of Mines, Laurentian University, 935 Ramsey Lake Road, Sudbury, Ontario P3E 2C6
[3]Ministère de l'Énergie et des Ressources naturelles, 82 Boul Québec, Rouyn-Noranda, Quebec J9X 6R1
[4]Manitoba Geological Survey, 360-1395 Ellice Avenue, Winnipeg, Manitoba R3G 3P2
*Corresponding author's e-mail: michel.houle@canada.ca

ABSTRACT

The Archean Superior Province is well known for its metal endowment. Ultramafic and mafic intrusions/flows are ubiquitous in greenstone belts across the Superior Province and are prospective hosts for magmatic Ni-Cu-(PGE), Cr-(PGE), and Fe-Ti-V deposits, although their abundance and endowment vary widely among the terranes/domains. For example, the Abitibi-Wawa terrane contains numerous but generally small Ni-Cu-(PGE) deposits, a few large Fe-Ti-V deposits, and only rare Cr mineralization. The Bird River–Uchi–Oxford-Stull–La Grande Rivière–Eastmain (BUOGE "superdomain") domains are characterized by several moderate to very large chromite deposits, a few moderate to small Ni-Cu-(PGE) deposits, and a few potentially large Fe-Ti-V deposits that are characterized as prospects due to the lack of definition drilling. The other terranes/domains in the Superior Province, including the Au and Cu-Zn-Au-rich Abitibi belt, contain some magmatic Ni-Cu-(PGE) and Fe-Ti-V mineralization, but no significant Cr-(PGE) mineralization. Many factors are responsible for the variable metal endowment, but some critical features appear to be particularly important and may define prospective Ni-Cu-(PGE), Cr-(PGE), and/or Fe-Ti-V metallotects. These include the presence of (1) abundant primitive mantle-derived magmas that were generated by large magmatic events over short durations; (2) magma compositions that favoured the generation of Ni-Cu-(PGE) (high-Mg komatiitic), Cr (low-Mg komatiitic), and Cu-Ni-PGE and Fe-Ti-V (basaltic) mineralization; (3) transcrustal discontinuities that focussed magma flow through the lower crust; (4) shallow structures and densities that favoured emplacement of channelized lava/magma conduits at relatively high levels, (5) high magma fluxes to promote thermomechanical erosion of crustal rocks; (6) high-level crustal rocks containing sulphur (e.g. sulphide-facies iron formation) and oxide (e.g. oxide-facies iron formation) reservoirs for generating and upgrading sulphide xenomelts and oxide xenocrysts; and (7) favourable deformation and erosion to preserve and expose prospective units for exploration. Targeting base and precious metals is challenging, even in well endowed but partially exposed greenstone belts. However, understanding these fundamental controls will help in the discover of additional resources in other frontier areas within the Superior Province and throughout the Canadian Shield.

INTRODUCTION

The Archean Superior Province, the largest coherent Archean craton in the world, is well known for its endowment of numerous base and precious metals occurring in world-class lode gold and zinc-copper volcanogenic massive sulphides deposits, and to lesser extent in orthomagmatic Ni-Cu-(PGE), Fe-Ti-V, and Cr-(PGE) deposits. The discovery, more than a decade ago, of world-class Cr-(PGE) deposits, a major Ni-Cu-(PGE) deposit, and significant Fe-Ti-V occurrences in the McFaulds Lake greenstone belt (a.k.a. "Ring of Fire") of northern Ontario has generated renewed interest in orthomagmatic mineralization associated with mafic-ultramafic rocks in the Superior Province. Despite this increase in mineral exploration for these types of deposits, only one significant discovery has been made since then: the Grasset magmatic Ni-Cu-(PGE) sulphide deposit (Tucker et al., 2019; Fig. 1) within the northeastern part of the Wawa-Abitibi terrane.

Mafic intrusions and ultramafic intrusions/flows are ubiquitous throughout the Superior Province and are prospective to host magmatic Ni-Cu-(PGE), Cr-(PGE), and Fe-Ti-V deposits, but their abundance and endowments vary widely within the terranes/domains across

Houlé, M.G., Lesher, C.M., Sappin, A.-A., Bédard, M.-P., Goutier, J., and Yang, X.M., 2020. Overview of Ni-Cu-(PGE), Cr-(PGE), and Fe-Ti-V magmatic mineralization in the Superior Province: Insights on metallotects and metal endowment; *in* Targeted Geoscience Initiative 5: Advances in the understanding of Canadian Ni-Cu-PGE and Cr ore systems – Examples from the Midcontinent Rift, the Circum-Superior Belt, the Archean Superior Province, and Cordilleran Alaskan-type intrusions, (ed.) W. Bleeker and M.G. Houlé; Geological Survey of Canada, Open File 8722, p. 117–139. https://doi.org/10.4095/326890

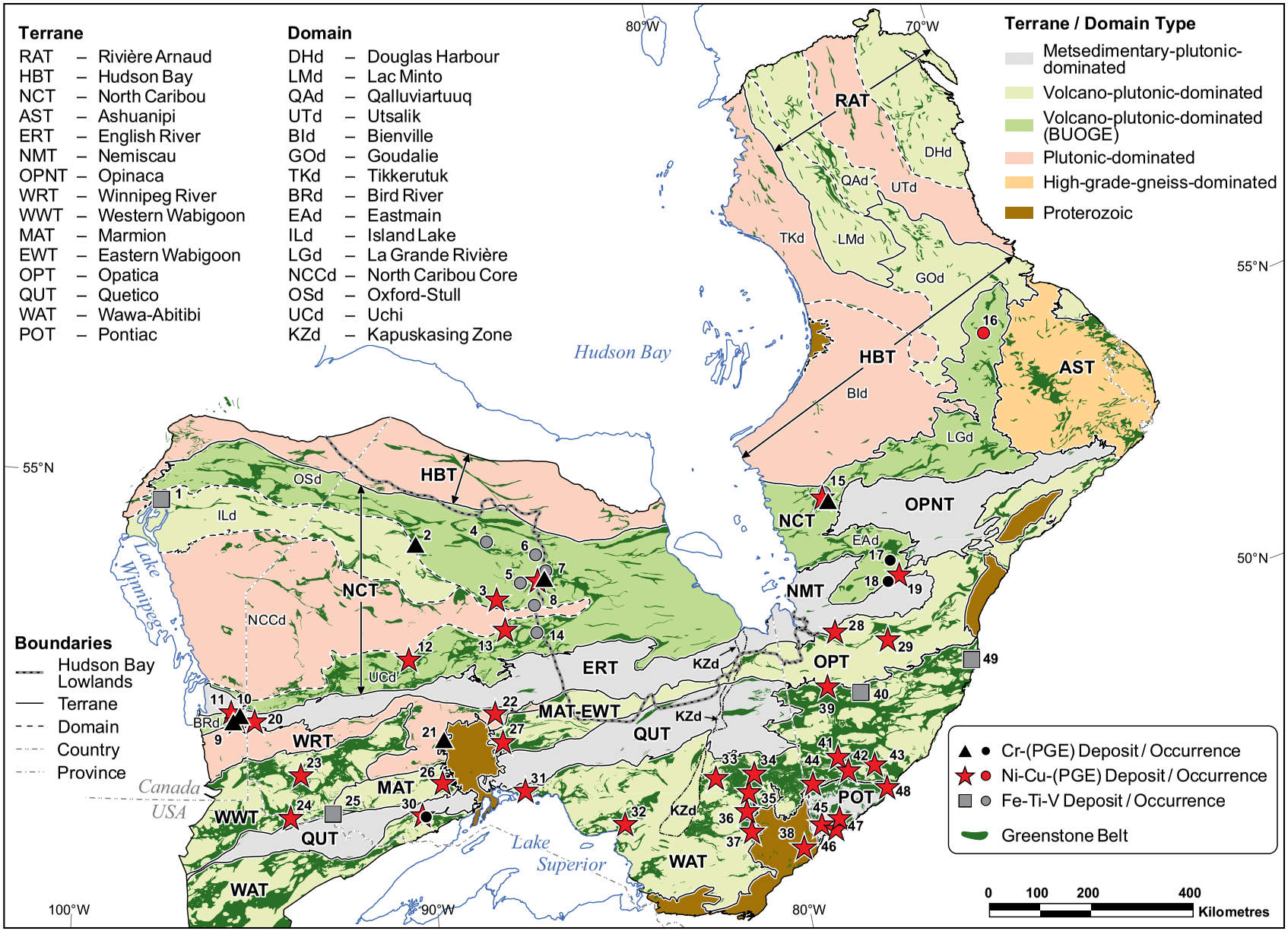

Figure 1. Simplified geological map of the Superior Province showing all Cr-(PGE), Ni-Cu-(PGE), and Fe-Ti-V deposits and selected significant mineral occurrences. Terranes, domains, and boundaries are adapted from Stott et al. (2010), Percival et al. (2012), and SIGÉOM (2020). Greenstone belts have been compiled from Wardle et al. (1997), Ontario Geological Survey (2011), Thériault and Beauséjour (2012), and Manitoba Geological Survey (2018). *See* Table 1 for more detailed information about each deposit and mineral occurrence.

the province. Houlé et al. (2015a) proposed the presence of a Cr-(PGE)-rich metallogenic province, referred to as the BUOGE[1] "superdomain", based on the distribution of almost all the Cr-(PGE) deposits and significant prospects in this part of the craton. Although the determinant factors behind this distinctive metal endowment remain to be resolved, Houlé et al. (2015a) have highlighted some critical features that may represent regional-scale metallotects for Cr-(PGE) mineralization, which are also applicable to Ni-Cu-(PGE) systems and, to a lesser extent, Fe-Ti-V mineralization. These factors include the presence of (1) primitive mantle-derived magmas emplaced by a large magmatic event over a short duration; (2) significant nearby transcrustal discontinuities that could have focussed the ascent of magma through the crust; and (3) favourable crustal architecture containing sulphur (e.g. sulphide-facies iron formation) and oxide reservoirs (e.g. oxide-facies iron formation) for generating the sulphides and chromitites within these ultramafic to mafic magmatic systems.

To advance our understanding and to determine which factors are critical for this distinctive type of metal endowment across the Superior Province, where metal discoveries have been made over more than a century, it is essential to build a database detailing the characteristics of the mafic and ultramafic intrusions throughout the province. In this contribution, we summarize the results of a compilation of the Ni-Cu-(PGE), Cr-(PGE), and Fe-Ti-V deposits and prospective mafic to ultramafic units that may host these types of orthomagmatic mineralization across the Superior Province. Identifying the characteristics of these mafic to ultramafic prospective units will aid in constraining integrated metallogenic models for these orthomagmatic mineralized systems and the likelihood of discovering additional mineral resources in established and emerging mining camps within or along the margin of the Superior Province.

COMPILATION METHODOLOGY

In the course of this research activity, a comprehensive, Superior Province-wide inventory of mafic and ultramafic prospective units has been initiated, which includes information about the spatial and temporal (when available) distribution of (1) mafic and ultramafic bodies (intrusions and flows including komatiitic rocks), (2) orthomagmatic Cr-(PGE), Ni-Cu-(PGE), and Fe-Ti-V deposits, and (3) surrounding country rocks (i.e. potential sulphur and oxide sources). This database will help constrain Ni, Cr, and Fe-Ti-V metallotects at various scales and promote key criteria for improving exploration models and exploration targeting not only across the BUOGE superdomain but also within the Superior Province as a whole.

As an initial step, a digital map of the units prospective to host these types of mineralization has been produced that covers the entire Superior Province in Manitoba, Ontario, Quebec, and Newfoundland and Labrador (Manitoba: Viljoen et al., 1999 supplemented by unpublished mafic and ultramafic polygons provided by the Manitoba Geological Survey in December 2017; Ontario: Ontario Geological Survey, 2011; Quebec: SIGÉOM, 2020; and Newfoundland and Labrador: Wardle et al., 1997). Subsequent steps of this compilation involved incorporating other data sets and maps, mainly from geological surveys and mining companies, to faithfully represent the majority of these occurrences across the Superior Province. However, the reader is cautioned that this representation is directly related to the information that has been compiled and does not include all known occurrences. For example, to avoid overcrowding, not all compiled mafic and ultramafic prospective units are shown in Figures 2 and 3. Each point may represent more than one closely spaced (~ 9 km radius) prospective unit. Nevertheless, the authors believe that this representation is realistic for the current distribution of these prospective mafic and ultramafic units across the Superior Province.

PROSPECTIVE UNITS ACROSS THE SUPERIOR PROVINCE

Although mafic intrusions and ultramafic intrusions/flows are ubiquitous throughout the Superior Province, they are irregularly distributed within its distinct terranes and domains. The lithotectonic nomenclature used herein for the Superior Province was adapted from Stott et al. (2010) and Percival et al. (2012)[2]. Each terrane/domain was assigned to one of the four types of terranes proposed by Card and Ciesielski (1986), such as metasedimentary-plutonic-dominated, volcano-plutonic-dominated, plutonic-dominated, and high-grade gneiss-dominated, which reflect the predominance of the lithological units in each type.

Several types of mafic to ultramafic prospective units that have been identified across the Superior Province have been grouped into four main categories (Fig. 2, 3): 1) mafic-dominated intrusions (M), 2) mafic to ultramafic intrusions (MUM), 3) ultramafic-domi-

[1] BUOGE "superdomain" = Bird River–Uchi–Oxford-Stull–La Grande Rivière–Eastmain domains of the North Caribou terrane.

[2] The use of this terminology is strictly for the purpose of the subdivision of the Superior Province and does not imply, in any way, a genetic connotation for the development of the Superior (accretion model versus cratonic rifting model), which is beyond the scope of this contribution.

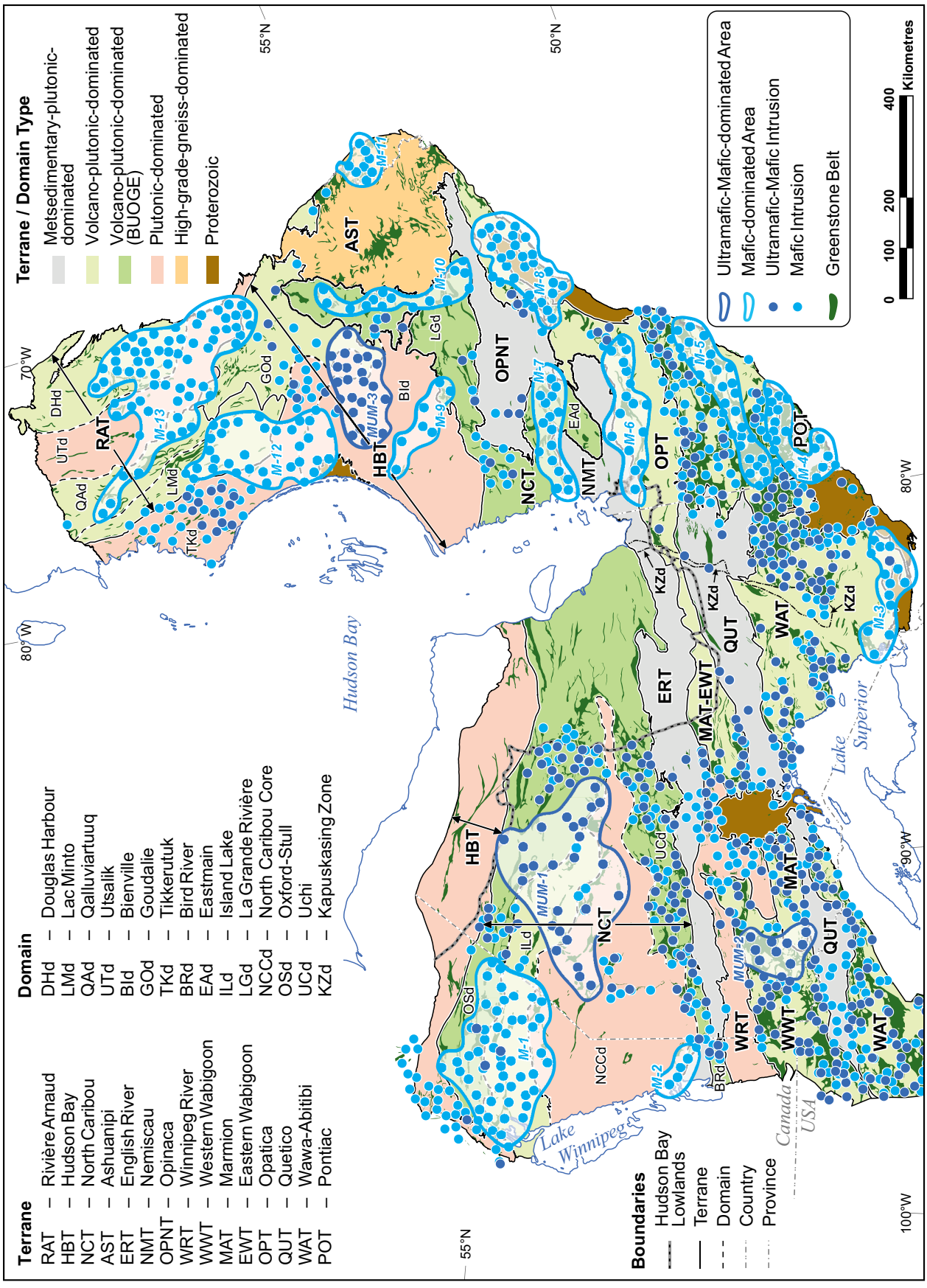

Figure 2. Map showing the distribution of mafic (M) and mafic to ultramafic intrusions (MUM) across the Superior Province. Unpublished data compiled by Houlé and Bédard (Geological Survey of Canada). Note that to avoid overcrowding, each point may represent more than one closely spaced prospective unit of this type. *See* Figure 1 for references.

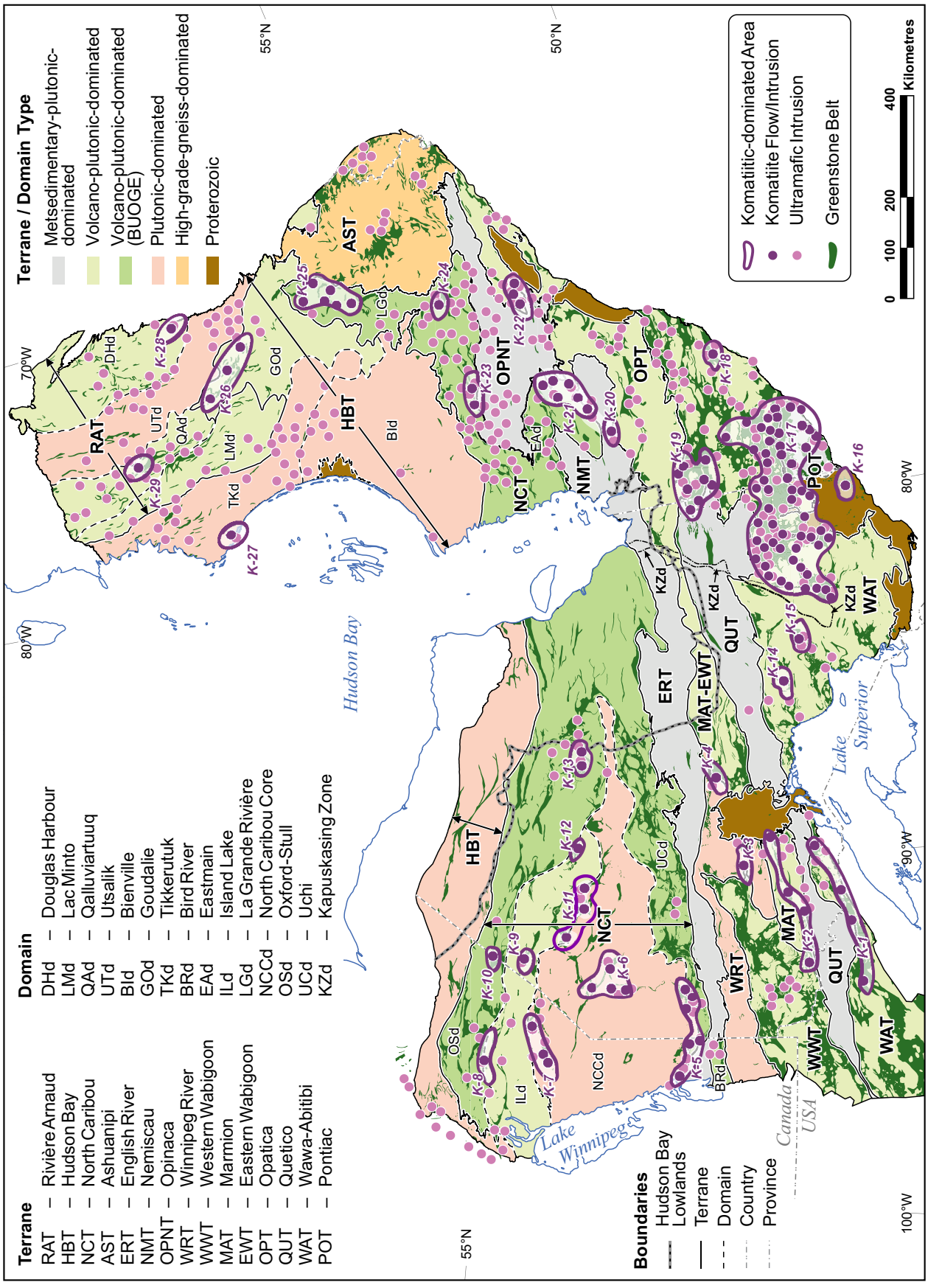

Figure 3. Map showing the distribution of ultramafic intrusions (UM) and komatiitic flows/intrusions (K) across the Superior Province. Unpublished data compiled by Houlé and Bédard (Geological Survey of Canada). Note that to avoid overcrowding, each point may represent more than one closely spaced prospective unit of this type. See Figure 1 for references.

nated intrusions (UM), and 4) ultramafic lavas and ultramafic intrusions of komatiitic affinity (K).

Spatial Distribution

Mafic intrusions and ultramafic intrusions/flows are very common throughout the Superior Province and although these units do not appear to be restricted to specific terranes and/or domains, the first order of control of mineral abundance is the type of terrane or domain. Indeed, regardless of the type of mafic and ultramafic prospective units, their abundance decreases from terranes/domains dominated by volcano-plutonic rocks through those dominated by plutonic rocks to those dominated by high-grade metamorphic rocks to those dominated by metasedimentary rocks (Fig. 2, 3). However, one area, referred to as the Hudson Bay Lowlands, is characterized by a paucity of documented mafic and ultramafic prospective units. This vast region is covered by a thin Paleozoic platform sequence and glacial deposits with few Archean rock exposures, making it difficult to identify any prospective units without extensive drilling.

Mafic-dominated intrusions (M) are the most common prospective units across the Superior Province, occurring most abundantly within supracrustal rock successions. Differentiated mafic to ultramafic intrusions (MUM) are the second most common prospective units (Fig. 2). In most cases, the distribution of mafic to ultramafic intrusions is similar to the distribution of the mafic-dominated intrusions. However, in a few areas, mafic to ultramafic intrusions predominate (e.g. MUM-1, MUM-2, and MUM-3 areas, Fig. 2) but in many other areas, mafic-dominated intrusions predominate (e.g. M-1 through M-13 areas, Fig. 2). In contrast, ultramafic-dominated intrusions (UM) are more restricted and appear to occur randomly across the province (Fig. 3). However, it is important to note that there are discrepancies in their distribution between the Quebec and the Ontario-Manitoba parts of the Superior Province, with an apparently higher abundance of ultramafic-dominated units in Quebec (Fig. 3). Of all prospective units, the komatiitic flows and intrusions (K) are spatially widespread but much more restricted across the province (e.g. K-1 through K-29, Fig. 3). Komatiitic rocks are most abundant in the eastern part of the Abitibi greenstone belt of the Wawa-Abitibi terrane but are also widespread across the Uchi and Oxford-Stull domains of the North Caribou terrane and its eastern extensions, which include the La Grande Rivière and Eastmain domains, all part of the BUOGE superdomain (*see* Houlé et al., 2015a, 2017). The highest volumes of komatiitic rocks within this superdomain occur within (1) the western part of the Uchi domain (e.g. Wallace Lake and Red Lake greenstone belts), (2) the central part of the Oxford-Stull domain (e.g. Muskrat Dam, Caribou Lake, and McFaulds Lake greenstone belts), and (3) the central and northern parts of the La Grande Rivière domain (e.g. Lac Guyer and Venus greenstone belts). Outside of these terranes and domains, more sporadic but significant occurrences of komatiitic rocks also occur within (1) the Western Wabigoon (e.g. Lake of the Woods greenstone belt and Grassy Portage area), (2) the central part of the North Caribou core (e.g. North Spirit Lake, Favourable, and Hornby greenstone belts), (3) the Goudalie (e.g. Vizien, Duvert, Natuak, and Morrice greenstone belts) and Tikkerutuk (e.g. Nuvvuagittuq greenstone belt) domains of the Hudson Bay terrane, and (4) also within the Qalluviartuuq (e.g. Qalluviartuuq-Payne greenstone belt) and Douglas Harbour (e.g. Papijjusaq greenstone belt) domains of the Arnaud River Terrane.

Temporal Distribution

It is important to note that despite the predominance of Archean ages, which are directly part of the evolution of the Superior Province, younger mafic to ultramafic units also occur within the province. These are mainly Paleoproterozoic dyke swarms, lamprophyre dykes, or kimberlite pipes, but include some Neoarchean dyke swarms (e.g. Mistassini: Ernst and Buchan, 2004). None of these are considered in Figure 4.

Compiled and recent geochronological results acquired from the Orthomagmatic Ni-Cu-PGE-Cu Ore Systems Project of the Targeted Geoscience Initiative Program (TGI) indicate that Archean ultramafic-mafic magmatism across the Superior Province spans more than 350 Ma, from ca. 3.0 to 2.6 Ga. The age distribution of the mafic to ultramafic prospective units is evident in Figure 4a. The oldest direct[3] U-Pb zircon crystallization age of 3.0 Ga (Stone, 2010) is related to the mafic phases of the Marmion batholith rather than a discrete mafic-dominated prospective unit. On the other hand, older ages for mafic and ultramafic rocks are inferred in some areas based on other methods. For example, minimum mantle extraction ages inferred from Nd isotopic systematics suggest that some of the gabbroic and ultramafic rocks of the Nuvvuagittuq greenstone belt within the Tikkerutuk domain of the Hudson Bay terrane may be as old as ca. 4.3 Ga (O'Neil et al., 2012). However, this age interpretation has been challenged and should not be taken without caveats (Caro et al., 2017). Effectively, direct dating using the U-Pb method on zircon suggests a maximum age of 3.8 Ga within and surrounding the Nuvvuagittuq greenstone belt (Greer et al., 2020), where ultramafic volcanic rocks, not preserving any spinifex texture,

[3] A U-Pb age obtained from the mafic or ultramafic intrusion itself and not inferred by other geological information.

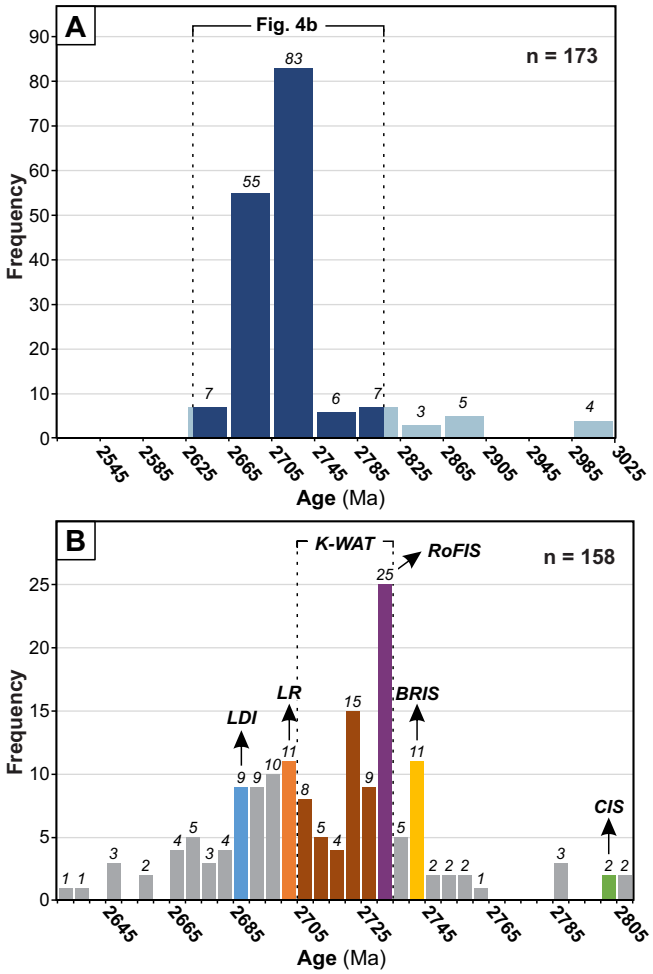

Figure 4. a) Age-frequency histogram for Mesoarchean to Neoarchean mafic to ultramafic prospective units across the Superior Province. Each bar represents a 40 Myr interval. **b)** Age-frequency histogram for mafic to ultramafic prospective units from 2.81 to 2.63 Ga. Each bar represents a 5 Myr interval. Data compiled from Manitoba Geological Survey (2018), Ontario Geological Survey (2019), SIGÉOM (2020), and TGI-4/5 unpublished data. Dark blue bars in Figure 4a represent the data that are highlighted in the histogram shown in Figure 4b; the pale blue bars are not shown. Colour bars in Figure 4b highlight the main mineralizing events in the Superior Province. Numbers above age intervals represent the number of ages in each interval. Abbreviations: BRIS (yellow bar) = Bird River intrusive suite, CIS (green bar) = Caumont intrusive suite, K-WAT (brown and purple bars) = Komatiitic rocks in the Wawa-Abitibi terrane, LDI (blue bar) = Lac des Iles, LR (orange bar) = Lac Rocher, RoFIS (purple bar) = Ring of Fire intrusive suite, n = total number of ages.

have been interpreted as potential komatiitic basalt units based on their geochemistry (Cates and Mojzsis, 2007). Regardless, if we factor in these ages for the Nuvvuagittuq greenstone belt, mafic and ultramafic magmatism appears to have a much larger age range (ca. 1.2 Ga) than what has been recognized in the remainder of the Superior Province. The youngest U-Pb zircon age is ca. 2630 Ma, which was obtained in the course of the TGI Program from an alkaline gabbroic rock that is part of a phlogopite-olivine metawebsterite intrusion in the Lac Pelletan area within the Opinaca terrane (Houlé et al., 2015b).

Despite this wide range for the temporal distribution of mafic to ultramafic units across the craton, the majority of these units formed between 2745 and 2685 Ma, with a peak at 2735–2730 Ma during which almost all the mineralized mafic to ultramafic units were emplaced (also corresponding to the Ring of Fire intrusive suite) (Fig. 4b).

Magma Compositions

Previous investigations in different parts of the Superior Province (e.g. Manitoba: Peck et al., 2000; Ontario: Sproule et al., 2002; Vaillancourt et al., 2003; and Québec: Houlé and Goutier, unpublished) have shown that the compositions of the mafic and ultramafic intrusions are quite variable. They range from komatiitic (high-Mg through low-Mg komatiitic) through komatiitic basaltic to basaltic, with various geochemical affinities ranging from alkaline and calc-alkaline through tholeiitic through komatiitic affinities. We have grouped these prospective units across the Superior into four end-members based on the predominant lithologies (e.g. mafic-dominated, mafic to ultramafic-dominated, ultramafic-dominated, and komatiitic-dominated units[4]), using the compositions of the parental mafic-ultramafic magmas estimated from the compositions of the most-magnesian olivine and the compositions of the most magnesian olivine cumulate rocks; however, this method was hampered by widespread serpentinization and talc-carbonation and incomplete data sets. The wider distribution and higher abundances of low-Mg magmas (mafic-dominated units) and intermediate-Mg magmas (mafic-dominated and ultramafic-dominated units) across the craton make drawing conclusions about the magma composition difficult. However, the much more restricted distribution of komatiitic rocks (Fig. 3) at least indicates which areas experienced higher heat and magmas fluxes, generating high-Mg magmas across the Superior Province.

Nd Isotopic Compositions

To characterize the origin and evolution of the magmas associated with some of the mafic intrusions and the ultramafic intrusions/flows of the Superior Province, new Sm-Nd isotope analyses were undertaken using 125 whole-rock samples from 34 intrusions across the BUOGE superdomain. The analyses were performed at

[4] Ultramafic-dominated units that contain or are associated with rocks containing typical textural (e.g. spinifex) and/or geochemical characteristics of komatiitic rocks have been assigned to komatiitic-dominated units.

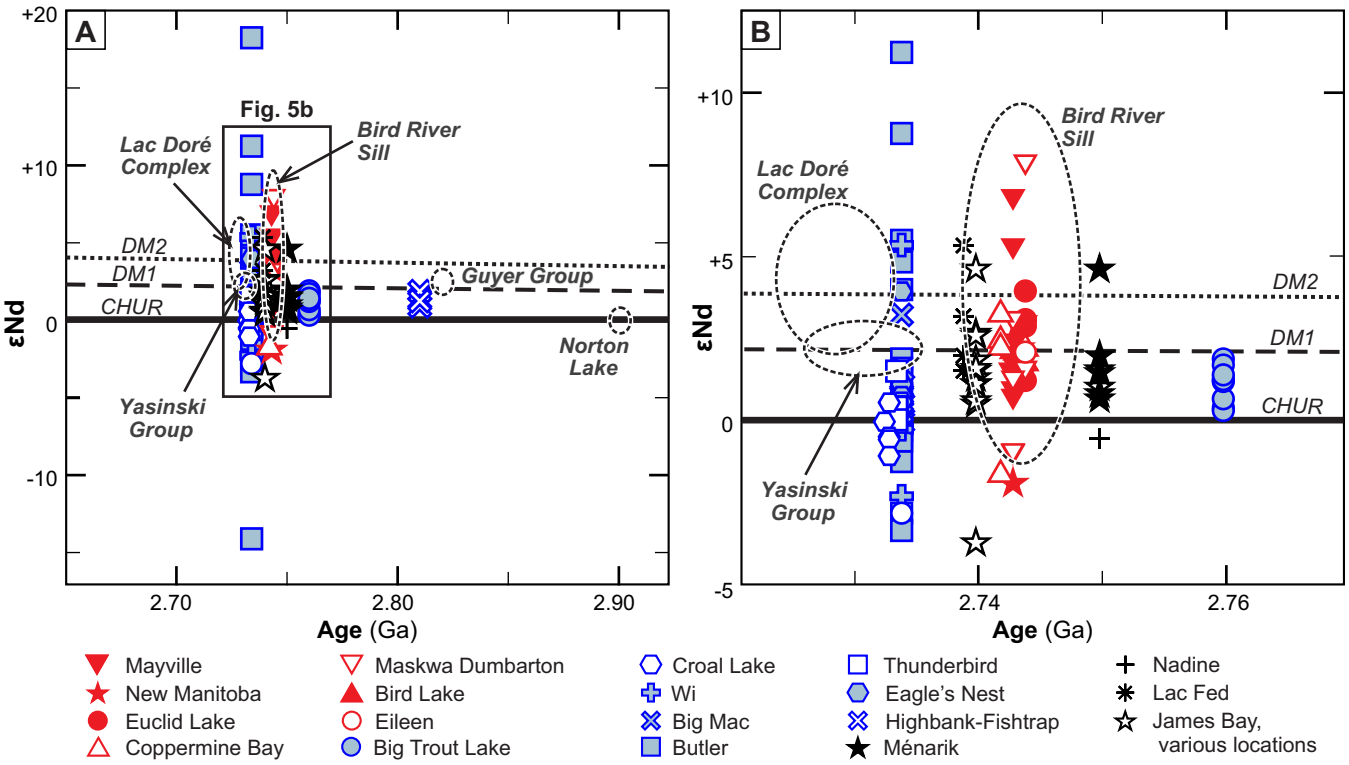

Figure 5. a) Initial $\varepsilon Nd_{(t)}$ versus age (Ma) for different intrusions across the BUOGE superdomain. **b)** Close-up of Figure 5a. The chondritic uniform reservoir model (CHUR) and depleted mantle 1 models (DM1) are from DePaolo (1981). The depleted mantle model 2 (DM2) is from Goldstein et al. (1984). Red, blue, and black symbols identify samples by their general location, such as the Bird River greenstone belt, Ring of Fire region, and various locations in the La Grande Rivière and Eastmain domains, respectively. Fields (dashed ellipses) represent data compiled for gabbroic rocks and peridotite of the Bird River Sill from Sotiriou et al. (2019), gabbroic rocks of the Norton Lake intrusion from Johnson (2005), gabbroic rocks of the Lac Doré complex peridotite of the Yasinski Group, and komatiite of the Guyer Group from Isnard (2003).

multiple laboratories (Carleton University, Ottawa; University of Texas, Austin; University of Copenhagen, Copenhagen), but duplicates were analyzed in each laboratory to confirm inter-laboratory agreement. Two main age groups of intrusions/flows were defined: Mesoarchean (ca. 2809 Ma) and Neoarchean (2760–2727 Ma). The gabbroic rocks of the Mesoarchean Highbank–Fishtrap intrusive complex have a narrow range of $\varepsilon Nd_{(t)}$ values, from +0.9 to +1.9 (Fig. 5a). In contrast, the various mafic to ultramafic lithologies of the Neoarchean intrusions/flows have a wide range of $\varepsilon Nd_{(t)}$ values that range from -14.1 to +18.2 (Fig. 5b). Values of $\varepsilon Nd_{(t)}$ greater than +5 are likely related to a disturbance of the Sm-Nd isotopic system by later alteration (e.g. Lahaye et al., 1995; Lesher and Arndt, 1995; Lahaye and Arndt, 1996; Sotiriou et al., 2019). The majority of $\varepsilon Nd_{(t)}$ values obtained for the mafic to ultramafic prospective units of the BUOGE superdomain are lower than values for the depleted mantle and many are even lower than CHUR (chondritic uniform reservoir) at ca. 2.8 to 2.7 Ga (Fig. 5b), suggesting that they contain a component of non-radiogenic upper crustal rocks. The most contaminated signatures are from the mafic-dominated intrusions of the Bird River intrusive suite (e.g. Coppermine and New Manitoba) and ferrogabbroic intrusions of the Ring of Fire intrusive suite (e.g. Butler and Croal Lake intrusions).

Metal Endowment

The overall spatial and temporal distribution of Ni-Cu-(PGE), Cr-(PGE), and Fe-Ti-V deposits and significant prospects and occurrences across the Superior Province are shown in Figures 1 and 4 and listed in Table 1.

As pointed out by Houlé et al. (2015a), the highest abundance of Ni-Cu-(PGE) deposits and metal endowment across the Superior Province is by far within the Wawa-Abitibi terrane (Fig. 1), which is mainly driven by the presence of the low grade but enormous geological resources associated with the differentiated komatiitic sill hosting the Dumont nickel deposit (Fig. 6a). However, the BUOGE superdomain contains numerous Ni-Cu-(PGE) deposits and in many cases, these deposits are spatially associated with Cr-(PGE) deposits/prospects within the same intrusive body (Fig. 1; Table 1). If the Dumont deposit is excluded, then the Ni-Cu-(PGE) endowment of the BUOGE superdomain exceeds the endowment of the Wawa-Abitibi terrane (Fig. 6b), which indicates the importance of this area within the overall Ni-Cu-(PGE) endowment of the province.

Table 1. Main characteristics of Cr-(PGE), Ni-Cu-(PGE), and Fe-Ti-V deposits and selected mineral occurrences within the Superior Province (*adapted from* Houlé et al., 2015a, 2019).

Map # ID	Deposits	Status	Intrusive Suite/ Assemblage	Intrusive/Extrusive Unit	Prospective Unit Type			Age (Ma)			Mineralization Type
North Caribou Terrane											
Cross Lake Greenstone Belt											
1	**Pipestone**	Dp		Pipestone Lake Anorthosite	M		A	2760	1	CA	Fe-Ti-V
Big Trout Lake - Swan Lake Greenstone Belt											
2	**Big Trout Lake**	Dp		Big Trout Lake	MUM	M > UM	A	*Pending*	2		Cr-PGE, *Ni-Cu-PGE*
Wunnummin Lake Greenstone Belt											
3	**Lavoie Lake**	Dp		Lansdowne House	MUM	M > UM		-			Cu-Ni-PGE, *Fe-Ti-V, PGE*
McFaulds Lake Greenstone Belt											
4	**Croal Lake**	Oc	Ring of Fire	Croal Lake	M		A	2733	3	CA	*Fe-Ti-V*
5	**Butler West**	Oc	Ring of Fire	Butler West	M	± UM	A	-	3	NZ	*Fe-Ti-V*
	Butler East	Oc	Ring of Fire	Butler East	M	± UM	A	-	3	NZ	*Fe-Ti-V*
6	**Big Mac**	Oc	Ring of Fire	Big Mac	M	± UM	A	2734	3	CA	*Fe-Ti-V*
7	**Blackbird 1**	Dp	Ring of Fire	Double Eagle	MUM	UM > M		-			Cr-PGE, *Ni-Cu-PGE*
	Blackbird 2	Dp	Ring of Fire	Double Eagle	MUM	UM > M		-			Cr-PGE, *Ni-Cu-PGE*
	Black Horse	Dp	Ring of Fire	Double Eagle	MUM	UM > M		-			Cr-PGE, *Ni-Cu-PGE*
	Eagle's Nest	Dp	Ring of Fire	Eagle's Nest dyke	UM			-			Ni-Cu-PGE
	Big Daddy	Dp	Ring of Fire	Black Thor	MUM	UM > M	A	2734	3	CA	Cr-PGE
	Black Creek	Dp	Ring of Fire	Black Thor	MUM	UM > M		-			Cr-PGE, *Ni-Cu-PGE*
	Black Label	Dp	Ring of Fire	Black Thor	MUM	UM > M	A	2734	3	CA	Cr-PGE, *Ni-Cu-PGE*
	Black Thor	Dp	Ring of Fire	Black Thor	MUM	UM > M	A	2734	3	CA	Cr-PGE, *Ni-Cu-PGE*
	Thunderbird	Oc	Ring of Fire	Thunderbird	M	± UM	A	2734	3	CA	*Fe-Ti-V*
8	**Highbank**	Oc		Highbank-Fishtrap	MUM	M >> UM	A	2810	3		*Fe-Ti-V*
Bird River Greenstone Belt											
9	**Chrome**	Dp	Bird River	Bird River Sill-Chrome	MUM	M > UM	A	2743	4	CA	Cr-PGE
	Page	Dp	Bird River	Bird River Sill-Page	MUM	M > UM		-			Cr-PGE
	Ore Fault	Dp	Bird River	Bird River Sill-Page	MUM	M > UM		-			Ni-Cu-PGE
	Makwa	Dp	Bird River	Bird River Sill-Makwa	MUM	M >> UM		-			Ni-Cu-PGE, *Cr-PGE*
	Dumbarton	Dp	Bird River	Bird River Sill-Makwa	MUM	M > UM		-			Ni-Cu-PGE
	Bird Lake	Dp	Bird River	Bird River Sill-Petra	MUM	M > UM	A	2743	3	CA	Cr-PGE
10	**Euclid**	Dp	Bird River	Euclid Lake	MUM	M ~ UM	A	2744	3	CA	Cr-PGE
	New Manitoba	Dp	Bird River	Cat Lake	M		A	2743	3	CA	Ni-Cu-PGE
11	**M2**	Dp	Bird River	Mayville	MUM	M >> UM	A	2743	3	CA	Cu-Ni-PGE, *Cr-PGE*
Pickle Lake Greenstone Belt											
12	**Thierry**	Dp	Kapkichi Lake		M	± UM		-		ND	Ni-Cu-PGE
Miminiska-Fort Hope Greenstone Belt											
13	**Norton**	Dp		Norton Lake	MUM	UM > M		-		ND	Ni-Cu-PGE
14	**Wabassi**	Oc		Wabassi Main	MUM	M >> UM	A	2727	5	CA	*Fe-Ti-V*

Table 1 continued.

Map # ID	Deposits	Status	Intrusive Suite/ Assemblage	Intrusive/Extrusive Unit	Prospective Unit Type		Age (Ma)			Mineralization Type
North Caribou Terrane										
Yasinski Greenstone Belt										
15	**Menarik-Cr**	Dp		Menarik	MUM	UM > M	A 2750	3	CA	Cr-PGE
	Menarik-Ni	Dp		Menarik	MUM	UM > M	-		ND	Ni-Cu-PGE
	Baie Chapus	Oc		Bais Chapus	MUM	UM > M	-		IA	*Fe-Ti-V*
Venus Greenstone Belt										
16	**Gayot**	Oc	Gayot Complex		MUM	UM > M	B 2880	6	CA	*Ni-Cu-PGE*
Eastmain Greenstone belt										
17	**Lac Fed**	Oc		Lac Fed	UM		B 2739	7	CA	*Cr-PGE*
Lac des Montagnes Greenstone Belt										
18	**Lac des Montagnes**	Oc	Caumont	Lac des Montagnes	MUM	UM > M	A 2802	3	CA	*Cr-PGE, Ni-Cu-PGE*
19	**Nisk**	Dp	Caumont	Levack	MUM	UM > M	A *Pending*	2	CA	Ni-Cu-PGE, *Cr-PGE*
English River Terrane										
Werner-Rex Belt										
20	**Gordon**	Dp			UM		-		ND	Ni-Cu-PGE
	Norpax	Dp			MUM	UM > M	-		ND	Ni-Cu-PGE
Winnipeg River Terrane										
Obanga Greenstone Belt										
21	**Puddy-Chrome Lakes**	Dp		Puddy-Chrome Lake	UM	-	-		ND	Cr-PGE
Caribou-Marshall Lake Greenstone Belt										
22	**B4-7 deposit**	Dp		Grassy Pond Sill	M		-		ND	Ni-Cu-PGE
	VW deposit	Dp		Carrot Top komaiites	UM	UM >> M	-		ND	Ni-Cu-PGE
Western Wabigoon Terrane										
Kakagi-Rowan Greenstone Belt										
23	**Kenbridge**	Dp			M±UM	M >> UM	-		ND	Ni-Cu-PGE, *Fe-Ti-V*
	Apex	Dp			M		-		ND	Ni-Cu-PGE
24	**Nico 1**	Dp		Dobie Intrusion	M±UM	M > UM	-		ND	Ni-Cu-PGE
Fort Francis-Mine Centre Greenstone Belt										
25	**Seine Bay**	Dp		Bad Vermillion	M±UM	M >> UM	B > 2716	8	CA	Fe-Ti-V
Marmion Terrane										
Bo Lake-Heavan Lake Greenstone Belt										
26	**Lac des Iles**	Dp	Lac des Iles	Mine Block	M		A 2689	9	CA	PGE-Cu-Ni
Elmhirst-Castlewood-Klotz Greenstone Belt										
27	**Jacobus**	Dp		Pinel Creek	M±UM	M >> UM	-		ND	Cu-Ni-PGE
Opatica Terrane										
Colomb-Chaboullié Greenstone Belt										
28	**Horden Lake**	Dp			MUM	M > UM	-		ND	Cu-Ni-PGE
Frotet-Evans Greenstone Belt										
29	**Lac Rocher**	Dp	Rocher-Quénonisca	Lac Rocher	MUM	UM >> M	A 2703	10	CA	Ni-Cu-PGE

Table 1 continued.

Map # ID	Deposits	Status	Intrusive Suite/ Assemblage	Intrusive/Extrusive Unit	Prospective Unit Type		Age (Ma)			Mineralization Type
Abitibi-Wawa Terrane										
Shebandowan Greenstone Belt - Wawa										
30	**Shebandowan**	Dp	Shebandowan		UM		B 2722–2219	11	CA	Ni-Cu-PGE, *Cr-PGE*
				Haines Gabbro	M		A 2722	11	CA	
Schreiber-Hemlo Greenstone Belt - Wawa										
31	**Nicopor**	Dp		Zenmac	M±UM	M >> UM	-		ND	Ni-Cu-PGE
Michipicoten Greenstone Belt - Wawa										
32	**Lakemount**	Dp		Sunrise	UM		-		ND	Ni-Cu-PGE
Timmins West Area - Abitibi										
33	**Montcalm**	Dp		Montcalm	M±UM	M >> UM	A 2702	12	CA	Ni-Cu-PGE
	Loveland	Dp			M		-		ND	Ni-Cu-PGE
	Enid Creek	Dp		Enid Creek	M		-		ND	Ni-Cu-PGE
	Warran Claims	Dp			M		-		ND	Ni-Cu-PGE
	Crawford	Dp			MUM	UM >>> M	-		ND	Ni-Cu-PGE
Dundonald District - Abitibi										
34	**Alexo/Kelex**	Dp	Kidd-Munro		UM		B 2720–2710	13	CA	Ni-Cu-PGE
	Dundeal	Dp	Kidd-Munro		UM		B 2720–2710	13	CA	Ni-Cu-PGE
	Dundonald South	Dp	Kidd-Munro		UM		B 2720–2710	13	CA	Ni-Cu-PGE
	Nickel Island	Dp	Kidd-Munro		UM		-		ND	Ni-Cu-PGE
Shaw Dome District - Abitibi										
35	**Redstone**	Dp	Tisdale		UM		B 2710–2704	13	CA	Ni-Cu-PGE
	McWatters	Dp	Tisdale		UM		B 2710–2704	13	CA	Ni-Cu-PGE
	Langmuir 1	Dp	Tisdale		UM		B 2710–2704	13	CA	Ni-Cu-PGE
	Langmuir 2	Dp	Tisdale		UM		B 2710–2704	13	CA	Ni-Cu-PGE
	Langmuir North	Dp	Tisdale		UM		B 2710–2704	13	CA	Ni-Cu-PGE
	Langmuir South	Dp	Tisdale		UM		B 2710–2704	13	CA	Ni-Cu-PGE
	Hart	Dp	Tisdale		UM		B 2710–2704	13	CA	Ni-Cu-PGE
	W4	Dp	Tisdale		UM		B 2710–2704	13	CA	Ni-Cu-PGE
Bartlett-Halliday-Bannockburn Area - Abitibi										
36	**Texmont**	Dp	Tisdale		UM		B 2710–2704	13	CA	Ni-Cu-PGE
	Sothman	Dp	Kidd-Munro		UM		B 2720–2710	13	CA	Ni-Cu-PGE
	Bannockburn	Oc	Kidd-Munro		UM		B 2720–2710	13	CA	*Ni-Cu-PGE*
Shining Tree Area - Abitibi										
37	**Shining Tree**	Dp			M		-		ND	Ni-Cu-PGE
Temagami Greenstone Belt - Abititbi										
38	**Kanichee**	Dp			MUM	UM >> M	-		ND	Ni-Cu-PGE
	Temagami	Dp			M		A 2732	14	CA	Ni-Cu-PGE
Matagami Area - Abitibi										
39	**Grasset**	Dp			MUM		A *Pending*	2	CA	Ni-Cu-PGE
40	**Iron-T**	Dp		Rivière Bell Complex	M±UM	M >>> UM	A 2725	15	CA	Fe-Ti-V
Amos Area - Abitibi										
41	**Dumont**	Dp			MUM		A *Pending*	2	CA	Ni-Cu-PGE

Table 1 continued.

Map # ID	Deposits	Status	Intrusive Suite/ Assemblage	Intrusive/Extrusive Unit	Prospective Unit Type		Age (Ma)			Mineralization Type
Abitibi-Wawa Terrane										
La Motte-Vassen Area - Abitibi										
42	**Marbridge 1**	Dp	Kidd-Munro		UM		B 2720–2710	[13]	CA	Ni-Cu-PGE
	Marbridge 2	Dp	Kidd-Munro		UM		B 2720–2710	[13]	CA	Ni-Cu-PGE
	Marbridge 3	Dp	Kidd-Munro		UM		B 2720–2710	[13]	CA	Ni-Cu-PGE
	Marbridge 4	Dp	Kidd-Munro		UM		B 2720–2710	[13]	CA	Ni-Cu-PGE
	Québec Moly	Dp	Kidd-Munro		UM		-		ND	Ni-Cu-PGE
	Bilson-Cubric	Dp	Kidd-Munro		UM		B 2720–2710	[13]	CA	Ni-Cu-PGE
43	**Vendôme**	Dp	Mont-Vidéo		MUM	M >> UM	-		ND	Ni-Cu-PGE
	Commander-Zulapa	Dp			FI±M		-		ND	Ni-Cu-PGE
Black River Area - Abitibi										
44	**R.M. Nickel**	Dp			M		A 2695	[16]	CA	Ni-Cu-PGE
Belleterre-Angliers Greenstone Belt - Abitibi										
45	**Alotta**	Dp			M		B 2712–2707	[17]	CA	Ni-Cu-PGE
	Midrim	Dp			M		-		ND	Ni-Cu-PGE
46	**Blondeau-Nickel**	Dp			M		-		ND	Ni-Cu-PGE
	Lorraine	Dp			M		-		ND	Ni-Cu-PGE
	Lac Kelly	Dp			M		-		ND	Ni-Cu-PGE
47	**La Force**	Dp			M		A 2692	[17]	CA	Ni-Cu-PGE
Lac Villebon Area - Abitibi										
48	**Villebon**	Dp			UM		-		ND	Ni-Cu-PGE
Chibougamau District - Abitibi										
49	**Lac Doré**	Dp		Lac Doré Complex-South Limb	M±UM	M >>> UM	A 2728	[15]	CA	Fe-Ti-V
	Armitage	Dp			M±UM	M >>> UM	A 2728	[15]	CA	Fe-Ti-V
	Southwest	Dp			M±UM	M >>> UM	A 2728	[15]	CA	Fe-Ti-V
	Ile Portage	Dp		Lac Doré Complex-North Limb	M±UM	M >>> UM	-		ND	Fe-Ti-V

References:

[1]Corkery et al., 1992; [2]This study; [3]Houlé et al., 2015a, 2020; [4]Scoates and Scoates, 2013; [5]Sappin et al., 2016; [6]David et al., 2009; [7]Moukhsil et al., 2007; [8]Zhou et al., 2016; [9]Stone et al., 2003; [10]Bandyayera and Sharma, 2001; [11]Corfu and Stott, 1998; [12]Barrie et al., 1990; [13]Houlé et al., 2017; [14]Ontario Geological Survey, unpublished; [15]Mortensen, 1993; [16]McNicoll et al., 2014; [17]Huffman, unpublished data.

Abbreviations:

Dp = deposit, Oc = occurrence; Mineralization type in italics = occurrence;
FI = felsic intrusion, M = mafic, MUM = mafic to ultramafic, UM = ultramafic;
A = direct age constraint, B = Indirect age contraint obtained via dated crosscutting dykes or subjacent host volcanic rocks;
CA = crystallization age, IA = inheritance age, ND = not dated, NZ = no zircon found.

Note:

Map ID #: refers only to a spatial association and does not imply any cogenetic correlation. All deposits are mainly compiled and modified from a provincial mineral occurrences database (Mineral Inventory Card in Manitoba, Mineral Deposit Inventory in Ontario, SIGÉOM in Québec). Deposits are defined as a mineral occurrences that contain actual or past geological resources. No distinction has been made among producing mines, past producers, and deposits. Mineral occurrences listed here are considered significant mineral occurrences; not all mineral occurrences are listed in this table or represented on Figure 1.

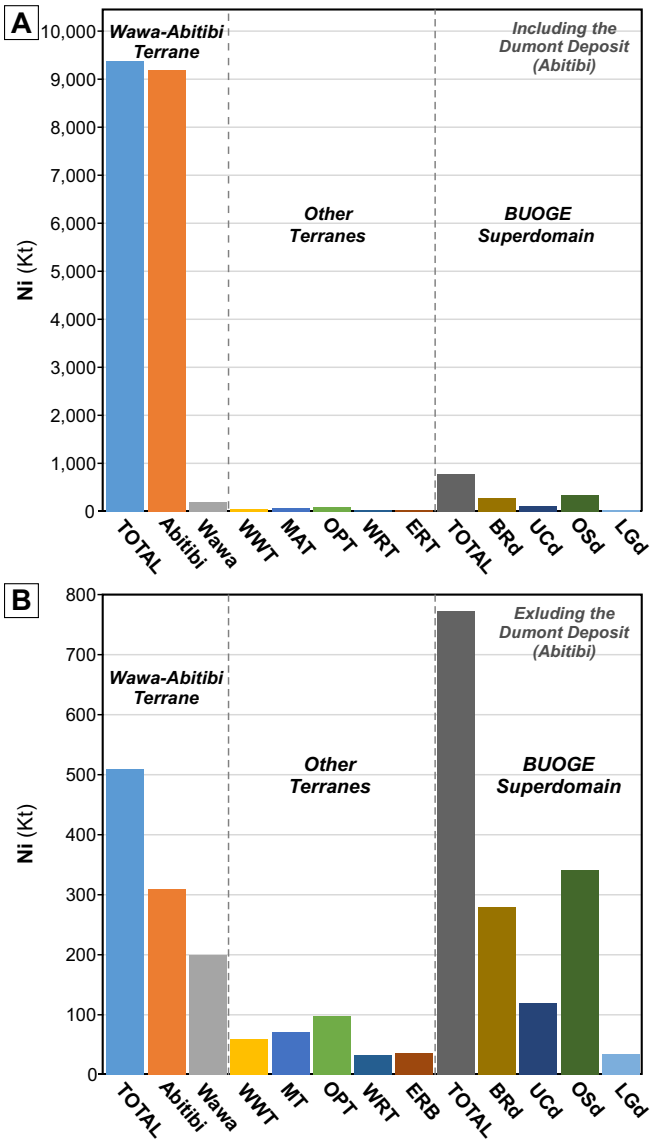

Figure 6. Estimated geological resources in kilotonnes of nickel across the Superior Province, including **(a)** and excluding **(b)** the contribution of the large low-grade Dumont nickel deposit in the Abitibi greenstone belt. Data for geological resources are from a variety of sources, including provincial geological survey reports and company reports (mostly available at www.sedar.com); geological resources include production, reserves (proven and probable), and resources (measured, indicated, and inferred), when available. The reader is cautioned that not all of the geological resources presented are compliant to Canadian Institute of Mining, Metallurgy and Petroleum's (CIM) standards as required by the NI 43-101 regulations and represent only historic geological resources. *See* Figure 1 for terrane and domain abbreviations.

The vast majority of Cr-(PGE) deposits/occurrences across the Superior Province occur within the Mesoarchean to Neoarchean supracrustal successions of the BUOGE superdomain, defining a major Cr-Ni-Cu-(PGE) metallotect (Fig. 1, Table 1; Houlé et al., 2015a). The Ring of Fire intrusive suite alone contains close to 90% of the known Cr budget of the entire craton (Fig. 7a). Outside of the BUOGE superdomain, only one other chromite deposit (Puddy-Chrome Lakes) is known within the Winnipeg River terrane. However, it is quite different from most other deposits in the Superior Province, exhibiting many similarities with podiform-type chromite deposits (e.g. Whittaker, 1986). On the other hand, a significant interval (up to ~30 feet thick) of massive to semi-massive chromitite occurs within a komatiitic ultramafic body at the Ni-Cu-(PGE) Shebandowan mine (M. Lavigne, A. Aubut, and T. Hart, pers. comm., 2013–2019) (Fig. 1).

It is difficult to make generalizations regarding the distribution of the Fe-Ti-V deposits, as they occur within a wider range of types of terranes and domains and because many of the significant occurrences do not have any geological resource estimates (Fig. 7b,c). As an example, the Pipestone deposit occurs in the Island Lake domain within the North Caribou terrane, the Bad Vermillion deposit is within the western Wabigoon terrane, and the Rivière Bell and Lac Doré deposits are in the Wawa-Abitibi terrane; in addition, numerous Fe-Ti-V prospects occur in the Ring of Fire area in the Oxford-Stull domain (Fig. 1). Furthermore, the Butler, Thunderbird, Big Mac, and a few other Fe-Ti-V prospects in the Ring of Fire area do not have any resource estimates due to the lack of closely spaced drilling, but vanadiferous oxide-layers (magnetite-ilmenite) have been intersected at depth in several diamond drillholes over a few kilometres of strike length, along with high-magnetic anomalies (Houlé et al., 2015a, 2020).

DISCUSSION

Targeting Ni-Cu-(PGE), Cr-(PGE), and Fe-Ti-V ore systems is challenging, especially in poorly exposed, highly deformed, and metamorphosed Archean cratons such as the Superior Province. Many factors can be responsible for the variable metal endowment across the province; however, several critical features appear to be important for identifying the most prospective areas to host economic orthomagmatic ore systems across the Superior Province.

Spatial Distribution and Magma Composition

As almost all of orthomagmatic Ni-Cu-(PGE), Cr-(PGE), and Fe-Ti-V deposits in the Superior Province occur within mafic and ultramafic bodies, the presence and estimated abundance of favourable rocks in a given sector greatly increases the likelihood of metal discovery, making this as a prime criterion to assess prospectivity. However, these units are common throughout the Superior Province, which makes it difficult to predict where the most prospective areas are using this criterion alone (Fig. 2, 3). Therefore, the presence of highly magnesian units and local crustal-contamination signa-

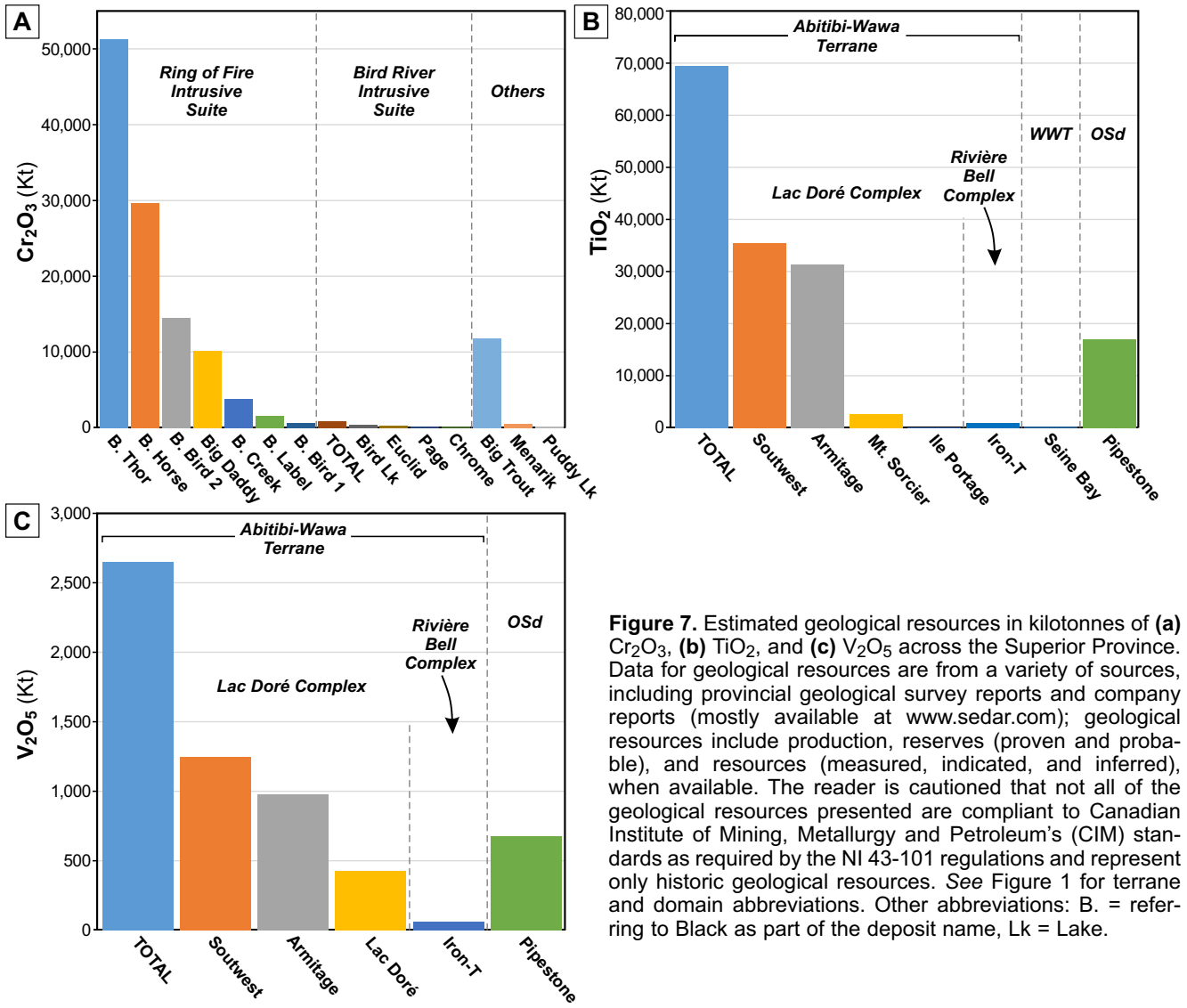

Figure 7. Estimated geological resources in kilotonnes of **(a)** Cr_2O_3, **(b)** TiO_2, and **(c)** V_2O_5 across the Superior Province. Data for geological resources are from a variety of sources, including provincial geological survey reports and company reports (mostly available at www.sedar.com); geological resources include production, reserves (proven and probable), and resources (measured, indicated, and inferred), when available. The reader is cautioned that not all of the geological resources presented are compliant to Canadian Institute of Mining, Metallurgy and Petroleum's (CIM) standards as required by the NI 43-101 regulations and represent only historic geological resources. *See* Figure 1 for terrane and domain abbreviations. Other abbreviations: B. = referring to Black as part of the deposit name, Lk = Lake.

tures, which are critical factors to generate sulphide (e.g. Lesher, 1989; Lesher et al., 2001; Houlé and Lesher, 2011) and chromite deposits (e.g. Lesher et al., 2019), could help to identify the most prospective area across the province. In any case, areas that contain a greater diversity of prospective units, in particular the most primitive ones (related to komatiitic and ultramafic magmatism: Fig. 3) appear to be more prospective, as they host most of the orthomagmatic Ni-Cu-(PGE), Cr-(PGE), and Fe-Ti-V deposits and significant occurrences within the province (e.g. BUOGE, Wawa-Abitibi terrane).

In addition, the generation of a specific deposit type seems to be dependent on the initial magma composition or at least favoured for the generation of specific deposit types. Ni-Cu-(PGE), Cr-(PGE), Cu-Ni-PGE, and Fe-Ti-V mineralization are preferentially associated with high-Mg komatiitic magmas (e.g. Abitibi), with low-Mg komatiitic to basaltic magmas (e.g. Ring of Fire and Bird River intrusive suites), with basaltic magmas (e.g. Abitibi), and with Fe-rich basaltic magmas (e.g. Abitibi), respectively (Fig. 1, 2, 3). Negative $\varepsilon Nd_{(t)}$ isotopic compositions (Fig. 5) combined with enrichment in highly incompatible lithophile elements (e.g. Th and light rare-earth elements) relative to moderately incompatible elements (e.g. Y-Zr-Hf and heavy to middle rare-earth elements) is a signature of crustal contamination in komatiitic rocks (*see* Lesher and Arndt, 1995; Lesher et al., 2001). However, crustal contamination alone is not a reliable indicator of prospectivity, as komatiitic magmas and, to a lesser extent, basaltic magmas may assimilate crustal material but not interact with any sulphur or oxide sources.

Temporal Distribution

Orthomagmatic Ni-Cu-(PGE), Cr-(PGE), and Fe-Ti-V deposits have formed during most of Earth's history (Naldrett, 2010). However, the majority and the most endowed deposits, especially those that are Ni-Cu-(PGE)-rich, cluster in four prominent time periods

(Late Archean, Middle to Late Paleoproterozoic, Middle Mesoproterozoic to Early Neoproterozoic, and Late Paleozoic), which most workers have linked to supercontinent cycles (Kenorland, Nuna, Rodinia, and Pangea) (e.g. Kerrich et al., 2005; Maier and Groves, 2011; Begg et al., 2018). Prospective mafic to ultramafic units across the Superior Province formed over more than 350 Ma, but almost all Ni-Cu-(PGE), Cr-(PGE), and Fe-Ti-V deposits occur within the time-interval generally assigned to the Kenorland Supercontinent (ca. 2.8–2.5 Ga: Williams et al. 1991; Goldfarb et al., 2010), or the Superia supercraton (ca. 2.7–2.5 Ga: Bleeker, 2003), which was the ancestral landmass to the Superior, Wyoming, Hearne, and Kola/Karelia cratons (Bleeker and Ernst, 2006; Ernst and Bleeker, 2010), among others.

More specifically, orthomagmatic ore systems in the Superior Province predominantly occur during a few short specific time intervals. These include ca. 2.88–2.87 Ga (e.g. Gayot complex); ca. 2.81–2.80 Ga (e.g. Caumont intrusive suite and Highbank-Fishtrap complex); ca. 2.74–2.71 Ga (e.g. Bird River and Ring of Fire intrusive suites, Wawa-Abitibi terrane komatiites); ca. 2.71–2.70 Ga (e.g. Lac Rocher); and 2.69–2.68 Ga (e.g. Lac des Iles) (Fig. 4b, Table 1). Indeed, several mineralizing events occur during this period across the Superior Province, which suggests that the most important factor driving the metal endowment is not the actual time of emplacement but more the presence of large magmatic events emplaced over a short time period. The Bird River intrusive suite (ca. 2743 Ma), Ring of Fire intrusive suite (ca. 2734 Ma), and Wawa-Abitibi terrane (2722 Ma: Greenwater komatiite; 2720–2710 Ma: Kidd-Munro komatiites; 2710–2704: Tisdale komatiites: Houlé and Lesher, 2011) are all good examples of these large magmatic mineralizing events across the Superior Province. Therefore, the most endowed period (ca. 2.75–2.70 Ga) in the Superior Province also appears to coincide with a peak of high-Mg magmas worldwide at ca. 2.73 Ga, as previously noted by Isley and Abbott (2002). Other large magmatic events that occur outside this peak period (e.g. Gayot komatiitic magmatism and Caumont Intrusive Suite), however, should not be neglected as potential targets.

Craton Margins, Translithospheric Structures, and Intracratonic Boundaries

To form well endowed orthomagmatic ore systems, the fertile magma must be transported rapidly through the lithosphere along the thinner margins of the craton (e.g. Sleep, 2006; Begg et al., 2010; Griffin et al., 2013) or through the lithosphere along translithospheric faults (e.g. Naldrett, 2004; Barnes and Lightfoot, 2005) or crustal sutures (Cassidy and Champion, 2004; Mole et al., 2013). Some Ni-Cu-(PGE) deposits appear to better fit a craton margin model (e.g. Pechenga, Raglan, Thompson, Sudbury), some appear to better fit a translithospheric fault model (e.g. Duluth, Noril'sk), and some appear to better fit a crustal suture model (e.g. Kambalda, Mt Keith, Perseverence). In the case of the Superior Province, at least two modes of localization are present. The 1.88 Ga Ni-Cu-PGE deposits in the Labrador Trough, Cape Smith belt, Fox River belt, Thompson Nickel Belt, and Sudbury occur along the 3,500 km long margin of the Superior (a.k.a. Circum-Superior Belt: Baragar and Scoates, 1981). On the other hand, almost all of the 2.8–2.7 Ga Ni-Cu-(PGE), Cr-(PGE), and Fe-Ti-V deposits within the Superior Province, including as the Abitibi and Ring of Fire intrusive suite deposits, occur on translithospheric structures or ancient sutures within the interior of the province (Fig. 1).

To further assess these models as they apply to the Superior Province, we examined the spatial distribution of Ni-Cu-(PGE), Cr-(PGE), and Fe-Ti-V deposits relative to the internal subdivisions (e.g. terrane, domain) defined by Stott et al. (2010), Percival et al. (2012), and SIGÉOM (2020) (Fig. 1). These internal domain or terrane boundaries are considered to be potential intracratonic boundaries independent of the geodynamic model preferred for the development of the Superior Province (i.e. accretion: Percival et al., 2012 versus cratonic rifting: Bédard and Harris, 2014), as both models used the same internal subdivisions. Additional constraints are provided by the alignment of komatiite flows along the northern and the southern margins of the North Caribou Core domain, which support—to some extent—a role for at least some of these boundaries in the emplacement of ultramafic to mafic magmatism across the province. Table 2 shows the spatial distribution of the main mineralized areas within the BUOGE superdomain in respect to these internal boundaries. Some deposits clearly occur on (e.g. Highbank-Fishtrap complex, Lac des Montagnes) or near (e.g. Bird River intrusive suite) these internal boundaries, whereas others occur in the central parts of terranes or domains (e.g. Ring of Fire intrusive suite). It is also difficult to establish whether the internal boundaries are translithospheric faults or sutures; for this, further assessment will be required that is beyond the scope of this contribution.

Dynamic Ore Systems

It has been well recognized that to generate sulphide-rich Ni-Cu-(PGE) deposits and Cr-(PGE) deposits, or at least magmatic conduit-hosted deposits, some several key elements are required, including the presence of bulk densities and shallow structures that favour high magma fluxes (e.g. Lesher, 1989; Lesher et al.,

Table 2. Spatial relationship of selected deposits/areas of the BUOGE superdomain from the internal domain/terrane interpreted as potential intra-cratonic boundaries in the Superior Province. *See* Figure 1 for the location of the main internal domain and terrane boundaries.

North Caribou Terrane		Cratonic-Margin Model – Internal domain/terrane boundaries		
# Deposit / Area	Location	Distance - Boundaries (km)		Boundaries
		South Margin	North Margin	
1 Pipestone	ON	105	18	ILd/OSd
2 Big Trout Lake	ON	6	95	ILd/OSd
3 Lavoie Lake	NR	18	160	ILd/OSd
4 Croal Lake	CE	101	75	OSd
5 Butler	CE	50	110	OSd
6 Big Mac	CE	100	48	OSd
7 Esker intrusive complex deposits	CE	50	95	OSd
8 Highbank-Fishtrap	ON	10	140	NCCd-OSd
9 Bird River sill deposits	NR	12	15 (45)	BRd/ERT and BRd/NCCd
10 Euclid-New Manitoba	ON	25	1 (32)	BRd/ERT and BRd/NCCd
11 M2-Mayville	ON	32	2 (42)	BRd/ERT and BRd/NCCd
12 Thierry	ON	58	6	UCd/NCCd
13 Norton	ON	60	9	UCd/NCCd
14 Wabassi Main	CE	34	38	UCd
15 Menarik	CE	35	25	LGd
16 Gayot	CE	36	45	LGd
17 Lac Fed	CE	33	70	EAd
18 Lac des Montagnes	ON	82	<1	NMT/EAd
19 Nisk	ON	4	<1	NMT/EAd

Abbreviations:
CE = located in the central part of the domain or terrane (>20 km), NR = located near the domain/terrane margin (10–20 km), ON = located on the domain/terrane margin (i.e. <10 km);
BRd = Bird River domain, EAd = Eastmain domain, ERT = English River Terrane, ILd = Island Lake domain, LGd = La Grande Rivière domain, NCCd = North Caribou Core domain, NMT = Nemiscau Terrane, OSd = Oxford-Stull domain, UCd = Uchi domain.

Note:
Numbers in parentheses for deposits 9, 10, and 11 correspond to the distance to the boundary with the North Caribou Core domain. *See* Table 1 for the number correspondance.

2001; Lesher and Keays, 2002) and emplacement of channelized lava/magma conduits at relatively high stratigraphic levels (Houlé et al., 2008; Layton-Matthews et al., 2010) to promote incorporation of S from crustal rocks (e.g. sulphide-facies iron formation: Groves et al., 1979; Green and Naldrett, 1981; sulfidic cherts/shales: Huppert et al., 1984; Lesher et al., 1984; VMS mineralization: Menard et al, 1996; sulphidic argillites: Houlé et al., 2012) but also oxide (e.g. oxide-facies iron formation) reservoirs (Lesher et al., 2019; *see* discussion in Houlé et al., 2020), which will allow large accumulations of sulphides or chromite.

A compilation of the degree of olivine enrichment (a measure of the degree of lava/magma flow-through and therefore more favourable to host mineralization) and differentiation (a measure of ponding or stagnation and therefore less favourable to host mineralization) is in progress and will be reported in due course, but it is clear that in many, if not most cases, these conditions have been met. These conditions occur definitively in many of the large magmatic events recognized across the BUOGE superdomain (e.g. Bird River and Ring of Fire intrusive suites, Gayot Lake and Lac Fed komatiitic sill-lava complexes) and the Wawa-Abitibi terrane (e.g. almost all komatiite-associated deposits in the Abitibi).

Large Magmatic Events within the BUOGE Superdomain

Numerous large and well endowed magmatic events, typically composed of several intrusions of the same age, have been identified within the BUOGE superdomain, including the Bird River intrusive suite within the Bird River domain and the Ring of Fire intrusive suite and the Highbank-Fishtrap intrusive complex within the Oxford-Stull domain (Houlé et al., 2015a). Smaller and more spatially restricted, but still significant, magmatic events also occur within the Eastmain domain, including the Caumont intrusive suite and the Lac Fed komatiitic sill-lava complex (Houlé et al., 2015b).

In the western Superior Province, the entire North Caribou terrane, which is composed of the North Caribou Core domain and flanked by the Uchi domain to the south and the Island Lake and the Oxford-Stull domains to the north, experienced widespread komatiitic magmatism (Fig. 3): For example, komatiitic volcanism occurred in the following areas:

- within the North Caribou Core domain in the McInnes Hornby, Favourable, and North Spirit Lake greenstone belts (K-6 on Fig. 3);
- within the Uchi domain in the Black Island, Rice Lake, Wallace Lake, and Red Lake greenstone belts (K-5 on Fig. 3);
- along the boundary between the North Caribou Core and the Island Lake domain in the Bigstone, Island Lake, Muskrat Dam, and North Caribou greenstone belts (K-7 and K-11 on Fig. 3);
- along the boundary between the Island Lake and Oxford-Stull domains in the Carrot River and Wunnummin greenstone belts (K-8 and K-12 on Fig. 3); and
- within the central part of the Island Lake or Oxford-Stull domains in the Pierce-Ponask-Sachigo, Stull Lake, and the McFaulds Lake greenstone belts (K-9, K-10, and K-13 on Fig. 3).

Overall, the distribution of the oldest komatiites in each domain—from the North Caribou Core (e.g. North Spirit Lake at 3.05–2.98 Ga: Préfontaine et al., 2008) to the Island Lake domain (e.g. Island Lake at ca. 2.85 Ga: Parks et al., 2014; Caribou Lake <2.9 Ga: McNicoll et al., 2016) to the Oxford-Stull domain (e.g. McFaulds Lake at ca. 2.73 Ga: Houlé et al., 2015a)—broadly suggests a younging of the komatiitic volcanism to the north (Fig. 8). The Oxford-Stull domain has been interpreted to have formed a major intracratonic rift, separating the North Caribou Core and the Hudson Bay terrane (Stott et al., 2010; Bédard and Harris, 2014). Therefore, it has been speculated that the northern margin might be defined by the North Kenyon fault, whereas the southern margin might be marked by the presence of a large mafic to ultramafic layered intrusion such as the 2809 Ma Highbank-Fishtrap complex, located along the Wunnummin greenstone belt (Stott et al., 2010). If this is correct, the Oxford-Stull intracratonic rift was most likely initiated by the komatiitic volcanism along the actual internal boundary between the Island Lake and Oxford-Stull domains, followed by the emplacement of large mafic to ultramafic intrusions (Fig. 8b). The rifting continued for at least another 75 Myr before the emplacement of the Ring of Fire intrusive suite at ca. 2736–2732 Ma (Houlé et al., 2015a; Metsaranta and Houlé, 2020: Fig. 8c). This long-lived intracratonic rifting might have played a crucial role in the metal endowment of the Ring of Fire intrusive suite by making its ascent through the crust more efficient due to sustained extension and thinning of the crust.

This succession of events in the Ring of Fire region is similar in some respects to the evolution of the Yilgarn Craton proposed by Cassidy and Champion (2004) and Mole et al. (2013, 2019), in which an ancient cratonic nucleus was subsequently rifted, expanded, and reworked by successive magmatic events from the Mesoarchean to Neoarchean. Repetitive emplacement of high-Mg magmas, from the Mesoarchean to the Neoarchean, most likely facilitated large, short-lived but episodic magmatic events promoting the formation of preferential magma pathways along this intracratonic architecture, subsequently driving the emplacement of large and well endowed ultramafic to mafic magmatic events such as the Ring of Fire intrusive suite.

Mantle plumes might help promoting this extensional environment (i.e. rifting). Decompression melting of a hotter ambient mantle can generate magmas containing up to 18–19% MgO (*see* Herzberg, 2004), but a mantle plume is required to generate high-Mg komatiites like those observed in the Abitibi (Sproule et al., 2002) and inferred for the parental magmas of the Ring of Fire (Houlé et al. 2020; Carson, in prep.). This sequence of events is in agreement with the initial proposition of Mungall et al. (2010) and Mungall (2013), in which a mantle plume came up underneath the North Caribou terrane and komatiitic magmatism was emplaced along thinner parts of the lithosphere.

IMPLICATIONS FOR EXPLORATION

Mafic to ultramafic units are ubiquitous across the Superior Province and are prospective to host magmatic Ni-Cu-(PGE), Cr-(PGE), and Fe-Ti-V deposits, but their abundance and metal endowment vary widely. Many factors could be responsible for the variable metal contents of these prospective units; however, it is still unclear which ones are the most critical. Below are some characteristics that define the most prospective areas in the Superior Province:

- Presence of large magmatic events that generated abundant primitive mantle-derived magmas for a short duration.
  - Occurrence of a large number of various prospective units including high-MgO units (komatiites and/or ultramafic units).
- Presence of specific magma compositions that favoured the generation of Ni-Cu-(PGE) (high-Mg komatiitic), Cr (low-Mg komatiitic), and Cu-Ni-PGE and Fe-Ti-V (basaltic) mineralization.
- Presence of transcrustal discontinuities that focussed magma flow through the lower crust.
  - Prospective units on or near terrane/domain margins (i.e. intracratonic margins) seems to be a favourable environment, but lavas and intrusions can flow laterally hundreds of kilometres from their magmatic centres (e.g. Magee et al., 2016), therefore, some of the most endowed regions are located further away

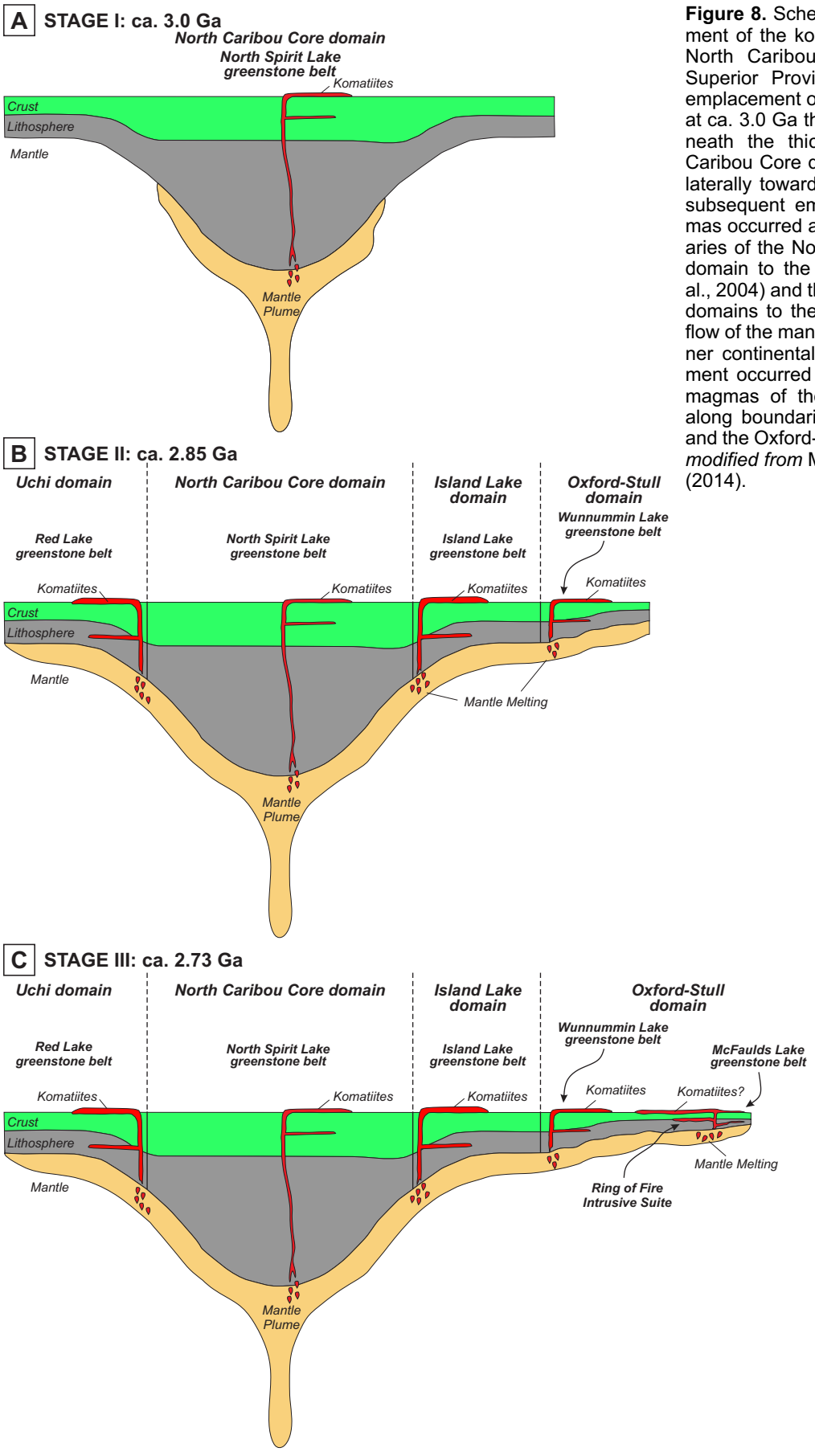

Figure 8. Schematic diagram of the emplacement of the komatiitic magmatism across the North Caribou terrane within the western Superior Province (not to scale). **a)** Initial emplacement of komatiitic magmas took place at ca. 3.0 Ga through mantle upwelling underneath the thick lithosphere of the North Caribou Core domain. **b)** Mantle melts flowed laterally toward thinner continental areas and subsequent emplacement of komatiitic magmas occurred at ca. 2.85 Ga along the boundaries of the North Caribou Core and the Uchi domain to the south (e.g. Sanborn-Barrie et al., 2004) and the Island Lake and Oxford-Stull domains to the north, respectively. **c)** Lateral flow of the mantle melts continued toward thinner continental areas and the final emplacement occurred at ca. 2.73 Ga with komatiitic magmas of the Ring of Fire intrusive suite along boundaries of the North Caribou Core and the Oxford-Stull domain. Schematic model *modified from* Mole et al. (2013) and Fiorentini (2014).

from these interpreted intracratonic margins (e.g. Ring of Fire intrusive suite).

- Presence of shallow structures and densities that favoured the emplacement of channelized lava/magma conduits at high crustal levels.
- Presence of high magma fluxes to promote thermo-mechanical erosion of crustal rocks.
- Presence of large magmatic events that generated abundant primitive mantle-derived magmas for a short duration.
- Presence of high-level crustal rocks containing sulphur (e.g. sulphide-facies iron formation) and oxide (e.g. oxide-facies iron formation) reservoirs for generating and upgrading sulphide xenomelts and oxide xenocrysts.
- Presence of favourable deformation and erosion environments to preserve and expose prospective units for exploration.

Thus far, the BUOGE superdomain and the Wawa-Abitibi terrane are the most endowed parts of the Superior Province for Ni-Cu-(PGE) and Cr-(PGE). However, these superdomain/terranes appear to be fundamentally different from each other in their metal endowment: Cr in BUOGE >>> Cr in Wawa-Abitibi; Ni in BUOGE <<< Ni in Wawa-Abitibi (including Dumont) or Ni in BUOGE > Ni in Wawa-Abitibi (excluding Dumont); and Fe-Ti-V in BUOGE << Fe-Ti-V in Wawa-Abitibi. Their distinct metal contents (Cr-Ni in BUOGE versus Ni only in Abitibi) might be related to the intrinsic characteristics of the prospective units and those associated with them. First, the proportion of sulphide-rich (e.g. sulphide-facies iron formation, VMS deposits) and oxide-rich (e.g. oxide-facies iron formation) country rocks could influence if Ni-Cu-(PGE) or Cr-(PGE) mineralization is generated, respectively. It is difficult to evaluate this point at the regional-scale, as both the BUOGE superdomain and the Wawa-Abitibi terrane contain both types of units interlayered within their respective supracrustal succession and many maps/reports do not distinguish between sulphide±silicate and oxide±silicate iron formation, but we are in the process of compiling all available information. Secondly, both areas exhibit a spatial concentration of mafic and ultramafic units. In the BUOGE superdomain, a large proportion of these are Neoarchean, but the presence of Mesoarchean units in the vicinity might suggest an interaction with older intrusions and supracrustal sequences. In comparison, in the Wawa-Abitibi terrane, all mafic and ultramafic units are Neoarchean within an age range of more than 55 Ma (e.g. Houlé et al., 2017). Furthermore, their geochemical signatures are generally considered to be very juvenile with the absence of older Mesoarchean isotopic signatures (e.g. Sproule et al., 2002; Houlé and Lesher, 2011). Further detailed work will be needed to validate the significance of these factors.

ONGOING AND FUTURE WORK

In this contribution, we summarize the spatial and temporal distribution of mafic and ultramafic prospective units in conjunction with new data collection from diverse localities across the Superior Province. However, to advance our understanding of the metal endowment of the different parts of the province, a more comprehensive geological data set is crucial. In the near future, a Superior Province-wide inventory of mafic and ultramafic prospective units, including almost all magmatic Ni-Cu-(PGE), Cr-(PGE), and Fe-Ti-V deposits associated with these units, will be made available (including those contain geological resources, both compliant and non-compliant to NI-43-101).

Numerous extra steps will be necessary to have a more complete and comprehensive data set for the mafic and ultramafic prospective units across the Superior Province. In line with this, several tasks are still on-going to further advance our geoscientific knowledge:

- Improvement of the geochronological characterization of more prospective units.
- Compiling geochemical and isotopic data that will provide a more accurate assessment of the parental magmas of these prospective units.
- Continuing the compilation of prospective units across the Superior Province.

A collaborative Ph.D. study between the Metal Earth project of Laurentian University (Sudbury) and the Targeted Geoscience Initiative of the Geological Survey of Canada is currently in progress to better understand the petrogenesis and metallogenesis of polymetallic Cr-Ni-Cu-(PGE) ore systems in specific parts of the Superior Province. This research aims to advance the understanding of the spatial and possible genetic link between the Cr-(PGE) and Ni-Cu-(PGE) mineralization related to the same large intrusive event, and even within the same intrusive body, at many localities in the BUOGE superdomain (e.g. Bird River, McFaulds Lake, and Nemiscau greenstone belts).

ACKNOWLEDGMENTS

This report is a contribution to NRCan's Targeted Geoscience Initiative Program (TGI). Support for this study was provided through the Orthomagmatic Ni-Cu-PGE-Cr Ore Systems Project's 'Activity NC-2.2: Ni-Cr metallotect: Synthesis, updates and revised models for the Superior Province'.

This work has been supported over the years by numerous mining companies, in particular, Azimut

Exploration Inc., Balmoral Resources Ltd., Cliffs Natural Resources Ltd., Critical Elements Lithium Corp., Gossan Resources Ltd., Grid Metals Corp. (formerly Mustang Minerals Corp.), Harfang Exploration Inc., KWG Resources Inc., Lasalle Exploration Corp., MacDonald Mines Ltd., Midland Exploration Inc., Monarch Resources Ltd./Nemaska Exploration Inc., Noront Resources Ltd., Northern Shield Resources Inc., and Royal Nickel Corp. First, we would like to acknowledge the contribution of Riku Metsaranta from the Ontario Geological Survey (OGS) for sharing his knowledge of the McFaulds Lake greenstone belt but also stimulating discussion and for its implication for the entire Superior Province. We also would like to express our appreciation to numerous colleagues from provincial geological surveys (Ontario Geological Survey, Manitoba Geological Survey, Ministère de l'Énergie et des Ressources naturelles) and academia (Laurentian University, University of Ottawa, Université Laval) for valuable discussions about the geology of the Superior Province. We are grateful to Vicki McNicoll and Nicole Rayner from the Geological Survey of Canada (GSC) for their inputs into this project and for generating the new geochronological constraints on mafic and ultramafic intrusions across the Superior. We also acknowledge the involvement and participation of numerous researchers, students, and mining company geologists in the Orthomagmatic Ni-Cr-PGE-Cu Ore Systems Project of the Targeted Geoscience Initiative Program. We are also grateful to John Ayer (Laurentian University) and Wouter Bleeker (GSC) for their prompt and constructive reviews that helped us improve the final version of this contribution and to Elizabeth Ambrose and Valérie Bécu (GSC) for technical reviews.

REFERENCES

Bandyayera, D. and Sharma, K.N.M., 2001. Minéralisations en Ni-Cu±ÉPG dans la bande volcano-sédimentaire de Frotet-Evans (SNRC 32K); Ministère des Ressources naturelles et de la Faune du Québec, MB 2001-06, 72 p.

Baragar, W.R.A. and Scoates, R.F.J., 1981. The Circum-Superior Belt: A Proterozoic Plate Margin?; Chapter 12 *in* Precambrian Plate Tectonics, (ed.) A. Kroner; Elsevier, Developments in Precambrian Geology, v. 4, p. 297–330.

Barnes, S.-J. and Lightfoot, P.C., 2005. Formation of Magmatic Nickel Sulfide Deposits and Processes Affecting Their Copper and Platinum Group Element Contents; *in* Economic Geology 100th Anniversary Volume, (ed.) J.W. Hedenquist, J.F.H. Thompson, R.J. Goldfarb, and J.P Richards; Society of Economic Geologists, p. 179–213.

Barrie, C.T., Naldrett, A., and Davis, D., 1990. Geochemical constraints on the genesis of the Montcalm Gabbroic Complex and Ni-Cu deposit, Western Abitibi Subprovince, Ontario; The Canadian Mineralogist, v. 28, p. 451–474.

Bédard, J.H. and Harris, L.B., 2014. Neoarchean disaggregation and reassembly of the Superior craton; Geology, v. 42, p. 951–954.

Begg, G.C., Hronsky, J.A.M., Arndt, N.T., Griffin, W.L., O'Reilly, S.Y., and Hayward, N., 2010. Lithospheric, cratonic and geodynamic setting of Ni-Cu-PGE sulfide deposits; Economic Geology, v. 105, p. 1057–1070.

Begg, G.C., Hronsky, J.A.M., Griffin, W.L., and O'Reilly, S.Y., 2018. Global- to deposit-scale controls on orthomagmatic Ni-Cu-(PGE) and PGE reef ore formation; *in* Processes and Ore Deposits of Ultramafic-Mafic Magmas through Space and Time, (ed.) S.K. Mondal and W.L.Griffin; Elsevier, Netherlands, p. 1–46.

Bleeker, W., 2003. The late Archean record: A puzzle in ca. 35 pieces; Lithos, v. 71, p. 99–134.

Bleeker, W. and Ernst, R. 2006. Short-lived mantle generated magmatic events and their dyke swarms: The key unlocking Earth's paleogeographic record back to 2.6 Ga; *in* Dyke Swarms — time markers of crustal evolution, (ed.) E. Hanski, S. Mertanen, T. Rämä, and J. Vuollo; Taylor and Francis/ Balkema, United Kingdom, p. 3–26.

Card, K.D. and Ciesielski, A., 1986. Subdivisions of the Superior Province of the Canadian Shield; Geoscience Canada, v. 13, p. 5–13.

Caro, G., Morino, P., Mojzsis, S.J., Cates, N.L., and Bleeker, W., 2017. Sluggish Hadean geodynamics: evidence from coupled ^{146,147}Sm–^{142,143}Nd systematics in Eoarchean supracrustal rocks of the Inukjuak domain (Québec); Earth and Planetary Science Letters, v. 457, p. 23–37.

Carson, H.J.E., in prep. Stratigraphy, geochemistry, and petrogenesis of the Black Thor intrusion and associated Cr and Ni-Cu-PGE mineralization, McFaulds greenstone belt, Ontario; Ph.D. thesis, Laurentian University, Sudbury, Ontario.

Cassidy, K.F. and Champion, D.C., 2004. Crustal evolution of the Yilgarn Craton from Nd isotopes and granite geochronology: Implications for metallogeny; *in* SEG 2004, Predictive Mineral Discovery Under Cover, (ed.) J.R. Muhling; Centre for Global Metallogeny. University of Western Australia, p. 317–320.

Cates, N.L. and Mojzsis, S.J., 2007. Pre-3750 Ma supracrustal rocks from the Nuvvuagittuq supracrustal belt, northern Québec; Earth and Planetary Science Letters, v. 255, p. 9–21.

Corfu, F. and Stott, G.M., 1998. Shebandowan greenstone belt, Western Superior Province: U-Pb ages, tectonic implications, and correlations; Geological Society America Bulletin, v. 110, p. 1467–1484.

Corkery, M.T., Davis, D.W., and Lenton, P.G., 1992. Geochronological constraints on the development of the Cross Lake greenstone belt, northwest Superior Province, Manitoba; Canadian Journal of Earth Sciences, v. 29, p. 2171–2185.

David, J., Maurice, C., and Simard, M., 2009. Datations isotopiques effectuées dans le Nord-Est de la Province du Supérieur – Travaux de 1998, 1999 et 2000; Ministère des Ressources naturelles et de la Faune du Québec, DV 2008-05, 88 p.

DePaolo, D.J., 1981. Neodymium isotopes in the Colorado Front Range and crust-mantle evolution in the Proterozoic; Nature, v. 291, p. 193–196.

Ernst, R. and Bleeker, W., 2010. Large igneous provinces (LIPs), giant dyke swarms, and mantle plumes: Significance for breakup events within Canada and adjacent regions from 2.5 Ga to the Present; Canadian Journal of Earth Sciences, v. 47, p. 695–739.

Ernst, R.E. and Buchan, K.L., 2004. Large Igneous Provinces (LIPs) in Canada and Adjacent Regions: 3 Ga to present; Geoscience Canada, v. 31, p. 103–126.

Fiorentini, M., 2014. Mineral exploration – Out of this world; Reasearch Highlights 2014, CCFS-ARC Centre of Excellence for Core to Crust Fluid Systems, Macquarie University, Australia. <http://ccfs.mq.edu.au/AnnualReport/14Report/ResHigh.html#Mineral> [accessed June 9, 2020]

Goldfarb, R.J., Bradley, D., and Leach, D.L., 2010. Secular variation in economic geology; Economic Geology, v. 105, p. 459–465.

Goldstein, S.L., O'Nions, R.K., and Hamilton, P.J., 1984. A Sm-Nd isotopic study of atmospheric dusts and particulates from major river systems; Earth and Planetary Science Letters, v. 70, p. 221–236.

Green, A.H. and Naldrett, A.J., 1981. Langmuir volcanic peridotite-associated nickel deposits: Canadian equivalents of the Western Australian occurrences; Economic Geology, v. 76, p. 1503–1523.

Greer, J., Caro, G., Cates, N.L., Tropper, P., Bleeker, W., Kelly, N.M., and Mojzsis, S.J., 2020. Widespread poly-metamorphosed Archean granitoid gneisses and supracrustal enclaves of the southern Inukjuak Domain, Québec (Canada); Lithos, v. 364-365, p. 2–19.

Griffin, W.L., Begg, G.C., and O'Reilly, S.Y., 2013. Continental-root control on the genesis of magmatic ore deposits; Nature Geoscience, v. 6, p. 905–910.

Herzberg, C., 2004. Geodynamic information in peridotite petrology; Journal of Petrology, v. 45, p. 2507–2503.

Houlé, M.G. and Lesher, C.M., 2011. Komatiite-associated Ni-Cu-(PGE) deposits, Abitibi greenstone belt, Superior Province, Canada; *in* Magmatic Ni-Cu and PGE Deposits: geology, geochemistry, and genesis, (ed.) C. Li and E.M. Ripley; Reviews in Economic Geology, v. 17, p. 89–121.

Houlé, M.G., Gibson, H.L., Lesher, C.M., Davis, P.C., Cas, R.A.F., Beresford, S.W., and Arntd, N. T. 2008. Komatiitic sills and multigenerational peperite at Dundonald Beach, Abitibi Greenstone Belt, Ontario: volcanic architecture and nickel sulfide distribution; Economic Geology, v. 103, p. 1269–1284.

Houlé, M.G., Lesher, C.M., and Davis, P.C., 2012. Thermomechanical erosion at the Alexo Mine, Abitibi greenstone belt, Ontario: implications for the genesis of komatiite-associated Ni-Cu-(PGE) mineralization; Mineralium Deposita, v. 47, p. 105–128.

Houlé, M.G., Lesher, C.M., McNicoll, V.J., Metsaranta, R.T., Sappin, A.-A., Goutier, J., Bécu, V., Gilbert, H.P., and Yang, X.M., 2015a. Temporal and spatial distribution of magmatic Cr-(PGE), Ni-Cu-(PGE), and Fe-Ti-(V) deposits in the Bird River–Uchi–Oxford-Stull–La Grande Rivière–Eastmain domains: a new metallogenic province within the Superior Craton; *in* Targeted Geoscience Initiative 4: Canadian Nickel-Copper-Platinum Group Elements-Chromium Ore Systems — Fertility, Pathfinders, New and Revised Models, (ed.) D.E. Ames and M.G. Houlé; Geological Survey of Canada, Open File 7856, p. 35–48.

Houlé, M.G., Goutier, J., Sappin, A.-A., and McNicoll, V.J., 2015b. Regional characterization of ultramafic to mafic intrusions in the La Grande Rivière and Eastmain domains, Superior Province, Quebec; *in* Targeted Geoscience Initiative 4: Canadian Nickel-Copper-Platinum Group Elements-Chromium Ore Systems — Fertility, Pathfinders, New and Revised Models, (ed.) D.E. Ames and M.G. Houlé; Geological Survey of Canada, Open File 7856, p. 125–137.

Houlé, M.G., Lesher, C.M., and Préfontaine, S., 2017. Physical volcanology of komatiites and Ni-Cu-(PGE) deposits of the southern Abitibi greenstone belt; *in* Abitibi Base and Precious Metal Deposits, southern Abitibi greenstone belt, Canada, (ed.) T. Monecke, P. Mercier-Langevin, and B. Dubé; Reviews in Economic Geology, v. 19, p. 103–132.

Houlé, M.G., Lesher, C.M., and Sappin, A.-A., 2019. Overview of chromium, Fe-Ti-V and metal endowment of the Superior Province; *in* Targeted Geoscience Initiative: 2018 report of activities, (ed.) N. Rogers; Geological Survey of Canada, Open File 8549, p. 433–440.

Houlé, M.G., Lesher, C.M., Metsaranta, R.T., Sappin, A.-A., Carson, H.J.E., Schetselaar, E.M., McNicoll, V., and Laudadio, A., 2020. Magmatic architecture of the Esker intrusive complex in the Ring of Fire intrusive suite, McFaulds Lake greenstone belt, Superior Province, Ontario: Implications for the genesis of Cr and Ni-Cu-(PGE) mineralization in an inflationary dyke-chonolith-sill complex; *in* Targeted Geoscience Initiative 5: Advances in the understanding of Canadian Ni-Cu-PGE and Cr ore systems – Examples from the Midcontinent Rift, the Circum-Superior Belt, the Archean Superior Province, and Cordilleran Alaskan-type intrusions, (ed.) W. Bleeker and M.G. Houlé; Geological Survey of Canada, Open File 8722, p. 141–163.

Isley, A.E. and Abbott, D.H., 2002. Implications of temporal distribution of High-Mg magmas for mantle plume volcanism through time; Journal of Geology, v. 111, p. 141–158.

Isnard, H., 2003. Application des traceurs isotopiques Pb-Pb, Sm-Nd et Lu-Hf à la compréhension de l'histoire Archéenne du Bouclier Canadien et à la formation de la croûte continentale; Ph.D. thesis, Université du Québec à Montréal, Montréal, Québec, 206 p.

Johnson, J.R., 2005. Mineralization and tectonic setting of the Norton Lake region, Uchi Subprovince; M.Sc. thesis, Lakehead University, Thunder Bay, Ontario, 171 p.

Kerrich, R., Goldfarb, R.J., and Richards, J.P., 2005. Metallogenic provinces in an evolving geodynamic framework; *in* Economic Geology 100th Anniversary Volume, (ed.) J.W. Hedenquist, J.F.H. Thompson, R.J. Goldfarb, and J.P Richards; Society of Economic Geologists, p. 1097–1136.

Lahaye, Y. and Arndt, N.T., 1996. Alteration of a komatiite flow from Alexo, Ontario, Canada; Journal of Petrology, v. 37, p. 1261–1284.

Lahaye, Y., Arndt, N.T., Byerly, G., Chauvel, C., Fourcade, S., and Gruau, G., 1995. The influence of alteration on the trace element and Nd isotopic compositions of komatiites; Chemical Geology, v. 126, p. 43–64.

Layton-Matthews, D., Lesher, C.M., Burnham, O.M., Hulbert, L., Peck, D.C., Golightly, J.P., and Keays, R.R., 2010. Exploration for komatiite-associated Ni–Cu–(PGE) mineralization in the Thompson nickel belt, Manitoba; Chapter 27 *in* The Challenge of Finding New Mineral Resources: Global metallogeny, innovative exploration, and new discoveries, Volume II: Zinc-lead, nickel-copper-PGE, ad uranium, (ed.) R.J. Goldfarb, E.E. Marsh, and T. Monecke; Society of Economic Geologists, Special Publication 15, p. 513–538.

Lesher, C.M. 1989. Komatiite-associated nickel sulfide deposits; *in* Ore Deposition Associated with Magmas; (ed.) J.A. Whitney and A.J. Naldrett; Reviews in Economic Geology, v. 4, p. 44–101.

Lesher, C.M., 2017. Roles of xenomelts, xenoliths, xenocrysts, xenovolatiles, residues, and skarns in the genesis, transport, and localization of magmatic Fe–Ni–Cu–PGE sulfides and chromite; Ore Geology Reviews, v. 90, p. 465–484.

Lesher, C.M., 2019. Up, down, or sideways: emplacement of magmatic Fe-Ni-Cu-PGE sulphide melts in large igneous provinces; Canadian Journal of Earth Sciences, v. 56, p. 756–773.

Lesher, C.M. and Arndt, N.T., 1995. REE and Nd isotope geochemistry, petrogenesis and volcanic evolution of contaminated komatiites at Kambalda, Western Australia. Lithos, v. 34, p. 127–157.

Lesher, C.M. and Keays, R.R., 2002. Komatiite-associated Ni-Cu-(PGE) deposits: Mineralogy, geochemistry, and genesis; *in* The Geology, Geochemistry, Mineralogy, and Mineral Beneficiation of the Platinum-Group Elements, (ed.) L.J. Cabri;

Canadian Institute of Mining, Metallurgy, and Petroleum, Special Volume 54, p. 579–617.

Lesher, C.M., Burnham, O.M., Keays, R.R., Barnes, S.J., and Hulbert, L., 2001. Trace-element geochemistry and petrogenesis of barren and ore-associated komatiites; The Canadian Mineralogist, v. 39, p. 673–696.

Lesher, C.M., Carson, H.J.E., and Houlé, M.G., 2019. Genesis of chromite deposits by dynamic upgrading of Fe+Ti oxide xenocrysts; Geology, v. 27, p. 207–210.

Magee, C., Muirhead, J.D., Karvelas, A., Holford, S.P., Jackson, C.A.L., Bastow, I.D., Schofield, N., Stevenson, C.T.E., McLean, C., McCarthy, W., and Shtukert, O., 2016. Lateral magma flow in mafic sill complexes; Geosphere, v. 12, p.809–841.

Maier, W.D. and Groves, D.I., 2011. Temporal and spatial controls on the formation of magmatic PGE and Ni-Cu deposits; Mineralium Deposita, v. 46, p. 841–857.

Manitoba Geological Survey, 2018. Manitoba Geochronology Database – Version 1.8. <https://www.gov.mb.ca/iem/geo/gis/databases.html> [accessed January, 2018]

McNicoll, V., Goutier, J., Dubé, B., Mercier-Langevin, P., Ross, P.-S., Dion, C., Monecke, T., Legault, M., Percival, J., and Gibson, H., 2014. U-Pb geochronology of the Blake River Group, Abitibi greenstone belt, Quebec, and implications for base metal exploration; Economic Geology, v. 109, p. 27–59.

McNicoll, V., Dubé, B., Castonguay, S., Oswal, W., Biczokd, J., Mercier-Langevin, P., Skulski, T., and Malo, M., 2016. The world-class Musselwhite BIF-hosted gold deposit, Superior Province, Canada: New high-precision U–Pb geochronology and implications for the geological setting of the deposit and gold exploration; Precambrian Research, v. 272, p. 133–149.

Menard, T., Lesher, C.M., Stowell, H.H., Price, D.P., Pickell, J.R., and Hulbert, L., 1996. Geology, genesis, and metamorphic history of the Namew Lake Fe-Ni-Cu-PGE deposit, Manitoba; Economic Geology, v. 91, p. 1394–1413.

Mole, D.R., Fiorentini, M.L., Cassidy, K.F., Kirkland, C.L., Thebaud, N., McCuaig, T.C., Doublier, M.P., Duuring, P., Romano, S.S., Maas, R., Belousova, E., Barnes, S.J., and Miller, J., 2013. Crustal evolution, intra-cratonic architecture and the metallogeny of an Archaean craton; *in* Ore Deposits in an Evolving Earth, (ed.) G.R.T. Jenkin, P.A.J. Lusty, I. McDonald, M.P. Smith, A.J. Boyce, and J.J. Wilkinson; Geological Society of London, Special Publications 393, p. 23–80.

Mole, D.R., Kirkland, C.L., Fiorentini, M.L., Barnes, S.J., Cassidy, K.F., Isaac, C., Belousova, E.A., Hartnady, M., and Thebaud, N., 2019. Time-space evolution of an Archean craton: A Hf-isotope window into continent formation; Earth-Science Reviews, v. 196, p. 1–46.

Mortensen, J.K., 1993. U-Pb geochronology of the eastern Abitibi Subprovince. Part 1: Chibougamau – Matagami – Joutel Region; Canadian Journal of Earth Sciences, v. 30, p. 11–28.

Moukhsil, A., Legault, M., Boily, M., Doyon, J., Sawyer, E., and Davis, D., 2007. Geological and metallogenic synthesis of the Middle and Lower Eastmain greenstone belt (Baie James); Ministère des Resources naturelles du Québec, ET-2007-01, 55 p.

Mungall, J.E., 2013. Polymetallic Ni-Cu-PGE-Cr-Fe-Ti-V and VMS mineralization in the Ring of Fire Intrusive Suite, Ontario; Prospectors and Developers Association of Canada Annual Convention–PDAC 2013, Technical Program, Toronto, March 5th, 2013.

Mungall, J.E., Harvey, J.D., Balch, S.J., Azar, B., Atkinson, J., and Hamilton, M.A., 2010. Eagle's Nest: A magmatic Ni-sulfide deposit in the James Bay Lowlands, Ontario, Canada; *in* Chapter 28 *in* The Challenge of Finding New Mineral Resources: Global metallogeny, innovative exploration, and new discoveries, Volume II: Zinc-lead, nickel-copper-PGE, ad uranium, (ed.) R.J. Goldfarb, E.E. Marsh, and T. Monecke; Society of Economic Geologists, Special Publication 15, p. 539–559.

Naldrett, A.J. 2004. Magmatic sulfide deposits: geology, geochemistry and exploration; Springer, Germany, 727 p.

Naldrett, A.J., 2010. Secular variation of magmatic sulfide deposits and their source magmas; Economic Geology, v. 105, p. 669–688.

O'Neil, J., Carlson, R.W., Paquette, J-L., and Francis, D., 2012. Formation Age and Metamorphic History of the Nuvvuagittuq Greenstone Belt; Precambrian Research, v. 220-221, p. 23–44.

Ontario Geological Survey, 2011. Bedrock geology of Ontario; Ontario Geological Survey, Miscellaneous Release–Data 126, Revision 1, scale 1:250 000.

Ontario Geological Survey, 2019. Geochronology Inventory of Ontario—2019. <http://www.geologyontario.mndm.gov.on.ca/mndmaccess/mndm_dir.asp?type=pub&id=GeochrON> [accessed June 30, 2019]

Parks, J., Lin, S., Davis, D.W., Yang, X.-M., Creaser, R.A., and Corkery, M.T., 2014. Meso- and Neoarchean evolution of the Island Lake greenstone belt and the northwestern Superior Province: Evidence from lithogeochemistry, Nd isotope data, and U-Pb zircon geochronology; Precambrian Research, v. 246, p. 160–179.

Peck, D.C., Theyer, P., Hulbert, L.J., Xiong, J., Fedikow, M.A.F., and Cameron, H.D.M., 2000. Preliminary Exploration Database for Platinum Group Elements (PGE) in Manitoba; Manitoba Geological Survey, Open File Report OF2000-5, (CD-ROM).

Percival, J.A., Skulski, T., Sanborn-Barrie, M., Stott, G.M., Leclair, A.D., Corkery, M.T., and Boily, M., 2012. Geology and tectonic evolution of the Superior Province, Canada; *in* Tectonic Styles in Canada: The LITHOPROBE Perspective, (ed.) J.A. Percival, F.A. Cook and R.M. Clowes; Geological Association of Canada, Special Paper 49, p. 321–378.

Préfontaine, S., Buse, S., Davis, D.W., Hamilton, M.A., and Stott, G.M., 2008. Geology of the North Spirit Lake area located in the North Spirit Lake greenstone belt, northwestern Ontario; *in* Summary of Field Work and Other Activities 2008; Ontario Geological Survey, Open File Report 6226, p.42-1 to 42-15.

Sanborn-Barrie, M., Rogers, N., Skulski, T., Parker, J., McNicoll, V., and Devaney, J., 2004. Geology and tectonostratigraphic assemblages, East Uchi Subprovince, Red Lake and Birch–Uchi belts, Ontario; Geological Survey of Canada, Open File 4256, or Ontario Geological Survey, Preliminary Map P.3460, scale 1:250 000.

Sappin, A.-A., Houlé, M.G., Lesher, C.M., McNicoll, V., Vaillancourt, C., and Kamber, B.S., 2016. Age constraints and geochemical evolution of the Neoarchean mafic–ultramafic Wabassi Intrusive Complex in the Miminiska–Fort Hope greenstone belt, Superior Province, Canada; Precambrian Research, v. 286, p. 101–125.

Scoates, J.S. and Scoates, R.F.J., 2013. Age of the Bird River Sill, southeastern Manitoba, Canada, with implications for the secular variation of layered intrusion-hosted stratiform chromite mineralization; Economic Geology, v. 108, p. 895–907.

SIGÉOM, 2020. Système d'information géominière du Québec. Ministère de l'Énergie et des Ressources naturelles. <http://sigeom.mines.gouv.qc.ca> [accessed February 9, 2020]

Sleep, N.H., 2006. Mantle plumes from top to bottom; Earth-Science Reviews, v. 77, p. 231–271.

Sotiriou, P., Polat, A., Frei, R., Yang, X.-M., and van Vessem, J., 2019. A back-arc origin for the Neoarchean megacrystic anorthosite-bearing Bird River Sill and the associated green-

stone belt, Bird River subprovince, Western Superior Province, Manitoba, Canada; International Journal of Earth Sciences, v. 108, p. 2177–2207.

Sproule, R.A., Lesher, C.M., Ayer, J.A., and Thurston, P.C., 2002. Spatial and temporal variations in the geochemistry of komatiitic rocks in the Abitibi greenstone belt and implications for their tectonic setting; Precambrian Research, v. 115, p. 153−186.

Stone, D., 2010. Precambrian geology of the central Wabigoon Subprovince area, northwestern Ontario; Ontario Geological Survey, Open File Report 5422, 130 p.

Stone, D., Lavigne, M.J., Schnieders, B., Scott, J., and Wagner, D., 2003. Regional geology of the Lac des Iles Area; *in* Summary of Field Work and Other Activities 2003; Ontario Geological Survey, Open File Report 6120, p.15-1 to 15-2.

Stott, G.M., Corkery, M.T., Percival, J.A., Simard, M., and Goutier, J., 2010. A revised terrane subdivision of the Superior Province; *in* Summary of Field Work and Other Activities 2010; Ontario Geological Survey, Open File Report 6260, p. 20-1 to 20-10.

Thériault, R. and Beauséjour, S., 2012. Geological map of Quebec, 2012 Edition; Ministère des Ressources naturelles du Quebec, DV 2012-07, scale 1 :2 000 000.

Tucker, M.J., Wagner, D., and Houlé, M.G., 2019. The Grasset Ultramafic Complex – A new nickel district in the northern Abitibi greenstone belt, Canada; Society for Geology Applied to Mineral Deposits, Proceedings of the 15th SGA Biennial Meeting, p. 497–500.

Vaillancourt, C., Sproule, R.A., MacDonald, C.A., and Lesher, C.M. 2003. Investigation of mafic-ultramafic intrusions in Ontario and implications for platinum group element mineralization: Operation Treasure Hunt; Ontario Geological Survey, Open File Report 6102, 335 p.

Viljoen, D., Chackowsky, L.E., and Lenton, P.G., 1999. Geology, magnetic and gravity maps of Manitoba: a digital perspective; Manitoba Energy and Mines, Geological Services, Open file 99-12, 1 CD-ROM.

Wardle, R.J., Gower, C.F., Ryan, B., Nunn, G.A.G., James, D.T., and Kerr, A., 1997. Geological Map of Labrador; Government of Newfoundland and Labrador, Department of Mines and Energy, Geological Survey, Map 97-07, scale 1:1 000 000.

Whittaker, P.J., 1986. Chromite deposits in Ontario; Ontario Geological Survey, Study 55, 97 p.

Williams, H., Hoffman, P.F., Lewry, J.F., Monger, J.W.H., and Rivers, T., 1991. Anatomy of North America: thematic geologic portrayals of the continent; Tectonophysics, v. 187, p. 117–134.

Zhou, S., Polat, A., Longstaffe, F. J., Yang, K.G., Fryer, B.J., and Weisener, C., 2016. Formation of the Neoarchean Bad Vermilion Lake Anorthosite Complex and spatially associated granitic rocks at a convergent plate margin, Superior Province, Western Ontario, Canada; Gondwana Research, v. 33, p. 134–159.

Magmatic architecture of the Esker intrusive complex in the Ring of Fire intrusive suite, McFaulds Lake greenstone belt, Superior Province, Ontario: Implications for the genesis of Cr and Ni-Cu-(PGE) mineralization in an inflationary dyke-chonolith-sill complex

Michel G. Houlé[1,*], C. Michael Lesher[2], Riku T. Metsaranta[3], Anne-Aurélie Sappin[1], Heather J.E. Carson[2], Ernst M. Schetselaar[4], Vicki McNicoll[4], and Alexandra Laudadio[5]

[1]Geological Survey of Canada, 490 rue de la Couronne, Québec, Quebec G1K 9A9
[2]Department of Earth Sciences, Mineral Exploration Research Centre, Goodman School of Mines, Laurentian University, 935 Ramsey Lake Road, Sudbury, Ontario P3E 2C6
[3]Ontario Geological Survey, 933 Ramsey Lake Road, Sudbury, Ontario P3E 6B5
[4]Geological Survey of Canada, 601 Booth Street, Ottawa, Ontario K1A 0E8
[5]Carleton University, Department of Earth Sciences, 1125 Colonel By Drive, Ottawa, Ontario K1S 5B6
[*]Corresponding author's e-mail: michel.houle@canada.ca

ABSTRACT

One of the dominant geological features in the arcuate, >175 km long, Mesoarchean to Neoarchean McFaulds Lake greenstone belt in northern Ontario is the semi-continuous trend of mafic to ultramafic intrusions belonging to the Ring of Fire intrusive suite, which hosts world-class Cr mineralization, major Ni-Cu-(PGE) mineralization, and potentially significant Fe-Ti-V-(P) mineralization. It appears to have been emplaced over a relatively short time interval of approximately 4 to 4.5 million years. The intrusive suite contains two subsuites: the less widely distributed Koper Lake subsuite, which consists of komatiitic ultramafic-dominated intrusions and typically hosts Cr and Ni-Cu-(PGE) mineralization (e.g. Esker intrusive complex), and the more widely distributed Ekwan River subsuite, which consists of tholeiitic high-Fe-Ti mafic-dominated intrusions and typically hosts Fe-Ti-V-(P) mineralization (e.g. Thunderbird intrusion).

The Esker intrusive complex contains the majority of the known Cr and Ni-Cu-(PGE) mineralization in the Ring of Fire intrusive suite. It is a semi-continuous, structurally rotated, subvertical ultramafic-mafic sill-like body that is composed of multiple intrusions with morphologies that vary from bladed dyke morphologies (e.g. Eagle's Nest), transitional dyke/chonolith morphologies (e.g. Double Eagle, AT-3, and AT-8), to some with transitional chonolith/sill morphologies (e.g. Black Thor). It extends over more than 16 km, youngs to the south-southeast, and is bordered to the north-northwest by several keel-like ultramafic intrusive bodies (e.g. AT-12, C-6, AT-5, AT-1). Clear connections between AT-12 and AT-1 and the overlying Black Thor and Double Eagle intrusions, respectively, and the continuous spectrum of intrusion morphologies suggest that the keels were originally subhorizontal blade-shaped dykes (e.g. Eagle's Nest), the upper parts of which expanded laterally to form transitional dykes/chonoliths (e.g. Double Eagle intrusion) and chonoliths/sills (e.g. Black Thor intrusion), which inflated laterally and coalesced over time to form the sill-like Esker intrusive complex.

Most of the Ni-Cu-(PGE) mineralization in the Esker intrusive complex appears to have formed by incorporation of sulphur from footwall oxide-silicate-sulphide iron formations, a process that is similar to most other komatiite-associated Ni-Cu-(PGE) deposits worldwide. A fundamental issue in the genesis of all stratiform chromite deposits is how to form thick layers of massive to semi-massive chromite, an issue exacerbated by the vast amounts of chromite in the Esker intrusive complex. A genetic model that resolves the mass balance problem involves partial melting of Fe±Ti oxide-rich rocks (oxide-facies iron formation or ferrogabbro) and conversion of fine-grained oxide xenocrysts to chromite by reaction with Cr-rich komatiitic magma in a dynamic magma conduit. This model has been recently challenged based on the capacity of komatiitic magma to dissolve large amounts of magnetite, which would prevent upgrading. However, alternative models cannot explain the presence of composite chromite-silicate-sulphide grains with textures like

Houlé, M.G., Lesher, C.M., Metsaranta, R.T., Sappin, A.-A., Carson, H.J.E., Schetselaar, E.M., McNicoll, V., and Laudadio, A., 2020. Magmatic architecture of the Esker intrusive complex in the Ring of Fire intrusive suite, McFaulds Lake greenstone belt, Superior Province, Ontario: Implications for the genesis of Cr and Ni-Cu-(PGE) mineralization in an inflationary dyke-chonolith-sill complex; *in* Targeted Geoscience Initiative 5: Advances in the understanding of Canadian Ni-Cu-PGE and Cr ore systems – Examples from the Midcontinent Rift, the Circum-Superior Belt, the Archean Superior Province, and Cordilleran Alaskan-type intrusions, (ed.) W. Bleeker and M.G. Houlé; Geological Survey of Canada, Open File 8722, p. 141–163. https://doi.org/10.4095/326892

those in footwall magnetite-silicate-sulphide facies iron formations. More research is required to reconcile the discrepancies.

Regardless of their origin, the wide diversity of mineral deposit types in the McFaulds Lake greenstone belt, including world-class Cr, significant Ni-Cu-(PGE), and potential Fe-Ti-V-(P) mineralization related to mafic and ultramafic rocks, make the Ring of Fire region an excellent exploration target to increase the world's supply of critical minerals.

INTRODUCTION

The Mesoarchean to Neoarchean McFaulds Lake greenstone belt (a.k.a. Ring of Fire region; Metsaranta and Houlé, 2020) in northern Ontario is recognized as one of the next emerging major mineral districts in Canada, containing world-class magmatic Cr deposits, a major Ni-Cu-(PGE) deposit and numerous occurrences, small volcanogenic massive Cu-Zn sulphide deposits, significant Fe-Ti-V-(P) prospects, and several kimberlitic diamond and orogenic Au occurrences (*see* Metsaranta and Houlé, 2020).

Over the past decade, the Geological Survey of Canada (GSC) and the Ontario Geological Survey (OGS), in collaboration with numerous exploration companies and academic collaborators, have undertaken a diverse range of geoscience activities in the Ring of Fire region. This research has significantly increased our knowledge of the Cr, Ni-Cu-(PGE) and Fe-Ti-V-(P) mineralized ultramafic to mafic intrusions and their overall geological context (Metsaranta and Houlé, 2020 and references therein).

In this contribution, we summarize the main characteristics of the McFaulds Lake greenstone belt, the Ring of Fire intrusive suite, and their associated orthomagmatic Cr, Ni-Cu-(PGE), and Fe-Ti-V mineralization, and briefly address some key components of the magmatic architecture of this well endowed ultramafic to mafic ore system in northern Ontario.

McFAULDS LAKE GREENSTONE BELT

The geology of the Ring of Fire region, located in the central part of the northern Superior Province, comprises a variety of Precambrian supracrustal and intrusive rocks, flat-lying Paleozoic cover rocks, and Quaternary deposits. The poorly exposed Precambrian geology includes Mesoarchean to Neoarchean supracrustal rocks of the McFaulds Lake greenstone belt and a variety of felsic to ultramafic intrusive rocks (Fig. 1), as well as Proterozoic dyke swarms (Matachewan, Marathon, Pickle Crow, Mackenzie: Stott and Josey, 2009) and kimberlitic intrusions (Kyle Lake kimberlites: Sage, 2000). The paucity of outcrop was one of the major reasons for the lack of interest in this region from the provincial/federal geological surveys and mineral explorers until the discoveries of the Kyle diamondiferous kimberlites in the mid-1990s. The subsequent discovery of the McFaulds Cu-Zn volcanogenic massive sulphide (VMS)-style mineralization in 2002 led to an increase of exploration efforts in the region and the discovery of the Big Daddy Cr mineralization in 2006 and the Eagle One (now known as Eagle's Nest) Ni-Cu-(PGE) mineralization in 2007 (*see* Exploration History for more details in Metsaranta and Houlé, 2020).

The McFaulds Lake greenstone belt is an arcuate (>175 km long) greenstone belt that records episodic volcanism and sedimentation spanning from ca. 2.83 Ga to 2.70 Ga (e.g. Metsaranta et al., 2015; Metsaranta and Houlé, 2020). It has been subdivided into eight lithotectonic assemblages: two late Mesoarchean to early Neoarchean assemblages comprising volcanic rocks of mostly tholeiitic affinity with lesser amounts of volcanic rocks of komatiitic and calc-alkalic affinities (Butler: ca. 2828 Ma; Attawapiskat: ca. 2820–2797 Ma); two early Neoarchean volcanic-dominated assemblages of tholeiitic and calc-alkalic affinities (Victory: ca. 2783–2780 Ma; Winiskisis: ca. 2757 Ma); three middle Neoarchean assemblages dominated by volcanic rocks of calc-alkalic affinity with minor amounts of volcanic rocks with tholeiitic and komatiitic affinities (Muketei: ca. 2737–2734 Ma; Oval: >2711 Ma; Kitchie: <2725 Ma); and one very poorly exposed sedimentary rock-dominated assemblage (Tappan: <2702 Ma) (Fig. 2; Metsaranta and Houlé, 2020).

One particularity of the McFaulds Lake greenstone belt that was highlighted by recent OGS and GSC work is that almost the entire metal endowment of the Ring of Fire region is closely associated with the 2737–2734 Ma Muketei assemblage and the widespread, coeval mafic to ultramafic magmatism of the Ring of Fire intrusive suite, which includes the well endowed ultramafic to mafic Esker intrusive complex (Fig. 2).

The McFaulds Lake greenstone belt, like most other Archean greenstone belts across the Superior Province, experienced several phases of deformation and metamorphism, up to upper amphibolite facies that affected, to varying degrees, the preservation of this greenstone belt (*see* Metsaranta and Houlé, 2020). In the central part of the McFaulds Lake greenstone belt, metamorphic grades appear to be lower than elsewhere in the belt. The Esker intrusive complex displays well preserved igneous textures, has been metamorphosed to the lower to middle greenschist facies, and is only

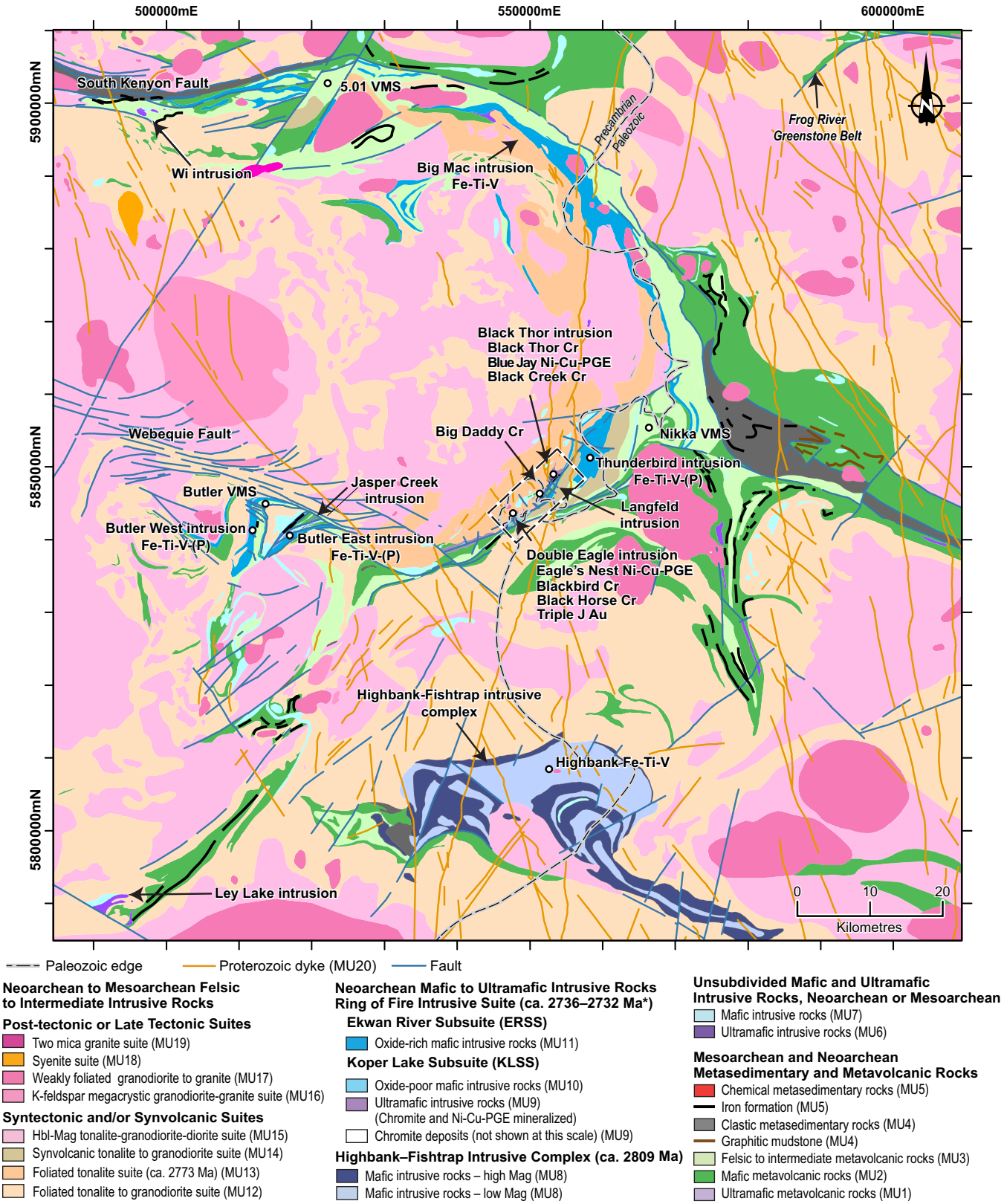

Figure 1. Geological map of the McFaulds Lake and southeast extension of the Frog River greenstone belts showing the location of the main mineral deposits and occurrences in the Ring of Fire region (*modified from* Metsaranta and Houlé, 2017a,b,c). Paleozoic cover rocks occur to the east of the Paleozoic edge line. Trace of the fold axial plane is omitted for clarity. Dashed black box indicates the location of Figure 5. Cooridnates in Universal Transverse Mercator (UTM)–North America Datum 1983 (NAD83)–Zone 16. Abbreviations: Hbl = hornblende, K-feldspar = potassium feldspar, Mag = magnetite, MU = map units used in Metsaranta and Houlé (2017a,b,c, 2020). *The age interval for the Ring of Fire intrusive suite is rounded and takes errors into account.

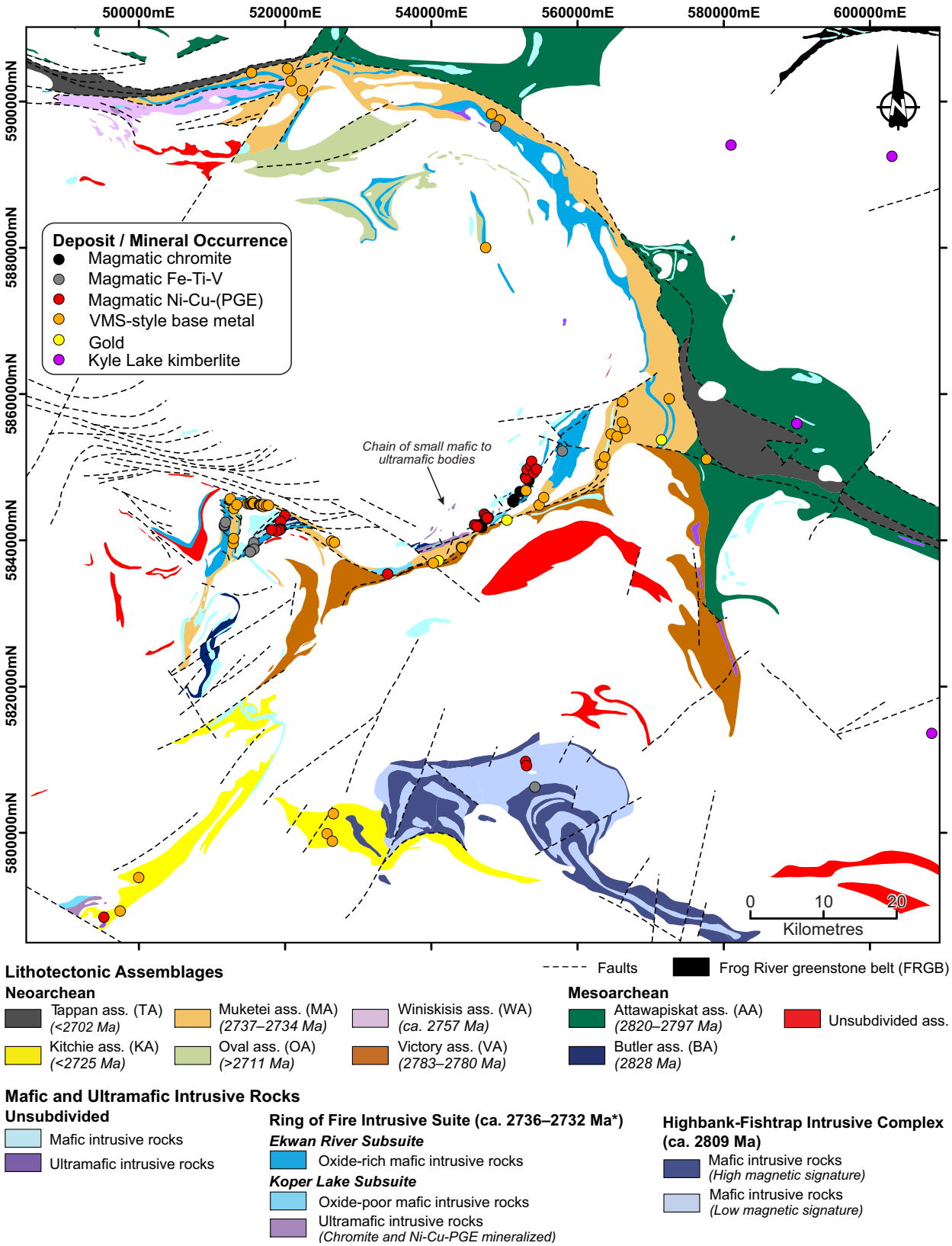

Figure 2. Simplified geological map showing the distribution of the lithotectonic assemblages for supracrustal rocks and the distribution of mafic to ultramafic intrusions in the McFaulds Lake greenstone belt (*modified from* Metsaranta and Houlé, 2020). Coordinates in UTM NAD83, Zone 16. Abbreviations: ass. = assemblage as defined by Metsaranta and Houlé (2020), VMS = volcanogenic massive sulphides. *The age interval for the Ring of Fire intrusive suite is rounded and takes errors into account.

locally deformed, in which most of the rocks do not exhibit any strong penetrative structural fabrics.

Ring of Fire Intrusive Suite

The dominant mafic and ultramafic intrusions in the Ring of Fire region represent a large mafic to ultramafic magmatic event recognized as the Ring of Fire intrusive suite (e.g. Mungall et al., 2011; Houlé et al., 2015; Metsaranta et al., 2015), which were emplaced along the entire strike length of the McFaulds Lake greenstone belt over a relatively short time period of a few million years (*see* Timing and Relationship of Koper Lake and Ekwan River Subsuites; Fig. 2). Two major types of mafic to ultramafic intrusions have been recognized in the McFaulds Lake greenstone belt (e.g. Metsaranta et al., 2015; Houlé et al., 2015) and have been subdivided by Houlé et al. (2019) into the Ekwan River and the Koper Lake subsuites based on their spatial distribution, lithological association, geochemical signature, and mineralization styles.

Ekwan River subsuite

The Ekwan River subsuite is dominated by Fe-oxide-bearing mafic rocks and is composed of abundant gabbro, melagabbro, and leucogabbro with lesser anorthosite and rare pyroxenite. This subsuite occurs over the entire length of the McFaulds Lake greenstone belt (Fig. 1, 2). It hosts most of the Fe-Ti-V-(P) mineralization in the region, the best examples being the Thunderbird, Butler West, Butler East (Kuzmich et al., 2015), and Big Mac (Sappin et al., 2015) intrusions, which are relatively continuous over significant strike lengths and exhibit strong geophysical anomalies (OGS–GSC, 2011). Almost all of these intrusions contain significant amounts of fine-grained disseminated and lesser semi-massive to massive Fe-Ti-V oxides (e.g. titanomagnetite, magnetite, ilmenite), whereas only a few contain phosphates (apatite). The mineralization is texturally similar from one intrusion to another and occurs in rocks ranging in composition from melagabbro to anorthosite. The Fe-Ti-V ore horizon in the Thunderbird intrusion generally occurs as a thick (100s of metres) interval of disseminated magnetite-ilmenite with sparse, thin (up to 45 cm thick), semi-massive to massive oxide layers (Kuzmich, 2014). In contrast, Fe-Ti-V ore horizons in the Butler intrusions (i.e. Butler East and West intrusions) generally occur as interlayered semi-massive to massive oxides (up to 24 m thick) and heavily disseminated oxides in gabbroic rocks (Kuzmich, 2014).

Rocks of the Ekwan River subsuite range from Mg-Cr-Ti-poor, Al-rich mesogabbro to Mg-Cr-poor, Al-Ti rich ferrogabbro, consistent with fractionation and accumulation of clinopyroxene-plagioclase-ilmenite (Fig. 3). They include Fe-Ti-V-rich, Mg-poor oxide mineralization (Fig. 3a,b,g,h).

Koper Lake subsuite

The Koper Lake subsuite is dominated by ultramafic rocks and is composed of variably serpentinized and/or talc-carbonate-altered dunite, peridotite, chromitite, pyroxenite, and gabbro. This subsuite is relatively restricted geographically, occurring predominantly in the central part of the McFaulds Lake greenstone belt but locally on its peripheries (e.g. Ley and Wi intrusions; Fig. 1, 2). It hosts most of the orthomagmatic Cr and Ni-Cu-PGE mineralization, the best examples of which occur in the Black Thor (Carson et al., 2015, 2016; Carson, in prep) and Double Eagle intrusions (Azar, 2010), and the Eagle's Nest dyke (Mungall et al., 2010; Zuccarelli et al., 2017, 2018a,b, 2020; Zuccarelli, in prep) of the Esker intrusive complex (Houlé et al., 2019). These styles of mineralization are briefly summarized below (*see* Orthomagmatic Mineralization).

Rocks of the Koper Lake subsuite range from Mg±Cr rich, Al-Ti-poor dunite, peridotite, and pyroxenite that exhibit trends consistent with fractionation and accumulation of olivine±chromite to Mg-Cr-poor, Al-Ti rich mesogabbro that exhibits trends consistent with fractionation of clinopyroxene-plagioclase± ilmenite. They include Cr-Al-Mg-rich, Ti-V-poor chromite mineralization (Fig. 3). Two distinct trends are shown in Figure 3 that are characteristic of the Koper Lake and Ekwan River subsuites. The Koper Lake subsuite generally exhibits higher values of Ni and Cr whereas the Ekwan River subsuite generally exhibits higher values of Ti and V (Fig. 3b,d–h). This clear geochemical distinction can be used to correctly discriminate between the two subsuites.

Timing and relationship of the Koper Lake and Ekwan River subsuites

U-Pb single zircon thermal ionization mass spectrometry (TIMS) dating indicates that the Ring of Fire intrusive suite was emplaced over a period of 4 to 4.5 million years between 2736.3 to 2731.8 Ma[1] (Table 1). The oldest date obtained is from the mafic component of the Big Daddy segment of the Black Thor intrusion at ca. 2735.5 ± 0.8 Ma, whereas the youngest dates are from the Wi intrusion at 2732.9 ± 0.6 Ma and the Croal Lake intrusion at 2732.6 ± 0.8 Ma, belonging to the Koper Lake and Ekwan River subsuites, respectively (Table 1). Attempts to date the ultramafic part of the Black Thor intrusion have thus far not been successful, but a late websterite phase that crosscuts the lower part

[1] This age interval for the emplacement of the Ring of Fire intrusive suite has been estimated from the oldest and youngest ages obtained, including the errors on these ages, making this a maximum time duration for its emplacement.

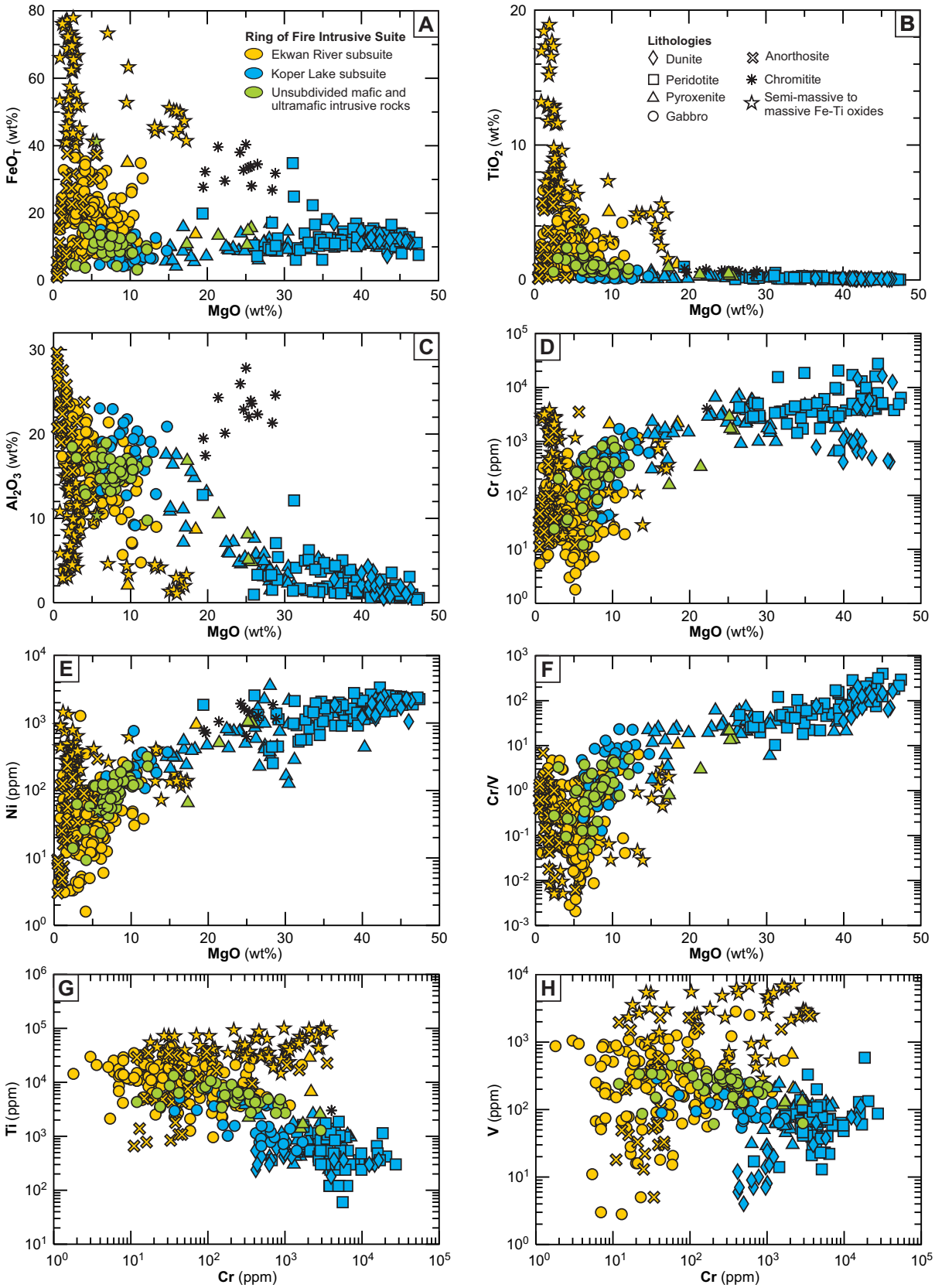

Figure 3. Binary plots of major and trace elements (anhydrous and normalized to 100%) of the mafic to ultramafic intrusions within the Koper Lake and Ekwan River subsuites of the Ring of Fire intrusive suite. **a)** FeO_T versus MgO, **b)** TiO_2 versus MgO, **c)** Al_2O_3 versus MgO, **d)** Cr versus MgO, **e)** Ni versus MgO, **f)** Cr/V versus MgO, **g)** Ti versus Cr, and **h)** V versus Cr. The shape of the symbol indicates the rock types whereas the colour indicates the subsuite to which they belong. Data are *from* Kuzmich et al. (2015), Metsaranta (2017), and Houlé, unpublished data.

Table 1. Lithodemic unit classification scheme as proposed by Houlé et al. (2019) for mafic-ultramafic intrusive rocks in the Ring of Fire intrusive suite with their associated mineralization and age constraints.

Suite	Subsuite	Complex	Lithodeme		U-Pb Age (Ma)	Magmatic Mineralization*
			Intrusion	Segment		
Ring of Fire Intrusive Suite (RoFIS)	Koper Lake Subsuite	Esker Intrusive Complex (EIC)	Black Thor	Black Thor	2734.1±0.6 and 2733.6±0.7	**BT, BL** BJ, BJE, BCZ, NEBZ, CBZ, SWBZ, NOT-08-2G15, NOT-08-2G28
				Black Creek	*Undated*	**BC**
				Big Daddy	2735.5±0.8 and 2733.7±0.8	**BD**
				C-3/C-4	*Undated*	FN-10-21
			C6		*Undated*	–
			AT-5		*Undated*	–
			Double Eagle	AT-1	*Undated*	**BH**, EZ, FN-08-10 FN-08-02, FN-10-01
				Blackbird	*Undated*	**BB1, BB2**, ET
			Eagle's Nest		*Undated*	**EN**
			Wi		2732.9±0.6	–
			Ley Lake		*Undated*	–
			Jasper Creek		*Undated*	–
	Ekwan River Subsuite		Butler West		*No zircon*	BP11-V01/V06/V07
			Butler East		*No zircon*	BP11-V05/V04, MN08-82, McNugget
			Thunderbird		2733.6±0.7	Thunderbird Anomaly
			Big Mac		2734.1±0.8	BM9B-04
			Langfeld		*Undated*	Unamed
			Croal Lake**		2732.6±0.8	Semple-Hulbert
			Pinay		*Pending*	Unamed

*Mineralization text: bold text = deposit, non-bold text = occurrence, black text = Cr-(PGE), red text = Ni-Cu-(PGE), green text = Fe-Ti-V-(P).

**Croal Lake intrusion is not shown on Figure 1. It is located approximately 50 km west-northwest of the northwest corner of the mapping area shown in Figure 1. Geochronology data *from* Houlé et al. (2015a) and this study.

See Figure 5 for abbreviations. NOT-08-2G15 or other combinations are drillhole identifications.

of the intrusion has been dated at 2733.6 ± 0.7 Ma. The textures along the contact between the late websterite phase and the lower part of the Black Thor intrusion suggest that they are more or less coeval (Spath, 2017), suggesting that the Esker intrusive complex was emplaced within an interval of 1.8 to 3.4 million years.

A younger age (2730.5 ± 0.8 Ma) was obtained in the McFaulds Lake greenstone belt for a biotite-bearing gabbro that crosscuts the Black Thor intrusion and it is therefore interpreted to be unrelated to the Ring of Fire intrusive suite (Houlé et al., 2019). Overall, no significant age differences have been observed between intrusions that belong to either the Koper Lake or the Ekwan River subsuites.

Esker intrusive complex

The Esker intrusive complex is a semi-continuous, subvertical ultramafic-mafic body comprising multiple intrusions (e.g. Black Thor, Double Eagle, AT-3, and AT-8) that extends for 16 km from Black Thor intrusion in the northeast to the AT-8 intrusion in the southwest (Fig. 4). The Esker intrusive complex includes several keel-like ultramafic intrusive bodies (e.g. AT-12, C-6, AT-5, AT-1, and Eagle's Nest) to the north-northwest that extend 650–900 m into the granitoid country rocks (Fig. 4). A few distinct magnetic anomalies, which are interpreted to correspond to other ultramafic to mafic intrusive bodies, potentially extend the footprint of the Esker intrusive complex for another 4 km to the southwest.

The base (northwest side) of the Esker intrusive complex is usually in contact with ca. 2773 Ma (e.g. Mungall et al., 2010; Metsaranta et al., 2015; Metsaranta and Houlé, 2020) tonalitic rocks that are locally baked and intruded by the Esker intrusive complex. However, the sparse geological information along the base of the Esker intrusive complex and the presence of thin granitoids within the complex cannot completely discount the possibility that locally younger granitoids may have been intruded along the basal con-

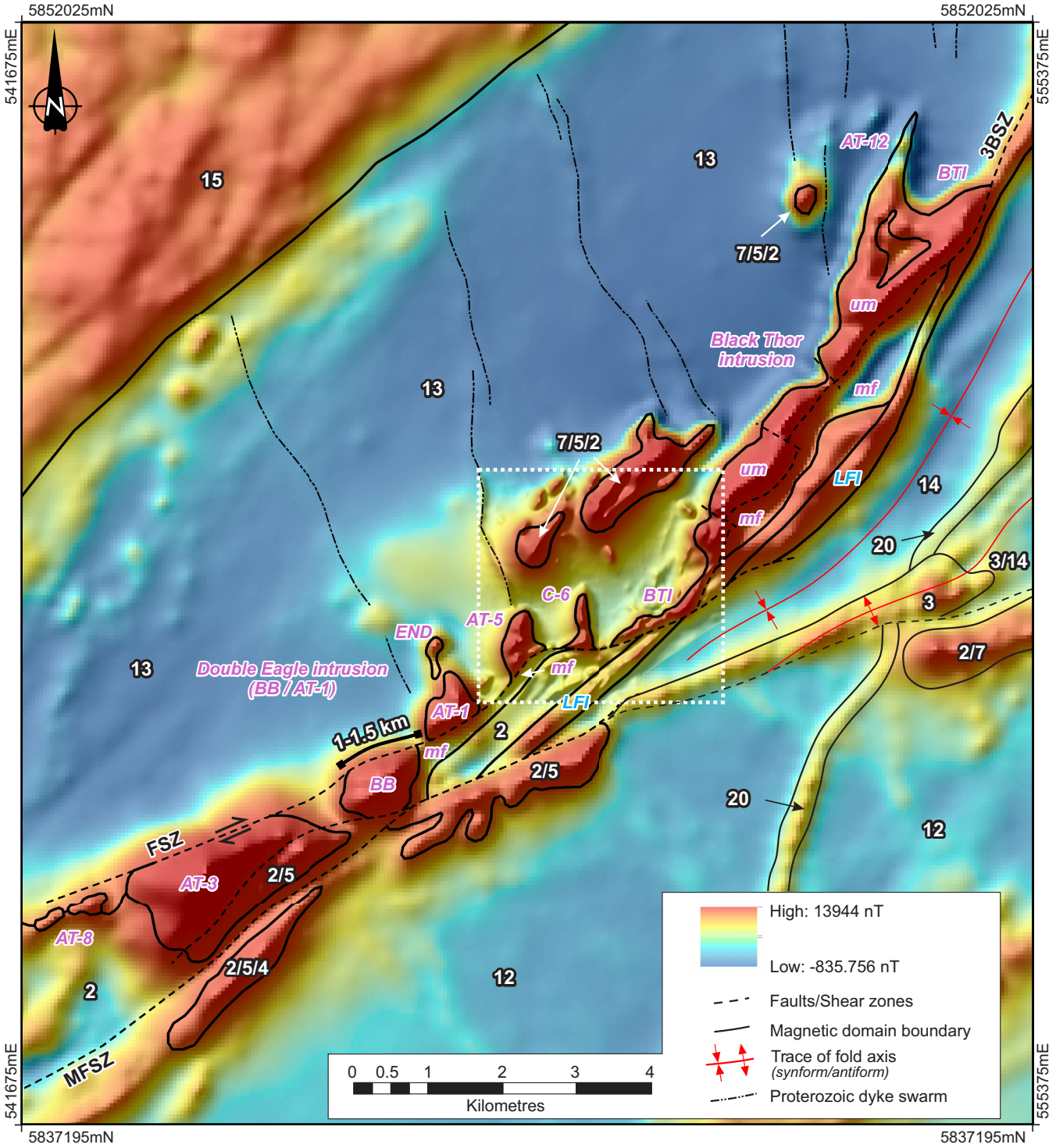

Figure 4. Colour-relief-shaded magnetic data, displayed with histogram equalization, overlain with the revised structural interpretation and magnetic domain boundaries showing the distribution of mafic to ultramafic intrusive bodies of the Esker intrusive complex (*modified from* Laudadio, 2019). White dotted box highlights proprietary high-resolution magnetic data (gridded from 75 m line spacing). Black text labels are faults: FSZ = Frank Shear Zone, MFSZ = McFaulds Lake Shear Zone, 3BSZ = Black Thor-Black Creek-Big Daddy Shear Zone. Purple text labels are part of the Koper Lake subsuite: BTI = Black Thor intrusion, DEI = Double Eagle intrusion, END = Eagle's Nest dyke, mf = mafic component, um = ultramafic component. Blue text labels are part of the Ekwan River subsuite: LFI = Langfeld intrusion. White text labels are map units: 2 = mafic metavolcanic rocks, 3 = felsic to intermediate metavolcanic rocks, 4 = graphitic mudstone, 5 = iron formation and graphitic mudstone, 7 = unsubdivided mafic intrusive rocks, 12 = foliated tonalite to granodiorite suite, 13 = foliated tonalite suite, 14 = synvolcanic tonalite to granodiorite suite, 15 = hornblende-magnetite tonalite-granodiorite-diorite suite, 20 = Proterozoic dyke swarm. Numbers are consistent with the map units in Figure 1.

tact. The tonalitic footwall rocks contain kilometric enclaves of supracrustal rocks, as shown on Figure 5, composed predominantly of mafic intrusive and volcanic rocks within oxide-facies iron formation, which are interpreted to be stratigraphically equivalent of the Butler assemblage by Metsaranta and Houlé (2020). Overall differentiation of the complex from dunitic and peridotitic in the northwest grading to more pyroxenitic to gabbroic in composition to the south-southeast strongly suggest a stratigraphic top in that direction (Fig. 5, 6). In addition, several small ellipsoidal magnetic anomalies trending northeast-southwest in the footwall of the complex (mostly north of AT-8), delineate a chain of mafic to ultramafic intrusions, a few of which have been determined to be peridotitic and ferrogabbroic bodies that most likely belong to the Koper Lake and Ekwan River subsuites, respectively (Fig. 2). Some of these intrusive bodies will be briefly described below, however, the reader is referred to previous (Metsaranta and Houlé, 2020 and references therein) and upcoming publications (Carson, in prep; Farhangi, in prep; Zuccarelli, in prep) from this project for more details about these well mineralized ultramafic to mafic intrusions. Almost all components of the Esker intrusive complex are composed of thick lower olivine-rich ultramafic zones that are normally, but not always, overlain by thinner upper mafic zones.

Black Thor intrusion

The Black Thor intrusion is the largest and the most continuous intrusive body of the Esker intrusive complex. It extends for more than 8 km along strike (Fig. 4, 5) and exhibits the most complete (potentially archetype) section throughout the Koper Lake subsuite. The present surface section (which approximates an original cross-section) consists of a broad trough-shaped sill comprising a thicker ultramafic component overlain by a thinner mafic component (Fig. 5). It appears to have formed by repeated influxes of komatiitic magmas accompanied by crystallization of olivine±orthopyroxene±chromite-rich cumulates and fractionation of the residual liquid (Carson, in prep). The result is a stratigraphy comprising interlayered (from base to top) dunite/harzburgite, harzburgite/websterite/chromitite, and websterite/gabbro (e.g. Tuchscherer et al., 2010; Carson et al., 2015, 2016). The Black Thor intrusive body can be subdivided into three main series: a Basal Series, an Ultramafic Series (with Lower, Middle, and Upper parts), and a Mafic Series, each of which can be further subdivided into several zones (Fig. 6). The reader is referred to Carson (in prep) for a more detailed description of the entire igneous stratigraphy of the Black Thor intrusion. The distribution and the thickness of the series and zones vary across the intrusion, indicating lateral facies variations, with the magma conduit located at the thickest part, at the AT-12 keel in the northeast, with the sequence thinning toward the Big Daddy deposit to the southwest (Fig. 5). The intrusion is cut by the 3B Shear Zone (3BSZ) to the east, but the oblique orientation of the AT-12 keel suggests that magma may have flowed toward the southwest, feeding the more distal (relative to the interpreted conduit) parts of the intrusion. We cannot completely rule out that this geometry could also result from a progressive non-coaxial deformation but it is unlikely based on the facies variations observed in drill cores. The AT-12 keel is ~100–1000 m wide (east-west) and ~1000 m long (north-south) in surface section, narrowing and apparently terminating into the footwall rocks toward the north-northwest (Fig. 5). It contains similar Black Thor Marginal Zone units along the sides grading gradually from pyroxenite at the margins to olivine pyroxenite to peridotite toward the interior. However, the AT-12 keel lithologies have been transgressed by a websterite to a feldspathic websterite (i.e. Late Websterite phase) that extends into the Black Thor intrusion; where it has intruded and brecciated the Lower Ultramafic and Middle Ultramafic Series, including the Black Label Chromite Zone (Spath, 2017). The Late Websterite phase appears to have been emplaced after the Basal Series and Lower Ultramafic Series but before complete solidification, producing a range of hybrid lithologies and incorporating numerous inclusions, including some chromitite inclusions, mainly within its peripheries (Fig. 7a; Spath, 2017). Multiple generations of peridotitic units also occur locally within the Black Thor intrusion, the younger of which contain numerous subrounded to subangular chromitite inclusions and the older of which are completely lacking of any chromitite inclusions or chromitite layers (*see* Fig. 7b). These observations suggest that the chromitite inclusions have been transported from "upstream" in the system. Olivine compositions in this intrusion range between Fo_{94} and Fo_{80} (Laarman, 2014; Spath 2017; Carson, in prep), with the most magnesian analyzed olivine occurring in the Black Label Chromitite Zone.

Double Eagle intrusion

The Double Eagle intrusion is principally composed of two ultramafic bodies (AT-1 and Blackbird) that are dissected by the Frank Shear Zone (Fig. 4, 5). The intrusions appear to correlate based on their magnetic signatures, suggesting 1–1.5 km of dextral displacement (Fig. 4), a correlation supported by 3-D modelling (Laudadio, 2019; also *see* Esker Intrusive Complex Structural Reconstruction). In surface section (which approximates an original cross-section), the restored intrusion has the form of a transitional dyke/chonolith (*see* discussion of morphologies by Barnes and

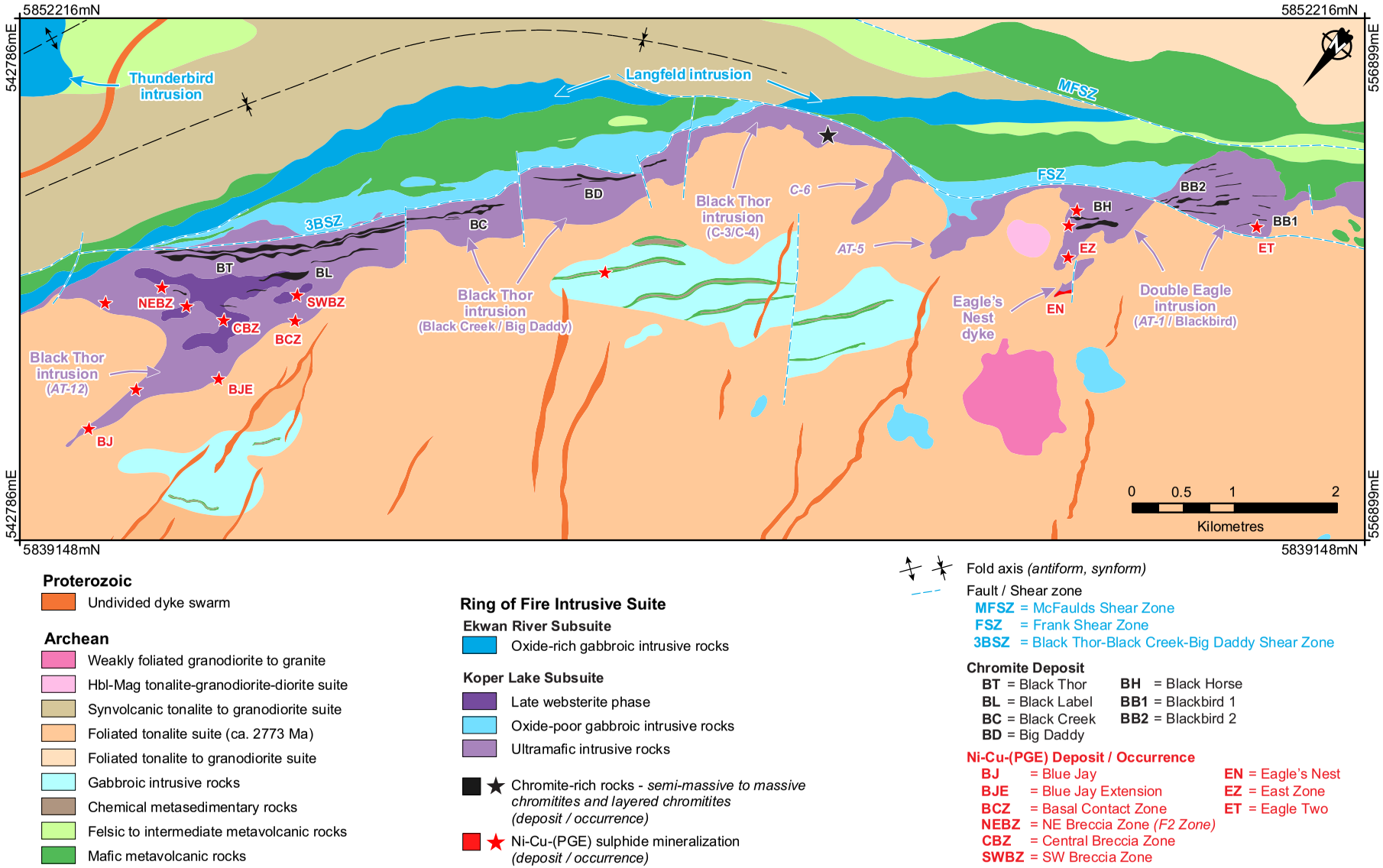

Figure 5. Geological map showing the Esker intrusive complex and associated mineral deposits and occurrences. Geology *adapted from* Metsaranta and Houlé (2017b), Houlé et al. (2017, 2019), Laudadio (2019), and Noront Resources Ltd. (unpub. data). Text in blue = intrusion of the Ekwan River subsuite, purple text = intrusion/keel (*italic*) of the Koper Lake subsuite. Abbreviations: Hbl = hornblende, Mag = magnetite. Chromite and Ni-Cu-(PGE) mineralization shown on the map represent the main mineralized intervals projected to surface. Note that the map has been rotated in order to put the stratigraphic top upward.

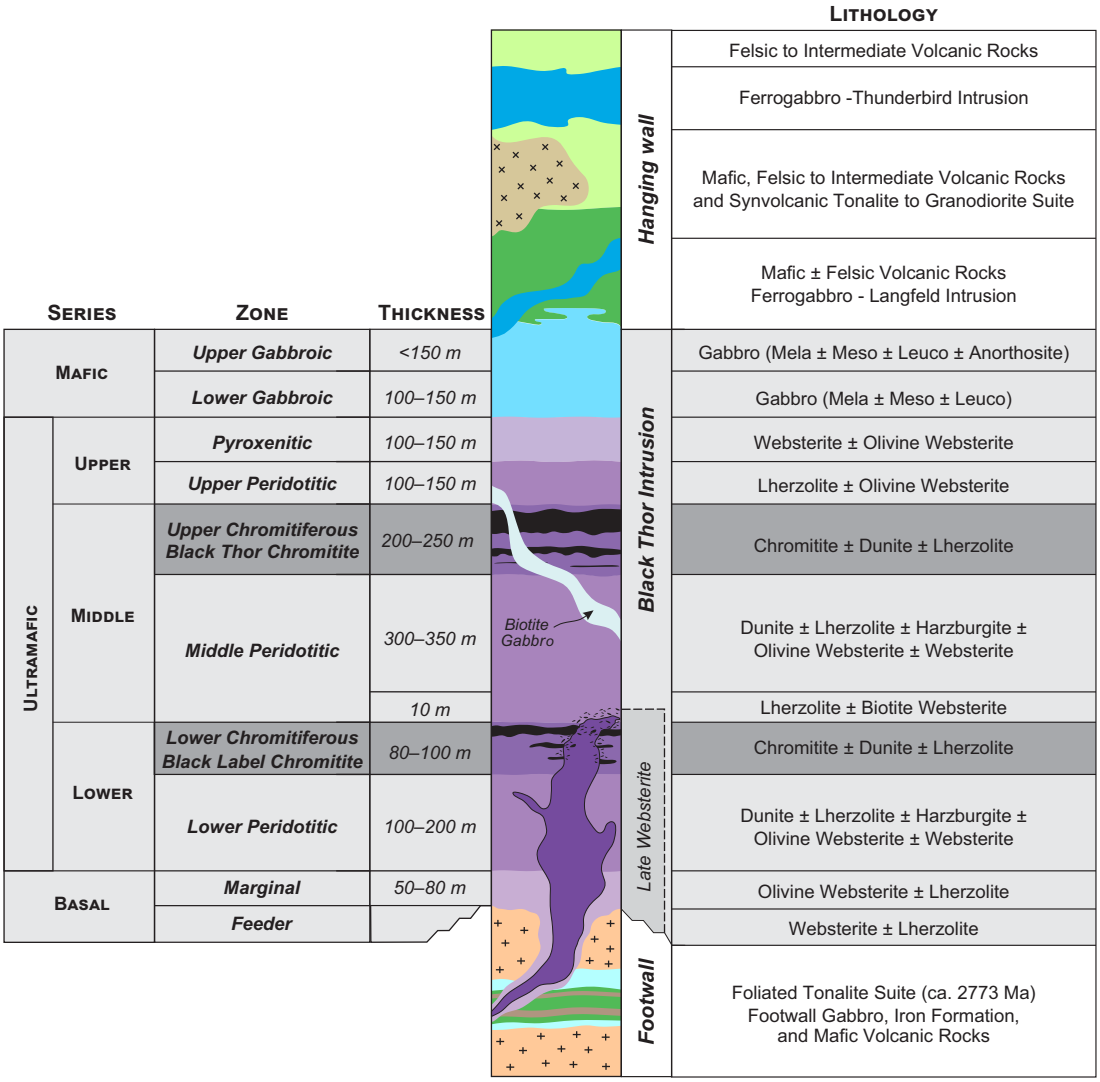

Figure 6. Idealized and schematic stratigraphic column of the Black Thor intrusion (Black Thor segment) in the Esker intrusive complex showing the various stratigraphic subdivisions (e.g. series and zones) and the confining lithological units of the footwall and hanging wall (*adapted from* Carson et al., 2015). Abbreviations: Leuco = leucogabbro; Mela = melagabbro, Meso = mesogabbro.

Mungall, 2018). South of the Frank Shear Zone, the Blackbird body is at least 1 km wide (east-west) and at least 700 m thick (north-south) between bounding faults (Fig. 5). To the north, the ultramafic body of AT-1 is interpreted to be the keel of the Double Eagle intrusion, where it is approximately 600 m wide (east-west) and 700 m thick (north-south) at its thickest. The ultramafic component of this intrusion is composed of variable proportions of dunite, harzburgite, and orthopyroxenite (Azar, 2010). There is little mafic component in this intrusion, except at the eastern end where it occurs as a thin layer approximately 100 m thick (north-south) at surface.

Eagle's Nest dyke

The Eagle's Nest dyke is a north-south-trending komatiitic ultramafic body with a flattened tube-shaped morphology that is interpreted to represent a structurally rotated subhorizontal blade-shaped dyke (Mungall et al., 2010; Zuccarelli et al., 2018a; Zuccarelli, in prep). In surface section (which approximates an original cross-section), it is ~500 m long (high) and ≤85 m wide (thick). The dyke has been drilled to a depth (length) of at least 1500 m. It is composed of an olivine-rich peridotite core flanked by more pyroxenitic margins (Zuccarelli et al., 2020; Zuccarelli, in prep). Mungall et al. (2010) described a marginal gabbro along parts of the contact, which might be explained by contamination and the presence of abundant xenoliths of country rocks (e.g. granodiorite, tonalite) in those areas. The ultramafic lithologies are mainly lherzolite, wehrlite, harzburgite, olivine pyroxenite, and pyroxenite that all contain orthopyroxene oikocrysts (Zuccarelli, in prep).

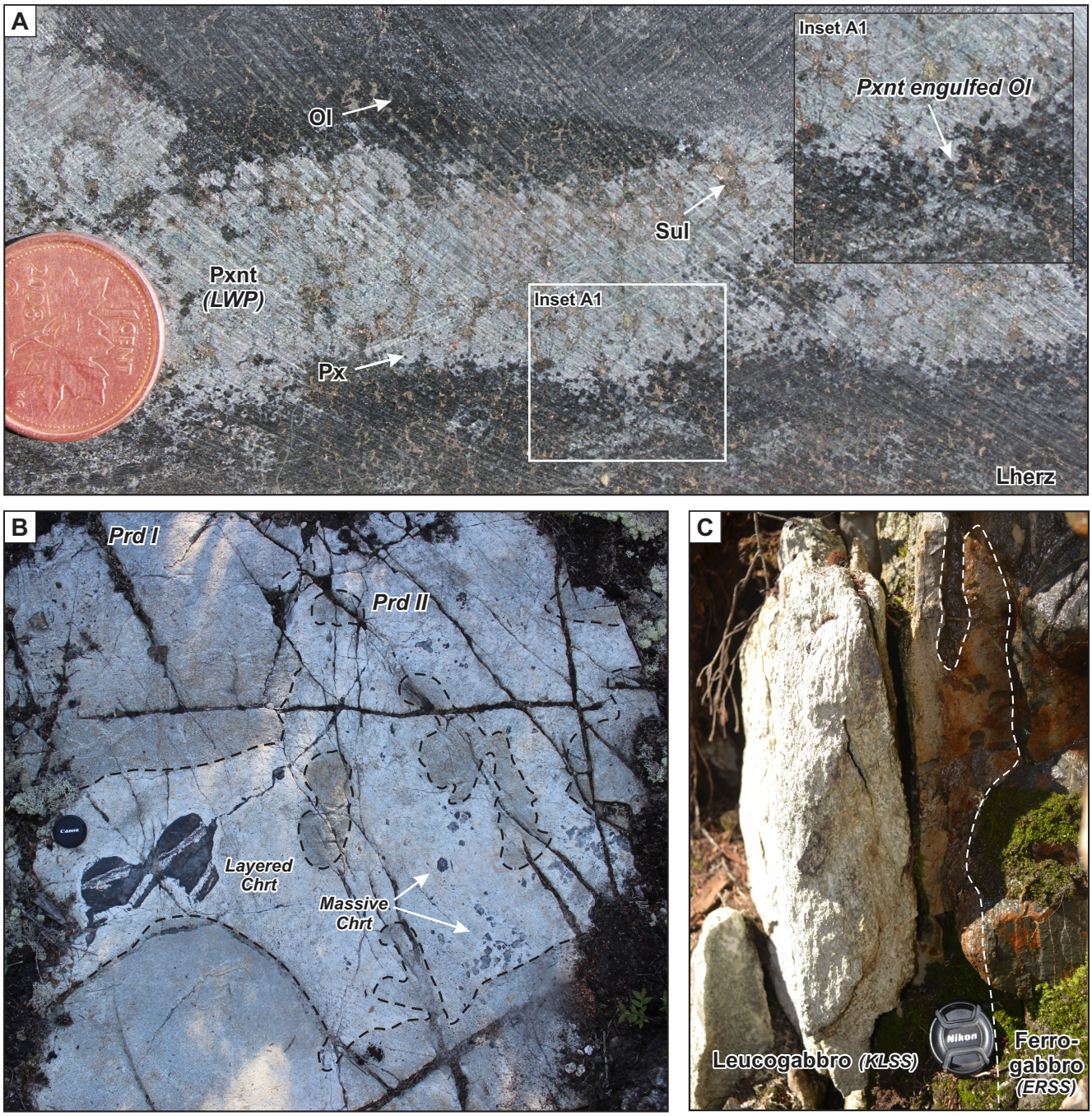

Figure 7. Field photographs showing some of the crosscutting relationships observed in the Black Thor intrusion within the Esker intrusive complex. **a)** Late Websterite phase injected into the lherzolite of the Black Thor intrusion. While the lherzolite was only partially unconsolidated, the pyroxenitic magma invaded the interstitial material, gradually engulfing the olivine crystals (*see* inset A1) of the lherzolite, producing hybrid rocks. Coin is 18 mm in diameter. **b)** Contact relationship between two peridotitic units in the Black Thor intrusion suggesting multi-generational emplacement of the komatiitic magma. Peridotitic unit II contains bimodal, subrounded to subangular chromitite inclusions: 1) numerous but small massive chromitite inclusions and 2) large but uncommon layered chromitite composed of massive chromitite and net-textured chromitite layers. Note that chromitite inclusions only occur within peridotitic unit II and are absent in peridotitic unit I. Lens cap is 6 cm in diameter. **c)** Iron- and titanium-enriched gabbroic dyke of the Ekwan River subsuite cutting leucogabbro (on the left) of the upper part of the Black Thor intrusion of the Koper Lake subsuite (KLSS). The white dashed line highlights the sharp intrusive contact between the two gabbroic rocks. Lens cap is 6 cm in diameter. Abbreviations: Chrt = chromitite; ERSS = Ekwan River subsuite; KLSS = Koper Lake subsuite; Lherz = lherzolite; LWP = Late Websterite phase; Ol = olivine; Prd I, Prd II = peridotitic unit, generation I and II, respectively; Px = pyroxene; Pxnt = pyroxenite; Sul = sulphide.

Other intrusive bodies

The C-6 intrusion is ~250 m wide (east-west) and ~750 m long (north-south) in surface section, narrowing and apparently terminating into the footwall rocks toward the north (Fig. 5) and cut off to the south by the Frank Shear Zone. It is poorly characterized but the magnetic signature combined with a few diamond drill core intersections suggests that it is composed mainly of ultramafic rocks.

The AT-5 intrusion is ~500 m wide (east-west) and up 650 m long (north–south) in surface section, narrowing and apparently terminating into the footwall rocks toward the north (Fig. 5). It consists mainly of peridotite to dunite with abundant relict igneous olivine (Fo_{91}–Fo_{86}: Houlé, unpubl. data), pyroxene, and subordinate gabbroic rocks.

Orthomagmatic Mineralization

Chromite mineralization correlation along strike

Chromite deposits are thus far restricted to the ultramafic-dominated Esker intrusive complex of the Koper Lake subsuite, which hosts at least six chromite deposits: the Black Thor, Black Label, Black Creek, and Big Daddy deposits in the Black Thor intrusion and the Black Horse, and Blackbird (including ore zones #1 and #2 referred as Blackbird 1 and Blackbird 2, respectively) deposits in the Double Eagle intrusion (Fig. 5). All six chromite deposits exhibit similar chromite textural facies, including finely disseminated, patchy disseminated, patchy net-textured, net-textured, semi-massive, and massive. These facies are commonly complexly interlayered, ranging from very thinly laminated (<1 mm) to very thickly bedded (>60 cm).

To aid in correlating the complex chromite-rich zones along strike, Laudadio (2019) subdivided them into (1) massive and semi-massive chromitite containing >35% Cr_2O_3 (~70 modal% chromite) and (2) disseminated, net-textured, and banded chromitite-dunite containing 15–35% Cr_2O_3 (~30–70 modal% chromite). Defined this way, the chromite mineralization within the Black Thor intrusion occurs as a relatively continuous and thick horizon that is broadly correlative over a strike length of 5 km. Mineralization up to 80 m thick occurs within the upper third of the Ultramafic Series, which is underlain by peridotitic units and overlain by olivine pyroxenitic to pyroxenitic units. Except for the Black Label Chromitite Zone that is predominantly composed of layered ore, all of the other chromitite zones (Black Thor, Black Creek, and Big Daddy) in the Black Thor intrusion consist of a relatively thin zone of massive and semi-massive chromitite surrounded by a thicker zone of disseminated, net-textured, and banded chromitite-dunite (Laudadio, 2019). In contrast, the main chromitite zones within the Double Eagle intrusion consist primarily of massive ores, although three layered chromitite horizons occur stratigraphically below the Blackbird 2 deposit (Laudadio, 2019).

Ni-Cu-(PGE) mineralization styles

Known Ni-Cu-(PGE) deposits are thus far also restricted to the ultramafic-dominated Esker intrusive complex of the Koper Lake subsuite. Only one deposit (Eagle's Nest) has geological resource estimates, but numerous Ni-Cu-(PGE) showings occur across the complex. Several types of Ni-Cu-(PGE) mineralization occur within the ultramafic component of the Esker intrusive complex (Farhangi et al., 2013; Houlé et al., 2015, 2017): 1) sulphide-rich conduit-style mineralization within feeder systems (e.g. Eagle's Nest, Blue Jay); 2) sulphide-rich contact-style mineralization along basal contacts (e.g. Black Thor intrusion Basal Contact, Blue Jay Extension); 3) sulphide-poor disseminated reef-style PGE-rich mineralization in chromitite horizons (e.g. Black Label, Black Thor); 4) sulphide-rich disseminated PGE-poor reef-style mineralization in fractionated gabbroic rocks in mafic zones (e.g. Black Thor intrusion); 5) sulphide-rich breccia mineralization associated with the emplacement of the slightly younger websteritic phase within the Black Thor intrusion (e.g. SW/Central/NE Breccia Zones); and 6) tectonically/hydrothermally mobilized sulphide-rich mineralization within shear zones (e.g. transition zone between ultramafic and mafic parts of intrusion; Fig. 5). More detailed work has been completed on these different types of mineralization at the Black Thor intrusion (Farhangi, in prep), and is currently ongoing at the Eagle's Nest deposit (Zuccarelli, in prep).

Summary

Although the mafic to ultramafic intrusive bodies of the Ring of Fire intrusive suite have similar emplacement/crystallization ages (Table 1; Houlé et al., 2015), they are significantly different in many respects: 1) the Koper Lake subsuite is spatially much more restricted than the Ekwan River subsuite (Fig. 1); 2) the Ekwan River subsuite does not contain any olivine-rich ultramafic rocks (Fig. 3); 3) the Koper Lake and Ekwan River subsuites show clear differences in their geochemical trends indicating a distinct geochemical evolution (Fig. 3); 4) the Ekwan River subsuite ferrogabbro locally crosscuts Black Thor leucogabbro (Fig. 7c), as well as other Koper Lake subsuite lithologies (evident in airborne magnetic maps), however, the opposite relationship is also observed locally in the Butler area; and 5) there are thin, highly deformed volcanic units between the Black Thor intrusion (i.e. Koper Lake subsuite) leucogabbro and Langfeld ferrogabbro (i.e.

Ekwan River subsuite; Fig. 5). Together, the above observations suggest discrete ultramafic-dominated (i.e. Koper Lake subsuite) and mafic-dominated (i.e. Ekwan River subsuite) intrusions with complex contact relationships, rather than a single, large, tectonically dismembered layered ultramafic-mafic intrusion, as previously suggested by Mungall et al. (2010).

DISCUSSION

Understanding the architecture of volcanic and intrusive plumbing systems of orthomagmatic mafic to ultramafic ore systems is critically important in determining their prospectivity and where chromite and Ni-Cu-(PGE) sulphide deposits might be located within these systems. However, the deposits and host units are normally small, making the task challenging, especially in deformed, metamorphosed, and glacially covered Archean greenstone belts like the McFaulds Lake greenstone belt.

Esker Intrusive Complex Structural Reconstruction

To improve our understanding of the plumbing systems of the Esker intrusive complex, a 3-D geological model was developed to better image the subsurface distribution and structural disposition of the Black Thor and the Double Eagle intrusions within the Esker intrusive complex (Laudadio et al., 2018a,b; Laudadio, 2019). The results mostly agree with the previous 2-D geological interpretation of Metsaranta and Houlé (2017b) but there are significant differences regarding the low-angle (i.e. to the stratigraphy) ductile shear zone (e.g. Frank Shear Zone) that transgresses the Esker intrusive complex subparallel to its internal stratigraphy (Fig. 5). The complex occurs entirely on the northern limb of a synform, so most of the stress appears to have been partitioned into these discrete low-angle shear zones (e.g. Frank Shear Zone and 3B Shear Zone), such that most of the ores and host rocks are not penetratively deformed and exhibit well preserved igneous textures. High-angle faults (i.e. to the stratigraphy) also transgress the complex but with apparent minor displacements (Fig. 5).

However, there are many features indicating that many—if not most—of the basal contacts of the Esker intrusive complex are primary features:

- Irregular contacts and hornfelsed footwall rocks along the basal contact of the Black Thor intrusion and at Eagle's Nest;
- Ultramafic protrusions extending from the ultramafic rocks into the footwall rocks at Eagle's Nest;
- Sulphide veinlets extending from mineralized peridotite into the footwall rocks at Eagle's Nest and the Basal Contact Zone of the Black Thor intrusion;
- The connection between the Basal Series of the AT-12 keel and the overlying Lower Ultramafic Series of the Black Thor intrusion;
- The continuity between the Late Websterite phase in the AT-12 keel and the Lower Ultramafic Series of the Black Thor intrusion; and
- The presence of mineralogically and geochemically similar Ni-Cu-(PGE) mineralization at Blue Jay, Blue Jay Extension, and Basal Contact Zone within the Black Thor intrusion.

At the northeast end of the complex, in the Black Thor intrusion, the amount of dextral displacement along the 3B Shear Zone is not well known, but it is inferred to be minimal based on a lack of offset along the geophysically interpreted contacts of the Langfeld intrusion but also by the apparent continuity of units on both side of the 3B Shear Zone within the Esker intrusive complex (Fig. 4, 5). Nonetheless, only within the northernmost part of the intrusion, the chromite horizon appears to be structurally repeated along 3B Shear Zone, roughly parallel to the stratigraphy (Tuchscherer et al., 2010). Conversely, at the opposite end of the complex, the C-6, AT-5, and AT-1 keels on the northwest side of the Frank Shear Zone are displaced from the Double Eagle and AT-3 chonoliths (Fig. 4). The conceptual restoration of deformation by Laudadio (2019) suggests dextral displacement of 1 to 1.5 km along the Frank Shear Zone. This would connect the AT-1 and Blackbird bodies to form the Double Eagle intrusion, and reconnect the gabbro units between the Black Thor and Double Eagle intrusions, which would bring the Double Eagle and AT-3 intrusions closer to the Black Thor intrusion (Fig. 4). However, this interpretation leaves the C-6 and AT-5 keels "stranded" with little or no overlying ultramafic components on the southeast side of the shear zone. An alternative scenario involves 3 to 4 km of dextral displacement along the Frank Shear Zone, which would connect C-6 with the Double Eagle complex, and AT-5 and AT-1 with AT-3 (*see* Fig. 4). Both scenarios support a linkage between the Black Thor and Double Eagle intrusions and their assignment to a single intrusive complex, as was proposed by Houlé et al. (2019).

Regardless of the magnitude of displacement along the Frank Shear Zone, the 3-D reconstruction of the Esker intrusive complex suggests that the Eagle's Nest dyke is not directly connected (Laudadio, 2019) and may therefore not be the magma conduit of the Double Eagle intrusion. We cannot completely rule out additional structural complexity as an explanation for this spatial relationship between these bodies, but this interpretation is supported by the much greater abundance of Fe-Ni-Cu sulphides in the Eagle's Nest dyke and the much greater abundance of chromite in the Double

Eagle intrusion, requiring an "upstream" (lateral or deeper) source for the rare chromitite clasts within the Eagle's Nest dyke (*see* the discussion about Ore Genetic Models; Zuccarelli et al., 2020).

Similarly, although the ~90º east-southeast structural rotation is well defined by younging directions inferred from textural, mineralogical, and lithogeochemical gradations in the Eagle's Nest dyke, Double Eagle intrusion, and Black Thor intrusion, the estimate of fault displacement relies heavily on geophysics and may require revision after more geological data about the relationship between the Double Eagle and the Black Thor intrusions become available.

Magmatic Architecture of the Esker Intrusive Complex

After removal of the superimposed deformation, the Esker intrusive complex consists of a semi-continuous sill-like ultramafic±mafic body that incorporates the Double Eagle transitional dyke/chonolith, which is underlain by the keel-shaped AT-1, AT-5, and C-6 bodies and the Eagle's Nest dyke (Fig. 8). It also contains the trough-shaped Black Thor sill, which is underlain by the keel-shaped AT-12 body.

All of the keel-shaped intrusive bodies along the north-northwest margin of the Esker intrusive complex appear to have been originally oriented at >60º to the basal contact of the Esker intrusive complex, emplaced along inferred synvolcanic faults, and thin rapidly northward, suggesting that they were all originally subhorizontal to slightly inclined blade-shaped dykes similar to unmineralized (e.g. Hawaii: Rubin and Pollard, 1987; New Zealand: Shelley, 1988) and mineralized (e.g. Expo-Méquillon: Mungall, 2007; Savannah: Barnes et al., 2016; Huangshan, Jinchuan, Jingbulake, Kalatongke #1, Hongqiling #1, Limahe, Qingkuangshan, Zhubu: Lu et al., 2019; *see* review by Lesher, 2019) subhorizontal dykes in many other subvolcanic systems. These keel-like bodies are interpreted to have fed the overlying Black Thor and Double Eagle intrusions. Subhorizontal blade-shaped dykes are interpreted to form at a level of neutral buoyancy (e.g. in this case near the contact between the less dense granitoid rocks and the denser mafic±felsic volcanic rocks and iron formations) in an extensional stress regime that facilitates lateral propagation (e.g. Rubin and Pollard, 1987; Townsend et al., 2017). The clear connections between the AT-12 and AT-1 intrusions and the overlying Black Thor and Double Eagle intrusions, respectively, suggest that over time the upper parts of the bladed dykes intruded laterally and expanded (as shown in the experiments by Kavanagh et al., 2015) to form a transitional dyke/chonolith (Double Eagle intrusion) and a trough-shaped sill (Black Thor intrusion). The Double Eagle and Black Thor intrusions are interpreted to have eventually coalesced to form the Esker intrusive complex (Fig. 8; Houlé et al., 2019; *see* discussion by Magee et al., 2016; Biggs and Annen, 2019). Thus, the Esker intrusive complex appears to preserve all components of the transition from bladed dykes through chonoliths to channelized sills.

Regardless of the mechanism and timing of growth and coalescence, Ni-Cu-(PGE) mineralization was localized in environments of linear propagation (blade-shaped dykes), whereas chromite mineralization was localized in environments of transitional (chonoliths) and subhorizontal (trough-shaped sill) propagation.

System Dynamics

Komatiite-associated Ni-Cu-(PGE) deposits form in high-flux lava channels, channelized sheet flows, chonoliths, and channelized sheet sills (e.g. Lesher et al., 1984; Lesher, 1989, 2017, 2019; Barnes, 2006; Lesher and Barnes, 2009; Barnes et al., 2016) and it is now recognized that some types of stratiform chromite deposits formed in similar environments (e.g. Prendergast, 2008; Lesher et al., 2019).

Ni-Cu-(PGE) ores typically occur at or near the base of their host units, suggesting that they form early, prior to the crystallization of the overlying rocks, which are typically olivine±pyroxene cumulates. Overlying olivine-rich cumulate rocks indicate continued high magma fluxes, whereas differentiation to more evolved gabbroic rocks indicates waning magma fluxes (e.g. Lesher and Keays, 2002). The ores are sometimes coarsely layered (e.g. Raglan: Lesher, 2007; Alexo: Houlé et al., 2012), but never finely layered and are commonly just zoned (e.g. Kambalda: Ewers and Hudson, 1972). The Ni-Cu-(PGE) ores at Eagle's Nest are overlain by barren peridotites and lesser pyroxenites, consistent with continued high magma fluxes, and have complexly zoned net-textured subfacies, but are not layered (Zuccarelli et al., 2020; Zuccarelli, in prep).

In contrast, Cr deposits occur above the base of the host units and are typically finely interlayered with barren or weakly mineralized olivine±pyroxene cumulate rocks. The origin of the layering is not well understood but is normally interpreted to reflect some combination of multiple influxes ± magma mixing (*see* review by Namur et al., 2015) rather than continuous or semi-continuous high-flux flow. Although both deposits form in dynamic systems, it appears that high-grade conduit-hosted Ni-Cu-(PGE) deposits form at higher magma fluxes than high-grade conduit-hosted Cr deposits.

It is not yet clear whether the sulphides and oxides in the Esker intrusive complex formed at more-or-less the same time in different environments under different fluid dynamic conditions (higher flux blade-shaped

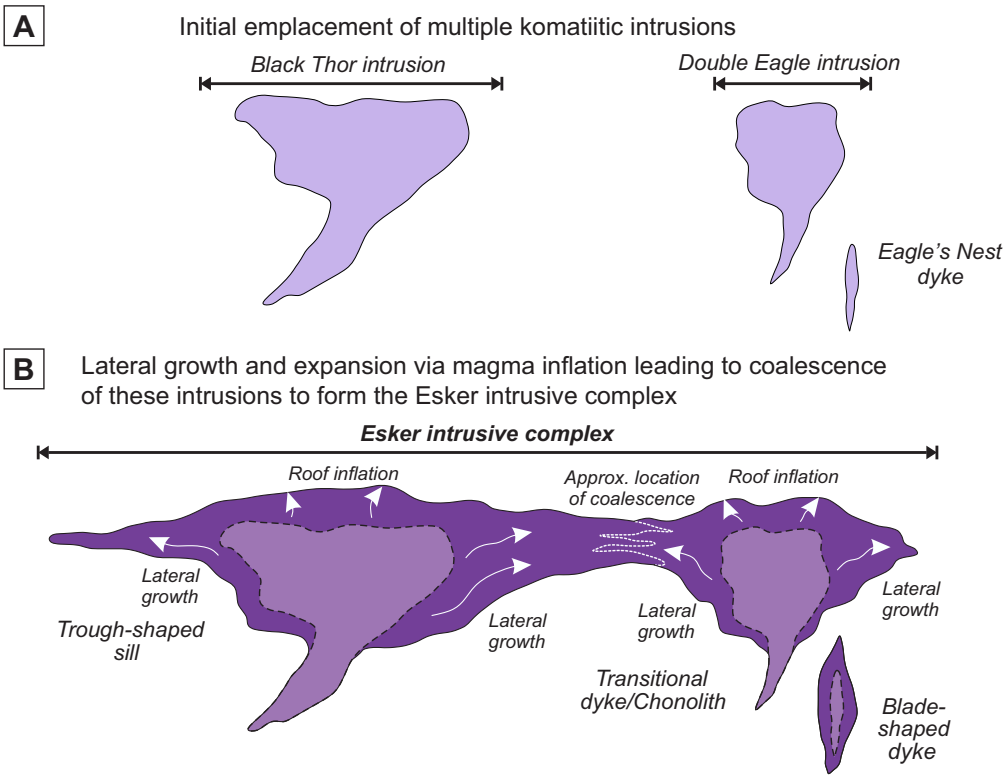

Figure 8. Schematic reconstruction (not to scale) of the evolution of the Esker intrusive complex (*modified from* Houlé et al., 2019). **a)** The light purple represents the initial individual emplacement of the Black Thor and Double Eagle intrusions and the Eagle's Nest dyke. **b)** The continuation of magma flux through each system resulted in the vertical inflation and lateral expansion of the Black Thor and the Double Eagle intrusions until eventually they coalesced to form the Esker intrusive complex. The dark purple represents the full extent of the intrusions that form the Esker intrusive complex; medium purple represents the trace of the initial magma bodies emplaced in (a). The white arrows indicate the displacement of magma throughout the inflation processes; the white dashed line indicates the approximate location of the coalescence of the Black Thor and Double Eagle intrusions. Not shown in this diagram is the Frank Shear Zone, which subsequently faulted the Esker intrusive complex. Note that for simplicity, the late websteritic phase has been omitted from this schematic reconstruction.

dykes versus lower flux channelized sills) or whether they formed at different times as the geometries and fluid dynamic conditions evolved within the system (higher flux blade-shaped dykes evolving into lower flux channelized sills). Additional U-Pb dating might be helpful to establish the geochronological relationships among the different intrusion types and whether any age gradation can be observed.

Ore Genesis

Magmatic chromite deposits

The chromite deposits in the McFaulds Lake greenstone belt of the Ring of Fire region do not exhibit the main geological characteristics of traditional stratiform deposits hosted by large periodically replenished magma chambers. They are considered to be part of a subtype hosted by smaller magmatic conduits (e.g. Prendergast, 2008; Lesher et al., 2019). One fundamental problem in the genesis of all stratiform chromite deposits is how layers of massive to semi-massive chromitite that are commonly up to 1 m thick (e.g. Bushveld Complex–South Africa; Stillwater Complex–USA; or Great Dyke–Zimbabwe), sometimes up to 10 m thick (e.g. Inyala and Railway Block–Zimbabwe; Ipueira-Medrado–Brazil; Uitkomst–South Africa; and Sukinda–India), and less commonly up to 100 m thick (e.g. Kemi–Finland; Esker intrusive complex–Canada) are generated from magmas that typically contain <0.35% Cr and crystallize very small amounts of chromite (normally <1 modal% of the cumulus assemblage; see discussion by Lesher et al., 2019). Although many models have been suggested over the years (see discussion by Lesher et al., 2019), and even if most of the suggested processes could have operated alone or in combination to generate thin layers of semi- to massive chromitites, none of these appear capable of generating the vast amounts of chromite that are present in the Esker intrusive complex relative to its preserved size. To solve this mass balance problem, Lesher et al. (2019) proposed a process involving partial melting of Fe±Ti oxide-rich rocks (oxide-facies iron formation or ferrogabbro) and conversion of fine-grained xenocrystic oxide to chromite by reaction with Cr-rich komatiitic magma in a dynamic magma conduit (Fig. 9). They demonstrated that this process was geologically, physically, and chemically feasible, and suggested that it

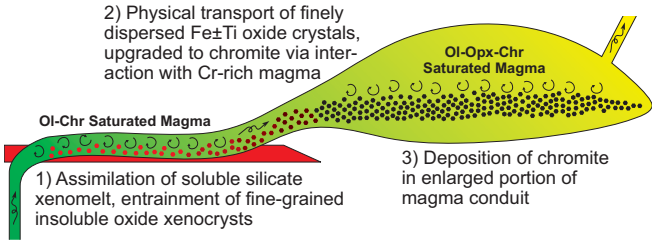

Figure 9. Schematic model of the dynamic upgrading of Fe±Ti oxides derived from oxide-facies iron formation or ferrogabbro via interaction with Cr-rich komatiitic magma (Lesher et al., 2019). Abbreviations: Chr = chromite, Ol = olivine, Opx = orthopyroxene.

probably occurred in the Black Thor intrusion.

Lesher et al. (2019) assumed that the magmas were saturated in chromite and could not dissolve significant amounts of xenocrystic magnetite or ilmenite from footwall oxide-facies iron formations or gabbros. Experiments by Keltie (2018) and MELTS models (Azar, 2010; Carson, in prep) suggest that high-Mg komatiites are able to assimilate significant amounts of magnetite (as much as 66 wt% FeO in the Keltie experiments) before saturating the komatiitic magma in magnetite. However, this seems difficult to reconcile with the worldwide paucity of Fe-rich komatiites (other than geochemically and isotopically distinct ferropicrites) and the presence of oxide-facies iron formation xenoliths within the Double Eagle intrusion (Blackbird deposit: Azar, 2010), the Black Thor intrusion (Carson et al., 2016; Carson, in prep), and elsewhere (e.g. Perring et al., 1995, 1996; Prendergast, 2001). Establishing the Fe contents of liquids that formed rocks containing cumulus olivine±chromite±orthopyroxene assemblages with negligible trapped liquid components is difficult, but relict igneous olivine compositions in the Black Thor intrusion range up to Fo_{94} (Laarman, 2014) and there is a subset of high-Mg, low-Fe peridotites in the Black Thor intrusion that must contain olivine ranging up to that composition (Carson, in prep). This olivine composition is similar to the most magnesian olivine in the Alexo komatiite of the Abitibi greenstone belt, which is inferred to have crystallized from a liquid containing ~28 wt% MgO and ~11 wt% FeO_{total} (Arndt, 1986). Many Black Thor cumulate rocks crystallized from more evolved magmas with higher Fe and lower Mg contents (Carson, in prep), but it is unlikely that the high-Mg olivine or high-Mg, low-Fe cumulate rocks crystallized from magmas with higher Fe contents, as this would require the magma to have proportionally higher Mg contents. Thus, the olivine and whole-rock data suggest a typical high-Mg, moderate-Fe komatiitic parental magma that evolved through a combination of fractional crystallization± assimilation of iron-formation to higher Fe, lower Mg compositions.

Table 2. Comparison of the characteristics of the mechanical sorting of the cotectic olivine-chromite crystallization model and the Fe±Ti oxide xenocryst upgrading model

	Mechanical Sorting of Cotectic Ol-Chr	Dynamic Upgrading of Fe±Ti Oxide Xenocrysts
V–Ga abundances and trends (and overall limited range in chromite compositions)	yes	yes
Composite chromite-silicate-sulphide grains containing Fe±Cu sulphides *(Ni-absent)* that are texturally and mineralogically similar to interlayered massive magnetite-silicate-sulphide (Fe±Cu) in the footwall iron formation	no	yes
Absence of proportionally (50x) large amounts of olivine cumulate rocks	no	yes
High solubility of Fe±Ti oxide in komatiite melt	yes	no

Abbreviations: Chr = chromite, Ol = olivine.

Brenan et al. (2019) showed that the V and Ga contents of Black Thor chromite are consistent with crystallization of olivine and chromite in more-or-less cotectic proportions (50:1), not with crystallization of olivine alone (which would produce higher V/Ga ratios) or of significant amounts of chromite (which would produce lower V/Ga ratios). These observations led Brenan et al. (2020) to propose that the chromite deposits within the Esker intrusive complex formed by cotectic crystallization of olivine-chromite, followed by subsequent crystal sorting, a variant of the H_2O-addition mechanical-sorting model proposed by Azar (2010).

A detailed evaluation of the two models is beyond the scope of this contribution and will be addressed by Carson (in prep), but a preliminary comparison of the ability of the models to explain some of the geological, textural, mineralogical, and geochemical observations are summarized in Table 2. There are several key points that should be considered.

- Both models can explain the abundances and broadly positive correlation between V and Ga in the Ring of Fire chromite. In the case of the xenocryst-upgrading model, V (*see* Lesher et al., 2019) and Ga increase with magma:oxide ratio and reach the observed levels at high magma:oxide and oxide: olivine ratios, provided that the initial V and Ga contents in the magma are similar to those of the most fractionated magma required in the cotectic fractionation model (Carson, in prep). A minor technical point is that fractional crystallization± assimilation models do not make allowances for diffusion, which Lesher et al. (2019) showed would be very rapid for such small (<0.2 mm) grain sizes. This results in a physical-chemical process more similar to equilibrium crystallization, which would reduce the degrees of fractionation in

the models to some degree and require higher initial V and Ga contents in the magma or higher chromite/melt partition coefficients to achieve the same enrichments.

- Both models can explain the massive and silicate melt inclusion-bearing chromite types (e.g. Carson et al., 2015), but only the xenocryst-upgrading model can explain the minor but significant Fe±Cu sulphide-bearing chromite grains within massive to disseminated chromite-rich lithofacies in the Black Thor intrusion, which closely match the textures and sulphide mineralogy of footwall iron formations (Carson et al., 2015, 2016; Lesher et al., 2019). Importantly, the absence of pentlandite as a component of the sulphide inclusions in the chromite grains indicates that the sulphide inclusions did not segregate from the komatiitic magma, as did other sulphides in the Esker intrusive complex (e.g. Eagle's Nest, Blue Jay, Blue Jay Extension, Black Label Breccia Zone: Farhangi et al., 2013; Zuccarelli et al., 2020).
- Azar (2010) and Brenan et al. (2019, 2020) did not indicate whether the proposed mechanical sorting process occurred below, within, or above the Esker intrusive complex, but a cotectic olivine-chromite crystallization and mechanical segregation model requires the production of 50x more olivine than chromite. The Black Thor intrusion does not contain significant amounts of excess olivine (Carson, in prep), so this model requires the formation of 50x larger or 50x more numerous barren dunite bodies (or larger or more numerous peridotite bodies), which have not been observed thus far in the Ring of Fire region, or in any of the other localities where deposits of this type occur. Alhough the Ring of Fire region is poorly exposed, such units should stand out on regional magnetic surveys, which does not appear to be the case. Similarly, the olivine-rich units could also have been eroded or structurally removed (e.g. McFaulds Shear Zone), but one would expect at least some of such large volumes of dunite to be preserved.
- A xenocryst-upgrading model is not consistent with the high solubility of magnetite predicted by MELTS models (Azar, 2010; Carson, in prep) and the Keltie (2018) experiments, and the moderate FeO_T contents of the parental magma. The high magma:oxide values inferred by Lesher et al. (2019) would dilute the effects of assimilation (*see* Lesher et al., 2001), but this would also maintain solubility.

At this stage both models have at least one serious deficiency (*see* Table 2) that must be reconciled to adequately explain the genesis of thick chromitite zones. In our opinion, the observed composite chromite-silicate-sulphide grains provide unambiguous evidence of an oxide-silicate-sulphide source for at least some of the chromite; we are presently evaluating explanations for the magnetite solubility.

Magmatic Ni-Cu-PGE deposits

The main ingredients required for the generation of high-grade magmatic Ni-Cu-PGE sulphide deposits appear to be (1) sulphide-undersaturated magmas derived by moderate to high degrees of melting of peridotitic or pyroxenitic asthenospheric mantle (e.g. Keays, 1982; Lesher and Stone, 1996; Arndt et al., 2005; Lu et al., 2019); (2) an external source of S (e.g. Lesher and Groves, 1986; Lesher and Campbell, 1993; Keays and Lightfoot, 2010; Ripley and Li, 2013); (3) a high-flux magma conduit (lava channel, channelized sheet flow, chonolith, channelized sheet sill) to facilitate thermomechanical erosion (e.g. Huppert et al., 1984; Lesher et al, 1984); and (4) a favourable site of deposition (e.g. Barnes et al., 2016; Lesher, 2017, 2019).

The Eagle's Nest deposit, the only known high-grade Ni-Cu-(PGE) deposit in the Ring of Fire region, exhibits all of these features (Zuccarelli, in prep). Although most of these features are also present in other parts of the Esker intrusive complex but, as noted above, most other parts (Black Thor and Double Eagle intrusions) appear not to have had high magma fluxes, which may explain why they contain only minor Ni-Cu-(PGE) sulphides (e.g. Black Thor intrusion: Farhangi, in prep).

The ^{34}S isotopic compositions of the Ni-Cu-(PGE) mineralization within the Esker intrusive complex (-3 to +2‰ $\delta^{34}S$; Farhangi, in prep) are much more variable than mantle values (0.1 ± 0.5‰; Sakai et al., 1982, 1984) but overlap footwall iron formation (-1 to +1.5‰ $\delta^{34}S$; Carson, in prep). These overlapping values suggest that footwall oxide-sulfide-silicate iron formations are a potential source for most of the S in the system. The amount of sulfide in the iron formations examined thus far is limited, so additional sources such as sulphidic graphitic argillites, should also be considered, but their distribution and abundance is poorly constrained at this stage.

IMPLICATIONS FOR EXPLORATION

Our knowledge in the Ring of Fire region has increased significantly since the beginning of collaborative efforts between the Geological Survey of Canada, the Ontario Geological Survey, academia, and industry partners under the Targeted Geoscience Initiative (Phases 4 and 5). Some guidelines are listed below that could help target the most prospective areas for orthomagmatic mineralization across the Superior Province.

- At the craton-scale, the well endowed McFaulds Lake greenstone belt lies within the Oxford-Stull domain, which is part of the larger Bird River–Uchi–Oxford-Stull–La Grande Rivière–Eastmain superdomain. It defines a large metallotect that is highly prospective for orthomagmatic Cr, Ni-Cu-PGE and Fe-Ti-V (Houlé et al., 2015, 2020).
- At the greenstone belt-scale, the regionally mappable Muketei assemblage is, thus far, the most prospective part recognized thus far, of the McFaulds Lake greenstone belt, as it hosts not only all of the known orthomagmatic Cr-(PGE), Ni-Cu-(PGE), and hydrothermal VMS deposits, but also significant orthomagmatic Fe-Ti-V prospects and orogenic gold mineralization (Metsaranta et al., 2015; Houlé et al., 2020; Metsaranta and Houlé, 2020).
- At the district-scale, almost all of the orthomagmatic deposits in the Ring of Fire region are intimately related to a large mafic to ultramafic magmatic event, recognized as the Ring of Fire intrusive suite, which is known to have been emplaced in a very restricted time between 2736 and 2732 Ma.
    - Ultramafic-dominated intrusions of the Koper Lake subsuite are the prime target for Cr and Ni-Cu-(PGE) mineralization.
    - Mafic-dominated intrusions of Ekwan River subsuite are the prime target for Fe-Ti-V mineralization.
- At the scale of an individual intrusive complex, the Esker intrusive complex
    - Comprises multiple discrete coeval and comagmatic intrusive bodies,
        - some of which contain high-grade, high-tonnage Ni-Cu-(PGE) mineralization (e.g. Eagle's Nest dyke),
        - some of which contain high-grade, high-tonnage Cr mineralization (e.g. Double Eagle and Black Thor intrusions).
        - which appears to have been initially emplaced as separate intrusions that coalesced over time through lateral growth and magma inflation within a dynamic komatiitic system.
    - Is a mafic to ultramafic ore system in which all the deposits recognized thus far, were originally subhorizontal and subconcordant to the regional stratigraphy.
        - Ni-Cu-(PGE) mineralization occurs predominantly within the very high magma flux and highly dynamic blade-shaped dykes of the system (e.g. Eagle's Nest).
        - Cr-(PGE) mineralization occurs predominantly within the high magma flux but slightly less dynamic transitional dykes/chonoliths (e.g. Double Eagle intrusion) to through-shaped sills (e.g. Black Thor intrusion) of the system.
        - Despite the strong association between mineralization and the host geometries, we cannot preclude that other mineralization could be found in other parts of the system given that the Esker intrusive complex is seen as having a complete continuum in their host geometry and also in their mineralization.

The wide diversity of mineral deposit types in the McFaulds Lake greenstone belt, and especially the Cr-(PGE), Ni-Cu-(PGE), and Fe-Ti-V-(P) mineralization related to mafic to ultramafic rocks, make the Ring of Fire region an unmatched exploration target of emerging world-wide economic importance as a source for critical minerals.

ONGOING AND FUTURE WORK

A little more than a decade ago, the Ring or Fire region was poorly known and did not represent a prime mineral exploration target within the Superior Province, even less so for orthomagmatic Ni-Cu-(PGE), Cr-(PGE) or Fe-Ti-V-(P) mineralization. Despite slow development, this region of the Superior Province is now regarded as one of Canada's future mining camps. Significant progress in our understanding of this mineralized system has been made in recent years as part of the Targeted Geoscience Initiative (TGI). There are, however, many unresolved questions that merit further research.

This contribution offers a current summary of some of the critical advances made over the years during the TGI program. A few graduate studies at Laurentian University (H.J.E. Carson, Ph.D candidate – Black Thor intrusion; N. Zuccarelli, M.Sc. candidate – Eagle's Nest deposit; and K. Kuster, Ph.D. candidate – Geochemical modelling of the Esker intrusive complex) are on-going. Furthermore, numerous contributions on various aspects of the Ring of Fire are currently underway, in addition to Ontario Geological Survey Open File report summarizing the regional mapping work conducted by the OGS in collaboration with the GSC Targeted Geoscience Initiative during the past decade (Metsaranta and Houlé, 2020).

ACKNOWLEDGMENTS

This report is a contribution to NRCan's Targeted Geoscience Initiative (TGI) Program. Support for this study was provided through the Orthomagmatic Ni-Cu-PGE-Cr Ore Systems Project's 'Activity NC-2.1: Architecture of magmatic conduits in Cr-(PGE)/Ni-Cu-

(PGE) ore systems' and has benefitted from financial support by NSERC and Cliffs Natural Resources (CRDPJ 446109 – 2012).

We are grateful to Noront Resources Ltd., Cliffs Natural Resources/Freewest Resources, KWG Resources Inc., MacDonald Mines Ltd., Fancamp Exploration Ltd., Bold Ventures Inc., Probes Mines, UC Resources, and Canterra Minerals for their generous assistance, providing access to properties, and permission to access diamond-drill cores and corporate geological databases over the years. We also greatly appreciated the involvement and participation of numerous researchers Pete Hollings (Lakehead University), Jim Mungall (Carleton University), and Claire Samson (Carleton University) and students (Naghmeh Farhangi, Ben Kuzmich, Jordan Laarman, Kaveh Merhmanesh, C.J. Spath, and Natascia Zuccarelli) from the Ring of Fire Targeted Geoscience Initiative research group that have facilitated advances in our understanding of the Ring of Fire geology. We are grateful to Nicole Rayner (GSC-Ottawa) for providing high-quality geochronological analysis throughout the TGI-5 program over the years. Furthermore, we express our appreciation to numerous academic researchers and mining company geologists for geological discussions over the years, but especially geologists of Cliffs Natural Resources (Richard Fink, Andrew Mitchell, Michael Orobona, Ryan Weston, and David Shinkle) and Noront Resources (Ryan Weston, Matt Downey, Stephen Flewelling, Matt Deller, and Geoff Heggie) and KWG Resources (Moe Lavigne). This report benefited from the scientific review of Martin Tuchscherer (Tascan Geosciences Inc.), and Wouter Bleeker (GSC) and editorial review by Elizabeth Ambrose and Valérie Bécu (GSC).

REFERENCES

Arndt, N.T., 1986. Differentiation of komatiite flows; Journal of Petrology, v. 27, p. 279–303.

Arndt, N.T., Lesher, C.M., and Czamanske, G.K., 2005. Mantle-derived magmas and magmatic Ni-Cu-(PGE) deposits; *in* Economic Geology 100th Anniversary Volume, (ed.) J.W. Hedenquist, J.F.H. Thompson, R.J. Goldfarb, and J.P. Richards; Society of Economic Geologists, p. 5–23.

Azar, B., 2010. The Blackbird chromite deposit, James Bay Lowlands of Ontario, Canada: Implications for chromitite genesis in ultramafic conduits and open magmatic systems; M.Sc. thesis, University of Toronto, Toronto, Ontario, 154 p.

Barnes, S.J., 2006. Komatiite-hosted nickel sulfide deposits: geology, geochemistry, and genesis; Chapter 3 *in* Nickel Deposits of the Yilgarn Craton: Geology, geochemistry, and geophysics applied to exploration, (ed.) S.J. Barnes; Society of Economic Geologists, Special Publication 13, p. 51–97.

Barnes, S.J. and Mungall, J.E., 2018. Blade-shaped dikes and nickel sulfide deposits: A model for the emplacement of ore-bearing small intrusions; Economic Geology, v. 113, p. 789–798.

Barnes, S.J., Cruden, A.R., Arndt, N.T., and Saumur, B.M., 2016. The mineral system approach applied to magmatic Ni-Cu-PGE sulphide deposits; Ore Geology Reviews, v. 76, p. 296–316.

Biggs, J. and Annen, C., 2019. The lateral growth and coalesence of magma systems; Royal Society A: Mathematical, Physical and Engineering Sciences, Philosophical Transactions, v. 377, 20180005, p. 1–20.

Brenan, J.M., Woods, K., Mungall, J.E., and Weston, R., 2019. Origin of chromitites in the Ring of Fire Part II: Trace element fingerprinting of contaminants; *in* Targeted Geoscience Initiative 5 Grant Program interim reports 2018–2019, (ed.) K.U. Rempel, A.E., Williams-Jones, and K. Fuller; Geological Survey of Canada, Open File 8620, p. 5–18.

Brenan, J.M., Woods, K., Mungall, J.E., and Weston, R., in press. Origin of chromitites in the Ring of Fire intrusive suite as revealed by chromite trace element chemistry and simple crystallization models; *in* Targeted Geoscience Initiative 5: Grant program final reports (2018–2020); Geological Survey of Canada, Open File 8734.

Carson, H.J.E., in prep. Stratigraphy, geochemistry, and petrogenesis of the Black Thor intrusion and associated Cr and Ni-Cu-PGE mineralization, McFaulds greenstone belt, Ontario; Ph.D. thesis, Laurentian University, Sudbury, Ontario.

Carson, H.J.E., Lesher, C.M., and Houlé, M.G., 2015. Geochemistry and petrogenesis of the Black Thor intrusive complex and associated chromite mineralization, McFaulds Lake greenstone belt, Ontario; *in* Targeted Geoscience Initiative 4: Canadian Nickel-Copper-Platinum Group Elements-Chromium Ore Systems—Fertility, Pathfinders, New and Revised Models, (ed.) D.E. Ames and M.G. Houlé; Geological Survey of Canada, Open File 7856, p. 87–102.

Carson, H.J.E., Lesher, C.M., and Houlé, M.G., 2016. Oxide chemostratigraphy of the Black Thor Chromitite Zone, Black Thor Intrusive Complex, McFaulds Lake, Canada; Geological Survey of Western Australia, 13th International Ni-Cu-PGE Symposium, Abstracts, Record 2016/13, p. 19.

Ewers, W.E. and Hudson, D.R., 1972. An interpretive study of a nickel-iron sulfide ore intersection, Lunnon shoot, Kambalda, Western Australia; Economic Geology, v. 67, p. 1075–1092.

Farhangi, N., in prep. Mineralogy, geochemistry, and petrogenesis of Ni-Cu-(PGE) mineralization in the Black Thor intrusion, McFaulds Lake greenstone belt, Ontario; M.Sc. thesis, Laurentian University, Sudbury, Ontario.

Farhangi, N., Lesher, C.M., and Houlé, M.G. 2013. Mineralogy, geochemistry and petrogenesis of nickel-copper-platinum group element mineralization in the Black Thor Intrusive Complex, McFaulds Lake greenstone belt, Ontario; *in* Summary of Field Work and Other Activities, 2013; Ontario Geological Survey, Open File Report 6290, p.55-1 to 55-7.

Houlé, M.G., Lesher, C.M., and Davis, P.C., 2012. Thermo-mechanical erosion and genesis of komatiite-associated Ni-Cu-(PGE) mineralization at the Alexo Mine, Abitibi Greenstone Belt, Ontario; Mineralium Deposita, v. 47, p. 105–128.

Houlé, M.G., Lesher, C.M., McNicoll, V.J., Metsaranta, R.T., Sappin, A.A., Goutier, J., Bécu, V., Gilbert, H.P., and Yang, X.M., 2015. Temporal and spatial distribution of magmatic Cr-(PGE), Ni-Cu-(PGE), and Fe-Ti-(V) deposits in the Bird River–Uchi–Oxford-Stull–La Grande Rivière–Eastmain domains: A new metallogenic province within the Superior Craton; *in* Targeted Geoscience Initiative 4: Canadian Nickel-Copper-Platinum Group Elements-Chromium Ore Systems —Fertility, Pathfinders, New and Revised Models, (ed.) D.E. Ames and M.G. Houlé; Geological Survey of Canada, Open File 7856, p. 37–48.

Houlé, M.G., Lesher, C.M., McNicoll, V.J., and Bécu, V., 2017. Ni-Cr metallotect: synthesis, updates, and revised models for the

Superior Province; *in* Targeted Geoscience Initiative–2016 Report of Activities, (ed.) N. Rogers; Geological Survey of Canada, Open File 8199, p. 59–61.

Houlé, M.G., Lesher, C.M., Metsaranta, R.T., and Sappin, A.-A., 2019. Architecture of magmatic conduits in chromium-PGE and Ni-Cu-PGE ore systems in Superior Province: example from the 'Ring of Fire' region, Ontario; *in* Targeted Geoscience Initiative: 2018 report of activities, (ed.) N. Rogers; Geological Survey of Canada, Open File 8549, p. 441–448.

Houlé, M.G., Lesher, C.M., Sappin, A.-A., Bédard, M.-P., Goutier, J., and Yang, X.-M., 2020. Overview of Ni-Cu-(PGE), Cr-(PGE), and Fe-Ti-V magmatic mineralization in the Superior Province: Insights on metallotects and metal Endowment; *in* Targeted Geoscience Initiative 5: Advances in the understanding of Canadian Ni-Cu-PGE and Cr ore systems—Examples from the Midcontinent Rift, the Circum-Superior Belt, the Archean Superior Province, and Cordilleran Alaskan-type intrusions, (ed.) W. Bleeker and M.G. Houlé; Geological Survey of Canada, Open File 8722, p. 117–139.

Huppert, H.E., Sparks, R.S.J., Turner, J.S., and Arndt, N.T., 1984. Emplacement and cooling of komatiite lavas; Nature, v. 309, p. 19–22.

Kavanagh, J., Boutelier, D., and Cruden, A. 2015. The mechanics of sill inception, propagation and growth: Experimental evidence for rapid reduction in magmatic overpressure; Earth and Planetary Science Letters, v. 421, p. 117–128.

Keays, R.R., 1982. Palladium and iridium in komatiites and associated rocks: Application to petrogenetic problems; *in* Komatiites, (ed.) N.T. Arndt and E.G. Nisbet; George Allen and Unwin, London, p. 435–457.

Keays, R.R. and Lightfoot, P.C., 2010. Crustal sulfur is required to form magmatic Ni–Cu sulfide deposits: evidence from chalcophile element signatures of Siberian and Deccan Trap basalts; Mineralium Deposita, v. 45, p. 241–257.

Keltie, E.E., 2018. An experimental study of the role of contamination in the formation of chromitites in the Ring of Fire intrusive suite; M.Sc. thesis, Dalhousie University, Halifax, Nova Scotia, 146 p.

Kuzmich, B. 2014. Petrogenesis of the ferrogabbroic intrusions and associated Fe-Ti-V-P mineralization within the McFaulds Lake greenstone belt, Superior Province, northern Ontario, Canada; M.Sc. thesis, Lakehead University, Thunder Bay, Ontario, 486 p.

Kuzmich, B., Hollings, P., and Houlé, M.G., 2015. Petrogenesis of the ferrogabbroic intrusions and associated Fe-Ti-V-(P) mineralization within the McFaulds greenstone belt, Superior Province, northern Ontario; *in* Targeted Geoscience Initiative 4: Canadian Nickel-Copper-Platinum Group Elements-Chromium Ore Systems—Fertility, Pathfinders, New and Revised Models, (ed.) D.E. Ames and M.G. Houlé; Geological Survey of Canada, Open File 7856, p. 115–123.

Laarman, J.E., 2014. A detailed metallogenic study of the McFaulds Lake chromite deposits, northern Ontario; Ph.D. thesis, University of Western Ontario, London, Ontario, 529 p.

Laudadio, A.B., 2019. 3D geological modelling of the Double Eagle – Black Thor intrusive complexes, McFaulds Lake greenstone belt, Ontario, Canada; M.Sc. thesis, Carleton University, Ottawa, Ontario, 107 p.

Laudadio, A.B., Schetselaar, E., and Houlé, M.G., 2018a. 3D geological modelling of the Double Eagle - Black Thor intrusive complexes, McFaulds Lake greenstone belt, Ontario, Canada; Geological Survey of Canada, Scientific Presentation 82, 1 poster.

Laudadio, A.B., Schetselaar, E., Houlé, M.G, and Samson, C., 2018b. 3D geological modelling of the Double Eagle – Black Thor intrusive complexes, McFaulds Lake greenstone belt, Ontario; *in* Targeted Geoscience Initiative: 2017 report of activities, volume 2, (ed.) N. Rogers; Geological Survey of Canada, Open File 8373, p. 35–41.

Lesher, C.M., 1989. Komatiite-associated nickel sulfide deposits; *in* Ore Deposition Associated with Magmas, (ed.) J.A. Whitney and A.J. Naldrett; Reviews in Economic Geology, v. 4, p. 45–101.

Lesher, C.M., 2007. Ni-Cu-(PGE) deposits in the Raglan area, Cape Smith Belt, New Québec; *in* Mineral Deposits of Canada: A Synthesis of Major Deposit-Types, District Metallogeny, the Evolution of Geological Provinces, and Exploration Methods, (ed.) W.D. Goodfellow; Geological Association of Canada, Mineral Deposits Division, Special Publication no. 5, p. 351–386.

Lesher, C.M., 2017. Roles of residues/skarns, xenoliths, xenocrysts, xenomelts, and xenovolatiles in the genesis, transport, and localization of magmatic Fe-Ni-Cu-PGE sulfides and chromite; Ore Geology Reviews, v. 90, p. 465-484.

Lesher, C.M., 2019. Up, down, or sideways: Emplacement of magmatic Ni-Cu±PGE sulfide melts in Large Igneous Provinces; Canadian Journal Earth Sciences, v. 56, p. 756–773.

Lesher, C.M. and Barnes, S.J., 2009. Komatiite-associated Ni-Cu-(PGE) deposits; *in* Magmatic Ni-Cu-PGE Deposits: Genetic Models and Exploration, (ed.) C. Li and E.M. Ripley; Geological Publishing House of China, p. 27–101.

Lesher, C.M. and Campbell, I.H., 1993. Geochemical and fluid dynamic modeling of compositional variations in Archean komatiite-hosted nickel sulfide ores in Western Australia; Economic Geology, v. 88, p. 804–816.

Lesher, C.M. and Groves, D.I., 1986. Controls on the formation of komatiite associated nickel–copper sulfide deposits; *in* Geology and Metallogeny of Copper Deposits, (ed.) G.H. Friedrich, A. Genkin, A.J. Naldrett, J.D. Ridge, R.H. Sillitoe, and F.M. Vokes; Proceedings of the Twenty-Seventh International Geological Congress, Moscow, Springer, Germany, p. 43–62.

Lesher, C.M. and Keays, R.R., 2002. Komatiite-associated Ni-Cu-(PGE) deposits: Mineralogy, geochemistry, and genesis; *in* The Geology, Geochemistry, Mineralogy, and Mineral Beneficiation of the Platinum-Group Elements, (ed.) L.J. Cabri; Canadian Institute of Mining, Metallurgy, and Petroleum, Special volume 54, p. 579–617.

Lesher, C.M. and Stone, W.E., 1996. Exploration geochemistry of komatiites; *in* Igneous Trace Element Geochemistry: Applications for Massive Sulphide Exploration, (ed.) D. Wyman; Geological Association of Canada, Short Course Notes 12, p. 153–204.

Lesher, C.M., Arndt, N.T., and Groves, D.I., 1984. Genesis of komatiite-associated nickel sulphide deposits at Kambalda, Western Australia: a distal volcanic model; *in* Sulphide Deposits in Mafic and Ultramafic Rocks, (ed.) D.L. Buchanan and M.J. Jones; Institute of Mining and Metallurgy, United Kingdom, p. 70–80.

Lesher, C.M., Burnham, O.M., Keays, R.R., Barnes, S.J., and Hulbert, L., 2001. Geochemical discrimination of barren and mineralized komatiites associated with magmatic Ni-Cu-(PGE) sulphide deposits; The Canadian Mineralogist, v. 39, p. 673–696.

Lesher, C.M., Carson, H.J.E, and Houlé, M.G., 2019. Genesis of chromite deposits by dynamic upgrading of Fe±Ti oxide xenocrysts; Geology, v. 47, p. 207–210.

Lu, Y., Lesher, C.M., and Deng, J., 2019. Geochemistry and genesis of magmatic Ni-Cu±PGE and PGE deposits in China; Ore Geology Reviews, v. 107, p. 863–887.

Magee, C., Muirhead, J.D., Karvelas, A., Holford, S.P., Jack-son, C.A.L., Bastow, I.D., Schofield, N.J., Stevenson, C.T.E.,

McLean, C., McCarthy, W., and Shtukert, O., 2016. Lateral magma flow in mafic sill complexes; Geosphere, v. 12, p. 809–841.

Metsaranta, R.T., 2017. Lithogeochemical data, magnetic susceptibility data and outcrop photographs from the Winiskisis Channel, McFaulds Lake and Highbank Lake areas, "Ring of Fire" region, northern Ontario; Ontario Geological Survey, Miscellaneous Release—Data 347.

Metsaranta, R.T. and Houlé, M.G., 2017a. Precambrian geology Winiskisis Channel area, "Ring of Fire Region", north sheet; Ontario Geological Survey, Preliminary Map P.3804; Geological Survey of Canada, Open File 8200, scale 1:100 000.

Metsaranta, R.T. and Houlé, M.G., 2017b. Precambrian geology of the McFaulds Lake area, "Ring of Fire Region" – central sheet; Ontario Geological Survey, Preliminary Map P.3805; Geological Survey of Canada, Open File 8201, scale 1:100 000.

Metsaranta, R.T. and Houlé, M.G., 2017c. Precambrian geology of the Highbank Lake area – "Ring of Fire Region", southern sheet; Ontario Geological Survey, Preliminary Map P.3806; Geological Survey of Canada, Open File 8202, scale 1:100 000.

Metsaranta, R.T. and Houlé, M.G., 2020. Precambrian geology of the McFaulds Lake "Ring of Fire" region, northern Ontario; Ontario Geological Survey, Open File Report 6359, 260 p.

Metsaranta, R.T., Houlé, M.G., McNicoll, V.J., and Kamo, S.L., 2015. Revised geological framework for the McFaulds Lake greenstone belt, Ontario; *in* Targeted Geoscience Initiative 4: Canadian Nickel-Copper-Platinum Group Elements-Chromium Ore Systems—Fertility, Pathfinders, New and Revised Models, (ed.) D.E. Ames and M.G. Houlé; Geological Survey of Canada, Open File 7856, p. 61–73.

Mungall, J.E., 2007. Crustal contamination of picritic magmas during transport through dikes: The Expo intrusive suite, Cape Smith Fold Belt, New Quebec; Journal of Petrology, v. 48, p. 1021–1039.

Mungall, J.E., Harvey, J.D., Balch, S.J., Azar, B., Atkinson, J., and Hamilton, M.A., 2010. Eagle's Nest: A magmatic Ni-sulfide deposit in the James Bay Lowlands, Ontario, Canada; *in* The Challenge of Finding New Mineral Resources: Global Metallogeny, Innovative Exploration, and New Discoveries, Volume I: Gold, Silver, and Copper-Molybdenum, (ed.) R.J. Goldfarb, E.E. Marsh, and T. Monecke; Society of Economic Geologists, Special Publication 15, p. 539–559.

Mungall, J.E., Azar, B., and Hamilton, M. 2011. Ni-Cu-PGE-Cr-Fe-Ti-V and VMS mineralisation of the Ring of Fire intrusive suite, Ontario; Geological Association of Canada–Mineralogical Association of Canada, Program with Abstracts, v. 34, p. 148.

Namur, O., Abily, B., Boudreau, A., Blanchette, F., Bush, J., Ceuleneer, G., Charlier, B., Donaldson, C., Duchesne, J.C., Higgins, M., Morata, D., Nielsen, T., O'Driscoll, B., Pang, K.-N., Peacock, T., Spandler, C., Toramaru, A., and Veksler, I., 2015. Igneous layering in basaltic magma chambers; *in* Layered Intrusions, (ed.) B. Charlier, O. Namur, R. Latypov, and C. Tegner; Springer Geology, p. 75–152.

Ontario Geological Survey–Geological Survey of Canada (OGS–GSC) 2011. Ontario airborne geophysical surveys, gravity gradiometer and magnetic data, grid and profile data (ASCII and Geosoft® formats) and vector data, McFaulds Lake area; Ontario Geological Survey, Geophysical Data Set 1068.

Perring, C.S., Barnes, S.J., and Hill, R.E.T., 1995. The physical volcanology of Archaean komatiite sequences from Forrestania, Southern Cross Province, Western Australia; Lithos, v. 34, p. 189–207.

Perring, C.S., Barnes, S.J., and Hill, R.E.T., 1996. Geochemistry of komatiites from Forrestania, Southern Cross Province, Western Australia: Evidence for crustal contamination; Lithos, v. 37, p. 181–197.

Prendergast, M.D., 2001. Komatiite-hosted Hunters Road nickel deposit, central Zimbabwe: physical volcanology and sulfide genesis; Australian Journal of Earth Science, v. 48, p.681–694.

Prendergast, M.D., 2008. Archean komatiitic sill-hosted chromite deposits in the Zimbabwe craton; Economic Geology, v. 103, p. 981–1004.

Ripley, E.M. and Li, C., 2013. Sulfide saturation in mafic magmas: Is external sulfur required for magmatic Ni-Cu-(PGE) ore genesis?; Economic Geology, v. 108, p. 45–58.

Rubin, A.M. and Pollard, D.D., 1987. Origins of blade-shaped dikes in volcanic rift zones; *in* Volcanism in Hawaii, (ed.) R.W. Decker, T.L. Wright, and P.H. Stauffer; United States Geological Survey, Professional Paper 1350, v 2, p. 1449–1470.

Sage, R.P., 2000. Kimberlites of the Attawapiskat area, James Bay lowlands, northern Ontario; Ontario Geological Survey, Open File Report 6019, 341 p.

Sakai, H., Casadevall, T.J., and Moore, J.G., 1982. Chemistry and isotope ratios of sulfur in basalts and volcanic gases at Kileuea volcano, Hawaii; Geochimica et Cosmochimica Acta, v. 46, p. 729–738.

Sakai, H., Des Marais, D.J., Ueda, A., and Moore, J.G., 1984. Concentrations and isotope ratios of carbon, nitrogen, and sulfur in ocean-floor basalts; Geochimica et Cosmochimica Acta, v. 48, p. 2433–2441.

Sappin, A.-A., Houlé, M.G., Lesher, C.M., Metsaranta, R.T., and McNicoll, V.J., 2015. Regional characterization of mafic-ultramafic intrusions in the Oxford-Stull and Uchi domains, Superior Province, Ontario; *in* Targeted Geoscience Initiative 4: Canadian Nickel-Copper-Platinum Group Elements-Chromium Ore Systems—Fertility, Pathfinders, New and Revised Models, (ed.) D.E. Ames and M.G. Houlé; Geological Survey of Canada, Open File 7856, p. 75–85.

Shelley D., 1988. Radial dikes of Lyttleton Volcano—their structure, form, and petrography; New Zealand Journal of Geology and Geophysics, v. 31, p. 65–75.

Spath, C.S., III, 2017. Geology and genesis of hybridized ultramafic rocks in the Black Label hybrid zone of the Black Thor intrusive complex, McFaulds Lake greenstone belt, Ontario, Canada; M.Sc. thesis, Laurentian University, Sudbury, Ontario, 94 p.

Stott, G.M. and Josey, S.D., 2009. Post-Archean mafic (diabase) dikes and other intrusions of northwestern Ontario, north of latitude 49°30′; Ontario Geological Survey, Miscellaneous Release—Data 241.

Townsend, M.R, Pollard, D.D., and Smith, R.P., 2017. Mechanical models for dikes: A third school of thought; Tectonophysics, v. 703-704, p. 98–118.

Tuchscherer, M.G., Hoy, D., Johnson, M., Shinkle, D., Kruze, R., and Holmes, M., 2010. Fall 2008 to winter 2009 Technical drill report on the Black Thor chromite deposit, Black Label chromite zone, and associated Ni-Cu-PGEs, McFaulds property (100%), James Bay Lowlands, northern Ontario, Latitude 52º78′ N, longitude -86º20′ W; Freewest Resources Canada Ltd., unpublished report, 62 p.

Zuccarelli, N., in prep. Sulfide textural variations and multiphase ore emplacement in the Eagle's Nest Ni-Cu-(PGE) deposit, McFaulds Lake greenstone belt, Superior Province, Ontario, Canada; M.Sc. thesis, Laurentian University, Sudbury, Ontario.

Zuccarelli, N., Lesher, C.M., Houlé, M.G., and Weston, R.J., 2017. Sulfide textural variations and multiphase ore emplacement in the Eagle's Nest Ni-Cu-PGE deposit, McFaulds Lake greenstone belt, Ontario, Canada; Society for Geology Applied to Mineral Deposits, Proceeding of the 14th SGA Biennial

Meeting, p. 583–586.

Zuccarelli, N., Lesher, C.M., Houlé, M.G., and Weston, R.J., 2018a. Sulfide textural variations and multiphase ore emplacement in the Eagle's Nest Ni-Cu-(PGE) deposit, McFaulds Lake greenstone belt, Superior Province, northern Ontario, Canada; Geological Society of America, Abstracts with Programs, v. 50. doi:10.1130/abs/2018AM-317024

Zuccarelli, N., Lesher, C.M., and Houlé, M.G., 2018b. Sulphide textural variations and multiphase ore emplacement in the Eagle's Nest Ni-Cu-(PGE) deposit, McFaulds Lake greenstone belt, Ontario; *in* Targeted Geoscience Initiative: 2017 report of activities, volume 2, (ed.) N. Rogers; Geological Survey of Canada, Open File 8373, p. 29–34.

Zuccarelli, N., Lesher, C.M., Houlé, M.G., and Barnes, S.J., 2020. Variations in the textural facies of sulphide minerals in the Eagle's Nest Ni-Cu-(PGE) deposit, McFaulds Lake greenstone belt, Superior Province, Ontario: Insights from microbeam scanning energy-dispersive X-ray fluorescence spectrometry; *in* Targeted Geoscience Initiative 5: Advances in the understanding of Canadian Ni-Cu-PGE and Cr ore systems—Examples from the Midcontinent Rift, the Circum-Superior Belt, the Archean Superior Province, and Cordilleran Alaskan-type intrusions, (ed.) W. Bleeker and M.G. Houlé; Geological Survey of Canada, Open File 8722, p. 165–179.

Variations in the textural facies of sulphide minerals in the Eagle's Nest Ni-Cu-(PGE) deposit, McFaulds Lake greenstone belt, Superior Province, Ontario: Insights from microbeam scanning energy-dispersive X-ray fluorescence spectrometry

Natascia Zuccarelli[1], C. Michael Lesher[1], Michel G. Houlé[2], and Stephen J. Barnes[3]

[1]Mineral Exploration Research Centre, Harquail School of Earth Sciences, Goodman School of Mines, Laurentian University, Sudbury, Ontario P3E 2C6
[2]Geological Survey of Canada, 490 rue de la Couronne, Québec, Quebec G1K 9A9
[3]Commonwealth Scientific and Industrial Research Organisation (CSIRO), Kensington, WA 6155, Australia
*Corresponding author's e-mail: nzuccarellipegoraro@laurentian.ca

ABSTRACT

The Eagle's Nest Ni-Cu-(PGE) deposit occurs within the 2.73 Ga Esker intrusive complex of the Ring of Fire intrusive suite, in the McFaulds Lake greenstone belt of northern Ontario. Sulphide mineralization occurs along the northwestern margin of a subvertical ~500 m wide (north-south) x ≤85 m thick (east-west) x >1500 m deep komatiitic ultramafic body composed of harzburgite±lherzolite±wehrlite that is interpreted to represent a structurally rotated, originally subhorizontal blade-shaped dyke. Disseminated (<15 wt% sulphide), net (15–35 wt% sulphide), and lesser semi-massive (50–80 wt% sulphide) and massive (>80 wt% sulphide) -textured sulphides have been characterized using microbeam scanning energy-dispersive X-ray fluorescence spectrometry (μXRF). The images produced by this process have identified the abundances and locations of Fe, Ni, Cu, Ca, Si, and Cr within different minerals in 11 samples with representative sulphide textures: disseminated, leopard net-textured (containing bimodal coarse- and fine-grained olivine), pinto net-textured (containing bimodal coarse orthopyroxene and fine olivine), inclusion net-textured (containing coarse inclusions of peridotite), disrupted net-textured (containing pyroxenite invading leopard and pinto net-textured sulphides), semi-massive (containing inclusions of peridotite, pyroxenite, gabbro, and net-textured sulphides), and massive. All sulphide textures typically contain magmatic assemblages of pyrrhotite-pentlandite-chalcopyrite-magnetite±chromite. Notable differences include small ellipsoidal chromite inclusions only in facies with disseminated textures, little to no clinopyroxene in leopard net-textures, abundant clinopyroxene in invasive pyroxenite in disrupted net-textures, high-Cr orthopyroxene oikocrysts in pinto net-textures, and variable degrees of segregation of Cu-rich residual sulphide liquid from fractionally crystallizing Fe-Ni-rich monosulphide solid solution, more in disrupted and inclusion net-textures than in disseminated textures or leopard or pinto net-textures. The wide variety of net textures, the abundance of inclusions, and the invasive pyroxenite indicate a complex history for the magmatic plumbing system. Inclusions and late-stage pyroxenitic melt may have physically facilitated migration of residual sulphide liquid from monosulphide solid solution, and the emplacement of the late pyroxenite may have slowed cooling and/or reheated the mineralization. Many of these details are less evident visually in slabbed cores or polished thin sections, highlighting the usefulness of μXRF in interpreting the genesis and beneficiation of texturally complex magmatic Ni-Cu-PGE ores.

INTRODUCTION

Most magmatic Ni-Cu-PGE ores form by the accumulation of an immiscible sulphide liquid that has scavenged chalcophile elements from a coexisting silicate liquid phase (*see* review by Naldrett, 2004). Most deposits contain multiple textural facies that reflect the mode(s) of emplacement of the sulphides (*see* review by Barnes et al., 2017). The Eagle's Nest Ni-Cu-(PGE) deposit in northern Ontario, contains a wide range of textures, some of which have previously not been described, making it a particularly good site to evaluate the importance of ore textures in constraining ore genesis and beneficiation.

The Eagle's Nest deposit occurs within the 2.73 Ga Esker intrusive complex of the Ring of Fire intrusive suite within the McFaulds Lake greenstone belt of the north-central Superior Province in northern Ontario (Fig. 1, inset). The McFaulds Lake greenstone belt records episodic volcanism, sedimentation, ultramafic to felsic intrusive activity, and tectonism spanning

Zuccarelli, N., Lesher, C.M., Houlé, M.G., and Barnes, S.J., 2020. Variations in the textural facies of sulphide minerals in the Eagle's Nest Ni-Cu-(PGE) deposit, McFaulds Lake greenstone belt, Superior Province, Ontario: Insights from the microbeam scanning energy-dispersive X-ray fluorescence spectrometry; *in* Targeted Geoscience Initiative 5: Advances in the understanding of Canadian Ni-Cu-PGE and Cr ore systems – Examples from the Midcontinent Rift, the Circum-Superior Belt, the Archean Superior Province, and Cordilleran Alaskan-type intrusions, (ed.) W. Bleeker and M.G. Houlé; Geological Survey of Canada, Open File 8722, p. 165–179. https://doi.org/10.4095/326895

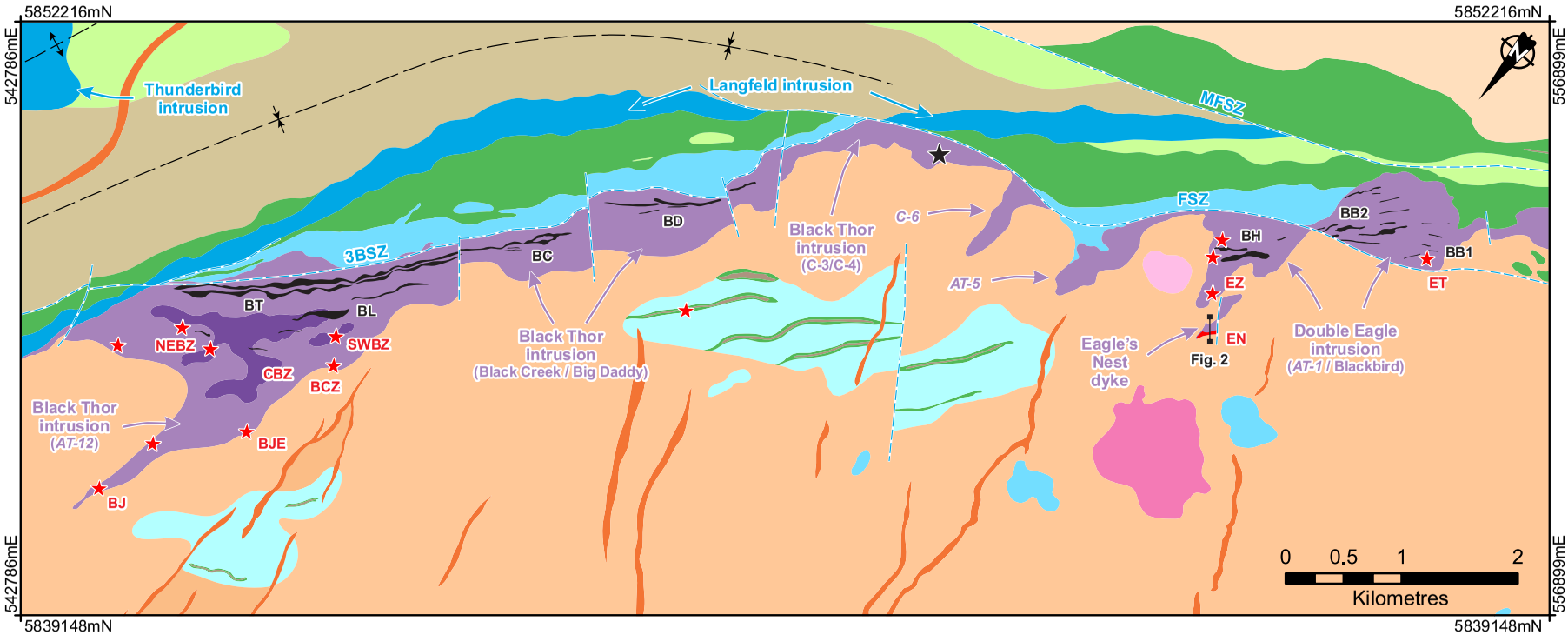

PROTEROZOIC

- Undivided dyke swarm

ARCHEAN

- Weakly foliated granodiorite to granite
- Hbl-Mag tonalite-granodiorite-diorite suite
- Synvolcanic tonalite to granodiorite suite
- Foliated tonalite suite (ca. 2773 Ma)
- Foliated tonalite to granodiorite suite
- Gabbroic intrusive rocks
- Chemical metasedimentary rocks
- Felsic to intermediate metavolcanic rocks
- Mafic metavolcanic rocks

RING OF FIRE INTRUSIVE SUITE

Ekwan River Subsuite

- Oxide-rich gabbroic intrusive rocks

Koper Lake Subsuite

- Late websterite phase
- Oxide-poor gabbroic intrusive rocks
- Ultramafic intrusive rocks
- Chromite-rich rocks - *semi-massive to massive chromitites and layered chromitites* *(deposit / occurrence)*
- Ni-Cu-(PGE) sulphide mineralization *(deposit / occurrence)*
- Fold axis *(antiform, synform)*

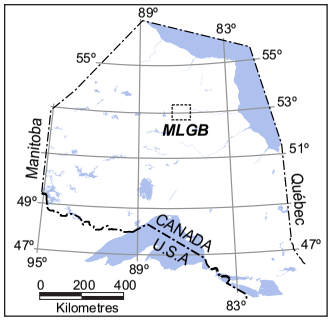

- Fault / Shear zone
  - **MFSZ** = McFaulds Shear Zone
  - **FSZ** = Frank Shear Zone
  - **3BSZ** = Black Thor-Black Creek-Big Daddy Shear Zone

Figure 1. Geological map of the Esker intrusive complex in the McFaulds Lake greenstone belt showing the location of the main mineral deposits and occurrences (*after* Houlé et al., 2020). Abbreviations: MLGB = McFaulds Lake greenstone belt, Hbl = hornblende, Mag = magnetite. Chromite deposits in black: BB1 = Blackbird 1, BB2 = Blackbird 2, BC = Black Creek, BD = Big Daddy, BH = Black Horse, BL = Black Label, BT = Black Thor. Ni-Cu-(PGE) deposits/occurrences in red: BCZ = Basal Contact Zone, BJ = Blue Jay, BJE = Blue Jay Extension, CBZ = Central Breccia Zone, EN = Eagle's Nest, ET = Eagle Two, EZ = East Zone, NEBZ = northeast Breccia Zone, SWBZ = southwest Breccia Zone. Note that the map has been rotated in order to put the stratigraphic top upward.

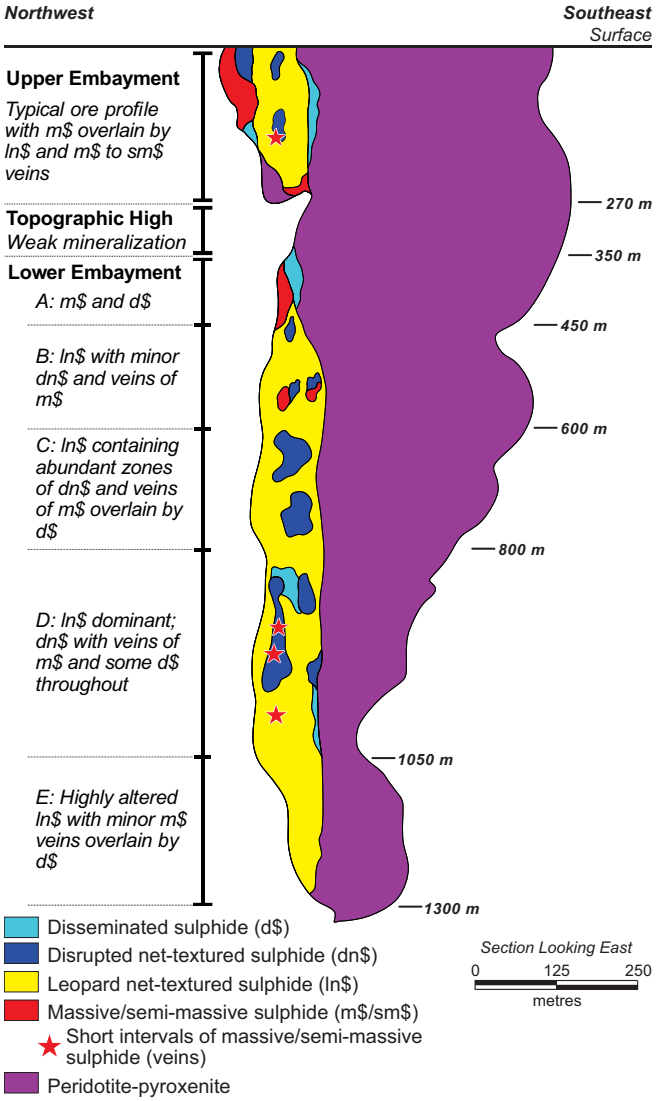

Figure 2. Schematic of a northwest-southeast section (NAD 83, Zone 16, UTM 547219 mE) through the Eagle's Nest dyke showing the sulphide facies and subfacies distributions. Note that the Eagle's Nest deposit occurs along the northwestern contact with the country rocks. The location of the section is shown in Figure 1.

from at least 2.83 to 2.66 Ga (Metsaranta et al., 2015; Metsaranta and Houlé, 2020). This Archean basement is overlain by flat-lying Paleozoic carbonate-dominated strata and unconsolidated Quaternary deposits, making exploration challenging.

The Esker intrusive complex, which comprises the komatiitic Black Thor intrusion, Double Eagle intrusion, Eagle's Nest dyke, and many other intrusive bodies (Fig. 1), represents an ultramafic-dominated intrusive complex that experienced high magma flux through and crystallization/ accumulation within originally smaller, dynamic, komatiitic intrusions/conduits that are interpreted to have coalesced laterally over time through magma inflation to form the present 16 km long Cr- and Ni-Cu-(PGE) mineralized complex (Houlé et al., 2019, 2020). The Eagle's Nest intrusion is a subvertical ~500 m wide (north-south) x ~85 m thick (east-west) x >1500 m deep body composed of harzburgite±lherzolite± wehrlite within tonalitic country rocks, with the deposit occurring along the northwestern margin of the dyke (Fig. 2). It is interpreted to have been emplaced as a subhorizontal blade-shaped dyke (Barnes and Mungall, 2018; Zuccarelli et al., 2018a) and to have been structurally rotated (along with the rest of the Esker intrusive complex) into its current subvertical orienta-tion (Mungall et al., 2010; Zuccarelli et al., 2018a,b; Laudadio, 2019). All of the rocks have been metamorphosed to greenschist facies and are locally deformed, but the stress was partitioned into discrete shear zones (e.g. Frank Shear Zone: Laudadio, 2019) so most of the ores and host rocks are not penetratively deformed and exhibit well preserved igneous textures.

The purpose of this contribution is to report the results of microbeam scanning energy-dispersive X-ray fluorescence spectrometry (µXRF) mapping of the representative textural sulphide facies at the Eagle's Nest Ni-Cu-(PGE) deposit to not only supplement the petrographic work undertaken by Zuccarelli (M.Sc. in prep) but also to provide insights on the mechanisms involved in the formation of textural sulphide facies within magmatic Ni-Cu-(PGE) deposits.

METHODS

During this M.Sc. project, the surfaces of two hundred representative samples of half NQ (47.6 mm diameter) core were ground on a diamond-bonded lap and examined mesoscopically using a stereomicroscope. Thin sections were prepared of representative parts of the cores and examined microscopically in reflected and transmitted light using a compound polarizing microscope. The mineralogical and textural information collected about these samples was used to guide textural classification and the selection of a subset of 11 samples (1 patchy/blebby disseminated, 3 leopard net-textured, 2 pinto net-textured, 1 inclusion net-textured, 2 disrupted net-textured, 1 semi-massive, and 1 massive sulphide) for chemical/mineralogical characterization using a Bruker Tornado™ high-resolution desktop µXRF at the Commonwealth Scientific and Industrial Research Organisation (CSIRO) in Perth (Western Australia). Analyses utilized a ~40 micron diameter collimated X-ray beam generated from an Rh target tube operating at 50 kV and 500 nA without filters and an XFlash VR silicon drift detector. The sample was rastered under the beam with dwell times typically 5 to 10 ms per pixel, at a spatial resolution of 40 microns. Each map is presented as a composite red-green-blue (RGB) image showing the distributions of combinations of three elements (Cr-Fe-Ca, Ni-Cu-S, and S-Fe-

Table 1. Principal characteristics of sulphide textural facies and subfacies in magmatic Ni-Cu-PGE deposits at the Eagle's Nest Ni-Cu-(PGE) deposit.

Sulphide Textural Facies	Nominal Sulphide Content (wt%)	Nominal Sulphur Content (wt%)	Eagle's Nest Deposit			
			Sulphide Content (wt%)	Proportion (%)	Thickness (m)	Strike Length[1] (m)
Disseminated*	**<15**	**<5.9**	**<15**	**5**		
Lightly**	<5	<2.0	0.5–5	*14*		
Medium**	5–10	2.0–3.9	5–10	*42*	***up to 20***	***up to 125***
Heavily**	10–15	4.0–5.9	10–15	*21*		
Patchy**	<15	<5.9	8–10	*9*		
Blebby**	<15	<5.9	2–5	*14*		
Net-Textured*	**15–60**	**5.9–23.4**	**15–35**	**80**		
Leopard**			15–35	*52*		
Patchy**			15–25	*14*	***up to 40***	***up to 130***
Inclusion**			15–30	*5*		
Pinto**			15–30	*1*		
Disrupted**			18–25	*28*		
Semi-Massive*	**50–80**	**19.5–31.2**	**50–80**	**15**	***up to 20***	***up to 40***
Massive*	**>80**	**>31.2**	**>80**			

*Based on Noront Resources Ltd. assay data set that contains more than 10,000 assays and assuming 39 wt% S in 100% sulphide; **based on 200 representative samples examined in this study. Sulphide textural facies and subfacies are generally gradational with some overlap of sulphide or sulphur contents, particularly in samples containing 50–60% sulphide. Thickness and strike length have been estimated based on a detailed geological map from Noront Resources Ltd. [1]Corresponds to the ore surface projection of each textural suphide facies.

Ca) at various scales. Minerals containing none of the elements appear black, minerals containing one of the three elements appear in the corresponding colour, minerals containing equal amounts of two or three of the elements appear in composite colours (e.g. 1 green + 1 blue = cyan, 1 red + 1 green = yellow, 1 red + 1 blue = magenta, 1 red + 1 green + 1 blue = white), and minerals containing unequal amounts of two or three of the elements appear in intermediate colours (e.g. 2 red + 1 green = orange). Each channel is normalized to the minimum and maximum count rate per pixel over the entire map; hence, where concentrations of a particular element are low, this normalization process will exaggerate backgrounds and can produce artifacts. Diffraction artefacts can also occur at low element concentrations, arising from geometry, whereby a particular crystal is aligned with a lattice plane making a Bragg angle with the input beam and the detector, although these are usually only evident in unaltered well crystalline rocks.

SULPHIDE TEXTURAL FACIES

The Eagle's Nest Ni-Cu-(PGE) deposit contains a wide range of sulphide textural facies: 1) disseminated, 2) net-textured, 3) semi-massive, and 4) massive sulphides (Table 1). The ore assemblage in all facies is a typical magmatic assemblage of pyrrhotite >> pentlandite > chalcopyrite >> magnetite±chromite. There is a general upward trend of the ore profile from discontinuous massive sulphide through more continuous net-textured to disseminated sulphide (Fig. 2). The contacts between the zones are generally relatively sharp; however, the contacts between the various net-textured facies vary from sharp to gradational. Most net-textured subfacies vary non-systematically on scales of 10 to 20 m, whereas disrupted net-textured sulphides vary on a scale of 2 to 10 cm.

Many crosscutting relationships and inclusions occur between and within the sulphide facies at Eagle's Nest (Mungall et al., 2010; Zuccarelli et al., 2017; Zuccarelli, in prep). Although the majority of massive sulphides are localized in shallow footwall embayments, massive sulphides veins (1–100 cm thick) containing inclusions of leopard and disrupted net-textured facies and barren gabbroic rocks crosscut disseminated and net-textured facies. Disrupted net-textured facies contain inclusions of net-textured olivine-sulphide cumulates, inclusion net-textured sulphides contain inclusions of barren peridotite, and disseminated sulphide facies contain inclusions of massive chromitite.

Disseminated Sulphide Facies

Disseminated sulphide facies generally contains <15 wt% sulphide and ≤6 wt% S. Mineralization is distributed heterogeneously across the deposit, most commonly between underlying net-textured sulphides and overlying barren host rocks. Disseminated sulphides occur as lightly, medium, heavily, patchy, and blebby disseminated subfacies. Lightly disseminated sulphide

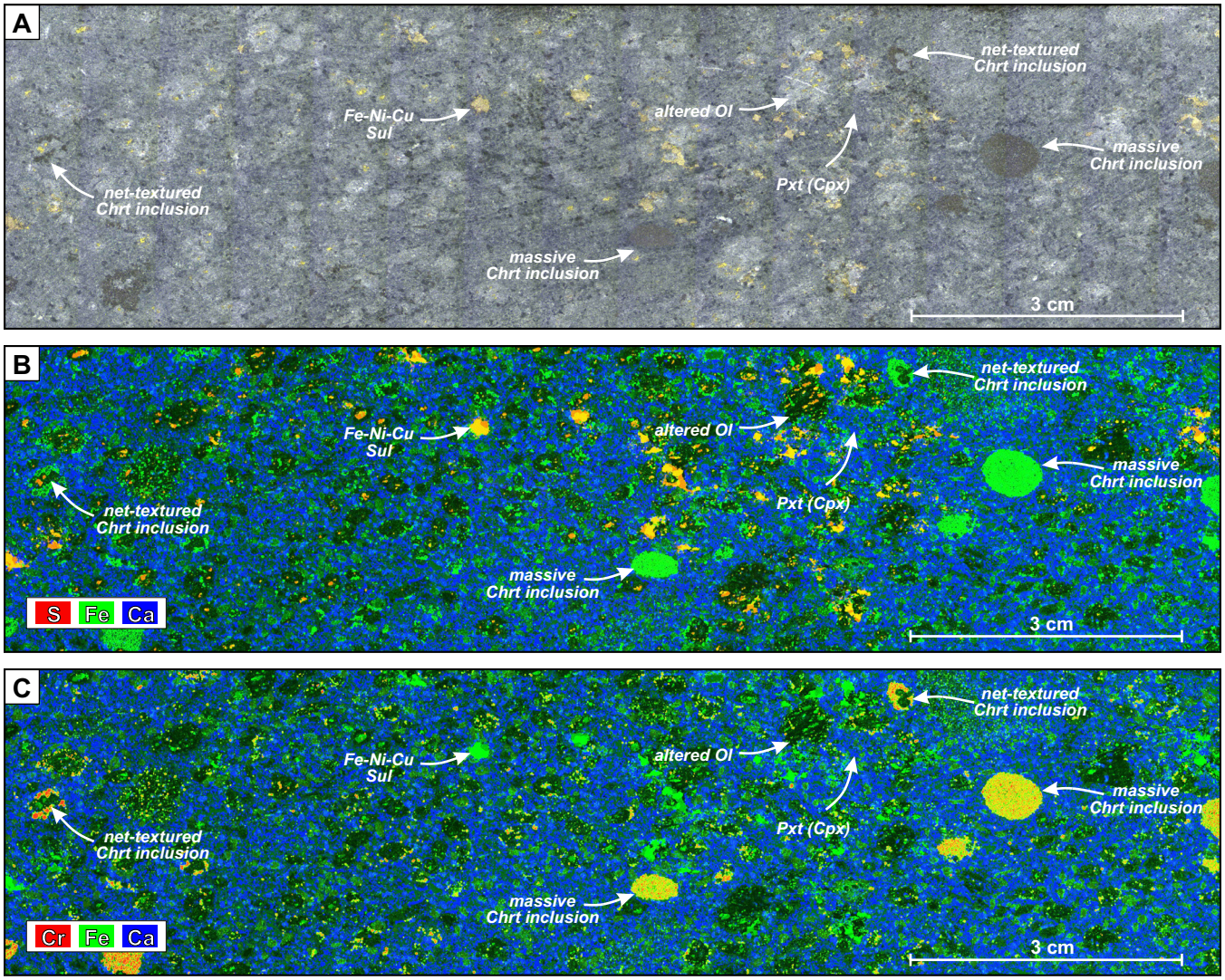

Figure 3. Disseminated sulphide facies at the Eagle's Nest deposit (drill core NOT-09-053W3 at 828.17 m, NQ core size). **a)** A scanned slab showing the typical disseminated sulphide texture within olivine pyroxenite. Black phases are chromite, dark grey phases are olivine, grey phases are pyroxene, and yellowish phases are sulphide. **b)** µXRF map, normalized relative concentrations of Ca (blue), Fe (green), and S (red). **c)** µXRF map, normalized relative concentrations of Cr (red), Fe (green), and Ca (blue). Chromite-magnetite aggregates in orange. Abbreviations: Chrt = chromitite, Cpx = clinopyroxene, Ol = olivine, Pxt = pyroxenite, Sul = sulphides.

occurs as 0.5–5 wt% sulphide distributed in very fine (0.2–0.5 mm) grains. Medium disseminated sulphide occurs as 5–10% sulphide in small to medium (0.5–10 mm) irregular wisps. Heavily disseminated sulphide occurs as 10–15 wt% sulphide in 10–30 mm irregular wisps. Patchy disseminated sulphide (8–10 wt% sulphide) occurs as very small to small (<0.5–40 mm), isolated, unevenly to uniformly dispersed, irregular patches. Blebby disseminated sulphide (2–5 wt% sulphide) occurs as small to medium (20–40 mm), rounded to subrounded blebs in the interstitial spaces between olivine and pyroxene in peridotite and pyroxenite. The sulphides within coarser blebs are occasionally fractionated with chalcopyrite-rich upperparts and pyrrhotite-pentlandite-rich lower parts, whereas finer blebs are rarely systematically fractionated.

A typical example of 8 wt% patchy disseminated sulphides within an olivine pyroxenite is shown in Figure 3 (optical scan in Fig. 3a and µXRF maps in Fig. 3b,c). The optical scan shows that sulphide is concentrated in domains containing abundant dark serpentinized olivine crystals and that several ellipsoidal chromitite inclusions are also present. However, these observations are much clearer in the µXRF maps. In the S-Fe-Ca map (Fig. 3b), it is obvious that sulphide phases (yellow and orange colours) are more abundant in olivine-rich domains (dark green), that there are few sulphides in clinopyroxene- (blue) and orthopyroxene- (green) rich domains, and that clinopyroxene-rich domains contain ellipsoidal peridotite (dark and medium green) and chromitite (bright green) inclusions. Some of the latter are embayed. In the Cr-Fe-Ca

map (Fig. 3c), it is possible to identify two types of chromitite inclusions: 1) net-textured chromitite, where chromite occurs as clusters of single crystals (red to yellow) within olivine-rich domains (dark to dark green) and 2) ellipsoidal massive chromitite inclusions exhibiting varying degrees of alteration to ferrichromite (i.e. red = Cr-rich core, yellow = Cr-poor rim). These textures are more complex than the more uniformly disseminated sulphides in most Ni-Cu-PGE deposits (*see* Barnes et al., 2017).

Net-Textured Sulphide Facies

Net-textured sulphide facies typically contains ~15–35 wt% sulphide and ~6–14 wt% S and occurs along the entire length of the deposit. It consists of ~65–85% mesocumulus olivine with ~15–35 wt% sulphides that form thin films between the olivine. However, these facies exhibit wide textural variations in the Eagle's Nest deposit, which can be subdivided into five subfacies that differ in their distribution of sulphide and silicate minerals.

Leopard net-textured sulphide subfacies

Leopard net-textured sulphide subfacies is the most common net-textured subfacies at Eagle's Nest. It consists of ~65–85% cumulus olivine and lesser intercumulus pyroxene with ~15–35 wt% interstitial sulphide that forms thin films between the olivine and triangular-shaped patches between olivine±pyroxene. Olivine and pyroxene are bimodal, ranging in size from 1–3 mm and 5–15 mm. The coarser crystals and lesser crystal aggregates define this as ''leopard net-textured'' because the large pseudomorphs of serpentine-magnetite after olivine appear as black spots among the network of yellowish sulphides giving the appearance of a leopard's coat. The sulphide assemblage is composed of pyrrhotite > pentlandite > chalcopyrite.

A typical example of the leopard net-textured sulphide subfacies rock is shown in Figure 4 (optical scan in Fig. 4a and μXRF maps in Fig. 4b,c). In the optical image (Fig. 4a), the sulphides are evenly distributed except within serpentinized olivine mesocrysts (dark black) and fine-grained aggregates (dark-greyish black phases). In the Ni-Cu-S map (Fig. 4b), abundant chalcopyrite (green) forms an anastomosing network around very fine and very coarse olivine (black), most of the pentlandite (magenta) occurs more sporadically, and most of the pyrrhotite (blue) defines a foliation oriented at ~60° to the core axis and ~60º to a weak igneous lamination defined by the olivine aggregates. This particular hole was drilled subparallel to the basal contact of the intrusion and the orientation of the sawn surface was not necessarily perpendicular to the foliation and as a result, the sulphide foliation may be a bit more perpendicular but the igneous lamination cannot be any less oblique. In the Cr-Fe-Ca map (Fig. 4c), coarse serpentinized olivine (black) is oikocrystic, containing fine chromite (red) and ferrichromite (yellow) chadacrysts, or is xenolithic comprising inclusions of chromite-bearing dunite. The matrix consists of fine disseminated clinopyroxene (blue) and Fe-bearing sulphides (green).

Pinto net-textured sulphide subfacies

Pinto net-textured sulphide subfacies, which is characterized by white (talc-altered orthopyroxene) rather than grey (clinopyroxene) or black (serpentinized olivine) "spots", is uncommon at Eagle's Nest. It comprises ~15–30 wt% sulphides and ~6–12 wt% S and most commonly occurs as 1–2 m zones within areas of disrupted net-textured sulphides and where domains of leopard net-textured sulphide facies rocks border pyroxene-rich domains. It is texturally similar to leopard net-textured subfacies rock and consists of small serpentinized olivine surrounded by interstitial sulphides with large (0.3–10 mm) subhedral-euhedral oikocrysts of talc-carbonate-altered orthopyroxene (appearing whitish-grey in the core). The oikocrysts contain both fresh and serpentinized olivine.

A typical example of pinto net-textured sulphide subfacies rock is shown in Figure 5 (optical scan in Fig. 5a, μXRF maps in Fig. 5b,c). In the optical image (Fig. 5a) the amount of sulphide is relatively small (~20–25%) and occurs almost exclusively in close association with small serpentinized olivine crystals (black) that are interstitial to coarse sulphide-free orthopyroxene oikocrysts (grey). In the Ni-Cu-S map (Fig. 5b), pyrrhotite (blue), pentlandite (magenta), and chalcopyrite (green) are more-or-less evenly disseminated throughout the sample except within the large weakly aligned pyroxene domains (black). Nevertheless, chalcopyrite is more common on the peripheries of the pyroxene oikocrysts. In the Cr-Fe-Ca map (Fig. 5c), the matrix is dominated by sulphides (green) and fine-grained olivine (greenish-black), and the pyroxene-rich domains include parts comprising mainly orthopyroxene (reddish-brown), chromite (red), and ferrichromite (orange and yellow) as well as parts comprising mainly clinopyroxene (blue).

Inclusion net-textured sulphide subfacies

Inclusion net-texture sulphide subfacies, which is another uncommon variety of net-textured sulphide at Eagle's Nest, contains ~15–30 wt% sulphide and ~6–12 wt% S. It is similar to the leopard net-textured sulphide subfacies except that it contains a greater abundance of clinopyroxene (~10–15% silicates) and is characterized by 4–300 mm silicate inclusions. The inclusions are typically dunite to peridotite, vary in shape from angular to rounded, and the contacts

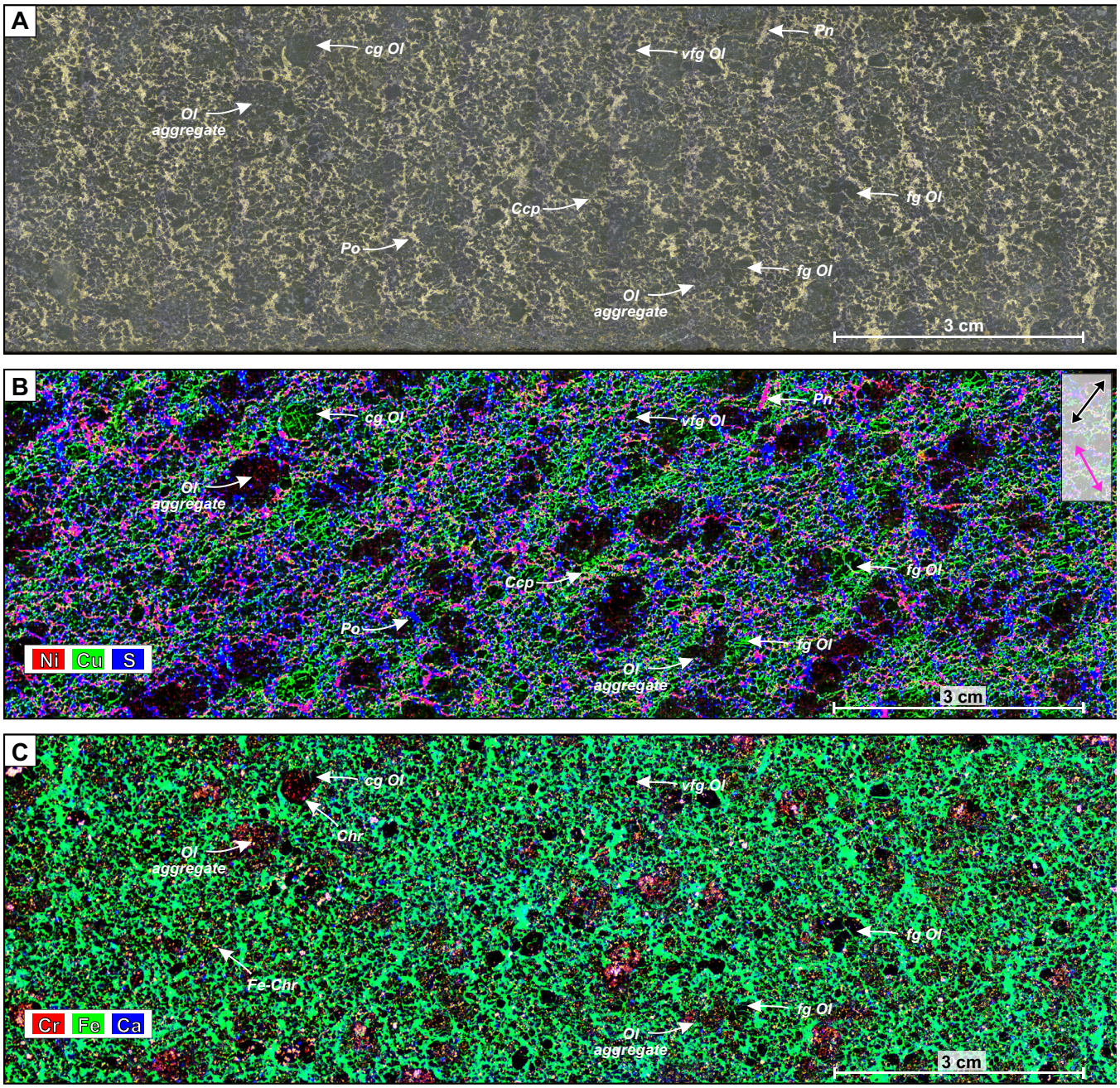

Figure 4. Leopard net-textured sulphide subfacies at Eagle's Nest deposit (drill core NOT-07-017 at 138.01 m, NQ core size). **a)** A scanned slab of a typical leopard net-textured sulphide. The black minerals are serpentinized olivine and the yellowish minerals are sulphide minerals including pyrrhotite, pentlandite, and chalcopyrite. However, these sulphide minerals are difficult to distinguish. **b)** µXRF map with normalized relative concentrations of Ni (red), Cu (green), and S (blue) resulting in olivine appearing as black, chalcopyrite as green, pyrrhotite as blue, and pentlandite as magenta. **c)** µXRF map with normalized relative concentrations of Cr (red), Fe (green), and Ca (blue) resulting in olivine appearing as black, chromite as red, ferrichromite as yellow, clinopyroxene as blue and Fe-bearing sulphides as green. The black arrow indicates the direction of a weak igneous lamination defined by the alignment of the olivine aggregates; the magenta arrow indicates the direction of the weak foliation defined by pentlandite±pyrrhotite veinlets. Abbreviations: cg = coarse-grained, fg = fine-grained, vfg = very fine-grained; Ccp = chalcopyrite, Chr = chromite, Fe-Chr = ferrichromite, Ol = olivine, Pn = pentlandite, Po = pyrrhotite.

between olivine and pyroxene along the margins are diffuse and infiltrated by sulphide (typically chalcopyrite). One particularly large (30 cm) inclusion is exceptionally angular but also exhibits irregular and diffuse margins (Zuccarelli, in prep).

A typical example of inclusion net-textured sulphide subfacies rock containing ~25 wt% sulphides is shown in Figure 6. In the optical image (Fig. 6a), sulphide is not evenly distributed and is controlled mainly by the distribution of inclusions and, to a lesser extent, olivine. The three main domains can be defined: 1) chalcopyrite-pentlandite-(pyrrhotite), 2) pentlandite-pyrrhotite-

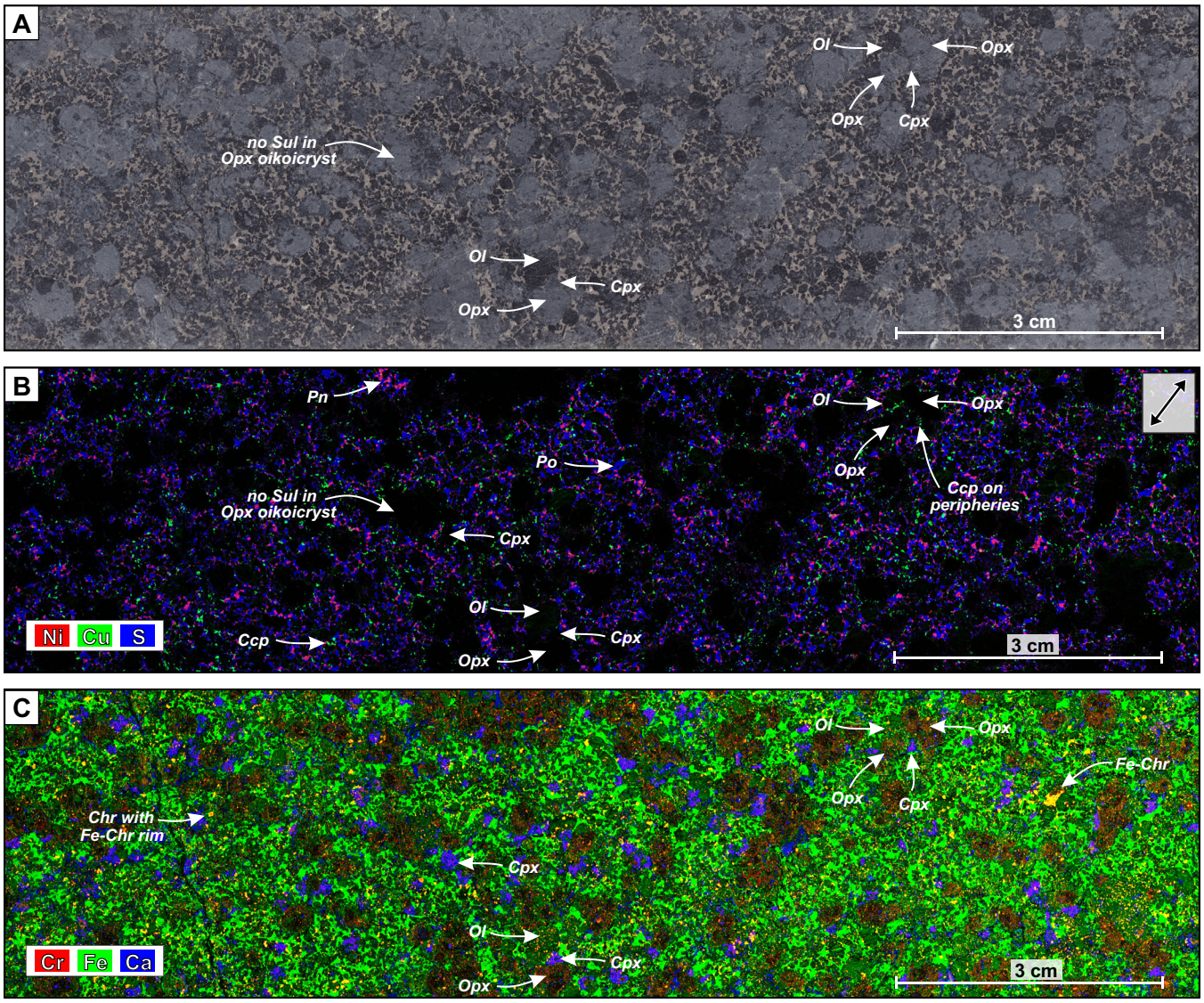

Figure 5. Pinto net-textured sulphide subfacies at the Eagle's Nest deposit (sample NOT-10-076-W1/557.1 m, NQ core size). **a)** A scanned slab of typical pinto net-textured sulphide. The black minerals are olivine, grey minerals are pyroxene, and yellowish minerals are sulphide. **b)** µXRF map with normalized relative concentrations of Ni (red), Cu (green), and S (blue) with pyrrhotite appearing as blue, pentlandite as magenta, and chalcopyrite as green. **c)** µXRF map with normalized relative concentrations of Cr (red), Fe (green), and Ca (blue) resulting in the sulphides appearing as green, olivine as greenish-black, orthopyroxene-rich domains as reddish-brown, chromite as red, ferrichromite as yellow and orange, and clinopyroxene as blue. The black arrow indicates the direction of the weak lamination defined by orthopyroxene oikocrysts. Abbreviations: Ccp = chalcopyrite, Cpx = clinopyroxene, Chr = chromite, Fe-Chr = ferrichromite, Ol = olivine, Opx = orthopyroxene, Pn = pentlandite, Po = pyrrhotite, Sul = sulphides.

(chalcopyrite), and 3) chalcopyrite-pyrrhotite-pentlandite. In the Ni-Cu-S map (Fig. 6b), pentlandite (magenta), pyrrhotite (blue), and lesser chalcopyrite (cyan or green) occur both in large domains with silicates (reddish-black in this image) and in fine pyrrhotite-pentlandite-rich veinlets oriented at ~90° to the core axis (subparallel to the dyke contact). Chalcopyrite, silicates, and lesser pyrrhotite-pentlandite dominate the other domains. In the Cr-Fe-Ca map (Fig. 6c), it is clear that the silicate phases include coarse-grained olivine (black) containing small inclusions of chromite (red), orthopyroxene (opalescent), medium-grained clinopyroxene (blue), and fine-grained olivine (black) within sulphide (green). The 1 cm dunite autolith in this sample is a serpentinized peridotite composed of serpentine (black) with magnetite (green) veinlets and fine chromite inclusions (red).

Disrupted net-textured sulphide subfacies

Disrupted net-textured sulphide subfacies is a localized but common form of net texture in Eagle's Nest, containing ~18–25 wt% sulphide and ~7–10 wt% S. It is characterized by highly irregular domains of grey talc-magnesite-altered pyroxenite that transgresses leopard net-texture and consists of coarse (up to 4 mm) serpentinized olivine in a matrix of fine serpentinized olivine

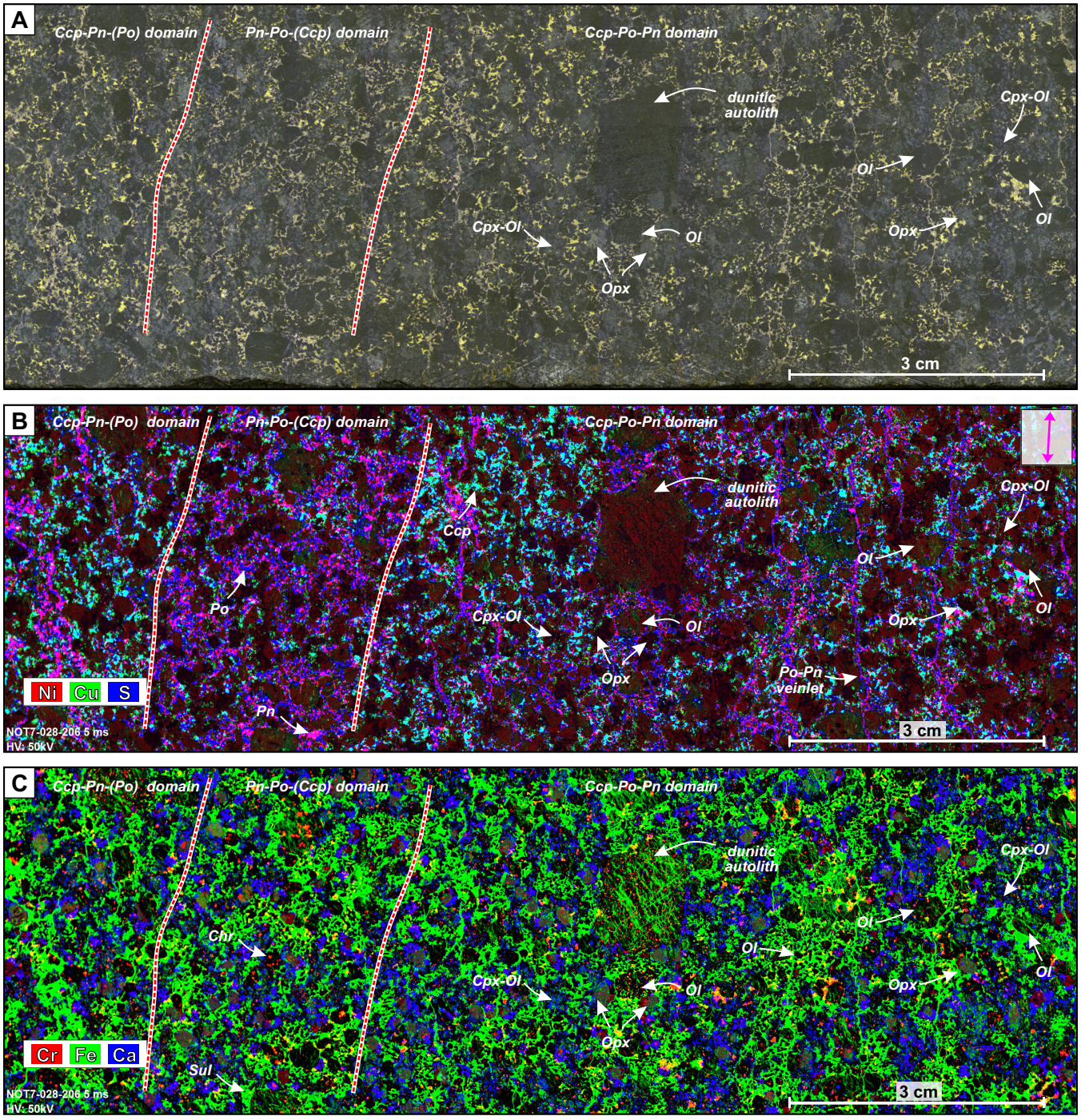

Figure 6. Inclusion net-textured sulphide subfacies at the Eagle's Nest deposit (drill core NOT-07-028 at 208.97 m, NQ core size). **a)** A scanned slab of a typical inclusion net-textured sulphide facies rock from the Eagle's Nest deposit. The black minerals are olivine and the yellowish minerals are sulphide. **b)** µXRF map with normalized relative concentrations of Ni (red), Cu (green), and S (blue). **c)** µXRF map with normalized relative concentrations of Cr (red), Fe (green), and Ca (blue). Red-dashed lines show the approximate limit between pentlandite-pyrrhotite-rich and chalcopyrite-rich domains; the magenta arrow in (b) indications the orientation of the fine veinlets of pentlandite and pyrrhotite. Abbreviations: Ccp = chalcopyrite, Chr = chromite, Cpx = clinopyroxene, Ol = olivine, Opx = orthopyroxene, Pn = pentlandite, Po = pyrrhotite.

and sulphides, often leaving isolated coarse unserpentinized olivine but not any fine-grained olivine or sulphides. The contacts between the pyroxenite domains and net-textured sulphides are very irregular. The most abundant sulphide mineral in this subfacies is pyrrhotite, with varying amounts of fine-grained pentlandite (0.1–0.5 mm) and chalcopyrite (0.1–3 mm). Magnetite occurs in both barren and mineralized areas, forming grains of up to 0.5 mm in apparent diameter that range from anhedral to euhedral. Minor chromite is also present.

A typical example of disrupted net-textured sulphide subfacies rock, containing ~25 wt% sulphides, is shown

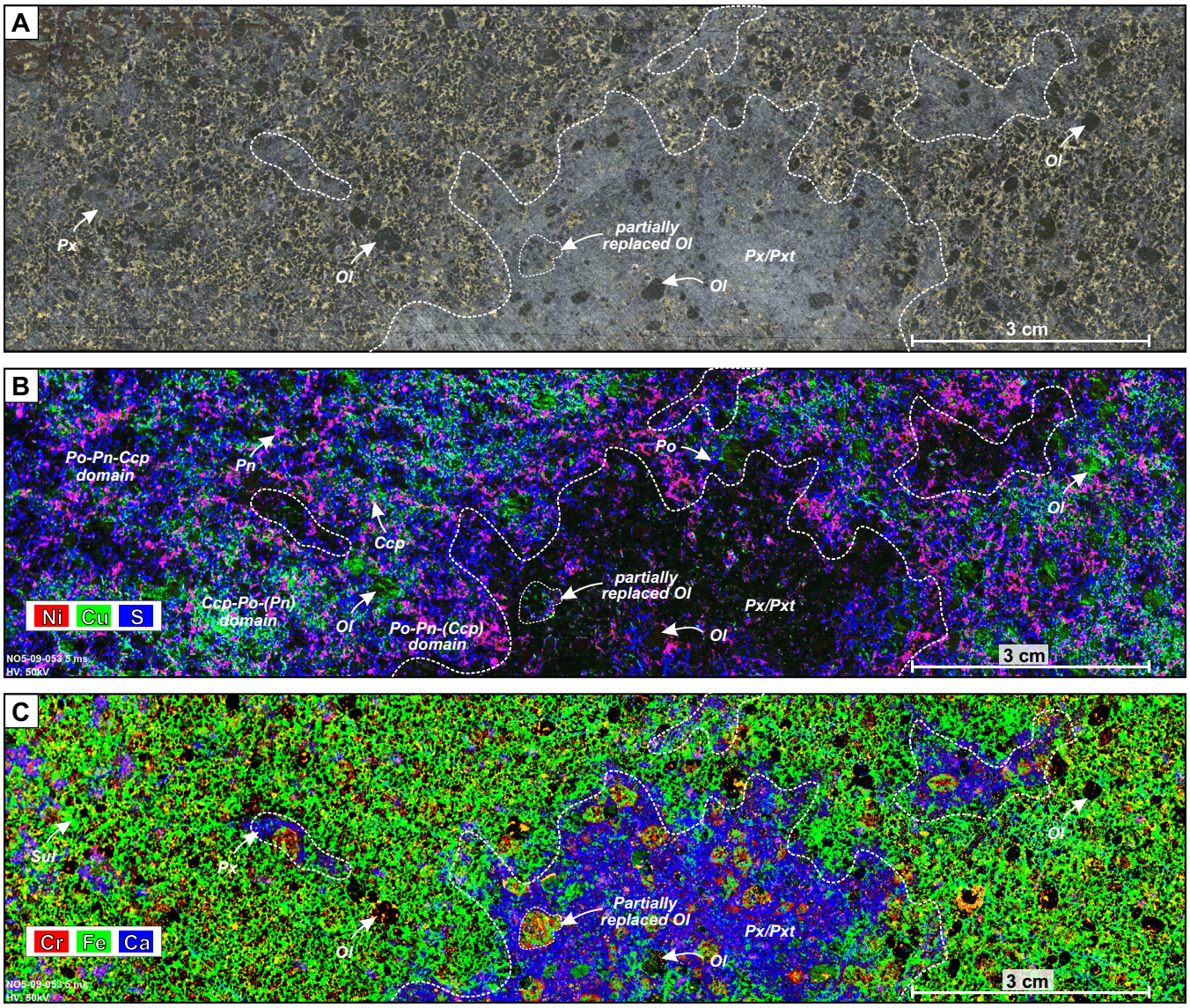

Figure 7. Disrupted net-textured sulphide subfacies from the Eagle's Nest deposit (drill core NOT-09-053 at 857.26 m, NQ core size). **a)** A scanned slab of typical disrupted net-textured sulphide. The black minerals are olivine and the yellowish minerals are sulphide. **b)** µXRF map with normalized relative concentrations of Ni (red), Cu (green), and S (blue) showing three main sulphide domains (*see* text for discussion). **c)** µXRF map with normalized relative concentrations of Cr (red), Fe (green), and Ca (blue). White dotted lines indicate the gradational contact between the pyroxenite and the net-textured sulphide facies into the disrupted net-textured sulphide subfacies rock. Abbreviations: Ccp = chalcopyrite, Ol = olivine, Pn = pentlandite, Po = pyrrhotite, Px = pyroxene, Pxt = pyroxenite.

in Figure 7. The optical image (Fig. 7a) indicates that sulphide is much more abundant in leopard net-textured domains containing abundant fine-grained serpentinized olivine (black) and much less abundant in areas where pyroxene (grey) occurs as pyroxenite. The Ni-Cu-S map (Fig. 7b), highlights three main sulphide domains that border the areas of pyroxenite, progressing outward from (1) pyrrhotite (blue) ≈ pentlandite (magenta) >> chalcopyrite (green) through (2) chalcopyrite >> pyrrhotite ≈ pentlandite to (3) pyrrhotite ≈ pentlandite > chalcopyrite. In the Cr-Fe-Ca map (Fig. 7c), the distinction between the pyroxenitic material (blue), which contain patches of residual olivine (black), ferrichromite (yellow), and chromite (red), and the surrounding net-textured sulphides (green; all sulphide species), is more distinct.

Massive to Semi-massive Sulphide Facies

Massive sulphide facies at Eagle's Nest contains >80 wt% sulphides and >31 wt% S and is localized mainly in two embayments along the (original) basal contact (Fig. 2). Gangue phases include inclusions of peridotite and calcite. Semi-massive sulphide, which is very uncommon in the Eagle's Nest deposit, contains 50–80 wt% sulphides and ~20–31 wt% S depending on the proportion of inclusions present. It occurs in the lower parts of the deposit in contact with country rocks (more common) and the upper parts of the deposit in contact

with barren ultramafic rocks (less common). The non-sulphide component is normally composed of gabbro or granodiorite xenoliths derived from the country rocks, and pyroxenite and peridotite anteliths or autoliths ("cognate xenoliths") derived from this or other phases of the intrusive system. Although much less common, sulphide-bearing inclusions also occur within this facies and are normally composed of leopard net-textured sulphides. Semi-massive sulphides contain no olivine and pyroxene crystals, except within ultramafic inclusions. The sulphides are similar to those found in the massive sulphide facies.

A contact between semi-massive and massive sulphide facies is shown in Figure 8 (optical scan in Fig. 8a, μXRF maps in Fig. 8b,c). The amount of sulphide varies from ~60% in semi-massive sulphides (left side of image) to ~95% in massive sulphides (right side of image). The semi-massive sulphide domain contains abundant inclusions of altered, recrystallized, and partially melted gabbro. In the Ni-Cu-S map (Fig. 8b), it is clear that the semi-massive sulphides are composed of pyrrhotite (blue) >> pentlandite (magenta) chalcopyrite (cyan) and that the massive sulphides are composed of pyrrhotite > pentlandite chalcopyrite. Pentlandite and chalcopyrite are finer grained and more dispersed (occurring as patches and along pyrrhotite grain boundaries) in semi-massive sulphides, and coarser grained and more segregated in massive sulphides. In the Cr-Fe-Ca map (Fig. 8c), pyrrhotite is bright green, and pentlandite and chalcopyrite are both dark green. The sulphide minerals display a combination of coarse granular pentlandite (at contacts with chalcopyrite) and thin (sub-mm) "loops" of exsolved pentlandite (commonly in semi-massive sulphide around pyrrhotite grain boundaries, Fig. 8c). The inclusions contain a Ca-rich phase (dark blue), likely altered clinopyroxene based on the mineral habit, and a Cr-Fe-Ca-poor phase (black), likely altered (albitic) plagioclase. Ferrichromite (orange-yellow) occurs as isolated crystals and as rims on inclusions.

DISCUSSION

Maps obtained by μXRF provide greatly enhanced textural, mineralogical, and geochemical characterizations compared that obtained from macroscopic core logging and microscopic petrographic examination. In particular, they provide detailed geochemical information that is not available by either of the other methods and at a scale larger than permitted by SEM-based ED-XRES, EPMA-based WD-XRES, or LA-ICP-MS methods[1].

Below we further discuss some of the textures in Eagle's Nest ores and their implications for the genesis of the mineralization.

Mineralogical Insights

Clinopyroxene and orthopyroxene in pinto and disrupted net-textured sulphide subfacies

Superimposed talc-carbonate alteration commonly hampers identifications of primary mineralogy, but μXRF maps make it possible to readily distinguish between serpentine-magnetite pseudomorphs after olivine in leopard net-textured sulphide, talc±anthophyllite pseudomorphs after orthopyroxene and Ca-rich amphibole pseudomorphs after clinopyroxene in pinto net-textured sulphide, and Ca-pyroxene pseudomorphs after clinopyroxene in disrupted net-textured sulphide.

In pinto net-textured sulphides (Fig. 5), the μXRF maps indicate that clinopyroxene occurs as evenly distributed, fine-grained (0.1–0.2 mm) subhedral crystals, whereas orthopyroxene occurs both as evenly distributed, medium-grained (0.3–10 mm) rounded crystals typically associated with clinopyroxene, and as coarse-grained (up to 15 mm) irregular aggregates. The composite orthopyroxene-clinopyroxene crystals are evenly distributed and appear to have nucleated more-or-less homogeneously, locally impinging on each other to form coarser aggregates. Both pyroxenes are devoid of sulphides, suggesting that they crystallized from the silicate melt prior to the introduction of sulphide liquid.

In disrupted net-textured (Fig. 7), the μXRF maps indicate that the clinopyroxene has replaced smaller olivine crystals and possibly sulphide, leaving behind coarser olivine crystals and aggregates. The nature of this process is discussed further below.

Sulphide inclusions in olivine

The presence of pyrrhotite as uncommon blebs within olivine and pyroxene may represent (1) mobilization of sulphides into fractures in olivine after serpentinization (large fracture in olivine seen in Fig. 6), or (2) sulphidation of magnetite formed during serpentinization, as observed at the Raglan mine in Quebec (Bazilevskaya, 2009).

Monosulphide Solid Solution Segregation

Small-scale monosulphide solid solution segregation

The greater segregation of Cu and Fe-Ni in inclusion net-textured (Fig. 6), disrupted net-textured (Fig. 7), and massive (Fig. 8) sulphide textures is attributed to segregation of Cu-rich residual sulphide liquid from Fe-Ni-rich monosulphide solid solution (mss) (*see* review of phase equilibria by Naldrett, 2004). In the net-textured sulphide subfacies, the inclusions may have phys-

[1] ED = energy dispersive, EPMA = electron probe microanalyzer, LA-ICP-MS = laser ablation-inductively coupled plasma-mass spectrometry, SEM = scanning electron microscope, WD = wavelength-dispersive, XRES = X-ray emission spectrometry.

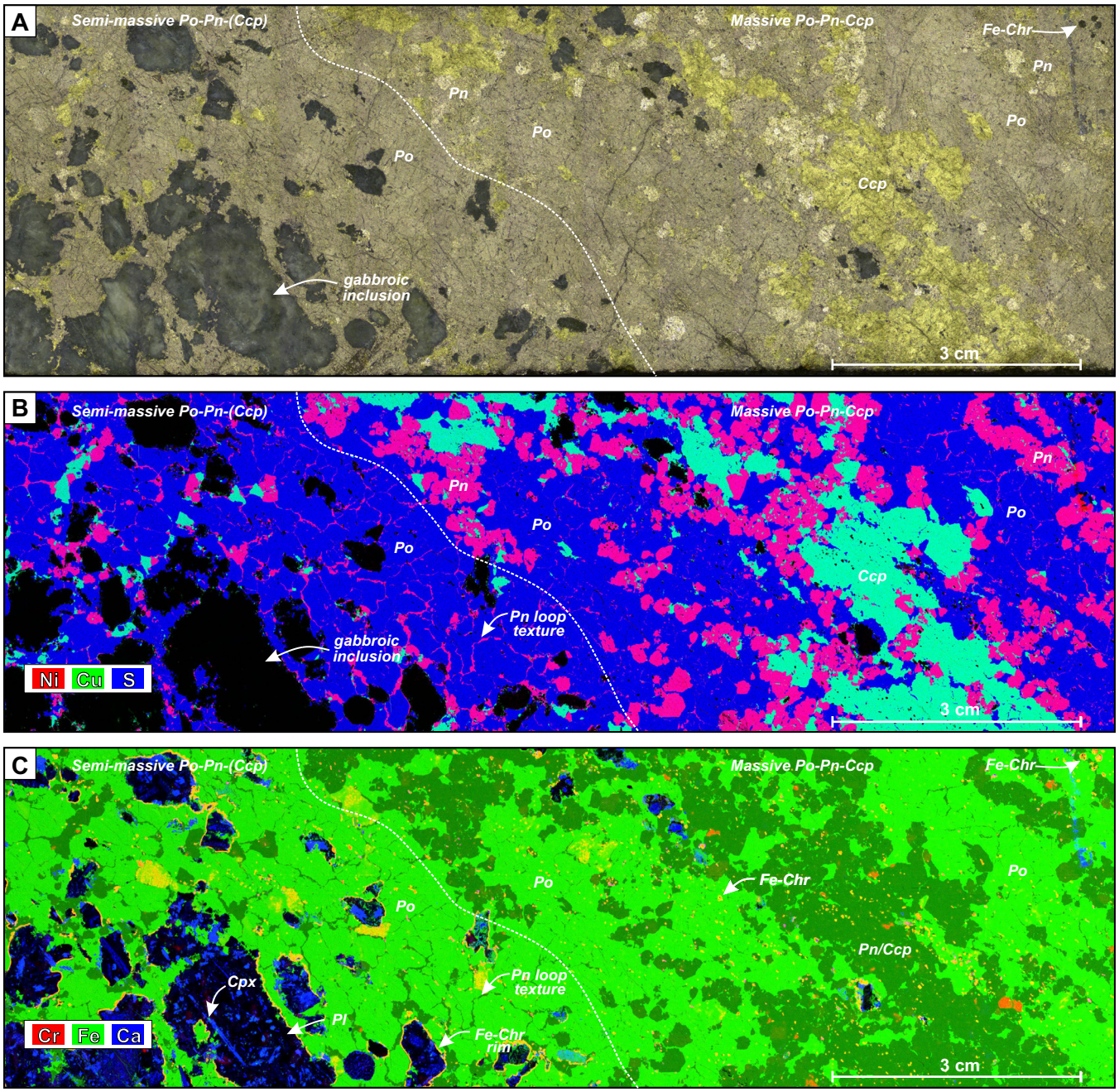

Figure 8. Massive and semi-massive sulphide facies at the Eagle's Nest deposit (drill core NOT-10-087A at 608 m, NQ core size). **a)** A scanned slab of typical semi-massive sulphides containing numerous gabbroic inclusions (dark grey on the left side) and massive sulphide (right side). The yellowish minerals are sulphide and fine black minerals are fine ferrichromite. **b)** μXRF map with normalized relative concentrations of Ni (red), Cu (green), and S (blue). **c)** μXRF map with normalized relative concentrations of Cr (red), Fe (green), and Ca (blue). The coarse yellow patches within the pyrrhotite crystals in this image are diffraction artifacts. Abbreviations: Ccp = chalcopyrite, Cpx = clinopyroxene, Fe-Chr = ferrichromite, Pl = plagioclase, Pn = pentlandite, Po = pyrrhotite.

ically facilitated migration of sulphide liquid from mss, and the emplacement of the late pyroxenite may have slowed cooling and/or reheated the mineralization.

Large-scale monosulphide solid solution-melt segregation

Pyrrhotite±pentlandite veinlets locally crosscut the fabrics of net-textured ores and locally also olivine and pyroxene grains (Fig. 4, 6). They appear to be oriented at steep angles to the basal contact of the intrusion. The abundance of pyrrhotite-pentlandite and paucity of chalcopyrite in the veinlets suggests that they represent the lower temperature equivalents of higher temperature Fe-Ni-(Co)-rich mss. Two possible origins are (1) solid-state mobilization of mss into the veinlets during volume expansion accompanying serpentinization of

olivine (which we consider less likely based on the mineralogy, textures, and orientation), and (2) crystallization of mss from a sulphide liquid as it percolated downward through the crystal network of olivine crystals, from which the residual Cu-rich sulphide liquid escaped (which we consider more likely based on the same features). In the latter case, some of the Cu-rich sulphide liquid may have infiltrated other areas, forming complementary chalcopyrite-rich mineralization represented by sporadic chalcopyrite-rich veins (e.g. Fig. 2). Further study of relationships between the veinlets and serpentine-magnetite alteration should provide better insights into the relative roles of each process.

Multistage Silicate-Sulphide Emplacement

Country-rock inclusions

The presence of barren gabbro inclusions only in semi-massive sulphide (Fig. 8) indicates that only this phase of mineralization incorporated gabbroic country rocks prior to reaching this part of the system. The reason for the restriction to these facies is not known but would require a separate phase of emplacement. The thin, semi-continuous ferrichromite rims along the margins of the gabbro inclusions against sulphide suggest reaction with sulphide liquid. These rims are similar to ferrichromites that occur along the basal and upper margins of massive sulphides in other komatiite-associated Ni-Cu-(PGE) deposits (e.g. Kambalda: Groves et al., 1977; Silver Swan: Dowling et al., 2004; Alexo: Houlé et al., 2012; *see also* Fonseca et al., 2008). Gabbroic inclusions have significantly lower densities (~2.9 g cm^{-3}) than sulphide liquid (~4.2 g cm^{-3}), so unless connected in 3-D, all but the smallest inclusions would rapidly rise through sulphide liquid (*see* Lesher, 2017). If so, this means (1) they could not have been transported over significant distances, and (2) they must have been incorporated shortly before the sulphide liquid began to crystallize. Alternatively, the gabbroic inclusions could also represent sulphide-silicate emulsion textures, which also exhibit fine chromite rims (e.g. Frost and Groves, 1989; Staude et al., 2017). In this case, the "inclusions" might be connected in 3-D to the original contact (*see* Dowling et al., 2004). However, thus far, no evidence of such a connection has been observed to support this interpretation.

Anteliths

The presence of inclusions of barren peridotite only within disseminated and inclusion net-textured sulphides (Fig. 6) indicates that only these phases of mineralization incorporated anteliths "upstream" in the system or within this part of the system. The latter is more likely because the angular margins of some of the inclusions would likely not have survived during transport-related thermochemical sulphide erosion.

Chromitite and chromite-peridotite inclusions

The presence of ellipsoidal inclusions of chromitite (Fig. 3) and net-textured chromitite in disseminated sulphide (Fig. 3), but not in any of the other textural types, indicates that the disseminated sulphides formed from a different magma or that chromite xenoliths were completely assimilated in other textures. The chromite inclusions were coarser and denser (1–2 cm, ~5.2 g cm^{-3}) than associated olivine (3–5 mm, ~3.2 g cm^{-3}), so should have settled much more rapidly (*see* Lesher, 2017). This suggests that the magmas that formed the disseminated mineralization were emplaced after the magma that formed the underlying net-textured mineralization and that the chromite inclusions were transported from "upstream" of the plumbing system. The chromite inclusions may represent chromitite that crystallized in a staging chamber and was mechanically eroded, or the inclusions may represent refractory magnetite layers (e.g. massive chromitite inclusions) that were disrupted and upgraded to chromite during transport, similar to the process envisioned for the chromite horizons in the overlying Esker intrusive complex (Lesher et al., 2019).

Disrupted net-textured sulphide facies

One of the main characteristics of the disrupted net-textured sulphide facies is its very localized and heterogeneous distribution throughout the deposit (Zuccarelli et al., 2017, 2018b). This heterogeneity is well illustrated at the deposit scale in Figure 2, but also at the mesoscopic scale in Figure 7 where domains (2–5 cm) of barren pyroxenite are surrounded by more typical net-textured sulphide. Several scenarios have been evaluated by Zuccarelli (in prep) to explain disrupted net-textured sulphide: 1) early downward gravitational percolation of molten sulphide; 2) invasion by a late magmatic pyroxenitic melt, as proposed by Spath (2017) for the Black Label chromite zone of the Black Thor intrusion of the Esker intrusive complex a few kilometres to the northeast; 3) infiltration by a late magmatic Ca-Si-rich fluid, converting olivine to pyroxene, as proposed for the Ntaka ultramafic complex, Tanzania by Barnes et al. (2016); and/or 4) variable degrees of metamorphic alteration.

A detailed discussion of each hypothesis is beyond the scope of this contribution; however, µXRF mapping (Fig. 7b,c) shows that some olivine has been transgressed by pyroxene rather than corroded by it. This favours physical invasion by a more fractionated magma that crystallized pyroxenite rather than the reaction of olivine with a Ca-Si-rich fluid to produce pyroxene, which is consistent with the occurrence of pyroxenite also crosscutting barren peridotite elsewhere within the Eagle's Nest intrusion (Zuccarelli, in prep) and in the nearby Black Label chromite zone (Spath, 2017).

The zonation of sulphides outward from pyroxenite in Figure 7b most likely reflects the partial melting of the Fe-Ni-Cu sulphides, mobilizing a Cu-rich sulphide melt and leaving behind a Cu-poor mss.

Late Sulphide Mobilization

The veins of massive pentlandite-pyrrhotite-chalcopyrite and chalcopyrite-pyrrhotite-pentlandite that crosscut disseminated and net-textured facies could represent separate late injections of massive sulphide liquids from upstream in the conduit, but more likely represent late mobilization of a molten sulphide liquid within the conduit. Fe-Ni-Cu sulphides crystallize at temperatures of between 1160 and 850ºC (*see* review of phase equilibria by Naldrett, 2004), which is below the 1360–1200ºC temperature over which the host rocks would have crystallized (*see* review by Arndt et al., 2008).

CONCLUSIONS

The wide variety of sulphide textures within the Eagle's Nest orebody have been characterized using μXRF, adding critical geochemical and mineralogical information that has greatly expanded and improved our understanding of the geological history and genesis of the ores.

The μXRF scans more clearly define the textural differences between each sulphide facies and subfacies as well as other distinguishing features: 1) chromitite inclusions in disseminated sulphides, 2) mesocrysts and aggregates of serpentinized olivine in leopard net-textured sulphides, 3) altered orthopyroxene oikocrysts in pinto net-textured sulphides, 4) peridotite anteliths in inclusion net-textured sulphides, 5) transgressive pyroxenite in disrupted net-textured sulphides, 6) gabbro inclusions in semi-massive sulphides, and 7) small- and large-scale segregation of mss and residual sulphide liquids in many of these facies. Different types of inclusions in disseminated, inclusion net-textured, and semi-massive sulphides, and the presence of late pyroxenite suggest that the inclusions were emplaced in separate "pulses".

ACKNOWLEDGMENTS

This report is a contribution to NRCan's Targeted Geoscience Initiative Program (TGI). Support for this study was provided through the Orthomagmatic Ni-Cu-PGE-Cr Ore Systems Project's 'Activity NC-2.1: Architecture of magmatic conduits in Cr-(PGE)/Ni-Cu-(PGE) ore systems'.

Natascia Zuccarelli is conducting a TGI-supported M.Sc. thesis at Laurentian University, Sudbury, Ontario. The authors are thankful to Noront Resources Ltd. (Alan Coutts, Ryan Weston, Matt Downey, and the Esker exploration team) for providing access to properties and geological information. We are also grateful to Ryan Weston, Matt Deller, and Geoff Heggie from Noront Resources Ltd. for their strong support throughout the project, insightful discussions, and sharing of knowledge on the geology and mineralization of the Eagle's Nest deposit. The μXRF mapping was carried out at the CSIRO characterization facility in Perth, Western Australia, and Michael Verrall is thanked for assistance and laboratory maintenance. This report benefited from scientific reviews by Charley Duran and Wouter Bleeker, and editorial review by Elizabeth Ambrose and Valérie Bécu.

REFERENCES

Arndt, N., Lesher, C.M., and Barnes, S.J., 2008. Komatiite; Cambridge University Press, Cambridge, United Kingdom, 467 p. (first edition)

Barnes, S.J. and Mungall, J.E., 2018. Blade-shaped dikes and nickel sulphide deposits: a model for the emplacement of ore-bearing small intrusions; Economic Geology, v. 113, p. 789–798.

Barnes, S.J., Mole, D.R., Le Vaillant, M., Campbell, M.J., Verrall, M.R., Roberts, M.P., and Evans, N.J., 2016. Poikilitic textures, heteradcumulates and zoned orthopyroxenes in the Ntaka Ultramafic Complex, Tanzania: Implications for crystallization mechanisms of oikocrysts; Journal of Petrology, v. 57, p. 1171–1198.

Barnes, S.J., Mungall, J.E., Le Vaillant, M.L., Godel, B., Lesher, C.M., Holwell, D.M., Lightfoot, P.C., Krivolutskaya, N., and Wei, B., 2017. Sulphide-silicate textures in magmatic Ni-Cu-PGE sulphide ore deposits: Disseminated and net-textured ores; American Mineralogist, v. 102, p. 473–506.

Bazilevskaya, E., 2009. Primary and secondary textures of Fe-Ni-Cu sulfide mineralization in the Katinniq member of the Raglan Formation, Cape Smith Belt, New Quebec; M.Sc. thesis, Laurentian University, Sudbury, Ontario, 59 p.

Dowling, S.E., Barnes, S.J., and Hill, R.E.T., 2004. Komatiites and nickel sulfide ores of the Black Swan area, Yilgarn Craton, Western Australia. 2: Geology and genesis of the orebodies; Mineralium Deposita, v. 39, p. 707–728.

Frost, K.M. and Groves, D.I., 1989. Magmatic contacts between immiscible sulfide and komatiitic melts; implications for genesis of Kambalda sulfide ores; Economic Geology, v. 84, p. 1697–1704.

Fonseca, R.O.C., Campbell, I.H., O'Neill, H.St.C., and Fitzgerald, J.D., 2008. Oxygen solubility and speciation in sulphide-rich mattes; Geochimica et Cosmochimica Acta, v. 72, p. 2619–2635.

Groves, D.I., Barrett, F.M., Binns, R.A., and McQueen, K.G., 1977. Spinel phases associated with metamorphosed volcanic-type iron-nickel sulfide ores from Western Australia; Economic Geology, v. 72, p. 1224–1244.

Houlé, M.G., Lesher, C.M., and Davis, P.C., 2012. Thermomechanical erosion at the Alexo mine, Abitibi greenstone belt, Ontario: Implications for genesis of komatiite-associated Ni-Cu-(PGE) mineralization; Mineralium Deposita, v. 47, p. 105–128.

Houlé, M.G., Lesher, C.M., Metsaranta, R.T., and Sappin, A.-A., 2019. Architecture of magmatic conduits in chromium-PGE and Ni-Cu-PGE ore systems in Superior Province: Example from the 'Ring of Fire' region, Ontario; *in* Targeted Geoscience Initiative: 2018 report of activities, (ed.) N. Rogers; Geological Survey of Canada, Open File 8549, p. 441–448.

Houlé, M.G., Lesher, C.M., Metsaranta, R.T., Sappin, A.-A., Carson, H.E.J., Schetselaar, E., McNicoll, V., and Laudadio, A., 2020. Magmatic architecture of the Esker intrusive complex,

Ring of Fire intrusive suite, McFaulds Lake greenstone belt, Superior Province, Ontario: Implications for the genesis of Cr and Ni-Cu-(PGE) mineralization in an inflationary dyke-chonolith-sill complex; *in* Targeted Geoscience Initiative 5: Advances in the understanding of Canadian Ni-Cu-PGE and Cr ore systems – Examples from the Midcontinent Rift, the Circum-Superior Belt, the Archean Superior Province, and Cordilleran Alaskan-type intrusions, (ed.) W. Bleeker and M.G. Houlé; Geological Survey of Canada, Open File 8722, p. 141–163.

Laudadio, A., 2019. 3D Geological Modeling of the Double Eagle–Black Thor Intrusive Complexes, McFaulds Lake Greenstone Belt, Ontario, Canada; M.Sc. thesis, Carleton University, Ottawa, Ontario, 107 p.

Lesher, C.M., 2017. Roles of residues/skarns, xenoliths, xenocrysts, xenomelts, and xenovolatiles in the genesis, transport, and localization of magmatic Fe-Ni-Cu-PGE sulfides and chromite; Ore Geology Reviews, v. 90, p. 465–484.

Lesher, C.M., Carson, H.J.E., and Houlé, M.G., 2019. Genesis of chromite deposits by dynamic upgrading of Fe±Ti oxide xenocrysts; Geology, v. 47, p. 207–210.

Metsaranta, R.T., Houlé, M.G., McNicoll, V.J., and Kamo, S.L., 2015. Revised geological framework for the McFaulds Lake greenstone belt, Ontario; *in* Targeted Geoscience Initiative 4: Canadian Nickel-Copper-Platinum Group Elements-Chromium Ore Systems — Fertility, Pathfinders, New and Revised Models, (ed.) D.E. Ames and M.G. Houlé; Geological Survey of Canada, Open File 7856, p. 61–73.

Mungall, J.E., Harvey, J.D., Balch, S.J., Azar, B., Atkinson, J., and Hamilton, M.A., 2010. Eagle's Nest: A Magmatic Ni-Sulfide Deposit in the James Bay Lowlands, Ontario, Canada; Chapter 28 *in* The Challenge of Finding New Mineral Resources: Global Metallogeny, Innovative Exploration, and New Discoveries, (ed.) R.J. Goldfarb, E.E. Marsh, and T. Monecke; Society of Economic Geologists, Special Publication 15, v. 1, p. 539–557.

Naldrett, A.J., 2004. Magmatic Sulfide Deposits: Geology, Geochemistry and Exploration; Springer, Berlin, Germany, New York, New York, 727 p. (first edition)

Spath, C.S., III, 2017. Geology and Genesis of Hybridized Ultramafic Rocks in the Black Label Hybrid Zone of the Black Thor Intrusive Complex, McFaulds Lake Greenstone Belt, Ontario, Canada; M.Sc. thesis, Laurentian University, Sudbury, Ontario, 94 p.

Staude, S., Barnes, S.J., and Le Vaillant, M., 2017. Thermo-mechanical excavation of ore-hosting embayments beneath komatiite lava channels: textural evidence from the Moran deposit, Kambalda, Western Australia; Ore Geology Review, v. 90, p. 446–464.

Zuccarelli, N., in prep. Textural sulphide facies at Eagle's Nest Ni-Cu-(PGE) deposit; M.Sc. thesis, Laurentian University, Sudbury, Ontario.

Zuccarelli, N., Lesher, C.M., Houlé, M.G., and Weston, R.J., 2017. Sulfide textural variations and multiphase ore emplacement in the Eagle's Nest Ni-Cu-PGE deposit, McFaulds Lake greenstone belt, Ontario, Canada; Society for Geology Applied to Mineral Deposits, Proceedings of the 14th SGA Biennial Meeting, p. 583–586.

Zuccarelli, N., Lesher, C.M., Houlé, M.G., and Weston, R.J., 2018a. Sulfide textural variations and multiphase ore emplacement in the Eagle's Nest Ni-Cu-(PGE) deposit, McFaulds Lake greenstone belt, Superior Province, northern Ontario, Canada; Geological Society of America, Abstracts with Programs, v. 50. doi:10.1130/abs/2018AM-317024

Zuccarelli, N., Lesher, C.M., and Houlé, M.G., 2018b. Sulphide textural variations and multiphase ore emplacement in the Eagle's Nest Ni-Cu-(PGE) deposit, McFaulds Lake greenstone belt, Ontario; *in* Targeted Geoscience Initiative: 2017 report of activities, volume 2, (ed.) N. Rogers; Geological Survey of Canada, Open File 8373, p. 29–34.

The composition of magnetite in Archean mafic-ultramafic intrusions within the Superior Province

A.-A. Sappin* and M.G. Houlé

Geological Survey of Canada, 490 rue de la Couronne, Québec, Quebec G1K 9A9
*Corresponding author's e-mail: anne-aurelie.sappin@canada.ca

ABSTRACT

The mineral chemistry of magnetite from eleven Archean mafic, mafic-ultramafic, and ultramafic intrusions within the Superior Province was determined to be used as a petrogenetic indicator and to identify the most prospective areas for exploration of Fe-Ti-V and Fe-Ti-P mineralization.

The composition of magnetite is influenced by the presence of exsolutions and inclusions (e.g. ilmenite, Al-spinel), the type of parental melt (e.g. komatiitic, basaltic) and its Ti contents (e.g. high-Ti or low-Ti parental magmas), and the element partitioning with co-crystallized minerals (e.g. clinopyroxene) or previously crystallized minerals (e.g. chromite). The overall composition of magnetite, however, appears to be mainly independent of the host-rock type. The composition of magnetite in compatible (e.g. Mg, Co, V, Ni, and Cr) and incompatible (e.g. Al, Ga, Mn, Ti, Zn) elements during fractionation processes also provides useful information about the degree of differentiation of the host intrusions. Among the studied intrusions with a mafic-dominated composition, the Rivière Bell and Lac Doré complexes appear to be the most evolved, whereas the Croal Lake, Big Mac, Butler, and Wabassi Main intrusions and the Highbank-Fishtrap intrusive complex are the most primitive. Furthermore, the variation of the minor and trace element contents of the magnetite could be used to determine the internal stratigraphy within the mafic to ultramafic intrusions. For example, in the mafic-dominated Big Mac intrusion and in the ultramafic-dominated Baie Chapus Pyroxenite, the more vent-proximal facies appear to be located to the north and to the east, respectively. In addition, the V and Ni+Cr contents of magnetite from the Big Mac intrusion suggest that the northern part of this intrusion is a prospective area for Fe-Ti-V mineralization, whereas the southern part has more potential for Fe-Ti-P mineralization. In the Baie Chapus Pyroxenite, the concentrations in V and Ni+Cr in magnetite support the prospectivity of this intrusion for Fe-Ti-V mineralization.

Magnetite from the oxide-bearing mafic to ultramafic rocks and the semi-massive to massive Fe-Ti oxide layers have lower Ti+V values than expected, with magnetite compositions plotting within the fields for hydrothermal deposits in Ni/(Cr+Mn) versus Ti+V, Ca+Al+Mn versus Ti+V, and Ni+Cr versus Ti+V discrimination diagrams. Considering that the Fe-Ti-V deposit fields in these diagrams were mostly defined based on Fe-oxides hosted within Proterozoic and Phanerozoic Fe-Ti deposits, the preliminary results presented here suggest there may be a specific signature for magnetite from Archean Fe-Ti-V-oxide-bearing intrusions. However, further work is required to confirm this distinct signature to the Archean.

INTRODUCTION

The concentration of minor and trace elements in Fe-oxides is controlled by their environment of formation, which makes magnetite a useful petrogenetic tracer and a suitable indicator mineral for mineral exploration (e.g. Dare et al., 2012, 2014). Ultramafic and mafic intrusions/flows are generally prospective units to host orthomagmatic ore deposits and are ubiquitous throughout the Superior Province, although their abundance is variable across the Province and only a limited number of these units host economic Ni-Cu-(PGE) or Fe-Ti-V-P deposits.

In this contribution, we report magnetite composition from 11 Mesoarchean to Neoarchean, mafic to ultramafic intrusions (i.e. Mayville, Croal Lake, Big Mac, Eagle's Nest, Butler, Highbank-Fishtrap, Oxtoby Lake, Wabassi Main, Baie Chapus, Rivière Bell, and Lac Doré) across the Bird River–Uchi–Oxford-Stull–La Grande Rivière–Eastmain (BUOGE "superdomain") domains and the Wawa-Abitibi terrane within the Superior Province (Fig. 1). The characterization of the minor and trace element contents of magnetite from each intrusion provided information about the factors that controlled the composition of this mineral, the degree of fractionation, and the internal stratigraphy of each intrusion, as well as information about the potential use of magnetite as a prospectivity indicator for Fe-Ti-V-P mineralization and the validity of magnetite discrimination diagrams to determine the mineral deposit environment in which these Fe-oxide grains formed (e.g. Dupuis and Beaudoin, 2011).

Sappin, A.-A. and Houlé, M.G., 2020. The composition of magnetite in Archean mafic-ultramafic intrusions within the Superior Province; *in* Targeted Geoscience Initiative 5: Advances in the understanding of Canadian Ni-Cu-PGE and Cr ore systems – Examples from the Midcontinent Rift, the Circum-Superior Belt, the Archean Superior Province, and Cordilleran Alaskan-type intrusions, (ed.) W. Bleeker and M.G. Houlé; Geological Survey of Canada, Open File 8722, p. 181–196. https://doi.org/10.4095/326896

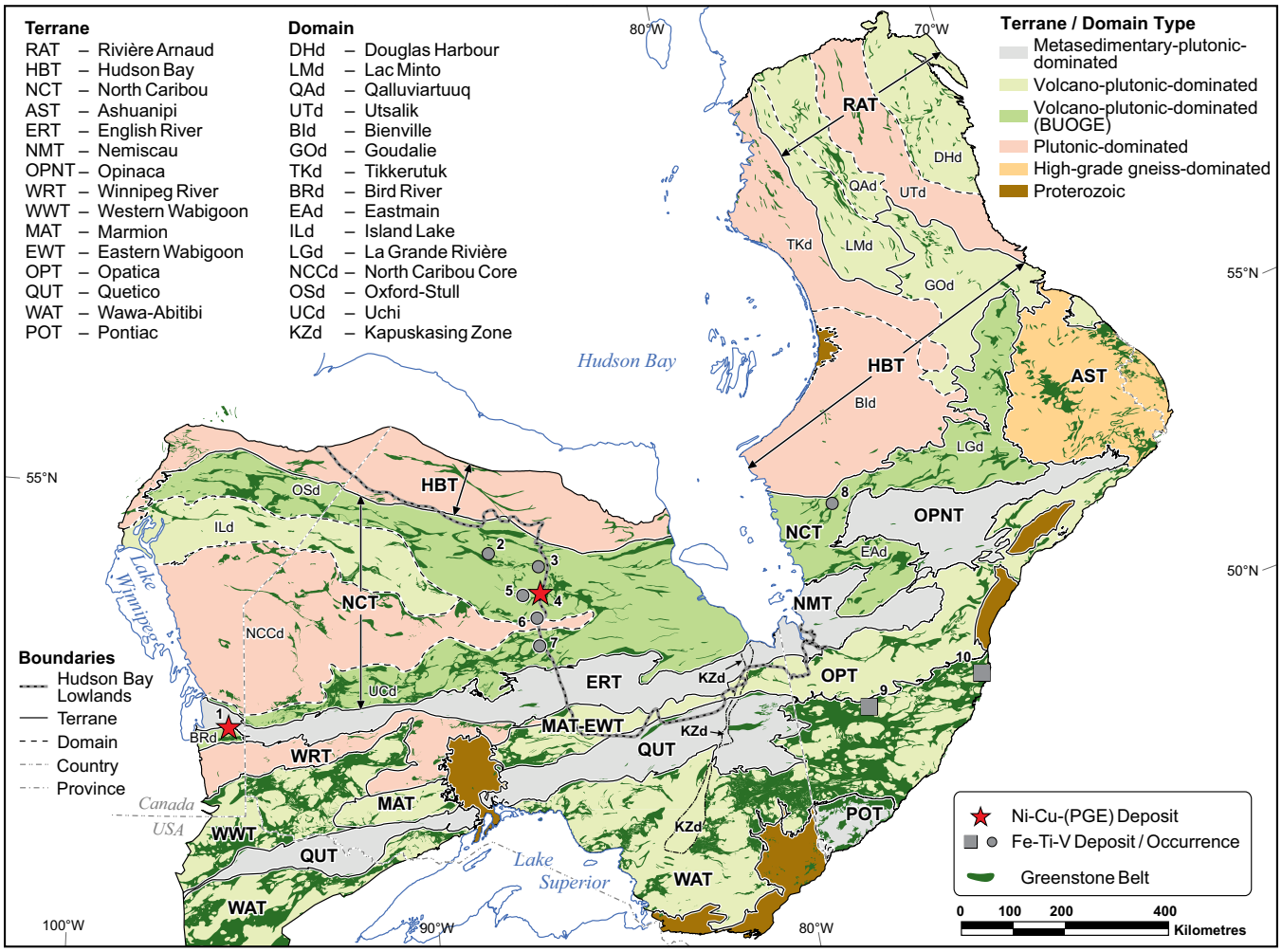

Figure 1. Geological map showing the locations of the mafic to ultramafic intrusions that were studied across the Bird River–Uchi–Oxford-Stull–La Grande Rivière–Eastmain (BUOGE) domains and the Wawa-Abitibi terrane (*after* Houlé et al., 2020). Terrane and domain boundaries are *modified from* Stott et al. (2010), Percival et al. (2012), and SIGÉOM (2020). Names of the host intrusions of the deposits/occurrences: 1 = Mayville intrusion, 2 = Croal Lake intrusion, 3 = Big Mac intrusion, 4 = Eagle's Nest dyke, 5 = Butler West and East intrusions, 6 = Highbank-Fishtrap intrusive complex, 7 = Oxtoby Lake and Wabassi Main intrusions, 8 = Baie Chapus Pyroxenite, 9 = Rivière Bell complex, 10 = Lac Doré complex.

SAMPLING AND METHODOLOGY

Sampling

A total of 83 representative drill core or grab samples were collected from 11 mafic to ultramafic intrusions across the Superior Province: the Mayville intrusion (n=2) of the Bird River intrusive suite within the Bird River domain in the North Caribou terrane (Manitoba); the Croal Lake (n=10), Big Mac (n=17), Eagle's Nest (n=1), and Butler (n=3) intrusions from the Ring of Fire intrusive suite and the Highbank-Fishtrap intrusive complex (n=19) within the Oxford-Stull domain in the North Caribou terrane (Ontario); the Oxtoby Lake (n=3) and Wabassi Main (n=11) intrusions within the Uchi domain in the North Caribou terrane (Ontario); the Baie Chapus Pyroxenite (n=11) within the La Grande Rivière domain in the North Caribou terrane (Quebec); and the Rivière Bell (n=5) and Lac Doré (n=1) complexes within the Abitibi greenstone belt in the Wawa-Abitibi terrane (Quebec) (Fig. 1, Table 1, 2). A total of 727 magnetite grains from 83 samples were analyzed by electron probe micro-analyzer (EPMA) and 240 magnetite grains from 36 samples were analyzed using laser ablation-inductively coupled plasma mass spectrometry (LA-ICP-MS) (Table 2).

Methodology

Minor and trace element contents of magnetite (Mg, V, Ni, Cr, Al, Mn, Ti, Zn, and Ca) were determined by EPMA at the Université Laval (Québec, Canada), using a method modified from Boutroy et al. (2014). Mg, Co, V, Ni, Cr, Al, Ga, Mn, Ti, Zn, and Ca were also determined by LA-ICP-MS spot analysis at the Geological Survey of Canada (Ottawa, Canada). The LA-ICP-MS analyses of magnetite included the ilmenite exsolutions formed during subsolidus exsolution-oxidation processes. However, the EPMA analyses of the mag-

Table 1. Summary of the main characteristics of the studied mafic to ultramafic intrusions across the Superior Province.

Intrusive Unit	Terrane/Domain	Magmatic Suite		Mineralization	Age	MF/UM Ratio	Lithology	Parental Magma
		Suite	Subsuite	Deposit/*Occurrence*				
Mayville intrusion	NCT - BRd	BRIS		Cu-Ni-PGE, *Cr-PGE*	ca. 2743 Ma[1]	MF >> UM	Gabbroic-anorthositic rocks, minor peridotite, pyroxenite, and chromitite layers	Basaltic[5]
Croal Lake intrusion	NCT - OSd	RoFIS	ERSS	*Fe-Ti-V*	ca. 2733 Ma[1]	MF >>> UM	Gabbroic rocks (±Ol), minor peridotite, anorthosite, and semi-massive to massive Fe-Ti oxides	-
Big Mac intrusion	NCT - OSd	RoFIS	ERSS	*Fe-Ti-V*	ca. 2734 Ma[1]	MF >>> UM	Gabbroic rocks, minor anorthosite, pyroxenite, and semi-massive to massive Fe-Ti oxides	-
Eagle's Nest dyke	NCT - OSd	RoFIS	KLSS	Ni-Cu-PGE	-	UM >>> MF	Komatiitic dunite, lherzolite, websterite, and minor gabbroic rocks	Komatiitic[6,7]
Butler West intrusion	NCT - OSd	RoFIS	ERSS	*Fe-Ti-V*	-	MF >>> UM	Gabbroic rocks, minor anorthosite, pyroxenite, and semi-massive to massive Fe-Ti oxides	Basaltic with high-Fe and Ti contents[8]
Butler East intrusion	NCT - OSd	RoFIS	ERSS	*Fe-Ti-V*	-	MF >>> UM	Gabbroic rocks, minor anorthosite, pyroxenite, and semi-massive to massive Fe-Ti oxides	Basaltic with high-Fe and Ti contents[8]
Highbank-Fishtrap intrusive complex	NCT - OSd			*Fe-Ti-V*	ca. 2808–2810 Ma[1]	MF >> UM	Gabbroic rocks, anorthosite, pyroxenite, and minor semi-massive Fe-Ti oxides	-
Oxtoby Lake intrusion	NCT - UCd			-	ca. 2717 Ma[2]	MF	Gabbroic rocks	Basaltic[2]
Wabassi Main intrusion	NCT - UCd			*Cu-Ni*	ca. 2727 Ma[2]	MF > UM	Gabbroic rocks (±Ol), anorthosite, minor peridotite	Basaltic[2]
Baie Chapus Pyroxenite	NCT - LGd			*Fe-Ti-V*	<2802 Ma[3]	UM >> MF	Clinopyroxenite (±Pl, ±Ol), minor gabbro, wehrlite, dunite, and semi-massive to massive Fe-Ti oxides	Relatively primitive, mantle-derived[9]
Rivière Bell complex	WAT			Fe-Ti-V	ca. 2725 Ma[4]	MF >>> UM	Gabbroic rocks, minor anorthosite, granophyre, pyroxenite (±Ol), and troctolite, and semi-massive to massive Fe-Ti oxides	Basaltic[10]
Lac Doré complex	WAT			Fe-Ti-V	ca. 2728 Ma[4]	MF >>> UM	Anorthosite, gabbroic rocks, diorite, tonalite, ultramafic rock, semi-massive to massive Fe-Ti oxides	Tholeiitic[11,12]

Abbreviations:
NCT = North Caribou terrane, WAT = Wawa-Abitibi terrane
BRd = Bird River domain, LGd = La Grande Rivière domain, OSd = Oxford-Stull domain, UCd = Uchi domain
BRIS = Bird River intrusive suite, RoFIS = Ring of Fire intrusive suite, ERSS = Ekwan River subsuite, KLSS = Koper Lake subsuite
MF = mafic, Ol = olivine, PGE = platinum-group elements, Pl = plagioclase, UM = ultramafic.

References:
[1]Houlé et al., 2015a; [2]Sappin et al., 2016; [3]Houlé et al., 2015b; [4]Mortensen, 1993; [5]Yang et al., 2013; [6]Mungall et al., 2010; [7]Zuccarelli et al., 2018; [8]Kuzmich, 2014; [9]Sappin et al., 2015a; [10]Maier et al., 1996; [11]Arguin et al., 2018; [12]Mathieu, 2019.

Table 2. Main compositions of magnetite (maximum values) from the studied mafic to ultramafic intrusions across the Superior Province.

Intrusive Unit	Mayville intrusion			Croal Lake intrusion			Big Mac intrusion			Eagle's Nest dyke			Butler West intrusion			Butler East intrusion		
Rock type	MF	UM	Massive sulphides	MF	UM	SM to M Fe-Ti oxides	MF	UM	SM to M Fe-Ti oxides	MF	UM	Massive sulphides	MF	UM	SM to M Fe-Ti oxides	MF	UM	SM to M Fe-Ti oxides
Mag/Ilm ratio	Mag > Ilm	Ilm > Mag	Mag > Ilm	Mag > Ilm	-	Mag > Ilm	Mag > Ilm	Mag > Ilm	Mag > Ilm	-	-	Mag >>> Ilm	Mag > Ilm	Mag > Ilm	Mag > Ilm	Mag > Ilm	Mag > Ilm	Mag > Ilm
Total of samples																		
Number of samples	0	0	2	7	No	3	10	1	6	0	No	1	1	0	0	1	1	0
Number of analyses	-	-	36	76	Prim Mag	78	73	20	68	-	Prim Mag	18	18	-	-	13	15	-
EPMA data (ppm)																		
Number of samples			2	7		3	10	1	6			1	1			1	1	
Number of analyses			20	61		58	63	12	50			10	10			7	7	
Mg			339	856		881	2,256	1,490	1,466			1,530	550			500	70	
V			1,604	17,584		10,331	9,319	2,830	8,653			1,830	5,250			10,870	6,300	
Ni			311	200		240	230	100	170			810	160			190	210	
Cr			231	5,360		5,665	11,077	9,530	6,568			35,190	750			520	8,390	
Al			1,272	3,864		3,820	24,494	3,932	14,713			120	1,100			600	410	
Mn			279	1,720		922	790	240	270			3,130	140			210	320	
Ti			800	12,236		6,040	14,090	1,190	3,640			790	2,380			590	1,050	
Zn			189	900		420	240	190	932			420	260			270	240	
Ca			27	170		736	450	70	40			800	60			70	50	
LA-ICP-MS data (ppm)																		
Number of samples			2	2		3	2	1	2			1	1			1	1	
Number of analyses			16	15		20	10	8	18			8	8			6	8	
Mg			294	184		2,020	1,273	721	3,188			2,345	814			1,502	952	
Co			14	65		170	71	69	56			39	30			43	34	
V			1,686	9,118		7,300	2,069	2,558	4,597			2,523	4,796			11,780	6,580	
Ni			240	189		159	119	81	99			803	68			95	84	
Cr			200	1,440		4,559	2,773	8,685	4,053			96,409	714			392	6,427	
Al			1,211	1,490		3,460	4,041	2,794	11,837			659	1,686			1,856	1,051	
Ga			27	50		49	57	49	56			25	54			53	24	
Mn			459	3,180		3,618	3,826	5,872	3,392			11,761	2,708			3,280	6,505	
Ti			2,470	107,072		129,063	150,651	124,564	151,145			1,534	67,525			70,749	96,211	
Zn			12	595		498	78	501	1,153			667	68			52	83	
Ca			109	107		105	46	26	63			1,229	47			83	3,809	

Intrusive Unit	Highbank-Fishtrap intrusive complex			Oxtoby Lake intrusion	Wabassi Main intrusion		Baie Chapus Pyroxenite			Rivière Bell complex			Lac Doré complex		
Rock type	MF	UM	SM Fe-Ti oxides	MF	MF	UM	MF	UM	SM to M Fe-Ti oxides	MF	UM	SM to M Fe-Ti oxides	MF	UM	SM to M Fe-Ti oxides
Mag/Ilm ratio	Ilm > Mag	Ilm > Mag	Mag > Ilm	Mag > Ilm	Ilm > Mag	-	Ilm > Mag	Mag > Ilm	Mag >>> Ilm	Mag > Ilm	Mag > Ilm	Mag > Ilm	Mag > Ilm	Mag > Ilm	Mag > Ilm
Total of samples															
Number of samples	11	5	3	3	11	No	0	7	4	0	0	5	1	0	0
Number of analyses	98	63	38	42	82	Prim Mag	-	84	56	-	-	77	12	-	-
EPMA data (ppm)															
Number of samples	11	5	3	3	11			7	4			5	1		
Number of analyses	84	57	31	27	58			84	40			41	7		
Mg	1,090	2,623	410	230	5,476			7,850	260			6,606	90		
V	10,120	7,749	12,309	3,711	12,380			1,740	7,440			9,710	nd		
Ni	580	786	731	1,290	1,713			1,500	620			330	60		
Cr	21,900	13,869	6,014	2,020	30,714			3,680	300			760	350		
Al	2,948	2,030	3,140	2,020	54,105			1,290	140			39,626	6,850		
Mn	860	590	150	1,180	3,830			450	750			4,167	810		
Ti	65,330	28,790	3,870	53,938	123,685			1,690	49,860			128,026	15,530		
Zn	830	1,280	610	2,030	10,347			280	540			1,516	4,240		
Ca	190	540	110	214	600			4,290	320			110	100		
LA-ICP-MS data (ppm)															
Number of samples	3	1	1	2	5			No sample	2			5	1		
Number of analyses	14	6	7	15	24				16			36	5		
Mg	188	179	677	88	5,590				404			6,128	1,042		
Co	82	58	132	67	182				41			292	57		
V	8,869	3,131	8,310	3,394	15,206				6,949			9,475	1,432		
Ni	476	13	658	337	547				366			665	15		
Cr	20,616	52	3,362	1,752	14,948				32			454	318		
Al	1,195	1,771	1,682	835	30,012				550			29,559	15,208		
Ga	44	70	44	52	85				14			61	58		
Mn	1,838	1,813	2,024	289	6,404				3,812			3,692	3,761		
Ti	67,969	118,914	76,364	296	224,453				101,402			169,773	88,265		
Zn	558	492	459	163	3,685				95			1,395	11,489		
Ca	218	235	127	14	150				417			133	21		

Abbreviations: EPMA = electron probe micro-analyzer, LA-ICP-MS = laser ablation-inductively coupled plasma-mass spectrometry; M = massive, MF = mafic, SM = semi-massive, UM = ultramafic; Ilm = ilmenite, Mag = magnetite, nd = not determined, Prim = primary.

netite excluded as much as possible any inclusions or exsolutions in order to analyze a single mineral species.

The EPMA analyses were undertaken with a CAMECA SX-100 five-spectrometer electron microprobe using 15 kV accelerating voltage, a 20 nA beam current forming a 5 μm diameter beam, and counting times of 20 s on peak and 10 s on background to determine the major and minor element contents of the magnetite grains. For the minor and trace element contents, an accelerating voltage of 15 kV, a 100 nA beam current forming a 10 μm diameter beam, counting times of 40 to 80 s on peak, and a background measured on both sides for 15 to 20 s at positions free of interferences were used. Simple oxides (GEO Standard Block, from P&H Developments) and minerals (Mineral Standard Mount MINM25-53, from Astimex Scientific Limited; reference samples from Jarosewich et al., 1980) were used as calibration standards.

The LA-ICP-MS system consisted of a Photon Machine Analyte 193 nm excimer laser ablation system coupled to an Agilent Technologies 7700x ICP-MS, which was operated using a laser frequency of 10 Hz and a spot size of 40 to 69 μm. Fe was used as the internal standard (concentrations determined by EPMA in Fe-oxides or a stoichiometric value was assumed when EPMA data were not available). Certified reference materials (GSE-1G, GSD-1G, Po726) and in-house standards of natural magnetite (BC28) were used for calibration and quality control.

In this study, only the minor and trace element concentrations at levels above EPMA and LA-ICP-MS detection limits were used. A selection of data obtained using both methods is provided in Table 2.

RESULTS

Magnetite Composition from Mafic to Ultramafic Intrusions

Magnetite grains in this study are hosted by different types of rocks, such as oxide-bearing mafic to ultramafic rocks, semi-massive to massive Fe-Ti oxide layers, and massive sulphides belonging to a wide range of mafic, mafic-ultramafic, and ultramafic intrusions (Table 2). These intrusions occur in a number of terranes/domains in the Superior Province (Bird River, Oxford-Stull, Uchi, La Grande Rivière, and Wawa-Abitibi) and have varying ages (Mesoarchean versus Neoarchean) and compositions (mafic-dominated versus ultramafic-dominated) (Table 1).

Magnetite in oxide-bearing mafic to ultramafic rocks

The oxide-bearing mafic to ultramafic rock samples (<40% Fe-Ti oxides) were collected from the mafic-dominated Croal Lake, Big Mac, Butler (East and West), Highbank-Fishtrap, Oxtoby Lake, Wabassi Main, and Lac Doré intrusions and the Baie Chapus Pyroxenite, an ultramafic-dominated intrusion (Table 2). These intrusions are all Neoarchean, except for the Highbank-Fishtrap intrusive complex, which is Mesoarchean (Table 1).

The results obtained for V and Cr contents in the magnetite determined using EPMA and LA-ICP-MS are similar (Fig. 2, Table 2). However, Mg, Al, Mn, and Ti contents determined by electron microprobe are generally lower than those determined by LA-ICP-MS, whereas Ni and Zn contents are mostly higher (Fig. 2, Table 2). During fractionation, Mg, Co, V, Ni, and Cr are compatible elements in mafic magmas and Al, Mn, Ti, and Zn are incompatible (e.g. Dare et al., 2014). In the oxide-bearing mafic to ultramafic rocks, the concentration of compatible and incompatible elements in magnetite varies from intrusion to intrusion (Fig. 2). Magnetite from the Croal Lake, Big Mac, Butler, and Highbank-Fishtrap intrusions shows high Cr and locally high V contents. Magnetite from the Oxtoby Lake intrusion has low Mg contents, relatively low Cr, Al, and Mn contents, and the lowest Ti contents of the intrusions studied. Magnetite from the Wabassi Main intrusion has the highest Mg and Co contents and high V, Ni, Cr, Al, Mn, and Ti contents. Magnetite from the Lac Doré complex has low V contents, relatively low Mg and Cr contents, and the lowest Ni contents, but high Mn, Ti, and Zn contents. Pyroxenite from the Baie Chapus intrusion contains magnetite with the highest Ni contents, relatively high Mg contents, and low V, Cr, and Al contents.

Magnetite in semi-massive to massive Fe-Ti oxides

The semi-massive and massive Fe-Ti oxide samples (40–80% and >80% Fe-Ti oxides, respectively) are from the Neoarchean mafic-dominated Croal Lake, Big Mac, and Rivière Bell intrusions, the Mesoarchean mafic-dominated Highbank-Fishtrap intrusion, and the Neoarchean ultramafic-dominated Baie Chapus Pyroxenite (Table 1, 2).

EPMA and LA-ICP-MS data for magnetite show similar concentration ranges, except for elements Mn, Ti, and, locally, Mg, Cr, and Zn (Fig. 3, Table 2). The chemical signature of the magnetite from the semi-massive to massive magnetite-ilmenite layers also varies by intrusions (Fig. 3). Magnetite from the Croal Lake and Big Mac intrusions have relatively high Mg and Cr contents, whereas magnetite from the Highbank-Fishtrap intrusive complex has relatively low Mg contents but high Cr contents. In the Rivière Bell complex, the magnetite has been affected by regional and local metamorphism and most of its primary composition, with the exception of V and Cr con-

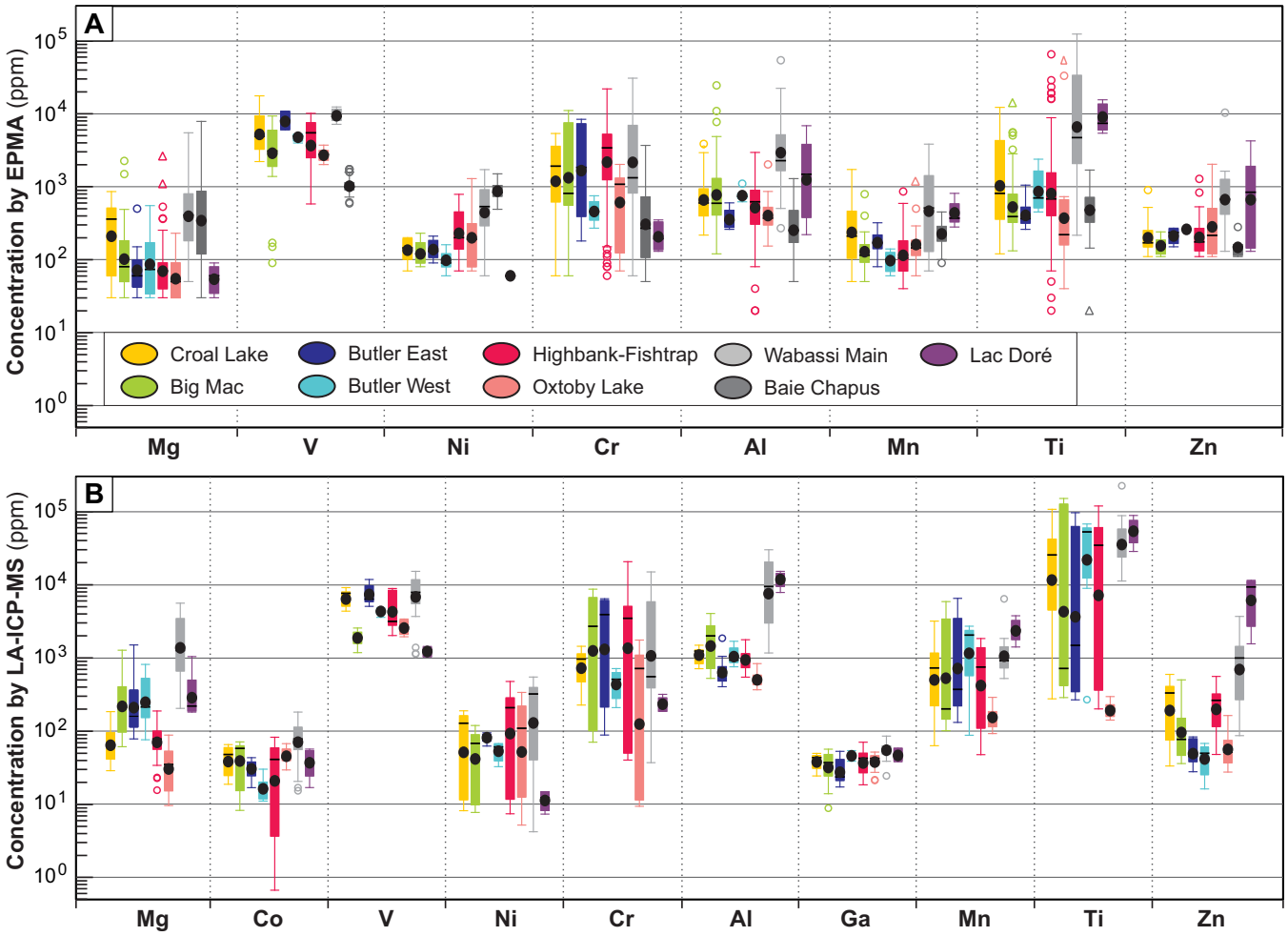

Figure 2. Box and whisker plots of selected minor and trace elements in magnetite from the Croal Lake, Big Mac, Butler (East and West), Highbank-Fishtrap, Oxtoby Lake, Wabassi Main, Baie Chapus, and Lac Doré intrusions. Magnetite in oxide-bearing mafic to ultramafic rocks were analyzed by **(a)** EPMA and **(b)** LA-ICP-MS. The upper and lower margins of the box represent the upper 75% and lower 25% of the data. The whiskers represent the upper and lower threshold values (95% of the data). Median values are shown as solid black lines and mean values as solid black circles. Outliers are shown as open circles and far outlier as open triangles along the whisker.

tents, has been modified (Polivchuk, 2017). The Fe-oxides from this complex have relatively low V and Cr contents. Semi-massive to massive Fe-Ti oxides from the Baie Chapus Pyroxenite host magnetite with intermediate Ni contents, relatively high Mn contents, locally low Mg and Zn contents, and the lowest contents of Co, Cr, Al, and Ga (an incompatible element during fractionation that is enriched in the residual liquid).

Magnetite in massive sulphides

The massive sulphide samples belong to the Neoarchean mafic-dominated Mayville and ultramafic-dominated Eagle's Nest Ni-Cu-(PGE)-bearing intrusions (Table 1, 2).

Analytical results for magnetite are similar and of the same order of magnitude, whether analyses were by EPMA or LA-ICP-MS, with the exception of results for Mn, Ti, and Zn (Fig. 4, Table 2). In general, magnetite in the Mayville intrusion contains very low concentrations of compatible elements (Mg, Co, V, and Cr; Fig. 4). In contrast, magnetite from the Eagle's Nest intrusion has higher Mg, Co, V, Ni, Cr, and Mn contents and lower Al, Ga, and Ti contents than the Mayville magnetite (Fig. 4).

Case Study: Magnetite Composition in the Big Mac Intrusion

The Big Mac mafic intrusion (ca. 2734 Ma: Houlé et al., 2015a) is part of the Ring of Fire intrusive suite within the Oxford-Stull domain (Ontario), in the central part of the Superior Province (Fig. 1). Based on geophysical data (OGS–GSC, 2011), the intrusion forms, at surface, an approximately 60 km long and 1 to 4 km wide elongate body oriented northwest-southeast (Fig. 5). It is a subconcordant sill that is broadly layered, as indicated by field observations. The Big Mac intrusion is composed of gabbro (*sensu lato*),

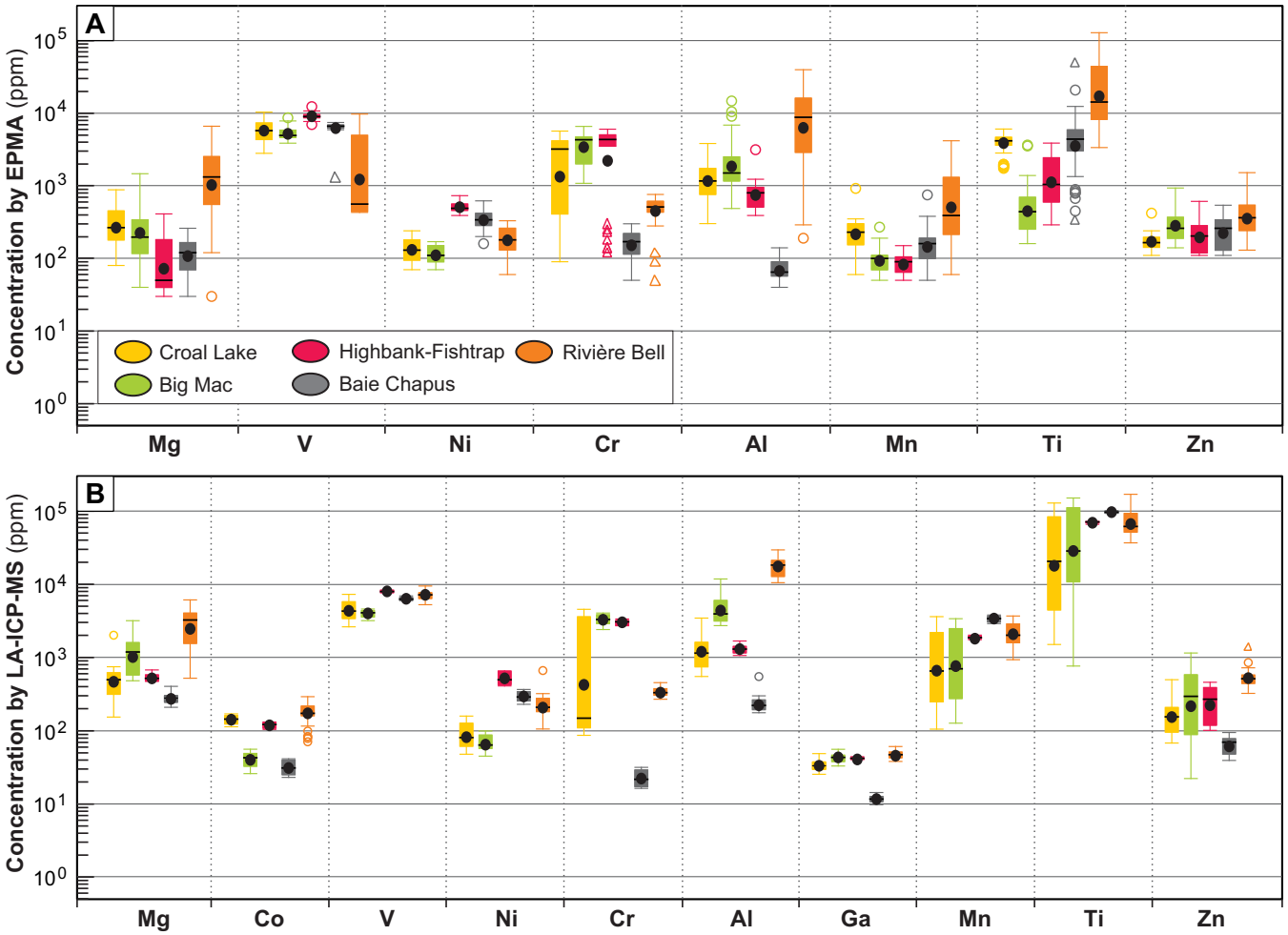

Figure 3. Box and whisker plots of selected minor and trace elements in magnetite from the Croal Lake, Big Mac, Highbank-Fishtrap, Baie Chapus, and Rivière Bell intrusions. Magnetite in semi-massive to massive Fe-Ti oxide layers were analyzed by **(a)** EPMA (a) and **(b)** LA-ICP-MS. *See* Figure 2 for the meaning of symbols in the plots.

minor anorthosite, and rare pyroxenite. It also contains a few decimetre- to metre-thick, semi-massive to massive, magnetite-ilmenite layers, which are restricted to the northern part of the intrusion.

In the Big Mac intrusion, the chemical composition of Fe-oxides varies with location. Magnetite in the northern part of the intrusion is rich in elements that are compatible in mafic magmas (i.e. Mg, V, Ni, Cr), whereas to the south, the concentration of these elements is low and it is locally rich in elements that are incompatible during fractionation process (i.e. Mn, Ti, Zn; Fig. 6). In addition, the mafic to ultramafic rocks in the northernmost part of the Big Mac intrusion have the most primitive geochemical signatures (Mg# ≤50, Cr = 2095–23 ppm, V = 1255–33 ppm, P_2O_5 = 0.14–0.03 wt%), have high magnetite/ilmenite ratios, contain plagioclase with the most primitive composition (up to An_{84}), and contain rare traces of apatite. In contrast, the southernmost part of this intrusion is characterized by mafic rocks with more evolved geochemical signatures (Mg# ≤35, Cr = 134–15 ppm, V = 453–16 ppm, P_2O_5 = 2.81–0.12 wt%), lower magnetite/ilmenite ratios, plagioclase with an evolved composition (as low as An_{25}), and up to 9 modal% apatite.

Case Study: Magnetite Composition in the Baie Chapus Pyroxenite

The Baie Chapus Pyroxenite (emplaced after 2802 Ma: Houlé et al., 2015b), is located within the La Grande Rivière domain (Quebec), in the eastern part of the Superior Province (Fig. 1). This intrusion is approximately 3 km long by 1 km wide at surface and is crudely layered, as indicated by field observations (Fig. 7). It is composed of clinopyroxenite, plagioclase clinopyroxenite, olivine clinopyroxenite, gabbro (*sensu lato*), and rare wehrlite and dunite. Significant accumulations of semi-massive to massive magnetite, which extend over at least 70 m with a thickness estimated to be a few metres, were found near the western part of the intrusion.

In the Baie Chapus Pyroxenite, the chemical composition of the magnetite also varies with location. Fe-

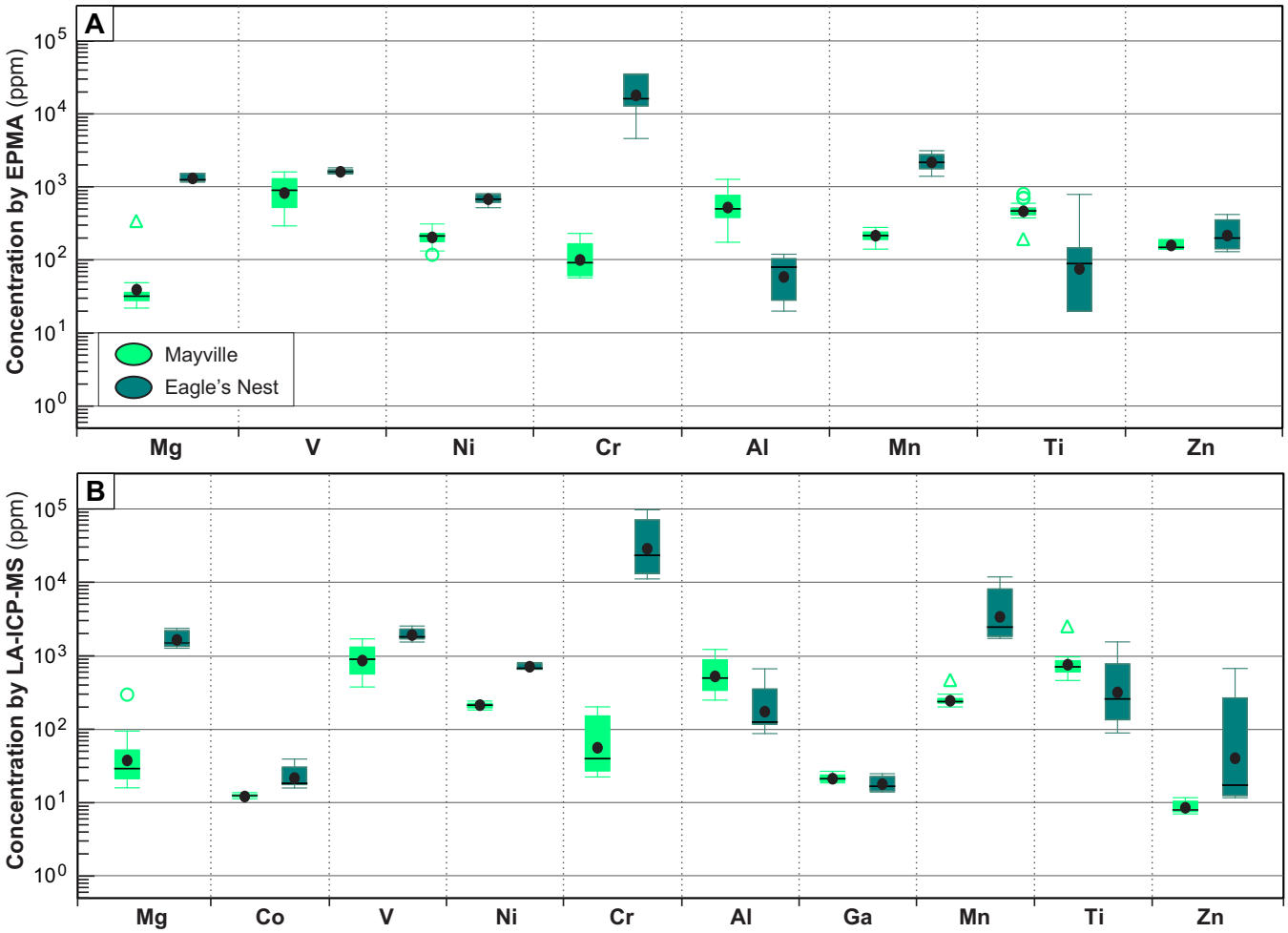

Figure 4. Box and whisker plots of selected minor and trace elements in magnetite from the Mayville and Eagle's Nest Ni-Cu-(PGE)-bearing intrusions. Magnetite in massive sulphides were analyzed by **(a)** EPMA and **(b)** LA-ICP-MS. *See* Figure 2 for the meaning of symbols in the plots.

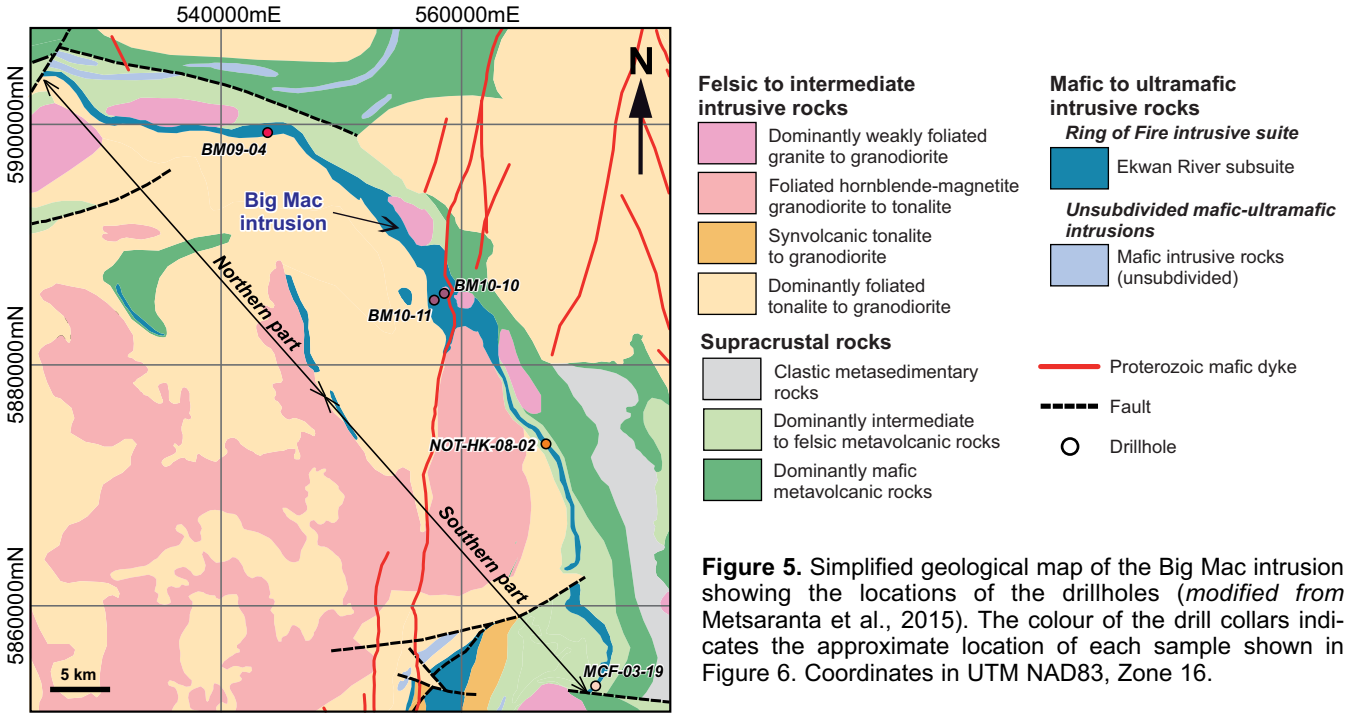

Figure 5. Simplified geological map of the Big Mac intrusion showing the locations of the drillholes (*modified from* Metsaranta et al., 2015). The colour of the drill collars indicates the approximate location of each sample shown in Figure 6. Coordinates in UTM NAD83, Zone 16.

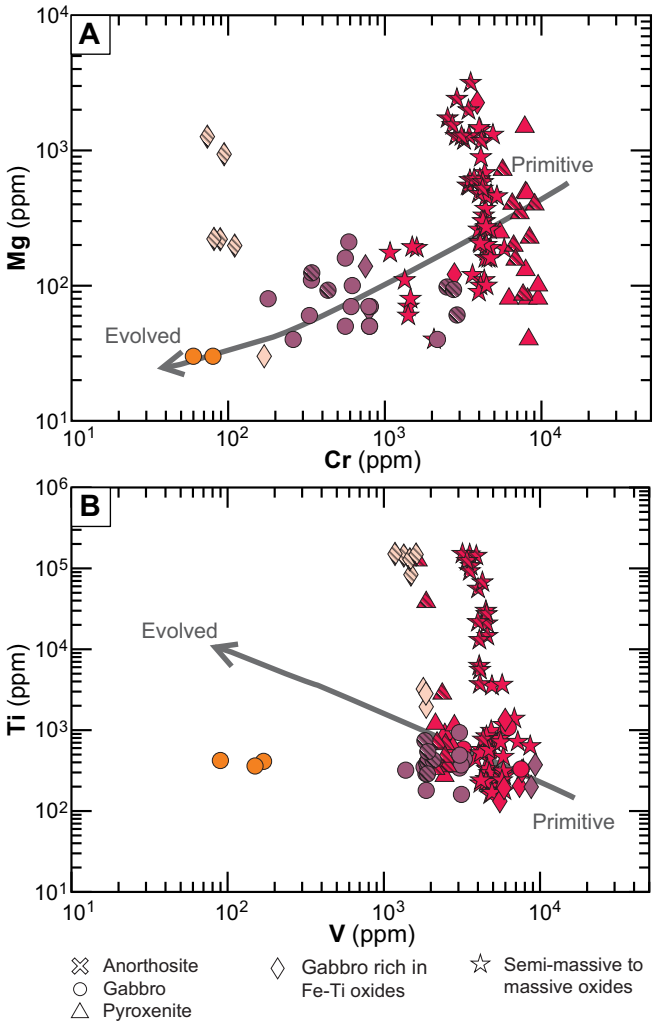

Figure 6. Composition of magnetite in anorthosite, gabbro, pyroxenite, and semi-massive to massive Fe-Ti oxide layers from the Big Mac intrusion. **a)** Mg versus Cr and **b)** Ti versus V. Each data point represents an individual magnetite grain analyzed by EPMA (nonhatched symbols) or LA-ICP-MS (hatched symbol). The fill colour of the symbols corresponds to the drill collars in Figure 5.

oxides in the eastern part of this intrusion are rich in elements that are compatible in mafic magmas, such as Mg and Cr, but to the west, the magnetite is poor in these elements and locally rich in incompatible elements (e.g. Ti, Zn) (Fig. 8a,b). Furthermore, the eastern part of the Baie Chapus Pyroxenite hosts mafic to ultramafic rocks with a relatively primitive geochemical composition (Mg# = 78–53, Cr = 703−245 ppm, V = 282−159 ppm, P_2O_5 = 0.05−0.02 wt%), clinopyroxene with a primitive composition (Mg# = 89–80), and is devoid of apatite. In contrast, the western part of this intrusion contains mafic to ultramafic rocks with a more evolved geochemical signature (Mg# = 76–41, Cr = 266−39 ppm, V = 427−41 ppm, P_2O_5 = 0.25−0.01 wt%), and up to 1 modal% apatite. Clinopyroxene in the westernmost part of this intrusion also has the most evolved composition (Mg# = 84–73).

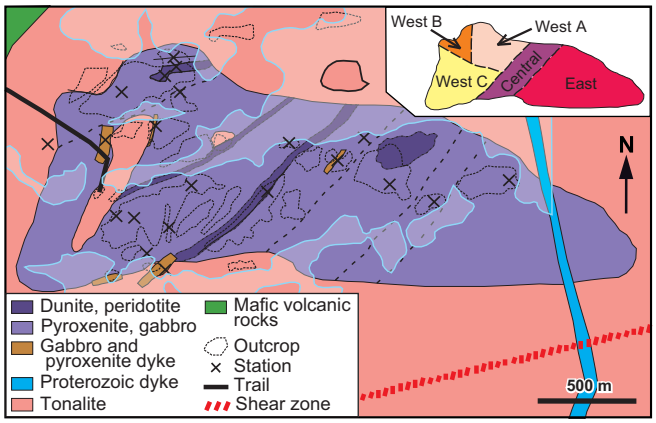

Figure 7. Simplified geological map of the Baie Chapus Pyroxenite (*modified from* Houlé and Goutier, unpubl. map). The inset indicates the different areas of this intrusion. The centre of the intrusion is approximately located at UTM (NAD83) Zone 18, 352746mE, 5928161mN.

Discrimination Diagrams of Magnetite Composition from Fe-Ti-V Deposits

Several diagrams have been proposed to classify magnetite grains based on their composition, such as the Ti versus Ni/Cr discrimination diagram for differentiating magnetite of magmatic and hydrothermal origin (Dare et al., 2014). This diagram also appears useful for identifying Ti-poor magnetite from magmatic settings (Duparc et al., 2016). The vast majority of the magnetite grains hosted by oxide-bearing mafic to ultramafic rocks and semi-massive to massive Fe-Ti oxide layers in this study have low Ni/Cr ratios, regardless of analytical method, and plot within the magmatic field of the diagram (Fig. 9). However, the magnetite from the Baie Chapus Pyroxenite, which has the highest Ni/Cr ratios, has EPMA data that plot almost entirely within the hydrothermal field (Fig. 9a). Furthermore, based on EPMA data (Fig. 9a), most of samples contain magnetite with Ti contents that are less or equal to 1 wt%. However, the LA-ICP-MS data (Fig. 9b) indicate that the Croal Lake, Big Mac, Butler, Highbank-Fishtrap, Wabassi Main, Baie Chapus, Rivière Bell, and Lac Doré intrusions host some Ti-rich magnetite (≥1 wt% Ti), whereas the Oxtoby Lake intrusion only hosts Ti-poor magnetite (mostly <0.1 wt% Ti).

Dupuis and Beaudoin (2011) defined two discrimination diagrams (Ni/(Cr+Mn) versus Ti+V and Ca+Al+Mn versus Ti+V) to distinguish magnetite associated with hydrothermal deposits (e.g. iron oxide copper-gold (IOCG) and porphyry deposits) from those associated with Fe-Ti-V deposits. In both diagrams, the field for Fe-Ti-V deposits was primarily defined based on the Fe-oxide compositions (individual grains and average compositions) determined by electron microprobe analyzer from a range of Proterozoic (General Electric mine, La Blache, and Girardville associated with Grenvillian anorthositic massif, Canada) and

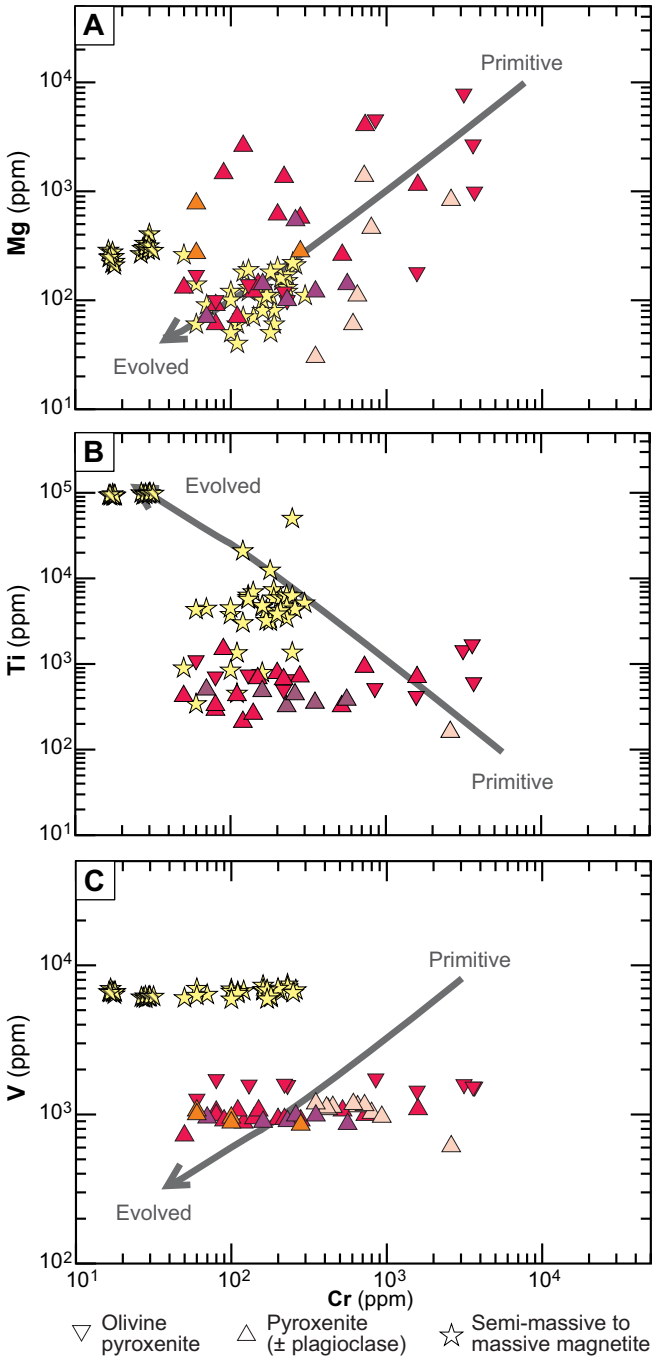

Figure 8. Composition of magnetite in pyroxenite and semi-massive to massive magnetite layers from the Baie Chapus Pyroxenite. **a)** Mg versus Cr, **b)** Ti versus Cr, and **c)** V versus Cr. Each data point represents an individual magnetite grain analyzed by EPMA (nonhatched symbols) or LA-ICP-MS (hatched symbol). The fill colour of the symbols, which corresponds to the inset map in Figure 7, indicates which area of the intrusion was sampled.

Phanerozoic (Routivare malmfält, Sweden) Fe-Ti deposits and from the Archean Lac Doré Fe-Ti-V deposit. Méric (2011) proposed an additional Ni+Cr versus Ti+V discrimination diagram to differentiate magnetite associated with hydrothermal deposits, Fe-Ti-V deposits, and Fe-Ti-P deposits using the general

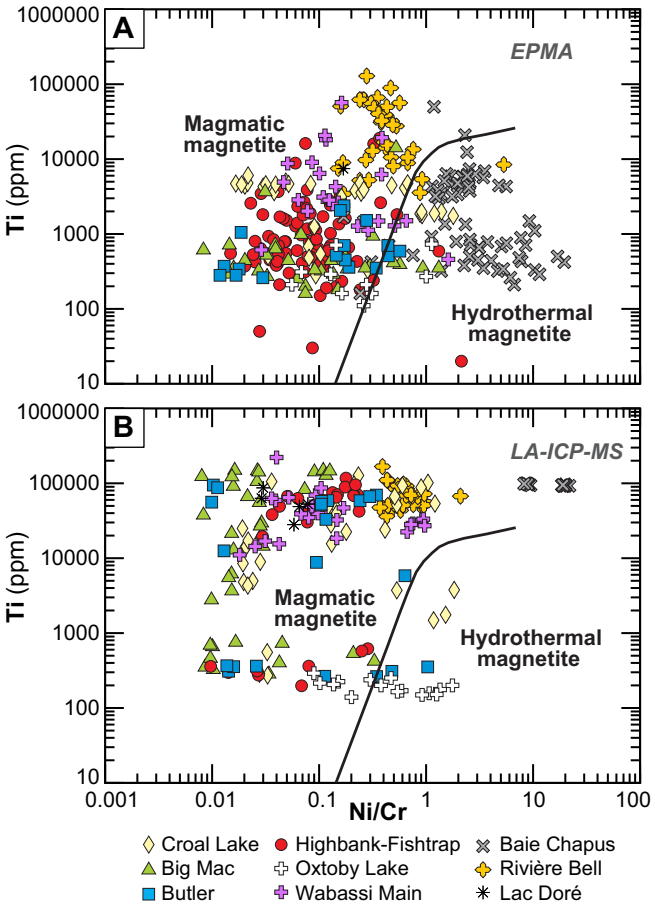

Figure 9. Ti versus Ni/Cr discrimination diagram for differentiated magmatic and hydrothermal magnetite of Dare et al. (2014) plotting magnetite from the oxide-bearing mafic to ultramafic rocks and the semi-massive to massive Fe-Ti oxide layers of the studied intrusions. **a)** Magnetite composition as determined by EPMA. **b)** Magnetite composition as determined by LA-ICP-MS. Each data point represents an individual magnetite grain.

Fe-Ti-V deposit field defined by Dupuis and Beaudoin (2011) for the Ni/(Cr+Mn) versus Ti+V diagram. In all these diagrams, the EPMA data for the magnetite from the oxide-bearing intrusive rocks and the semi-massive to massive Fe-Ti oxide layers of the studied Archean intrusions have significantly lower Ti+V contents than expected and plot predominantly within the field for hydrothermal deposits rather than within the field for Fe-Ti-V and Fe-Ti-P deposits (Fig. 10a,c,e). An exception is the Rivière Bell magnetite, which plots predominantly within the Fe-Ti-V deposit field (Fig. 10a,c,e). Interestingly, the LA-ICP-MS data for the magnetite grains generally plot within the Fe-Ti-V and Fe-Ti-P deposit fields in the three discrimination diagrams (Fig. 10b,d,f). However, significant LA-ICP-MS analyses from many of the intrusions of this study still plot within the hydrothermal field, in particular those for magnetite from the Oxtoby Lake intrusion (Fig. 10b,d,f), which also shows similar results when determined by EPMA (Fig. 10a,c,e).

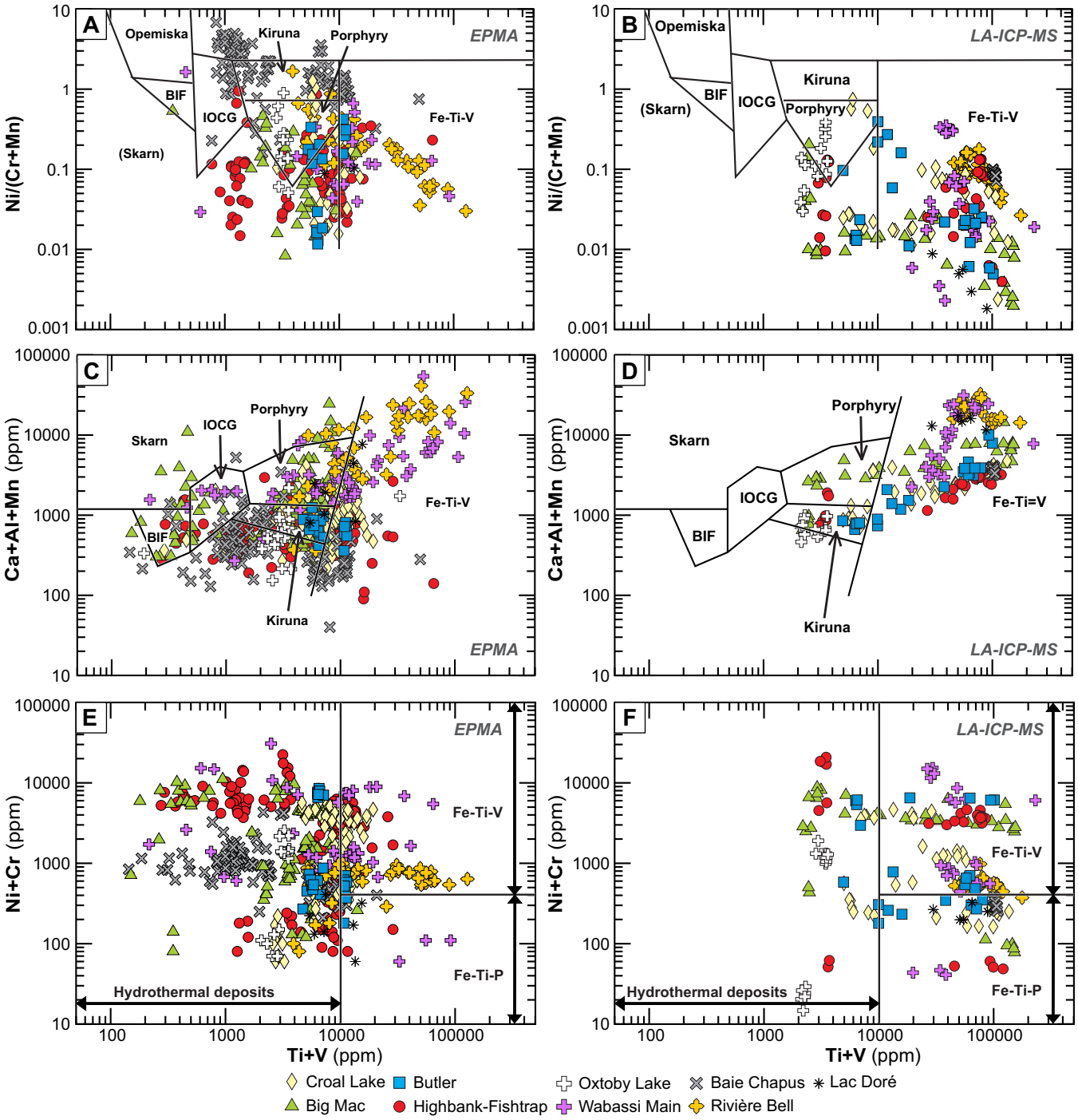

Figure 10. Discrimination diagrams of magnetite composition from hydrothermal and Fe-Ti-V deposits determined by EPMA and LA-ICP-MS. **a)** Ni/(Cr+Mn) versus Ti+V diagram for results determined by EPMA. **b)** Ni/(Cr+Mn) versus Ti+V diagram for results determined by LA-ICP-MS. **c)** Ca+Al+Mn versus Ti+V diagram for results determined by EPMA. **d)** Ca+Al+Mn versus Ti+V diagram for results determined by LA-ICP-MS. **e)** Ni+Cr versus Ti+V diagram for results determined by EPMA. **f)** Ni+Cr versus Ti+V diagram for results determined by LA-ICP-MS. Each data point represents an individual magnetite grain. Abbreviations: BIF = banded iron formation, IOCG = iron oxide copper-gold. The fields in discrimination diagrams (a), (b), (c), and (d) are from Dupuis and Beaudoin (2011), and those in (e) and (f) are from Méric (2011).

In the discrimination diagrams of Dupuis and Beaudoin (2011), Méric (2011), and Dare et al. (2014), it appears that the minor and trace element contents of magnetite from the oxide-bearing mafic and ultramafic rocks and the semi-massive to massive Fe-Ti oxide units are locally related to the type of lithology, such as in the Baie Chapus Pyroxenite (EPMA data: Fig. 9a, 10a,c,e, Table 2) and the Big Mac intrusion (EPMA and LA-ICP-MS data: Fig. 9, 10, Table 2).

DISCUSSION

Influence of the Exsolutions and/or Inclusions

Magnetite commonly contains ilmenite exsolutions that form during the subsolidus exsolution-oxidation processes (e.g. Dare et al., 2012, 2014). Unlike the electron microprobe (~5–10 µm beam size), the LA-ICP-MS uses larger beam sizes (>40 µm) that could incorporate some of these exsolutions during analyses, thus yielding a mixed analysis combining magnetite and ilmenite. However, these mixed analyses provide an estimate of the initial magnetite composition, before the Fe-oxide grains underwent subsolidus exsolutions. As a result, the EPMA and LA-ICP-MS data could show significant variations for some of the minor and trace element contents of the magnetite. For example, Ti, Mn, and Mg preferentially partition into ilmenite (Méric, 2011; Dare et al., 2014) and therefore are generally underestimated in the EPMA data (e.g. Fig. 2, 3, 9, Table 2).

The differing results for Ti contents obtained by the different analytical methods could explain the hydrothermal signature in the discrimination diagram of Dare et al. (2014) for the Baie Chapus magnetite, which was analyzed by EPMA (Fig. 9a). Indeed, LA-ICP-MS data show that these Fe-oxide grains were initially rich in Ti (>9 wt%) and plot within the magmatic field (Fig. 9b). The higher Ti contents of the Baie Chapus magnetite when determined by LA-ICP-MS could be the result of numerous Ti-enriched ilmenite exsolutions being present in the magnetite that could have been included in the LA-ICP-MS analyses but not in the EPMA results.

Other exsolutions (e.g. Al-spinel, Cr-spinel) or inclusions (e.g. sulphide) are commonly observed in magmatic magnetite (e.g. Dare et al., 2014; Huang et al., 2019). These exsolutions/inclusions could have been incorporated during LA-ICP-MS analysis, or during EPMA analysis in the case of micro- to nano-scale exsolutions/inclusions. This could explain the local variations in the minor and trace element contents of magnetite reported by the two analytical methods.

Influence of the Composition of the Parental Magma

Most of the intrusions studied that have a mafic-dominated composition (Croal Lake, Big Mac, Butler, Highbank-Fishtrap, Wabassi Main, Rivière Bell, and Lac Doré) or an ultramafic-dominated composition (Baie Chapus Pyroxenite) appear to have crystallized, at least in part, from high-Ti parental magmas. These intrusions contain some original Ti-rich magnetite (≥1 wt% Ti; Fig. 9b), suggesting that they were associated with high-Ti parental magmas. This confirms the previous results of Kuzmich (2014) about the nature of the parental magmas of the Butler intrusions (Table 1). In contrast, the low-Ti contents of the Oxtoby Lake magnetite as determined by EPMA and by LA-ICP-MS (mostly <0.1 wt% Ti, Fig. 9) indicate that these Ti-poor Fe-oxides likely crystallized from low-Ti parental magmas. It also suggests that the Ti-poor magmatic Fe-oxides could have higher Ni/Cr ratios than is predicted by the discrimination diagram of Dare et al. (2014; Fig. 9). This was previously reported by Duparc et al. (2016) for magnetite from Archean felsic intrusions and could reflect the initial composition of the parental magmas.

The nature of the parental magmas (e.g. basaltic, picritic, komatiitic) of the mafic to ultramafic intrusions could affect the chemical composition of magnetite. For example, magnetite from massive sulphides of the Eagle's Nest ultramafic-dominated intrusion has higher concentrations of compatible elements and lower concentrations of incompatible elements than magnetite from the Mayville intrusion (Fig. 4). The Mayville intrusion crystallized from basaltic parental magmas (Yang et al., 2013). In contrast, the Eagle's Nest dyke is associated with a komatiitic parental magma (Mungall et al., 2010; Zuccarelli et al., 2018), resulting from a higher degree of partial melting and, therefore, initially enriched in the most compatible elements and depleted in incompatible elements relative to a basaltic magma. Thus, the trace element contents of the magnetite from the Eagle's Nest dyke suggest that magnetite that crystallizes from an ultramafic parental magma will have a more primitive chemical signature than that which forms from a mafic parental magma.

Influence of the Co-crystallizing Minerals

The nature of the minerals that crystallize with magnetite also affects the minor and trace element composition of Fe-oxides (e.g. Dare et al., 2014). The composition of the magnetite from the Baie Chapus Pyroxenite is a good example of this co-crystallizing effect. The Baie Chapus Pyroxenite is associated with a relatively primitive, mantle-derived parental magma (Sappin et al., 2015a) and the magnetite from this ultramafic-dominated intrusion has a relatively primitive composition, with high Mg and Ni contents and low Al, Ga, and Zn contents (Fig. 2, 3). However, the magnetite also has lower Cr and V contents than expected (Fig. 2, 3). The lower Cr contents could be explained by the fractional crystallization of chromite at depth from this primitive silicate liquid, which would have resulted in a significant decrease in the amount of Cr available in the magma for the Fe-oxides formed later. Furthermore, the low V contents of the magnetite from the pyroxenite relative to that from the semi-massive to massive Fe-Ti oxides of the Baie Chapus Pyroxenite

(Fig. 2, 3, 8c, Table 2) could be explained by the competition for the partitioning of V between magnetite and co-crystallizing clinopyroxene. During magmatic processes, V is strongly partitioned into magnetite ($D_V^{Mag/Silicate\ melt}$ = 26.0: Esperança et al., 1997), but V also has a compatible behaviour with clinopyroxene ($D_V^{Cpx/Basaltic\ melt}$ = 3.1: Hart and Dunn, 1993). The pyroxenite is mainly composed of clinopyroxene with magnetite occurring as an accessory phase, whereas the semi-massive to massive oxide layers are primarily composed of magnetite with minor clinopyroxene. Thus, the high proportion of clinopyroxene in the pyroxenite could explain the depletion in V in magnetite from the ultramafic rocks relative to magnetite from the semi-massive to massive oxide layers.

Fe-Oxide Composition as a Fractionation and Stratigraphic Indicator

Regional scale

The chemical composition of Fe-oxides with respect to compatible and incompatible elements during fractionation processes is a good indicator of the degree of magmatic fractionation of the mafic to ultramafic intrusions in the Superior Province. Based on the magnetite composition of the oxide-bearing mafic to ultramafic rocks and the semi-massive to massive Fe-Ti oxides from the mafic-dominated intrusions, it appears that the Rivière Bell and Lac Doré complexes in the Wawa-Abitibi terrane have the most evolved composition, containing magnetite that is poor in compatible elements and rich in incompatible elements (Fig. 2, 3). The Oxtoby Lake intrusion, located in the Uchi domain, hosts magnetite with intermediate composition of compatible and incompatible elements (Fig. 2). On the other hand, the Croal Lake, Big Mac, Butler, and Highbank-Fishtrap intrusions, in the Oxford-Stull domain, appear to have a more primitive composition, as magnetite from these intrusions are rich in compatible elements (Fig. 2, 3), and magnetite from the Wabassi Main intrusion, in the Uchi domain, shows the most primitive signature of compatible elements (Fig. 2). Its high concentrations of incompatible elements, Al, Mn, and Ti (Fig. 2), could be related to the presence of numerous micro- to nano-scale exsolutions of ilmenite (for Mn and Ti) and Al-spinel (for Al) in the magnetite grains. Indeed, in magnetite from the Wabassi Main intrusion, Al-Mn-Ti contents increase with decreasing Fe contents (EPMA data). Identifying the most primitive and evolved intrusions in the Superior Province may help identify which intrusions in the area are most likely to host Ni-Cu-(PGE) and Fe-Ti-V-P mineralization.

Local scale

In the Big Mac and Baie Chapus intrusions, the chemical composition of magnetite, in terms of compatible and incompatible elements in mafic magmas, shows a strong geographical control that is mostly independent of the lithologies and the proportion of Fe-oxides in the rocks (Fig. 6, 8) and efficiently tracks the magmatic fractionation and indicates the way-up of each intrusion. Magnetite in the northern part of the Big Mac intrusion has a more primitive composition than in the southern area, suggesting that the northern intrusive rocks represent more vent-proximal facies and that the southern rocks are more distal facies. Similarly, the stratigraphic base of the Baie Chapus Pyroxenite appears to be located in the eastern part of the intrusion, as suggested by the occurrence of the most primitive magnetite in this area. These results are also supported by lithofacies distribution, geochemistry, and silicate mineral chemistry. Together these data help to constrain the internal stratigraphy and thus to target the most prospective areas to host Fe-Ti-V mineralization within these intrusions.

Magnetite Composition as an Indicator of the Fe-Ti-V or Fe-Ti-P Prospectivity

The Big Mac mafic intrusion is recognized as an area prospective for Fe-Ti-V mineralization (e.g. Metsaranta and Houlé, 2013; Sappin et al., 2015b; Houlé et al., 2019). In particular, the northern part of this intrusion appears to have the highest potential to host Fe-Ti-V mineralization. The semi-massive to massive oxide layers are restricted to this northern area and show high Fe, Ti, and V contents. In these magnetite-bearing horizons, the best mineralized interval (9.5 m thick) has an average composition of 68 wt% FeO_t, 17 wt% TiO_2, and 0.5 wt% V_2O_5, with a maximum of 76 wt% FeO_t, 19 wt% TiO_2, and 0.6 wt% V_2O_5. Magnetite from the mafic and ultramafic rocks and the semi-massive to massive Fe-Ti oxide layers in the northernmost area also have the most primitive composition, with high V contents (8653–1653), a composition favourable to the formation of Fe-Ti-V deposits. In addition, based on the Ni+Cr versus Ti+V discrimination diagram, the Ni+Cr values are mostly >400 ppm in magnetite from the intrusive rocks and from the Fe-Ti oxide layers in the northernmost and north-central parts of the Big Mac intrusion and are the same as Ni+Cr values in magnetite from Fe-Ti-V deposits (Fig. 10e,f). In contrast, in the southern area, the semi-massive to massive oxide layers are absent and magnetite from the mafic rocks shows a more evolved composition, with lower V contents (1870–90 ppm). These Fe-oxides also have Ni+Cr contents (<400 ppm) similar to that of more evolved magnetite from Fe-Ti-P deposits, according to the Ni+Cr versus Ti+V diagram (Fig. 10e,f). In

the southernmost part of the intrusion, magnetite is also hosted by rocks rich in apatite, suggesting that this area has more potential for Fe-Ti-P mineralization.

The Baie Chapus Pyroxenite, which is known for its potential to host Fe-Ti-V mineralization, contains semi-massive to massive oxide layers with high Fe, Ti, and V contents (up to 66 wt% Fe_2O_{3t}, 9 wt% TiO_2, and 0.7 wt% V_2O_5: Sappin et al., 2015a). Furthermore, the magnetite from the pyroxenite and the semi-massive to massive Fe-Ti oxide layers has a primitive composition with high V contents (up to 7440 ppm) and Ni+Cr contents similar to magnetite from Fe-Ti-V deposits in the Ni+Cr versus Ti+V diagram (Fig. 10e), confirming the prospectivity of the Baie Chapus Pyroxenite to host Fe-Ti-V mineralization.

These results confirm that the chemical composition of magnetite in mafic to ultramafic intrusions can serve as an indicator of the Fe-Ti-V or Fe-Ti-P prospectivity of these types of intrusions.

Archean Signature of Magnetite?

The EPMA analytical results of magnetite from samples of oxide-bearing mafic to ultramafic rocks and semi-massive to massive Fe-Ti oxides suggest that the magnetite from these rock types may have a distinctive Archean signature. For example, in the Ni/(Cr+Mn) versus Ti+V and Ca+Al+Mn versus Ti+V discrimination diagrams of Dupuis and Beaudoin (2011) and the Ni+Cr versus Ti+V discrimination diagram of Méric (2011), magnetite from the Archean intrusions containing the intrusive rocks and the Fe-Ti oxide layers of this study has significantly lower Ti+V contents than magnetite from the Proterozoic and Phanerozoic Fe-Ti deposits used to construct the diagrams (Fig. 10a,c,e). As can be seen on these discrimination diagrams (Fig 10a,c,e), the Rivière Bell magnetite displays a distinct chemical signature, with higher Ti+V contents, which could be due to ubiquitous fine ilmenite exsolutions in the Fe-oxide grains and/or remobilization of Ti during the greenschist-amphibolite-facies metamorphism that affected the intrusion after its emplacement (Polivchuk, 2017). The dichotomy between the Archean and Proterozoic magnetite composition does not appear to be related to an analytical error, as our Lac Doré magnetite has similar Ti+V values as the Lac Doré magnetite, which was analyzed previously (*see* Fig. 5 and 6 in Dupuis and Beaudoin, 2011). One explanation for this difference could be that there is lower Ti and/or V contents in magnetite from Archean Fe-Ti deposits than from younger deposits.

Another trend visible from the discrimination diagrams is that the LA-ICP-MS data appear better at correctly predicting the deposit type as the Ti contents determined by LA-ICP-MS are often higher than those determined by EPMA. However, a fair amount of the LA-ICP-MS data points still fall into other hydrothermal deposit types, especially data for Ti-poor magnetite from the Oxtoby Lake intrusion and also some data for magnetite from intrusions in the Ring of Fire area (Fig. 10b,d,f).

In the light of all these results, further investigations are needed to better understand which factors control this distinctive Archean signature of magnetite and to constrain the use of discrimination diagrams for magnetite to fingerprint the mineral deposit types, as they appear to be sensitive to other factors than solely the chemical composition of magnetite.

IMPLICATIONS FOR EXPLORATION

The chemical composition of magnetite is useful for determining the degree of fractionation and the internal stratigraphy of the intrusions hosting orthomagmatic mineralization and to identify the areas most prospective for this style of mineralization. Coupled with the fact that Fe-oxides are ubiquitous in mafic to ultramafic rocks and are resistant to mechanical and chemical weathering, magnetite could be used efficiently to gain useful information about the intrusions themselves within structurally deformed and metamorphosed Archean and Proterozoic greenstone belts. Furthermore, even though some of the minor and trace element contents of magnetite can be affected by the presence of exsolutions and/or inclusions, the nature of the parental magmas, or the type of co-crystallizing minerals, on the whole, the composition of this Fe-oxide is independent of the nature of its host rocks. This suggests that it is not necessary to have heavily mineralization samples to identify which unit(s) might be prospective for hosting orthomagmatic mineralization. In particular, the Ni+Cr contents of the magnetite appear to be a very interesting tool for determining the prospectivity of mafic to ultramafic intrusions to host Fe-Ti-V or Fe-Ti-P mineralization, irrespective of the amount of Fe-oxides in the rocks. However, the use of discrimination diagrams to estimate which type of mineralized environment is associated with the magnetite should be undertaken with caution.

ONGOING AND FUTURE WORK

Future research in the context of this project would include the study of ilmenite compositions analyzed by EPMA and LA-ICP-MS and the partial least squares-discriminant analysis (PLS-DA) of the minor and trace element contents of Fe-Ti oxides to confirm our preliminary results regarding the chemical signatures of magnetite from the mafic to ultramafic intrusions in the Superior Province. Comparison of the Fe-Ti oxides data from this study with magnetite and ilmenite compositions from previous work on these intrusions (e.g. Polivchuk, 2017; Arguin et al., 2018) and on other

mafic and ultramafic intrusions in the Superior Province, as well as in other geological provinces, would also help clarify if there is a specific regional signature of these oxides across the Superior. Additional studies are also required to identify the factors controlling the possible Archean-specific signature of Fe-oxides and discuss the applicability of discrimination diagrams to fingerprint Archean magnetite.

ACKNOWLEDGMENTS

This report is a contribution to NRCan's Targeted Geoscience Initiative Program (TGI-5). Support for this study was provided through the Orthomagmatic Ni-Cu-PGE-Cr Ore Systems Project's 'Activity NC-2.2: Ni-Cr metallotect: Synthesis, updates, and revised models for the Superior Province'.

We would like to thank Northern Shield Resources Inc. (C. Vaillancourt, I. Bliss, R.-L. Simard, and G. Budulan), R. Metsaranta from the Ontario Geological Survey (OGS), and V. Bécu from the Geological Survey of Canada (GSC) for providing representative samples. Thanks are also extended to M. Choquette (Université Laval) for his assistance with EPMA analyses, and Z. Yang, D. Petts, and S.E. Jackson (GSC) for their assistance with LA-ICP-MS analyses. This report benefited from the scientific review of Sarah Dare (Université du Québec à Chicoutimi) and Wouter Bleeker (GSC) and editorial review by Elizabeth Ambrose and Valérie Bécu.

REFERENCES

Arguin, J.-P., Pagé, P., Barnes, S.-J., Girard, R., and Duran, C., 2018. An integrated model for ilmenite, Al-spinel, and corundum exsolutions in titanomagnetite from oxide-rich layers of the Lac Doré Complex (Québec, Canada); Minerals, v. 8, 39 p.

Boutroy, E., Dare, S.A.S., Beaudoin, G., Barnes, S.-J., and Lightfoot, P.C., 2014. Magnetite composition in Ni-Cu-PGE deposits worldwide: application to mineral exploration; Journal of Geochemical Exploration, v. 145, p. 64–81.

Dare, S.A.S., Barnes, S.-J., and Beaudoin, G., 2012. Variation in trace element content of magnetite crystallized from a fractionating sulfide liquid, Sudbury, Canada: Implications for provenance discrimination; Geochimica et Cosmochimica Acta, v. 88, p. 27–50.

Dare, S.A.S., Barnes, S.-J., Beaudoin, G., Méric, J., Boutroy, E., and Potvin-Doucet, C., 2014. Trace elements in magnetite as petrogenetic indicators; Mineralium Deposita, v. 49, p. 785–796.

Duparc, Q., Dare, S.A.S., Cousineau, P.A., and Goutier, J., 2016. Magnetite chemistry as a provenance indicator in Archean metamorphosed sedimentary rocks; Journal of Sedimentary Research, v. 86, p. 542–563.

Dupuis, C. and Beaudoin, G., 2011. Discriminant diagrams for iron oxide trace element fingerprinting of mineral deposit types; Mineralium Deposita, v. 46, p. 319–335.

Esperança, S., Carlson, R.W., Shirey, S.B., and Smith, D., 1997. Dating crust-mantle separation: Re-OS isotopic study of mafic xenoliths from central Arizona; Geology, v. 25, p. 651–654.

Hart, S.R. and Dunn, T., 1993. Experimental cpx/melt partitioning of 24 trace elements; Contributions to Mineralogy and Petrology, v. 113, p. 1–8.

Houlé, M.G., Lesher, C.M., McNicoll, V.J., Metsaranta, R.T., Sappin, A.-A., Goutier, J., Bécu, V., Gilbert, H.P., and Yang, X.M., 2015a. Temporal and spatial distribution of magmatic Cr-(PGE), Ni-Cu-(PGE), and Fe-Ti-(V) deposits in the Bird River–Uchi–Oxford-Stull–La Grande Rivière–Eastmain domains: a new metallogenic province within the Superior Craton; *in* Targeted Geoscience Initiative 4: Canadian Nickel-Copper-Platinum Group Elements-Chromium Ore Systems — Fertility, Pathfinders, New and Revised Models, (ed.) D.E. Ames and M.G. Houlé; Geological Survey of Canada, Open File 7856, p. 35–48.

Houlé, M.G., Goutier, J., Sappin, A.-A., and McNicoll, V.J., 2015b. Regional characterization of ultramafic to mafic intrusions in the La Grande Rivière and Eastmain domains, Superior Province, Quebec; *in* Targeted Geoscience Initiative 4: Canadian Nickel-Copper-Platinum Group Elements-Chromium Ore Systems — Fertility, Pathfinders, New and Revised Models, (ed.) D.E. Ames and M.G. Houlé; Geological Survey of Canada, Open File 7856, p. 125–137.

Houlé, M.G., Lesher, C.M., Metsaranta, R.T., and Sappin, A.-A., 2019. Architecture of magmatic conduits in chromium-(PGE) and Ni-Cu-(PGE) ore systems in Superior Province: example from the 'Ring of Fire' region, Ontario; *in* Targeted Geoscience Initiative: 2018 report of activities, (ed.) N. Rogers; Geological Survey of Canada, Open File 8549, p. 441–448.

Houlé, M.G., Lesher, C.M., Sappin, A.-A., Bédard, M.-P., Goutier, J., and Yang, X.M., 2020. Overview of Ni-Cu-(PGE), Cr-(PGE), and Fe-Ti-V magmatic mineralization in the Superior Province: Insights on metallotects and metal endowment; *in* Targeted Geoscience Initiative 5: Advances in the understanding of Canadian Ni-Cu-PGE and Cr ore systems – Examples from the Midcontinent Rift, the Circum-Superior Belt, the Archean Superior Province, and Cordilleran Alaskan-type intrusions, (ed.) W. Bleeker and M.G. Houlé; Geological Survey of Canada, Open File 8722, p. 117–139.

Huang, X.-W., Sappin, A.-A., Boutroy, E., Beaudoin, G., and Makvandi, S., 2019. Trace element composition of igneous and hydrothermal magnetite from porphyry deposits: relationship to deposit subtypes and magmatic affinity; Economic Geology, v. 114, p. 917–952.

Jarosewich, E., Nelen, J.A., and Norberg, J.A., 1980. Reference samples for electron microprobe analysis; Geostandards Newsletter, v. 4, p. 43–47.

Kuzmich, B., 2014. Petrogenesis of the ferrogabbroic intrusions and associated Fe-Ti-V-P mineralization within the McFaulds Lake greenstone belt, Superior Province, northern Ontario, Canada; M.Sc. thesis, Lakehead University, Thunder Bay, Ontario, 486 p.

Maier, W.D., Barnes, S.-J., and Pellet, T., 1996. The economic significance of the Bell River Complex, Abitibi subprovince, Quebec; Canadian Journal of Earth Sciences, v. 33, p. 967–980.

Mathieu, L., 2019. Origin of the vanadiferous serpentine–magnetite rocks of the Mt. Sorcerer area, Lac Doré layered intrusion, Chibougamau, Québec; Geosciences, v. 9, p. 1–36.

Méric, J., 2011. Caractérisation géochimique des magnétites de la zone critique de l'intrusion magmatique de Sept-Îles (Québec, Canada) et intégration à une base de données utilisant la signature géochimique des oxydes de fer comme outil d'exploration; Internship report, Université du Québec à Chicoutimi, Chicoutimi, Quebec, 48 p.

Metsaranta, R.T. and Houlé, M.G., 2013. An update on regional bedrock geology mapping in the McFaulds Lake ("Ring of Fire") region; *in* Summary of Field Work and Other Activities 2013; Ontario Geological Survey, Open File Report 6290, p. 50-1–50-12.

Metsaranta, R.T., Houlé, M.G., McNicoll, V.J., and Kamo, S.L., 2015. Revised geological framework for the McFaulds Lake

greenstone belt, Ontario; *in* Targeted Geoscience Initiative 4: Canadian Nickel-Copper-Platinum Group Elements-Chromium Ore Systems — Fertility, Pathfinders, New and Revised Models, (ed.) D.E. Ames and M.G. Houlé; Geological Survey of Canada, Open File 7856, p. 61–73.

Mortensen, J.K., 1993. U-Pb geochronology of the eastern Abitibi Subprovince. Part 1: Chibougamau – Matagami – Joutel Region; Canadian Journal of Earth Sciences, v. 30, p. 11–28.

Mungall, J.E., Harvey, J.D., Balch, S.J., Azar, B., Atkinson, J., and Hamilton, M.A., 2010. Eagle's Nest: a magmatic Ni-sulfide deposit in the James Bay Lowlands, Ontario, Canada; *in* The Challenge of Finding New Mineral Resources: Global metallogeny, innovative exploration, and new discoveries. Volume II: Zinc-lead, nickel-copper-PGE, and uranium, (ed.) R.J. Goldfarb, E.E. Marsh, and T. Monecke; Society of Economic Geologists, Special Publication 15, p. 539–557.

Ontario Geological Survey–Geological Survey of Canada (OGS-GSC), 2011. Ontario airborne geophysical surveys, gravity gradiometer and magnetic data, grid and profile data (ASCII and Geosoft® formats) and vector data, McFaulds Lake area; Ontario Geological Survey, Geophysical Data Set 1068.

Percival, J.A., Skulski, T., Sanborn-Barrie, M., Stott, G.M., Leclair, A.D., Corkery, M.T., and Boily, M., 2012. Geology and tectonic evolution of the Superior Province, Canada; *in* Tectonic Styles in Canada: The LITHOPROBE Perspective, (ed.) J.A. Percival, F.A. Cook, and R.M. Clowes; Geological Association of Canada, Special Paper 49, p. 321–378.

Polivchuk, M., 2017. The formation of vanadium deposits in the Archean Rivière Bell Complex, Quebec: Insights from Fe-Ti oxide chemistry; M.Sc. thesis, University of Ottawa, Ottawa, Ontario, 146 p.

Sappin, A.-A., Houlé, M.G., Goutier, J., and McNicoll, V., 2015a. Caractérisation pétrographique et géochimique de la Pyroxénite de baie Chapus, Baie-James: Un exemple de minéralisation en Fe-Ti-V dans la Province du Supérieur; Geological Survey of Canada, Open File 7745, 1 sheet.

Sappin, A.-A., Houlé, M.G., Lesher, C.M., Metsaranta, R.T., and McNicoll, V.J., 2015b. Regional characterization of mafic-ultramafic intrusions in the Oxford-Stull and Uchi domains, Superior Province, Ontario; *in* Targeted Geoscience Initiative 4: Canadian Nickel-Copper-Platinum Group Elements-Chromium Ore Systems — Fertility, Pathfinders, New and Revised Models, (ed.) D.E. Ames and M.G. Houlé; Geological Survey of Canada, Open File 7856, p. 75–85.

Sappin, A.-A., Houlé, M.G., Lesher, C.M., McNicoll, V., Vaillancourt, C., and Kamber, B.S., 2016. Age constraints and geochemical evolution of the Neoarchean mafic–ultramafic Wabassi Intrusive Complex in the Miminiska–Fort Hope greenstone belt, Superior Province, Canada; Precambrian Research, v. 286, p. 101–125.

SIGÉOM, 2020. Système d'information géominière du Québec. Ministère de l'Énergie et des Ressources naturelles du Québec. <http://sigeom.mines.gouv.qc.ca> [accessed February 9, 2020]

Stott, G.M., Corkery, M.T., Percival, J.A., Simard, M., and Goutier, J., 2010. A revised terrane subdivision of the Superior Province; *in* Summary of Field Work and Other Activities 2010; Ontario Geological Survey, Open File Report 6260, p. 20-1–20-10.

Yang, X.M., Gilbert, H.P., Houlé, M.G., Bécu, V., McNicoll, V.J., and Corkery, M.T, 2013. The Neoarchean Mayville mafic-ultramafic intrusion in the Bird River greenstone belt, southeastern Manitoba: Geological setting, geochemical variation and the implications for Cu-Ni-PGE-Cr mineral exploration; Geological Association of Canada-Mineralogical Association of Canada, Program with Abstracts, v. 36, p. 200–201.

Zuccarelli, N., Lesher, C.M., and Houlé, M.G., 2018. Sulphide textural variations and multiphase ore emplacement in the Eagle's Nest Ni-Cu-(PGE) deposit, McFaulds Lake greenstone belt, Ontario; *in* Targeted Geoscience Initiative: 2017 report of activities, volume 2, (ed.) N. Rogers; Geological Survey of Canada, Open File 8373, p. 29–34.

Convergent margin Ni-Cu-PGE-Cr ore systems: U-Pb petrochronology and environments of Cu-PGE versus Cr-PGE mineralization in Alaskan-type intrusions

Graham T. Nixon[1*], James S. Scoates[2], Dejan Milidragovic[1], James Nott[2], Nichole Moerhuis[2], Thomas J. Ver Hoeve[2], Matthew J. Manor[2†], and Ingrid M. Kjarsgaard[3]

[1]British Columbia Geological Survey, Ministry of Energy, Mines and Petroleum Resources, PO Box 9333 Stn Prov Govt, Victoria, British Columbia V8W 9N3

[2]Pacific Centre for Isotopic and Geochemical Research (PCIGR), Department of Earth, Ocean and Atmospheric Sciences, 2020-2207 Main Mall, University of British Columbia, Vancouver, British Columbia V6T 1Z4

[3]Consulting Mineralogist, 15 Scotia Place, Ottawa, Ontario K1S 0W2

†Present address: Department of Earth Sciences, 9 Arctic Avenue, Memorial University of Newfoundland, St. John's, Newfoundland A1B 3X5

*Corresponding author's e-mail:graham.nixon@gov.bc.ca

ABSTRACT

Magmatic Ni-Cu-PGE deposits hosted by ultramafic-mafic intrusions in convergent margin or supra-subduction/post-subduction tectonic settings are becoming an increasingly important global resource. In the northern Cordillera, this class of intrusions is restricted to the accreted arc terranes of the continental margin of North America where the Alaskan-type subclass is particularly prevalent. This report describes recent research on the Tulameen and Polaris Alaskan-type intrusions in British Columbia that contain orthomagmatic Ni-Cu-PGE mineralization. Preliminary U-Pb geochronological results and trace element analyses of zircon from the Tulameen intrusion are interpreted using an integrated petrochronological approach to distinguish crystallization from post-crystallization events and to constrain the duration of magmatism.

Magmatic Cu-PGE mineralization (predominantly chalcopyrite-bornite) in the Tulameen intrusion is hosted by hornblende-magnetite-bearing ultramafic rocks near its periphery. Preliminary results suggest that emplacement and crystallization of the Tulameen intrusion occurred ca. 204–205 Ma (latest Triassic), coincident with a 6 million year period centred on 205 Ma that produced the most important porphyry Cu-Au deposits in British Columbia. The Cu-PGE mineralization constitutes a unique deposit type for Alaskan-type intrusions and has some attributes in common with stratiform or 'reef-style' mineralization in tholeiitic layered intrusions.

Magmatic Ni-Cu-PGE sulphides (mainly pyrrhotite, chalcopyrite, minor pentlandite) in the Early Jurassic (ca. 186 Ma) Polaris intrusion are hosted by the more evolved ultramafic and mafic rocks. Remobilized ultramafic cumulates form a distinctive component of both intrusions: plastically deformed and dismembered olivine-chromite cumulates are widely distributed in dunite, and what are interpreted as synmagmatic avalanche deposits are well exposed at Tulameen. The remobilization of pre-existing cumulate sequences is rationalized in terms of an open-system magma recharge model that accounts for some of the key textural features exhibited by ultramafic rocks in Alaskan-type intrusions.

INTRODUCTION

The most important Ni-Cu-platinum group element (PGE) resources on Earth are hosted by ultramafic-mafic intrusions and volcanic rocks in various rift-related tectonic settings (e.g. Naldrett, 2004). In the past, magmatic Ni-Cu-PGE sulphide deposits at convergent margins have been regarded as unfavourable environments for nickel exploration due to a perceived lack of economically exploitable deposits. However, over the last 15 years or so, discoveries of significant Ni-sulphide deposits in convergent margin or supra-subduction/post-subduction settings have established this class of intrusions as an increasingly important economic resource. For example, production at the Carboniferous Aguablanca deposit in the Variscan orogenic belt in Spain, Europe's only orthomagmatic nickel mine, began in 2004 with a resource of 15.7 million metric tonnes (Mt) at 0.66 wt% Ni, 0.46 wt% Cu, and 0.47 g/t PGE (Piña, 2019); the Silurian-Devonian Xiarihamu deposit in the Central Asian Orogenic Belt (Eastern Kunlun arc terrane), the second largest Ni-sulphide deposit in China, constitutes a resource of 157 Mt at an average grade of 0.65 wt% Ni, 0.14 wt% Cu, and 0.013 wt% Co (Li et al., 2015; Song et al., 2016).

Nixon, G.T., Scoates, J.S., Milidragovic, D., Nott, J., Moerhuis, N., Ver Hoeve, T.J., Manor, M.J., and Kjarsgaard, I.M., 2020. Convergent margin Ni-Cu-PGE-Cr ore systems: U-Pb petrochronology and environments of Cu-PGE versus Cr-PGE mineralization in Alaskan-type intrusions; *in* Targeted Geoscience Initiative 5: Advances in the understanding of Canadian Ni-Cu-PGE and Cr ore systems – Examples from the Midcontinent Rift, the Circum-Superior Belt, the Archean Superior Province, and Cordilleran Alaskan-type intrusions, (ed.) W. Bleeker and M.G. Houlé; Geological Survey of Canada, Open File 8722, p. 197–218. https://doi.org/10.4095/326897

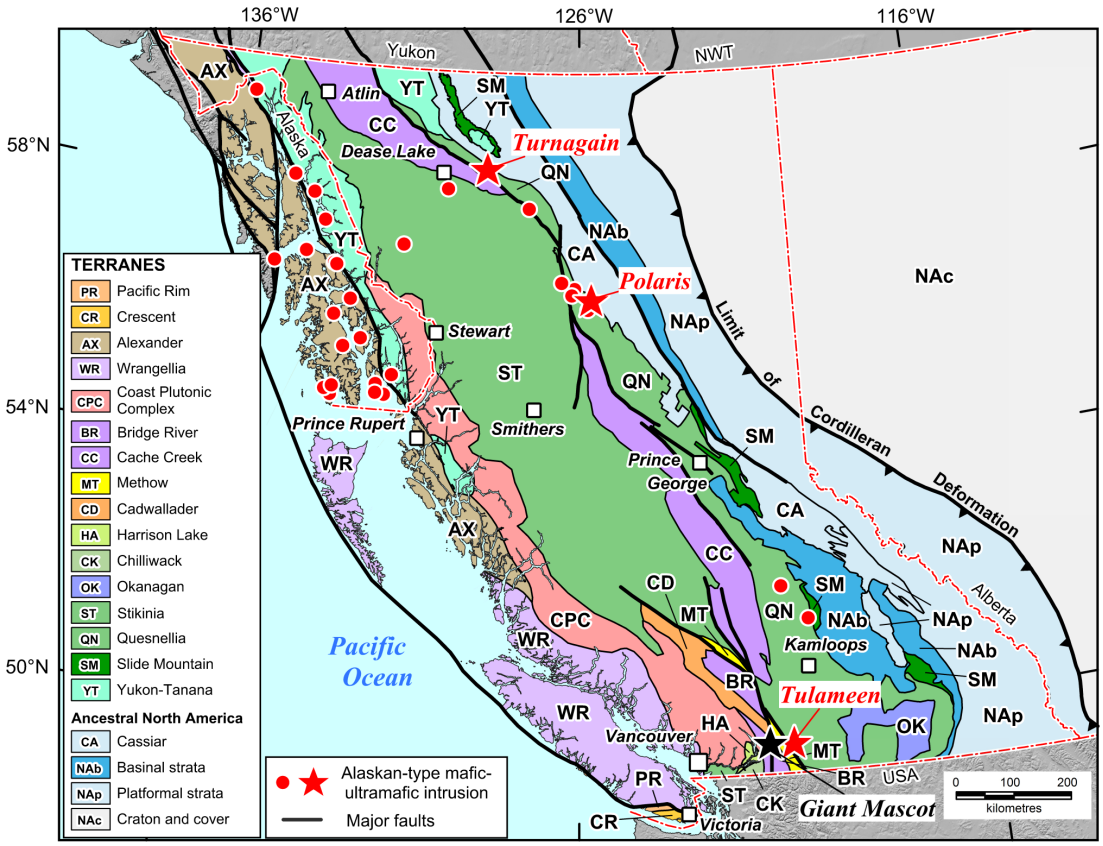

Figure 1. Terrane map of British Columbia and southeastern Alaska (*after* Colpron and Nelson, 2011) showing the distribution of Alaskan-type intrusions (*after* Himmelberg and Loney, 1995; Nixon et al., 1997). Current research on the Tulameen and Polaris intrusions is documented in this report. The subjects of previous studies, the Turnagain Alaskan-type intrusion (Scheel, 2007; Jackson-Brown, 2017; Nixon et al., 2020) and Late Cretaceous Giant Mascot ultramafic-mafic intrusion and Ni-Cu-PGE deposit (black star; Manor et al., 2016, 2017) are shown for reference. The Giant Mascot intrusion contains abundant orthopyroxene and is not an Alaskan-type body according to the mineralogical classification used in this report (Irvine, 1974; Nixon et al., 2015).

An overview of the characteristics and global distribution of Neoarchean to Mesozoic ultramafic-mafic intrusions with Ni-Cu-PGE mineralization in convergent margin settings is given by Nixon et al. (2015), who recognized two principal mineralogical subtypes of convergent-margin intrusions: Alaskan-type intrusions, which characteristically lack orthopyroxene (Irvine, 1974); and intrusions that carry abundant cumulus and/or postcumulus orthopyroxene. Both subtypes may exhibit a zonal arrangement of lithologies extending from dunite in the core of the intrusive body through orthopyroxene-bearing (harzburgite/lherzolite) or orthopyroxene-free (wehrlite) peridotite to hornblende-bearing pyroxenite and hornblendite±gabbro at the margin. The type example of a zoned, orthopyroxene-rich ultramafic body in British Columbia that hosts Ni-sulphide mineralization is the Late Cretaceous (ca. 93 Ma) Giant Mascot intrusion (Fig. 1). The Giant Mascot Ni-Cu sulphide deposit, the province's only former nickel mine (1958–1974), produced 4.2 Mt of ore grading 0.77 wt% Ni and 0.34 wt% Cu (Pinsent, 2002) from a series of subvertical ore shoots interpreted as representing conduit-style mineralization (Manor et al., 2016, 2017).

Regardless of tectonic setting, magmatic Ni-Cu-PGE deposits may be divided into two major groups: deposits mined primarily for their Ni and Cu, which tend to be rich in sulphide (10–90 vol.%, comprising mainly pyrrhotite, pentlandite, chalcopyrite, and minor pyrite); and PGE-rich deposits that are typically poor in sulphides (<0.1–5 vol.%; e.g. Naldrett, 2004; Maier, 2005). Alaskan-type intrusive suites are commonly perceived to evolve in sulphide-deficient magmatic environments and are primarily known for their chromitite-PGE mineralization in the dunite core and derivative platinum placers, some of which have been exploited economically (e.g. Tulameen, Nixon et al., 1990; *see* also reviews by Johan, 2002 and Weiser, 2002). In British Columbia, Late Triassic to Early Jurassic Alaskan-type intrusions are well represented in the accreted arc terranes of Quesnellia and Stikinia (Nixon et al., 1997; Fig. 1).

Perhaps in recognition of the growing economic potential of ultramafic-mafic intrusions at convergent margins, Naldrett (2010) introduced a new class of Ni-Cu sulphide deposit (NC-7, Ural-Alaskan-type) in his petrotectonic classification scheme, and cited the Early

Jurassic Turnagain ultramafic-mafic intrusion in northern British Columbia as the type example (Fig. 1). The Turnagain intrusion contains a large-tonnage, low-grade Ni-sulphide resource of 1842 Mt at an average grade of 0.21 wt% Ni and 0.013 wt% Co, and ranks ninth in the world for contained Ni metal (Scheel, 2007; Mudd and Jowitt, 2014). The unusual, currently subeconomic endowment of Ni-sulphide mineralization at Turnagain has been related to contamination of primitive high-Mg magmas by carbonaceous and sulphide-bearing sedimentary wallrocks that are also implicated in the origin of Cu-PGE mineralization in a younger intrusive phase (Nixon, 1998; Scheel, 2007; Jackson-Brown, 2017). Crustal contamination has also played an important role in the genesis of the Ni-Cu ores hosted by orthopyroxene-rich cumulates in the Giant Mascot deposit (Manor et al., 2016).

One prime objective of our studies of ultramafic-mafic intrusions at convergent margins is to establish the nature and timing of Ni-Cu-PGE mineralization within the context of the temporal and magmatic evolution of the host intrusion. Recently completed U-Pb and $^{40}Ar/^{39}Ar$ geochronological studies of the Turnagain intrusion have provided the first published absolute calibration of the multistage assembly of a zoned Alaskan-type intrusion (Nixon et al., 2020). The Turnagain body is a composite intrusion comprising four compositionally, spatially, and temporally distinct intrusive phases that were emplaced over approximately 4 million years in the Early Jurassic (ca. 189–185 Ma), concomitant with the accretion of major arc terranes in the northern Cordillera (Nixon et al., 2020). The main Ni resource given above is hosted by early stage dunite-wehrlite-clinopyroxenite cumulates (Scheel, 2007), whereas Cu-PGE mineralization is restricted to the youngest clinopyroxenite-hornblendite-(wehrlite-leucodiorite) intrusive component of the complex (Jackson-Brown, 2017).

This report describes recent work on the Tulameen and Polaris Alaskan-type intrusions in British Columbia (Fig. 1). Herein, we (1) present preliminary high-precision U-Pb crystallization ages and trace element concentrations of zircon from the Tulameen intrusion and frame them in an integrated petrochronological context; (2) describe the textures and mineralogy of a zone of Cu-PGE mineralization hosted by evolved ultramafic rocks in the Tulameen intrusion, mineralization that has affinities with stratiform Cu-PGE horizons in layered intrusions; and (3) adopt a magma recharge model to rationalize the physical reworking of cumulate sequences in the core of the Tulameen and Polaris intrusions. The results have significant implications for Ni-Cu-PGE exploration in convergent margin settings, and specifically for Alaskan-type intrusive complexes.

TULAMEEN INTRUSION

The Late Triassic Tulameen ultramafic-mafic intrusion (60 km^2) in southern British Columbia (Fig. 1) is a classically zoned Alaskan-type intrusion with a dunite core passing outwards through olivine clinopyroxenite/clinopyroxenite to hornblende clinopyroxenite and hornblendite at the margin (Findlay, 1963, 1969; Fig. 2). Gabbroic rocks are widely distributed, though concentrated in the eastern, central, and south-central parts of the intrusion, and a voluminous dioritic phase occupies the southeastern margin (Fig. 2). The intrusion has a dyke- or sill-like form (18 km long x 6 km maximum width) that is broadly concordant with the regional structural grain. Bedding attitudes in metavolcanic and metasedimentary host rocks of the Upper Triassic Nicola Group strike north-northwesterly and dip moderately to steeply (40–70°) to the west (Nixon, 2018). Contacts with the Nicola Group are defined by ductile (mylonitic) and brittle fault zones (Nixon and Rublee, 1988; Rublee, 1989). Rafts of hornfelsed metasedimentary rocks correlated with the Nicola Group occur within the Tulameen intrusion and establish the intrusive nature of the complex. A post-Triassic upper greenschist to lower amphibolite facies metamorphism in the Nicola Group overprints the Tulameen intrusion. The age of the metamorphism is considered to be broadly synchronous with the intrusion of the Eagle granodiorite-tonalite pluton situated a kilometre to the west (Greig et al., 1992). The pluton has been dated by U-Pb (zircon) at ca. 148–157 Ma (Late Jurassic: Greig et al., 1992).

In the following sections, we (1) present new petrochronological results for the Tulameen intrusion and discuss their significance; (2) illustrate the textural features of remobilized chromitites in the dunite core and fragmental dunite-clinopyroxenite cumulates peripheral to the core that are interpreted as magmatic avalanche deposits; and (3) describe the nature of recently discovered Cu-PGE mineralization in the Tulameen intrusion, and compare this Alaskan-type mineral occurrence with a specific type of stratiform or 'reef-style' mineralization hosted by layered intrusions.

Petrochronology

A framework for the crystallization history of the Tulameen intrusion is being established and refined using a petrochronological approach by combining scanning electron microscope-cathodoluminescence (SEM-CL) imaging, laser ablation-inductively coupled plasma-mass spectrometry (LA-ICP-MS) trace element analysis, and chemical abrasion-isotope dilution-thermal ionization mass spectrometry (CA-ID-TIMS) of individual zircon crystals or fragments thereof. Petrochronology links the petrology and geochemistry of zircon crystals to their chronometric data with the

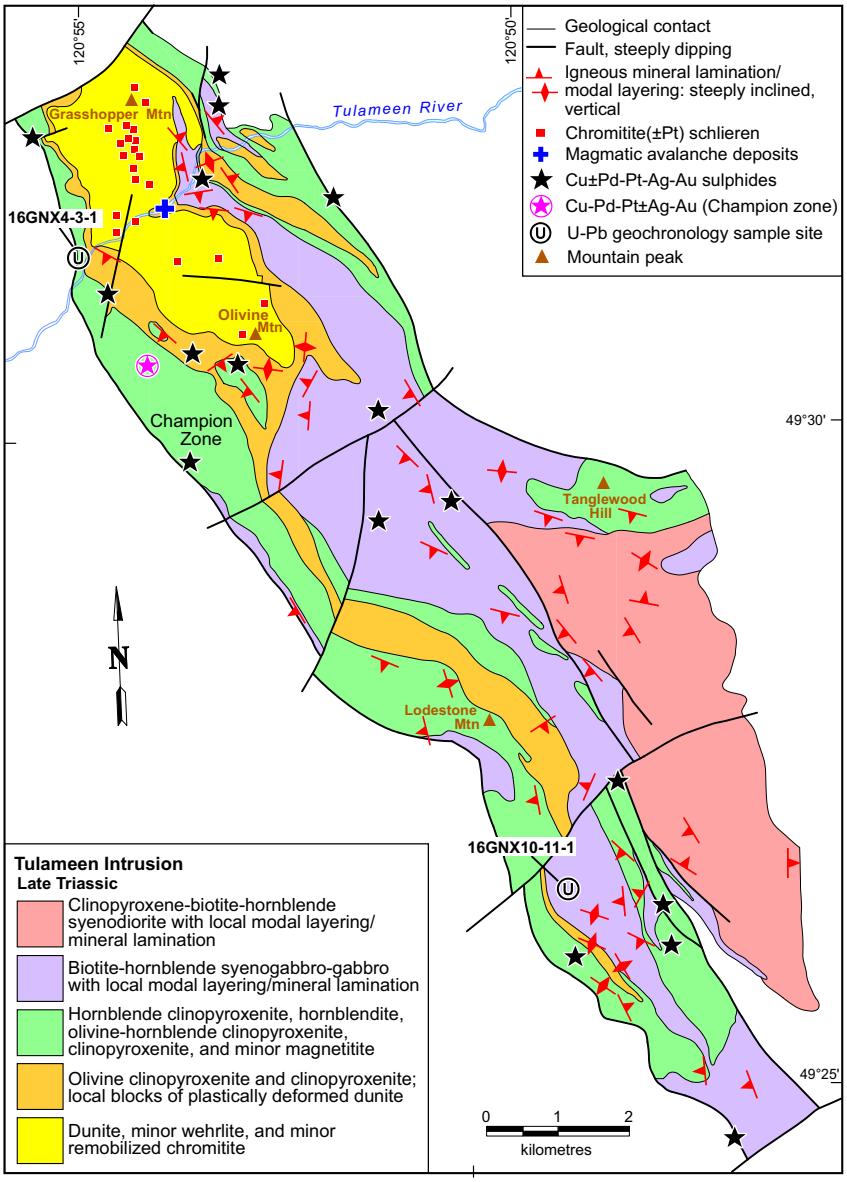

Figure 2. Generalized geological map of the Tulameen Alaskan-type intrusion, south-central British Columbia, showing chromitite (±PGE) localities in the dunite core (Nixon et al., 1997; Nixon, 2018) and Cu±PGE-Ag-Au sulphide occurrences, including the recently discovered Cu-Pd-Pt-rich Champion zone documented in this report. Abbreviation: Mtn = mountain.

goal of defining the specific conditions under which the analyzed zircon grains crystallized (Engi et al., 2017). Compared to our previous geochronological studies of convergent margin ultramafic-mafic intrusions in British Columbia (Giant Mascot intrusion: Manor et al., 2017; Turnagain intrusion: Nixon et al., 2020), the current study utilizes a workflow where the selection of zircon grains for high-precision CA-TIMS dating is determined by SEM-CL imaging and trace element compositions to ensure an internally consistent set of data from each analyzed zircon. From 20 geochronological samples representing major lithological units of the Tulameen intrusion, 11 yielded sufficient zircon grains for analysis. All analytical work is being conducted at the Pacific Centre for Isotopic and Geochemical Research at the University of British Columbia. Analytical techniques follow those described in detail in Scoates and Wall (2015), Ver Hoeve et al. (2018), and Wall et al. (2018).

The major accessory minerals in the Tulameen intrusion include zircon, apatite, and titanite. Euhedral apatite is present in most samples, whereas titanite is typically present in samples with no zircon. Titanite occurs in a variety of textural settings (e.g. wedge-shaped euhedral crystals, granular aggregates, rims around Fe-Ti oxides) and occurs in about 50% of the samples collected. Zircon from the Tulameen intrusion is characterized by a diverse range of internal structures under SEM-CL (Fig. 3). Herein we highlight the petrochronological attributes of two contrasting samples to demonstrate the potential for extracting information related to magmatic processes from the petrology, geochemistry, and geochronology of individual zircon grains. One is an ultramafic rock from the northwestern margin of the intrusion, adjacent to upper greenschist to lower amphibolite facies country rocks (biotite-hornblende clinopyroxenite, sample 16GNX4-3-1); the other is a monzodiorite from a gabbro-

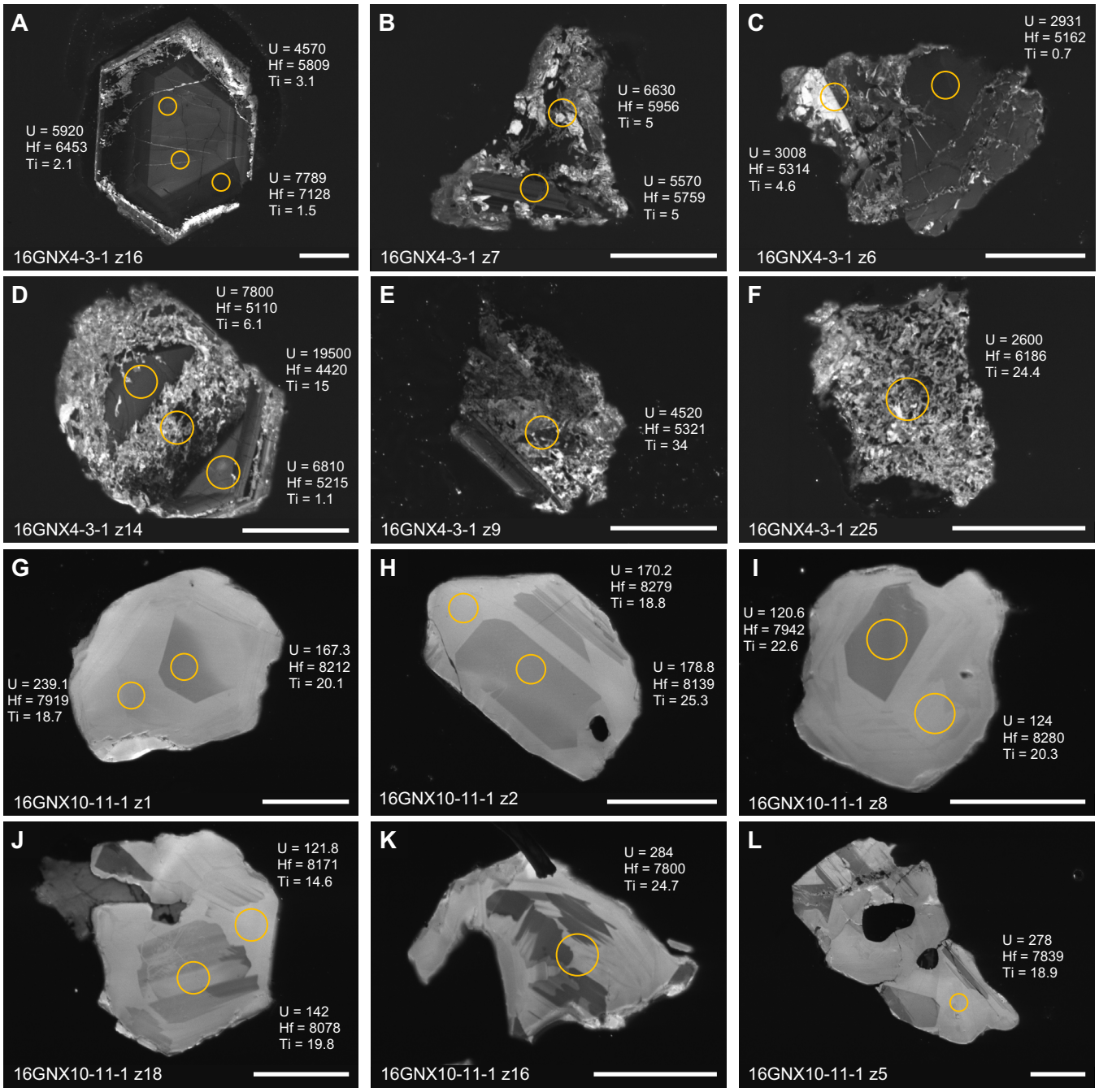

Figure 3. Scanning electron microscopy-cathodoluminescence (SEM-CL) images of zircon grains from representative samples of the Tulameen Alaskan-type intrusion. The circles indicate the locations of spot analysis by LA-ICP-MS (circle diameter is 34 µm). Values for U, Hf, and Ti (all in ppm) are shown adjacent to each spot. **a–f)** Zircon grains from sample 16GNX4-3-1 (biotite-hornblende clinopyroxenite). **g–l)** Zircon grains from sample 16GNX10-11-1 (monzodiorite). Note the presence of secondary and recrystallized CL-bright domains around and within the zircon grains from the clinopyroxenite sample compared to the essentially pristine zircon grains from the monzodiorite sample. Scales as indicated by the white bars (100 µm) on each photograph.

syenogabbro unit from the far southern end of the intrusion (monzodiorite, sample 16GNX10-11-1; Fig. 2). Zircon from the clinopyroxenite contains vestiges of oscillatory zoned magmatic zircon, generally with low CL response, that are enveloped or transected, or completely obliterated, by irregular and patchy domains and veins of CL-bright material (Fig. 3a-f). The domains and veins are interpreted to represent recrystallized and metamict (now strongly altered) zircon produced during deformation and associated metamorphism and hydrothermal activity (e.g. Scoates et al., 2017) that occurred after the Tulameen intrusion had solidified. In contrast, zircon from the monzodiorite is mostly pristine, showing only very minor effects of secondary processes along grain edges (CL-bright regions), and is dominated by simple zoning with CL-grey cores and

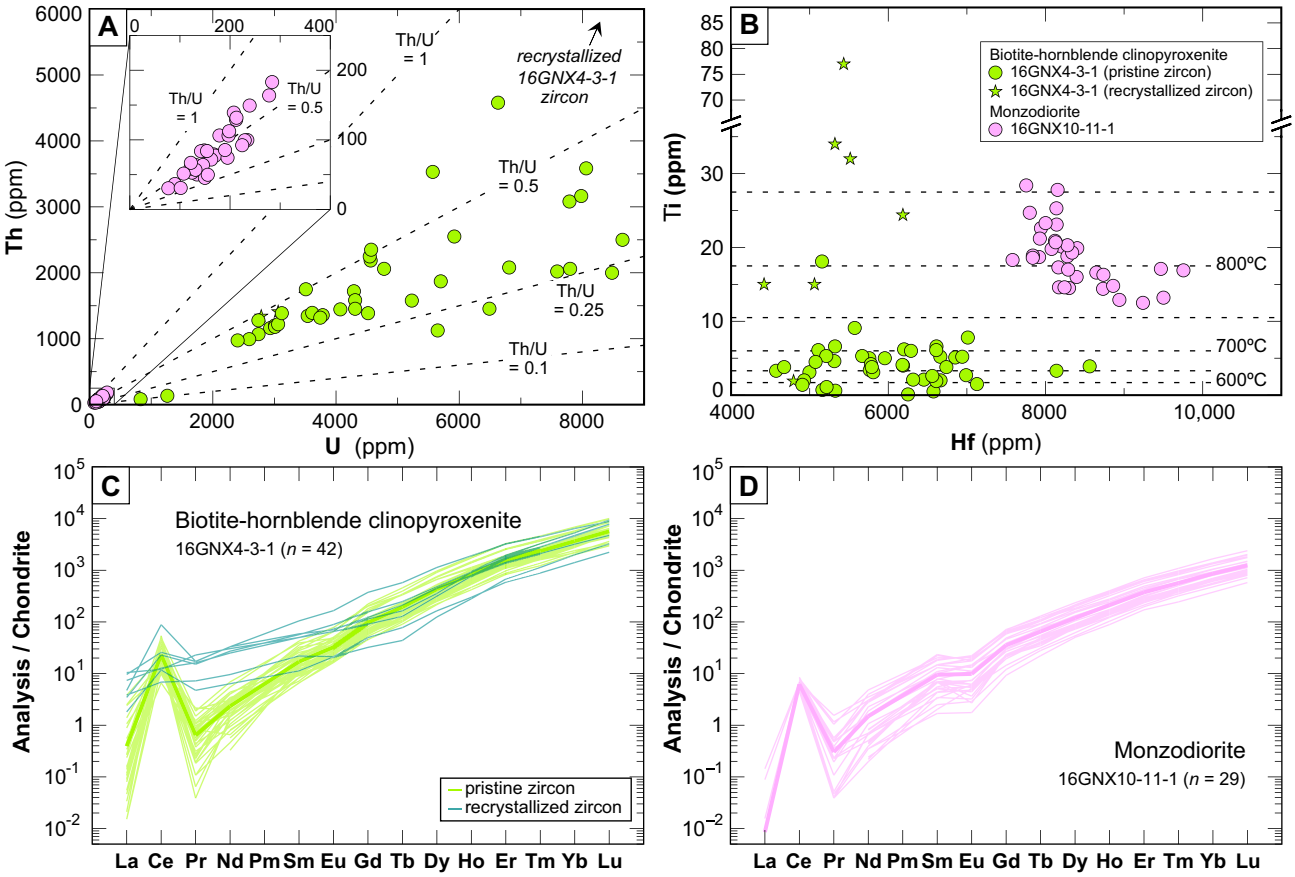

Figure 4. Trace element variations determined by LA-ICP-MS in zircon from representative samples of the Tulameen Alaskan-type intrusion. **a)** Plot of Th versus U with lines of constant Th/U indicated for reference. Anomalously high Th and U concentrations from the CL-bright recrystallized domains plot well off the scale of the graph. **b)** Plot of Ti versus Hf concentrations with horizontal dashed lines that are Ti-in-zircon temperatures calculated from Ferry and Watson (2007) using assumed a_{SiO_2} = 0.3 and a_{TiO_2} = 0.5 (i.e. no quartz or rutile are present in these samples; titanite is abundant). Note the break in scale on the Ti axis. Recrystallized zircon from the clinopyroxenite is indicated with the star symbol and is characterized by anomalously high Ti contents. **c)** Chondrite-normalized rare earth element (REE) patterns for zircon from sample 16GNX4-3-1 (biotite-hornblende clinopyroxenite). Patterns for CL-bright recrystallized zircon are shown in light blue and characterized by LREE enrichment. **d)** Chondrite-normalized rare earth element (REE) patterns for zircon from sample 16GNX10-11-1 (monzodiorite). Normalization values are from McDonough and Sun (1995).

broad CL-light rims (Fig. 3g-l). Inclusions of apatite occur in some zircon grains from the monzodiorite.

The geochemistry of zircon determined by LA-ICP-MS on mineral separates from the two samples is distinctive and highlights their different crystallization and post-crystallization histories (Fig. 4). Zircon from the clinopyroxenite has high but variable concentrations of U (850–8500 ppm) and Th (5–4500 ppm) with variable Th/U values (0.1–0.7; average = 0.4; Fig. 4a), consistent with derivation from an extremely fractionated interstitial melt. In contrast, zircon from the monzodiorite has relatively low and restricted concentrations of U and Th (U = 80–290 ppm; Th = 25–190 ppm; Th/U ≈ 0.5). Zircon from the two different rock types shows distinctive Ti-Hf systematics where Ti is a monitor of temperature (Ferry and Watson, 2007) and Hf is a proxy for the extent of fractionation (Grimes et al., 2009; Ver Hoeve et al., 2018; Fig. 4b). In the clinopyroxenite, zircon defines a nearly horizontal Ti-Hf trend with a limited range of very low Ti concentrations, and a wide range of Hf concentrations (4500–8500 ppm), a feature taken to indicate crystallization at near-solidus conditions. Anomalously high Ti contents (15–80 ppm) correlate with analyses of recrystallized, CL-bright zircon (Fig. 4b), indicating the addition of Ti to the magmatic zircon during secondary processes. In contrast, zircon from the monzodiorite defines the typical curvilinear Ti-Hf relationship that indicates the crystallization of zircon from a melt undergoing progressive fractionation (i.e. increasing Hf) during cooling (i.e. decreasing Ti; Fig. 4b). Estimates of crystallization temperatures based on Ti-in-zircon thermometry (Ferry and Watson, 2007) are cooler (average = 650ºC) for zircon from the clinopyroxenite compared to zircon from the monzodiorite (850–760°C). This confirms the near-solidus crystallization of zircon in the ultramafic rock relative to the higher temperatures of zircon crystallization as a liquidus phase in the monzodiorite; a similar

relationship was observed for zircon from ultramafic and dioritic rocks in the Giant Mascot and Spuzzum intrusions of southwestern British Columbia (Manor et al., 2017). Chondrite-normalized rare earth element (REE) patterns of zircon from the two samples from the Tulameen intrusion display typical igneous zircon patterns with relatively depleted light REE (LREE) and relatively enriched heavy REE, strong positive Ce anomalies (most significant in the clinopyroxenite), and subtle negative Eu anomalies (more negative in the monzodiorite; Fig. 4c,d). Zones of recrystallized zircon from the clinopyroxenite are characterized by anomalously flat LREE patterns indicating the addition of LREE during secondary processes. Overall, the absolute abundances of REE are higher, and REE profiles are more fractionated (i.e., higher Lu/Nd values) in zircon from the clinopyroxenite, compared to zircon from the monzodiorite (Fig. 4c,d).

The CA-ID-TIMS U-Pb zircon geochronology from the Tulameen intrusion reveals a range of $^{206}Pb/^{238}U$ dates for each sample at ca. 204–205 Ma (Fig. 5). The ability to date individual zircon crystals, or fragments of grains, to high precision by CA-ID-TIMS now systematically reveals dispersed zircon dates where it is no longer adequate to simply calculate weighted mean dates from a population, typically the oldest, and use them to infer crystallization ages (e.g. Samperton et al., 2015; Manor et al., 2017). The chemical abrasion technique (CA-ID-TIMS) of Mattinson (2005) allows for the removal of zircon domains that have lost Pb from the interior of grains and for the subsequent analysis of low-U+Th, closed-system residues with concordant results and ages with significantly improved accuracy. The U-Pb results for analyses completed to date for both samples are concordant to slightly normally and reversely discordant and they span a range of $^{206}Pb/^{238}U$ dates from 205.36 ± 0.28 Ma to 204.79 ± 0.24 Ma (Δt ≈ 0.57 Ma) for the clinopyroxenite (n = 5) and from 205.01 ± 0.29 Ma to 203.36 ± 0.72 Ma (Δt ≈ 1.74 Ma) for the monzodiorite (n = 8; Fig. 5). A single zircon from the monzodiorite yields an anomalously young concordant date of 178.26 ± 1.03 Ma (not shown in Fig. 5), reflecting the effects of Pb loss since crystallization, not mitigated by chemical abrasion pretreatment. The dispersion in the dates of both samples is provisionally attributed to protracted, autocrystic zircon crystallization following the approach outlined by Samperton et al. (2015), where autocryst refers to zircon associated exclusively with a distinct pulse or increment of magma (Miller et al., 2007). Except for recrystallized zircon in the clinopyroxenite, both samples contain what appear to be single populations of autocrystic zircon grains with relatively simple internal structures, no growth discontinuities or cores, and coherent trace element variations.

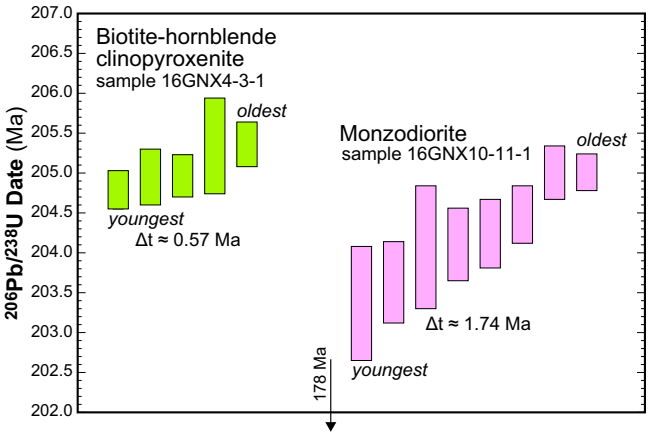

Figure 5. Preliminary chemical abrasion-isotope dilution-thermal ionization mass spectrometry (CA-ID-TIMS) U-Pb zircon geochronological results from the Tulameen Alaskan-type intrusion presented as rank-order plots of $^{206}Pb/^{238}U$ dates for sample 16GNX4-3-1 (biotite-hornblende clinopyroxenite) and for sample 16GNX10-11-1 (monzodiorite). Each bar represents the result of the analysis of a single zircon grain or fragment; the height of the bar corresponds to the 2σ uncertainty. Both samples show a range of $^{206}Pb/^{238}U$ dates at ca. 204–205 Ma. This dispersion (Δt) is provisionally attributed to protracted autocrystic zircon crystallization in the magmas that crystallized to produce clinopyroxenite and monzodiorite. Note that a single analysis from the monzodiorite with a much younger $^{206}Pb/^{238}U$ date of ca. 178 Ma is off the scale of the plot and is attributed to Pb loss since crystallization.

The preliminary U-Pb geochronological results indicate emplacement and crystallization of the Tulameen Alaskan-type ultramafic-mafic intrusion over a relatively restricted interval of time (204–205 Ma) in the Late Triassic. It is increasingly recognized that many plutonic rocks, spanning the spectrum of compositions from mafic to felsic, were emplaced into the middle to upper crust incrementally through the amalgamation of smaller volume batches in the form of horizontal sheets or sills (e.g. Matzel et al., 2006; Schoene et al., 2012; Annen et al., 2015; Wall et al., 2018). In British Columbia, the geochronology of composite ultramafic-mafic intrusions now demonstrates a range of emplacement and crystallization timescales, from relatively short (ca. 93 Ma for the Giant Mascot intrusion: Manor et al., 2017; ca. 204–205 Ma for Tulameen: this study) to extended (ca. 185–189 Ma for Turnagain: Nixon et al., 2020). These ultramafic-mafic intrusions represent the crystallized products of magmatic systems in arc environments where individual arcs may be active for prolonged periods of up to several million years, but may also be episodic with discrete periods of enhanced magmatism separated by lulls during which magma productivity is significantly reduced (e.g. DeCelles et al., 2009; Gehrels et al., 2009; Paterson and Ducea, 2015). The new dates for the Tulameen intrusion are also coincident with a 6 million year magmatic flare-up centred on 205 Ma in the Stikine and Quesnel arcs

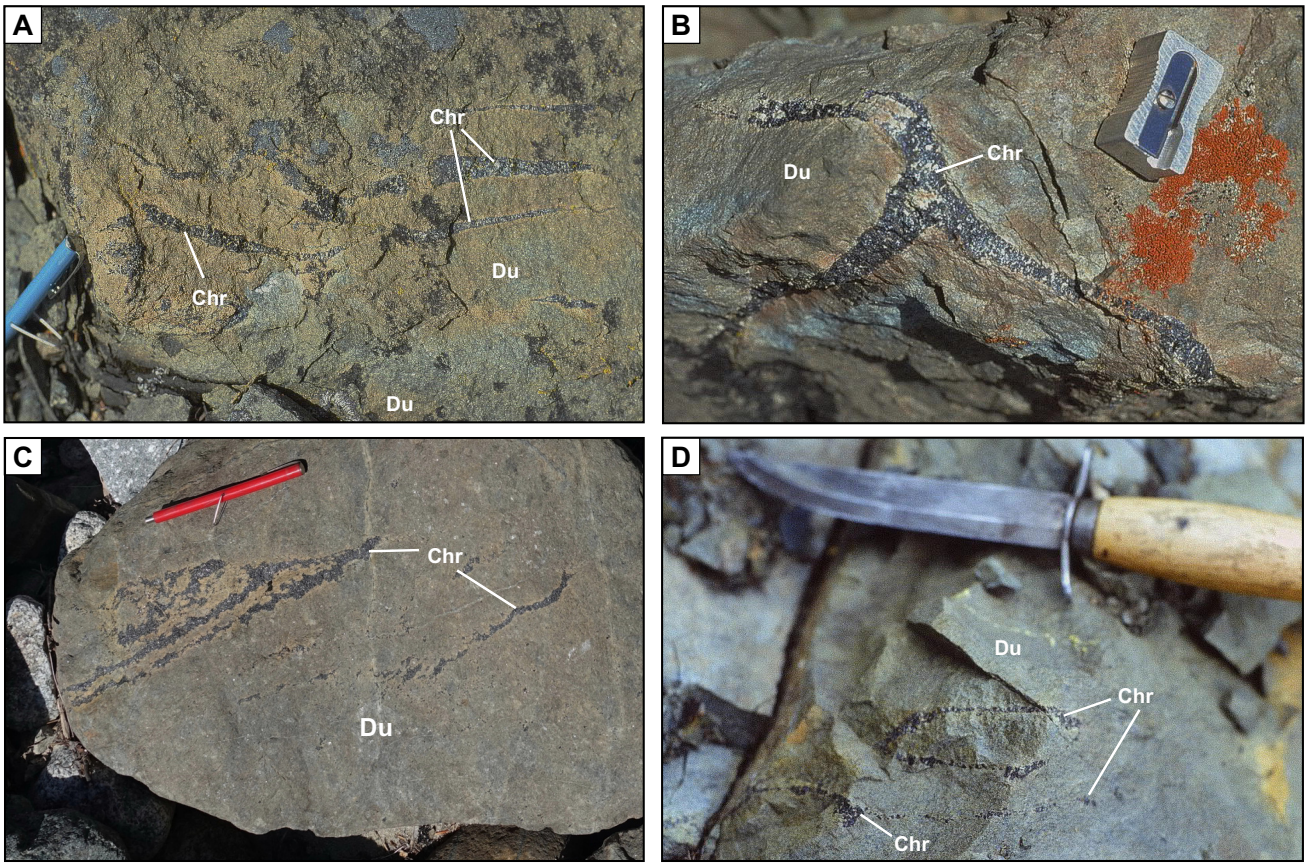

Figure 6. Photographs showing remobilized chromitites in the dunite core of the Tulameen intrusion. **a)** Massive chromitite schlieren (Chr) in dunite (Du) showing typical curvilinear morphology. The visible part of the pencil magnet is 6 cm in length. **b)** Contorted "wishbone" chromitite in dunite. The pencil sharpener is 3 cm in length. **c)** Layered chromitite-dunite inclusion and fine stringers of chromitite in a loose boulder of dunite at the confluence of Britton Creek with the Tulameen River. The pencil magnet is 13 cm in length. **d)** Circular chromitite body proximal to a fine seam of chromitite that shows no evidence of such deformation. The visible part of knife is 20 cm in length.

(Logan and Mihalynuk, 2014). During this time, more than 90% of the known copper endowment of the Stikine and Quesnel arc terranes was produced, resulting in the most prolific Cu-Au porphyry mineralization epoch in British Columbia. Enhanced magmatic activity at this time has been related to stalled subduction, arc-parallel tearing of the subducting slab that lead to early (ca. 210 Ma) production of picritic magmas followed by lower degree partial melts parental to the alkalic Cu-Au porphyries (Logan and Mihalynuk, 2014). The geochronological results from the Tulameen intrusion suggest a direct petrogenetic relationship between Alaskan-type ultramafic-mafic intrusions, the cumulate products of hydrous primitive mantle-derived arc magmas (e.g. up to Fo_{92} olivine at Tulameen: Nixon et al., 1990; Rublee, 1994; and Turnagain, Scheel, 2007), and the formation of Late Triassic Cu-Au porphyry deposits within the northern Cordilleran Stikine-Quesnel arc systems.

Chromitite

Chromitites in the dunite core of the Tulameen intrusion have attracted exploration interest in the past during the search for the origin of historic platinum-rich placers in the Tulameen River. The global platinum exploration boom in the mid-1980s lead to activity primarily focused on Grasshopper Mountain, and later research established platiniferous chromitites in bedrock as the source of platinum in the placers (Nixon et al., 1990). The dunite core of the Tulameen intrusion hosts chromitites with Pt abundances of up to 9.3 g/t Pt and high Pt/Pd values (~127: Nixon et al., 1990). The platinum group minerals are predominantly Pt-Fe alloys that crystallized directly from parental melts in equilibrium with chromite and laurite in a low-fS_2 environment (Nixon et al., 1990; Brenan and Andrews, 2001).

The features exhibited by chromitites in Tulameen dunite (Fig. 6) appear common to other Alaskan-type bodies in British Columbia and elsewhere (e.g. Nixon et al., 1997; Anikina et al., 2014). Chromitites are confined to the dunite core (Fig. 2), and their distribution, as mapped, is more a function of the time spent scouring the more easily accessible outcrops than their true spatial distribution within the dunite. The chromitites

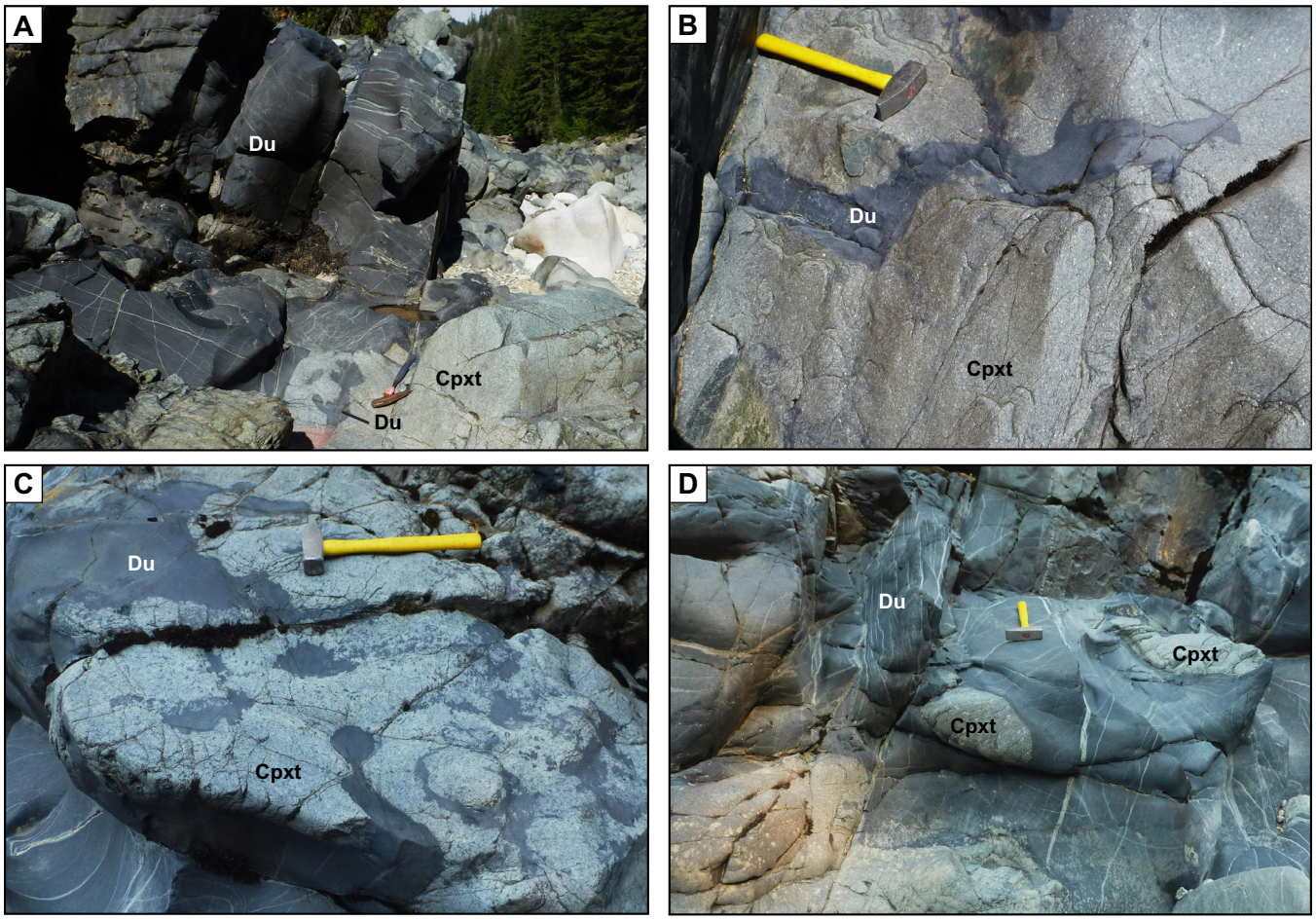

Figure 7. Photographs showing inclusions of dunite in 'magmatic avalanche' deposits exposed in the Tulameen River bed at the eastern periphery of the dunite core. **a)** A large (15 m across) block of dunite (Du) showing irregular contacts with olivine clinopyroxenite/clinopyroxenite (Cpxt) and intricately shaped dunite inclusions in adjacent clinopyroxenite. **b)** Elongate inclusion of dunite in clinopyroxenite exhibiting small protrusions into its host (right end of the dunite). **c)** Bulbous, ragged, and finely disaggregated inclusions of dunite in clinopyroxenite. Note the preferred orientation of dunite disaggregation trails (parallel to the hammer) and a round inclusion of clinopyroxenite (lower right) that has been almost completely exhumed from the dunite. **d)** Rounded inclusions of clinopyroxenite in a dunite pod. Note the highly crenulated and disaggregated dunite-clinopyroxenite contact at the bottom of the photograph. Hammers for scale are 37 cm in length.

generally occur as massive schlieren that reach over a metre in length, however, they are commonly less than 30 cm long by 4 cm wide (Fig. 6a). There is ample evidence for disruption and ductile deformation of formerly layered chromitite-dunite sequences, and some deformed chromitites defy a simple in situ structural explanation for their geometry (Fig. 6b,d). Rare inclusions of layered chromitites attest to the origin of the more common isolated chromitite schlieren (Fig. 6c). These features provide evidence for ductile disaggregation, transport, and redeposition of hot, malleable chromitite-olivine cumulates during crystallization of the dunite core. Similar features in chromitites of the Polaris intrusion are described below.

Magmatic Avalanche Deposits

Remobilized dunite-clinopyroxenite cumulates, herein interpreted as 'magmatic avalanche' deposits, are well exposed at the eastern margin of the dunite core along a 400 m stretch of the Tulameen River bed (Fig. 2). The deposits comprise dunite inclusions, up to 15 m across, immersed in an olivine clinopyroxenite/clinopyroxenite unit in sheared contact with variably serpentinized dunite. Displacement on this contact does not appear to be significant.

The dunite inclusions are generally weakly serpentinized and exhibit some unique features. The largest block of dunite has irregular contacts with the host clinopyroxenite; the latter contains dunite inclusions with intricate shapes that may have spalled off the neighbouring large dunite block (Fig. 7a). Some dunite inclusions are distinctly elongate and exhibit relatively smooth contacts with their clinopyroxenite host except for a few small protuberances (Fig. 7b). Locally, the dunite inclusions show smooth bulbous, as well as ragged morphologies with crenulated margins that dissipate into elongate trains of cm- to mm-size crystal clots dispersed in the clinopyroxenite matrix. The pre-

ferred orientation of these clots likely formed during deposition (Fig. 7c). Bulbous protrusions of dunite in clinopyroxenite and inclusions of clinopyroxenite in dunite are also evident (Fig. 7d) and provide evidence for the viscous intermingling of cumulates during crystallization of the host clinopyroxenite. These processes also appear to be operating in the chaotically intermingled units at Polaris (described below).

Champion Zone: Cu-PGE Mineralization

The Champion zone is a 700 m long zone of intermittent Cu-sulphide mineralization exposed near the western margin of the Tulameen intrusion along a logging road overlooking Champion Creek, for which the showing is named (Fig. 2). The mineralization is hosted in magnetite-hornblende±biotite clinopyroxenite and hornblendite with minor, thin (several cm) horizons of magnetitite. Textural evidence in the least altered rocks indicates that the mineralization is magmatic in origin; however, a metamorphic overprint is evident locally as are restricted zones of intense pyritic hydrothermal alteration. Scattered occurrences of Cu±Ag-Au-PGE mineralization are hosted by ultramafic and gabbroic rocks in other parts of the intrusion (Fig. 2) and may have similar origins as the Champion zone sulphides described below.

Cu sulphides (trace to 2 vol.%) are sparsely distributed throughout the Champion zone and are practically invisible in outcrop, except where weak malachite staining betrays their presence. The primary sulphide minerals are chalcopyrite and lesser bornite accompanied by minor covellite, digenite/chalcocite, and rare pyrrhotite. Pyrite is locally abundant as a hydrothermal overprint replacing magmatic sulphides (mainly chalcopyrite). Four principal textural groupings of sulphide minerals are recognized: 1) inclusions (mostly <30 μm across but reaching 60 μm in diameter) hosted by silicates (clinopyroxene, amphibole) and oxide (magnetite) (Fig. 8a); 2) primary sulphides that occur interstitially within the cumulate framework (Fig. 8b); 3) interstitial sulphides recrystallized and intergrown with metamorphic minerals (Fig. 8c); and 4) secondary Fe sulphides that replace primary Cu-sulphide minerals (Fig. 8d).

Inclusions of chalcopyrite, bornite, minor pyrite, and rare pyrrhotite are found in unaltered silicates and oxides (Fig. 8a). Chalcopyrite commonly forms inclusions in hornblende, clinopyroxene, and magnetite; rare pyrrhotite is confined to inclusions in clinopyroxene where it coexists with chalcopyrite. Bornite occurs in hornblende and magnetite and may be accompanied by chalcopyrite; bornite has not been observed to coexist with pyrrhotite.

Interstitial chalcopyrite and bornite occur as primary sulphides adjacent to unaltered cumulus clinopyroxene and cumulus or postcumulus hornblende and magnetite. Internal features commonly observed in the sulphides include crystallographically controlled, fine exsolution lamellae of chalcopyrite in bornite, and vermicular intergrowths of bornite and chalcopyrite (Fig. 8b). The sulphides locally display alteration rims of covellite and digenite/chalcocite, possibly developed during metamorphism. Malachite and Fe-oxide/hydroxide rims on sulphides are locally well developed as a result of weathering.

Recrystallized interstitial sulphides, predominantly chalcopyrite, are locally intergrown with actinolite, epidote, chlorite, and secondary titanite (Fig. 8c). Sulphide morphologies are typically angular due to control by secondary silicate grain boundaries. Locally, sulphides are remobilized along microfractures and cleavage planes of primary silicates. These textures are attributed to recrystallization and partial replacement of sulphides at upper greenschist-facies conditions, promoted by localized penetration of circulating metamorphic fluids along grain boundaries.

Late-stage hydrothermal pyrite locally occupies fractures and veinlets, and forms narrow (metre-scale) zones of more pervasive replacement of primary interstitial sulphides (Fig. 8d). These zones are typically steeply dipping and appear to crosscut the general trend of the Cu-sulphide mineralization. Rarely, the more pervasive hydrothermal assemblages involve pyrite, chalcopyrite, and pyrrhotite replacing primary silicate minerals.

In addition to the base-metal sulphides, platinum group minerals (PGM) identified in the Champion zone include mertieite (Pd_8Sb_3), sperrylite ($PtAs_2$), and an unknown Pd-Sb-telluride phase that may be a mixture of mertieite and a Pd-telluride (e.g. kotulskite or keithconnite). The PGM form small discrete grains (<7 μm) that are mainly distributed among secondary minerals (chlorite, actinolite, titanite rims on magnetite), except for the Pd-Sb-Te phase(s), which is enclosed in chalcopyrite. These observations suggest that the PGM were remobilized during metamorphism.

Preliminary geochemical results for bulk-rock samples from the Champion zone with low amounts (<2 vol.%) of sulphides yield up to 5200 ppm Cu, 1.15 ppm Pd, 0.79 ppm Pt, and 531 ppb Au with Pd/Pt ≈ 1.5. The abundance of sulphur is consistently low (<530 ppm) throughout the zone. The Cu-rich nature of the sulphides and their low modal proportions, the depletion in sulphur and relative enrichment in Pd, are attributes of Cu-PGE mineralization documented in stratiform or 'reef-style' mineralization in tholeiitic layered intrusions.

The mineralogical and geochemical traits of mineralization in the Champion zone and selected layered intrusions are compared in Table 1. The layered intru-

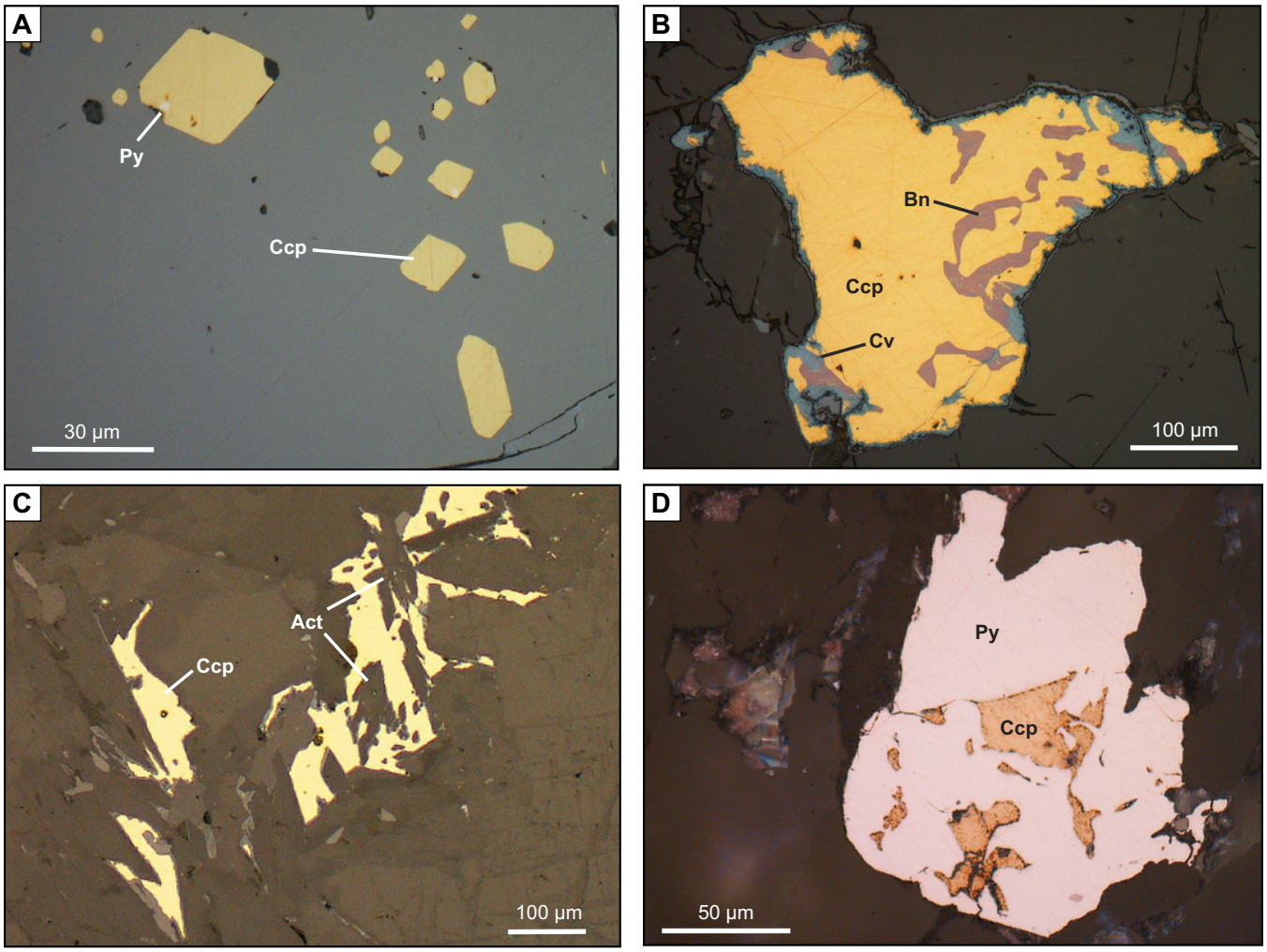

Figure 8. Reflected light photomicrographs showing textural features exhibited by Cu sulphides in ultramafic rocks of the Champion zone. **a)** Chalcopyrite inclusions (Ccp) displaying negative crystal shapes with minor inclusions of pyrite (Py) in cumulus magnetite (magnetite-hornblende clinopyroxenite, sample 16GNX15-7-3). **b)** Interstitial chalcopyrite (Ccp) with vermicular inclusions of bornite (Bn) and partly altered to covellite (Cv). Note the minor chalcopyrite exsolution lamellae that are barely visible in the bornite (magnetite-hornblende clinopyroxenite, sample 17GNX20-3-7). **c)** Recrystallized interstitial chalcopyrite (Ccp) partly replaced by/intergrown with actinolite (Act) (magnetite-hornblende clinopyroxenite, sample 17GNX20-7-1). **d)** Hydrothermal pyrite (Py) replacing interstitial chalcopyrite (Ccp) preserved as irregular relict grains (biotite-hornblende-magnetite clinopyroxenite, sample 17GNX20-12-1). Scales as noted on each photograph.

sions are considered to represent crystallization in closed systems, except for Rincón del Tigre in Bolivia, which has been interpreted as a periodically replenished open-system (Prendergast, 2000), and the W Horizon in the Marathon deposit, Ontario, where spectacular grades may reflect metal upgrading of sulphides via magma flow in conduits (Ames et al., 2017; Good et al., 2017). Remarkable PGE grades (Pt+Pd = 15 g/t, Table 1) are also documented in a 1 metre thick magnetite layer in the Stella intrusion, South Africa (Maier et al., 2003). In the Skaergaard intrusion in Greenland, one of the most intensively studied layered intrusions in the world, the Platinova Reef has an estimated (subeconomic) resource of 23 Mt at 2.3 g/t Au, 0.7 g/t Pd, and 0.1 g/t Pt (contained metal 1.7 Moz Au, 0.5 Moz Pd, and 0.04 Moz Pt) at a cut-off grade of 1.5 g/t equivalent Au (Holwell and Keays, 2014; Holwell et al., 2015).

The Cu-PGE stratiform mineralization is commonly associated with evolved, Fe-Ti oxide-rich gabbro or ferrogabbro cumulates that occur high in the stratigraphy after crystallization of two-thirds or more of the parental magma. Chalcopyrite and/or bornite generally account for the very low amount (<0.2 vol.%) of sulphide typically present in the reefs along with minor digenite, covellite, and chalcocite (Table 1). However, base-metal sulphides are commonly not the most important hosts for PGE but rather discrete platinum group minerals (PGM) such as alloys, PGE-rich sulphides, bismuthides, arsenides, tellurides, and bismuthotellurides (e.g. Godel, 2015).

In comparison to layered intrusions, Cu-rich sulphide mineralization in the Champion zone occurs in evolved ultramafic rocks (magnetite-rich hornblende

Table 1. Cu-PGE reefs in layered intrusions versus Tulameen Alaskan-type intrusion (Champion zone).

Name	Age	Sulphides		Maximum (ppm)						Host rock	Oxide	Ref.
	(Ma)	Type	vol.%	S	Cu	Pd	Pt	Au	Pd/Pt		(vol.%)	
Stella, South Africa	3033	Ccp, Py	m	1150	1096	7.6	7.3	0.67	~1	magt	>50	1
Nuasahi, India	3100	Ccp, Cc, Cv	tr–m	bdl	826	3.8	0.24	0.358	15.8	magt	70	2
PMZ, Sonju Lake, USA	1096	Ccp (Bn)	<0.2	400	<200	1	0.1	0.085	10	Fe-Ti-oxide gabbro	≤12	3, 4, 5
Marathon W Horizon, Coldwell, ON	1105–1108	Ccp, Bn (rare Pn, Po, Py, Mi, Cbt)	1–5	<1 (wt%)	5613	42.2*	8.9*	2.4	4.7*	gabbro		6, 7
PMZ, Rincon del Tigre, Bolivia	990	Ccp, Bn, Cc, Cv (Py, rare Po, Pn)	tr–m	nd	~100	1.8	0.68	0.35	2.6	Mag gabbro	5–30	8
Platinova Reef (Pd zone), Skaergaard, Greenland	56	Bn, Dg (Ccp)	<0.1	<100	300	4	0.2	0.3	20	oxide-rich gabbro	10–40	9, 10, 11
Champion Zone, Tulameen, BC	ca. 204–205	Ccp, Bn, Cv, Dg, Py (rare Po)	tr–2	530	5200	1.15	0.79	0.531	~1.5	Mag-Hbl cpxite; Mag hbt (magt)	5–50	this study

*Conservative values, maximum abundances reported: 67 ppm Pd and 39 ppm Pt (Pd/Pt = 1.7) over 2 m.

Abbreviations: bdl = below detection limit, Bn = bornite, Cbt = colbaltite, Cc = chalcocite, Ccp = chalcopyrite, cpxite = clinopyroxenite, Cv = covellite, Dg = digenite, Hbl = hornblende, hbt = hornblendite, m = minor, Mag = magnetite, magt = magnetitite, Mi = millerite, PMZ = precious-metal zone, Pn = pentlandite, Po = pyrrhotite, Py = pyrite, Ref. = reference, tr = trace, vol.% = volume percent.

References: 1) Maier et al., 2003; 2) Prichard et al., 2018; 3) Miller, 1999; 4) Li et al., 2008; 5) Miller and Ripley, 1996; 6) Good et al., 2017; 7) Ames et al., 2017; 8) Prendergast, 2000; 9) Holwell and Keays, 2014; 10) Holwell et al., 2015; 11) Godel et al., 2014.

clinopyroxenites and hornblendites) at the zoned margin of the intrusion. The Ni-poor nature of magmatic sulphides at Tulameen may be explained by early depletion of Ni by olivine fractionation in silicate melts prior to the onset of sulphide liquid immiscibility. The timing of sulphide saturation in fractionating silicate melts is dependent on a number of factors, some of which appear to have ramifications for sulphide mineralization at Tulameen. Fractional crystallization combined with progressive magmatic oxidation, at oxygen fugacities extending through the sulphide-sulphate transition (Jugo et al., 2010), results in equilibrium sulphide melts with increasingly higher Cu/Fe ratios (Wohlgemuth-Ueberwasser et al., 2013). Under these conditions, and where sulphide saturation of a silicate melt is delayed, the first equilibrium sulphide melts to form are expected to be Cu-rich, leading to bornite and/or chalcocite crystallization (Wohlgemuth-Ueberwasser et al., 2013). Fractionation of magnetite would serve to reduce the FeO content, Fe^{3+}/Fe^{2+}, fO_2 and SO_4^{2-}/S^{2-} of a silicate melt, all effects that would bring the melt closer to sulphide saturation (e.g. Haughton et al., 1974; Jenner et al., 2010; Keays and Tegner, 2015). Degassing of hydrous magmas in shallow crustal reservoirs would also drive the melt towards sulphide saturation (Fortin et al., 2015). Further mineralogical and geochemical studies are needed to resolve which of these and other factors are critical to the origin and timing of Cu-PGE mineralization at Tulameen and other Alaskan-type intrusions in hydrous and oxidizing supra-subduction zone settings.

POLARIS INTRUSION

The Early Jurassic Polaris ultramafic-mafic intrusion (45 km^2) in north-central British Columbia (Fig. 1) is one of the best exposed Alaskan-type intrusions in the North American Cordillera, and second in size only to Tulameen. The Polaris intrusion is a westerly dipping (30–50°) sill-like body (Nixon et al., 1997; Nott et al., 2020) emplaced into Late Paleozoic metasedimentary and metavolcanic rocks of the Lay Range assemblage (Fig. 9). The host rocks of the Lay Range assemblage (Mississippian-Permian: Ferri, 1997) are correlative with the Harper Ranch subterrane in southern British Columbia, and they form the substrate for the composite Middle Triassic-Early Jurassic volcanic arc that forms the bulk of Quesnel terrane. Emplacement of the Polaris intrusion into the Quesnel terrane (ca. 186 Ma: Nixon et al., 2019) was coeval with emplacement of the Turnagain Alaskan-type intrusion in the Yukon-Tanana terrane (ca. 189–185 Ma: Nixon et al., 2020), and marks the initial accretion of peri-Laurentian arc terranes to the western continental margin of ancestral North America in the Early Jurassic (Nelson et al., 2013; Monger and Gibson, 2019; Nixon et al., 2020).

Internal Zonation

The Polaris intrusion is composed of adcumulate to heteradcumulate (clinopyroxene-bearing) dunite(-chromitite), wehrlite, olivine clinopyroxenite, clinopyroxenite, hornblende clinopyroxenite, hornblendite, and gabbro-diorite (Fig. 9; Nott et al., 2020). Hornblende clinopyroxenite and gabbro-diorite contain accessory (<2 vol.%) apatite, titanite, and zircon. Minor amounts of disseminated orthomagmatic sulphides are found locally in clinopyroxene- and hornblende-rich rocks.

Along the eastern thrust margin of the Polaris intrusion, a narrow belt of ultramafic cumulates is preserved locally and passes gradationally (east to west) from olivine clinopyroxenite, through wehrlite and olivine

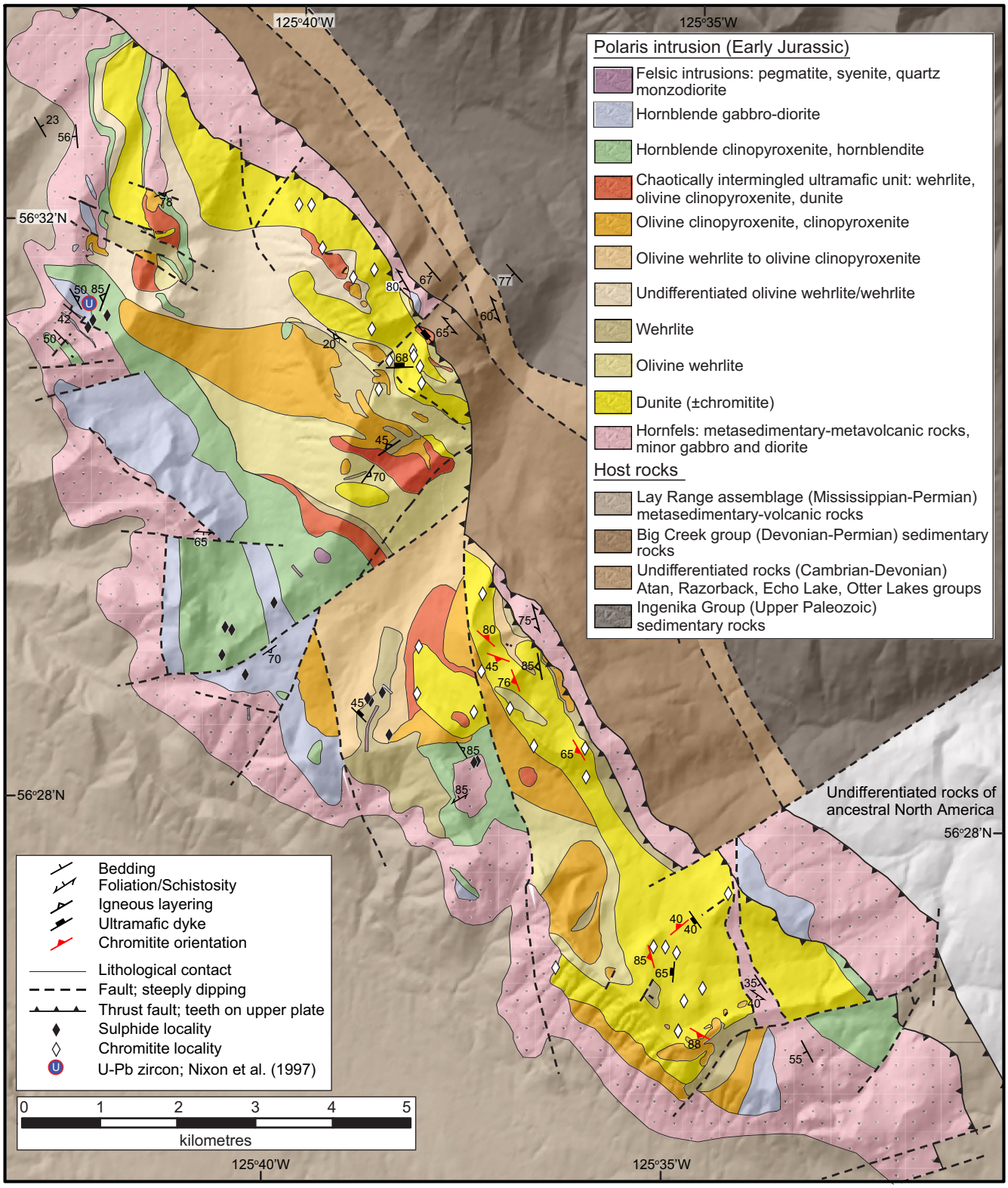

Figure 9. Generalized geological map of the Polaris Alaskan-type ultramafic-mafic intrusion showing regional geology, contact relationships, and chromitite and magmatic sulphide localities (*modified from* Nixon et al., 1997; and Nott et al., 2020).

wehrlite into dunite (Fig. 9). This zonation may have developed at the intrusive contact with the Lay Range assemblage, which has been removed by faulting. The overall internal distribution of rock types in the Polaris intrusion shows the opposite sense of zonation, with ultramafic rocks predominant in the eastern part of the intrusion and the more evolved feldspathic and hornblende-rich rocks concentrated in the west (Fig. 9). This

intrusion-scale distribution of ultramafic-mafic rock types appears to represent a crude internal stratigraphy that has been disrupted locally by faulting and zones of chaotically intermingled cumulates (discussed below).

Contact Relationships

Despite the disruption by syn- to post-emplacement ductile and brittle faulting (Fig. 9), igneous contacts between the mafic-ultramafic rock types of the Polaris intrusion are generally well preserved (Fig. 10). Where primary lithological zonation is exposed, most commonly at the transition from dunite through wehrlite to olivine clinopyroxenite, regular and continuous lithological contacts are gradational on the metre-scale (Fig. 10a). The more evolved, hornblende-rich and feldspathic rocks are typically heterogeneous on both hand- and outcrop-scale (Fig. 10h). Some igneous contacts between mafic and ultramafic rocks are intrusive and marked by what are interpreted as partially cannibalized enclaves of clinopyroxenite in a gabbro-diorite matrix.

Chaotically Intermingled Cumulates

Chaotically intermingled ultramafic cumulates on decametre- to metre-scale are a prominent feature in parts of the Polaris intrusion, especially near the margins of clinopyroxenite and wehrlite units, and less commonly dunite (Fig. 9). Contacts between intermingled rock types are commonly irregular and vary from sharp to gradational or diffuse. Dykes of coarse-grained to pegmatitic olivine clinopyroxenite/clinopyroxenite cut dunite and wehrlite, and foliated planar dykes of dunite or olivine wehrlite to wehrlite locally cut olivine clinopyroxenite (Fig. 10b–e). Local dense swarms of olivine clinopyroxenite/clinopyroxenite dykes with centimetre-scale offshoots cut dunite and olivine wehrlite. Centimetre- to metre-scale irregular, patchy, clinopyroxenite pods and dykes that have gradational to diffuse contacts with olivine-rich wallrocks may indicate reactive replacement of dunite/olivine wehrlite cumulates by clinopyroxene-rich magmas. The intermingled zones also contain fragmental cumulates, some composed of subrounded dunite-wehrlite clasts in sharp to diffuse contact with a clinopyroxene-rich host, whereas others comprise tabular blocks of wehrlite with a pronounced foliation set in a similar matrix (Fig. 10f,g).

The textural and ambivalent intrusive relationships in the chaotically intermingled units indicate both ductile and brittle behaviour of ultramafic cumulates involved in the mingling and intrusive activity. Ductile behaviour is apparent in the highly irregular, sharp to diffuse contacts and necking features observed among ultramafic rock types (Fig. 10b,e). Injection of dunite dykes with planar to curvilinear contacts appears to have taken place in a consolidated host capable of sustaining brittle fracture, and angular clasts of wehrlite attest to brittle disaggregation of pre-existing cumulates (Fig. 10c,d,g). Overall, the chaotically intermingled units are interpreted to represent zones of episodic mingling and intrusion involving variably crystallized and/or consolidated cumulates in differing thermal/rheological states.

Chromitite

The textural features displayed by chromitites in the Polaris intrusion are analogous to those described above for Tulameen. Chromitite at Polaris occurs in dunite, and less commonly in olivine wehrlite and wehrlite, as centimetre- to metre-scale schlieren of massive chromite and as disrupted blocks of variably deformed chromitite interlayered with dunite (Fig. 11). Layered samples show strong evidence of ductile deformation such as folding (Fig. 11a), and obliteration and/or coalescence of fine layering and reworking of chromite seams into more massive, irregular pods (Fig. 11c). Some outcrops exhibit a jumbled concentration of clasts comprising plastically deformed chromitite layering, massive schlieren, and subrounded fragments of layered chromitite-dunite that show no evidence of ductile deformation (Fig. 11d). These features are consistent with both ductile breakup/reworking and brittle fragmentation of pre-existing chromitite-dunite cumulates followed by transport and redeposition in their current dunite host. In some cases, early ductile deformation/disaggregation and redeposition of layered chromitite-dunite fragments are succeeded by injection

Figure 10 opposite page. Photographs showing contact relationships and textural features exhibited by ultramafic-mafic rocks of the Polaris intrusion. **a)** Metre-scale gradational contacts of olivine clinopyroxenite, olivine wehrlite to wehrlite, and dunite. **b)** Intermingled dunite and olivine clinopyroxenite. The contacts between the ultramafic rocks are sharp and irregular. **c)** Dykes of foliated dunite cutting massive olivine clinopyroxenite. **d)** Complex relationships among dunite, olivine wehrlite, wehrlite, and locally pegmatitic olivine clinopyroxenite. An offset dunite dyke is delineated by a fine-dashed line. **e)** Coarse-grained olivine clinopyroxenite blocks in wehrlite, cut by/intermingled with fine-grained dunite. **f)** Subrounded fragments (<30 cm) of fine- to medium-grained dunite and olivine wehrlite with diffuse boundaries set in a medium-grained wehrlite to olivine-clinopyroxenite matrix. **g)** Angular to subangular tabular xenoliths of wehrlite showing a distinct (flow?) foliation in a coarse-grained phlogopite-hornblende clinopyroxenite. **h)** Heterogeneous fine(fn)- to coarse(crs)-grained hornblende diorite, locally foliated. Hammer for scale in photographs (a–c) is 37 cm in length; pencil magnet in photographs (f–h) is 13 cm in length. Diffuse contacts are shown using a dot-dash line and sharp contacts with a solid line. Abbreviations: Du = dunite, HD = hornblende diorite, OPx = olivine clinopyroxenite, OWe = olivine wehrlite, Peg-OPx = pegmatitic olivine clinopyroxenite, phl-hbl-Cpxt = phlogopite-hornblende clinopyroxenite, We = wehrlite.

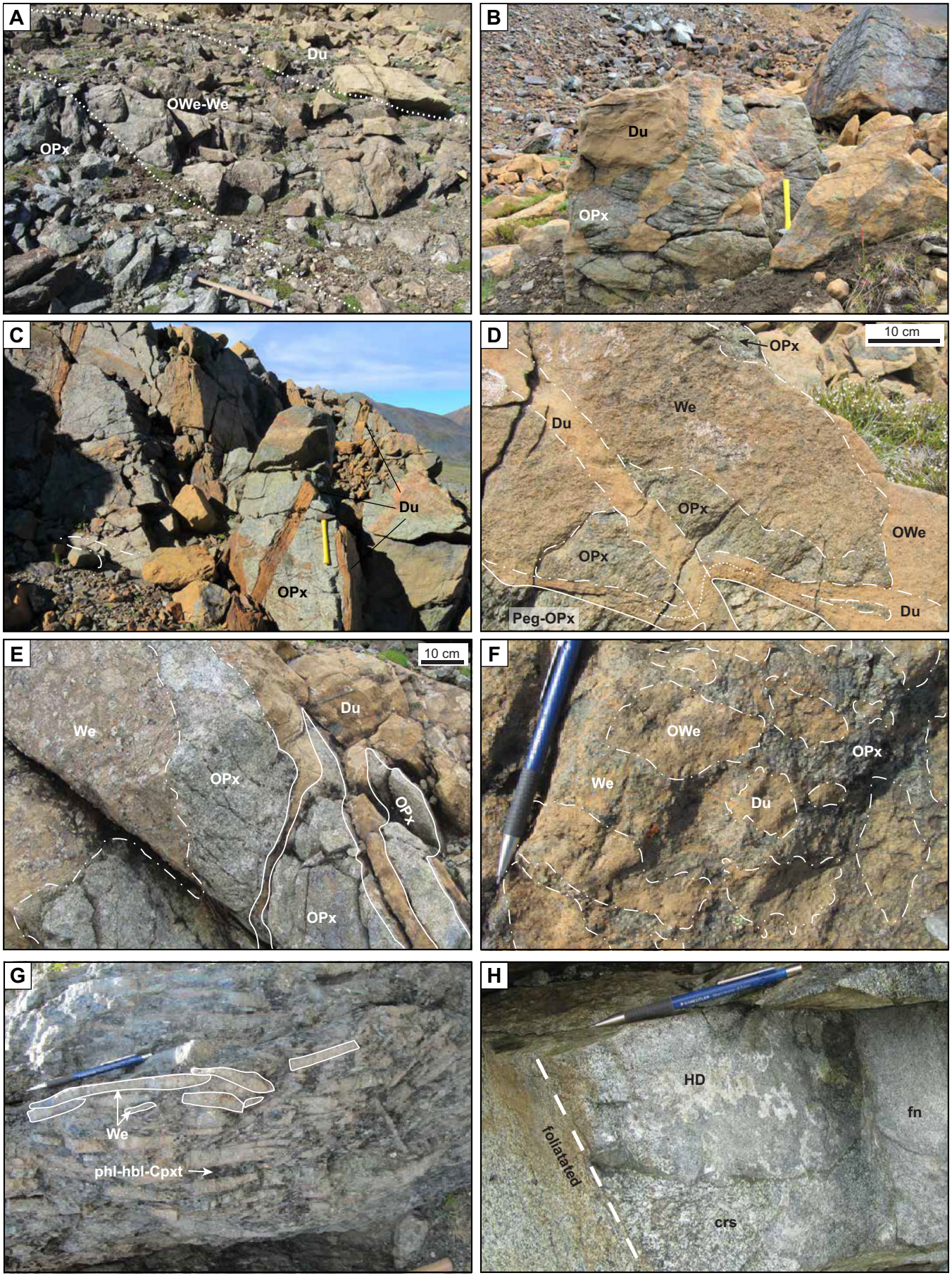
A
Du
OWe-We
OPx
B
Du
OPx
C
Du
OPx
D
10 cm
OPx
We
Du
OPx
OWe
OPx
Peg-OPx
Du
E
10 cm
Du
We
OPx
OPx
OPx
F
OWe
OPx
We
Du
G
We
phl-hbl-Cpxt
H
HD
fn
foliated
crs

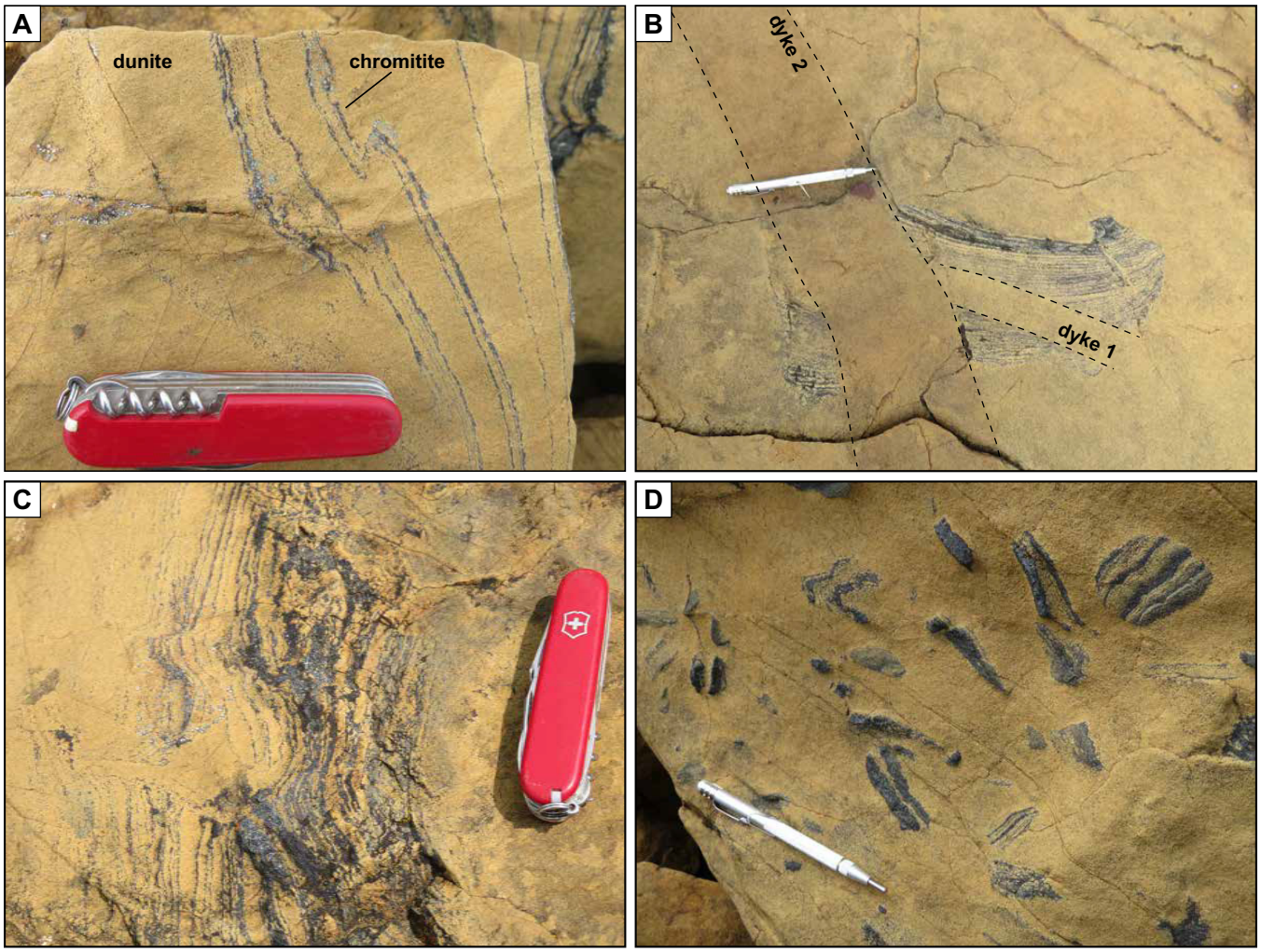

Figure 11. Photographs showing remobilized chromitite in the Polaris intrusion. **a)** Ductile deformation of adcumulate dunite containing thin laminae of chromitite and showing an isolated fold. **b)** Fragment of layered chromitite cut by two generations of dunite (1) and wehrlite (2) dykes, illustrating early ductile deformation/fragmentation of chromitite-dunite followed by late injection of dunite and wehrlite into a consolidated brittle host. **c)** Plastically deformed fragment of well layered chromitite in dunite showing reworking of thin, malleable chromitite layers into more massive, irregular pods of chromitite. **d)** Concentration of fragments comprising plastically deformed chromitite layering, massive schlieren, and subrounded fragments of layered chromitite-dunite showing no evidence of ductile deformation. The variety of textural features is compatible with both ductile breakup/reworking and brittle fragmentation of pre-existing chromitite-dunite cumulates followed by transport and redeposition in their current dunite host. Knife in photographs (a) and (c) is 10 cm in length; pencil magnet in photographs (b) and (d) is 13 cm in length.

of dunite dykes into a consolidated brittle host (Fig. 11b), features similar to those found in the chaotically intermingled units (Fig. 10d). Brittle fragmentation, or possibly early dyke emplacement in coherent layered chromitite-dunite sequences, may account for sharply truncated chromitite schlieren and angular to subangular, centimetre-sized chromitite fragments.

Ni-Cu-PGE Sulphides

Magmatic Ni-Cu(-PGE) sulphides in the Polaris intrusion generally occur in the more evolved ultramafic and mafic rocks in the northwestern and central parts of the intrusion (Fig. 9). The sulphides are hosted by wehrlite, olivine clinopyroxenite, hornblende clinopyroxenite, pegmatitic hornblendite, and gabbro-diorite. The mineralized rocks commonly weather reddish to rusty brown and display prominent malachite staining. The disseminated to locally blebby sulphides comprise mainly pyrrhotite and chalcopyrite with minor pentlandite, pyrite and rare bornite, and may constitute up to 15–20 vol.% of mineralized samples. The composition and textures of the sulphides are demonstrably magmatic as evidenced by ovoid inclusions of formerly immiscible sulphide melt in clinopyroxene and hornblende primocrysts, and irregular films and pockets of interstitial sulphides trapped within the cumulus silicate framework (Fig. 12a–c). Bornite, where present, is magmatic and occurs with chalcopyrite as composite interstitial grains and inclusions in magnetite with negative-crystal outlines. Coexistence of bornite and

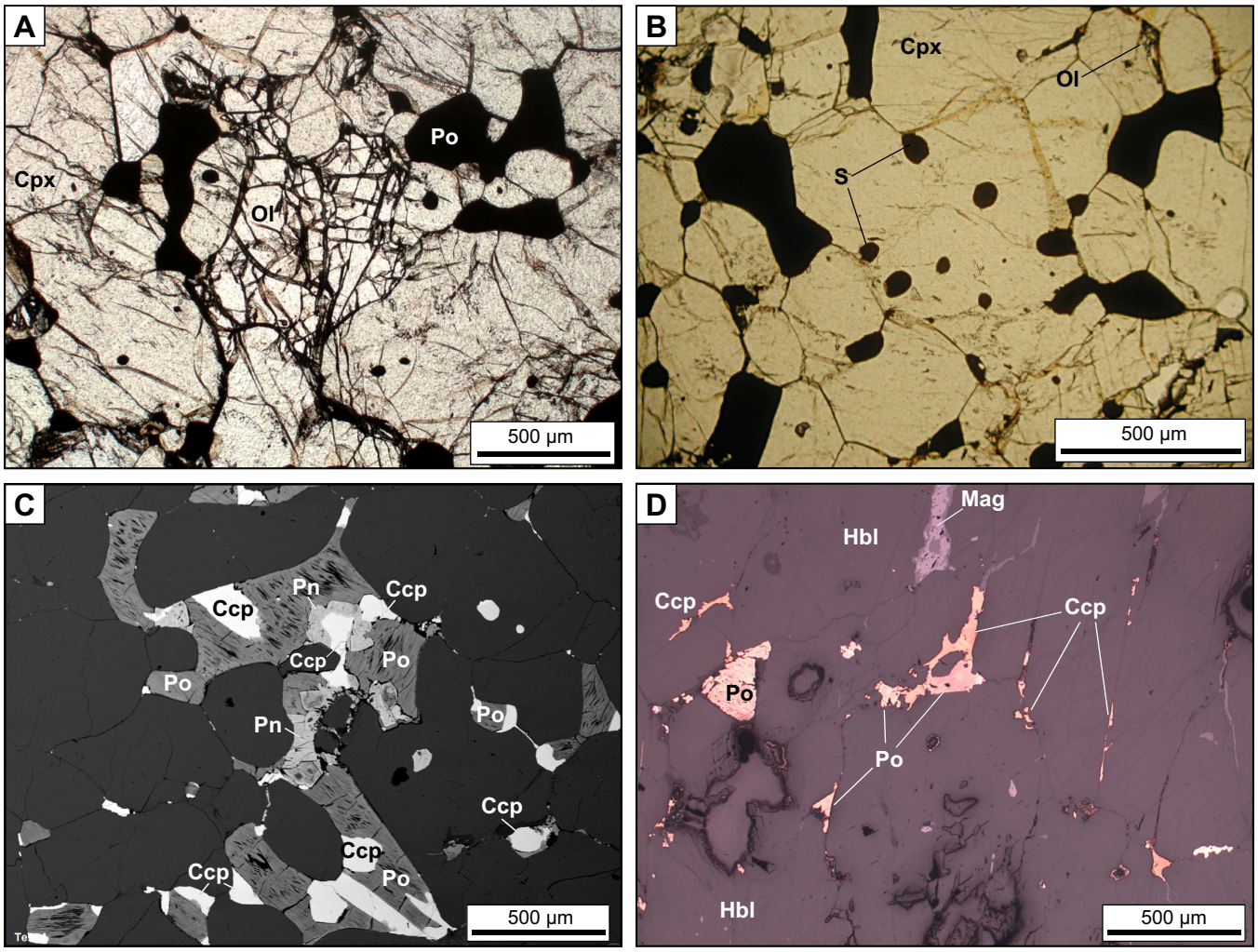

Figure 12. Photographs and images of sulphide-bearing samples from the Polaris intrusion. **a)** Plane-polarized light image of interstitial pyrrhotite in olivine clinopyroxenite. **b)** Plane-polarized light image of disseminated magmatic sulphides in olivine-bearing clinopyroxenite. The rounded shapes of sulphide inclusions in clinopyroxene and along silicate grain boundaries indicate trapping of immiscible sulphide liquid during silicate crystallization and accumulation. **c)** Backscatter electron image of composite interstitial sulphides in olivine clinopyroxenite. **d)** Reflected light image of primary and remobilized fracture-filling sulphides in hornblendite. Scales as noted on each photograph. Abbreviations: Ccp = chalcopyrite, Cpx = clinopyroxene, Hbl = hornblende, Mag = magnetite, Ol = olivine, Pn = pentlandite, Po = pyrrhotite, S = undifferentiated sulphide.

chalcopyrite implies the existence of a Cu-rich sulphide melt, analogous to sulphide assemblages documented above in the Champion zone of the Tulameen intrusion. The copper-rich sulphides commonly display thin alteration rims of covellite. Locally remobilized sulphides occupy thin veinlets or form fine films lining cleavage planes and/or fractures in amphibole (Fig. 12d). The presence of pentlandite and common occurrence of pyrrhotite distinguish Polaris sulphides from the Cu-rich sulphides in the Champion zone. A collection of chalcopyrite-bearing bulk-rock samples from a number of mineralized zones have maximum values of 1.18 wt% Cu, 1.8 g/t Pd and 1.3 g/t Pt (Mowat, 2015), and yield PGE signatures (Pd/Pt = 1.4), similar to those reported herein for Cu-PGE mineralized rocks in the Champion zone. Further work is needed to more completely characterize the mineralogical and geochemical attributes of the mineralization.

REMOBILIZED CUMULATES: VESTIGES OF MAGMA RECHARGE?

The textural features documented above for chromitites, intermingled ultramafic cumulates, and magmatic avalanche deposits in the Tulameen and Polaris intrusions provide evidence for ductile to brittle disaggregation, reworking, and redeposition of pre-existing cumulates in a dynamic magmatic environment. In this section, we have adapted a magma recharge model to explain the commonality of features exhibited by the remobilized cumulates. The model may have general applicability because, for example, chromitites with similar characteristics have been described in many Alaskan-type intrusions (e.g. Nixon et al., 1997; Garuti et al., 2003; Scheel et al., 2009; Anikina et al., 2014).

The mechanical and temporal evolution of an open-system magma-recharge event have been simulated

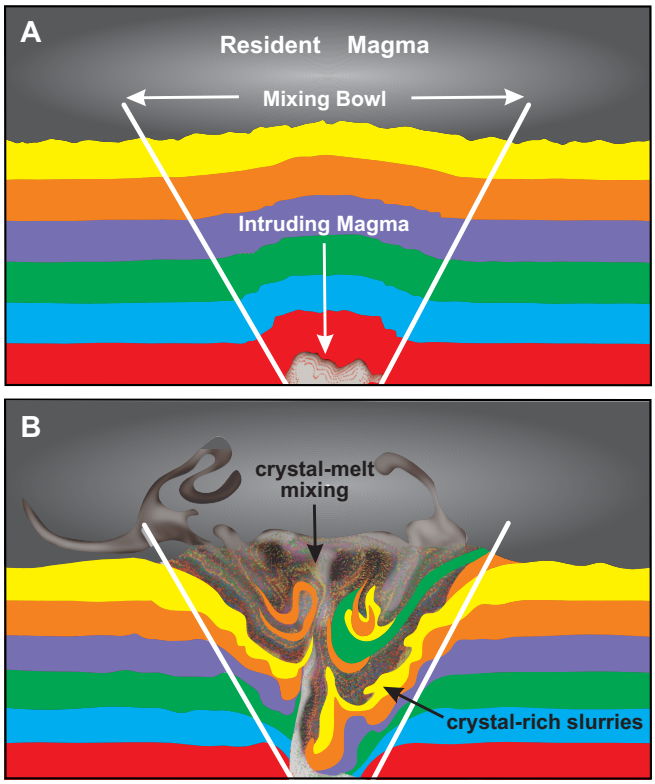

Figure 13. Schematic diagram depicting two stages in the computer simulation of an open-system recharge event (*redrawn from* Schleicher and Bergantz, 2017). **a)** Basaltic magma intrudes an olivine crystal mush with 40% interstitial melt. Crystal cumulates in the mush zone are multi-coloured for tracking purposes; an intruding basaltic melt is shown in mixed grey tones. The intruding magma induces a viscoplastic response in the cumulate pile that creates a mixing bowl. **b)** Hydrogranular dynamics subsequently create a fluidized, well mixed region of crystals and melt in the central part of the mixing bowl. The inferred environments of remobilized ultramafic cumulates in the Tulameen and Polaris Alaskan-type intrusions are discussed in the text within the framework of this model. For a full appreciation of the open-system dynamics, the reader is encouraged to view the video in the online Supplementary Data of Schleicher and Bergantz (2017).

using a computer algorithm to account for the complex interactions of the granular and fluid dynamics of basaltic liquid intruding a partially consolidated olivine-rich cumulate mush (Bergantz et al., 2015; Schleicher et al., 2016; Schleicher and Bergantz, 2017; Fig. 13). Basaltic liquid is injected into the base of crystal mush (crystal:melt ratio = 60:40) as a dyke under isothermal conditions at a constant momentum flux at a sufficiently high rate to overcome the resistance of the mush zone, which behaves as a viscoplastic material (Fig. 13a). The addition of basaltic liquid to the system is accommodated by internal inflation (ballooning) of the magma reservoir or eruption of the resident magma. The mush responds to the new magma influx by vertical expansion and fluidization along bounding crystal-liquid faults of relatively stable configuration that define a region of the mush unlocked by fluidization: referred to as the "mixing bowl" (Fig. 13a). This initial response is followed by block uplift of the crystal mush within the mixing bowl. The intruding liquid eventually penetrates the mush to form a high-porosity chimney for continued throughput of magma carrying entrained crystals from the base to the top of the cumulate pile where the new liquid mixes with resident magma and deposits its remaining crystal cargo on top of the mush (Fig. 13b). After the initial influx, the system reaches a quasi-steady state as the position of the chimney meanders through the mush zone generating granular vortices that expand the well fluidized region in the centre of the mixing bowl. Expansion of this fluidized region is accompanied by crystal slurries moving down the destabilized sides of the mixing bowl towards the base of the magma chamber (Fig. 13b). Termination of the new magma influx causes the mixing bowl to defluidize and collapse leaving a fossil kinematic and compositional footprint distinct from the surrounding undisturbed crystal mush.

Although the geometry of the Tulameen and Polaris magma chambers is not known, two key elements of this open-system recharge model can potentially explain the diversity of features exhibited by remobilized cumulates in these Alaskan-type intrusions: the upward transport and redistribution of material throughout the fluidized, well mixed core of the mixing bowl, and the counterbalanced downward movement of material along the unstable sidewalls.

Olivine-chromite cumulates in the core of the Tulameen intrusion exhibit textural features definitive of mechanical disruption, ductile reworking, and redeposition during crystallization of the dunite (Fig. 6). Framing the natural system in terms of the recharge model, formation of the dunite core involves recycling of early formed, coherent olivine-chromite cumulates, and mixing of recycled crystals from the mush and newly formed crystals from the intruding and/or hybrid melt, leading to the deposition of olivine-chromite cumulates of mixed age and heritage. Although this process must involve disaggregated fragments of dunite, chromitite and layered chromitite-dunite, as well as potentially separated crystals, only the presence of chromitite preserves overt macroscopic evidence of this heritage. The recycled material may be sourced from the unstable sidewall of the magma chamber and/or derived from compacted cumulates below the mush zone that has been disrupted by new magma influx. Ductile deformation of cumulate inclusions is probably initiated during disaggregation shortly after the initial magma influx, and deformation is sustained on termination of the recharge event as the fluidized core of the mush zone deflates and the recycled olivine(-chromite) crystals and inclusion cargo are redeposited. The relatively small size of chromitite schlieren

and layered chromitite-dunite inclusions observed in the dunite core would appear amenable to upward transport and dispersion by hydrogranular currents, depending on the momentum of new magma influx.

The textural relationships between plastically deformed dunite blocks (up to 15 m across) and host clinopyroxenite are interpreted above as evidence for synmagmatic avalanche deposits that involve the gravitational collapse of hot, malleable pre-existing cumulates. These deposits occur throughout the clinopyroxenite unit peripheral to the dunite core (Fig. 2) and include both coherent dunite and clinopyroxenite cumulates. Clasts of the latter are macroscopically visible where enclosed by dunite blocks, which are key markers of the recycling and deformation processes (Fig. 7).

In the recharge model, an environment conducive to the generation of the avalanche deposits is manifest at the margins of the mixing bowl where crystal-charged slurries move downslope towards the conduit (Fig. 13b). In the natural system, thermal gradients would exist between the hot centre of the mixing bowl and cooler wallrocks. By the time the avalanche deposits were generated, the peripheral zones of the intrusion must have cooled sufficiently via heat conduction through the wallrocks to form hot coherent dunite and clinopyroxenite cumulates. These cumulates were subsequently dislodged from the walls of the magma chamber and disrupted blocks cascaded downslope embroiled in the crystal mush to form the avalanche deposits. Ductile deformation of dunite inclusions likely began during disaggregation and continued during transport and deposition in the deeper, hotter regions near the base of the magma chamber. Such processes operating in the sidewall environment may also account for the features exhibited by chaotically intermingled ultramafic cumulates in the Polaris intrusion where the lack of extensive fragmentation may indicate limited downslope movement of cumulates and/or slumping *en masse*.

IMPLICATIONS FOR EXPLORATION

The Cu-PGE mineralization in the Tulameen ultramafic-mafic intrusion represents a unique deposit type for Alaskan-type intrusions, which are better known for chromite-associated platinum mineralization in dunite and the derivative placer deposits. The mineralization has certain attributes in common with Cu-PGE stratiform or reef-style occurrences in layered intrusions. Given the current historic high for the price of Pd (more than double the price of Pt and one and a half times that of Au as of March, 2020), the Pd-enriched nature of the Cu-sulphide mineralization at Tulameen may well become a significant factor in promoting exploration for this deposit style in Alaskan-type intrusions.

The magma-recharge model described above provides an explanation for the occurrence of Pt-rich and Pt-poor chromitites in close proximity in the dunite core of the Tulameen intrusion. The disaggregation of pre-existing olivine-chromite cumulates by an intruding magma, and their entrainment and redistribution by hydrogranular currents throughout the interior of the mixing bowl, as represented by the dunite core, results in the redeposition of dismembered, variably platiniferous chromitites derived from different parts of the original cumulate sequence. The small size and apparently chaotic distribution of the Pt-rich chromitites in bedrock is not conducive to economic exploitation. Unless laterally continuous, platiniferous chromitite horizons in the dunite can be identified, the associated placer deposits are more amenable targets.

FUTURE RESEARCH

U-Pb zircon geochronological and trace element geochemical studies are continuing for representative samples from the Tulameen intrusion, including those collected from Cu-PGE sulphide mineralization in the Champion zone. Samples collected by James Nott for his M.Sc. research at the University of British Columbia on the Polaris intrusion are currently being processed for U-Pb zircon LA-ICP-MS and CA-ID-TIMS geochronology following established workflows.

ACKNOWLEDGMENTS

Funding for this study was provided by NRCan's Targeted Geoscience Initiative Program (TGI- 5) under the Orthomagmatic Ni-Cu-PGE-Cr Ore Systems Project's 'Convergent margin Ni-Cu-PGE-Cr temporal and magmatic evolution', the British Columbia Geological Survey, and a NSERC Discovery Grant to James Scoates. James Nott's research at Polaris is partially supported by a NSERC Canada Graduate Scholarship. Dylan Spence and Abigail Fraser expedited field preparations and provided support throughout the 2018 and 2019 field seasons at Polaris, respectively. Ursula Mowat is thanked for providing a suite of mineralized samples from her claims on Polaris. We thank Wouter Bleeker for thorough and careful review of the manuscript and Valérie Bécu and Elizabeth Ambrose for technical editing and formatting of the final layout.

REFERENCES

Ames, D.E., Kjarsgaard, I.M., McDonald, A.M., and Good, D.J., 2017. Insights into the extreme PGE enrichment of the W Horizon, Marathon Cu-Pd deposit, Coldwell Alkaline Complex, Canada: Platinum-group mineralogy, compositions and genetic implications; Ore Geology Reviews, v. 90, p. 723–747.

Anikina, E., Malitch, K.N., Pushkarev, E.V., and Shmelev, V.R., 2014. The Nizhny Tagil and Volkovsky massifs of the Uralian Platinum Belt, and related deposits; Field Trip Guidebook, Zavaritsky Institute of Geology and Geochemistry, Russian Academy of Sciences, 12th International Platinum Symposium, Yekaterinburg, 48 p.

Annen, C., Blundy, J.D., Leuthold, J., and Sparks, R.S.J., 2015. Construction and evolution of igneous bodies: Towards an integrated perspective of crustal magmatism; Lithos, v. 230, p. 206–221.

Bergantz, G.W., Schleicher, J.M., and Burgisser, A., 2015. Open-system dynamics and mixing in magma mushes; Nature Geoscience, v. 8, p. 793–796.

Brenan, J.M. and Andrews, D., 2001. High-temperature stability of laurite and Ru–Os–Ir alloy and their role in PGE fractionation in mafic magmas; The Canadian Mineralogist, v. 39, p. 341–360.

Colpron, M. and Nelson, J.L., 2011. A digital atlas of terranes for the Northern Cordillera; British Columbia Ministry of Energy and Mines, British Columbia Geological Survey, Geofile 2011–11.

DeCelles, P.G., Ducea, M.N., Kapp, P., and Zandt, G., 2009. Cyclicity in Cordilleran orogenic systems; Nature Geoscience, v. 2, p. 251–257.

Engi, M., Lanari, P., and Kohn, M.J., 2017. Significant ages; an introduction to petrochronology; *in* Reviews in Mineralogy and Geochemistry, (ed.) M.J. Kohn, M., Engi, and P. Lanari;, Mineralogical Society of America and Geochemical Society, Washington, DC, p. 1–12.

Ferri, F., 1997. Nina Creek Group and Lay Range Assemblage, north-central British Columbia: remnants of late Paleozoic oceanic and arc terranes; Canadian Journal of Earth Sciences, v. 34, p. 854–874.

Ferry, J.M. and Watson, E.B., 2007. New thermodynamic models and revised calibrations for the Ti-in-zircon and Zr-in-rutile thermometers; Contributions to Mineralogy and Petrology, v. 154, p. 429–437.

Findlay, D.C., 1963. Petrology of the Tulameen ultramafic complex, Yale District, British Columbia; Ph.D. thesis, Queen's University, Kingston, Ontario, 415 p.

Findlay, D.C., 1969. Origin of the Tulameen ultramafic-gabbro complex, southern British Columbia; Canadian Journal of Earth Sciences, v. 6, p. 399–425.

Fortin, M.-A., Riddle, J., Desjardins-Langlais, Y., and Baker, D.R., 2015. The effect of water on the sulfur concentration at sulfide saturation (SCSS) in natural melts; Geochimica et Cosmochimica Acta, v. 160, p. 100–116.

Garuti, G., Pushkarev, E.V., Zaccarini, F., Cabella, R., and Anikina, E., 2003. Chromite composition and platinum-group mineral assemblage in the Uktus Uralian-Alaskan-type complex (Central Urals, Russia); Mineralium Deposita, v. 38, p. 312–326.

Gehrels, G., Rusmore, M., Woodsworth, G., Crawford, M., Andronicos, C., Hollister, L., Patchett, J., Ducea, M., Butler, R., Klepeis, K., Davidson, C., Friedman, R.M., Haggart, J.W., Mahoney, J.B., Crawford, W., Pearson, D., and Girardi, J., 2009. U-Th-Pb geochronology of the Coast Mountains batholith in north-coastal British Columbia: Constraints on age and tectonic evolution; Geological Society of America Bulletin, v. 121, p. 1341–1361.

Godel, B., 2015. Platinum-group element deposits in layered intrusions: Recent advances in the understanding of the ore forming processes; *in* Layered Intrusions, (ed.) B. Charlier, O. Namur, R. Latypov, and C. Tegner; Springer, Netherlands,,p. 379–432.

Godel, B., Rudashevsky, N.S., Nielsen, T.F.D., Barnes, S.J., and Rudashevsky, V.N., 2014. New constraints on the origin of the Skaergaard intrusion Cu–Pd–Au mineralization: Insights from high-resolution X-ray computed tomography; Lithos, v. 190–191, p. 27–36.

Good, D.J., Cabri, L.J., and Ames, D.E., 2017. PGM Facies variations for Cu-PGE deposits in the Coldwell Alkaline Complex, Ontario, Canada; Ore Geology Reviews, v. 90, p. 748–771.

Greig, C.J., Armstrong, R.L., Harakal, J.E., Runkle, D., and van der Heyden, P., 1992. Geochronometry of the Eagle Plutonic Complex and the Coquihalla area, southwestern British Columbia; Canadian Journal of Earth Sciences, v. 29, p. 812–829.

Grimes, C.B., John, B.E., Cheadle, M.J., Mazdab, F.K., Wooden, J.L., Swapp, S., and Schwartz, J.J., 2009. On the occurrence, trace element geochemistry, and crystallization history of zircon from in situ ocean lithosphere; Contributions to Mineralogy and Petrology, v. 158, p. 757–783.

Haughton, D.R., Roeder, P.L., and Skinner, B.J., 1974. Solubility of sulfur in mafic magmas; Economic Geology, v. 69, p. 451–467.

Himmelberg, G.R. and Loney, R.A., 1995. Characteristics and petrogenesis of Alaskan-type ultramafic-mafic intrusions, southeastern Alaska; United States Geological Survey, Professional Paper 1564, 47 p.

Holwell, D.A. and Keays, R.R., 2014. The formation of low-volume, high-tenor magmatic PGE-Au sulfide mineralization in closed systems: evidence from precious and base metal geochemistry of the Platinova Reef, Skaergaard intrusion, East Greenland; Economic Geology, v. 109, p. 387–406.

Holwell, D.A., Keays, R.R., McDonald, I., and Williams, M.R., 2015. Extreme enrichment of Se, Te, PGE and Au in Cu sulfide microdroplets: evidence from LA-ICP-MS analysis of sulfides in the Skaergaard intrusion, East Greenland; Contributions to Mineralogy and Petrology, v. 170, p. 53.

Irvine, T.N., 1974. Petrology of the Duke Island ultramafic complex, southeastern Alaska; Geological Society of America, Memoir 138, 240 p.

Jackson-Brown, S., 2017. Origin of the Cu-PGE-rich sulphide mineralization in the DJ/DB zone of the Turnagain Alaskan-type intrusion, British Columbia; M.Sc. thesis, University of British Columbia, Vancouver, British Columbia, 290 p.

Jenner, F.E., O'Neill, H.S.C., Arculus, R.J., and Mavrogenes, J.A., 2010. The magnetite crisis in the evolution of arc-related magmas and the initial concentration of Au, Ag and Cu; Journal of Petrology, v. 51, p. 2445–2464.

Johan, Z., 2002. Alaskan-type complexes and their platinum-group-element mineralization; *in* The Geology, Geochemistry, Mineralogy and Mineral Beneficiation of Platinum-group Elements, (ed.) L.J. Cabri; Canadian Institute of Mining, Metallurgy and Petroleum, Special Volume 54, p. 669–719.

Jugo, P.J., Wilke, M., and Botcharnikov, R.E., 2010. Sulfur K-edge XANES analysis of natural and synthetic basaltic glasses: Implications for S speciation and S content as function of oxygen fugacity; Geochimica et Cosmochimica Acta, v. 74, p. 5926–5938.

Keays, R.R. and Tegner, C., 2015. Magma chamber processes in the formation of the low-sulphide magmatic Au–PGE mineralization of the Platinova Reef in the Skaergaard intrusion, East Greenland; Journal of Petrology, v. 56, p. 2319–2340.

Li, C., Ripley, E.M., Oberthür, T., Miller, J.D., and Joslin, G.D., 2008. Textural, mineralogical and stable isotope studies of hydrothermal alteration in the main sulfide zone of the Great Dyke, Zimbabwe and the precious metals zone of the Sonju Lake Intrusion, Minnesota, USA; Mineralium Deposita, v. 43, p. 97–110.

Li, C., Zhang, Z., Li, W., Wang, Y., Sun, T., and Ripley, E.M., 2015. Geochronology, petrology and Hf–S isotope geochemistry of the newly-discovered Xiarihamu magmatic Ni–Cu sulfide

deposit in the Qinghai–Tibet plateau, western China; Lithos, v. 216–217, p. 224–240.

Logan, J.M. and Mihalynuk, M.G., 2014. Tectonic controls on early Mesozoic paired alkaline porphyry deposit belts (Cu-Au±Ag-Pt-Pd-Mo) within the Canadian Cordillera; Economic Geology, v. 109, p. 827–858.

Maier, W.D., 2005. Platinum-group element (PGE) deposits and occurrences: Mineralization styles, genetic concepts, and exploration criteria; Journal of African Earth Sciences, v. 41, p. 165–191.

Maier, W.D., Barnes, S.-J., Gartz, V., and Andrews, G., 2003. Pt-Pd reefs in magnetitites of the Stella layered intrusion, South Africa: A world of new exploration opportunities for platinum group elements; Geology, v. 31, p. 885–888.

Manor, M.J., Scoates, J.S., Nixon, G.T., and Ames, D.E., 2016. The Giant Mascot Ni-Cu-PGE deposit, British Columbia: mineralized conduits in a convergent margin tectonic setting; Economic Geology, v. 111, p. 57–87.

Manor, M.J., Scoates, J.S., Wall, C.J., Nixon, G.T., Friedman, R.M., Amini, M., and Ames, D.E., 2017. Age of the Late Cretaceous ultramafic-hosted Giant Mascot Ni-Cu-PGE deposit, southern Canadian Cordillera: integrating CA-ID-TIMS and LA-ICP-MS U-Pb geochronology and trace element geochemistry of zircon; Economic Geology, v. 112, p. 1395–1418.

Mattinson, J.M., 2005. Zircon U–Pb chemical abrasion ("CA-TIMS") method: Combined annealing and multi-step partial dissolution analysis for improved precision and accuracy of zircon ages; Chemical Geology, v. 220, p. 47–66.

Matzel, J.E., Bowring, S.A., and Miller, R.B., 2006. Time scales of pluton construction at differing crustal levels: Examples from the Mount Stuart and Tenpeak intrusions, North Cascades, Washington; Geological Society of America Bulletin, v. 118, p. 1412–1430.

McDonough, W.F. and Sun, S.-S., 1995. The composition of the Earth; Chemical Geology, v. 120, p. 223–253.

Miller, J.D., Jr., 1999. Geochemical evaluation of platinum group element (PGE) mineralization in the Sonju Lake intrusion, Finland, Minnesota; Minnesota Geological Survey, Information Circular 44, 32 p.

Miller, J.D., Jr., and Ripley, E.M., 1996. Layered intrusions of the Duluth Complex, Minnesota, USA; *in* Layered Intrusions, Developments in Petrology, (ed.) R.G. Cawthorn; Elsevier, v. 15, p. 257–301.

Miller, J.S., Matzel, J.E.P., Miller, C.F., Burgess, S.D., and Miller, R.B., 2007. Zircon growth and recycling during the assembly of large, composite arc plutons; Journal of Volcanology and Geothermal Research, v. 167, p. 282–299.

Monger, J.W.H. and Gibson, H.D., 2019. Mesozoic-Cenozoic deformation in the Canadian Cordillera: The record of a "Continental Bulldozer"?; Tectonophysics, v. 757, p. 153–169.

Mowat, U., 2015. Sampling on the Star 1, 3, 8, 10, 11 and 12 claims; British Columbia Geological Survey, Assessment Report 35680, 88 p.

Mudd, G.M. and Jowitt, S.M., 2014. A detailed assessment of global nickel resource trends and endowments; Economic Geology, v. 109, p. 1813–1841.

Naldrett, A.J., 2004. Magmatic Sulfide Deposits: Geology, Geochemistry and Exploration; Springer-Verlag, Germany, 727 p.

Naldrett, A.J., 2010. Secular variation of magmatic sulfide deposits and their source magmas; Economic Geology, v. 105, p. 669–688.

Nelson, J.L., Colpron, M., and Israel, S., 2013. The Cordillera of British Columbia, Yukon, and Alaska: Tectonics and metallogeny; *in* Tectonics, Metallogeny, and Discovery: The North American Cordillera and Similar Accretionary Settings, (ed.) M. Colpron,T. Bissig, B.J. Rusk, and J.F.M. Thompson; Society of Economic Geologists, Special Paper 17, p. 53–109.

Nixon, G.T., 1998. Ni-Cu sulfide mineralization in the Turnagain Alaskan-type complex; a unique magmatic environment; *in* Geological Fieldwork 1997; Ministry of Employment and Investment, British Columbia Geological Survey, Paper 1998-1, p. 18.1–18.11.

Nixon, G.T., 2018. Geology of the Tulameen Alaskan-type ultramafic-mafic intrusion, British Columbia; British Columbia Ministry of Energy, Mines and Petroleum Resources, British Columbia Geological Survey, Open File 2018-2, scale 1: 20 000.

Nixon, G.T. and Rublee, V.J., 1988. Alaskan-type ultramafic rocks in British Columbia: new concepts of the structure of the Tulameen complex; *in* Geological Fieldwork 1987; British Columbia Ministry of Energy, Mines and Petroleum Resources, British Columbia Geological Survey, Paper 1988-1, p. 281–294.

Nixon, G.T., Cabri, L.J., and Laflamme, J.H.G., 1990. Platinum-group-element mineralization in lode and placer deposits associated with the Tulameen Alaskan-type complex, British Columbia; The Canadian Mineralogist, v. 28, p. 503–535.

Nixon, G.T., Hammack, J.L., Ash, C.H., Cabri, L.J., Case, G., Connelly, J.N., Heaman, L.M., Laflamme, J.H.G., Nuttall, C., Paterson, W.P.E., and Wong, R.H., 1997. Geology and platinum group element mineralization of Alaskan-type ultramafic-mafic complexes in British Columbia; British Columbia Ministry of Employment and Investment, British Columbia Geological Survey, Bulletin 93, 142 p.

Nixon, G.T., Manor, M.J., Jackson-Brown, S., Scoates, J.S., and Ames, D.E., 2015. Magmatic Ni-Cu-PGE sulphide deposits at convergent margins; *in* Targeted Geoscience Initiative 4: Canadian Nickel-Copper-Platinum Group Elements-Chromium Ore Systems - Fertility, Pathfinders, New and Revised Models, (ed.) D.E. Ames and M.G. Houlé, Geological Survey of Canada, Open File 7856, p. 17–34.

Nixon, G.T., Milidragovic, D., and Scoates, J.S., 2019. Convergent margin Ni-Cu-PGE-Cr ore systems: temporal and magmatic evolution; *in* Targeted Geoscience Initiative 5, Grant Program Interim Reports 2018-2019; Geological Survey of Canada, Open File 8620, p. 49–61.

Nixon, G.T., Scheel, J.E., Scoates, J.S., Friedman, R.M., Wall, C.J., Gabites, J., and Jackson-Brown, S., 2020. Syn-accretionary multistage assembly of an Early Jurassic Alaskan-type intrusion in the Canadian Cordillera: U-Pb and $^{40}Ar/^{39}Ar$ geochronology of the Turnagain ultramafic-mafic intrusive complex, Yukon-Tanana terrane; Canadian Journal of Earth Sciences, v. 57, p. 575–600.

Nott, J., Milidragovic, D., Nixon, G.T., and Scoates, J.S., 2020. New geological investigations of the Early Jurassic Polaris ultramafic-mafic Alaskan-type intrusion, north-central British Columbia; *in* Geological Fieldwork 2019; British Columbia Ministry of Energy, Mines, and Petroleum Resources, British Columbia Geological Survey, Paper 2020-01, p. 59–76.

Paterson, S.R. and Ducea, M.N., 2015. Arc magmatic tempos; gathering the evidence; Elements, v. 11, p. 91–98.

Piña, R., 2019. The Ni-Cu-(PGE) Aguablanca Ore Deposit (SW Spain); SpringerBriefs in World Mineral Deposits, Springer International Publishing, Switzerland, 78 p.

Pinsent, R.H., 2002. Ni-Cu-PGE potential of the Giant Mascot and Cogburn ultramafic-mafic bodies, Harrison-Hope area, southwestern British Columbia (092H); *in* Geological Fieldwork 2001; British Columbia Ministry of Energy, Mines and Petroleum Resources, British Columbia Geological Survey, Paper 2002-01, p. 211–236.

Prendergast, M.D., 2000. Layering and precious metals mineralization in the Rincón del Tigre Complex, eastern Bolivia; Economic Geology, v. 95, p. 113–130.

Prichard, H.M., Mondal, S.K., Mukherjee, R., Fisher, P.C., and Giles, N., 2018. Geochemistry and mineralogy of Pd in the magnetitite layer within the upper gabbro of the Mesoarchean Nuasahi Massif (Orissa, India); Mineralium Deposita, v. 53, p. 547–564.

Rublee, V.J., 1989. The structural control of the Tulameen Complex and outlying ultramafic bodies, 92H/7, 10; *in* Exploration in British Columbia 1988; British Columbia Ministry of Energy, Mines and Petroleum Resources, British Columbia Geological Survey,, p. B71–B81.

Rublee, V.J., 1994. Chemical petrology, mineralogy and structure of the Tulameen Complex, Princeton area, British Columbia; M.Sc. thesis, University of Ottawa, Ottawa, Ontario, 183 p.

Samperton, K.M., Schoene, B., Cottle, J.M., Brenhin Keller, C., Crowley, J.L., and Schmitz, M.D., 2015. Magma emplacement, differentiation and cooling in the middle crust: Integrated zircon geochronological-geochemical constraints from the Bergell Intrusion, Central Alps; Chemical Geology, v. 417, p. 322–340.

Scheel, J.E., 2007. Age and origin of the Turnagain Alaskan-type intrusion and associated Ni-sulphide mineralization, north-central British Columbia, Canada; M.Sc. thesis, University of British Columbia, Vancouver, British Columbia, 210 p.

Scheel, J.E., Scoates, J.S., and Nixon, G.T., 2009. Chromian spinel in the Turnagain Alaskan-type ultramafic intrusion, northern British Columbia, Canada; The Canadian Mineralogist, v. 47, p. 63–80.

Schleicher, J.M. and Bergantz, G.W., 2017. The mechanics and temporal evolution of an open-system magmatic intrusion into a crystal-rich magma; Journal of Petrology, v. 58, p. 1059–1072.

Schleicher, J.M., Bergantz, G.W., Breidenthal, R.E., and Burgisser, A., 2016. Time scales of crystal mixing in magma mushes: Crystal mixing; Geophysical Research Letters, v. 43, p. 1543–1550.

Schoene, B., Schaltegger, U., Brack, P., Latkoczy, C., Stracke, A., and Guenther, D., 2012. Rates of magma differentiation and emplacement in a ballooning pluton recorded by U-Pb TIMS-TEA, Adamello Batholith, Italy; Earth and Planetary Science Letters, v. 355–356, p. 162–173.

Scoates, J.S. and Wall, C.J., 2015. Geochronology of Layered Intrusions; *in* Layered Intrusions, (ed.) B. Charlier, O. Namur, R. Latypov, and C. Tegner; Springer, Netherlands, p. 3–74.

Scoates, J.S., Scoates, R.F.J., Wall, C.J., Friedman, R.M., and Couëslan, C.G., 2017. Direct dating of ultramafic sills and mafic intrusions associated with Ni-sulfide mineralization in the Thompson Nickel Belt, Manitoba, Canada; Economic Geology, v. 112, p. 675–692.

Song, X.-Y., Yi, J.-N., Chen, L.-M., She, Y.-W., Liu, C.-Z., Dang, X.-Y., Yang, Q.-A., and Wu, S.-K., 2016. The giant Xiarihamu Ni-Co Sulfide deposit in the East Kunlun Orogenic Belt, northern Tibet Plateau, China; Economic Geology, v. 111, p. 29–55.

Ver Hoeve, T.J., Scoates, J.S., Wall, C.J., Weis, D., and Amini, M., 2018. A temperature-composition framework for crystallization of fractionated interstitial melt in the Bushveld Complex from trace element systematics of zircon and rutile; Journal of Petrology, v. 59, p. 1383–1416.

Wall, C.J., Scoates, J.S., Weis, D., Friedman, R.M., Amini, M., and Meurer, W.P., 2018. The Stillwater Complex: integrating zircon geochronological and geochemical constraints on the age, emplacement history and crystallization of a large, open-system layered intrusion; Journal of Petrology, v. 59, p. 153–190.

Weiser, T.W., 2002. Platinum-group minerals (PGM) in placer deposits; *in* The Geology, Geochemistry, Mineralogy and Mineral Beneficiation of Platinum-group Elements, (ed.) L.J. Cabri; Canadian Institute of Mining, Metallurgy and Petroleum, Special Volume 54, p. 721–756.

Wohlgemuth-Ueberwasser, C.C., Fonseca, R.O.C., Ballhaus, C., and Berndt, J., 2013. Sulfide oxidation as a process for the formation of copper-rich magmatic sulfides; Mineralium Deposita, v. 48, p. 115–127.

Appendix
Publications related to the TGI-5 Ni-Cu-PGE-Cr Project (2015–2020) and legacies of the TGI-4 Ni-Cu-PGE-Cr Project (2010–2015)

PEER-REVIEWED JOURNAL PUBLICATIONS

Ames, D.E., Kjarsgaard, I.M., McDonald, A.M., and Good, D.J., 2017. Insights into the extreme PGE enrichment of the W Horizon, Marathon Cu-Pd deposit, Coldwell Alkaline Complex, Canada: platinum-group mineralogy, compositions and genetic implications; Ore Geology Reviews, v. 90, p. 723–747.

Brzozowski, M.J., Samson, I.M., Gagnon, J.E., Linnen, R.L., Good, D.J., Ames, D.E., and Flemming, R., 2018. Controls on the chemistry of minerals in late-stage veins and implications for exploration vectoring tools for mineral deposits: An example from the Marathon Cu-Pd deposit, Ontario, Canada; Journal of Geochemical Exploration, v. 190, p. 109–129.

Davey S.C., Bleeker, W., Kamo, S.L., Vuollo, J., Ernst, R.E., and Cousens, B.L., 2020. Archean block rotation in Western Karelia: Resolving dyke swarm patterns in metacraton Karelia-Kola for a refined paleogeographic reconstruction of supercraton Superia; Lithos, v. 368–369, p. 1–24.

Davey, S.C., Bleeker, W., Kamo, S.L., Ernst, R.E., Cousens, B., Chamberlain, K., Vuollo, J., and Huhma, H., submitted. Evidence for a single large igneous province at 2.11 Ga across supercraton Superia; Journal of Petrology.

Kastek, N., Ernst, R.E., Cousens, B.L., Kamo, S.L., Bleeker, W., Söderlund, U., Baragar, W.R.A., and Sylvester, P., 2018. U-Pb Geochronology and geochemistry of the Povungnituk Group of the Cape Smith Belt: Part of a craton-scale circa 2.0 Ga Minto-Povungnituk large igneous province, northern Superior craton; Lithos, v. 320, p. 315–331.

Hiebert, R.S., Bekker, A., Houlé, M.G., and Rouxel, O.J., 2018. Depositional setting of the late Archean Fe oxide- and sulfide-bearing chert and graphitic argillite in the Shaw Dome, Abitibi greenstone belt, Canada; Precambrian Research, v. 311, p. 98–116.

Hiebert, R.S., Bekker, A., Houlé, M.G., Wing, B.A., and Rouxel, O.J., 2016. Tracing sources of crustal contamination using multiple S and Fe isotopes in the Hart komatiite-associated Ni–Cu–PGE sulfide deposit, Abitibi greenstone belt, Ontario, Canada; Mineralium Deposita, v. 51, p. 919–935. https://doi.org/10.1007/s00126-016-0644-1

Houlé, M.G., Lesher, C.M., and Préfontaine, S., 2017. Physical Volcanology of Komatiites and Ni-Cu-(PGE) Deposits of the southern Abitibi Greenstone Belt; *in* Abitibi Base and Precious Metal Deposits, southern Abitibi Greenstone Belt, Canada, (ed.) T. Monecke, P. Mercier-Langevin, and B. Dubé; Reviews in Economic Geology, v. 19, p. 103–132.

Huang, X.-W., Sappin, A.-A., Boutroy, É., Beaudoin, G., and Makvandi, S., 2019. Trace element composition of igneous and hydrothermal magnetite from porphyry deposits: Relationship to deposit subtypes and magmatic affinity; Economic Geology, v. 114, p. 917–952.

Lesher, C.M., Carson, H.J.E., and Houlé, M.G., 2019. Genesis of chromite deposits by dynamic upgrading of Fe±Ti oxide xenocrysts; Geology, v. 47, p. 207–210 https://doi.org/10.1130/G45448.1

Manor, M.J., Scoates, J.S., Nixon, G.T., and Ames, D.E., 2016. The Giant Mascot Ni-Cu-PGE deposit, British Columbia: mineralized conduits in a convergent margin tectonic setting; Economic Geology, v. 111, p. 57–87.

Manor, M.J., Scoates, J.S., Wall, C.J., Nixon, G.T., Friedman, R.M., Amini, M., and Ames, D.E., 2017. Age of the Late Cretaceous ultramafic-hosted Giant Mascot Ni-Cu-PGE deposit, southern Canadian Cordillera: integrating CA-ID-TIMS and LA-ICP-MS U-Pb geochronology and trace element geochemistry of zircon; Economic Geology, v. 112, p. 1395–1418.

McClenaghan, M.B., Plouffe, A., Paulen, R.C., Houlé, M.G., Jackson, S.E., and Peter, J.M., 2016. Overview of Indicator Mineral Research at the Geological Survey of Canada - An Update; EXPLORE, Newsletter for the Association of Applied Geochemists, v. 170, p. 1–15.

Motomura, K., Kiyokawa, S., Ikehara, M., Sano, T., Bleeker, W., Tanaka, K., Miki, T., and Sano, Y., submitted. A redox fluctuation and δ^{13}Corg and δ^{34}S perturbations recorded in the 1.9 Ga Nuvilik Formation of the Cape Smith belt, Canada; Earth and Planetary Science Letters.

Sappin, A.-A., Houlé, M.G., Lesher, C.M., McNicoll, V., Vaillancourt, C., and Kamber, B.S., 2016. Age constraints and geochemical evolution of the Neoarchean mafic-ultramafic Wabassi Intrusive Complex in the Miminiska-Fort Hope greenstone belt, Superior Province, Canada; Precambrian Research, v. 286, p. 101–125.

Sappin, A.-A., Guilmette, C., Goutier, J., and Beaudoin, G., 2018. Geochemistry of Mesoarchean felsic to ultramafic

Appendix: Publications related to the TGI-5 Ni-Cu-PGE-Cr Project (2015–2020) and legacies of the TGI-4 Ni-Cu-PGE-Cr Project (2010–2015); *in* Targeted Geoscience Initiative 5: Advances in the understanding of Canadian Ni-Cu-PGE and Cr ore systems – Examples from the Midcontinent Rift, the Circum-Superior Belt, the Archean Superior Province, and Cordilleran Alaskan-type intrusions, (ed.) W. Bleeker and M.G. Houlé; Geological Survey of Canada, Open File 8722, p. 219–225.

volcanic rocks of the Lac Guyer area, La Grande Subprovince (Canada): Evidence for plume-related magmatism in a rift setting; Precambrian Research, v. 316, p. 83–102.

Shahabi Far, M., Samson, I.M., Gagnon, J.E., Good, D.J., Linnen, R.L., Layne, G.D., and Wing, B.A., 2018. Identifying externally derived sulfur in conduit-type Cu-platinum-group element deposits; the importance of multiple sulfur isotope studies; Geology, v. 46, p. 235–238.

GOVERNMENT PUBLICATIONS

Adibpour, M., Jugo, P.J., and Ames, D.E., 2015. Trace element distribution in sulphide assemblages of the Levack-Morrison ore system, Sudbury, Ontario: Looking for chemical fingerprints of mineralization processes; *in* Targeted Geoscience Initiative 4: Canadian NickelCopper-Platinum Group Elements-Chromium Ore Systems — Fertility, Pathfinders, New and Revised Models, (ed.) D.E. Ames and M.G. Houlé; Geological Survey of Canada, Open File 7856, p. 257–268.

Ames, D.E. and Houlé, M.G., 2015. A synthesis of the TGI-4 Canadian nickel-copper-platinum group elements-chromium ore systems project — revised and new genetic models and exploration tools for Ni-Cu-PGE, Cr-(PGE), Fe-Ti-V-(P), and PGE-Cu deposits; *in* Targeted Geoscience Initiative 4: Canadian Nickel-Copper-Platinum Group Elements-Chromium Ore Systems — Fertility, Pathfinders, New and Revised Models, (ed.) D.E. Ames and M.G. Houlé; Geological Survey of Canada, Open File 7856, p. 1–15.

Ames, D.E. and Tuba, G., 2015. Epidote-amphibole and accessory phase mineral chemistry as a vector to low-sulphide platinum group element mineralization, Sudbury: laser ablation ICP-MS trace element study of hydrothermal alteration; *in* Targeted Geoscience Initiative 4: Canadian Nickel-Copper-Platinum Group Elements-Chromium Ore Systems — Fertility, Pathfinders, New and Revised Models, (ed.) D.E. Ames and M.G. Houlé; Geological Survey of Canada, Open File 7856, p. 269–286.

Bécu, V. and Houlé, M.G., 2015. Chromite occurrences of the E-Ext stripped outcrop, Mayville intrusion, Bird River greenstone belt, southeastern Manitoba; Geological Survey of Canada, Scientific Presentation 28, 1 sheet, https://doi.org/10.4095/296135

Bécu, V., Houlé, M.G., McNicoll, V.J., Yang, X.M., and Gilbert, H.P., 2015. Mafic intrusive rocks from the Bird River intrusive suite, Bird River greenstone belt, southeast Manitoba; *in* Targeted Geoscience Initiative 4: Canadian Nickel-Copper-Platinum Group Elements Chromium Ore Systems — Fertility, Pathfinders, New and Revised Models, (ed.) D.E. Ames and M.G. Houlé; Geological Survey of Canada, Open File 7856, p. 49–60.

Bécu, V., Houlé, M.G., McNicoll, V.J., Yang, X.M., and Gilbert, H.P., 2015. New insights from textural, petrographic, and geochemical investigation of the gabbroic rocks of the Bird River intrusive event within the Bird River greenstone belt, southeastern Manitoba; Geological Survey of Canada, Scientific Presentation 27, 1 sheet. https://doi.org/10.4095/296133

Bédard, M.-P., Houlé, M.G., Hébert, R., Goutier, J., 2017. Étude pétrographique de l'intrusion ultramafique chromitifère du lac des Montagnes, Baie-James, Québec; Geological Survey of Canada, Scientific Presentation 55, 1 sheet. https://doi.org/10.4095/299839

Bédard, M.-P., Houlé, M.G., and Huot, F., 2018. Caractérisation des filons-couches mafiques et ultramafiques de la Zone de Gerido dans la région des Lacs Qamaniik, Fosse du Labrador, Nunavik, Québec; Geological Survey of Canada, Scientific Presentation 89, 1 sheet.

Bleeker, W., 2020. Preface; *in* Targeted Geoscience Initiative 5: Advances in the understanding of Canadian Ni-Cu-PGE and Cr ore systems – Examples from the Midcontinent Rift, the Circum-Superior Belt, the Archean Superior Province, and Cordilleran Alaskan-type intrusions, (ed.) W. Bleeker and M.G. Houlé; Geological Survey of Canada, Open File 8722, p. 1–6. https://doi.org/10.4095/326835

Bleeker, W. and Ames, D.E., 2017. System-scale and deposit-scale controls on Ni-Cu-PGE mineralization in cratonic areas and their margins; *in* Targeted Geoscience Initiative – 2016 Report of Activities, (ed.) N. Rogers; Geological Survey of Canada, Open File 8199, p. 47-53. https://doi:10.4095/299573

Bleeker, W. and Houlé, M.G. (ed.), 2020. Targeted Geoscience Initiative 5: Advances in the understanding of Canadian Ni-Cu-PGE and Cr ore systems – Examples from the Midcontinent Rift, the Circum-Superior Belt, the Archean Superior Province, and Cordilleran Alaska-type intursions; Geological Survey of Canada, Open File 8722, 225 p. https://doi.org/10.4095/326702

Bleeker, W. and Kamo, S.L., 2018. Extent, origin, and deposit-scale controls of the 1883 Ma Circum-Superior large igneous province, northern Manitoba, Ontario, Quebec, Nunavut and Labrador; *in* Targeted Geoscience Initiative: 2017 report of activities, volume 2, (ed.) N. Rogers; Geological Survey of Canada, Open File 8373, p. 5–14. https://doi.org/10.4095/306592

Bleeker, W. and Kamo, S., 2020. Structural-stratigraphic setting and U-Pb geochronology of Ni-Cu-Co-PGE ore environments in the central Cape Smith Belt, Circum-Superior Belt; *in* Targeted Geoscience Initiative 5: Advances in the understanding of Canadian Ni-Cu-PGE and Cr ore systems – Examples from the Midcontinent Rift, the Circum-Superior Belt, the Archean Superior Province, and Cordilleran Alaskan-type intrusions, (ed.) W. Bleeker and M.G. Houlé; Geological Survey of Canada, Open File 8722, p. 65–98. https://doi.org/10.4095/326882

Bleeker, W., Kamo, S.L., Ames, D.E., and Davis, D., 2015. New field observations and U-Pb ages in the Sudbury

area: toward a detailed cross-section through the deformed Sudbury Structure; *in* Targeted Geoscience Initiative 4: Canadian Nickel-Copper-Platinum Group Elements-Chromium Ore Systems — Fertility, Pathfinders, New and Revised Models, (ed.) D.E. Ames and M.G. Houlé; Geological Survey of Canada, Open File 7856, p. 151–166.

Bleeker, W., Liikane, D.A., Smith, J., Hamilton, M., Kamo, S.L., Cundari, R., Easton, M., and Hollings, P., 2018. Controls on the localization and timing of mineralized intrusions in intra-continental rift systems, with a specific focus on the ca. 1.1 Ga Mid-continent Rift system; *in* Targeted Geoscience Initiative: 2017 report of activities, volume 2, (ed.) N. Rogers; Geological Survey of Canada, Open File 8373, p. 15–27. https://doi.org/10.4095/306594

Bleeker, W., Smith, J., Hamilton, M., Kamo, S., Liikane, D., Hollings, P., Cundari, R., Easton, M., and Davis, D., 2020. The Midcontinent Rift and its mineral systems: Overview and temporal constraints of Ni-Cu-PGE mineralized intrusions; *in* Targeted Geoscience Initiative 5: Advances in the understanding of Canadian Ni-Cu-PGE and Cr ore systems – Examples from the Midcontinent Rift, the Circum-Superior Belt, the Archean Superior Province, and Cordilleran Alaskan-type intrusions, (ed.) W. Bleeker and M.G. Houlé; Geological Survey of Canada, Open File 8722, p. 7–35. https://doi.org/10.4095/326880

Brzozowski, M.J., Samson, I.M., Gagnon, J.E., Linnen, R.L., Good, D.J., Ames, D.E., and Flemming, R.L., 2015. Variation in vein mineralogy and mineral chemistry around the Marathon Cu-Pd deposit, Ontario: Insights into the development of an exploration tool; *in* Targeted Geoscience Initiative 4: Canadian Nickel-Copper-Platinum Group Elements-Chromium Ore Systems — Fertility, Pathfinders, New and Revised Models, (ed.) D.E. Ames and M.G. Houlé; Geological Survey of Canada, Open File 7856, p. 245–255.

Carson, H.J.E., Lesher, C.M., and Houlé, M.G., 2015. Geochemistry and petrogenesis of the Black Thor intrusive complex and associated chromite mineralization, McFaulds Lake greenstone belt, Ontario; *in* Targeted Geoscience Initiative 4: Canadian Nickel-Copper-Platinum Group Elements-Chromium Ore Systems — Fertility, Pathfinders, New and Revised Models, (ed.) D.E. Ames and M.G. Houlé; Geological Survey of Canada, Open File 7856, p. 87–102.

Chung, C.-J., Franklin, J.M., Hillary, E., and Houlé, M.G., in prep. Technical Report on Development of a GIS-based System for Assessment of Discovery Potential Using an Expert-Defined Nickel Deposit Model and Digital Geological Maps Including Nickel potential maps in Shaw Dome and Dundonald areas (Timmins, ON), Melville Peninsula and Committee Bay areas (Nunavut) and Slave Province (Northwest Territories); Geological Survey of Canada, Open File 8661.

Dare, S.A.S., Ames, D.E., Lightfoot, P.C., Barnes, S.-J., and Beaudoin, G., 2015. Trace elements in Fe-oxide minerals from fertile and barren igneous complexes: Investigating their use as a vectoring tool for Ni-Cu-PGE sulphide mineralization; *in* Targeted Geoscience Initiative 4: Canadian Nickel-Copper-Platinum Group Elements-Chromium Ore Systems — Fertility, Pathfinders, New and Revised Models, (ed.) D.E. Ames and M.G. Houlé; Geological Survey of Canada, Open File 7856, p. 175–185.

Davey, S., Bleeker, W., Kamo, S., Davis, D., Easton, M., and Sutcliffe, R.H., 2019. Ni-Cu-PGE potential of the Nipissing sills as part of the ca. 2.2 Ga Ungava large igneous province; *in* Targeted Geoscience Initiative: 2018 report of activities, (ed.) N. Rogers; Geological Survey of Canada, Open File 8549, p. 403–419. https://doi.org/10.4095/313675

Hanley J.J., MacMillan, M.A., Kerr, M.J., Watts, K.M., Warren, M.R., and Ames, D.E., 2015. Recent advances in fluid and melt inclusion and applied mineralogical research in the Sudbury mining camp: improving ore genesis models and exploration success; *in* Targeted Geoscience Initiative 4: Canadian Nickel-Copper-Platinum Group Elements-Chromium Ore Systems — Fertility, Pathfinders, New and Revised Models, (ed.) D.E. Ames and M.G. Houlé; Geological Survey of Canada, Open File 7856, p. 209–231.

Hiebert, R.S., Bekker, A., Houlé, M.G., Rouxel, O.J., and Wing, B.A., 2015. Identifying and tracing crustal contamination in the Hart komatiite-associated Ni-Cu-(PGE) deposit using multiple S and Fe isotopes: Abitibi greenstone belt, Ontario; *in* Targeted Geoscience Initiative 4: Canadian Nickel-Copper-Platinum Group Elements-Chromium Ore Systems — Fertility, Pathfinders, New and Revised Models, (ed.) D.E. Ames and M.G. Houlé; Geological Survey of Canada, Open File 7856, p. 197–207.

Houlé, M.G. and Préfontaine, S, 2017. Geology and mineralization in the Potter Mine area, Munro Township (Day 2 - part 1): Precious- and base-metal deposits of the southern Abitibi greenstone belt, Superior Province, Ontario and Quebec, 14th Biennial Society for Geology Applied to Mineral Deposits meeting field trip guidebook, (ed.) P. Mercier-Langevin, J. Goutier, and B. Dubé; Geological Survey of Canada, Open File 8317, p. 13–28. https://doi.org/10.4095/306254

Houlé, M.G., Goutier, J., Sappin, A.-A., and McNicoll, V.J., 2015. Regional characterization of ultramafic to mafic intrusions in the La Grande Rivière and Eastmain domains, Superior Province, Quebec; *in* Targeted Geoscience Initiative 4: Canadian Nickel-Copper-Platinum Group Elements-Chromium Ore Systems — Fertility, Pathfinders, New and Revised Models, (ed.) D.E. Ames and M.G. Houlé; Geological Survey of Canada, Open File 7856, p. 125–137.

Houlé, M.G., Lesher, C.M., McNicoll, V.J., Metsaranta, R.T., Sappin, A.-A., Goutier, J., Bécu, V., Gilbert, H.P., and Yang, X.M., 2015. Temporal and spatial distribution of magmatic Cr-(PGE), Ni-Cu-(PGE), and Fe-Ti-(V) deposits in the Bird River–Uchi–OxfordStull–La

Grande Rivière–Eastmain domains: a new metallogenic province within the Superior Craton; *in* Targeted Geoscience Initiative 4: Canadian Nickel-Copper-Platinum Group Elements-Chromium Ore Systems — Fertility, Pathfinders, New and Revised Models, (ed.) D.E. Ames and M.G. Houlé; Geological Survey of Cana da, Open File 7856, p. 35–48.

Houlé, M.G., Lesher, C.M., McNicoll, V.J., and Bécu, V., 2017. Ni-Cr Metallotect: Synthesis, updates, and revised models for the Superior Province; *in* Targeted Geoscience Initiative – 2016 Report of Activities, (ed.) N. Rogers; Geological Survey of Canada, Open File 8199, p. 59–61. https://doi:10.4095/299573

Houlé, M.G., Lesher, C.M., Schetselaar, E.M., Metsaranta, R.T., and McNicoll, V.J., 2017. Architecture of magmatic conduits in Cr-(PGE)/Ni-Cu-(PGE) ore systems; *in* Targeted Geoscience Initiative – 2016 Report of Activities, (ed.) N. Rogers; Geological Survey of Canada, Open File 8199, p. 55–58. https://doi:10.4095/ 299573

Houlé, M.G., Lesher, C.M., and Sappin, A.-A., 2019. Overview of chromium, Fe-Ti-V and Ni-Cu-PGE metal endowment of the Superior Province; *in* Targeted Geoscience Initiative: 2018 report of activities, (ed.) N. Rogers; Geological Survey of Canada, Open File 8549, p. 433–440. https://doi.org/10.4095/313677

Houlé, M.G., Lesher, C.M., Metsaranta, R.T., and Sappin, A.-A., 2019. Architecture of magmatic conduits in chromium-PGE and Ni-Cu-PGE ore systems in Superior Province: example from the 'Ring of Fire' region, Ontario; *in* Targeted Geoscience Initiative: 2018 report of activities, (ed.) N. Rogers; Geological Survey of Canada, Open File 8549, p. 441–448. https://doi.org/ 10.4095/313678

Houlé, M.G., Lesher, C.M., Sappin, A.-A., Bédard, M.-P., Goutier, J., and Yang, X.M., 2020a. Overview of Ni-Cu-(PGE), Cr-(PGE), and Fe-Ti-V magmatic mineralization in the Superior Province: Insights on metallotects and metal endowment; *in* Targeted Geoscience Initiative 5: Advances in the understanding of Canadian Ni-Cu-PGE and Cr ore systems – Examples from the Midcontinent Rift, the Circum-Superior Belt, the Archean Superior Province, and Cordilleran Alaskan-type intrusions, (ed.) W. Bleeker and M.G. Houlé; Geological Survey of Canada, Open File 8722, p. 117–139. https://doi.org/ 10.4095/326890

Houlé, M.G., Lesher, C.M., Metsaranta, R.T., Sappin, A.-A., Carson, H.J.E., Schetselaar, E.M., McNicoll, V., and Laudadio, A., 2020b. Magmatic architecture of the Esker intrusive complex in the Ring of Fire intrusive suite, McFaulds Lake greenstone belt, Superior Province, Ontario: Implications for the genesis of Cr and Ni-Cu-(PGE) mineralization in an inflationary dyke-chonolith-sill complex; *in* Targeted Geoscience Initiative 5: Advances in the understanding of Canadian Ni-Cu-PGE and Cr ore systems – Examples from the Midcontinent Rift, the Circum-Superior Belt, the Archean Superior Province, and Cordilleran Alaskan-type intrusions, (ed.) W. Bleeker and M.G. Houlé; Geological Survey of Canada, Open File 8722, p. 141–163. https://doi.org/10.4095/ 326892

Houlé, M.G., Bandyayera, D., Bécu, V., and Bédard, M.-P., in press. Minéralisations chromifères et nickélifères associées à la Suite mafique-ultramafique de Caumont dans le secteur de Nemiscau, Eeyou Istchee Baie-James, Québec, Canada; Geological Survey of Canada; Scientific Presentation.

Kontak, D.J., MacInnis, L.M., Ames, D.E., Rayner, N.M., and Joyce, N., 2015. A geological, petrological, and geochronological study of the Grey Gabbro unit of the Podolsky Cu-(Ni)-PGE deposit, Sudbury, Ontario, with a focus on the alteration related to the formation of sharp-walled chalcopyrite veins; *in* Targeted Geoscience Initiative 4: Canadian Nickel-Copper-Platinum Group Elements-Chromium Ore Systems — Fertility, Pathfinders, New and Revised Models, (ed.) D.E. Ames and M.G. Houlé; Geological Survey of Canada, Open File 7856, p. 287–301.

Kuzmich, B., Hollings, P., and Houlé, M.G., 2015a. Petrogenesis of the ferrogabbroic intrusions and associated Fe-Ti-V-(P) mineralization within the McFaulds greenstone belt, Superior Province, northern Ontario; *in* Targeted Geoscience Initiative 4: Canadian Nickel-Copper-Platinum Group Elements-Chromium Ore Systems — Fertility, Pathfinders, New and Revised Models, (ed.) D.E. Ames and M.G. Houlé; Geological Survey of Canada, Open File 7856, p. 115–123.

Kuzmich, B., Hollings, P., and Houlé, M.G., 2015b. Lithogeochemistry of iron-titanium-vanadium-phosphorus mineralized mafic intrusions in the McFaulds Lake area, northern Ontario; Ontario Geological Survey, Miscellaneous Release—Data 318.

Laudadio, A.B., Schetselaar, E., Houlé, M.G., and Samson, C., 2018a. 3D geological modelling of the Double Eagle – Black Thor intrusive complexes, McFaulds Lake greenstone belt, Ontario; *in* Targeted Geoscience Initiative: 2017 report of activities, volume 2, (ed.) N. Rogers; Geological Survey of Canada, Open File 8373, p. 35–41. https://doi.org/10.4095/306599

Laudadio, A.B, Schetselaar, E., and Houlé, M.G., 2018b. 3D geological modelling of the Double Eagle-Black Thor intrusive complexes, McFaulds Lake Greenstone Belt, Ontario, Canada; Geological Survey of Canada, Scientific Presentation 82, 1 sheet.

Lesher, C.M. and Houlé, M.G., in press. Geology, physical volcanology, and Ni-Cu-(PGE) deposits of the Raglan area, Cape Smith Belt, Nunavik, Québec, Canada; A Field Trip to the 14th Biennial Society for Geology Applied to Mineral Deposits meeting; Geological Survey of Canada, Open File 8350, 110 p.

McKevitt, D.J., Houlé, M.G., and Lesher, C.M., 2018a. Investigation of ultramafic to mafic komatiitic units within the Raglan Block within the Cape Smith Belt, Nunavik, northern Quebec; *in* Targeted Geoscience

Initiative: 2017 report of activities, volume 1, (ed.) N. Rogers; Geological Survey of Canada, Open File 8358, p. 169–172. http://doi.org/10.4095/306470

McKevitt, Lesher, C.M., and Houlé, M.G., 2018b. Geology and geochemistry of mafic-ultramafic sills in the Northern Permits, Raglan Ni-Cu-(PGE) District, Cape Smith Belt, Nunavik, Quebec; Geological Survey of Canada, Scientific Presentation 90, 1 sheet., https://doi.org/10.4095/308353

McKevitt, D.J., Lesher, C.M. and Houlé, M.G., 2019. Volcanology, geochemistry and petrogenesis of the Expo-Raglan magmatic system in the eastern Cape Smith Belt, Nunavik, northern Quebec; *in* Targeted Geoscience Initiative: 2018 report of activities, (ed.) N. Rogers; Geological Survey of Canada, Open File 8549, p. 393–401. https://doi.org/10.4095/313674

McKevitt, D.J., Lesher, C.M., and Houlé, M.G., 2020. Regional lithogeochemical synthesis of mafic-ultramafic volcanic and intrusive rocks in the Cape Smith Belt, Nunavik, northern Quebec; *in* Targeted Geoscience Initiative 5: Advances in the understanding of Canadian Ni-Cu-PGE and Cr ore systems – Examples from the Midcontinent Rift, the Circum-Superior Belt, the Archean Superior Province, and Cordilleran Alaskan-type intrusions, (ed.) W. Bleeker and M.G. Houlé; Geological Survey of Canada, Open File 8722, p. 99–115. https://doi.org/10.4095/326883

Metsaranta, R.T., Houlé, M.G., McNicoll, V.J., and Kamo, S.L., 2015. Revised geological framework for the McFaulds Lake greenstone belt, Ontario; *in* Targeted Geoscience Initiative 4: Canadian Nickel-Copper-Platinum Group Elements-Chromium Ore Systems — Fertility, Pathfinders, New and Revised Models, (ed.) D.E. Ames and M.G. Houlé; Geological Survey of Canada, Open File 7856, p. 61–73.

Metsaranta, R.T. and Houlé, M.G., 2017a. Geochronology, mineral deposit, drill-core relogging and drill-core compilation data from the Winiskisis Channel, McFaulds Lake and Highbank Lake areas, "Ring of Fire" region, northern Ontario; Ontario Geological Survey, Miscellaneous Release—Data 343.

Metsaranta, R.T. and Houlé, M.G., 2017b. Precambrian geology of the Winiskisis Channel area, "Ring of Fire" region, Ontario—Northern sheet; Ontario Geological Survey, Preliminary Map P.3804; Geological Survey of Canada, Open File 8200, scale 1:100 000. http://doi.org/10.4095/ 299708229

Metsaranta, R.T. and Houlé, M.G., 2017c. Precambrian geology of the McFaulds Lake area, "Ring of Fire" region, Ontario—Central sheet; Ontario Geological Survey, Preliminary Map P.3805; Geological Survey of Canada, Open File 8201, scale 1:100 000. http://doi.org/10.4095/299711

Metsaranta, R.T. and Houlé, M.G., 2017d. Precambrian geology of the Highbank Lake area, "Ring of Fire" region, Ontario—Southern sheet; Ontario Geological Survey, Preliminary Map P.3806 (also Geological Survey of Canada, Open File 8202), scale 1:100 000. http://doi.org/10.4095/299712.

Metsaranta, R.T. and Houlé, M.G. 2020. Precambrian Geology of the McFaulds Lake "Ring of Fire" Region, Northern Ontario; Ontario Geological Survey, Open File Report 6359, 260 p.

Nixon, G.T., Manor, M.J., Jackson-Brown, S., Scoates, J.S., and Ames, D.E., 2015. Magmatic Ni-Cu-PGE sulphide deposits at convergent margins; *in* Targeted Geoscience Initiative 4: Canadian Nickel-Copper-Platinum Group Elements-Chromium Ore Systems — Fertility, Pathfinders, New and Revised Models, (ed.) D.E. Ames and M.G. Houlé; Geological Survey of Canada, Open File 7856, p. 17–34.

Nixon, G.T., Scoates, J.S., Milidragovic, D., Nott, J., Moerhuis, N., Ver Hoeve, T.J., Manor, M.J., and Kjarsgaard, I.M., 2020. Convergent margin Ni-Cu-PGE-Cr ore systems: U-Pb petrochronology and environments of Cu-PGE versus Cr-PGE mineralization in Alaskan-type intrusions; *in* Targeted Geoscience Initiative 5: Advances in the understanding of Canadian Ni-Cu-PGE and Cr ore systems – Examples from the Midcontinent Rift, the Circum-Superior Belt, the Archean Superior Province, and Cordilleran Alaskan-type intrusions, (ed.) W. Bleeker and M.G. Houlé; Geological Survey of Canada, Open File 8722, p. 197–218. https://doi.org/10.4095/326897

Pagé, P., Barnes, S.-J., Méric, J., and Houlé, M.G., 2015. Geochemical composition of chromite from Alexo komatiite in the western Abitibi greenstone belt: Implications for mineral exploration; *in* Targeted Geoscience Initiative 4: Canadian Nickel-Copper-Platinum Group Elements-Chromium Ore Systems — Fertility, Pathfinders, New and Revised Models, (ed.) D.E. Ames and M.G. Houlé; Geological Survey of Canada, Open File 7856, p. 187–195.

Pilkington, M. and Keating, P., 2015. Gravity gradiometer data analysis in mineral exploration; *in* Targeted Geoscience Initiative 4: Canadian Nickel-Copper-Platinum Group Elements-Chromium Ore Systems — Fertility, Pathfinders, New and Revised Models, (ed.) D.E. Ames and M.G. Houlé; Geological Survey of Canada, Open File 7856, p. 167–173.

Sappin, A.-A. and Houlé, M.G., 2020. The composition of magnetite in Archean mafic-ultramafic intrusions within the Superior Province; *in* Targeted Geoscience Initiative 5: Advances in the understanding of Canadian Ni-Cu-PGE and Cr ore systems – Examples from the Midcontinent Rift, the Circum-Superior Belt, the Archean Superior Province, and Cordilleran Alaskan-type intrusions, (ed.) W. Bleeker and M.G. Houlé; Geological Survey of Canada, Open File 8722, p. 181–196. https://doi.org/10.4095/326896

Sappin, A.-A., Houlé, M.G., Lesher, C.M., Metsaranta, R.T., and McNicoll, V.J., 2015a. Regional characterization of mafic-ultramafic intrusions in the Oxford-Stull and

Uchi domains, Superior Province, Ontario; *in* Targeted Geoscience Initiative 4: Canadian Nickel-Copper-Platinum Group Elements-Chromium Ore Systems — Fertility, Pathfinders, New and Revised Models, (ed.) D.E. Ames and M.G. Houlé; Geological Survey of Canada, Open File 7856, p. 75–85.

Sappin, A.-A., Houlé, M.G., Goutier, J., and McNicoll, V., 2015b. Caractérisation pétrographique et géochimique de la Pyroxénite de Baie Chapus, Baie-James: Un exemple de minéralisation en Fe-Ti-V dans la Province du Supérieur; Geological Survey of Canada, Open File 7745, 1 sheet, https://doi.org/10.4095/295612

Sappin, A.-A., Houlé, M.G. and Clark, T., 2018. Minéralisations en Ni-Cu-(EGP) dans la Province de Grenville: État des connaissances et nouvelles perspectives; Commission géologique du Canada, Présentation scientifique 78, 1 fichier.pdf. https://doi.org/10.4095/306387

Shahabi Far, M., Samson, I.M., Gagnon, J.E., Linnen, R.L., Good, D.J., and Ames, D.E., 2015. Textural character and chemistry of plagioclase and apatite in the Marathon Cu-PGE deposit, Ontario: Implications for mineralizing processes; *in* Targeted Geoscience Initiative 4: Canadian Nickel-Copper-Platinum Group Elements-Chromium Ore Systems — Fertility, Pathfinders, New and Revised Models, (ed.) D.E. Ames and M.G. Houlé; Geological Survey of Canada, Open File 7856, p. 233–243.

Smith, J., Bleeker, W., Liikane, D.A., Hamilton, M., Cundari, R., and Hollings, P., 2019. Characteristics of Ni-Cu-PGE sulphide mineralization within the 1.1 Ga Midcontinent Rift; *in* Targeted Geoscience Initiative: 2018 report of activities, (ed.) N. Rogers; Geological Survey of Canada, Open File 8549, p. 421–432. https://doi.org/10.4095/313676

Smith, J.W., Bleeker, W., Hamilton, M., Petts, D., Kamo, S.L., and Rossell, D., 2020. Timing and controls on Ni-Cu-PGE mineralization within the Crystal Lake Intrusion, 1.1 Ga Midcontinent Rift; *in* Targeted Geoscience Initiative 5: Advances in the understanding of Canadian Ni-Cu-PGE and Cr ore systems – Examples from the Midcontinent Rift, the Circum-Superior Belt, the Archean Superior Province, and Cordilleran Alaskan-type intrusions, (ed.) W. Bleeker and M.G. Houlé; Geological Survey of Canada, Open File 8722, p. 37–63. https://doi.org/10.4095/326881

Spath, C.S. III, Lesher, C.M., and Houlé, M.G., 2015. Hybridized ultramafic rocks in the Black Label hybrid zone of the Black Thor intrusive complex, McFaulds Lake greenstone belt, Ontario; *in* Targeted Geoscience Initiative 4: Canadian Nickel-Copper-Platinum Group Elements-Chromium Ore Systems — Fertility, Pathfinders, New and Revised Models, (ed.) D.E. Ames and M.G. Houlé; Geological Survey of Canada, Open File 7856, p. 103–114.

Trevisan, B.E., Hollings, P., Ames, D.E., and Rayner, N.M., 2015. The petrology, mineralization, and regional context of the Thunder mafic to ultramafic intrusion, Midcontinent Rift, Thunder Bay, Ontario; *in* Targeted Geoscience Initiative 4: Canadian Nickel-Copper Platinum Group Elements-Chromium Ore Systems — Fertility, Pathfinders, New and Revised Models, (ed.) D.E. Ames and M.G. Houlé; Geological Survey of Canada, Open File 7856, p. 139–149.

Zuccarelli, N., Lesher, C.M., and Houlé, M.G., 2018a. Sulphide textural variations and multiphase ore emplacement in the Eagle's Nest Ni-Cu-(PGE) deposit, McFaulds Lake greenstone belt, Ontario; *in* Targeted Geoscience Initiative: 2017 report of activities, volume 2, (ed.) N. Rogers; Geological Survey of Canada, Open File 8373, p. 29–34. https://doi.org/10.4095/306598

Zuccarelli, N., Lesher, C.M., Houlé, M.G., and Weston, R., 2018b. Textural variations in the Eagle's Nest Ni-Cu-(PGE) deposit in Ontario and implications for magma dynamics in a blade-shaped dike; Geological Survey of Canada, Scientific Presentation 83, 1 sheet, https://doi.org/10.4095/308255

Zuccarelli, N., Lesher, C.M., Houlé, M.G., and Barnes, S.J., 2020. Variations in the textural facies of sulphide minerals in the Eagle's Nest Ni-Cu-(PGE) deposit, McFaulds Lake greenstone belt, Superior Province, Ontario: Insights from microbeam scanning energy-dispersive X-ray fluorescence spectrometry; *in* Targeted Geoscience Initiative 5: Advances in the understanding of Canadian Ni-Cu-PGE and Cr ore systems – Examples from the Midcontinent Rift, the Circum-Superior Belt, the Archean Superior Province, and Cordilleran Alaskan-type intrusions, (ed.) W. Bleeker and M.G. Houlé; Geological Survey of Canada, Open File 8722, p. 165–179. https://doi.org/10.4095/326895

THESES

Brzozowski, M.J., 2018. Applications of mineral chemistry to petrogenesis and exploration in conduit-type Cu-PGE deposits; Ph.D. thesis, University of Windsor, Windsor, Ontario, 301 p.

Carson, H.J.E., in prep. Stratigraphy, geochemistry, and petrogenesis of the Black Thor intrusion and associated Cr and Ni-Cu-PGE mineralization, McFaulds greenstone belt, Ontario; Ph.D. thesis, Laurentian University, Sudbury, Ontario.

Davey, S.C., 2019. Testing the paleogeography of late Archean supercraton Superia using pre-breakup 2.51–1.98 Ga dyke and sill provinces—with a focus on the relationship between the Karelia-Kola and Superior cratonic fragments; Ph.D. thesis, Carleton University, Ottawa, Ontario, 313 p.

Farhangi, N., in prep. Mineralogy, geochemistry, and petrogenesis of Ni-Cu-(PGE) mineralization in the Black Thor intrusion, McFaulds Lake greenstone belt, Ontario; M.Sc. thesis, Laurentian University, Sudbury, Ontario.

Hiebert, R.S., 2018. Contamination of mafic to ultramafic magmas by sulfur-bearing sediments: evaluation of the environment of deposition and tracing the unique signature of the contaminants through the magma using multiple sulfur and iron isotope data; Ph.D. thesis, University of Manitoba, Winnipeg, Manitoba, 167 p.

Laudadio, A., 2019. 3-D Geological Modelling of the Double Eagle – Black Thor Intrusive Complexes, McFaulds Lake Greenstone Belt, Ontario, Canada; M.Sc. thesis, Carleton University, Ottawa, Ontario, 107 p.

MacInnis, L., 2019. Constraining alteration in the footwall of the Sudbury igneous complex: a case study of the alteration footprint to the Podolsky, Cu(-Ni)-PGE deposit, Sudbury; M.Sc. thesis, Laurentian University, Sudbury, Ontario, 204 p.

McKevitt, D.J., in prep. Localization of Ni-Cu-(PGE) mineralization in an early Proterozoic trans-crustal dike-sill-lava channel system, Cape Smith Belt, Nunavik; Ph.D. thesis, Laurentian University, Sudbury, Ontario.

Mehrmanesh, K., in prep. Stratigraphy of the Black Label Chromitite Horizon, Black Thor intrusion, McFaulds Lake Greenstone Belt, Ontario, Canada; M.Sc. thesis, Laurentian University, Sudbury, Ontario.

Méric, J., 2018. Le ruthénium (Ru), iridium (Ir), osmium (Os) et rhodium (Rh) et les éléments traces dans des chromites de komatiites issues de la zone Alexo et de la zone Hart, (Abitibi, Ontario): un outil diagnostique pour l'exploration de systèmes fertiles; M.Sc. thesis, Université du Québec à Chicoutimi, Saguenay, Québec, 185 p.

Paré, A., 2019. Origine d'un gabbro minéralisé issu de carottes de forages provenant de la Zone 5-8 de la Mine Raglan, Nunavik, Québec; B.Sc., Université Laval, Québec, Québec, 33 p.

Shahabi Far, M., 2016. The magmatic and volatile evolution of gabbros hosting the Marathon PGE-Cu deposit: Evolution of a conduit system; Ph.D. thesis, University of Windsor, Windsor, Ontario, 240 p.

Spath, C.S., III, 2017. Geology and Genesis of Hybridized Ultramafic Rocks in the Black Label Hybrid Zone of the Black Thor Intrusive Complex, McFaulds Lake Greenstone Belt, Ontario, Canada; M.Sc. thesis, Laurentian University, Sudbury, Ontario, 94 p.

Zuccarelli, N., in prep. Sulfide textural variations and multiphase ore emplacement in the Eagle's Nest Ni-Cu-(PGE) deposit, McFaulds Lake greenstone belt, Superior Province, Ontario, Canada; M.Sc. thesis, Laurentian University, Sudbury, Ontario.